AN EXPERIMENTAL AND NUMERICAL INVESTIGATION OF EVAPORATING WATER SPRAYS INJECTED INTO FLOWING SUPERHEATED STEAM

A THESIS

Presented to

The Academic Faculty

By

Kevin George Schoonover

In Partial Fulfillment

Of the Requirements for the Degree

Masters of Science in Mechanical Engineering

Georgia Institute of Technology

December 2001

AN EXPERIMENTAL AND NUMERICAL INVESTIGATION OF EVAPORATING WATER SPRAYS INJECTED INTO FLOWING SUPERHEATED STEAM

Approved:

Said I. Abdel-Khalik, Advisor

Sheldon M. Jeter

S. Mostafa Ghiaasiaan

Date Approved by Chairmen 10/12/01

ACKNOWLEDGEMENTS

Guidance and support from several important individuals has played an important role in the successful completion of this thesis. Foremost, I would like to thank my advisor, Dr. S. I. Abdel-Khalik. His instruction, counsel, and friendship have served as an invaluable source of inspiration throughout the duration of this project. I would also like to thank my additional committee members, Dr. Sheldon M. Jeter and Dr. S. Mostafa Ghiaasiaan for their assistance and recommendations in the development of this thesis.

Additional thanks are due to Mr. Mike Dowling for his assistance in the construction of the test apparatus and in the creation of the data sorting software. Likewise, thanks are in order for Dr. Guang-Fa Yao, at Georgia Tech, and Dr. Ted Long, at Fisher Controls International, Inc., for their support and guidance in the creation of the SteamCFD code and associated model generation. A special thanks is in order for Mr. Bill Lowrey, Plant Engineer – UNC Cogeneration Facility, for his acceptance of the project scope within the UNC steam plant and his flexibility in incorporating the necessary hardware and software for the experimental phase of the project.

Finally, I would like to thank my family, especially my wife Teresa, for their encouragement and patience throughout my graduate career at Georgia Tech. Their love and understanding has helped ease the completion of this thesis. I would also like to dedicate this paper to the memory of my father, George H. Schoonover, whose inspiration and mechanical abilities directed me toward the engineering field of study.

TABLE OF CONTENTS

TABLE OF CONTENTS (cont'd)

TABLE OF CONTENTS (cont'd)

LIST OF TABLES

LIST OF ILLUSTRATIONS

LIST OF ILLUSTRATIONS (cont'd)

LIST OF ILLUSTRATIONS (cont'd)

LIST OF ILLUSTRATIONS (cont'd)

LIST OF ILLUSTRATIONS (cont'd)

LIST OF ILLUSTRATIONS (cont'd)

LIST OF ILLUSTRATIONS (cont'd)

NOMENCLATURE

Cv	liquid flow coefficient [3.2]
P	pressure (psi) [3.1], [3.2]
Q	volumetric liquid flow rate (gpm) [3.1], [3.2]
SG	liquid specific gravity [3.2]

Greek Letters

Δ	differential

Subscripts

w	liquid
x	condition variable
1	initial condition
2	secondary condition

SUMMARY

The increased focus on improved reliability, flexibility, and efficiency in commercial and utility power plants has placed a strong emphasis on system performance. Integral to this is the operation of devices used for proper conditioning of steam temperature. These devices normally utilize sprays of sub-cooled water to regulate or control the temperature of superheated steam. Despite its widespread application, fundamental aspects of spray cooling in this manner remain essentially empirical. Considerable effort has recently been devoted to mechanistic modeling of the transport phenomena involved in such systems. Without the fundamental understanding to be gained from such efforts, prediction of system performance and accurate temperature control for the various operating conditions remains highly uncertain.

The objective of this research was to experimentally observe, within a controlled environment, and computationally simulate the various heat, mass, and momentum transport processes taking place in a steam conditioning or desuperheating system. A large-scale test facility was constructed within the low-pressure turbine extraction steam system of the University of North Carolina – Chapel Hill Cogeneration Plant. Before distribution to the academic and medical facilities on campus, the steam temperature needed to be reduced to more acceptable levels. To accomplish this, sub-cooled water was injected into the flowing superheated steam via a series of variable geometry back-pressure activated spray nozzles placed radially across the 30" diameter flow cross-section. Temperature, pressure, and mass flow data were collected and analyzed to

determine the extent of vaporization, droplet fall-out, and thermal stratification at two different axial and 48 radial locations along the downstream pipe. Experiments were conducted utilizing different control schemes, nozzle configurations, and steam flow conditions to determine the influence of various design and operational parameters on system performance including the creation of highly stratified steam flows in large diameter pipelines.

The collected experimental data were compared with predictions of the SteamCFD computer code developed at Georgia Tech. This code is based on rigorous, transient, three-dimensional, two-fluid representation of the conservation equations. Unlike most commercial computational fluid dynamic codes, SteamCFD was developed solely to evaluate the thermal and fluid dynamics affects of spray injections of water into flowing steam. Application of this computational tool was used to provide insight and graphical representation of the physical environment downstream of the injection point as well as utilize the data as a means for code verification. Computational and experimental thermal profiles were compared for each of the individual data sets. Based on this comparison, modifications in the system's design and instrumentation were implemented to reduce the extent of thermal stratification and improve the vaporization performance. The results of this investigation demonstrate the usefulness of the SteamCFD code as a computational tool to provide improved reliability, flexibility, and efficiency for many different steam systems within commercial and utility power plants.

CHAPTER I

INTRODUCTION

I.1 UNC Cogeneration Facility

The UNC Cogeneration Facility is one of the most modern energy production facilities of its kind with construction and start-up completed in 1992. The principal purpose of the Cogeneration Facility is to generate steam for distribution to the University Of North Carolina at Chapel Hill campus, and to the UNC Hospitals. The steam is used for heating, cooling (via heat absorption), domestic hot water, humidification, sterilization, cooking, and cleaning. The Cogeneration Facility also generates electricity as a by-product of steam production.

Figure I.1 - UNC Cogeneration Facility

Plant equipment includes two 250,000 pounds per hour circulating fluidized bed (CFB) coal burning boilers, one 150,000 pounds per hour oil/gas package boiler, and one

28 megawatt steam turbine generator. The plant is completely operated and controlled via a Westinghouse Process Control distributive control operating system.

Figure I.2 - Plant Distributed Control System (DCS)

The Cogeneration Facility generates steam in two large circulating fluidized bed (CFB) boilers. Steam exits the coal-fired boilers at roughly 900° F and 1,300 PSIG. The turbine-generator reduces the steam pressure and temperature in multiple stages and provides steam to a high and low-pressure extraction system. Discharge conditions are normally 420° F at 150 PSIG and 330° F at 40 PSIG, respectively. The lower pressure steam is used for space and water heating and as a heat source for 11,100 tons of steam absorption chillers for space cooling. The higher-pressure steam is used for process loads such as medical research projects and surgical instrument sterilization.

I.2 The Steam Bypass System

During design and construction of the plant, the UNC engineers realized that the likelihood of a turbine trip or load rejection would be inevitable. The complexity of the operating and control systems of the turbine-generator, and associated systems, makes the probability of malfunction much higher than that for the boiler. However, regardless of the turbine-generator's operating situation, the campus would still require an uninterrupted flow of steam at the desired pressure and temperature.

To assure the ability to deliver an uninterrupted flow of steam, at the desired conditions, a bypass system was implemented. This system included a series of large pressure reducing valves and desuperheaters that are capable of duplicating the depressurization and enthalpy reduction processes normally provided by the turbine. Depending on the application, equipment was provided to handle either or both of the control parameters, i.e., temperature and/or pressure. Thus, a means of providing the desired steam conditions to all the campus facilities, on an uninterrupted basis, was assured.

Figure I.3 - Plant Extraction Headers & Bypass System

I.3 Problem Definition and Objectives

Under normal operating conditions, the turbine efficiently and consistently reduces the steam pressure and temperature as the steam is expanded through each stage and the thermal energy is converted to mechanical energy. However, when the turbine is not operational, the bypass system must perform the desired depressurization and temperature reduction before the steam can be delivered to the various process applications.

From an expansion standpoint, much is known about the handling of compressible fluids, such as steam, and pressure control is a relatively easy task to accommodate. Utilizing elementary feedback control systems, today's pressure reducing valves can provide the accuracy and response time needed for such applications. However, when there is also a requirement for temperature control, the same levels of performance can be difficult to achieve.

The design and construction of spray systems, desuperheaters, and attemporators requires much more analysis and empirical data. Unlike the pressure-reducing valve, the desuperheater is not a final control element. Thus, its performance is highly susceptible to the environment or control volume that it must operate within. Parameters such as water temperature, water quantity, pipe size, spray geometry, droplet size and distribution, penetration velocity, orientation, and required rangeability can all impact positively or negatively on the overall performance envelope of the device.

The low-pressure extraction line at the UNC Cogeneration Plant is a 30" diameter-Standard Wall pipe. To control the downstream temperature, when variations above the

specified norm were detected, a Fisher Controls DVG/AF-1E self-contained variable geometry desuperheater nozzle was installed. To regulate the quantity of injected spray water, a simple feedback control system was employed using a single J-Type thermocouple installed in the centerline of the pipe approximately 50 diameters downstream of the injection point. Based on empirical models normally used to design such systems, it was expected that this would be a sufficient distance for the injected water to vaporize and mix, thus providing a homogenous flow stream in thermal equilibrium. Proposed application specifications at different conditions are listed in Table I.1.

Table I.1 - Low Pressure Extraction Steam Desuperheater Specifications

Operating Parameters	Units	Case 1 Conditions	Case 2 Conditions	Case 3 Conditions
Steam Pressure	PSIA	69.7	69.7	49.7
Steam Inlet Temperature	°F	375	650	405
Steam Outlet Temperature	°F	317	317	317
Water Pressure	PSIA	290	290	290
Water Temperature	°F	275	275	275
Inlet Steam Flow	PPH	350,000	50,000	130,000
Water Mass Flow	PPH	11,412	8,891	6,087
Inlet Steam Velocity	FPS	144.4	28.0	78.8
Inlet Enthalpy	BTU/LBm	1,219.1	1,356.3	1,237.5
Outlet Enthalpy	BTU/LBm	1,188.4	1,188.4	1,193.0
Water Enthalpy	BTU/LBm	244.1	244.1	244.1
Saturation Pressure	PSIA	45.4	45.4	45.4
Initial Superheat	°F	72.4	347.4	124.4
Final Superheat	°F	14.4	14.4	14.4
Steam Side Turndown	-/-	1	7	2.7
Water Side Turndown	-/-	1	1.3	1.9
Velocity Turndown	-/-	1	5.2	1.8

Plant data indicates that, at or near the maximum specified steam flows, the unit provided acceptable levels of performance. However, as steam flow was reduced, the temperature control system was unable to maintain the downstream temperature even though all systems appeared to be working in an acceptable manner. The reason for such degradation in performance can be traced to the presence of significant thermal stratification downstream of the injection point. This is especially evident in large diameter pipes, where large radial temperature gradients exist and thus render the single point control method inadequate and meaningless.

I.4 Experimental Scope

Many things in nature stratify naturally as a result of differences in density, temperature, or size. However, most of these situations are related more to natural convection conditions. The phenomenon of thermal stratification in highly turbulent, forced convection, compressible flow streams is far less understood and documented. Its relevance in the world today is far more important as factories and power stations continue to grow in size, and as demand for more efficient operation is increased.

The purpose of this experiment was two-fold. The first was to determine whether or not thermal stratification existed within the piping system downstream of a desuperheater. To accomplish this, the LP extraction pipeline at the UNC Cogeneration plant was instrumented in such a manner that radial temperature distributions could be recorded at several specific axial and radial locations in the pipeline. These reading would be collected and compared at various steam and water mass flows and steam pressures to determine the extent of vaporization, droplet fall-out, and thermal

stratification. The second objective was to determine if the stratification phenomenon could be computationally simulated and verified, quantified parametrically, and recommendations made to reduce its negative impacts. To accomplish this objective, the SteamCFD code, developed at Georgia Tech, was utilized to model the conditions observed in the field.

CHAPTER II

LITERATURE REVIEW

II.1 Introduction

Liquid atomization is used in many technical processes that require efficient heat and mass transfer between the injected liquid and the gas/vapor medium. The process of controlling steam temperatures with the injection of water is a common example of just such a process and one that is routinely found in most all power, chemical, and pulp & paper plants around the world. However, considering its widespread utilization, the processes and parameters required for efficient operation are not that widely analyzed or understood.

In early power stations, the process was very much a base load operation. The mass of steam flowing through the system was nearly constant every hour of the day. Likewise, the temperatures and pressures that were associated with sub-critical plant development did not warrant extremes in the design of the spray mechanism. Neither the spray quantity nor the steam temperature created any significant design or metallurgical concerns for the engineer. Some industrial plants produced their own designs of nozzles that involved little more then a capped pipe section with some flow orifices drilled in the side. Similarly, the large base loaded power stations utilized large fixed geometry simplex or pressure swirl atomizers to perform the task. The need for high performance and extreme turndown had not yet reached the commercial and power utility sites.

In the late 50's and early 60's, pressures and temperatures, and the resultant efficiencies began to rise significantly with the introduction of the super-critical boiler. With these changes came more challenges. Along with the increase in pressure and temperatures, the flow also increased drastically as did the size of the piping systems that had to deliver this flow stream to the turbine or other mechanical drive location.

At that point, performance started to become an issue. Besides plant efficiency, the treatment of the various heavy wall piping material grades, thermal expansion, thermal shock, and two-phase flow phenomenon brought new constraints to the design engineer. The old designs did not work and the pressure to continue the upward drive in flow conditions was not ending.

II.2 The Desuperheating Process

Compared to the many other components in a power station, i.e., turbine, boiler, pumps, valves, etc., the desuperheater is conceptually a relatively simple device. However, with only a minimum of review, one can readily understand the complexity of the application. If, for instance, we compared a desuperheater to a control valve assembly, we could see some major functional differences in assemblies that can appear very similar in arrangement. First, the valve is classified as a final or primary control element. By this, we define the system boundary to include the valve inlet and outlet. All flow within the control volume is contained within the valve and the valve has direct influence on the condition of the flow whether it is directional, capacity, or pressure related. Additionally, the valve, or the throttling process it is applied to, undertakes no

appreciable energy transfer, i.e., the process is Isenthalpic, and deals with a single flow stream of constant state and of single phase.

In contrast, the desuperheater is a secondary control element. Its system boundary does not encompass the majority flow stream that it is associated with. Flow through its control volume exits into a separate flow stream that materially governs the overall performance of the system. Thus, the desuperheater regulates and conditions a specific secondary flow stream that flows into the primary or majority flow stream. Once the two streams are combined, the resultant and expected function of the desuperheater, i.e., temperature control, is dependent on the condition of the secondary flow stream and its independent interaction with the primary flow stream. Additionally, the desuperheating process involves real energy transfer, a complex two-phase mixing flow, and transient transport phenomena with a phase change.

When one compares the actions or requirements of the valve assembly to the desupeheater, the complexity of the process becomes quite apparent. In designing a functional desuperheater installation, the design engineer must contend with considerable complexity in a number of specialty areas. Many of these areas are difficult to quantify. These include, but are not limited to, the following:

- Spray Penetration/Momentum Transfer
- Global Mixing Efficiency
- Instrumentation Location
- Pipeline Thermal Transients
- Nozzle Installation Geometry

- Spray Particle Size & Distribution
- Spray Water Temperature & Quantity
- Pipeline Size & Velocity
- Expected System Rangeability

II.3 Applicable Research

Spray and atomization research has been going on for a considerable period of time with the majority of studies being directed to the understanding of fuel injection in internal combustion engines. Additionally, most atomization investigations are conducted in a stagnant, non-condensable gas, such as free air, rather than in a flowing mediun within confined areas with possible phase change. While free air studies are important to understand the mechanics of the spray nozzle itself, it leaves much to interpretation as to what transpires when the classical spray pattern in immersed in a highly turbulent superheated vapor of the same substance, within a physically constrained environment.

General research can be divided into four main categories. These include nozzle design, fluid dynamic considerations, heat transfer, and application experience. Unfortunately, these individual components are rarely cross-correlated for direct application to the present study. In each case, specific components or results can be extracted and experimental or computational studies conducted to determine the resultant interaction of the parts and applicability of the hypothesis.

II.4 Nozzle Design

The field is rich with books, papers, and reports concerning the design of nozzles of every type and configuration. Liao et al. (1999) provided mathematical methods to effectively evaluate geometric variations in a simplex atomizer or pressure swirl nozzle. This style of nozzle is prevalent within the desuperheater industry due to its ability to generate a hollow cone spray pattern. Reitz et al. (1982) examined the impact of specific spray patterns requirements, such as spray angle and fluid distribution, on the resultant nozzle design process. It amounted to a means of reverse engineering to achieve specific fluid conditions. Additionally, in Rizkalla et al. (1975) the emphasis was on both design and results when mixing various liquid properties with airblast atomization techniques. Airblast or steam atomized styles of desuperheaters are another configuration that has gained technical popularity in recent years, however, quantified performance and rangeability data are not readily available. These studies, along with those of Hardalupas et al. (1996) and Palaszewski et al. (1981), all provide descriptions of the operating aspects of specific nozzle geometries. The research provided data on the physical interaction of liquid and vapor flow streams.

Studying nozzle geometry and performance are essential in quantifying geometric parameters for the CFD code. In addition, the information, even though it may be mainly based on stagnant air tests, is important for comparison of nozzle geometries' effects with experimental or application sensitivity studies.

II.5 Fluid Dynamics

The fluid dynamics of sprays is an important area of interest in the desuperheating design arena. A clear understanding of how the fluid will react and how flows combine is essential for any real research to proceed. Dent (1971) provided a methodology to predict, based on experimental methods, the penetration of sprays. While his methods did not cover the highly turbulent environment of today's desuperheating and bypass applications, his basic relationships provide guidelines for low flow applications. Schelling (1998) did considerable research into the interaction of confined sprays in downward air streams. His work did not include any phase change or heat transfer, but it did look at various spray nozzle types and geometries, and related their performance with respect to penetration and radial distribution. Another important fluid dynamic aspect of desuperheating is the understanding of what occurs when the droplets fully penetrate the flow stream and impact the confining walls. Tropea et al. (2000) provided some modeling techniques for spray impacts on solid surfaces. Finally, the Technical University in Delft, Holland, C.A.A. van Paassen (1995) generated a comprehensive volume on spray interactions in flow streams. The text is the result of numerous tests and experiments conducted at the university using various pipelines and spray nozzles. Reitz et al. (1982) examined the mechanism of atomization of a liquid jet. While the work concentrated on round liquid jets, the author did describe the basic mechanism that combines liquid-gas aerodynamic interaction as a function of nozzle geometry.

II.6 Heat Transfer

The purpose of the desuperheater or bypass system is to change the temperature of the flowing medium (steam). Needless to say, the heat transfer aspects are highly important in any study on the subject. Among the earliest studies on droplet evaporation are those of Ranz, et al. (1952) and Ingebo (1953). Ingebo (1953) provides basic information on vaporization rates and heat transfer coefficients for pure liquid drops. While the study did not deal with flowing media and ablation/forced convection processes, it provides detailed data on droplet heat transfer within a specific environment. In a similar manner, Ranz et al. (1952) investigated numerous factors that would influence the rate of evaporation of pure liquid drops. This paper limited gas/liquid flow interactions to flow streams with Reynolds Numbers of less then 200. In another paper, Ingebo (1953) investigated the effects of pressure on the vaporization rate of drops in a gas stream. While none of these papers provided direct correlation with the present experiment, incremental data and influences were beneficial in developing the procedures and interpreting data. In Chow et al. (1983), data on the rate of water evaporation into a superheated steam flow stream are provided. The study is more applicable to film or pool evaporation, but still addresses steam and water heat transfer. In Guo et al. (2000) the effects of the confined channel geometry on the resultant heat transfer and thermal profile are examined. The study includes an examination of thermal transients within a 180° tube bend. Geometric parameters of this type are always of concern when dealing with a two-phase flow and momentum transfer. Aggarwal et al. (1995) reviews the methodologies for representing the droplet motion and vaporization history in two-phase

flow computations. The focus is on the use of droplet models that are realistic in terms of their efficient implementation in comprehensive spray simulations. In Hubbard et al. (1975) droplet evaporation was studied relative to various transients and physical properties. While the research concentrated mostly on single droplet of fuel in stagnant air, much could be translated into the dynamics of heat transfer and evaporation within the flow particles of a desuperheating process. In a similar manner, Dwyer (1989) examined fuel droplet vaporization, however his focus was more toward measuring variations as a function of temperature and included the combustion process. Aggarwal et al. (1991) provided additional research on flow dynamics and evaporating flows. In this later paper, the research focused on the study of the structure of turbulent evaporating sprays and to examine the sensitivity of their vaporization behavior to transient liquid-phase processes.

II.7 Desuperheater Operating Experiences

The literature contains relatively few papers and articles dealing with real life experiences or experiments concerning desuperheaters and bypass applications. However, the subject is of high enough interest to provide some relevant technical papers. Amano et al. (1997) performed a CFD simulation of a bypass application. The model uses multiple spray injection points radially mounted on complex pipe geometry. The study includes heat transfer expectations and some interesting momentum correlations of normally directed flow streams. Kauer (1998) examined desuperheater applications within a thermal power station and provided installation guidelines to optimize heat and mass transfer. Likewise, the Power Industry has published numerous

guidelines for system design and implementation. In Sebald et al. (1982), the thermal and fluid aspects of high-energy admissions to a steam condenser are examined. Kals (1992), who studied the reaction of water-cooled and wet-surface air-cooled condensers to a bypass of the steam turbine, complimented the work of Sebald. Stelz et al. (1984), studied performance issues associated with steam bypass systems. However, his work concentrated more on the fluid and control aspects of the bypass valve. In either case, the desuperheating process was still integral to the paper and its importance in condenser protection was emphasized. Hellington (1985) describes use of desuperheaters for steam cycle temperature control. He focuses on the performance aspects of various styles of desuperheater and how they perform parametrically when compared one against the other.

Examination of the literature points to a clear need for mechanistic investigation of the heat and mass transfer process taking place in steam conditioning equipment. The SteamCFD code, Yao (2000), developed at Georgia Tech provides the means for the conduct of such investigations. Together with experimental data from carefully controlled prototypical systems, such a code can provide a valuable tool for designers of steam conditioning equipment. To this end, this investigation has been undertaken.

CHAPTER III

EXPERIMENTAL APPARATUS AND PROCEDURES

III.1 Introduction

In this chapter, we will describe the physical layout of the experimental installation and how the tests were conducted. This will include a description of the piping arrangement that exists within the UNC Cogeneration Facility, the desuperheater, or spray injection device, that was utilized and modified to provide a controlled variable, the thermocouple array, and the data acquisition system. Each of these components was integral to the performance of the system and the results achieved.

III.2 Piping Configuration

For the purposes of this experiment, the control volume utilized is comprised of 72.0 feet (22.0m) of 30" (762mm) diameter standard-weight carbon steel pipe. This constitutes a significant portion of the LP Extraction piping of the UNC Cogeneration Facility. The initial run is a 49'-7" (15.1m) length of horizontal pipe, see Figure III.1 for piping layout details. Within this section the various spray generating apparatus were installed. At the end of this section, the piping takes a 90° turn in the horizontal plane via a 30" radius elbow. The piping continues for another 8'-6" (2.6m) before encountering another 30" radius elbow that redirects the flow into a vertical downward direction. The control volume terminates approximately 15 feet (4.6m) downstream, where the control steam is mixed with other steam sources in a common distribution header. The control volume is terminated at that point to avoid the need to include these "uncontrolled"

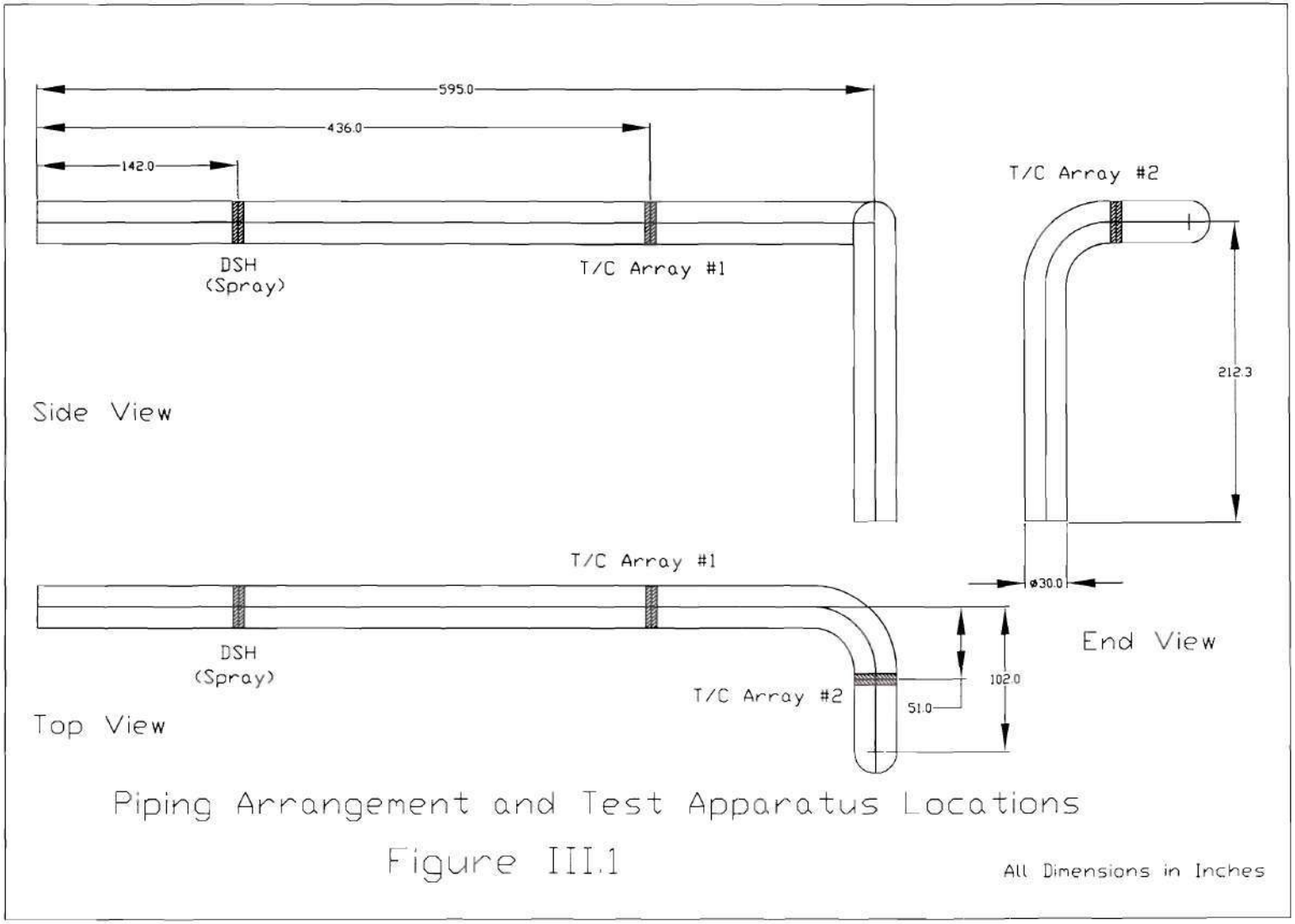

Piping Arrangement and Test Apparatus Locations

Figure III.1

All Dimensions in Inches

streams in the analysis. All measurements were taken within the LP Extraction piping configuration.

In order to determine the critical point of incipient stratification, temperature distribution data are required at various axial and radial locations along the pipe section. However, it is important to note that significant changes in the temperature distribution are expected to take place before and after flow disrupting devices such as elbows. The collection of the temperature distribution data would provide a detailed thermal profile of the flow stream. Additionally, analysis of such data for various flow conditions would allow one to determine how the development of thermal stratification is affected by various design and operational parameters, particularly flow velocity and spray injection quantity.

III.3 Desuperheater

One of the goals of this experiment is to determine how the configuration of the desuperheater, or spray injection device, contributes to the development of thermal stratification. Desuperheater devices can be configured in many ways to affect such parameters as spray angle, penetration velocity, droplet size, spray density, and overall spray distribution. Most of this is accomplished by altering the type and size of spray nozzle employed and by changing its physical location within the pipe cross-section. In this study, three different spray apparatus configurations were used to determine the impact on the system's performance and the degree of stratification generated.

For the test program, two different types of nozzles were utilized. The first nozzle had a special configuration designed to provide a consistent style of spray pattern

characteristic over a wide range of flow conditions. It was a back-pressure activated, variable geometry, hollow cone spray assembly. The hollow cone spray pattern was created by the acceleration of the spray water through a converging annular flow passage that was directed outwards at an angle of 40-45° to the nozzle centerline. The water exited through the nozzle discharge in the form of a thin sheet with an initial outside diameter in the 0.39-0.79" (10-20mm) range. Still air examinations of this type nozzle performance indicated that the sheet later disintegrated into ligaments and then fine droplets in the order of 200-500μm. To assure continuity in the distribution of the fluid as it entered the converging annular flow area, the entrance flow passages were given a compound angle of 20° inward off the centerline and pitched 18° to the side. This produced a radial flow component to the stream and increased the residence time within the nozzle. This additional residence time permitted the individual fluid jets to recombine into a more homogenous flow pattern before being discharged out of the nozzle. Also, to provide greater resistance, and thus better spray generation, to the flow at lower flows and decreased pressure differentials, the control element of the nozzle was spring-loaded. This design feature prevented the discharge of water without the generation of a minimum spray water differential pressure. A photograph of a typical spray pattern created by this type of nozzle is shown in Figure III.2 while a cross-sectional view is illustrated in Figure III.3.

The second type of nozzle utilized in this investigation was a more typical fixed geometry pressure swirl arrangement. In this design, the water is accelerated into the nozzle housing in a tangential manner. The driving force is the pressure differential of

the fluid across the nozzle assembly. Centrifugal force pushes the fluid outwards thus creating an air core in the center. As the fluid is displaced through the nozzle, it encounters a single cylindrical discharge orifice. If the fluid radial velocity is kept at sufficiently high levels, the air core is maintained as the fluid is accelerated through the orifice and the fluid is thrust outwards in a radial manner. The combination of radial and axial velocity components results in the formation of a hollow cone spray pattern of approximately the same discharge angle as the variable geometry backpressure nozzles previously described. The disadvantage of such nozzles is that their efficiency and capacity are dependent on the total differential pressure. Since the discharge geometry is fixed, the capacity varies with the square root of the pressure differential ratio, i.e.,

$$\frac{Qw_1}{Qw_2} = \frac{\sqrt{\Delta P_1}}{\sqrt{\Delta P_2}} \qquad [3.1]$$

where Qw_x is the volumetric liquid flow rate and ΔP_x is the available differential pressure.

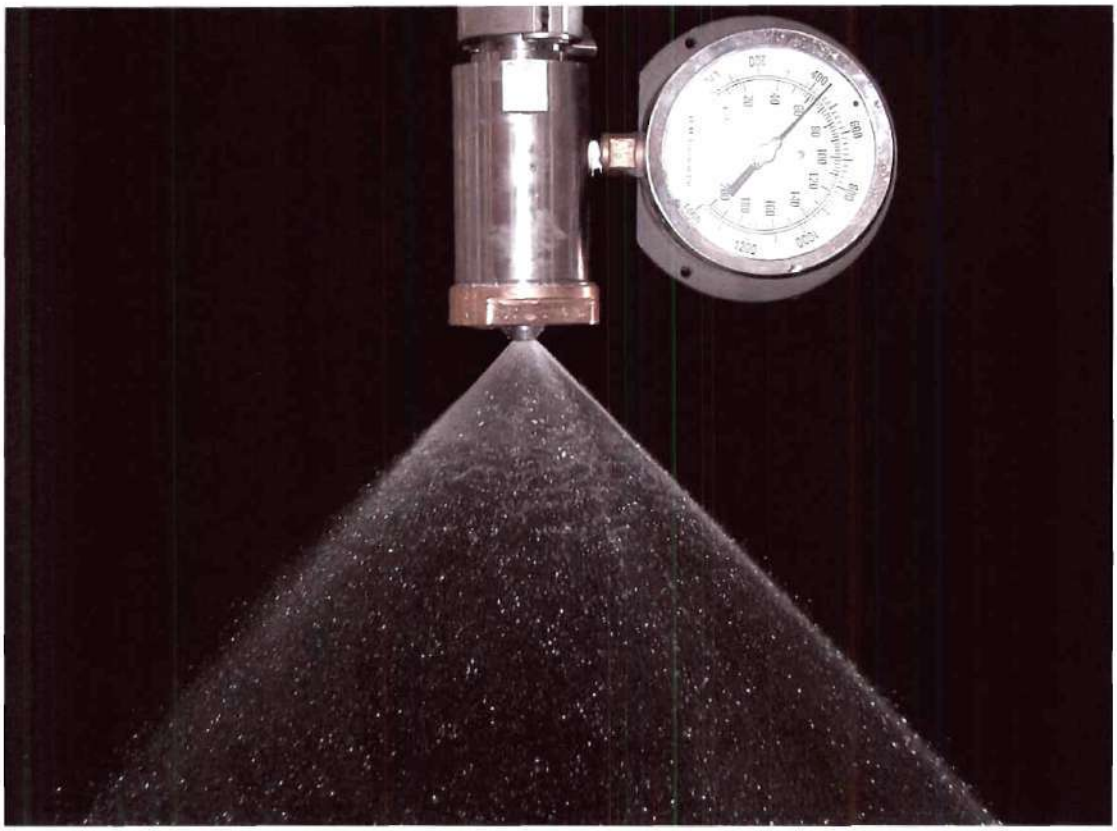

Figure III.2 – Variable Geometry Nozzle Spray Pattern

The first unit tested utilized a single variable geometry nozzle. The capacity of the nozzle was sized to accommodate the requirements of the flow conditions specified by the UNC Cogeneration Facility. In this way, the nozzle would be capable of handling the full range of spray injection needed to satisfy the steam and temperature needs of the campus. The calculated flow coefficient, Cv, of the nozzle was 2.0, where,

$$Cv = Q_w * \sqrt{\frac{SG}{\Delta P}} \qquad [3.2]$$

Here, SG is the respective fluid specific gravity and ΔP is the available pressure differential across the nozzle. The nozzle has a linear stroke length of 0.036" (0.91mm)

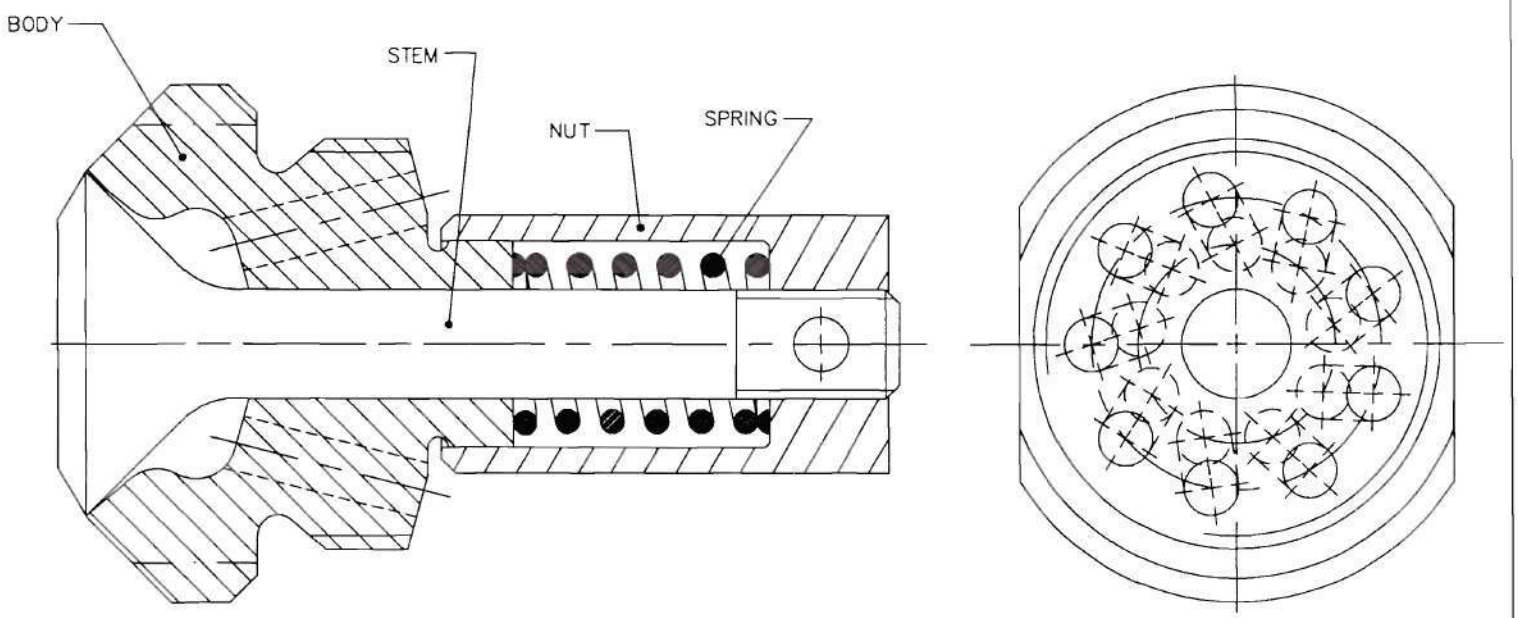

Spring Loaded Variable Geometry Spray Nozzle

Figure III.3

and produced a maximum sheet thickness of 0.025" (0.64mm) on a diameter of 0.79" (20mm). The nozzle was placed on the end of a fluid transfer tube that, when attached to the mounting flange on the outside of the main pipe, accurately positioned the axis of the nozzle in line with the horizontal axis of the pipe, 11.8 feet from the inlet section of the control volume (See Figure III.1). The other end of the fluid transfer pipe was attached to an integral control element. A pneumatic spring and diaphragm actuator was used to position the integral control element. When the system was in the automatic mode, this actuator received an input signal from the control room and the quantity of injected spray water was regulated based on a particular temperature set point. The unit could also be run in the manual mode and positioned anywhere from closed to fully open. Thus, the control system permitted the operator to run the injector at nearly any position regardless of the steam flow conditions.

The second injector or desuperheater tested was similar in design to the first one; however, instead of using only a single nozzle, the injected water flow was divided between four nozzles. As before, these nozzles were of the spring loaded, backpressure activated, variable geometry type. However, in this case, their flow coefficient was 0.5 each and created only a 0.014' (0.36mm) thick sheet on a 0.39" (10mm) diameter. The four nozzles, having a combined Cv of 2.0, were spaced out equally over the length of the fluid transfer pipe. The two inner nozzles were also given a slight radial adjustment in their alignment and were oriented 15° off the axial centerline in the horizontal plane. The purpose of this design was two-fold. The first was to see whether or not the spray distribution would affect the degree of thermal stratification produced in the large

pipeline. The second was to see if the smaller nozzles, generating smaller particles, would mix more evenly, evaporate faster, and thus prevent the onset of thermal stratification.

The third unit tested would exaggerate the concept of the second unit. By this, the fluid transfer pipe would house 28 fixed geometry micro spray nozzles. Once again the hypothesis was that by creating ever-smaller droplets, the localized turbulent action of the surrounding steam flow would more evenly distribute the particles within the flow stream. The resultant smaller particles would then vaporize more quickly thus producing a more homogenous temperature distribution and preventing the formation of thermal stratification. Due to the extremely small size of the discharge orifice, the degree of decay in spray pattern formation was minimized and not considered detrimental or inconsistent when compared to the variable geometry nozzles.

In every case, the same type of control scheme and mechanism were employed. Illustrations of the three desuperheater units can be seen in Figures III.4, III.5, and III.6, respectively.

III.4 Thermocouples

The initial temperature measurement arrangement was comprised of a series of three thermocouples installed at different locations along the pipeline. The first was in the horizontal run of pipe some 32.0 feet (9.75m) after the desuperheater. This was followed by a temperature indicator an additional 12" (305mm) downstream. The next thermocouple was located at the end of the test section near the inlet to the mixing header. The last thermocouple was located in the steam distribution system feeding the

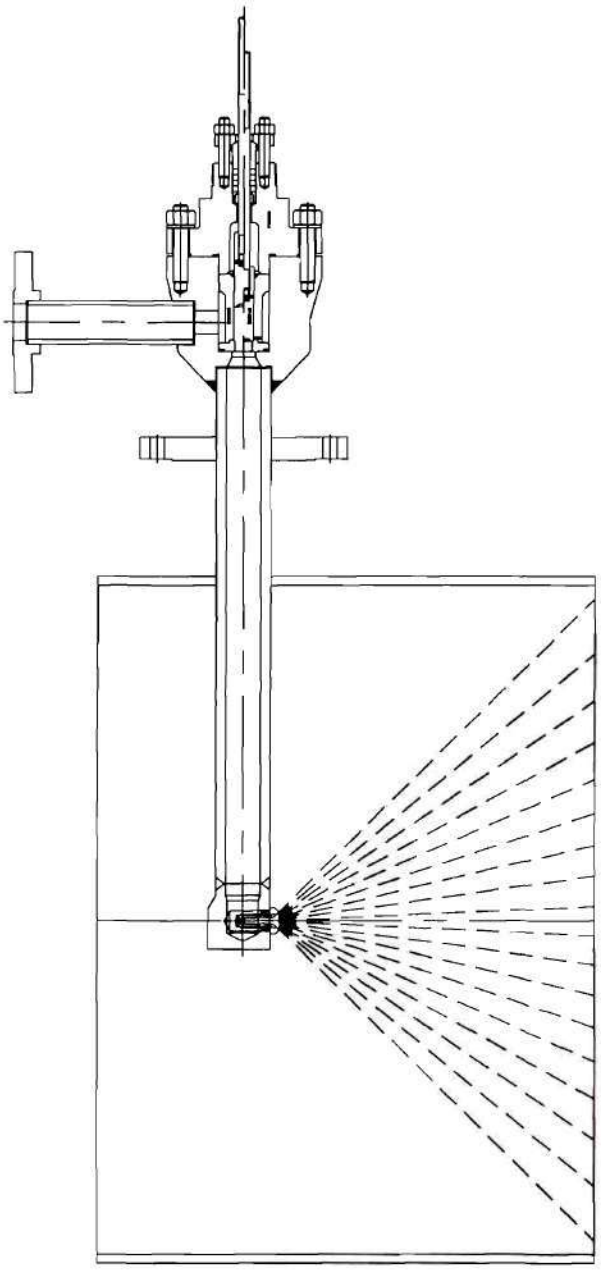

Test Unit #1
Single Variable Geometry Nozzle

Figure III.4

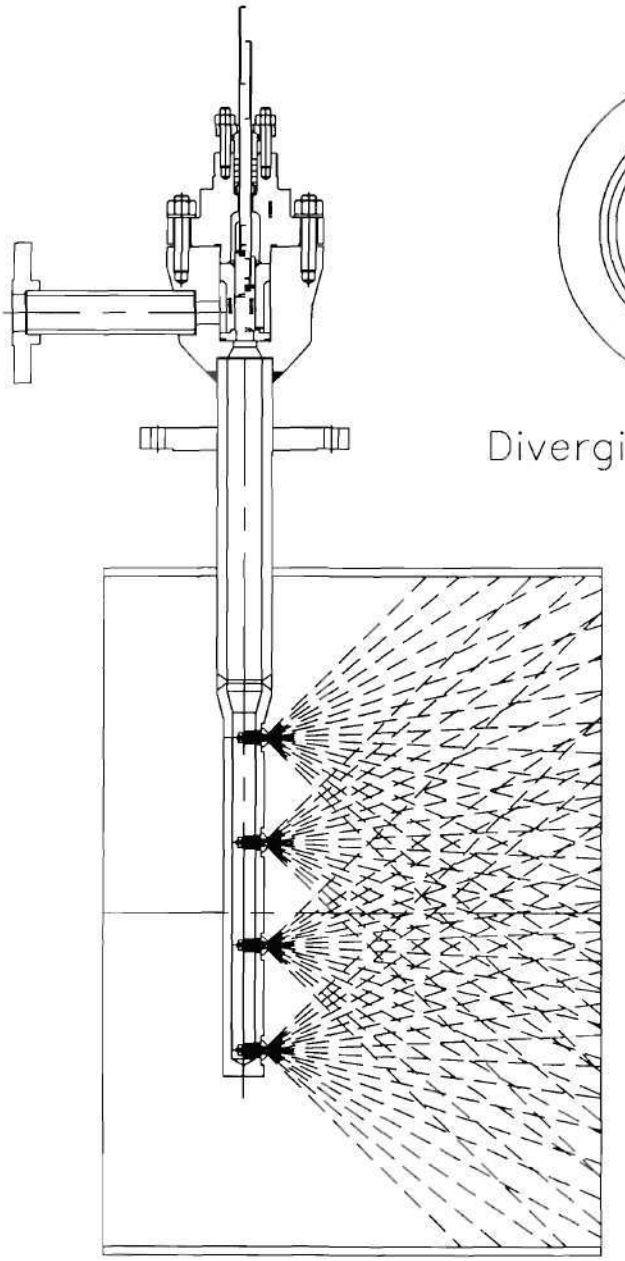

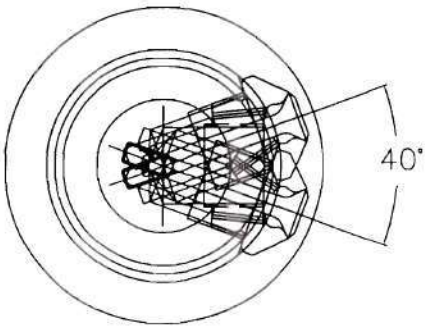

Diverging Inner Nozzles

Test Unit #2
Multiple Variable Geometry Nozzle

Figure III.5

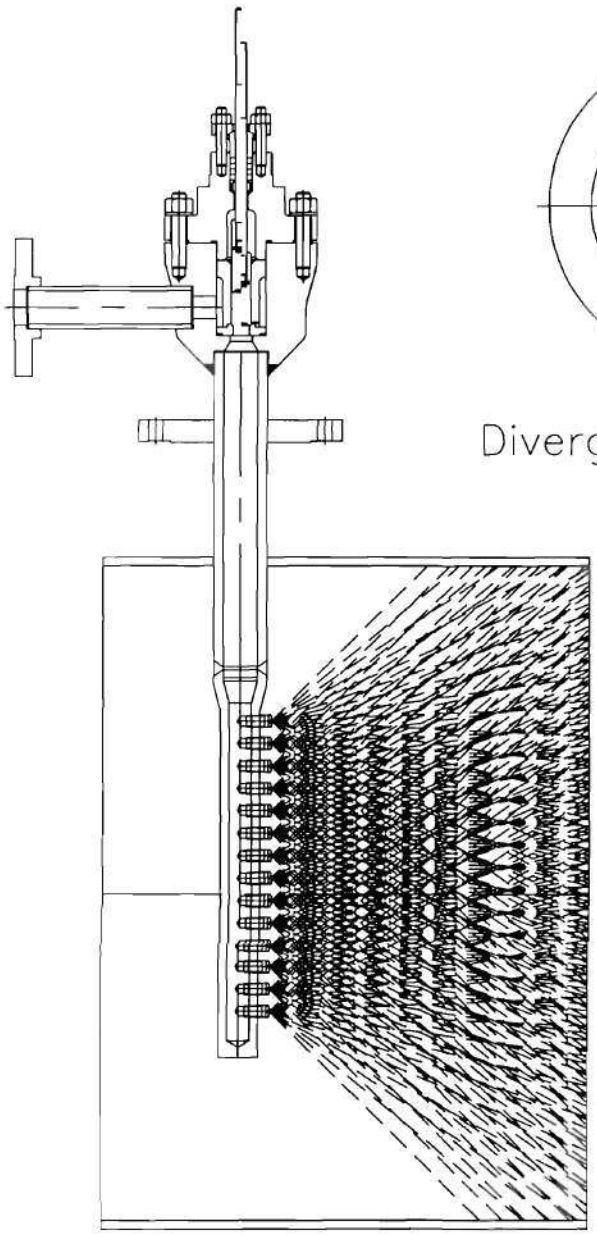

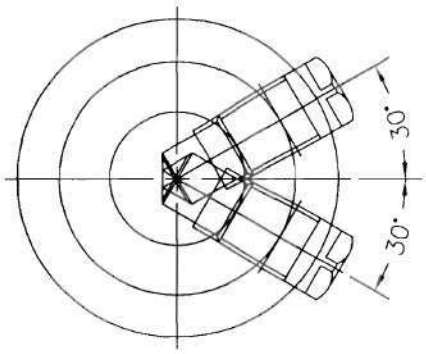

Diverging Inner Nozzles

Test Unit #3
Multiple Fixed Geometry Nozzle

Figure III.6

campus. This system of temperature measurement was utilized with the single nozzle desuperheater arrangement. If everything was working according to empirical estimates, each of these temperature-measuring devices should have read the same temperature. However, it was quite apparent that this was not the case and that even within the short span of 12" (305mm) between the thermocouple and the temperature indicator the readings varied. This was surely the result of significant thermal stratification in the system. Unfortunately, the limited instrumentation available in the original system was insufficient to generate the quantitative data that was required to effectively evaluate the phenomenon in question. The large cross-sectional flow area of the pipe and the directional temperature changes produced necessitated the use of multiple temperature measurement instruments.

Alltemp Senors, Inc., in Houston, Texas, was contacted and consulted as to the fabrication of some specialty thermocouple probes. They were able to design some thermocouple lances that housed six individual 1/8" Diameter, Type K, Ungrounded thermocouple contacts within a length that was less then the inner radius of the pipe. It was decided that an array of four of these lances, each with six contact points, would be inserted in the pipeline to give us 24 data points, 12 each on the horizontal axis and 12 each on the vertical axis. In this manner, a complete temperature profile could be obtained.

Since we were interested in both the thermal stratification as well as the vaporization process within the flow stream, it was decided to install the lances in two planes of the pipeline for a total of 48 thermocouples. The first would be within the

initial straight pipe length just downstream of the desuperheater. This measurement point would give us good indication of the vaporization process purely as a function of the flow dynamics. The second plane of sensors was located just after the first elbow but still in the horizontal plane. This measurement point would provide information relative to momentum effects on the suspended particulate as well as the inherent mixing advantages or disadvantages of this type of flow direction change. A photograph of a completed thermocouple lance assembly can be seen in Figure III.7. Figure III.8 is a photograph from the UNC Cogeneration Facility showing the installation orientation of the thermocouple lances after having been placed in the pipeline. Figure III.9 illustrates the dimensional details of the thermocouple lance, while Figure III.10 shows the physical layout of the four lances as they were installed in the pipeline.

Figure III.7 Thermocouple Lance Assembly

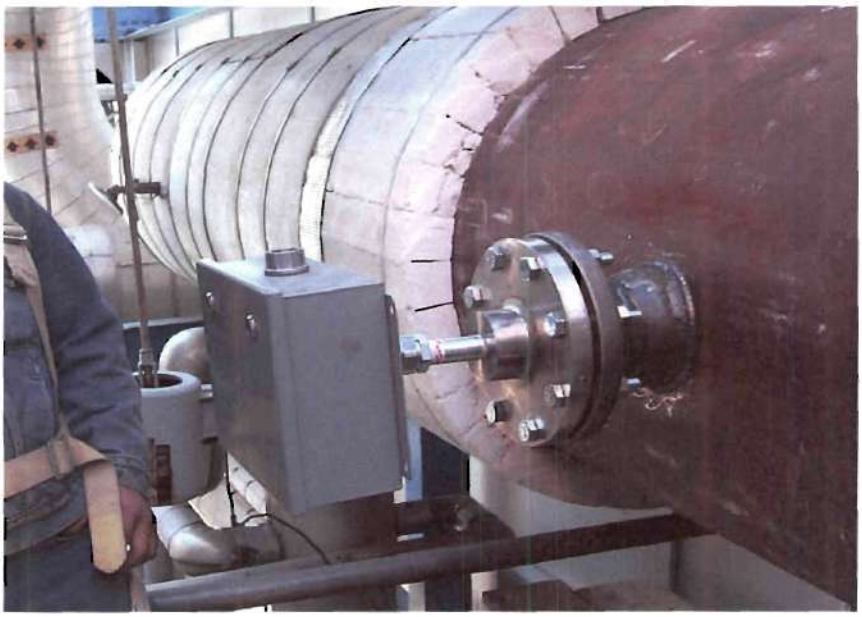

Figure III.8 Installed Thermocouple Lance

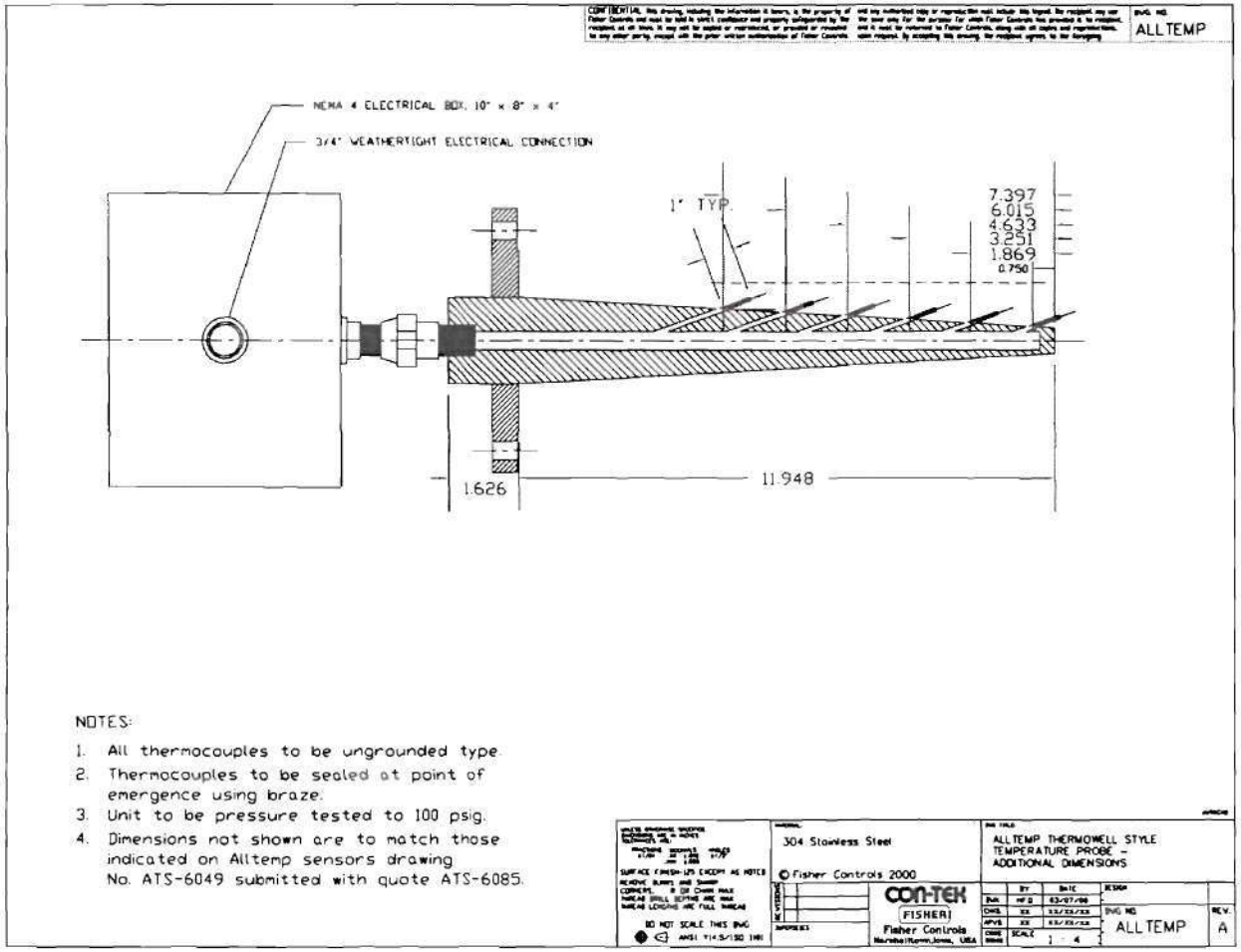

Figure III.9 Thermocouple Design Layout

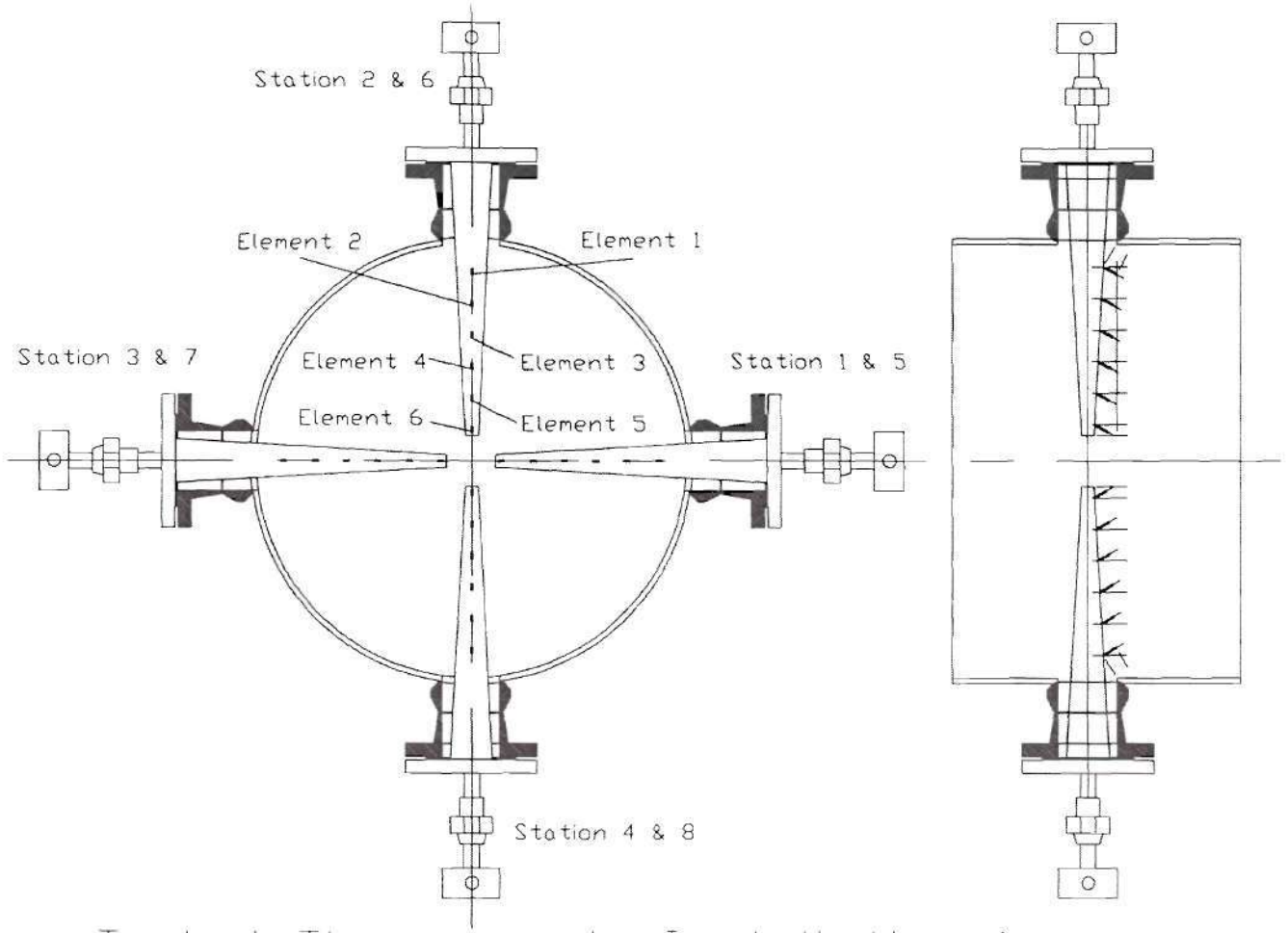

Typical Thermocouple Installation Arrangement

Figure III.10

III.5 Data Acquisition

In order to gather all the operational and performance data of the desuperheater, the distributed control system, DCS, in the UNC-Cogeneration Facility Control Room was utilized. The Westinghouse Process Control DCS was already configured to provide the majority of information needed to allow evaluation of the main process. However, with the addition of the eight-thermocouple lances and 48 additional temperature inputs, its capability to record all the inputs was challenged. To accommodate the additional input, eight Westinghouse QAV-G02 modules were installed in the control room. The system was already equipped with sufficient modules for the cold junction compensation measurement.

With the inclusion of the new thermocouple modules, the system was implemented and data collection begun. The system was configured to capture specific data that was pertinent to the process being evaluated as can be seen in Table III.1. This data is collected continuously and new data entries are only a function of system update times. Each data point is registered and archived for a period of 30 days.

For the purposes of this research, UNC permitted Internet access to their control room displays and data library. This allowed live viewing of system performance data on a real time basis, as well as the capture and downloading of all applicable data from a specific time sequence within the active archive window. Examples of the on-line graphics and data acquisition can be seen in Figures III.11 and III.12.

Table III.1 UNC Cogeneration Facility DCS Output Variables

Point Identification	Output Description
IPI041B	Turbine LP Extraction Pressure (PSIG)
IFT037	Turbine LP Extraction Flow (KPPH)
ITE042	Turbine LP Extraction Temperature (F)
IPT084	LP Steam Header Pressure (PSIG)
ITT086	LP Steam Header Local RTD (F)
ITT086A	LP Steam Header Local RTD @ 200 Ft Downstream (F)
ITCV090	LP Extraction Desuperheater - % Open (%)
FPT323	Desuperheater Inlet Water Pressure (PSIG)
FTE322	Desuperheater Inlet Water Temperature (F)
ITE09011-16	Radial Temperature Probe, Station 1, Element 1-6
ITE09021-26	Radial Temperature Probe, Station 2, Element 1-6
ITE09031-36	Radial Temperature Probe, Station 3, Element 1-6
ITE09041-46	Radial Temperature Probe, Station 4, Element 1-6
ITE09051-56	Radial Temperature Probe, Station 5, Element 1-6
ITE09061-66	Radial Temperature Probe, Station 6, Element 1-6
ITE09071-76	Radial Temperature Probe, Station 7, Element 1-6
ITE09081-86	Radial Temperature Probe, Station 8, Element 1-6

Data sets were normally collected in 24 hours segments. In order to evaluate the data and trend the process changes, a data-logger was created using Microsoft Excel. This spreadsheet would input all the saved data, sort it by time, and provide a means to visually assess the transient variation of conditions within the system.

Based on the output received, and computational capabilities of Excel, it was decided to add some additional fields to calculate additional values for trending and evaluation. The list of additional calculations can be seen in Table III.2. These values were also trended as a function of time and listed along side the directly inputted data.

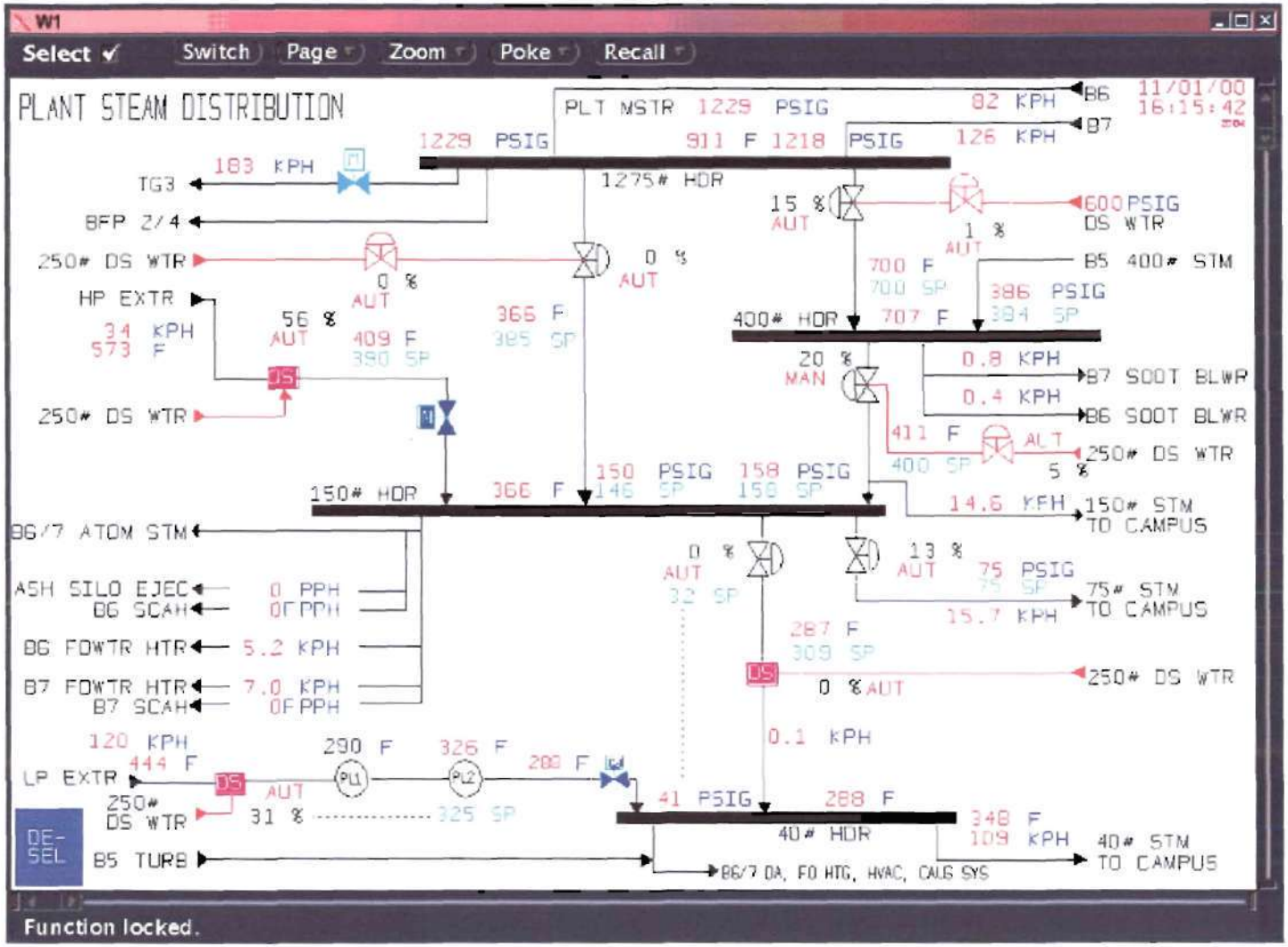

Figure III.11 On-Line System Graphics – UNC Cogeneration Facility

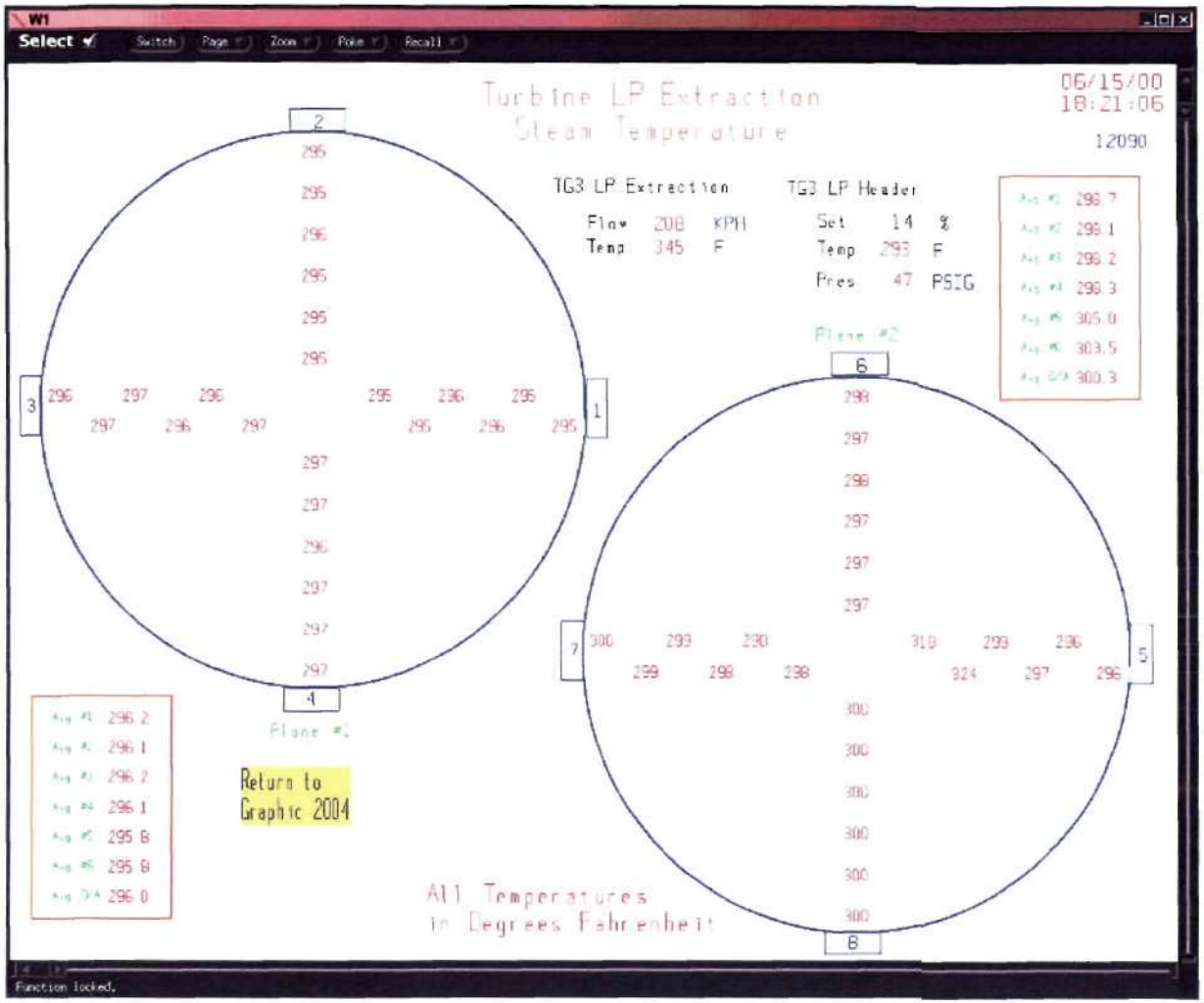

Figure III.12 On-Line Data Output Graphics – UNC Cogeneration Facility

The data-logger provided plotting capabilities for all inputted and calculated values during a specified time period. The time period could be changed to view details in as small an interval as 5 minutes or as long as 24 hours.

Table III.2 UNC Cogeneration Facility DCS Output Calculated Values

Point Identification	Point Description
Desup_SG	Calculation – Specific Gravity of DSH Water (-/-)
Desup_DP	Calculation – Differential Pressure Across DSH (PSID)
Desup_Cv	Calculation – DSH Flow Coefficient (-/-)
Desup_Qa	Calculation – Mass Flow from DSH – Actual (KPPH)
Desup_Qi	Calculation – Mass Flow From DSH – Ideal (KPPH)
Desup_Tse	*Calculation – DSH Temperature Setpoint (F)*
LPS_H	Calculation – Enthalpy of LP Steam (BTU/Lbm)
LPS_H_Ts	Calculation – Enthalpy of LP Steam at Setpoint Tse (BTU/Lbm)
Desup_H	Calculation – Enthalpy of DSH Water (BTU/Lbm)
LPS_V	Calculation – Steam Specific Volume at P1 and T1 (FT^3/Lbm)
PipeArea	Calculation – Cross-Sectional Flow Area of Pipe (FT^2)
LPS_Veloci	Calculation – Steam Velocity in LP Steam Header (FPS)
Sat_Temp	Calculation – LP Steam Saturation Temperature (F)

The data-logger is also capable of sorting all the thermocouple inputs and color coding the temperature outputs in a near graphically correct array. Thus the existence of thermal differences across the pipe can be easily observed over 5-minute increments. Examples of the data-logger output can be seen in Figure III.13, III.14, and III.15.

III.6 Experimental Procedures

III.6.1 Instrument Calibration

Each radial thermocouple probe included six individual temperature sensors. The sensors were standard 1/8" diameter, type-K, stainless steel-sheathed thermocouples with ungrounded tips. When assembled in the radial profile probe, the tip of each thermocouple extended approximately one inch beyond the conical surface of the probe

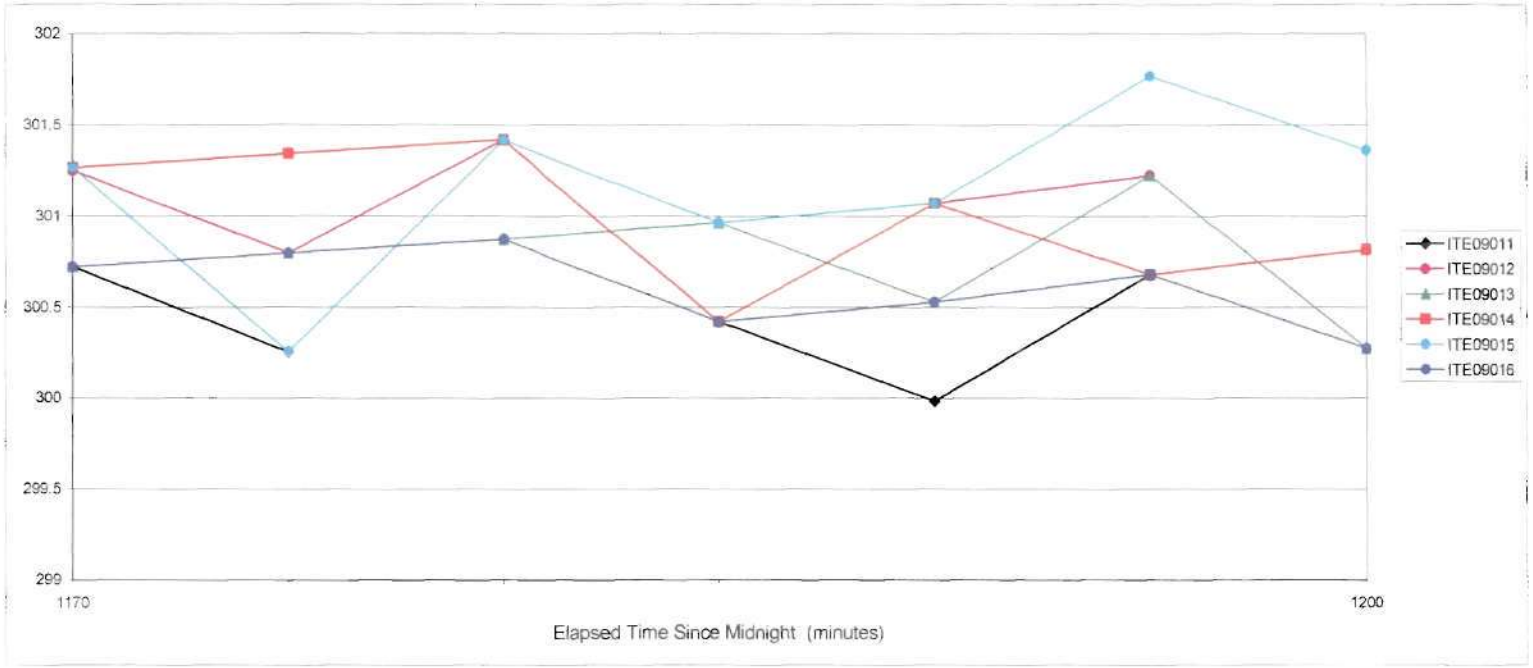

Series 1	ITE09011	Temperature - Con-Tek radial probe, station 1, element 1	F	22	
Series 2	ITE09012	Temperature - Con-Tek radial probe, station 1, element 2	F	23	
Series 3	ITE09013	Temperature - Con-Tek radial probe, station 1, element 3	F	24	
Series 4	ITE09014	Temperature - Con-Tek radial probe, station 1, element 4	F	25	
Series 5	ITE09015	Temperature - Con-Tek radial probe, station 1, element 5	F	26	
Series 6	ITE09016	Temperature - Con-Tek radial probe, station 1, element 6	F	27	

Figure III.13 Data Logger Output – Individual Probe Measurements

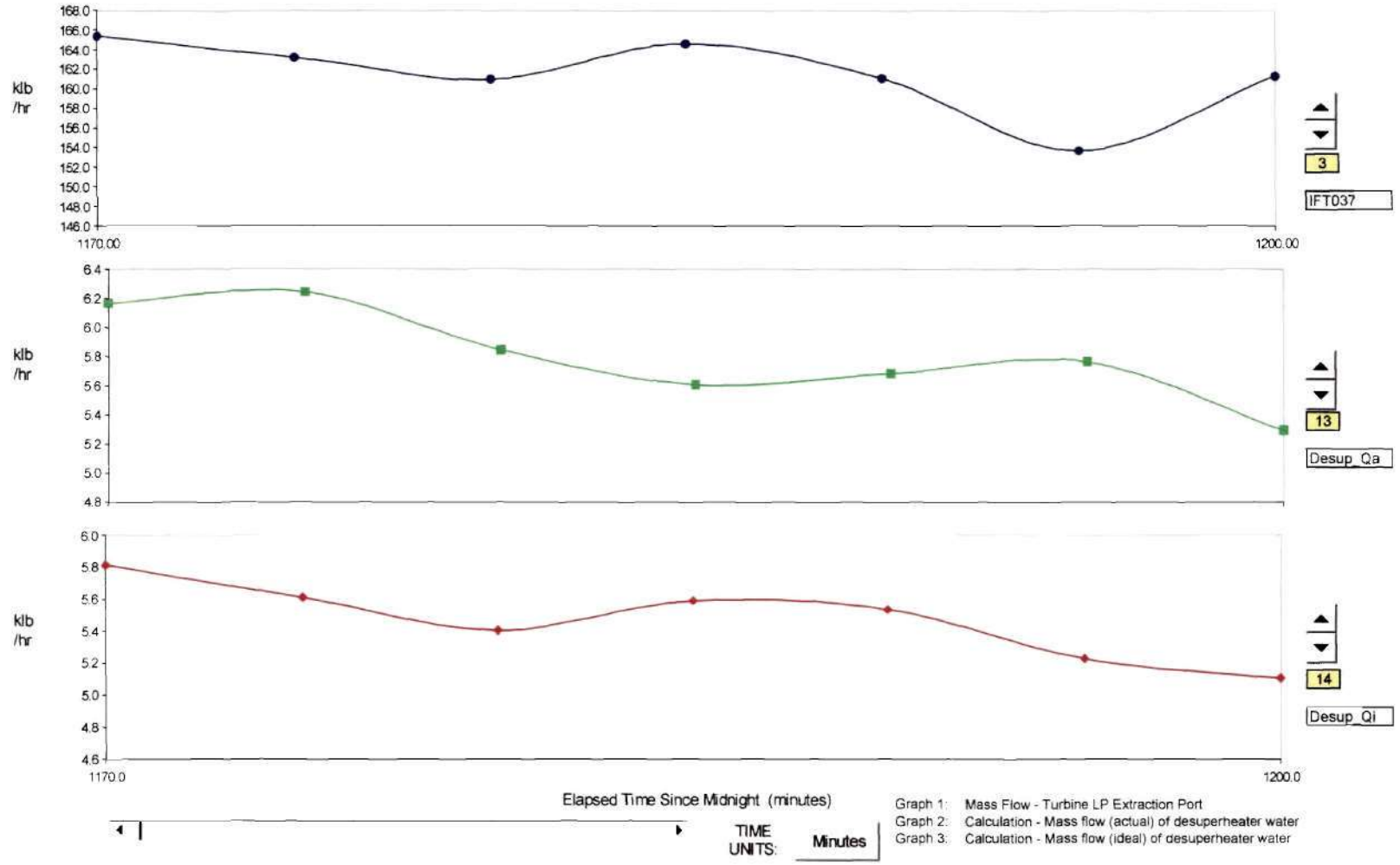

Figure III.14 Data Logger Output – Process Analysis

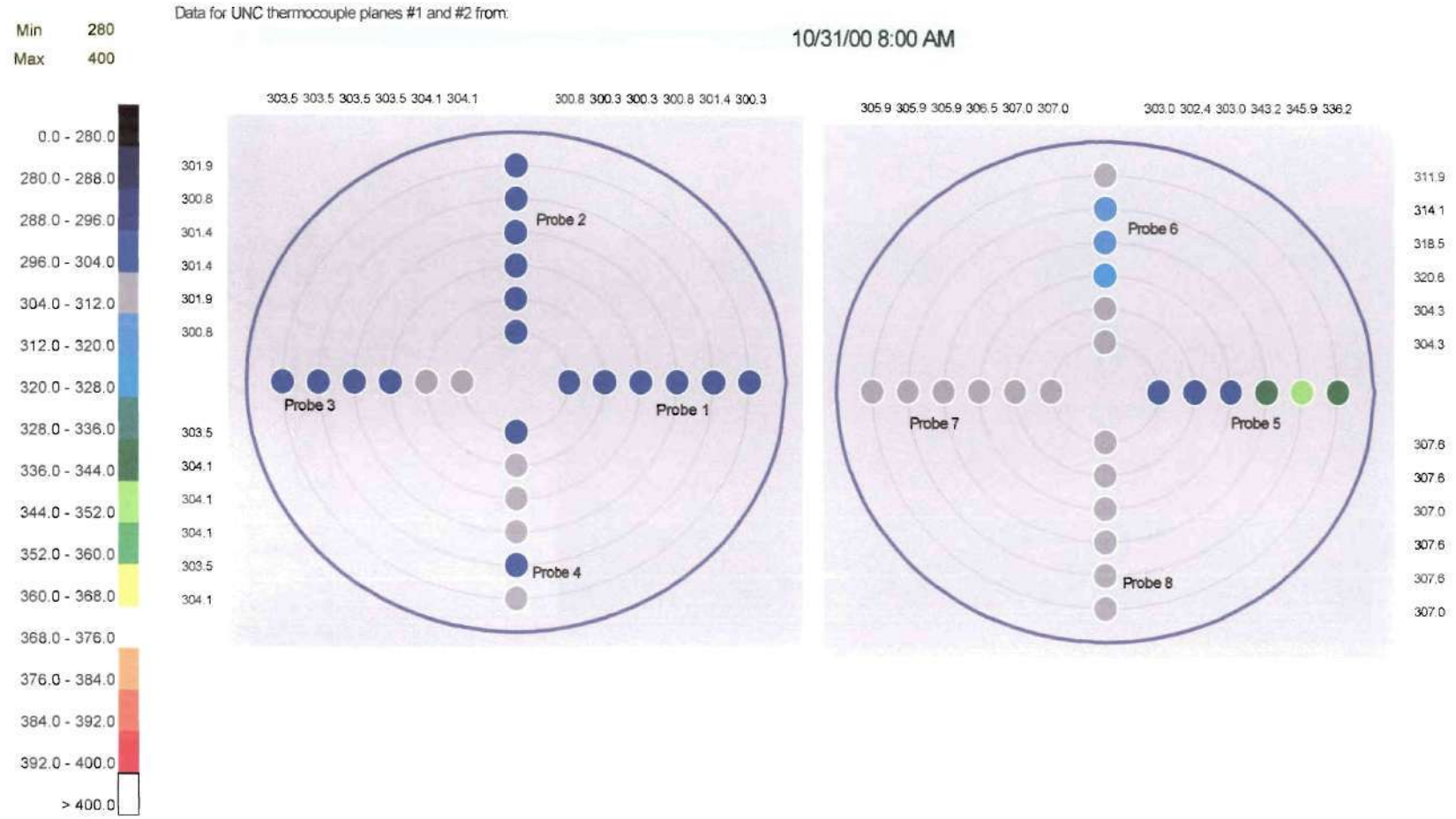

Figure III.15 Data Logger Output – Thermocouple Arrays

body. This extension provided thermal isolation between the probe tip and the heavy body of the probe and ensured that the sensors exhibited a sufficiently fast time response for the desired measurements while retaining adequate physical support; the extension length was selected after consultation with the manufacturer of the temperature sensors.

To eliminate potential errors in the thermocouple signals due to various sources, careful attention was paid during the design of the radial thermocouple probes to several thermal and electrical considerations. To minimize errors resulting from mismatched thermocouple wire, all of the sensors were purchased together and came from the same production lot. All thermocouples were made from thermocouple-grade wire. Each radial profile probe included a weatherproof electrical enclosure permanently mounted to its top, approximately one foot above the flanged connection by which it was attached to the steam pipe. Wires from the individual sensors terminated inside this sealed enclosure at a common junction block, ensuring that each terminal connection was at the same temperature. The enclosures were quite large and offered a large surface area for cooling in the ambient air, and they sat atop small diameter stainless steel pipe sections welded to the probe's flange. The extension length provided a buffer between the pipe's hot outer wall and the enclosure. These construction features ensured that the terminal junctions for all of the eight radial probes were at essentially the same temperature, minimizing errors between probes. Finally, all sensor wiring from the field into the data acquisition equipment located inside the plant was made using individual runs of shielded, twisted pair, extension grade thermocouple wire from a common spool. The field wiring ran

inside dedicated grounded conduit separate from any power-carrying conductors. The length of the field wiring was approximately 500 feet for each of the radial probes.

Temperature data for all thermocouple sensors was collected using a Westinghouse-brand data acquisition system already in use at the UNC Cogeneration Facility for plant data logging. Model QAV-G02 analog signal input boards were used to condition and digitize all temperature signals. Each QAV-G02 board included inputs for six individual thermocouple sensors. Thus, all the sensors for a given radial probe could be attached to the same input module. The analog input modules provided signal isolation and conditioning, signal amplification, and A/D conversion to 13 bit digital signals (1 bit for polarity, 12 bit resolution). Other pertinent specifications are listed below:

Input voltage range:	-12.5 to +50 mVDC
Normal mode rejection:	30 dB (minimum)
Sampling rate:	4 samples per second (all channels sampled simultaneously)
Resolution:	12 bit (plus additional voltage polarity bit)
Sample period:	0.20 sec

In the UNC data logging configuration, each of the channels was sampled at 1-second intervals rather than at the maximum rate of 4 samples per second.

Thermocouples require Cold Junction Compensation (CJC), that is, a correction of the observed sensor voltage to account for the small voltage offset that occurs at the electrical junction between the thermocouple field wiring and the copper conductors on

the analog input module circuit board. The QAV-G02 does not have an integrated CJC sensor. Instead, a separate, common CJC sensor module is used for all of the analog input modules mounted inside of a particular data acquisition enclosure. The CJC modules introduce a +/- 1° C temperature uncertainty in the final values. If all analog input modules are located in the same physical housing and share a CJC sensor, this introduced error is systematic and is not evident when comparing temperature values between thermocouples. For this installation, the analog input modules for all sensors were mounted in two enclosures, five modules in one enclosure, three in the other. This introduces a slight offset of less than 1 degree into readings when comparing data for thermocouples connected in one enclosure versus the other when actual steam conditions could reasonably be assumed constant.

Following the analog-digital conversion, the 12-bit voltage values were transferred onto a digital data bus (DIOB) for further temperature calculation and data storage. Temperature calculation was accomplished by first using the CJC value to correct the raw voltage, then using a standard 5^{th}-order polynomial calculation to convert from thermocouple voltage to temperature. Sensor temperature values for each time step (i.e., every second) were then stored as database records. Due to the enormous quantity of data points, this complete set of data was retained only for a 24-hour period. On the day following their date of generation, the data were condensed and stored in a different database format that could be accessed at later times.

III.6.2 Conduct of Experiments

Since the test apparatus and data collection system were an integral part of a working power generating facility, the conduct of the experiment had to be modified. The load on the turbine and the steam needs of the UNC community affected the quality of the available data. If the turbine/generator was fully loaded, the extraction steam contained very little residual superheat. This significantly reduced the need for desuperheating and thus rendered little data of interest for the investigation. If the turbine/generator was not loaded, the extraction temperature increased significantly, but steam flow was dependent on the seasonal demands of campus heating and cooling. This resulted in the summer and winter months as being the periods when conditions were best and the majority of the testing and data collection could be effectively accomplished. Additionally, special plant operations and mechanical shutdowns sometimes restricted test periods. Thus, rather then having complete control of the data stream and control variables, the experiment consisted of a mass collection of data.

During periods of high mass flow and residual superheat, the data historian at the plant would be initialized to collect all pertinent data and store it in the plants operational database. The data dumps were stored in 24-hour segments that could be FTP'd to our computers at any time for review. Once the data was collected, it was examined on a minute to minute basis to determine when and where conditions existed that would meet specific criteria for further analysis. These criteria included relatively high magnitudes of coordinated mass flow, inlet steam temperature, line velocity, and desuperheating water. Pressure was minimized in importance since the extraction pressure was relatively

constant during operation and only varied slightly for any set of operating conditions. Another important factor was that the data set would be compiled from a relatively stable period of operation. The desire was to capture conditions that exhibited nearly steady state conditions, thus eliminating the concern that the test data was not well coordinated due to transient affects.

III.6.3 Data Analysis

As previously stated, the operating data from the UNC Cogeneration Facility was FTP'd to use from the plant computers. The data was received in a tabulated time stamped format. Review and analysis of the information was difficult in this format as specific trends and stability were difficult to ascertain. For that reason, an Excel spreadsheet was created that sorted the data, as a function of time and date, and produced a graphical output for analysis. The spreadsheet contained three sections. The first section provided a means of displaying up to six input series. This was normally used to illustrate the changes in steam temperature with respect to the individual thermocouples on an individual lance mounted in one of the two measurement planes. By knowing the probe station and element number its location in the test array could be identified. Trends could be monitored and early indications of momentum transfer and thermal stratification noted. The examination time frame could be modified to display data contained in time increments from 5 minutes to 24 hours. A 30 minute time increment was found to be most suitable for the purposes of data review and analysis.

The second set of graphs consisted of a series of three independent charts that could be configured to illustrate the performance of any other output variable within the

same time period. These graphs were used to look at all the data other then the temperature outputs from thermocouple lances. As mentioned previously, one of the critical variables for evaluation and determination of viable test data was the steam mass flow rate. Thus, this was the first variable plotted.

Once periods of increased steam mass flow rate were identified, other variables, such as inlet steam temperature, desuperheater valve position, and line steam velocity were also plotted with respect to the flow. In this way, the key variables could be compared to the magnitude of steam mass flow. Likewise, the stability of the conditions could also be evaluated. The ideal situation was to achieve minimal or relatively no change in conditions for a period of at least 30 minutes. In viewing the data, this criteria was only coarsely achieved, as demand on the system was never that stable. However, two distinct and relatively stable periods were identified and used for the analysis in this experiment. The first, Case 1, occurred on October 31, 2000 between 1170 and 1200 minutes into the test period, or from 07:30 to 08:00. This interval was being supported by the four-nozzle desuperheater arrangement. The second, Case 2, occurred on May 2, 2001 between 1380 and 1410 minutes into the test period, or from 11:00 to 11:30. This interval was being supported by the 28-nozzle desuperheater arrangement.

For control purposes, it was desirable to have the two sets of conditions be as close to one another as possible. Under ideal circumstances, with complete control over all variables, this would not have been that difficult a task. However, since the data was from a full production power facility, the best we could achieve was relatively similar data with high mass flows and inlet steam temperatures. The selected data for both cases can be seen in

Table III.3. For purposes of analysis, the data achieved similarity thresholds with only a 1.7% variance in the inlet enthalpies and a 13.1% difference in the inlet steam mass flow. A complete printout of the two 24-hour intervals can be seen in Appendix A and B respectively.

Table III.3 Selected Operating Data

Input Variable	**Case 1: October 31, 2000 1182 Minutes Elapsed Time (07:42) 4 Nozzles**	**Case 2: May 2, 2001 1400 Minutes Elapsed Time (11:20) 28 Nozzles**
Steam Mass Flow (PPH)	164000	142500
Inlet Pressure (PSIA)	65.1	47.4
Inlet Temperature (°F)	378	415
Line Velocity (FPS)	86.7	97.1
Spray Water Flow (PPH)	5402	7346

The third set of graphs provided in the spreadsheet provided color-coded depictions of the 24 individual thermocouples within the control array. The color coding was done as a function of temperature. The thermal variation across the pipeline flow area could easily be seen. The program allowed for viewing of the thermal profiles in five-minute increments. One of the goals of this experiment is to see how well the computational tools can replicate the thermal profiles recorded for the time increments selected. The analysis of this portion of the data was integral in determining whether or not the degree of thermal stratification was sufficient in magnitude when compared with all the other variables.

CHAPTER IV

COMPUTATIONAL ANALYSIS

IV.1 Introduction

The data gathered at the UNC Cogeneration facility was beneficial in providing real information about the performance and installed characteristics of the system. However, since we did not have full control over the operating parameters at the site, an alternative approach was required. The decision was made to attempt to simulate the process with the use of available computational fluid dynamics (CFD) codes. This could facilitate two very important results. First, if the code could effectively simulate the complexity of the process, we could utilize its computational capabilities to simulate other flow conditions, desuperheater designs, and perform a system parametric study on all the variables involved. Secondly, by inputting the known data and computing a steady state solution, we could use the application to assist in verifying the code itself.

IV.2 SteamCFD

SteamCFD is a proprietary CFD code developed by Georgia Tech, Yao (2000) for CON-TEK Valves, Inc. It is a variant of the Kiva3 internal combustion code developed by Los Alamos National Laboratory, Amsden et al. (1993). Like Kiva3, SteamCFD uses the Arbitrary Lagrangian-Eulerian (ALE) method to solve the basic conservation equations governing fluid flow and heat transfer in complex two-phase flow systems. In addition, SteamCFD, as well as Kiva3, include models for droplet injection, evaporation, and transport. Where Kiva3 bases evaporation on concentration gradients, (as with all

the major commercial CFD codes) SteamCFD has been modified to consider the evaporation of water into steam due to heat transfer, thus distinguishing it from all known CFD codes.

In the creation of the code, mathematical models have been developed to simulate droplet condensation and evaporation, droplet breakup and coalescence, and droplet-wall interaction particularly associated with sprays within piping systems. Additionally, the Kiva3 code was modified to use real steam properties rather than making an ideal gas assumption.

For this analysis, two versions of the code were employed, SteamCFD Version 1.2 and 2.0. The purpose of this was to evaluate and determine the performance differences and sensitivity of the computation to spray impacting and fluid collection on hard surfaces. SteamCFD2.0 was identical to SteamCFD1.2 except for the addition of a newly developed spray impaction – film model. It was anticipated that the addition of this new sub-routine would improve the accuracy and validity of the code.

IV.3 Model Creation

Before any computational work can be conducted, the system in question must be represented in a three-dimensional grid structure model. In this particular case the geometry of the UNC Cogeneration Facility LP Extraction Steam Pipeline was represented using the K3Prep software package, which is a part of the original Kiva3 code. The smooth shaded boundary surfaces as well as the geometric mesh of the model can be seen in Figures IV.1 and IV.2, respectively. A cross-sectional coordinate surface is illustrated in Figure IV.3. In order to limit the computation time required, a 10 x 10

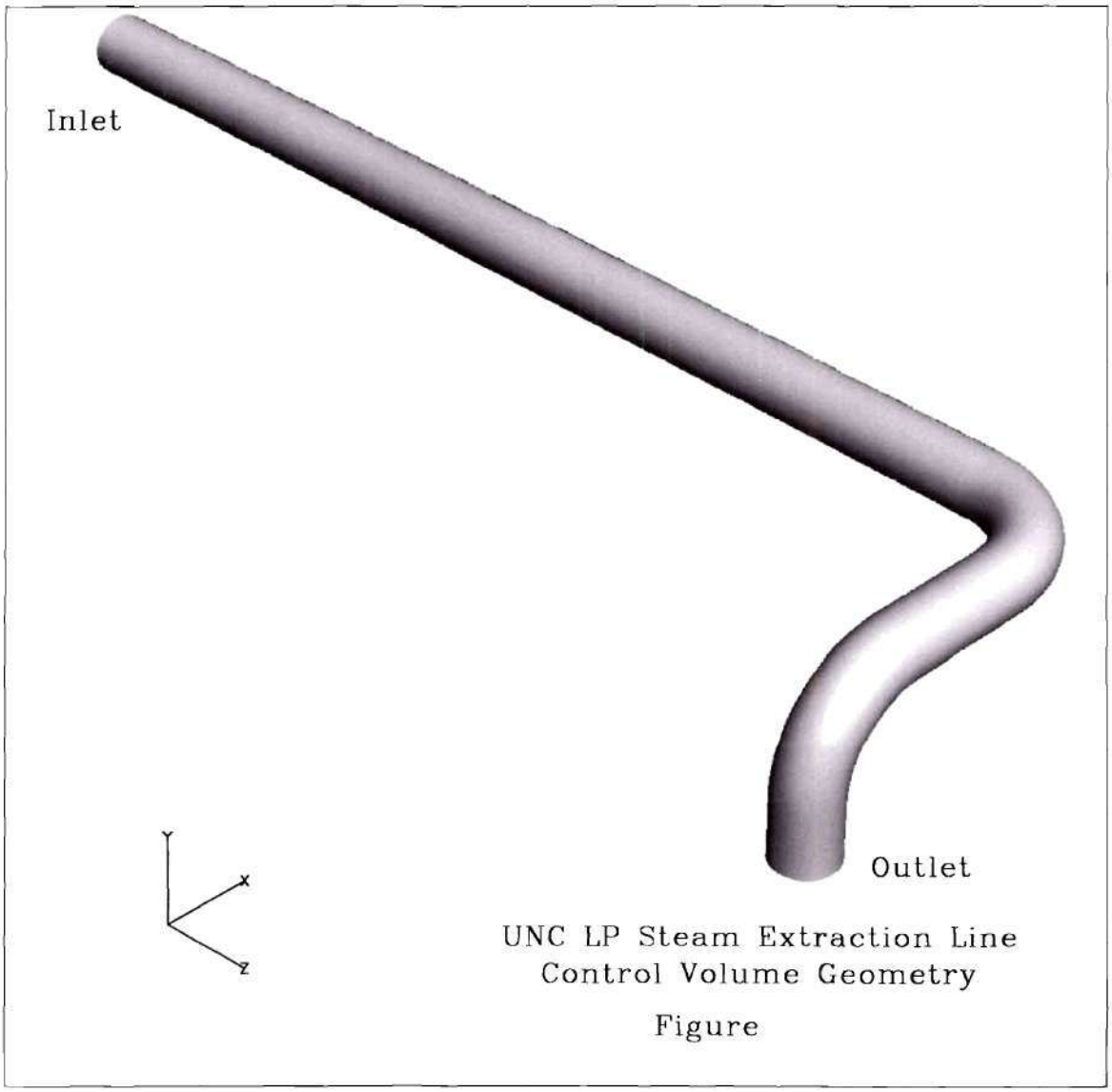
Inlet
Outlet
Y
X
Z
UNC LP Steam Extraction Line
Control Volume Geometry
Figure

Figure IV.1

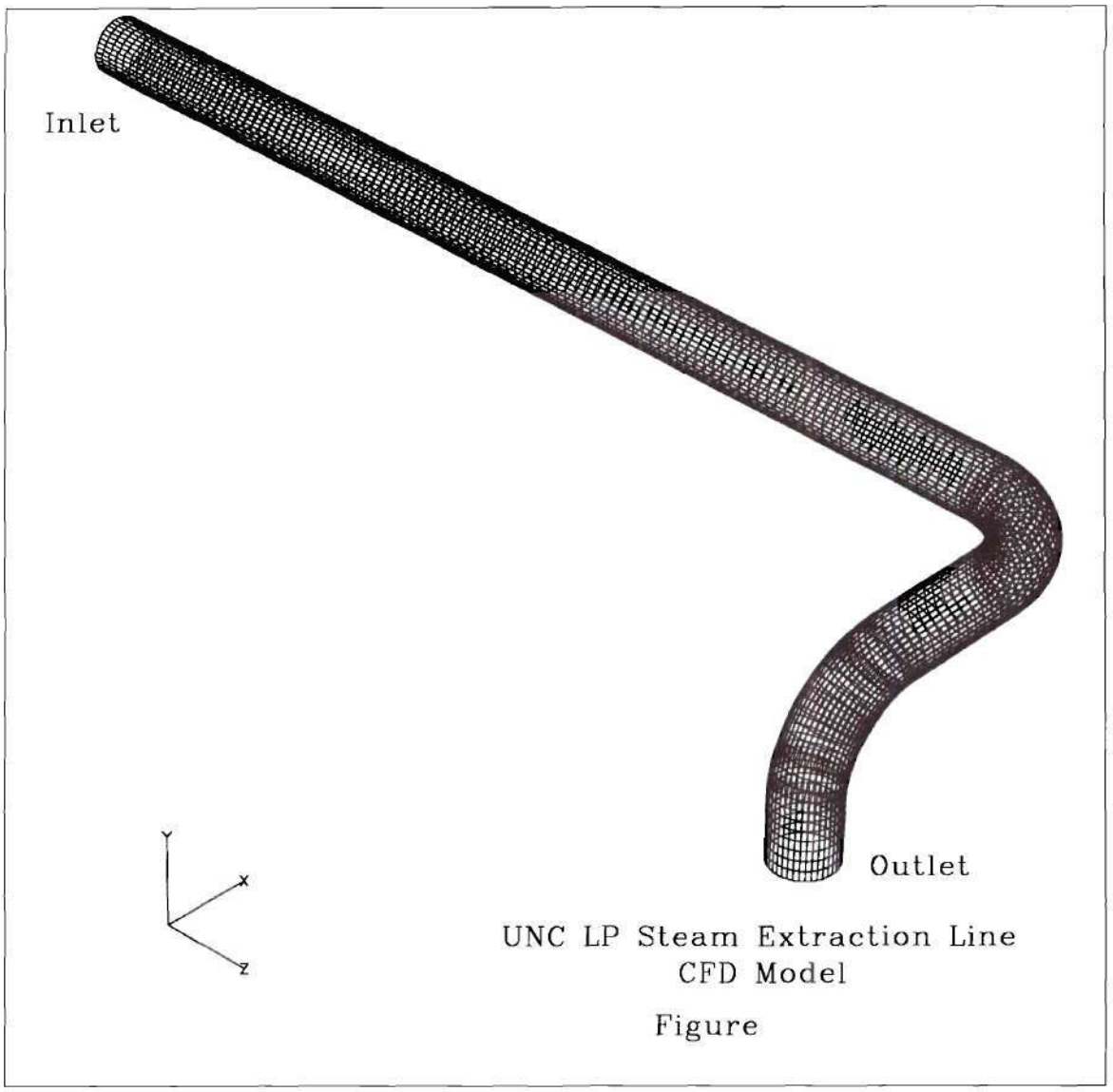
Inlet
Outlet
Y
X
Z
UNC LP Steam Extraction Line
CFD Model
Figure

Figure IV.2

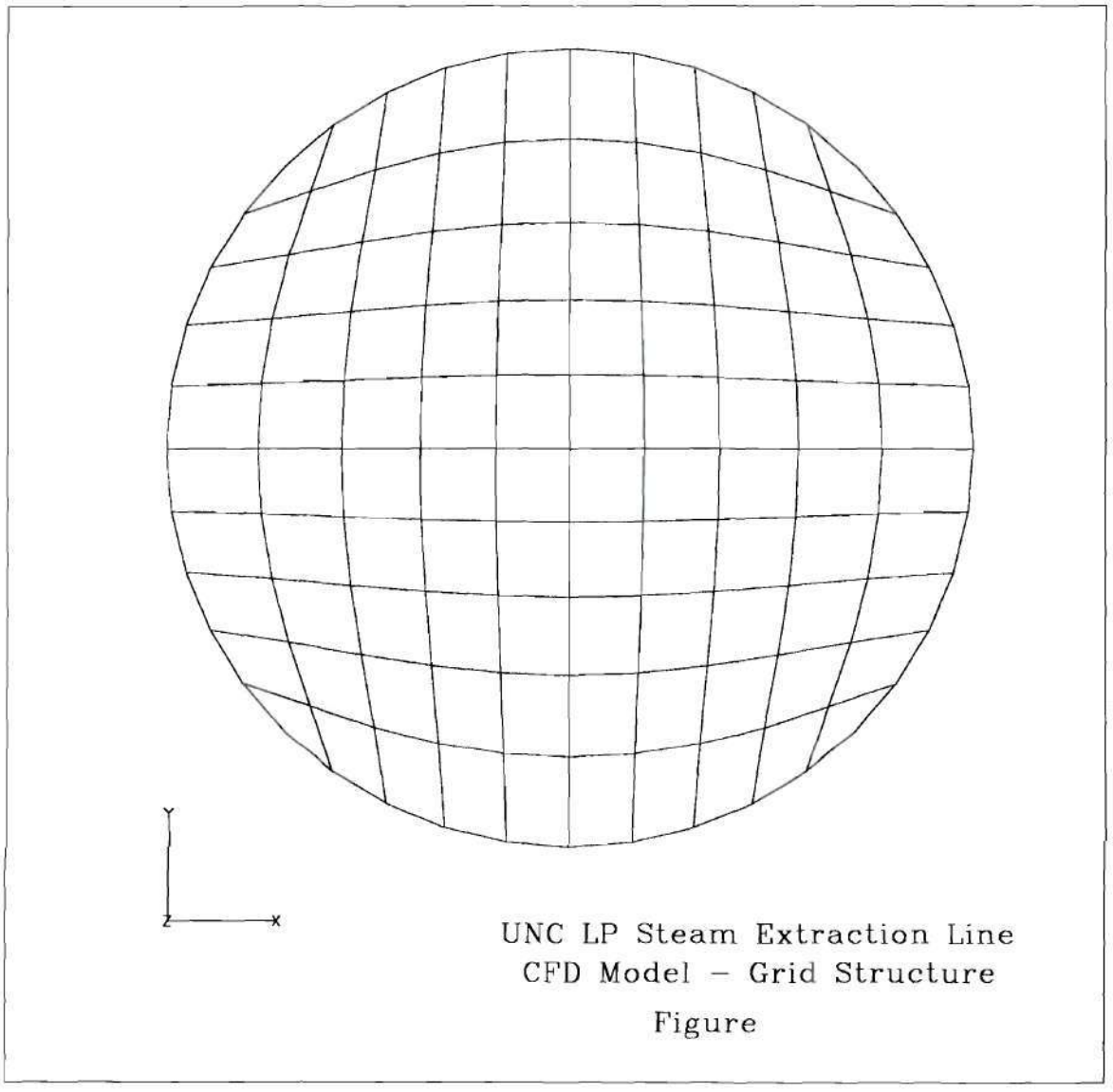
Y
Z
X
UNC LP Steam Extraction Line
CFD Model – Grid Structure
Figure

Figure IV.3

hexagonal grid was utilized. Skewness of the grid was considered satisfactory even considering the elements on the boundary perimeter at 45° to the axial centerline. The grid is kept as a separate input file called Tape17 that is accessed by the SteamCFD program.

IV.4 Input Variables

With the completion of the grid file, the next step was to enter the input variables that define the conditions and parameters to be computationally simulated in the code. Since the code can replicate a steady-state solution following a transient with a specified initial and boundary condition, it was desirable to find a set of actual conditions that were both stable and at the same time provided sufficiently complex input variables relative to the water injection and desuperheating process. Upon reviewing the output data supplied by UNC, two specific time intervals were identified that met both the complexity and steady-state criteria.

For the four-spray nozzle arrangement, information from the 10/30/00 to 10/31/00 data dump was located. During the time interval of 1170 to 1200 minutes of elapsed time, 07:30 to 08:00, the data compiled and graphed in the data-logger illustrated reasonable stability in the inlet temperature, pressure, and mass flow. At the same time, the outlet temperatures exhibited pronounced differences between the upstream array of thermocouples and the ones further downstream. Additionally, the downstream array also demonstrated evidence of thermal stratification, as evidenced by the considerable temperature differentials along both the vertical and horizontal axis of the pipe cross-section. A copy of the inlet flow, temperature, and pressure output graph for this time

period can be seen in Figure IV-4. The complete set of output data graphics can be found in the appendix A.

Similar data were identified for computational simulation of the 28-spray nozzle arrangement. In this case, the conditions simulated corresponded to the data collected between 5/2/01 and 5/3/01 with specific steady-state data identified between 1380 and 1410 minutes elapsed time, or 11:00 to 11:30. A copy of the inlet flow, temperature, and pressure output graph for this time period can be seen in Figure IV.5. The complete set of output data graphics can be found in the appendix B.

A comparison of the conditions used in the computational analysis can be seen in Table IV.1. It was desired, but not always practical, to have the two conditions as similar as possible. In this way, the true impact of the change in nozzle geometry could be most effectively evaluated as to its importance or significance in the evaporation process. It is widely known among practitioners in the field that by dividing the flow amongst smaller nozzles, the resultant spray pattern distribution and particle size generated is finer. However, since these nozzles were so closely packed geometrically, the net result of this refinement may not be totally realized.

Table IV.1 Specific Case Input Operating Data

Input Variable	Case 1: 4 Nozzles	Case 2: 28 Nozzles
Steam Mass Flow (PPH)	164000	142500
Inlet Pressure (PSIA)	65	47.4
Inlet Temperature (°F)	378	415
Line Velocity (FPS)	86.7	97.1
Spray Water Flow (PPH)	5402	7346

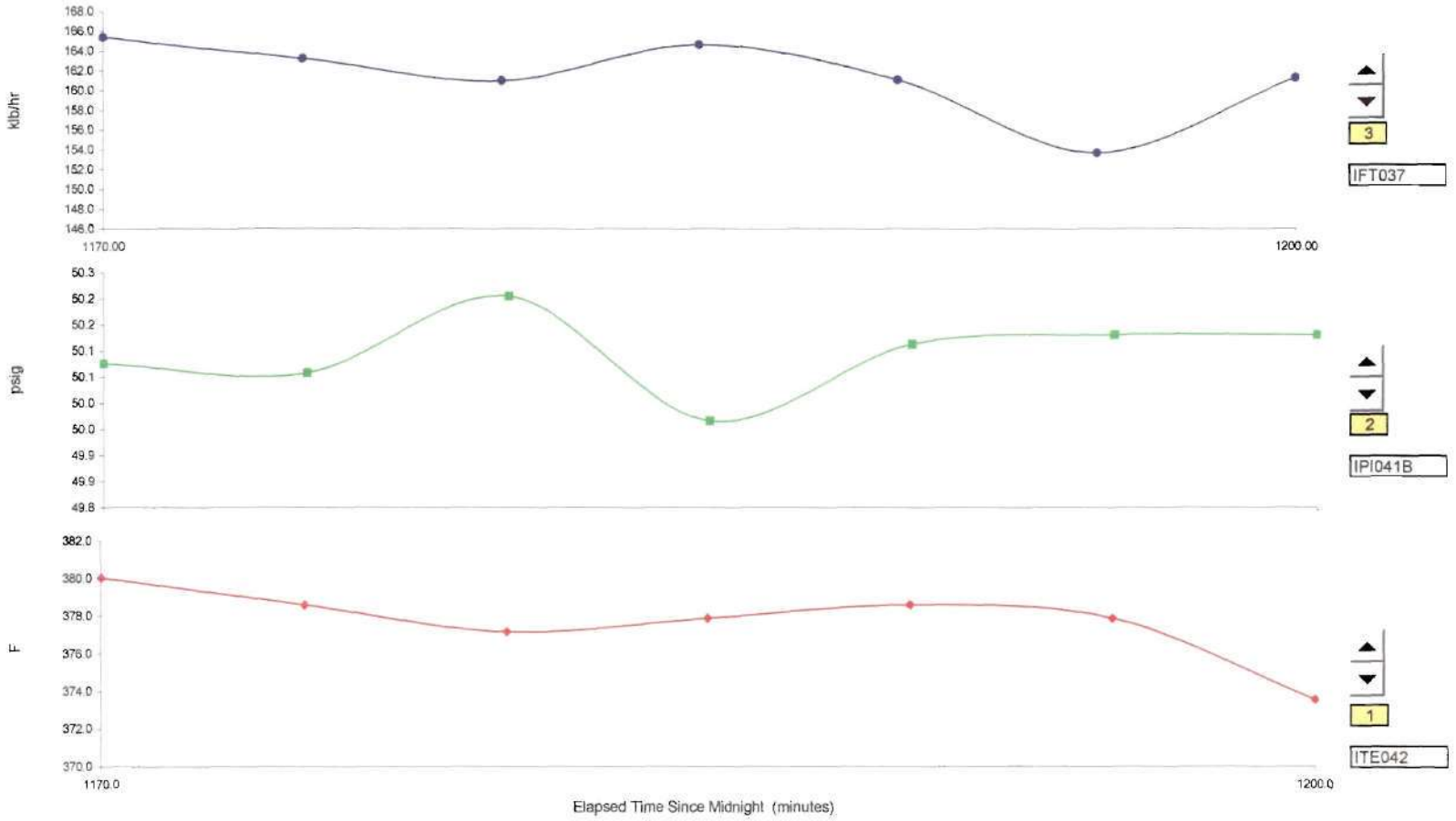

Graph 1: Mass Flow - Turbine LP Extraction Port
Graph 2: Pressure - Turbine LP Extraction Port
Graph 3: Temperature - Turbine LP Extraction Port

Figure IV.4 Inlet Flow, Pressure, and Temperature for Case 1 Time Interval

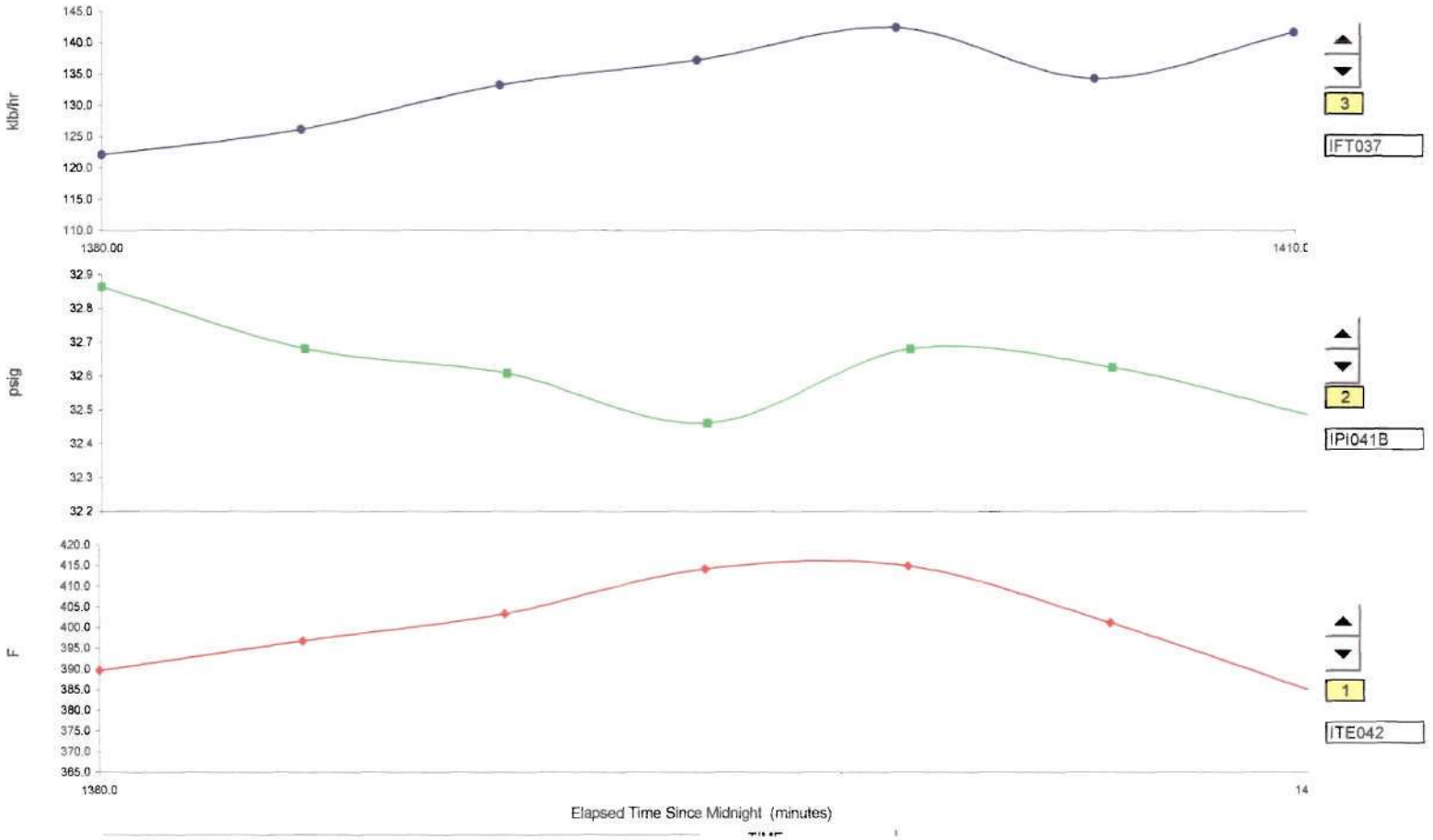

Graph 1: Mass Flow - Turbine LP Extraction Port
Graph 2: Pressure - Turbine LP Extraction Port
Graph 3: Temperature - Turbine LP Extraction Port

Figure IV.5 Inlet Flow, Pressure, and Temperature for Case 2 Time Interval

The SteamCFD code reads data input from a separate file. This file is identified as the itape file and contains all the operating conditions and piping/nozzle geometry identifiers. However, before the data can be input into the itape file, it has to be configured both dimensionally and physically to make it understandable to the main code. To assist in this task, a simple Microsoft Excel spreadsheet was constructed that allowed the input of information directly from the data-logger and made the correct dimensional conversion, as well as performing a heat balance, and then configured the data in a manner that was correct for the itape file. The respective spreadsheets for cases 1 and 2 can be seen in Figure IV.6 and Figure IV.7.

Of specific note here is the section of the spreadsheet that defines the nozzle geometry. In particular, the variables drnoz, dznoz, dthnoz, tiltxy, tiltxz, cone, dcone, anoz, and smr need to be defined. For each nozzle employed in the problem, these variables have to be specified to not only identify the geometric location of the nozzle, but to also describe the direction and performance characteristics of the spray pattern. The variables drnoz, dznoz, dthnoz, tiltxy, and tiltxz all deal with the physical layout of the nozzle with respect to the pipeline that it is installed in. With these variables, the nozzles can be oriented in any physical direction, i.e., axial, radial, co-current, counter-current, etc. The variables of cone, dcone, and smr all deal with defining the spray characteristics of the nozzle. Cone specifies the included cone angle of the spray. If dcone is not specified, then the spray pattern is considered to be full and the particle distribution is more widely spaced with the particle tracks covering the full range of the cone angle. When dcone is given a value, which must be less than cone, the code

SteamCFD Worksheet

Project: UNC - Chapel Hill **File Name:** 10-30 to 10-31 Data
Time: 1170-1200

Inlet	Steam Inlet Mass Flow:	**164000**	[PPH]	**20663.7**	[Gm/Sec]
	Steam Pressure:	**55**	[PSIA]		
	Steam Temperature:	**378**	[F]		
	Steam Specific Volume:	8.877	[Ft3/Lbm]		
	Steam Specific Heat @ Const P:	0.502	[BTU/Lbm/F]		
	Steam Sonic Velocity:	1720.03	[Ft/Sec]		
	Insentropic Expansion Coefficient:	1.308	[-/-]		
	Specific Thermal Conductivity:	0.0192	[BTU/Hr/Ft/F]		
	Dynamic Viscocity:	0.0381	[Lbm/Ft/Hr]		
	Laminar Prandtl Number:	0.997	[-/-]		
Outlet	Steam Outlet Temperature:	**317**	[F]	**287.06**	[Tsat-F]
				414.70	[Tsat-K]
	Steam Outlet Mass Flow:	169402	[PPH]	**21344.3**	[Gm/Sec]
Water	Water Mass Flow:	5402	[PPH]	**Mass Quan.**	**3.3%**
	Water Pressure:	**290**	[PSIA]		
	Water Temperature:	**275**	[F]		
	AF Nozzle Size:	**10**	[MM]	# of Nozzles:	**4**
Line	ID Steam Line:	**29.25**	[IN]		
	Inlet Line Velocity:	86.71	[FPS]		
	Inlet Mach Number:	0.05	[-/-]		
	Inlet Reynolds Number:	2.25E+06	[-/-]		

bore:	74.30	[Cm]	breakup:	**0.0**	
tcylwl:	465.37	[K]	ievap:	**1**	
thead:	465.37	[K]	drnoz:	**0**	[Cm]
tpistn:	465.37	[K]	dznoz:	**16**	[Cm]
tvalve:	465.37	[K]	dthnoz:	**0**	[Deg]
tempi:	465.37	[K]	tiltxy:	**0**	[Deg]
tkei:	34922	[Cm2/Sec2]	tiltxz:	**180**	[Deg]
tke-factor:	**1**	[1-10%]	cone:	**80**	[Deg]
pr1:	0.997	[-/-]	dcone:	**10**	[Deg]
rpr:	1.11	[-/-]	anoz:	0.15	[Cm2]
rprq:	1.0	[-/-]	smr:	**1.00E-02**	[Cm]
rpre:	0.769231	[-/-]	amp0:	0.0	
rsc:	1.11	[-/-]	velinj:	1199	[Cm/Sec]
numnoz:	**4**		h2o rho1:	1.804E-03	[Gm/Cm3]
numvel:	**1**		pamb:	3.793E+06	[Gm/Cm/Sec2]
injdist:	**1**		tkeamb:	3600.0	[Cm2/Sec2]
kolide:	**0**		sclamb:	1.0	[Cm]
tspmas:	681	[Gm/Sec]	spdam1:	1.964E-03	[Gm/Cm3]
pulse:	0.0		velin:	2643	[Cm/Sec]
tpi:	408.15	[K]	spdin1:	1.804E-03	[Gm/Cm3]

Figure IV.6 SteamCFD Input Worksheet For Case 1 Data

SteamCFD Worksheet

Project: UNC - Chapel Hill **File Name:** 5/2 to 5/3 Data
Time: 1380-1410

Inlet	Steam Inlet Mass Flow:	**142500**	[PPH]	**17954.7**	[Gm/Sec]
	Steam Pressure:	**47.4**	[PSIA]		
	Steam Temperature:	**415**	[F]		
	Steam Specific Volume:	10.824	[Ft3/Lbm]		
	Steam Specific Heat @ Const P:	0.491	[BTU/Lbm/F]		
	Steam Sonic Velocity:	1762.85	[Ft/Sec]		
	Insentropic Expansion Coefficient:	1.307	[-/-]		
	Specific Thermal Conductivity:	0.0202	[BTU/Hr/Ft/F]		
	Dynamic Viscocity:	0.0402	[Lbm/Ft/Hr]		
	Laminar Prandtl Number:	0.977	[-/-]		
Outlet	Steam Outlet Temperature:	**317**	[F]	**277.64**	[Tsat-F]
				409.47	[Tsat-K]
	Steam Outlet Mass Flow:	149846	[PPH]	**18880.3**	[Gm/Sec]
Water	Water Mass Flow:	7346	[PPH]	**Mass Quan.**	**5.2%**
	Water Pressure:	**290**	[PSIA]		
	Water Temperature:	**275**	[F]		
	AF Nozzle Size:	**7**	[MM]	# of Nozzles:	**28**
Line	ID Steam Line:	**29.25**	[IN]		
	Inlet Line Velocity:	91.86	[FPS]		
	Inlet Mach Number:	0.05	[-/-]		
	Inlet Reynolds Number:	1.85E+06	[-/-]		

bore:	74.30	[Cm]	breakup:	**0.0**	
tcylwl:	485.93	[K]	ievap:	**1**	
thead:	485.93	[K]	drnoz:	**0**	[Cm]
tpistn:	485.93	[K]	dznoz:	**16**	[Cm]
tvalve:	485.93	[K]	dthnoz:	**0**	[Deg]
tempi:	485.93	[K]	tiltxy:	**0**	[Deg]
tkei:	39196	[Cm2/Sec2]	tiltxz:	**180**	[Deg]
tke-factor:	**1**	[1-10%]	cone:	**80**	[Deg]
pr1:	0.977	[-/-]	dcone:	**10**	[Deg]
rpr:	1.11	[-/-]	anoz:	0.05	[Cm2]
rprq:	1.0	[-/-]	smr:	**5.00E-03**	[Cm]
rpre:	0.769231	[-/-]	amp0:	0.0	
rsc:	1.11	[-/-]	velinj:	661	[Cm/Sec]
numnoz:	**28**		h2o rho1:	1.480E-03	[Gm/Cm3]
numvel:	**1**		pamb:	3.269E+06	[Gm/Cm/Sec2]
injdist:	**1**		tkeamb:	3600.0	[Cm2/Sec2]
kolide:	**0**		sclamb:	1.0	[Cm]
tspmas:	926	[Gm/Sec]	spdam1:	1.685E-03	[Gm/Cm3]
pulse:	0.0		velin:	2800	[Cm/Sec]
tpi:	408.15	[K]	spdin1:	1.480E-03	[Gm/Cm3]

Figure IV.7 SteamCFD Input Worksheet For Case 2 Data

reconfigures the nozzle to represent the characteristics of a hollow cone style. The resulting spray pattern is restricted to a narrower range of cone angle and the particle tracks are aligned within that range. The variable smr describes the Sauter Mean Radius of the particles generated by the nozzle. The anoz variable is used only to determine the mass distribution amongst a multiple nozzle arrangement. As long as anoz remains constant, the program will evenly distribute the total specified spray water quantity to each nozzle. It is important to note that these nozzle geometry variables must be repeated for every nozzle, both type and quantity, which resides in the desuperheater or spray arrangement. Details of these geometric variables can be seen in Figures IV.8, IV.9, and IV.10.

One could ask as to what significance such a variation in flow pattern might have on the performance of a desuperheater. While it may appear that the full cone spray would provide better coverage across the pipe, in reality one only needs to look at the potential momentum transfer to the particles on the outer periphery of the cone. Since the mass flux has been reduced, momentum transfer, i.e. drag, with the flowing steam would cause the outer most particles to collapse onto the flow stream. The resulting cross-sectional flow would be far denser because of the already more centrally directed particles. Within the hollow cone spray, all the mass is directed radially outward in a direction closely resembling the cone angle. Momentum transfer also occurs here, but the collapsing spray pattern would force the droplets to move towards a void not previously populated by particles. The exact sensitivity of a particular piping

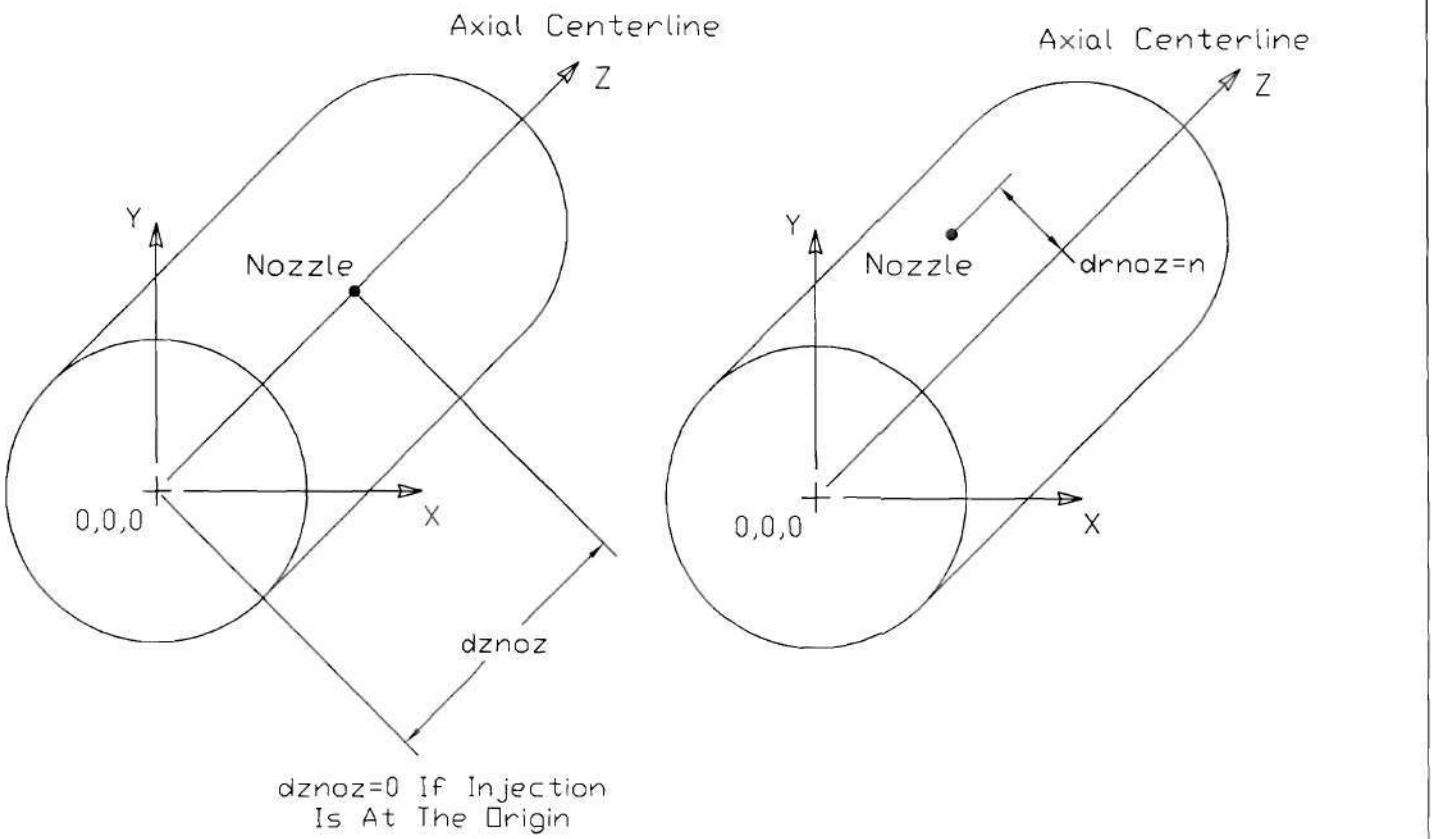

Nozzle Location

Figure IV.8

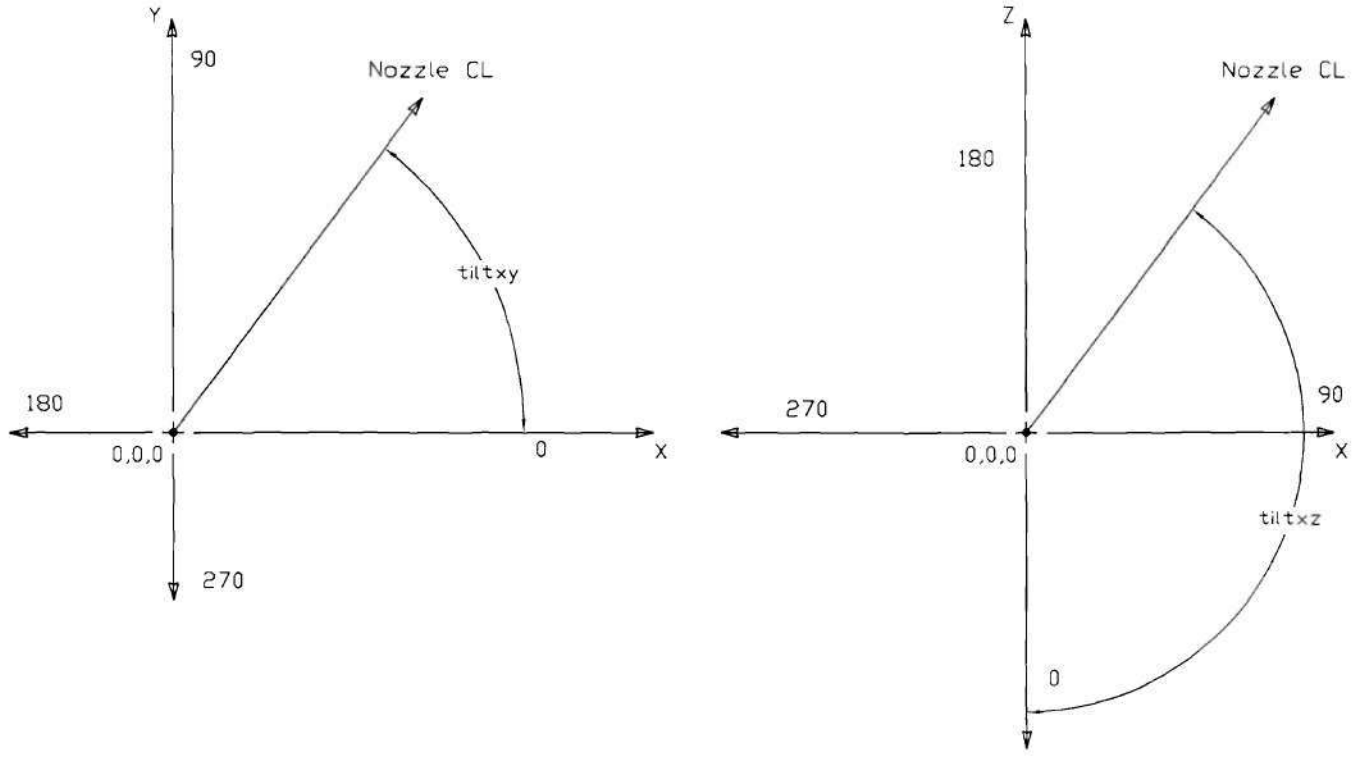

Nozzle Orientation

Figure IV.9

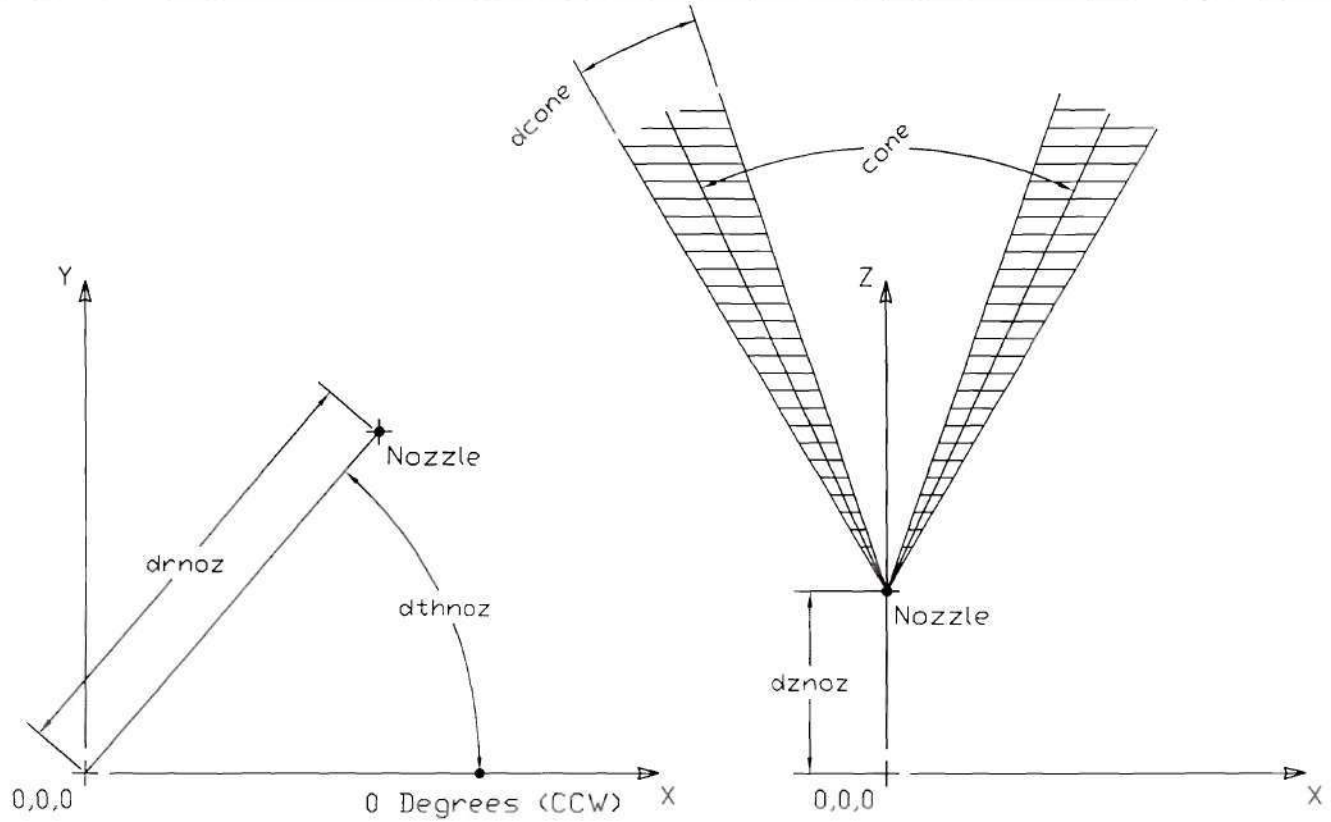

Nozzle Orientation & Spray Geometry

Figure IV.10

arrangement and style of nozzle used is one of the many variables this code was written to evaluate.

Once the input data is converted, it can be input into the itape file. The present itape is comprised of numerous variables, some of which have been written specifically for the SteamCFD code and others that are solely associated with the original Kiva3 code. Only those variables identified for use with the SteamCFD application are modified. Table IV.2 identifies all the variables and describes their numerical and technical significance to the code.

Table IV.2 Itape Input Variables

Variable Name	Typical Value	Description/Units
irest	0	Restart file number
lwall	0 or 1	0 = Slip, 1 = Use Law of the Wall BC
lpr	1	1= Detailed output
irez	0	0 = Eulerian, 1 = Lagrangian, 2 = Special (Leave set to 0)
ncfilm	9999	# of cycles between file outputs
nctap8	9999	# of cycles between restart file writes
nclast	9999	# of last cycle in calculation
cafilm	9999.0	ignore
catfin	9999.0	ignore
angmom	0.0	ignore
pgssw	1.0	0.0 = disable pressure gradient scaling, 1.0 = enable, forced to 0.0 if pressure boundaries present (Used for low Mach number flows)
sampl	0.0	ignore
dti	1.00000e-4	Initial Time Step, seconds
dtmxca	9999.0	ignore
dtmax	9.99e+9	Max. time step
tlimd	0.0	If set = 1.0, forces write of restart file at end of calculation
twfilm	0.25e-0	Time interval for print out of data, seconds
twfin	1.00e+0	Final time, seconds
stpmax	3.00e-4	Maximum Time Step
fchsp	0.25	ignore
bore	73.66	Pipe ID (cm)
stroke	8.0	ignore
squish	1.5	ignore
rpm	0.0	ignore
atdc	-180.0	ignore
datdct	0.0	ignore
conrod	16.269	ignore
swirl	0.0	Initial swirl = ratio of fluid swirl to crankshaft
swipro	3.11	Defines swirl profile (see p. 82 of KIVA II manual)
thsect	360.0	# of degrees in cyclinder model, 360.0 = full pipe
sector	0.0	Used with thsect to define partial model of

		cylinder (or pipe)	
epsy	1.0e-3	Mass diffusion relative error	
epsv	1.0e-4	Velocity relative error, (u,v,w,)	Always e-4 or e-5
epsp	1.0e-4	Pressure relative error	
epst	1.0e-4	Temperature relative error	
epsk	1.0e-4	Turbulent Kinetic Energy	
epse	1.0e-4	Turbulent Dissipation Rate	
gx	0.0	Gravitational Constant, gram cm/sec^2 (Be consistent with Coordinate System)	
gy	980.0		
gz	0.0		
tcylwl	717.1	Wall Temperature, K	
thead	717.1		
tpistn	717.1		
tvalve	717.1		
tempi	717.1	Initial Steam temperature, K	
pardon	0.0	Set = 1.0 for partial donor cell fluxing, = 0.0 for Quasi-2nd order upwind fluxing (Leave = 0.0)	
a0	0.0	Advective flux controls, only used when pardon = 1.0	
b0	1.0		
anc4	0.05	Alternate Node Coupler, 0.0<=anc4<=0.05	
adia	1.0	1.0 = Adiabatic Boundary Conditions, 0.0 = Fixed Temp. at wall	
anu0	0.0	Viscosity ratio, use 0.0 with k-e model	
visrat	-.66666667	Ratio of lambda to mu, use –2/3 for zero bulk viscosity	
tcut	9.99e+9	Ignore	
tcute	9.99e+9	Ignore	
epschm	0.02	Ignore	
omgchm	1.0	Ignore	
tkei	19656.45	Initial Turbulent K.E. in cm^2/sec^2 Use 1-10% of the mean flow kinetic energy.	
tkesw	1.0	Set = 1.0 if turbulence is on, Set = 0.0 if turbulence is off	
sgsl	0.0	SGS Length scale, typically 4-5 dz. = 0.0 for k-e turbulence model	
uniscal	0.0	If not 0.0 this is the initial turbulent length scale, leave = 0.0	
airmu1	1.457e-5	Ignore	
airmu2	110.0	Ignore	
airla1	252.0	Ignore	
airla2	200.0	ignore	
pr1	0.92	Laminar Prandtl Number – Rec. by Lit.	

rpr	1.11	1/ Turbulent Prandtl Number
rprq	1.0	Rpr for tke diffusion
rpre	0.769231	Rpr for epsilon diffusion
rsc	1.11	1/ turbulent Schmidt Number
xignit	0.0	ignore
tlign	9.99e+9	ignore
tdign	9.99e+9	ignore
calign	-27.0	ignore
cadign	9.6	ignore
xignl1	0.0	ignore
xignr1	0.623	ignore
yignf1	0.0	ignore
yignd1	0.238	ignore
zignb1	11.75	ignore
zignt1	12.50	ignore
xignl2	0.0	ignore
xignr2	0.0	ignore
yignf2	0.0	ignore
yignd2	0.0	ignore
zignb2	0.0	ignore
zignt2	0.0	ignore
kwikeq	0	ignore
icoll	1	1 = track quantity of unvaporized liquid leaving the system (tape26)
numnoz	1	Number of Nozzles
numvel	1	# of entries in velocity injection table following amp0 below, use 1 to input single velocity
injdist	1	0 = Uniform Droplet Size 1 = Follows specified Droplet Size Distr.
kolide	0	0 = Neglects Collision Model 1 = Utilizes Collision Model
tlinj	0.00e+0	Time injection begins, seconds
tdinj	9.99e+9	Time injection ends, seconds
calinj	999.0	ignore
cadinj	999.0	ignore
tspmas	11270.0	Injected Liquid Mass Flow Rate, gm/sec
pulse	0.0	=0.0 for continuous spray injection =1.0 for half sine wave injection =2.0 for square wave injection =3.0 for custom profile using velinj
tnparc	10000.0	Number of Computational Particles Not less then 5000. Not more than npar in

		comkiva.i.
tpi	420.0	Initial Droplet Temperature, K
turb	1.0	0 = Steam Turbulence Included 1 = Steam Turbulence Neglected
breakup	0.0	0 = No Droplet Break-Up 1 = Active Droplet Break-Up
evapp	1.0	0 = No Evaporation (Single Phase Problem) 1 = Liquid Evaporates
ievap	2	1 = Most general model including liquid heating 2 = Simplified model neglecting liquid heating 3 = Simplified model neglecting effect of local pressure change on droplet surface temperature
drnoz	0.0	Radius of nozzle from x0,y0, in cm.
dznoz	100.0	z coordinate of nozzle, in cm.
dthnoz	0.0	Azimuthal angle, in degrees, from the xz plane viewed from the +y direction. Positive direction is counterclockwise.
tiltxy	0.0	Nozzle rotation in the x-y plane, in degrees, where 0.0 points in the +y direction. Positive direction is counterclockwise.
tiltxz	0.0	Nozzle rotation in the xz plane, in degrees, where 0.0 points in the **negative** z direction. Positive direction is counterclockwise.
cone	80.0	Mean Spray Cone Angle in degrees
dcone	20.0	Spray Thickness (Degrees) For solid cone = Cone
anoz	4.084	Nozzle Area, cm^2
smr	1.00e-2	Sauter Mean Radius of Droplet, cm
amp0	0.0	Initial amplitude of droplet oscillation at injector based on Weber number
velinj	7500	Droplet velocity in cm/s
nsp	1	ignore
h2o rho1	1.57e-3	Internal Density of Steam – CGS this parameter has been altered from the Kiva3 usage and needs to be removed or at least cleaned up.
nrk	0	Leave as 0
nre	0	Leave as 0
distamb	0.0	If > than 0.0, distamb applies the outflow

		pressure distamb downstream of the boundary in an attempt to reduce acoustic wave reflection. Only applies to out-flow boundaries. Use a characteristic dimension of the grid.
pamb	5.1698e+6	Ambient pressure in gram/cm sec^2 at open boundary
tkeamb	3600.0	Ambient turbulent Kinetic Energy at open boundary, cm^2/sec^2
sclamb	1.0	Ambient turbulent length scale at open boundary, cm
spdam1	1.5700e-3	Ambient density at open boundary, $gram/cm^3$
velin	6270.0	Steam Velocity at Inlet, cm/sec
reedin	1.0	1 = Prevents Reverse Flow condition
reedout	1.0	0 = allows reverse flow at boundaries
spdin1	1.5700e-3	Density of Steam at velocity inlet, $gram/cm^3$

The typical itape file format can be seen in Table IV.3. As the title indicates, this itape was used in the computational analysis of the four-nozzle desuperheating arrangement. Note that the geometry factors have been quadrupled in order to correctly depict the layout and performance envelope of the unit.

Prior to initialization of the program, a test is performed to verify the location of the nozzles within the pipeline. Normally, the program is allowed to iterate for 50-100 cycles with the water injection turned on. Then the output files are run through the post processor to graphically display the layout and initial injection of the water particles. Examples of this check can be seen for the one, four, and 28-nozzle arrangements in Figures IV.11, 12,13, 14, 15, and 16.

When the checks are complete and the files located in the correct directories, the code is initialized and begins iterating the problem variables. In practice, it has been

found that the best results are gained when the water is not immediately injected into the problem, but rather that the steam flow is allowed to pass through the pipe for a short period of time. This allows for pressure and flow fluctuations to subside and steady-state conditions to prevail prior to water injection. The real time for this pre-run varies from 1 to 2 seconds and is a function of the pipe length and flow velocity.

Table IV.3 Typical itape File Format

```
irest      2
lwall      1
lpr        1
gmv        0.0
irez       0
ncfilm    25
nctap8   250
nclast99999
cafilm99999.0
cafin 99999.0
angmom     0.0
pgssw      0.0
sampl      0.0
dti    1.00000e-5
dtmxca 9999.0
dtmax     9.99e+9
tlimd      1.0
twfilm    0.25e-1
twfin     2.0e+0
stpmax    5.00e-5
fchsp      0.25
bore      72.39
stroke  1308.0
squish   149.5
rpm        0.0
atdc    -180.0
datdct     0.0
conrod    16.269
swirl      0.0
swipro     3.11
thsect   360.0
sector     0.0
epsy       1.0e-5
epsv       1.0e-5
epsp       1.0e-5
epst       1.0e-5
epsk       1.0e-5
epse       1.0e-5
gx         0.0
gy      -980.0
gz         0.0
tcylwl   464.0
thead    464.0
tpistn   464.0
tvalve   464.0
tempi    464.0
pardon     0.0
a0         0.0
b0         1.0
anc4       0.05
adia       1.0
anu0       0.0
visrat-.66666667
tcut      9.99e+9
tcute     9.99e+9
epschm     0.02
omgchm     1.0
tkei   97018.10
tkesw      1.0
sgsl       0.0
uniscal    0.0
airmu1   1.457e-5
airmu2   110.0
airla1   252.0
airla2   200.0
prl        1.012
rpr        1.11
rprq       1.0
rpre     0.769231
rsc        1.11
xignit     0.0
tlign     9.99e+9
tdign     9.99e+9
calign   -27.0
cadign     9.6
xignl1     0.0
xignr1     0.623
yignf1     0.0
yignd1     0.238
zignb1    11.75
zignt1    12.50
xignl2     0.0
xignr2     0.0
yignf2     0.0
yignd2     0.0
zignb2     0.0
zignt2     0.0
kwikeq     0
 icoll     1
 iavet     1
 ncvs    100
numnoz     4
numvel     1
injdist    1
kolide     0
tlinj      0.75
tdinj     9.99e+9
calinj   999.0
cadinj   999.0
tspmas 1436.0
pulse      0.0
tnparc 6000.0
tpi      408.0
turb       1.0
breakup    0.0
evapp      1.0
ievap      2
drnoz     19.4
dznoz     80.00
dthnoz    90.0
tiltxy     0.0
tiltxz -180.0
cone      80.0
dcone     10.0
anoz       0.15
smr       0.75e-2
amp0       0.0
drnoz      7.8
dznoz     80.00
dthnoz    90.0
tiltxy     0.0
tiltxz -160.0
cone      80.0
dcone     10.0
anoz       0.15
smr       0.75e-2
amp0       0.0
drnoz      3.8
dznoz     80.00
dthnoz   -90.0
tiltxy     0.0
tiltxz -200.0
cone      80.0
dcone     10.0
anoz       0.15
smr       0.75e-2
amp0       0.0
drnoz     15.4
dznoz     80.00
dthnoz   -90.0
tiltxy     0.0
tiltxz -180.0
cone      80.0
dcone     10.0
anoz       0.15
smr       0.75e-2
amp0       0.0
velinj 2529.0
nsp        1
h2o   rho1  2.310e-3
nrk        0
nre        0
distamb    0.0
pamb    4.80e+6
tkeamb   360.0
sclamb     1.0
spdam1   2.512e-3
velin    4405.3
reedin     1.0
reedout    1.0
spdin1   2.310e-3
```

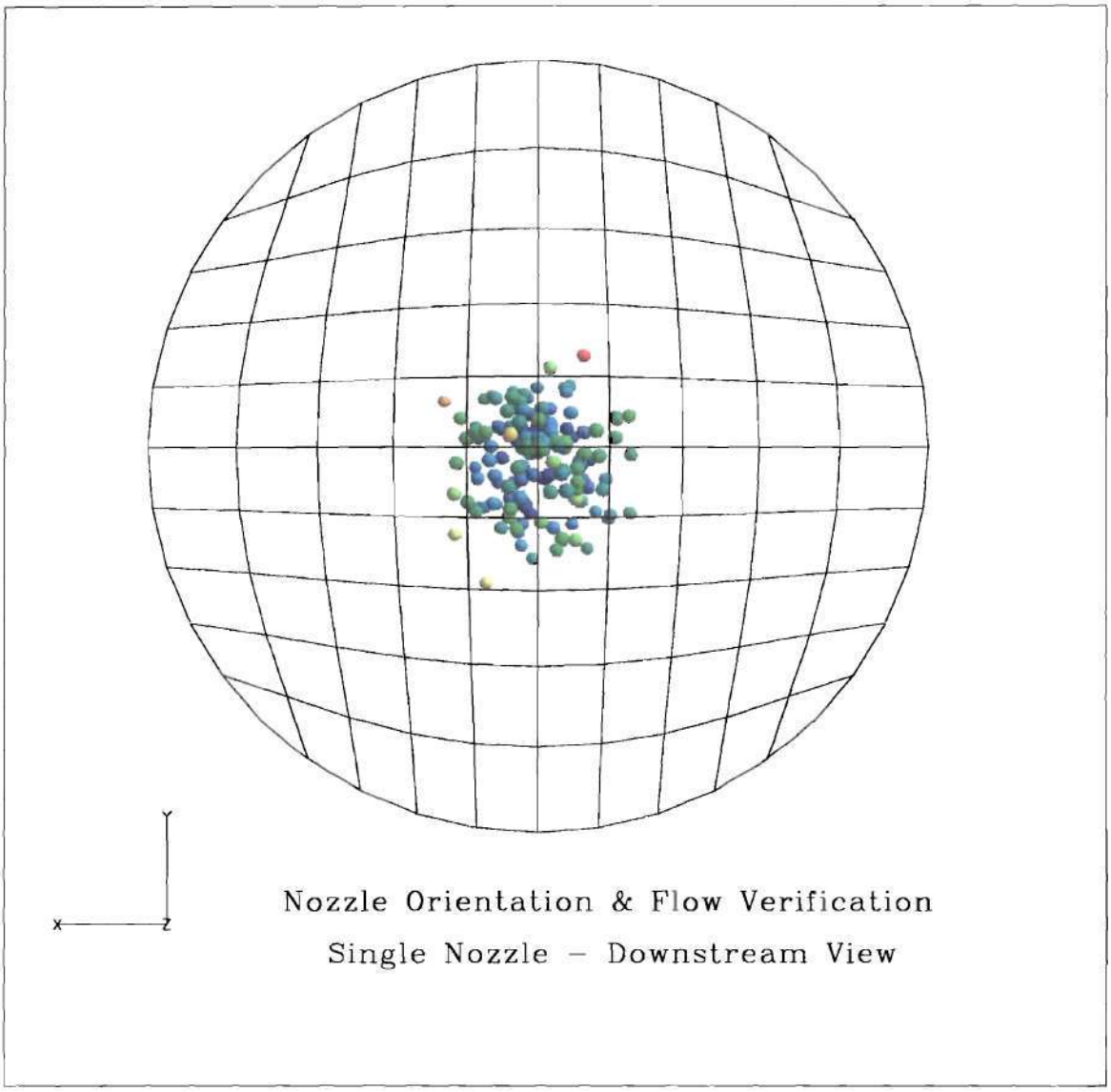
Y
X
Z
Nozzle Orientation & Flow Verification
Single Nozzle – Downstream View

Figure IV.11

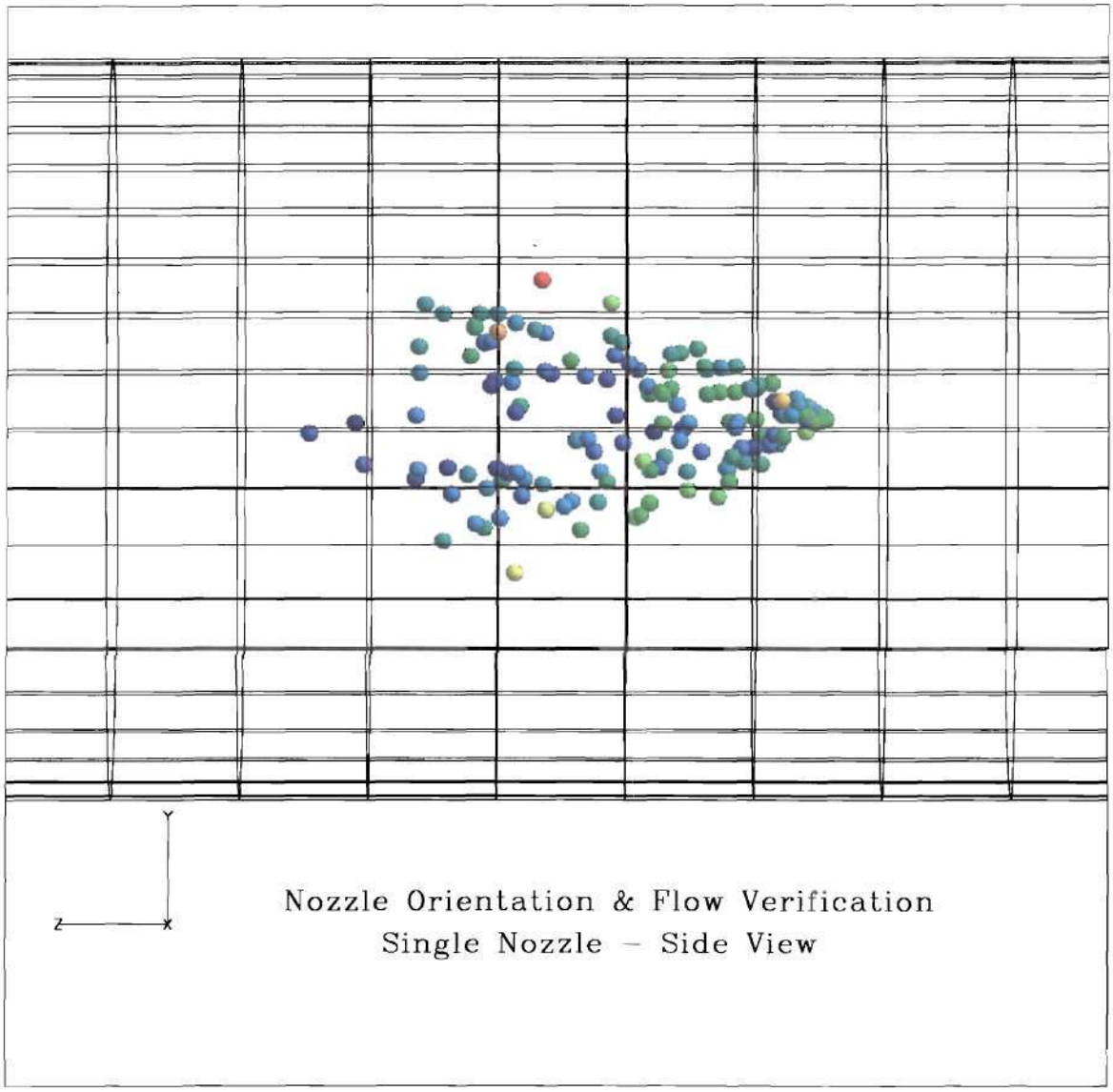
Y
Z
X
Nozzle Orientation & Flow Verification
Single Nozzle – Side View

Figure IV.12

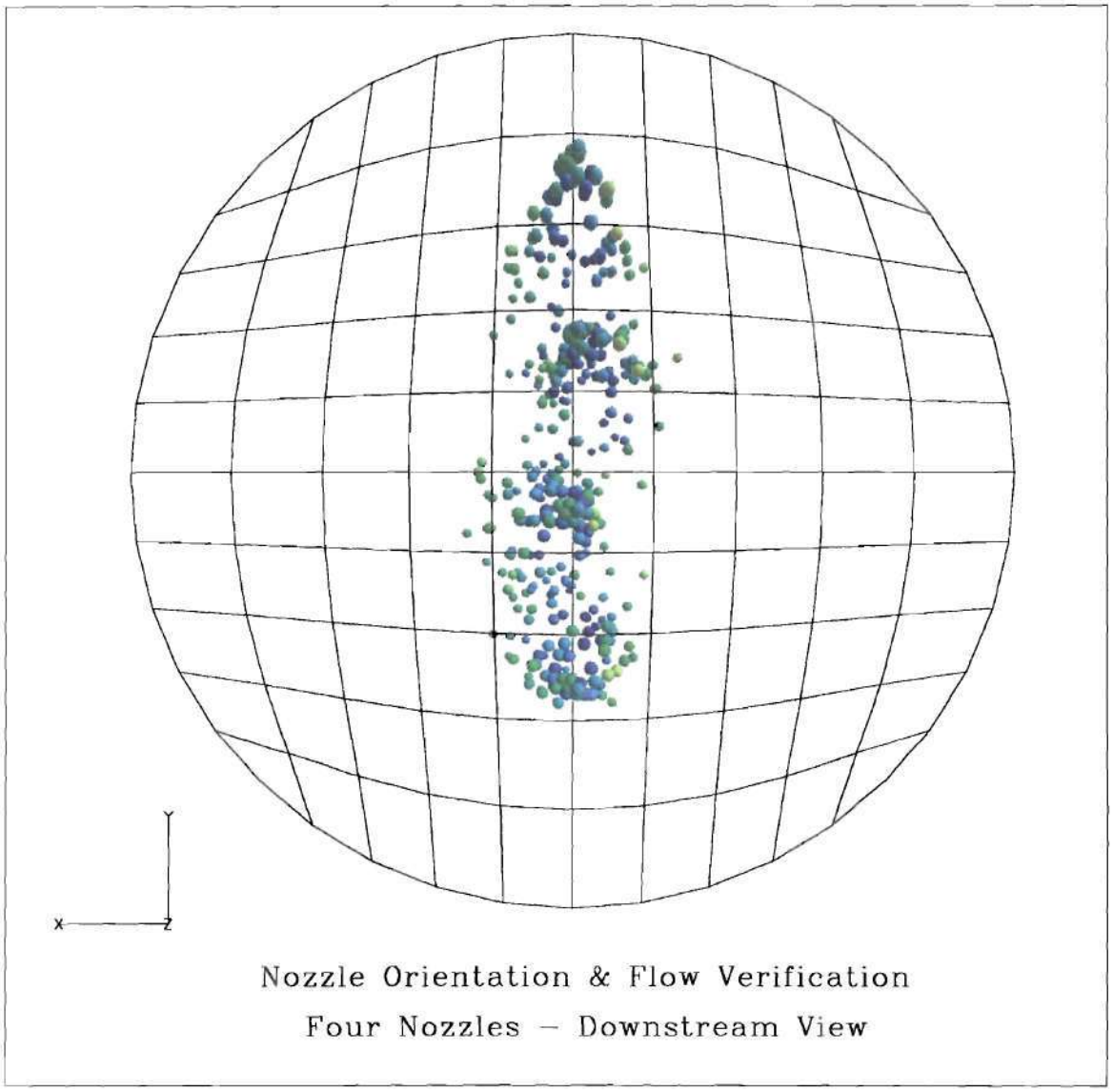
Y
X
Z
Nozzle Orientation & Flow Verification
Four Nozzles – Downstream View

Figure IV.13

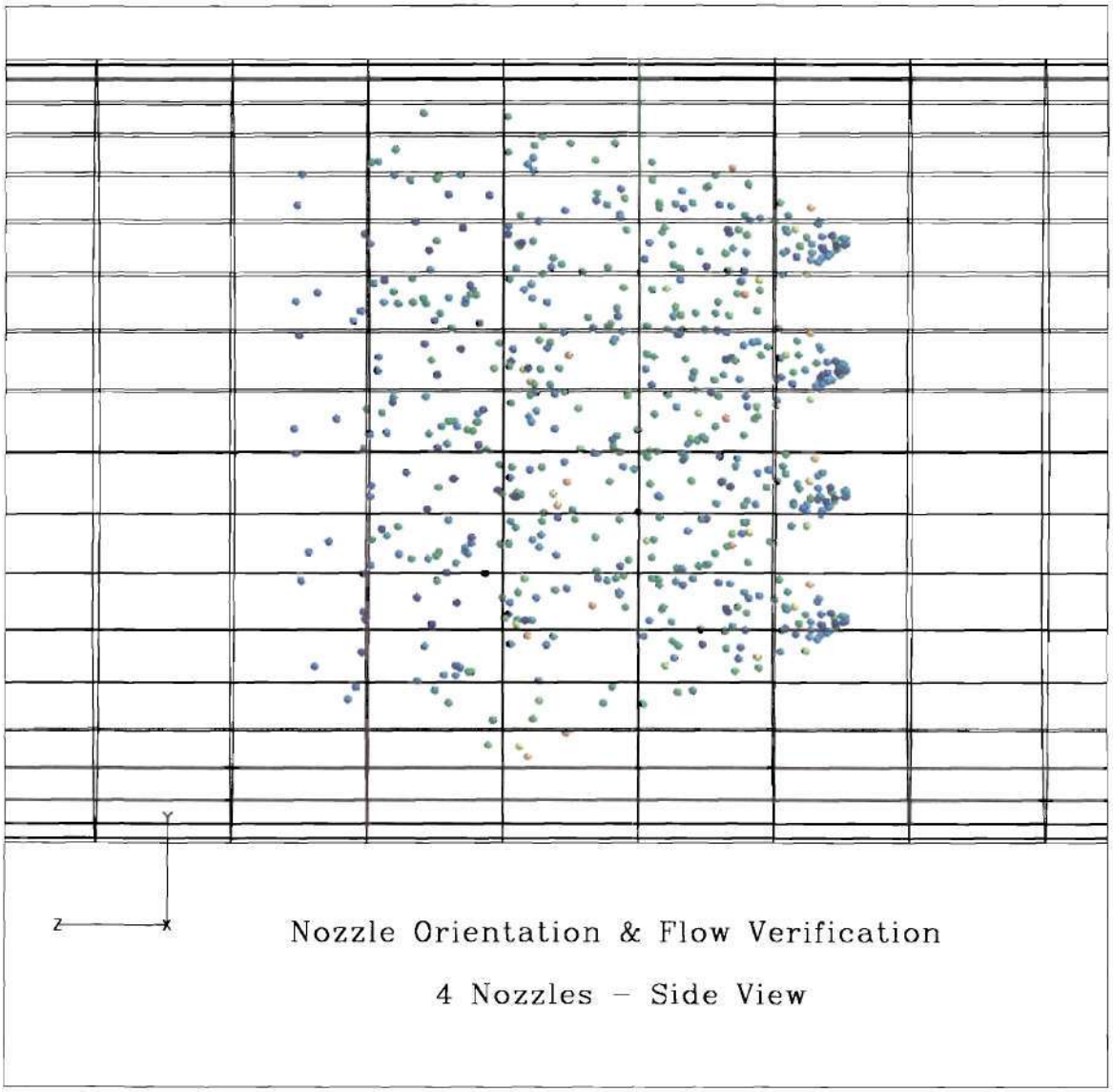
Y
Z
X
Nozzle Orientation & Flow Verification
4 Nozzles – Side View

Figure IV.14

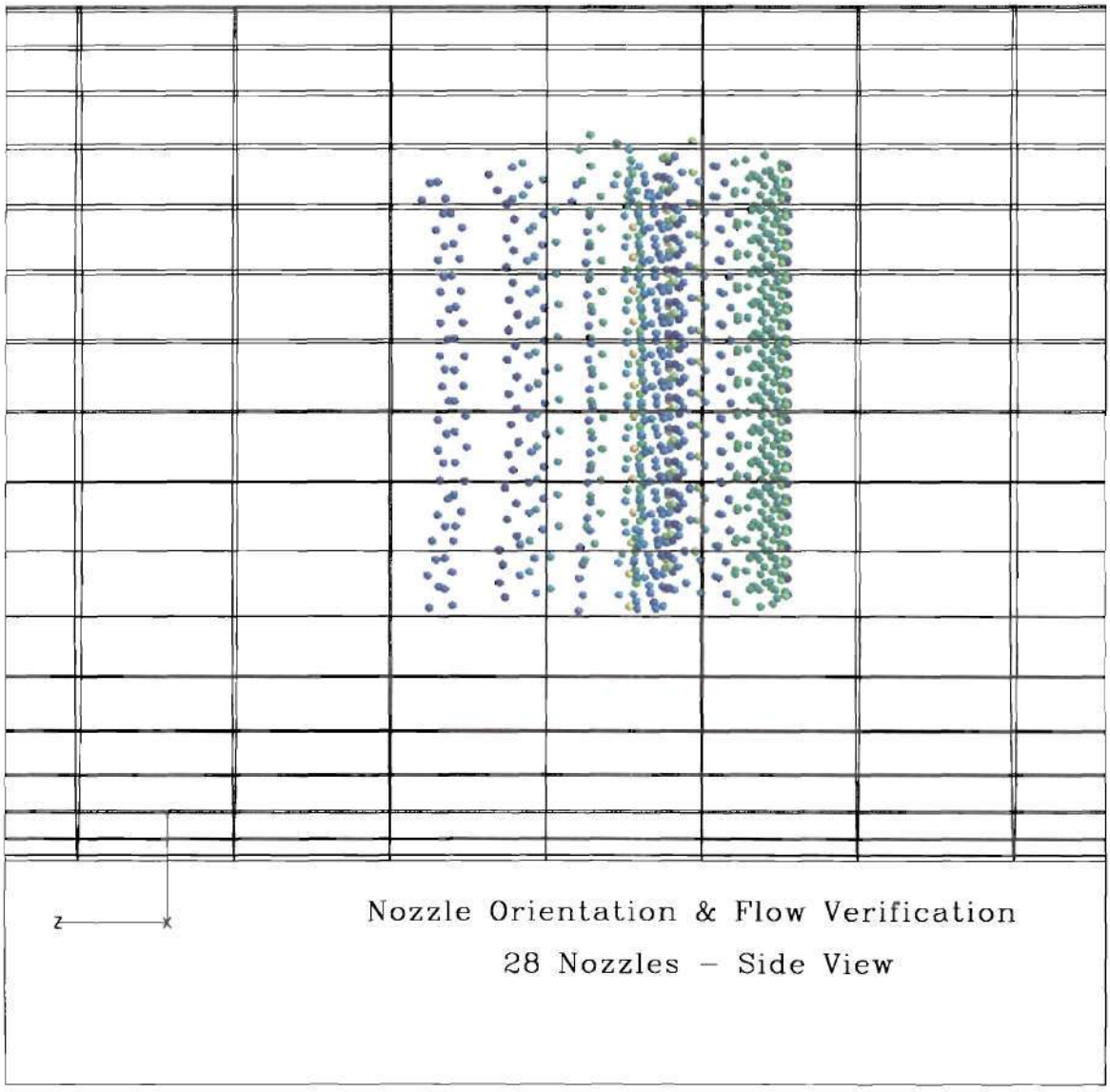
z
x
Nozzle Orientation & Flow Verification
28 Nozzles – Side View

Figure IV.15

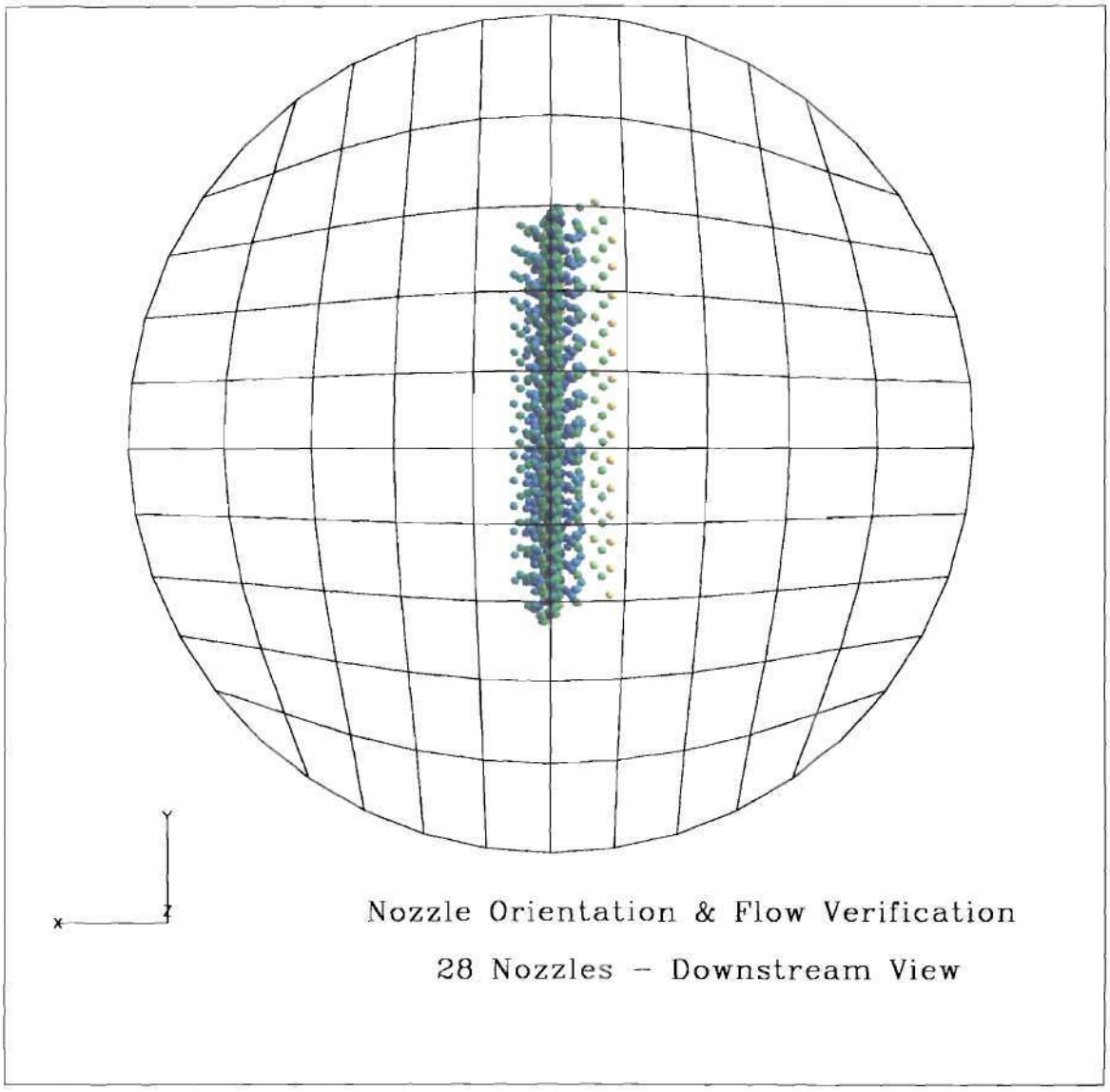
Y
Z
X
Nozzle Orientation & Flow Verification
28 Nozzles - Downstream View

Figure IV.16

CHAPTER V

RESULTS AND DISCUSSION

V.1 Introduction

In this chapter, the computational results obtained during this investigation will be compared with the experimental data collected from the test site. A total of five computational runs were conducted for this analysis. In four of the cases, the input data for the computer simulation was that which had been collected from the UNC test site and was directly applicable to the specific nozzle arrangement. In the fifth case, input data from the four-nozzle arrangement was utilized to examine the expected performance characteristics of the single nozzle arrangement for which detailed experimental data was unavailable. In every case, the program was allowed to progress 0.75 seconds before the injection of any water particles. In this way, steady state steam flow and pressure conditions were realized prior to the introduction of the particles and heat transfer routines.

The computational analysis for each case was divided into five categories. The first category was a dynamic assessment of the flow and temperature through the system. The goal here was to determine when the flow conditions, both steam and water, reached thermal equilibrium or steady state operation within the specified system control volume. The second was the Boundary Temperature Conditions. Here, the affects of thermal changes in the pipe wall could be examined as the particles advanced down the pipeline. The next category was the Temperature Profiles. Coordinate surfaces at the inlet, outlet,

and 1st & 2nd Thermocouple Array axial locations were established and the change in thermal profile and particle distribution with time were determined. The use of the two coordinate surfaces associated with the thermocouple arrays was important in making the necessary comparisons with the experimental data. The third category was the Spray Water Particle Flow. Here the size and flow path of the individual particle bundles could be examined and position changes noted for correlation with the previously mentioned thermal profiles. It also made the visual determination of gravitational and momentum effects very clear. The final category involved the direct comparison of the computational data as related to the collected experimental data. Radar graphs were used to compare the magnitude and variation of temperature at each of the 48 thermocouple, at a common time step, after it was determined that steady state flow had been achieved throughout the model.

Based on mass flow data and fluid velocity, the transient time of the steam and water particles through the system is approximately 0.7 seconds. In order to look at both the transient and steady state conditions within the pipe, computational measurements for all cases and categories were made at 1.10, 1.25, 1.45, 1.60, and 1.75 seconds. Dynamic conditions within the system were monitored by recording the average temperature of the four specified coordinate surfaces every 0.05 seconds. Thermal equilibrium was assumed when the calculated surface plane temperatures attained a near zero slope.

The first two computational runs utilized the original Version 1.2 of the SteamCFD software to examine the performance of the four-nozzle desuperheater and then again for the 26 nozzle arrangement. The analysis was then repeated utilizing the

same physical device geometry, but incorporating the latest version of the code that included a revised liquid film and particle impact model. Finally, a fifth run was undertaken to examine the performance of the original single nozzle device. Even though no experimental data existed to compare and contrast the device performance, it was desirable to examine the respective output relative to the other computational models based on similar flow and geometry constraints.

V.2 The Four Nozzle Device

V.2.1 Thermal Equilibrium

The first task was to determine the equilibrium conditions for each of the four coordinate surfaces. These surfaces were integrated to determine the average profile temperature at time increments of 0.1 seconds between 0.75 to 1.80 seconds. The results of this exercise can be seen in Figures V.1 and V.2. The inlet provided a near constant value of 377° F throughout the prescribed time period. However, in the case using Version 1.2, the latter three coordinate surface showed a 2-3° F greater initial surface temperature. The noted discrepancy in the initial surface temperatures relates to a known problem with Version 1.2 of the code. The thermodynamic properties of the flow are initialized based on the inputted boundary conditions for the problem. Under steady state, single-phase conditions, the correct properties are normally calculated. However, once the spray water is injected, multiphase properties must be considered. Due to Version 1.2's simplistic splash model, considerably more fluid is allowed to collect on the bottom of the pipe. This can result in several problems for the program. The first is a displacement of flow area due to the pooling liquid and the second is the possibility of

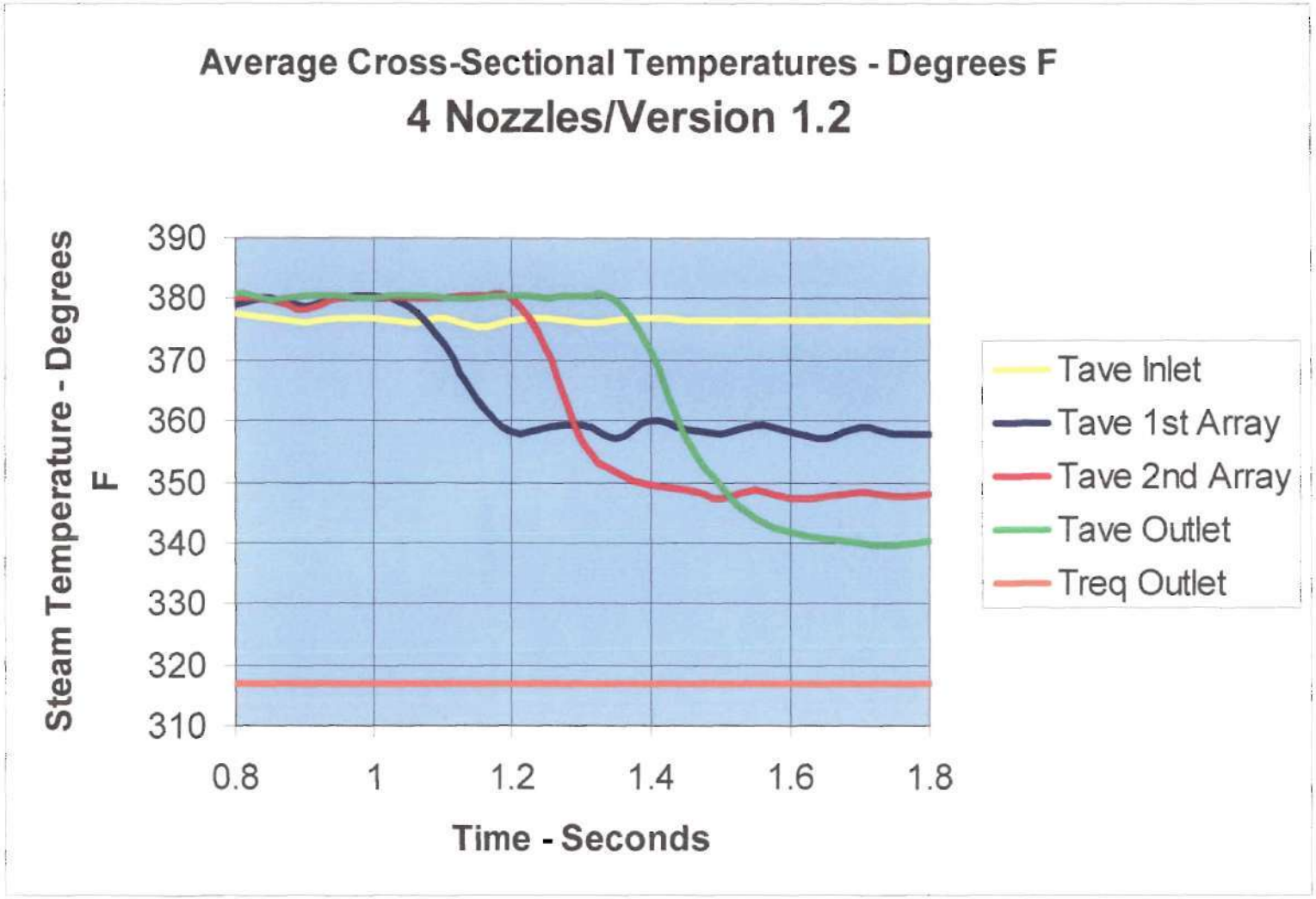
Average Cross-Sectional Temperatures - Degrees F
4 Nozzles/Version 1.2
Steam Temperature - Degrees F
390
380
370
360
350
340
330
320
310
0.8
1
1.2
1.4
1.6
1.8
Time - Seconds
Tave Inlet
Tave 1st Array
Tave 2nd Array
Tave Outlet
Treq Outlet

Figure V.1

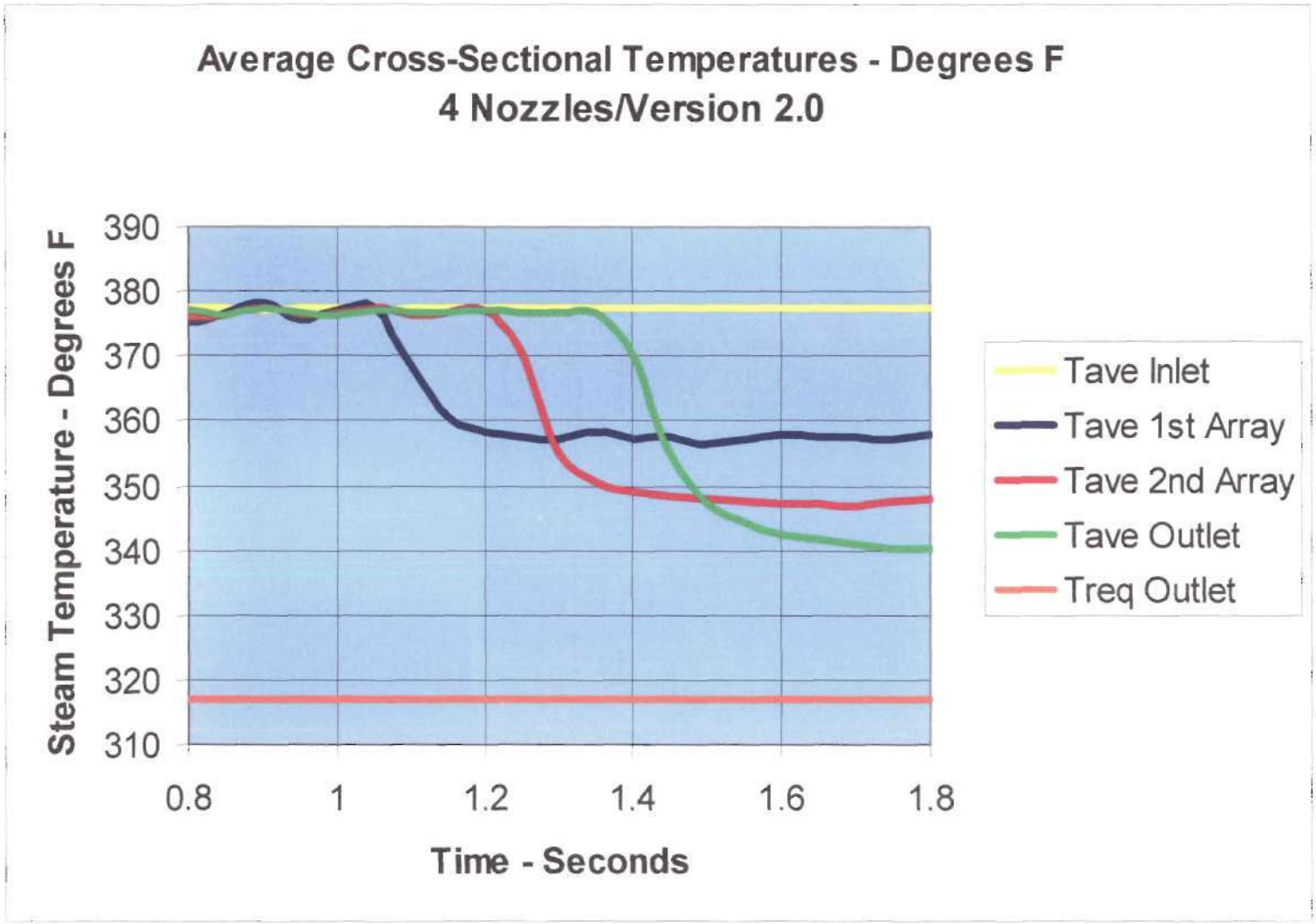
Average Cross-Sectional Temperatures - Degrees F
4 Nozzles/Version 2.0
Steam Temperature - Degrees F
390
380
370
360
350
340
330
320
310
0.8
1
1.2
1.4
1.6
1.8
Time - Seconds
Tave Inlet
Tave 1st Array
Tave 2nd Array
Tave Outlet
Treq Outlet

Figure V.2

further condensation of the steam flow. In an effort to reach thermodynamic equilibrium, the program adjusts certain variables accordingly. In this case, a pressure fluctuation, or depression, was created that resulted in an elevated steam temperature. If the order of magnitude is high, the program is re-initialized with smaller time steps between interations. In this case, the order of magnitude difference would not adversely affect the computations and thus the output was used as generated.

Both cases, run in Version 1.2 and 2.0 respectively, reached thermal equilibrium at about the same time. The 1st and 2nd array of thermocouples reached equilibrium at approximately 1.15-1.2 and 1.35 seconds respectively. The outlet plane reached thermal equilibrium at approximately 1.60 seconds. Thus, all the surfaces achieved relatively constant average temperature profiles within the 1.75-second period of analysis.

V.2.2 Boundary Temperature Conditions

The boundary temperature conditions through 1.25 seconds appear to be relatively constant between the two versions. Only slight differences in temperature are noted on the top portions of the pipe associated with Version 1.2. These are probably associated with the higher initial downstream steam temperatures noted previously and a slight scale difference in the color-coding. Major changes are noted when we reach 1.45 seconds. In viewing Figures V.3 and V4, both at 1.45 seconds, temperature differences at the outlet can be seen. The flow through the two elbows seems to generate similar thermal patterns. However, the magnitude of the surface temperatures is quite different. In Version 1.2, Figure V.3, there is indication of wall temperatures at or near the desired set point of 317 ° F. This is illustrated by the streaks of deep blue profiling on the lower and

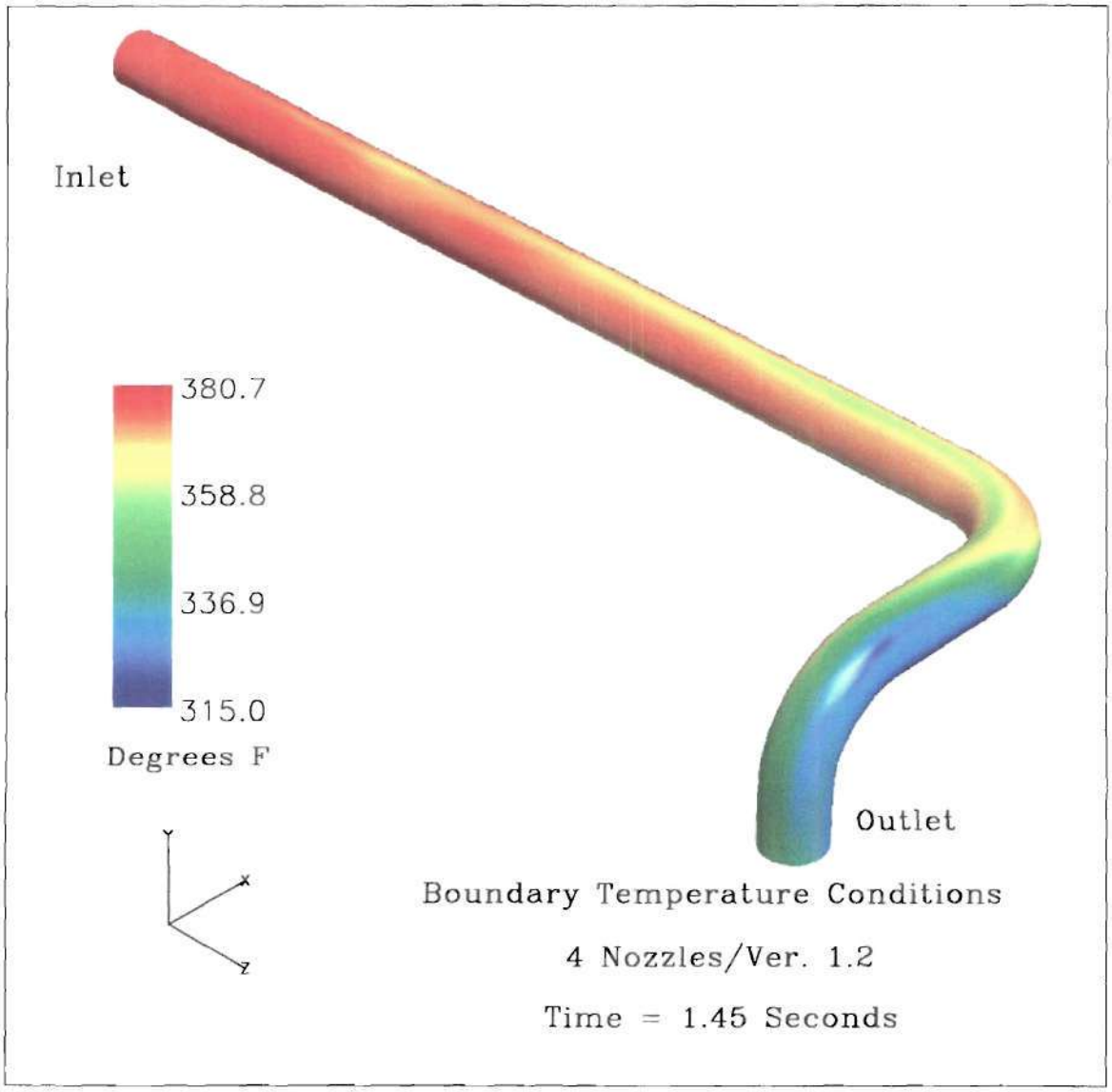
Inlet
380.7
358.8
336.9
315.0
Degrees F
Outlet
Boundary Temperature Conditions
4 Nozzles/Ver. 1.2
Time = 1.45 Seconds

Figure V.3

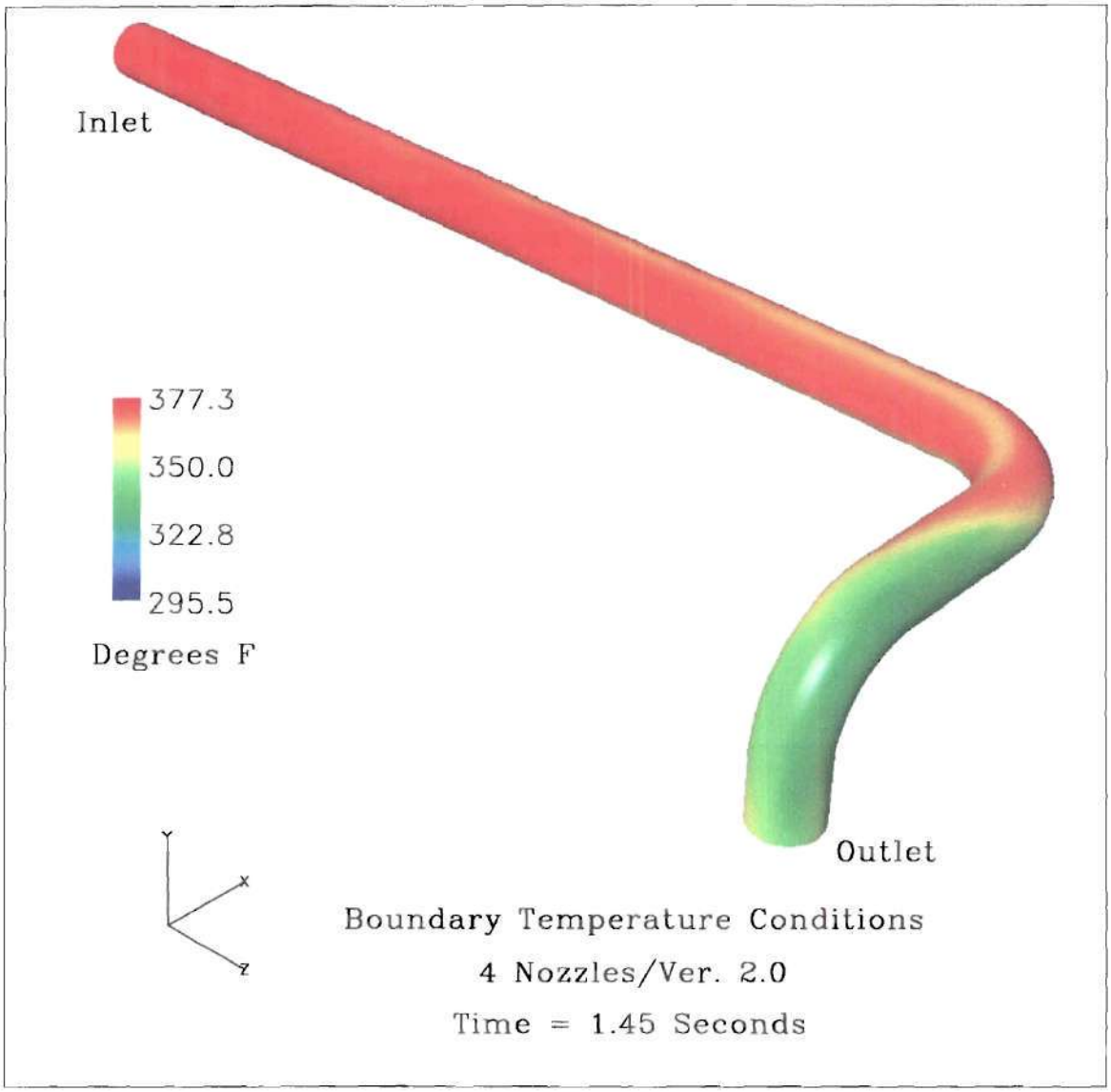
Inlet
377.3
350.0
322.8
295.5
Degrees F
Outlet
Boundary Temperature Conditions
4 Nozzles/Ver. 2.0
Time = 1.45 Seconds

Figure V.4

outer surfaces just past the first elbow. In contrast, in Version 2.0, Figure V.4, the same surfaces are in the 330-350° F range. This difference could certainly be the result of the improved film model and the fact that much less water is contained in this initial flow stream reaching the outlet.

The boundary temperature distributions between 1.60 and 1.75 seconds begin to show a convergence between the two versions. At 1.60 seconds, Version 1.2 shows greater thermal stabilization and temperature similarity to Version 2.0 on the same surfaces mentioned above. This can be seen by comparing Figure V.5 and V.6. In contrast, the profiles in Version 2.0 have changed little since 1.45 seconds. This can be seen by looking at Figures V.4 and V.7. At 1.75 seconds, the temperature distributions predicted by the two versions are almost identical, see Figures V.7 and V.8. Version 1.2 still indicates a very distinct region of lower temperatures just downstream of the second elbow. Version 2.0 shows a similar streak but at a much lower magnitude. This streak could be the result of several factors. It could actually relate to the manner in which the code handles the excess water in the region and thus it is not exhibited in the later version containing the improved film heat transfer model. It could also be a grid-related effect as it appears in a region at 45° to the main axis. This is the region of maximum skewness in the grid generation of the model.

The complete graphical output of the boundary temperature conditions for the four-nozzle arrangement, using both Version 1.2 and Version 2.0, can be viewed in Appendix C.

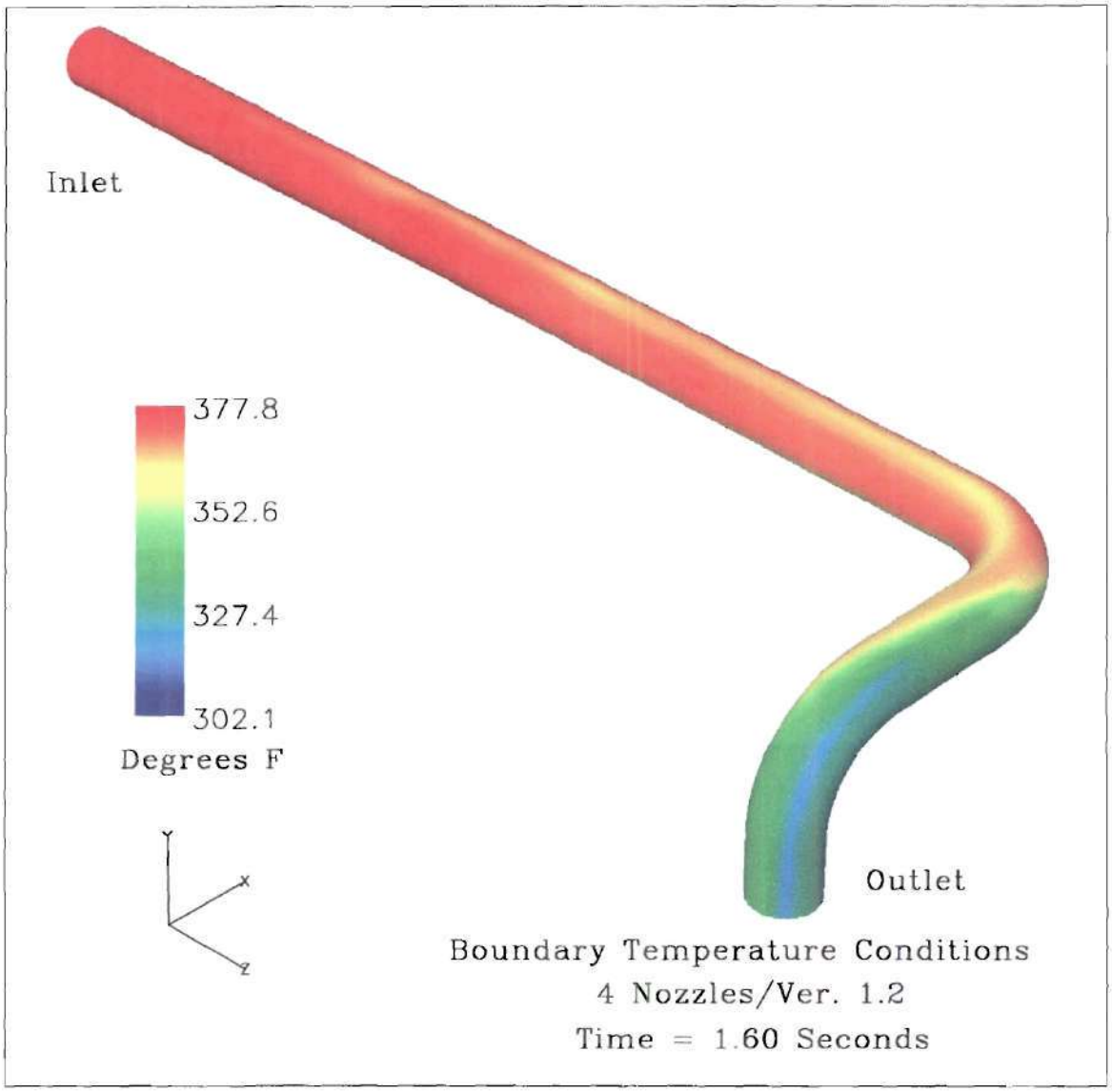
Inlet
377.8
352.6
327.4
302.1
Degrees F
Y
X
Z
Outlet
Boundary Temperature Conditions
4 Nozzles/Ver. 1.2
Time = 1.60 Seconds

Figure V.5

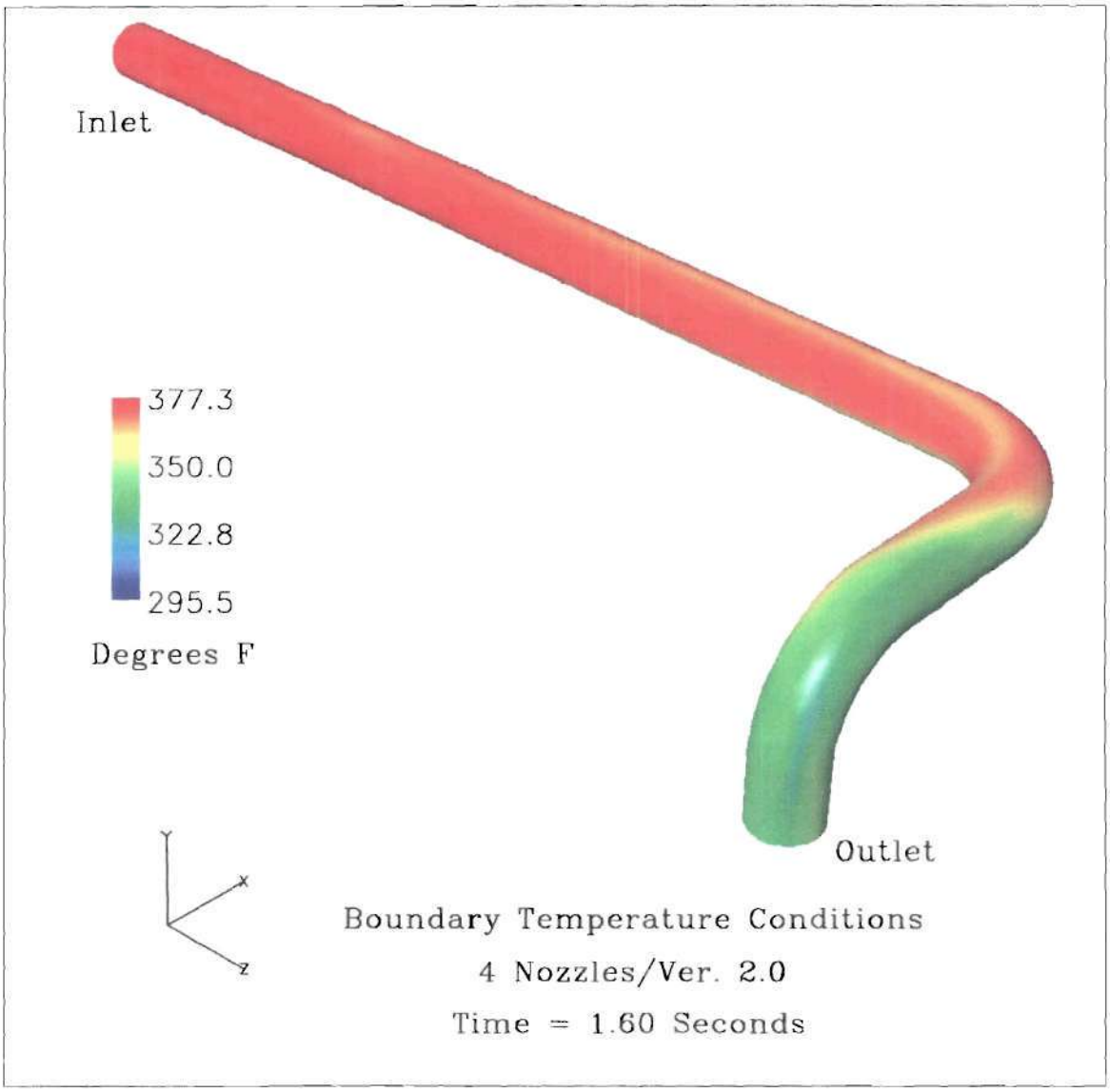
Inlet
377.3
350.0
322.8
295.5
Degrees F
Outlet
Boundary Temperature Conditions
4 Nozzles/Ver. 2.0
Time = 1.60 Seconds

Figure V.6

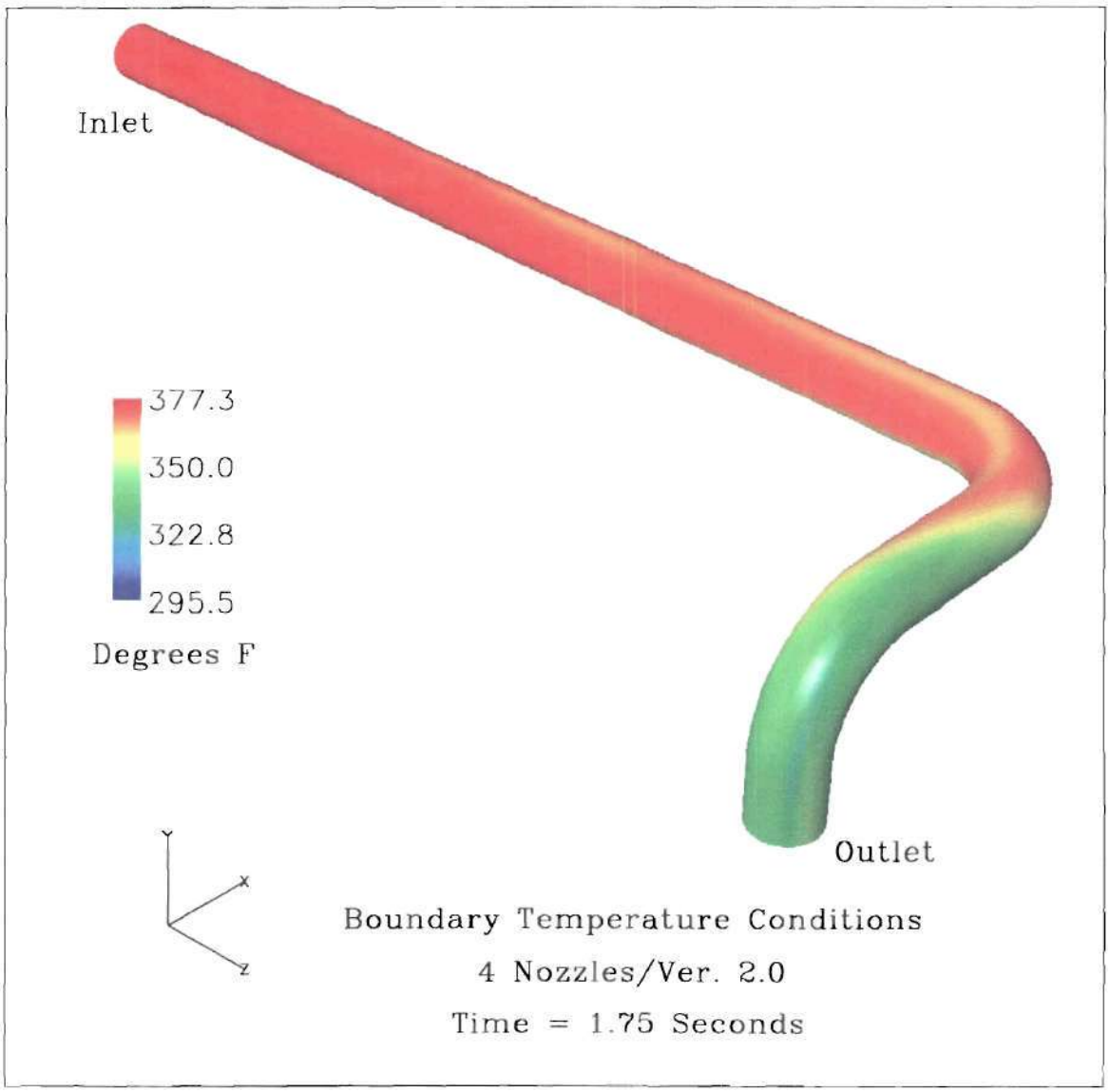
Inlet
377.3
350.0
322.8
295.5
Degrees F
Outlet
Boundary Temperature Conditions
4 Nozzles/Ver. 2.0
Time = 1.75 Seconds

Figure V.7

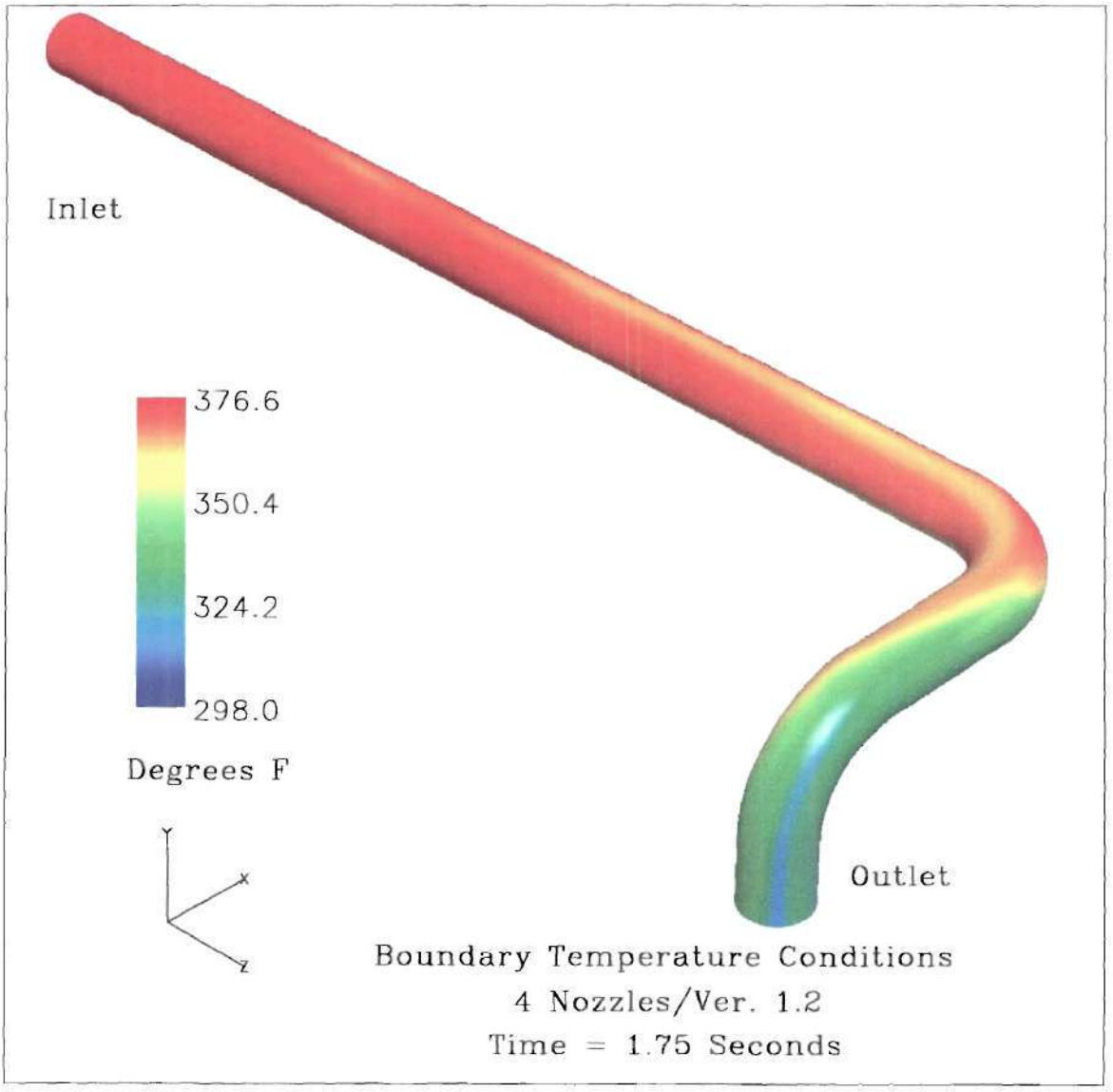
Inlet
376.6
350.4
324.2
298.0
Degrees F
Y
X
Z
Outlet
Boundary Temperature Conditions
4 Nozzles/Ver. 1.2
Time = 1.75 Seconds

Figure V.8

V.2.3 Temperature Profiles

The temperature profiles for both versions show very little variation through 1.10 seconds. However, it is interesting to examine the initial temperature profiles at the 1st thermocouple array at this time period. In Figure V.9, using Version 1.2, the concentration of fluid in the center of the pipeline is much greater and as such the temperature is also much lower. In Figure V.10, from Version 2.0, the thermal profiles are much less defined and more diffused. Since the initiation time of spray water flow for both examples is exactly the same, the only reason for this difference would be in the developments and improvements in particle management associated with the later code. The shape of the entrained particle flow as it reaches the 1st thermocouple array is also interesting to note. Of particular note is the elliptical shape of the flow profile, thus depicting very little lateral expansion of the particle flow stream after the injection nozzles. The elongation of the flow pattern along the vertical axis matches the shape and arrangement of the four-nozzles used to inject the spray water particles. It was assumed that the radial component of the nozzle holder, along with the multiple number of nozzles, and the spray angle of the individual nozzles would have provided better coverage at this point in the flow. However, it would appear that far greater mass and momentum transfer has occurred between the particulate and the steam flow, as well as drop coalescence, thus collapsing the anticipated ideal spray pattern into a more concentrated flow stream, and resultant thermal stratification. Additionally, the affects of gravity can also be seen, see Figures V.11 and V.12, as the profile is distinctly shifted toward the lower edge of the pipeline. However, the condition seems to be more

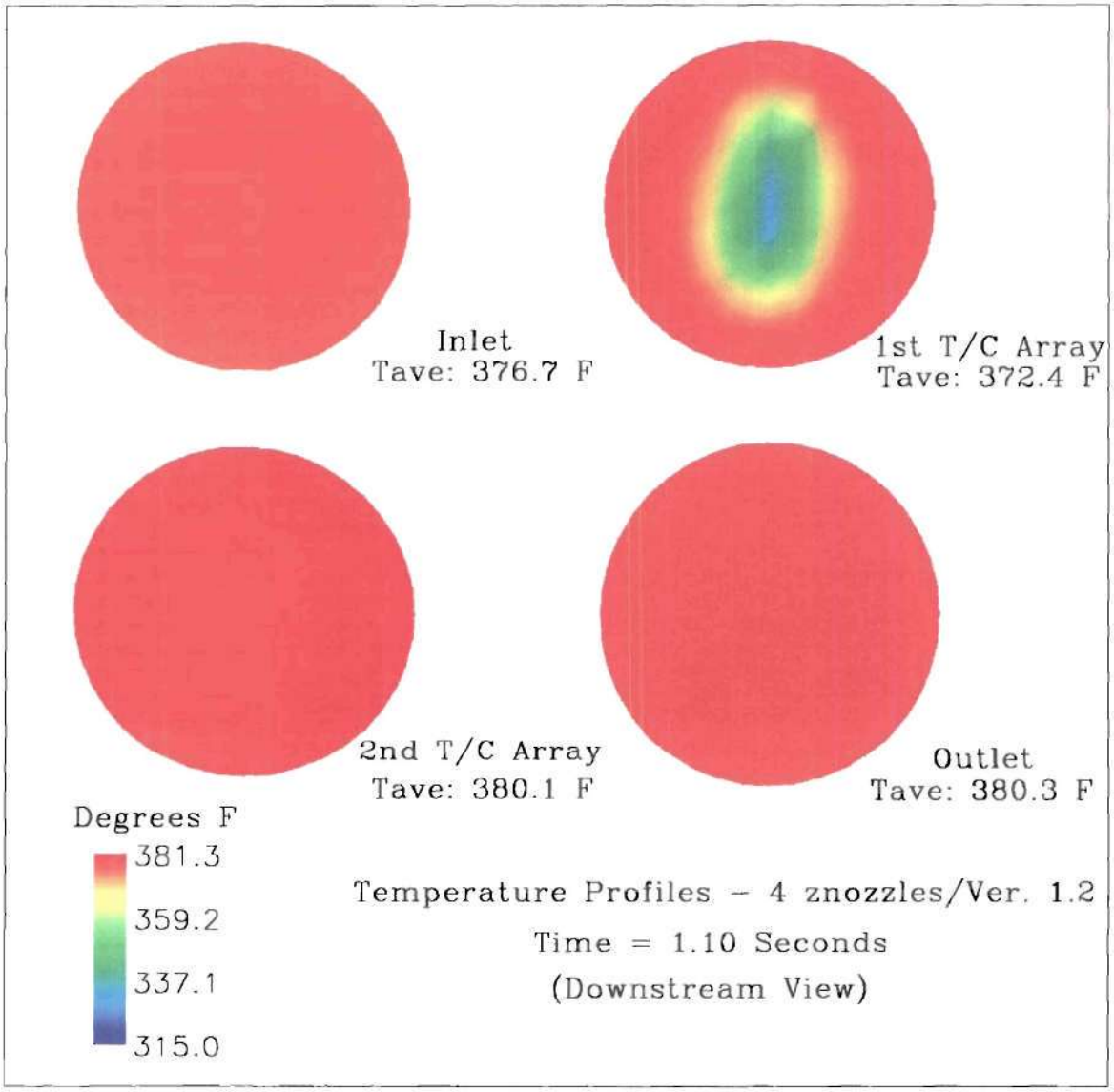
Inlet
Tave: 376.7 F
1st T/C Array
Tave: 372.4 F
2nd T/C Array
Tave: 380.1 F
Outlet
Tave: 380.3 F
Degrees F
381.3
359.2
337.1
315.0
Temperature Profiles - 4 znozzles/Ver. 1.2
Time = 1.10 Seconds
(Downstream View)

Figure V.9

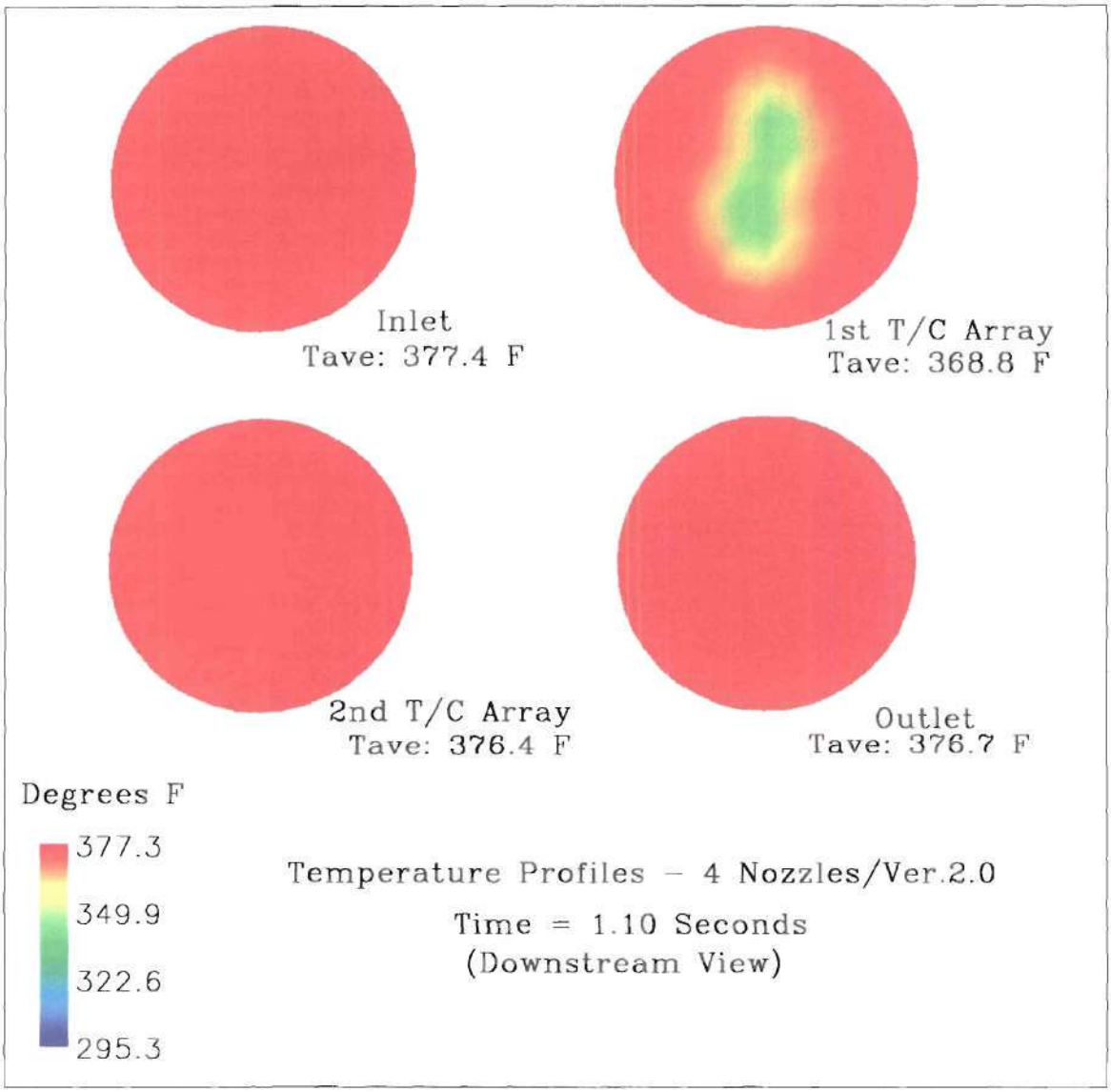
Inlet
Tave: 377.4 F
1st T/C Array
Tave: 368.8 F
2nd T/C Array
Tave: 376.4 F
Outlet
Tave: 376.7 F
Degrees F
377.3
349.9
322.6
295.3
Temperature Profiles - 4 Nozzles/Ver.2.0
Time = 1.10 Seconds
(Downstream View)

Figure V.10

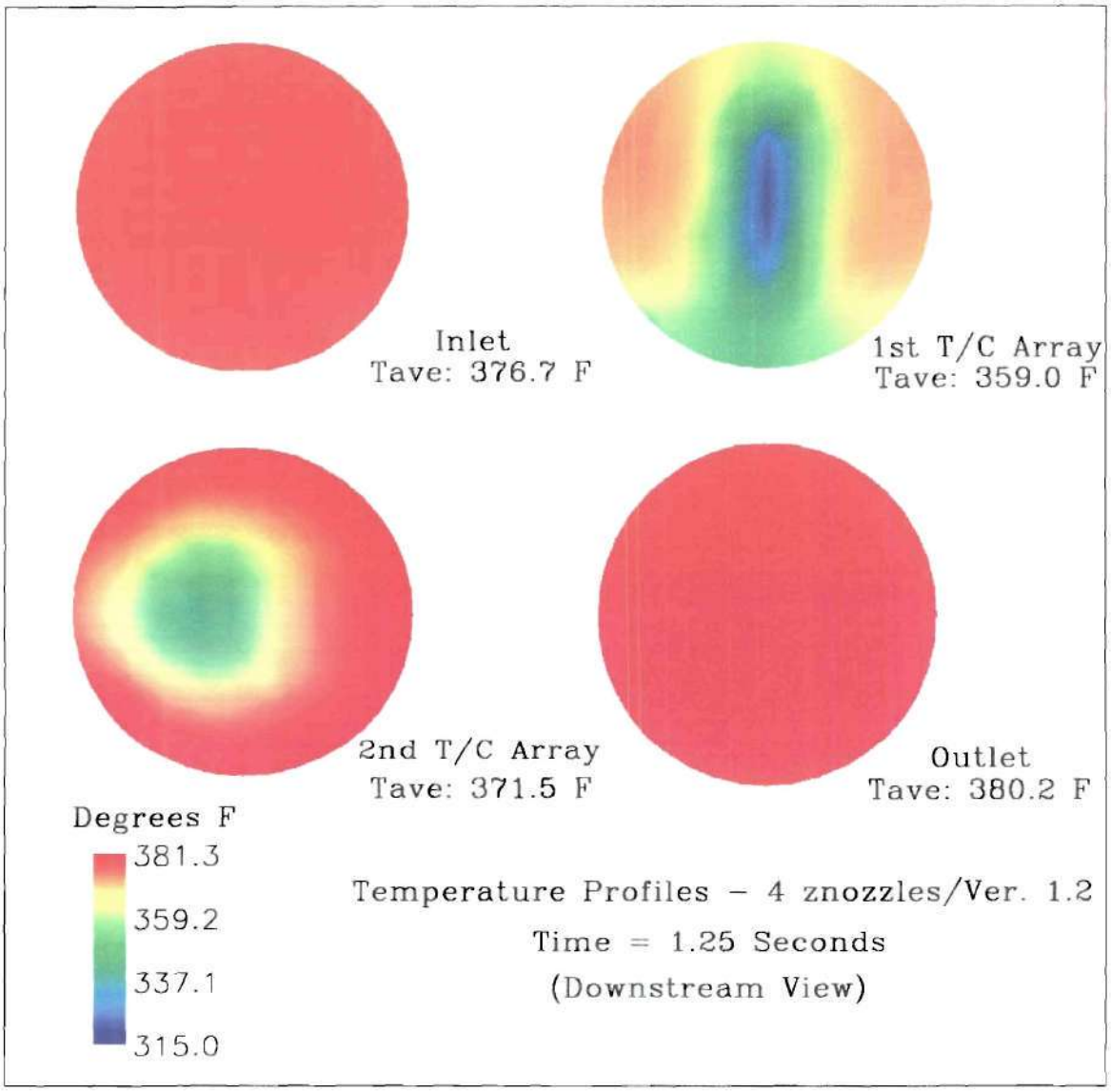
Inlet
Tave: 376.7 F
1st T/C Array
Tave: 359.0 F
2nd T/C Array
Tave: 371.5 F
Outlet
Tave: 380.2 F
Degrees F
381.3
359.2
337.1
315.0
Temperature Profiles - 4 znozzles/Ver. 1.2
Time = 1.25 Seconds
(Downstream View)

Figure V.11

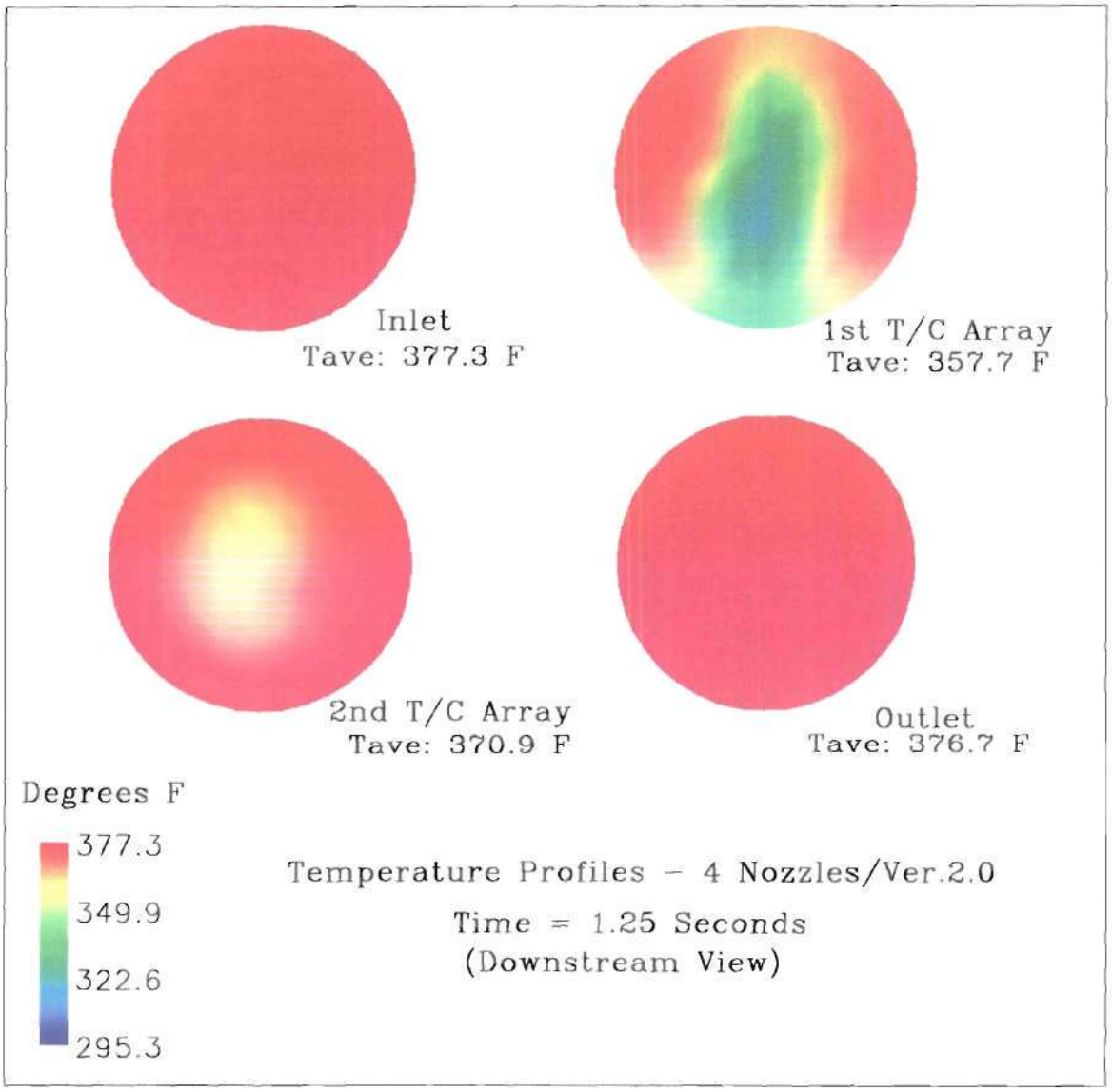
Inlet
Tave: 377.3 F
1st T/C Array
Tave: 357.7 F
2nd T/C Array
Tave: 370.9 F
Outlet
Tave: 376.7 F
Degrees F
377.3
349.9
322.6
295.3
Temperature Profiles - 4 Nozzles/Ver.2.0
Time = 1.25 Seconds
(Downstream View)

Figure V.12

profound in Version 1.2 of the code. This is probably due to the excess pooling and carry over of water on the bottom of the pipeline. With the inclusion of the film and droplet impaction model, more fluid particles are re-inserted into the flow stream as a result of rebound and splash from the pipe walls.

The break-up of this symmetric and concentric flow stream is evident when viewing the thermal profiles at the 2nd thermocouple array from time step 1.45 seconds and higher. The profile is no long centrally located but rather has been shifted to the outside edge of the pipeline. While the temperature continues to drop and the profiling becomes more dispersed, the thermal stratification phenomenon is still quite visible and contains extreme values from both ends of the allowable thermal spectrum.

When Figures V.13 and V.14 are examined, the similarities noted previously on the boundary temperature conditions, for the same time step, are clearly evident in the thermal profiles. At 1.45 seconds, the thermal profiles at the inlet, 1st thermocouple array, the 2nd thermocouple array, and the outlet are nearly identical. This agrees well with the thermal equilibrium analysis described in Section V.3.2, and this similarity of temperature profiles and average temperatures continues throughout the example at later time steps. Thus, for the four-nozzle arrangement, the system performance and output of the code is nearly identical for the two versions.

The complete graphical output of the temperature profiles for the four-nozzle arrangement, using both Version 1.2 and Version 2.0, can be viewed in Appendix C. In each case, the view is always in the direction of flow or looking downstream.

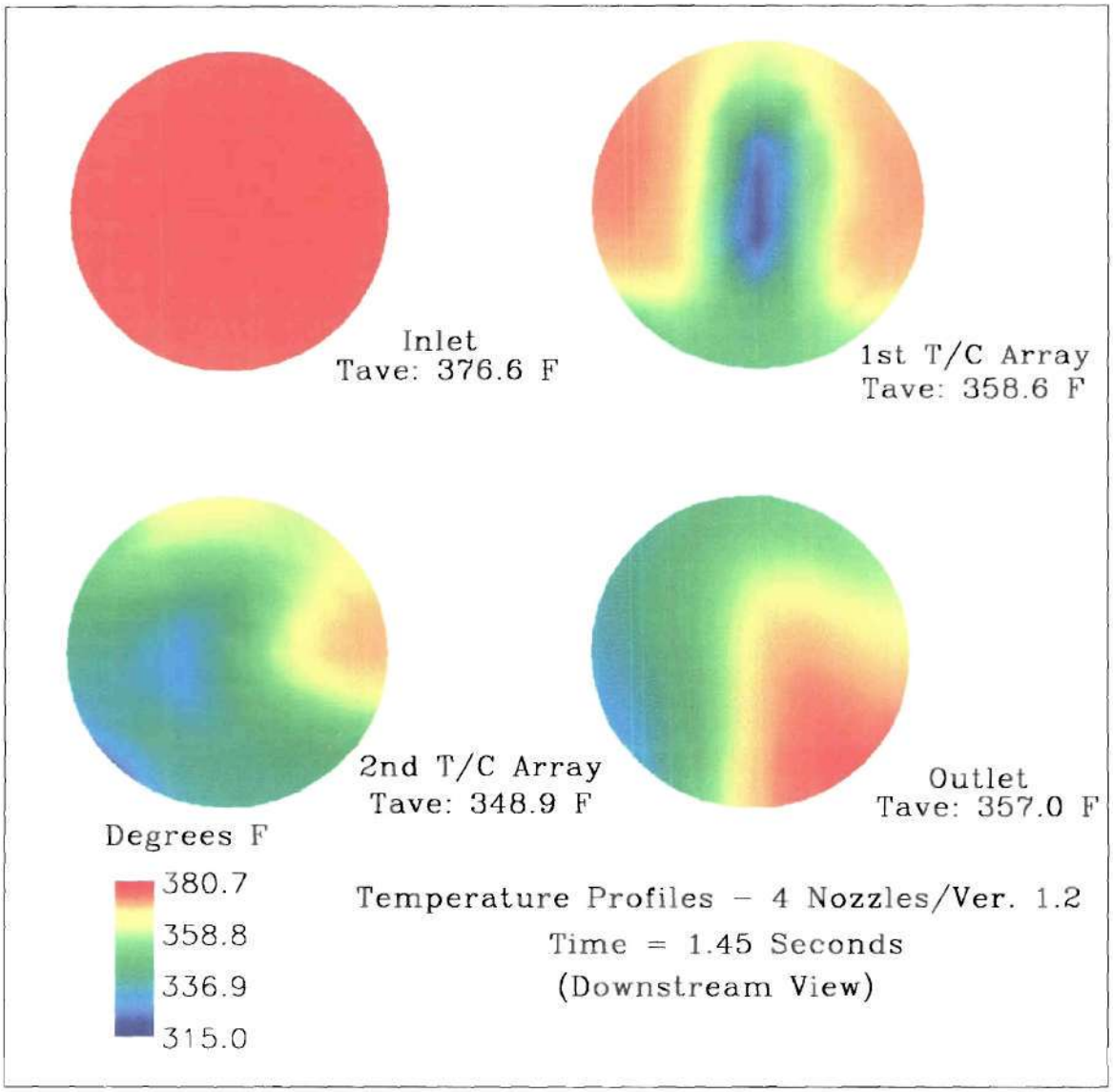
Inlet
Tave: 376.6 F
1st T/C Array
Tave: 358.6 F
2nd T/C Array
Tave: 348.9 F
Outlet
Tave: 357.0 F
Degrees F
380.7
358.8
336.9
315.0
Temperature Profiles - 4 Nozzles/Ver. 1.2
Time = 1.45 Seconds
(Downstream View)

Figure V.13

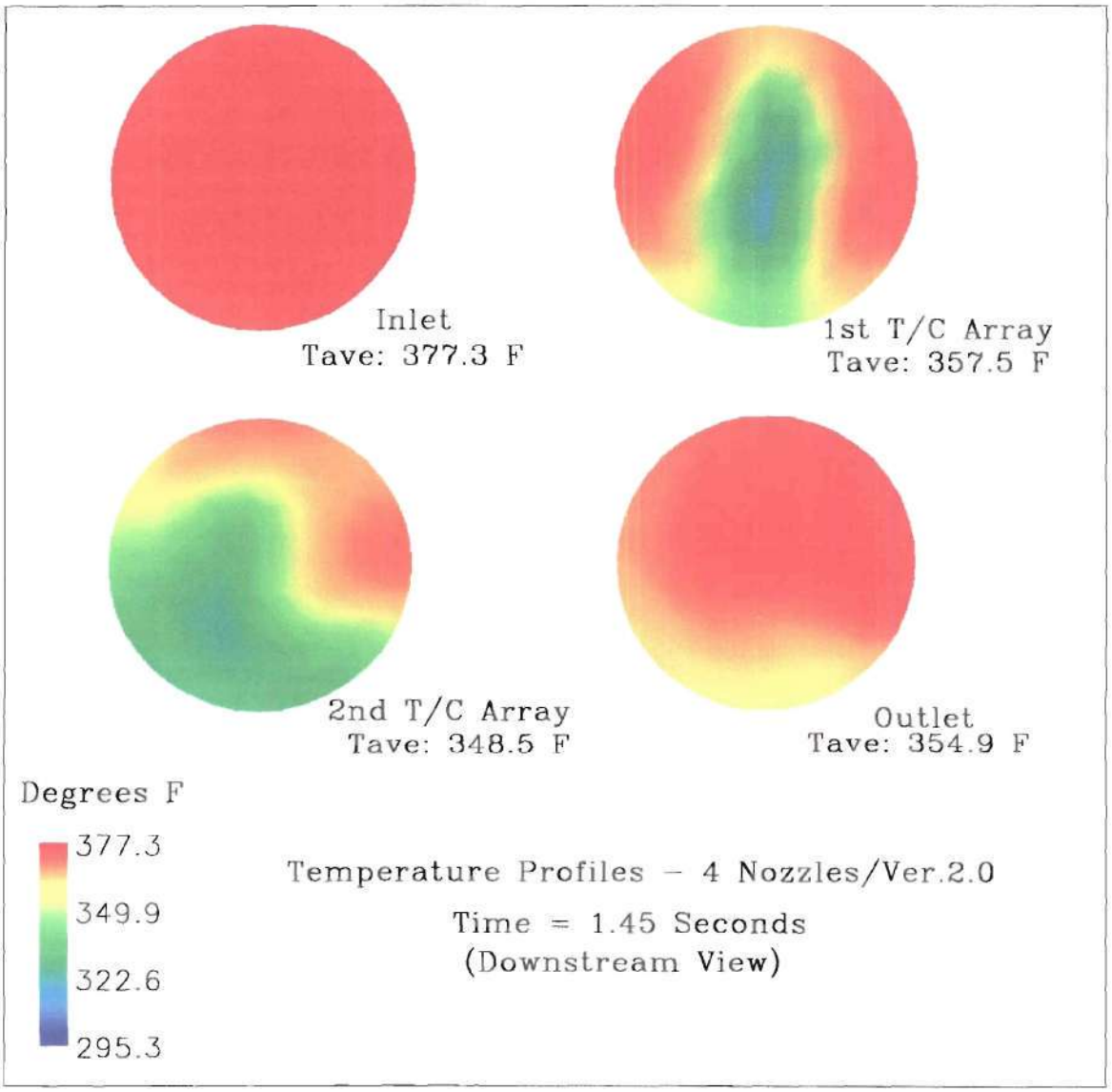
Inlet
Tave: 377.3 F
1st T/C Array
Tave: 357.5 F
2nd T/C Array
Tave: 348.5 F
Outlet
Tave: 354.9 F
Degrees F
377.3
349.9
322.6
295.3
Temperature Profiles - 4 Nozzles/Ver.2.0
Time = 1.45 Seconds
(Downstream View)

Figure V.14

V.2.4 Spray Water Particle Flow

The spray water particle flow graphics do not contribute substantially to the purpose of this work. However, they do assist in graphically depicting the flow and direction of the particles relative to the piping geometry. By examining the droplets flow, a better understanding of the spray dynamics and interpretation of the thermal profiles can be achieved.

Figures V.15 and V.16 illustrate the initial spray pattern as interpreted by the code at 0.85 seconds. As previously mentioned, and depicted in the thermal profiles at the 1st thermocouple array, the flow pattern is very compact and representative of the devices general geometry, i.e., vertically concentrated. It is interesting to examine the break-up of the dense spray pattern as the particles progress downstream and the droplets begin to spread and become smaller.

In Figures V.17 and V.18 the control volume is completely filled with the particulate bundles. In viewing the pipeline from this perspective, it is interesting to note the changes in the flow structure. Of particular note is the continuous reduction in particulate size. Shortly after injection, the bulk of the particles are green, yellow, and red. Thus placing them in the 1.9-3.0e^{-2} cm size category. As we progress down the pipeline, we see the size of the particles shift to the blue and purple scales or in the range of 1.0e^{-2} to 1.5e^{-4} cm. If one compares the particle flow illustrations at 1.75 seconds, Figures V.17 and V.18, it can be seen that the Version 2.0 code seems to predict smaller particle sizes in the outlet pipe then does the Version 1.2. The increased number of dark blue and purple particle packets in the Version 2.0 graphics visually demonstrates this

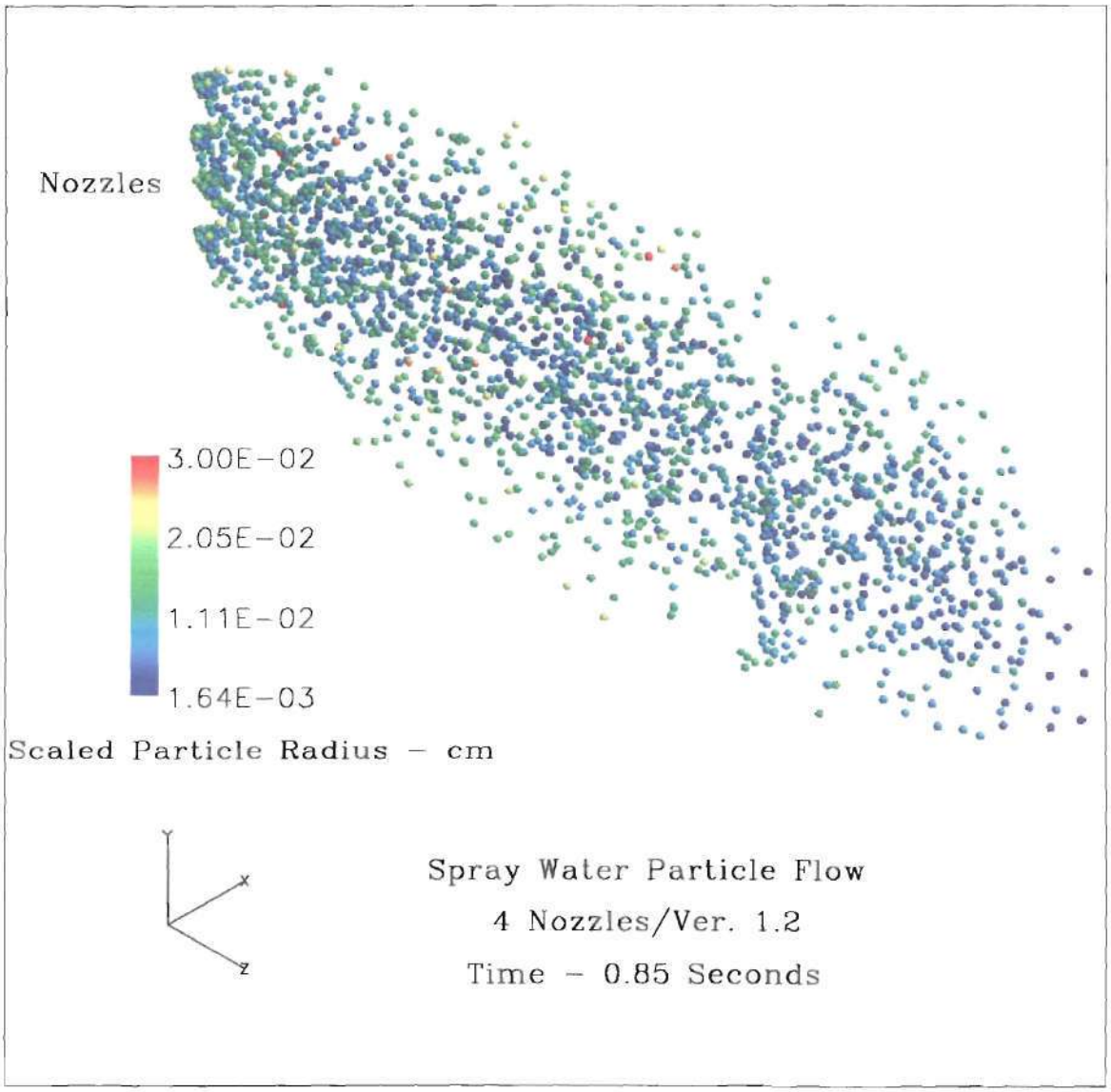
Nozzles
3.00E-02
2.05E-02
1.11E-02
1.64E-03
Scaled Particle Radius - cm
Y
X
Z
Spray Water Particle Flow
4 Nozzles/Ver. 1.2
Time - 0.85 Seconds

Figure V.15

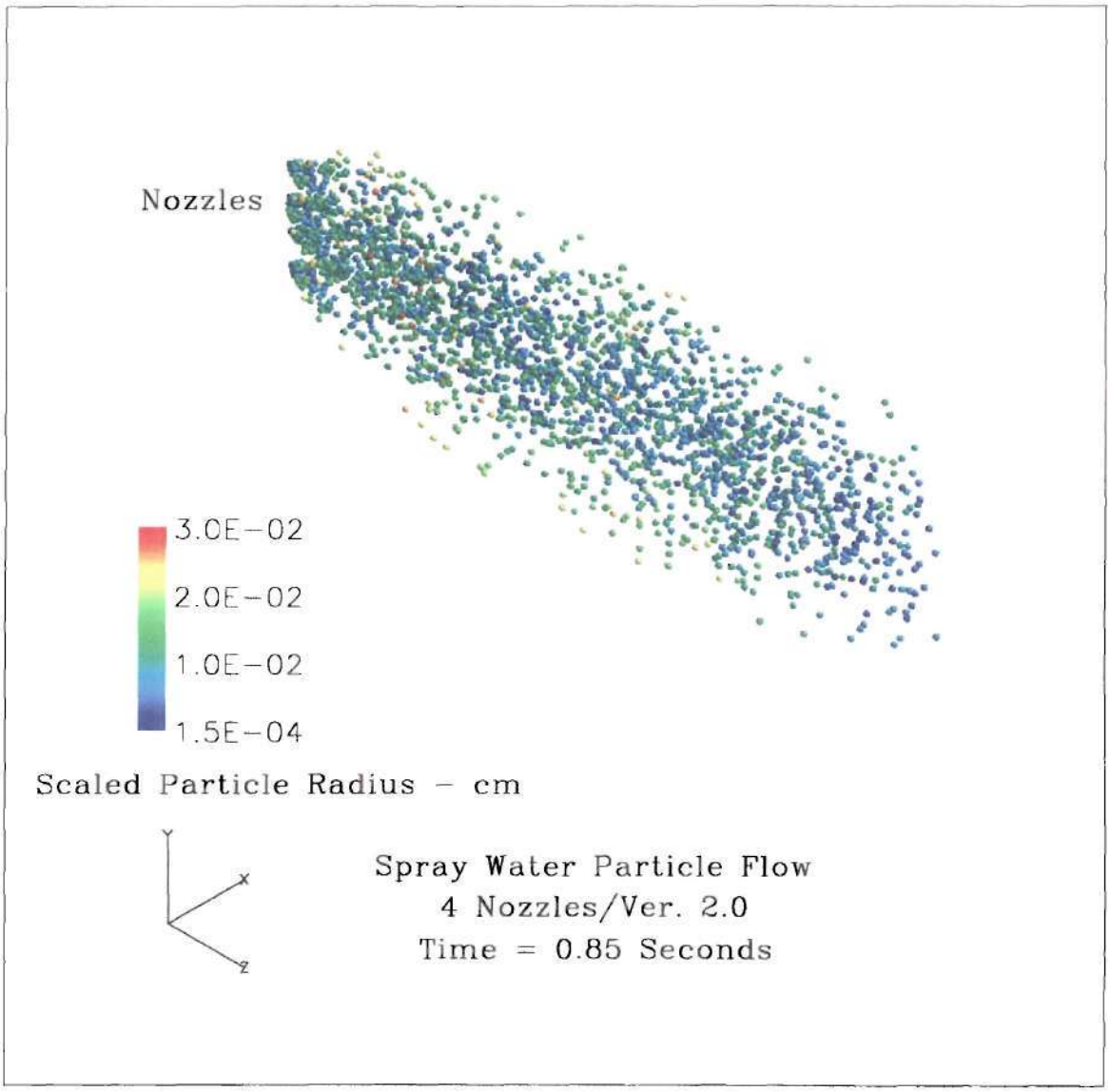
Nozzles
3.0E−02
2.0E−02
1.0E−02
1.5E−04
Scaled Particle Radius − cm
Y
X
Z
Spray Water Particle Flow
4 Nozzles/Ver. 2.0
Time = 0.85 Seconds

Figure V.16

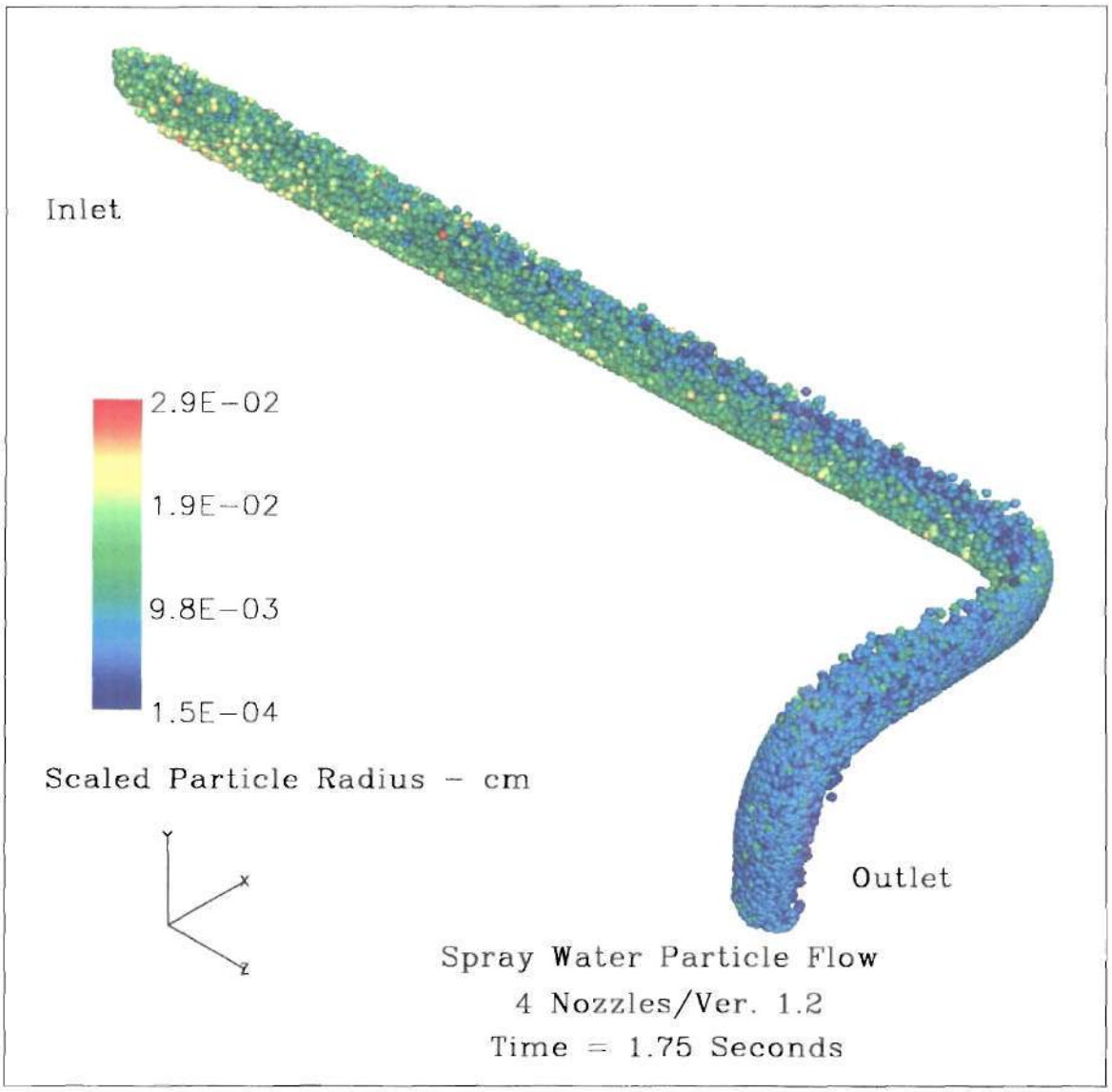
Inlet
2.9E-02
1.9E-02
9.8E-03
1.5E-04
Scaled Particle Radius - cm
Outlet
Spray Water Particle Flow
4 Nozzles/Ver. 1.2
Time = 1.75 Seconds

Figure V.17

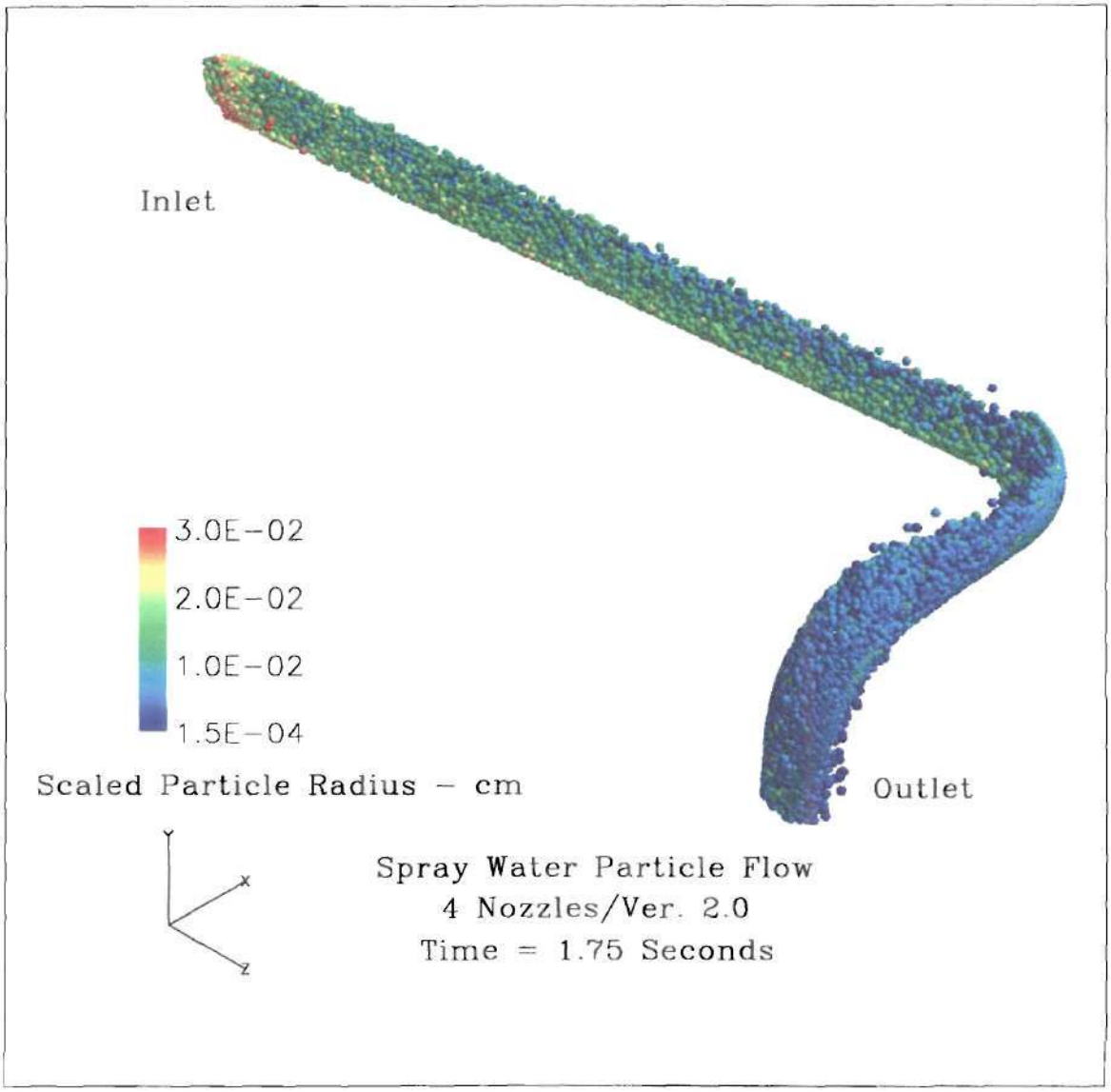
Inlet
3.0E-02
2.0E-02
1.0E-02
1.5E-04
Scaled Particle Radius - cm
Outlet
Y
X
Z
Spray Water Particle Flow
4 Nozzles/Ver. 2.0
Time = 1.75 Seconds

Figure V.18

computational result. This reduction in size can be the result of several factors. The first is that the entrained droplets have lost mass due to heat transfer and vaporization. The second possibility relates to the droplets trajectory and impaction on the pipe walls. The result, depending on the angle of impact, would be the splashing and break-up of the droplets prior to rebounding back into the flow stream. While these improvements would be expected in the later version of the code, and result in better overall performance, it is interesting to note that the thermal profiles show nearly identical temperatures within the individual planes for both codes.

Other characteristics of note include the gravitational affects as seen in the long horizontal length of pipe. Just prior to the first elbow, the upper half of the pipe has a noticeably lower number of particles entrained in the flow stream. This would be expected considering the L/D ratio of the pipeline and the velocity as which the particles are traveling.

The flow altering affects of both elbows is clearly visible within the model results. Similarly, the swirl created by the close proximity of the two elbows is likewise visible. In both cases, the particles' impaction on the walls along with momentum transfer has produced the noted affect and has separated the two flow streams. While the impact of elbows and other flow redirecting piping components is known, an understanding of the true dynamics and potential recovering in an important energy transfer process is not.

V.2.5 Comparison Between Computational And Experimental Temperature Data

In this section, the results of the experimental tests run at the UNC Cogeneration Facility utilizing the four-nozzle desuperheater arrangement will be compared with those

generated by the two versions of the SteamCFD code. The graphs used to relate the data refer to the specific thermocouples by a position number from 1 to 6. In our test apparatus, the outer most ring of thermocouples is designated as 1 and the inner most is 6. The placements of thermocouples are on the vertical and horizontal axis of the measurement plane. In every case, the view is always downstream. For further clarification, refer to Figure II.8.

Figures V.19 and V.20 illustrate the 1st thermocouple array experimental results as compared to the computational results obtained from Version 1.2 and 2.0, respectively, for the four-nozzle device. Unfortunately, it is quite apparent that the use of thermocouples for the measurement of particle-laden vapor-liquid flow stream is not acceptable. The thermocouples installed in this first array could only detect the saturation temperature of the unevaporated droplets. In contrast, the code was designed to only register the temperature of the superheated vapor. However, even with these differences, some notable observations can be rendered.

In the 1st thermocouple array graphs, there are distinct differences in the computational results. In positions 1 and 2, Version 2.0 indicates much lower temperatures in the lower quadrant then does Version 1.2. This is in contrast to the previously mentioned increase in particulate drop fall-out and lower temperature profiles noted for Version 1.2 as compared to 2.0.

This phenomenon for the lower quadrant is repeated for positions 3 and 4, however, the opposite is observed when we compare the upper quadrants. The temperatures in this quadrant are marginally lower for Version 1.2 than for 2.0. These

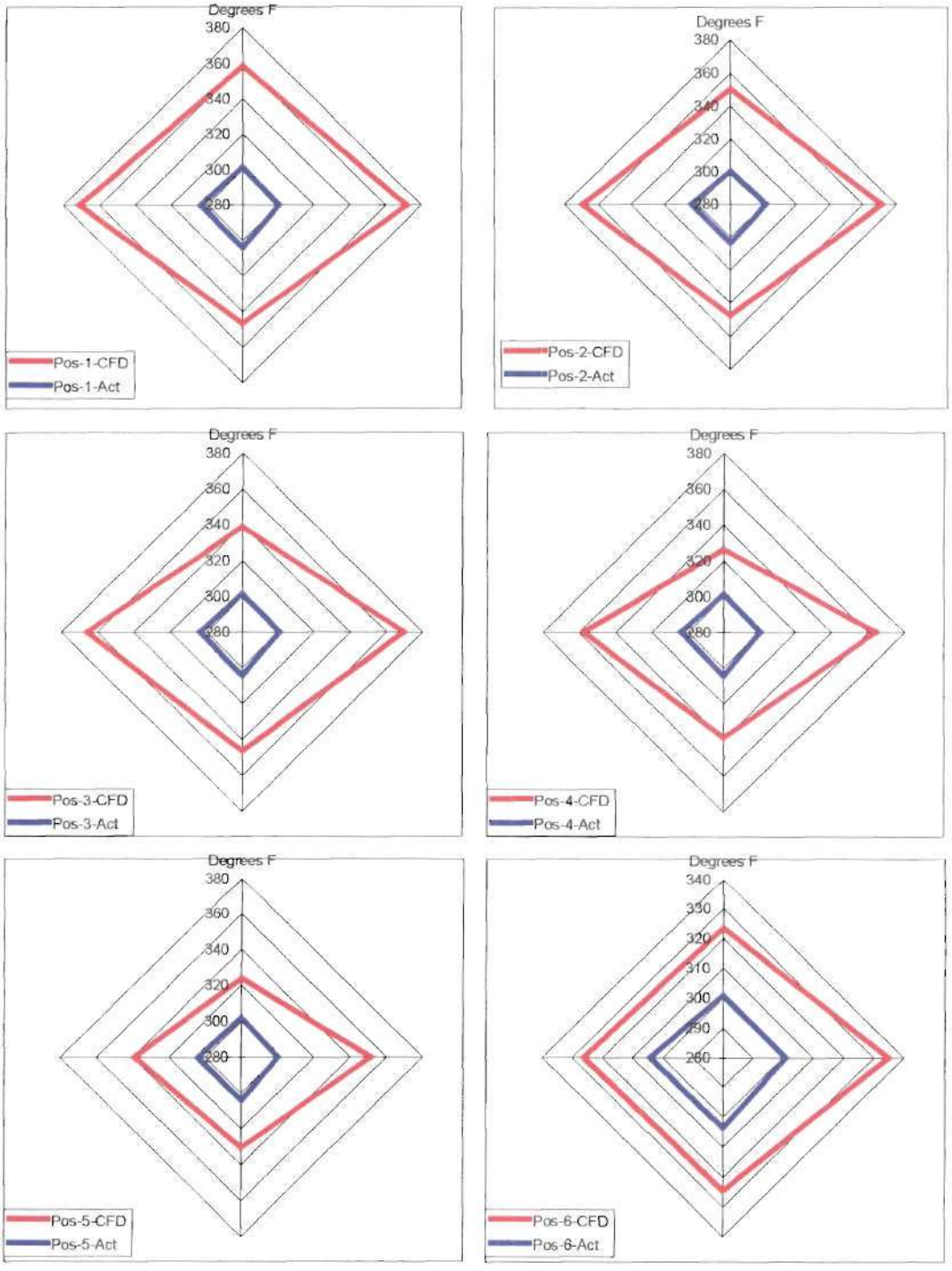

Comparison of Actual vs. Computational Thermocouple Readings - 1st Array, 4 Nozzles, Version 1.2

Figure V.19

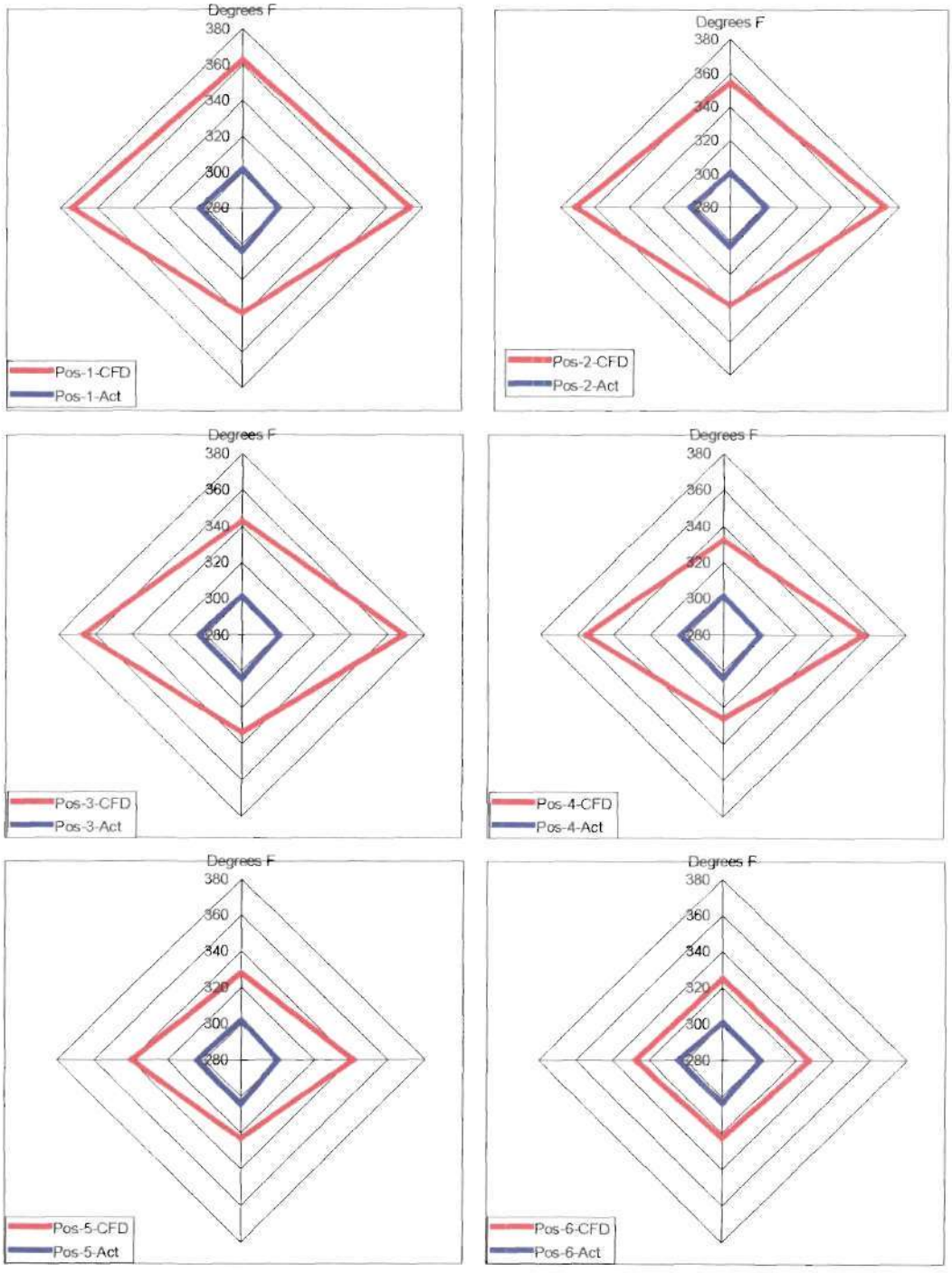

Comparison of Actual vs. Computational Thermocouple Readings - 1st Array, 4 Nozzles, Version 2.0

Figure V.20

differences are most likely the result of code improvements and the dynamic handling of the particles and vaporization processes. In Version 2.0, due to the inclusion of the film and splash models, there is more interaction and vaporization in the lower quadrant than for the same conditions in Version 1.2. Rebounding and splashing particles are being re-introduced to the flow stream, rather then just pooling on the bottom, and result in the lower steam temperatures presented in Version 2.0.

In viewing positions 1-5 of the 1st thermocouple array, the graphs clearly illustrate the lack of lateral or radial cooling in the flow at this early stage. This was evidenced also in the thermal profiles and substantiates the critical need for proper placement of the nozzles, especially in large pipelines, to reduce or eliminate thermal stratification. One case of interest is position 5 in Version 1.2. Here, the radial distribution has become considerably non-symmetric and the outer quadrant has cooled substantially more then has the inner quadrant, i.e., right side versus left side. This same condition is not observed in the Version 2.0 rendering of position 5. The cause of this may relate to pressure fluctuations generated in the program, especially in Version 1.2.

When we reach the position 6 ring, the general thermal symmetry returns. However, it would appear that Version 2.0 is showing far lower temperatures in the inner and outer quadrants then does Version 1.2. The inner quadrant of Version 1.2 shows a steam temperature of 335° F while the corresponding region under Version 2.0 is closer to 325° F.

In looking at the actual experimental values plotted, the shape of all the profiles at the 1st thermocouple are strangely non-symmetric regardless of what position it

represents. In each case, the left side of the pipe seems to be hotter then the right and the shape, somewhat trapezoidal, would appear to be the same regardless of the location. This would indicate that the particles may actually be distributed across the entire flow cross-section, but registering different values due to the fact that even a small amount of liquid on the thermocouple tips would result in saturation temperatures. The variations are mostly likely the result of flow variations as a result of the upstream elbow prior to water injection that was not made a part of this examination.

In Figures V.21 and V.22 the computational results are substantially different. By the time the steam reaches the 2nd thermocouple array, there is sufficient vaporization and flow disruption to provide temperature outputs from the sensing devices. The graphics clearly show the impact of the liquid separation due to the first elbow. The left side of the graphs, in both figures, is severely depressed temperature wise while the right side is at or near the initial inlet temperature, particularly in the outer rings of measurement.

In the case of the experimental data, the graphs show similar affects of momentum transfer as the mixture of vapor and liquid goes around the elbow. However, the actual data does show further reduction in steam temperature then the computational output. This can be caused by a number of potential differences including secondary affects of the cooling water impinging on the probes, particle size and distribution differences in the computational model versus reality, and refinement in the heat transfer routines presently in place. In contrast to the differences, it is important to note that the actual data was fully contained with the boundary of the computational results, thus

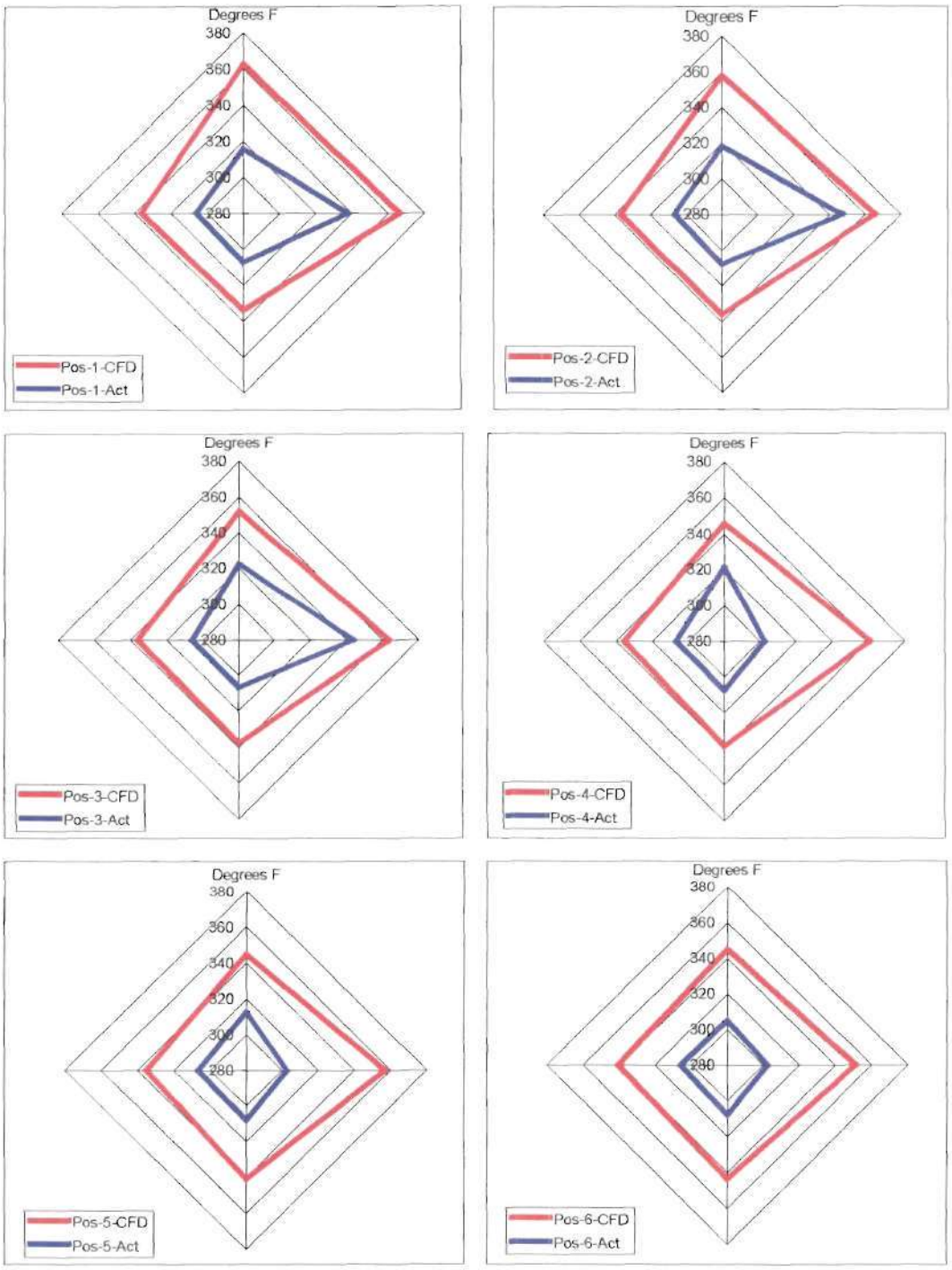

Comparison of Actual vs. Computational Thermocouple Readings - 2nd Array, 4 Nozzles, Version 1.2

Figure V.21

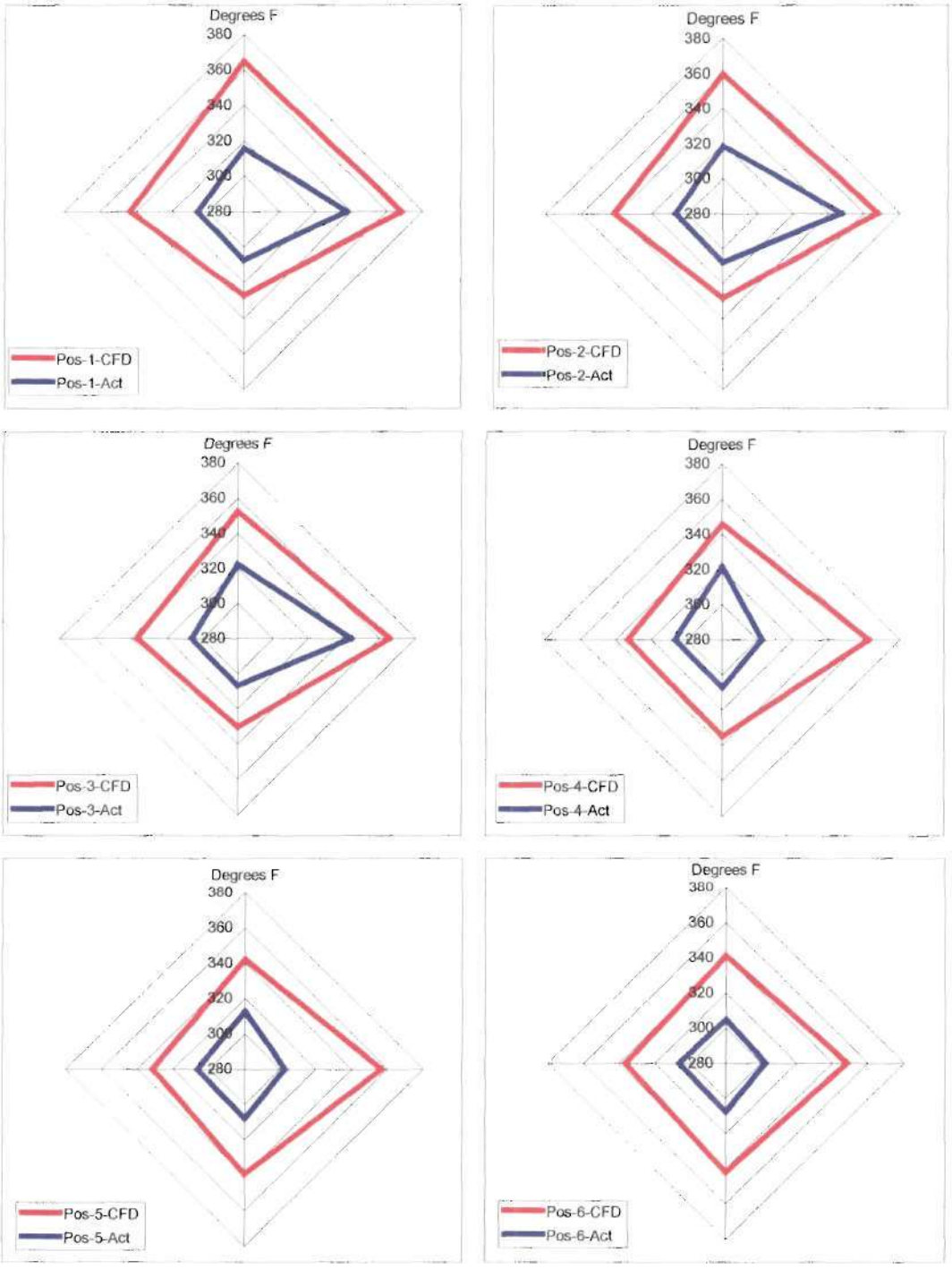

Comparison of Actual vs. Computational Thermocouple Readings - 2nd Array, 4 Nozzles, Version 2.0

Figure V.22

indicating that no major mass, momentum, or energy discrepancies existed within the program logic.

V.3 The 28 Nozzle Device

V.3.1 Thermal Equilibrium

As in the case for the four-nozzle arrangement, the first task was to establish thermal equilibrium for each of the four coordinate surfaces. These surfaces were integrated to determine the average profile temperature at time increments of 0.1 seconds between 0.75 to 1.80 seconds. The results of this exercise can be seen in Figures V.23 and V.24. Both cases, Version 1.2 and 2.0, reached equilibrium at about the same time. The inlet provided a near constant value of 415° F throughout the prescribed time period. The 1st and 2nd array of thermocouples reached equilibrium at approximately 1.15 and 1.35 seconds respectively. The outlet plane reached thermal equilibrium at approximately 1.60 seconds. Thus, all the surfaces achieved relatively constant average temperature profiles within the 1.75-second period of analysis.

While the time to equilibrium was relatively constant between the two versions, the actual equilibrium temperature was not. In particular, the outlet plane exhibited a 10° F difference between Version 1.2 and 2.0. This differential was expected due to the program changes made to the earlier version of the code. With a more advanced film and droplet impaction model, far less fluid was allowed to collect on the bottom of the pipe. As a result, the thermodynamic property and heat transfer routines were more stable and provided a more accurate depiction of the two-phase flow stream.

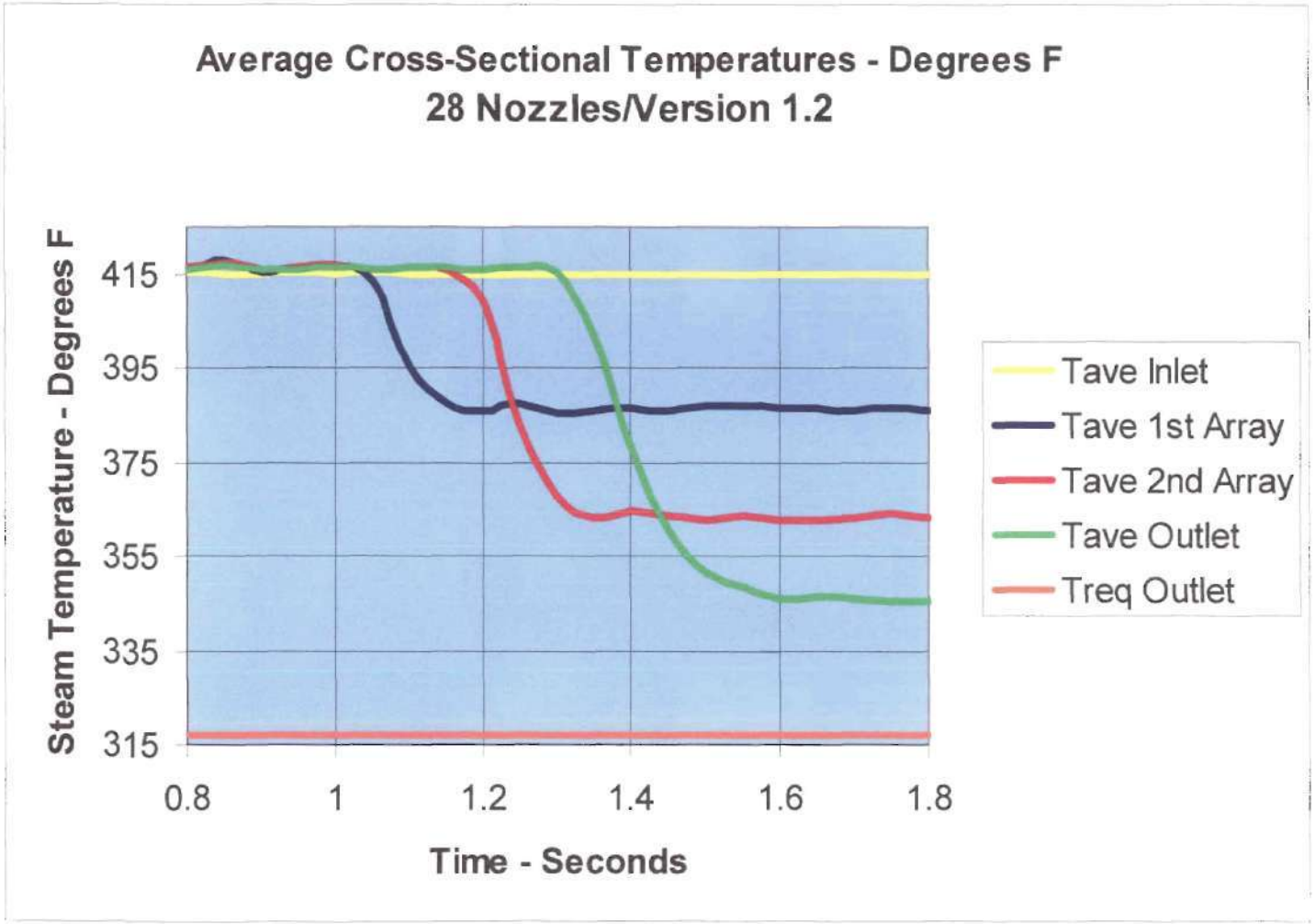
Average Cross-Sectional Temperatures - Degrees F
28 Nozzles/Version 1.2
Steam Temperature - Degrees F
415
395
375
355
335
315
0.8
1
1.2
1.4
1.6
1.8
Time - Seconds
Tave Inlet
Tave 1st Array
Tave 2nd Array
Tave Outlet
Treq Outlet

Figure V.23

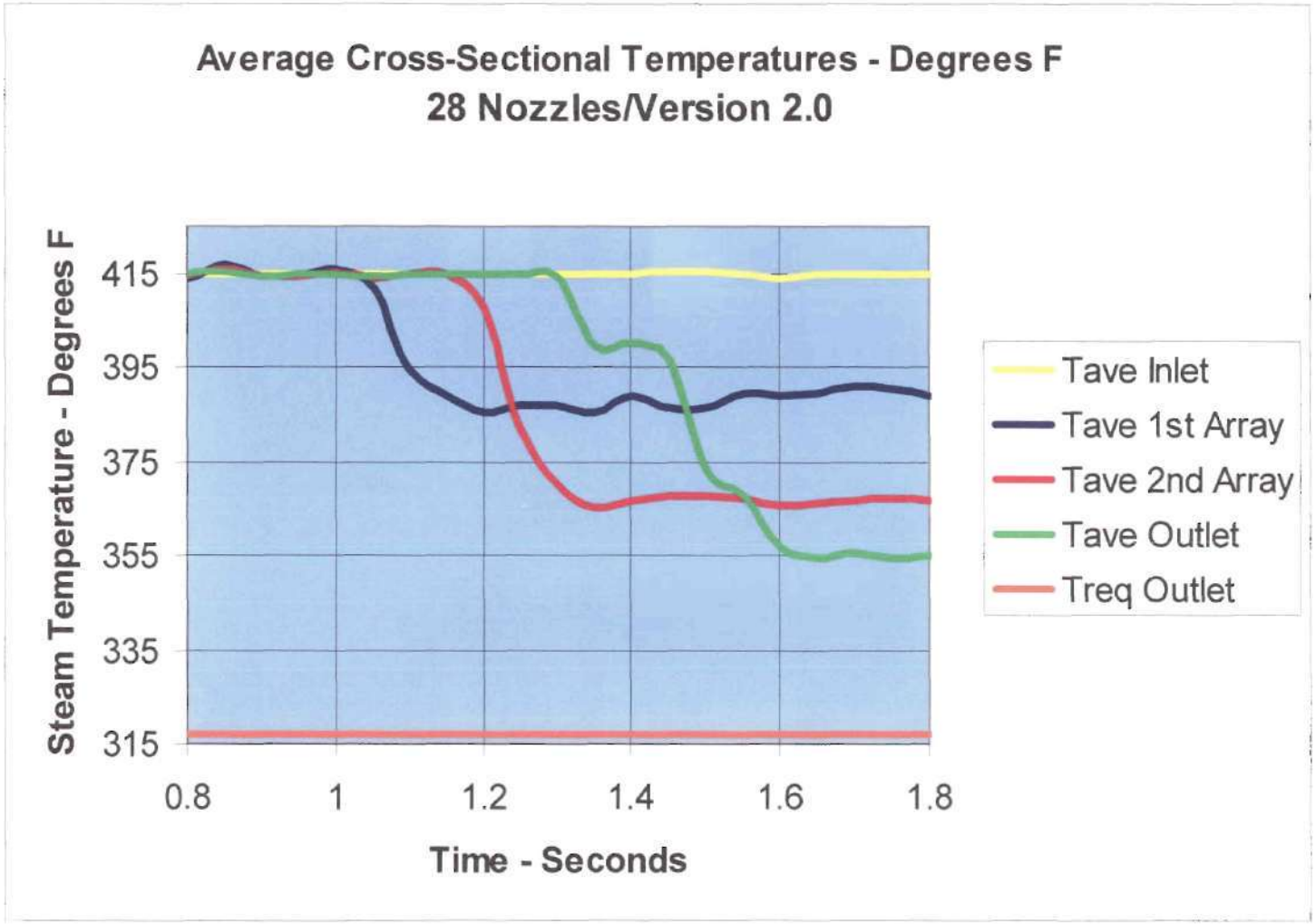
Average Cross-Sectional Temperatures - Degrees F
28 Nozzles/Version 2.0
Steam Temperature - Degrees F
415
395
375
355
335
315
0.8
1
1.2
1.4
1.6
1.8
Time - Seconds
Tave Inlet
Tave 1st Array
Tave 2nd Array
Tave Outlet
Treq Outlet

Figure V.24

V.3.2 Boundary Temperature Conditions

The boundary temperature conditions appear to be relatively constant between the two versions until we reach 1.45 seconds. In viewing Figures V.25 and V.26, both at 1.45 seconds, the thermal differences at the outlet can begin to be seen. The flow through the two elbows seems to generate the same temperature profiles. However, as we approach the outlet plane, the model run under Version 2.0 clearly shows the transfer of water particulate to the outside wall just below the second elbow. The consequence is a much higher region of pipe boundary temperature on the inside surface. This could be the result of the improved film model and the fact that much less water is contained in this initial flow stream reaching the outlet.

The boundary temperatures at 1.60 and 1.75 are nearly identical for the two versions. However, it would appear that the momentum and mass transfer to the particulate is far more pronounced in Version 2.0 as compared to Version 1.2. In comparing Figures V.27 and V.28, the vertical down leg of pipe, just after the second elbow, exhibits a much lower wall temperature in the later version of the code. The difference is quite pronounced especially considering the fact that the outlet temperature profile has already been noted as 10°F higher then for the earlier version. However, it is important to remember that the boundary temperature is far more susceptible to thermal variances as a result of particulate impaction then the steam flow. This is evident by comparing the saturated liquid temperature of the particulate versus the steam temperature. Additionally, in the determination of the average steam temperature, the

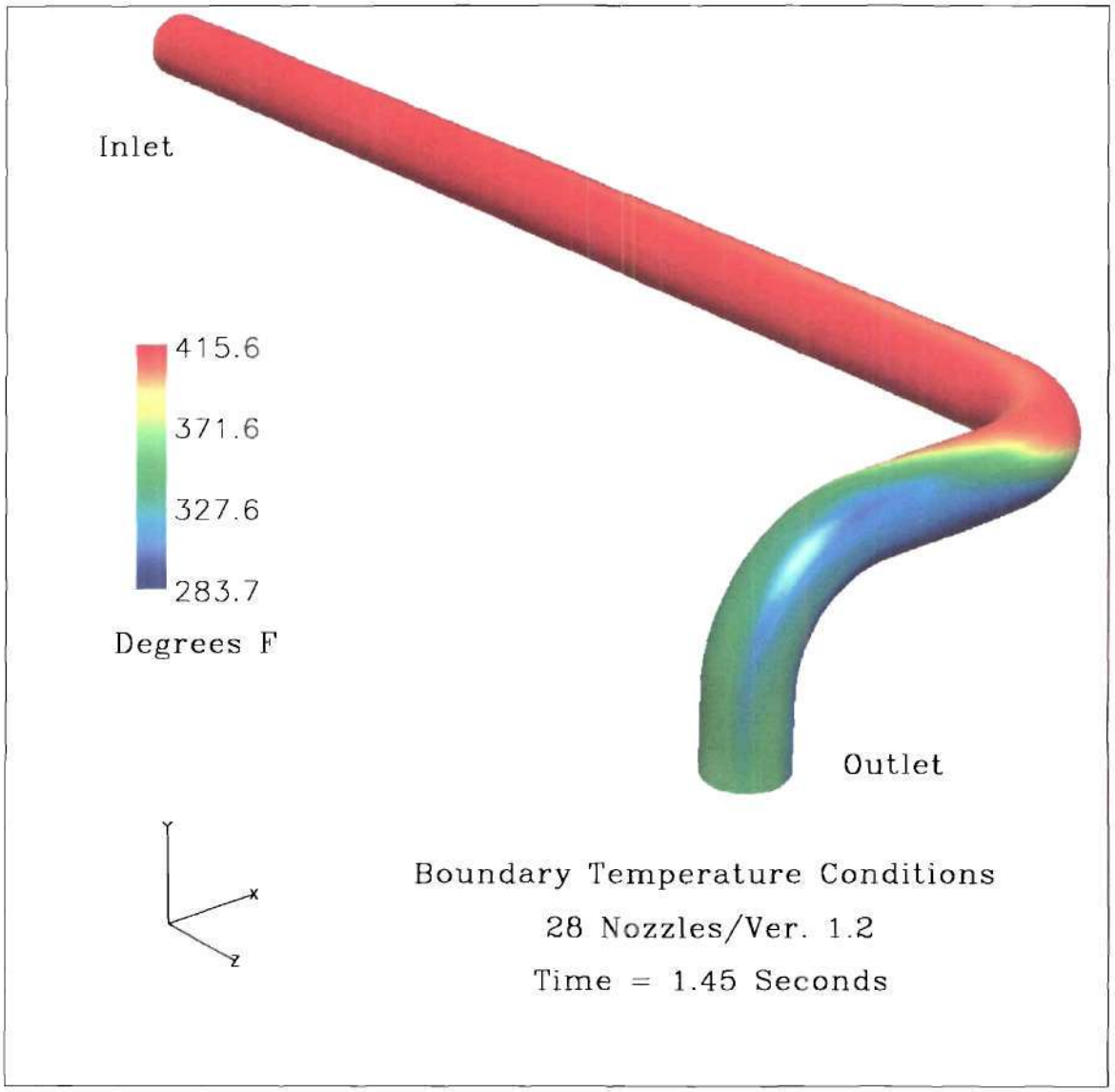
Inlet
415.6
371.6
327.6
283.7
Degrees F
Outlet
Y
X
Z
Boundary Temperature Conditions
28 Nozzles/Ver. 1.2
Time = 1.45 Seconds

Figure V.25

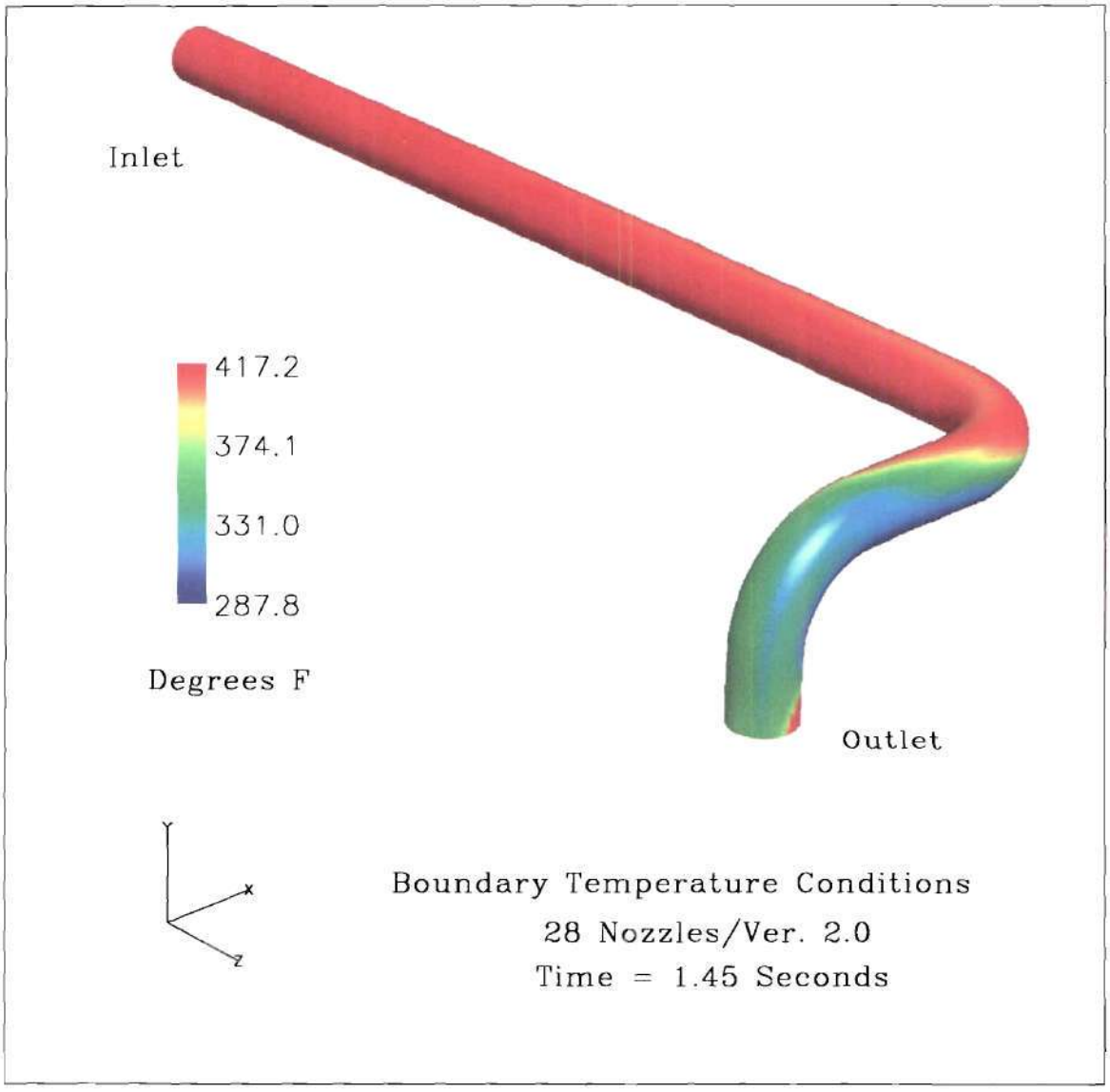
Inlet
417.2
374.1
331.0
287.8
Degrees F
Outlet
Y
X
Z
Boundary Temperature Conditions
28 Nozzles/Ver. 2.0
Time = 1.45 Seconds

Figure V.26

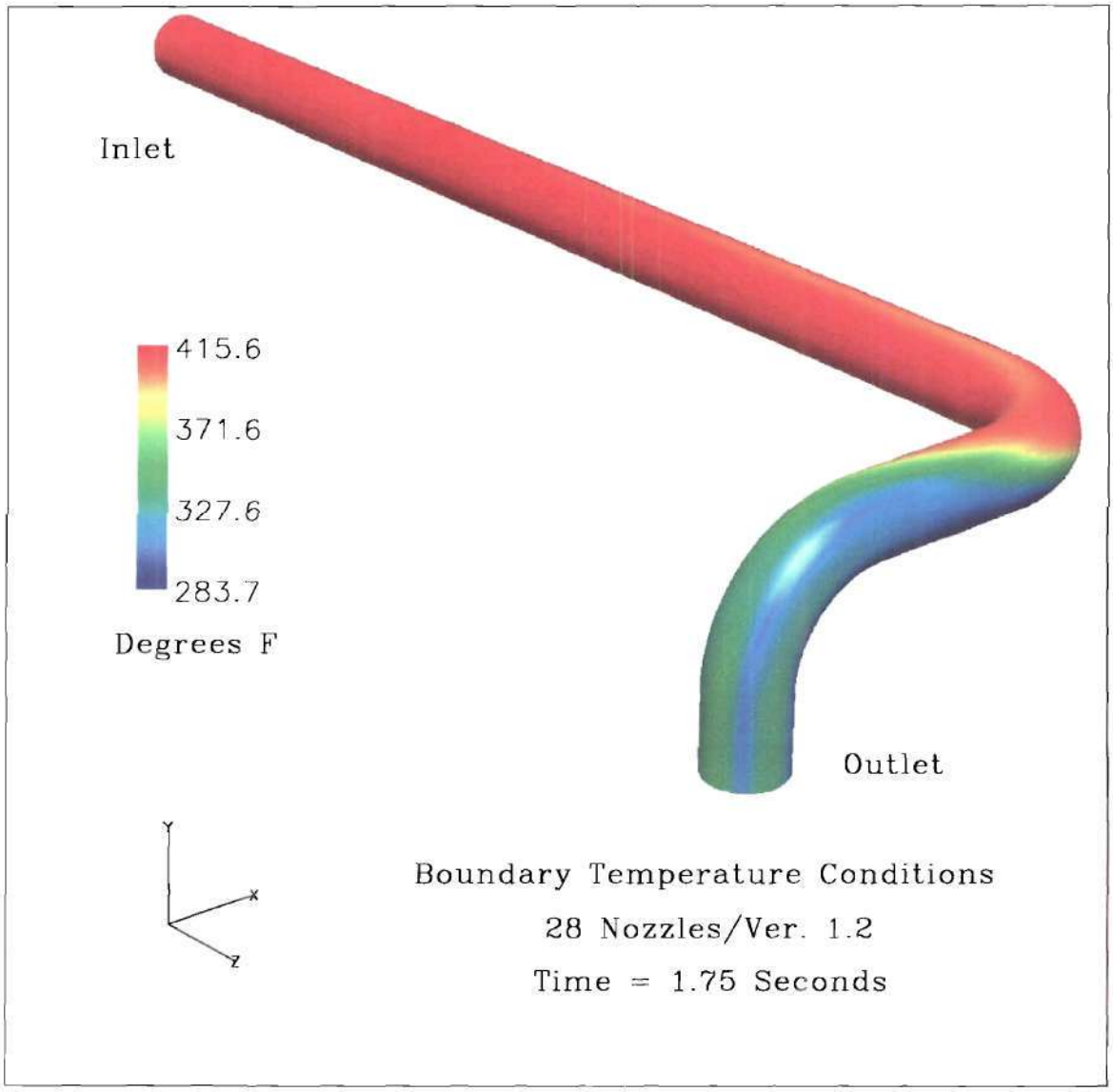
Inlet
415.6
371.6
327.6
283.7
Degrees F
Outlet
Y
X
Z
Boundary Temperature Conditions
28 Nozzles/Ver. 1.2
Time = 1.75 Seconds

Figure V.27

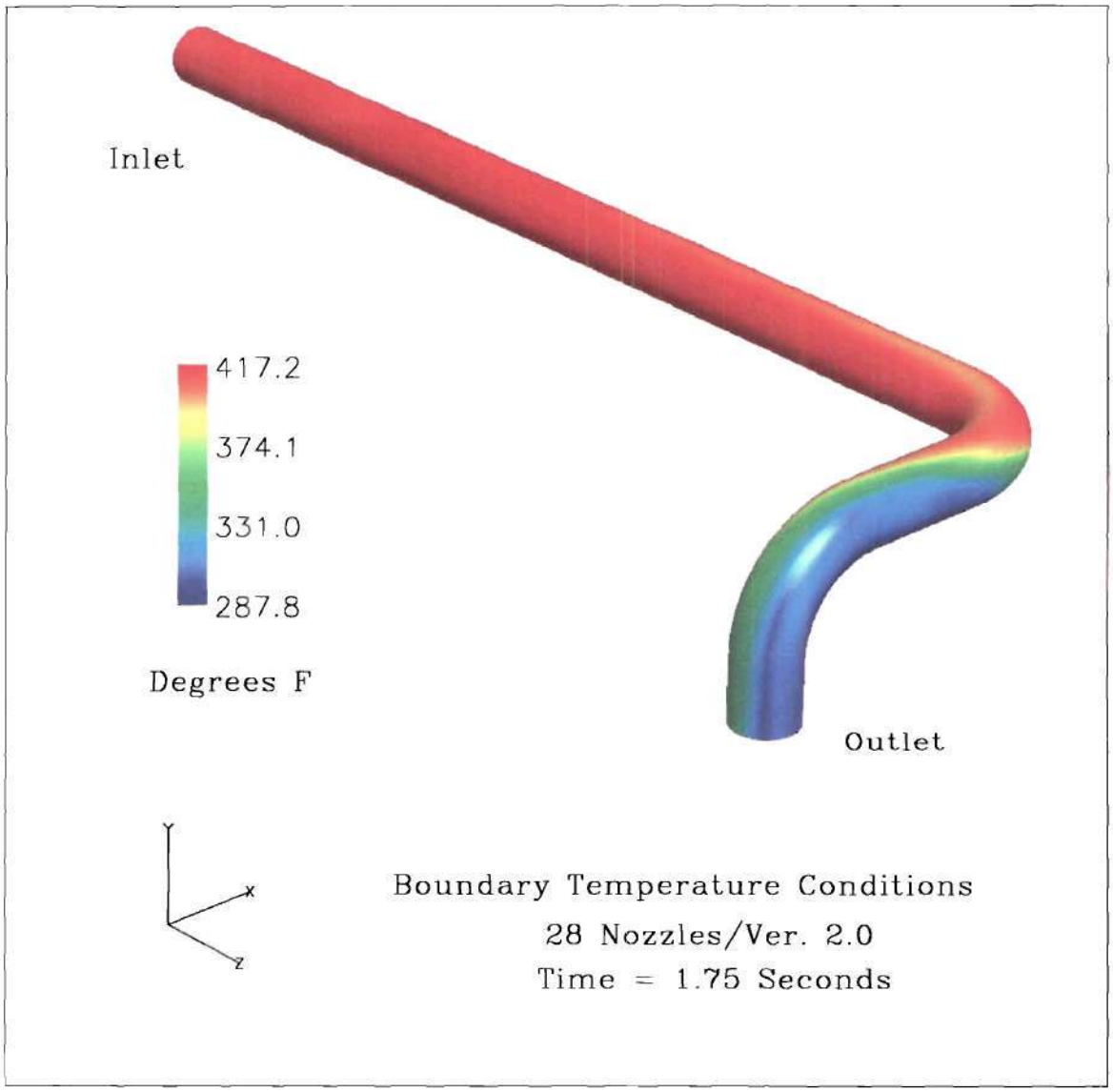
Inlet
417.2
374.1
331.0
287.8
Degrees F
Outlet
Y
X
Z
Boundary Temperature Conditions
28 Nozzles/Ver. 2.0
Time = 1.75 Seconds

Figure V.28

program only looks at the vapor portion of the flow, thus all unevaporated particulate is ignored.

The complete graphical output of the boundary temperature conditions for the four-nozzle arrangement, using both Version 1.2 and Version 2.0, can be viewed in Appendix D.

V.3.3 Temperature Profiles

The temperature profiles for both versions show very little variation through 1.25 seconds. It is interesting to note the shape of the entrained particle flow as it reaches the 1st thermocouple array. Of particular note is the elliptical shape of the flow profile, thus depicting very little lateral expansion of the particle flow stream after the injection nozzles. The elongation of the flow pattern along the vertical axis matches the shape and arrangement of the 28 nozzles used to inject the spray water particles. It was assumed that the radial component of the nozzle holder, along with the increased number of nozzles, and the spray angle of the individual nozzles would have provided better coverage at this point in the flow. However, it would appear that far greater mass and momentum transfer has occurred between the particles and the steam flow, as well as drop coalescence, thus collapsing the anticipated ideal spray pattern into a more concentrated flow stream, and resultant thermal stratification. Additionally, the affects of gravity can also be seen as the profile is distinctly shifted toward the lower edge of the pipeline.

The break-up of this symmetric and concentric flow stream is evident when viewing the thermal profiles at the 2nd thermocouple array from time step 1.25 and

higher. The profile is no long centrally located but rather has been shifted to the outside edge of the pipeline. While the temperature continues to drop and the profiling becomes more dispersed, the thermal stratification phenomenon is still quite visible and contains extreme values from both ends of the allowable thermal spectrum.

When Figures V.29 and V.30 are examined, the differences noted previously on the boundary temperature conditions, at this time step, are clearly evident in the thermal profiles. At 1.45 seconds, the thermal profiles at the inlet, 1st thermocouple array and the 2nd thermocouple array are nearly identical. This complies well with the thermal equilibrium analysis described in Section V.3.1. However, when we view the outlet profile, the average temperature varies by 36.5° F, which is representative of the 1.45-second boundary temperature profile mentioned in Section V.3.2. In Version 1.2, there is evidence of greater heat transfer interaction with the flowing particulate than in Version 2.0. It is anticipated that this is also the result of the programming changes made to the latest version of the code. It is also interesting to note that the thermal profiling has one again shifted in accordance with the expected mass and momentum transfer associated with the particles flow around the second elbow. The lower thermal profiles are now located more towards the outside surface of the pipeline.

In Figures V.31-32 and V.33-34, the thermal profiles at the outlet continue to change with respect to the different versions of the code as compared to the other three locations. At 1.60 and 1.75 seconds, the outlet temperature profiles of the outlet are distinctly different between Version 1.2 and 2.0. It is surmised that these differences are the result of code changes and the manner in which the thermodynamic properties are

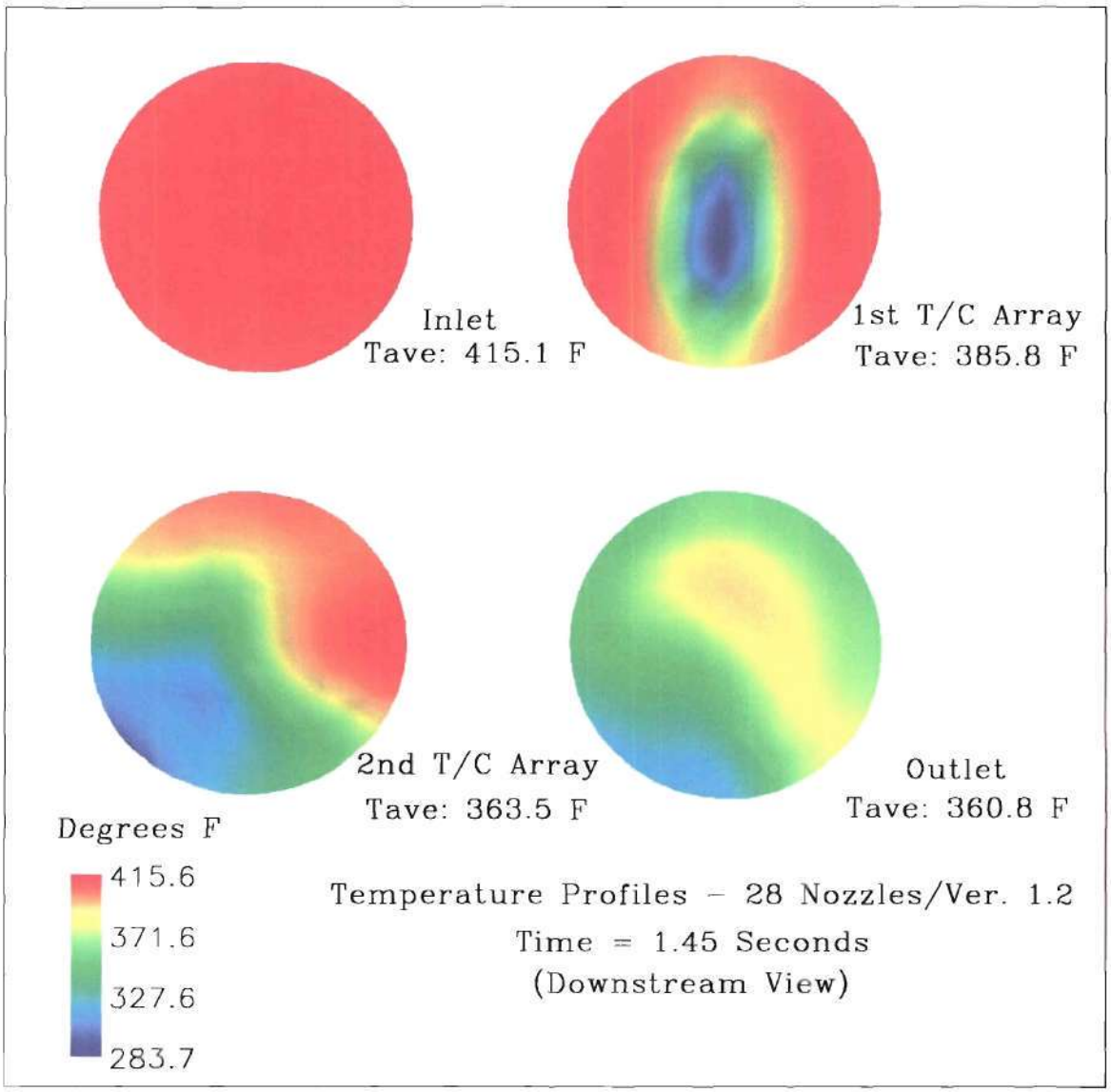
Inlet
Tave: 415.1 F
1st T/C Array
Tave: 385.8 F
2nd T/C Array
Tave: 363.5 F
Outlet
Tave: 360.8 F
Degrees F
415.6
371.6
327.6
283.7
Temperature Profiles - 28 Nozzles/Ver. 1.2
Time = 1.45 Seconds
(Downstream View)

Figure V.29

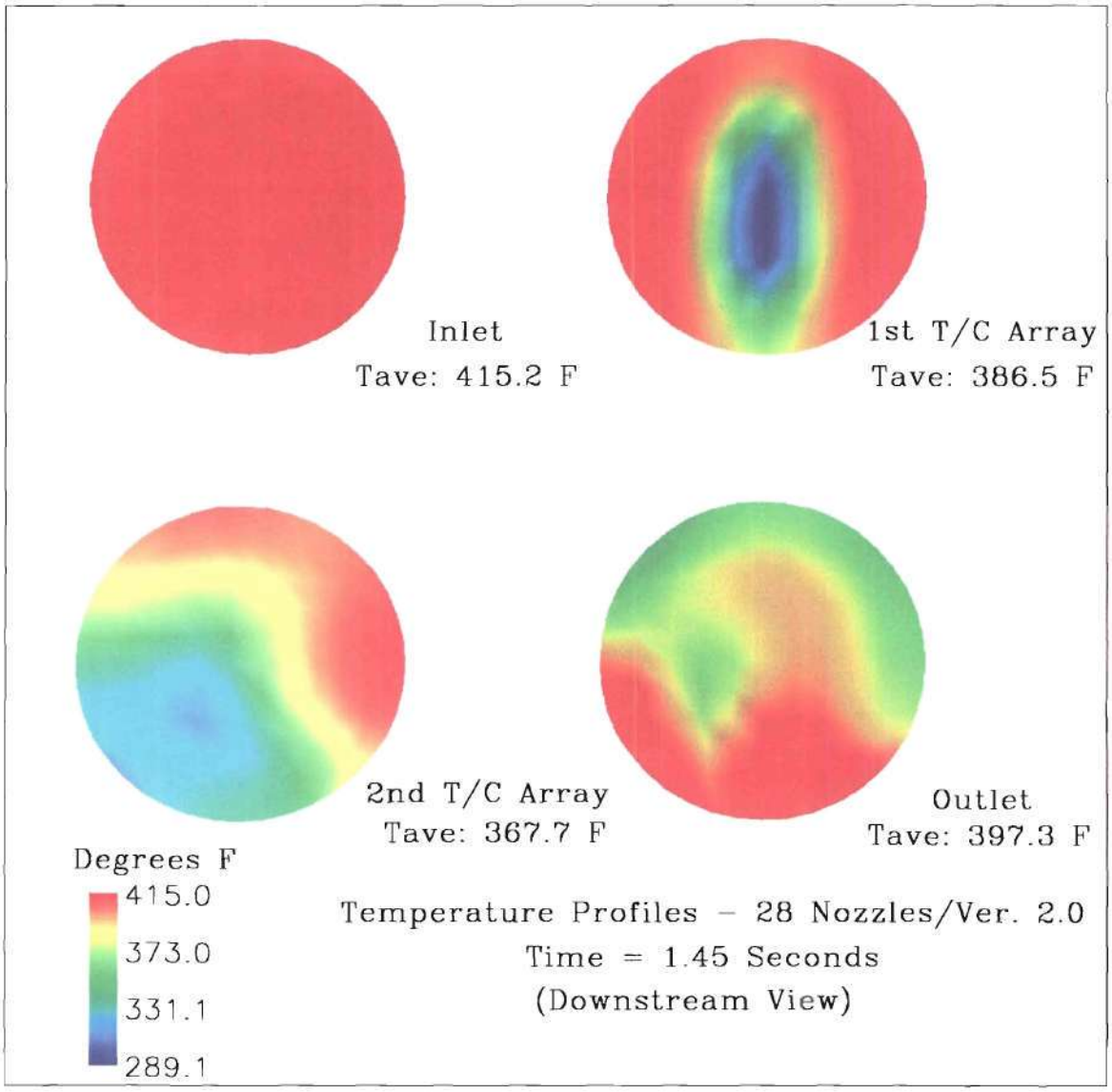
Inlet
Tave: 415.2 F
1st T/C Array
Tave: 386.5 F
2nd T/C Array
Tave: 367.7 F
Outlet
Tave: 397.3 F
Degrees F
415.0
373.0
331.1
289.1
Temperature Profiles - 28 Nozzles/Ver. 2.0
Time = 1.45 Seconds
(Downstream View)

Figure V.30

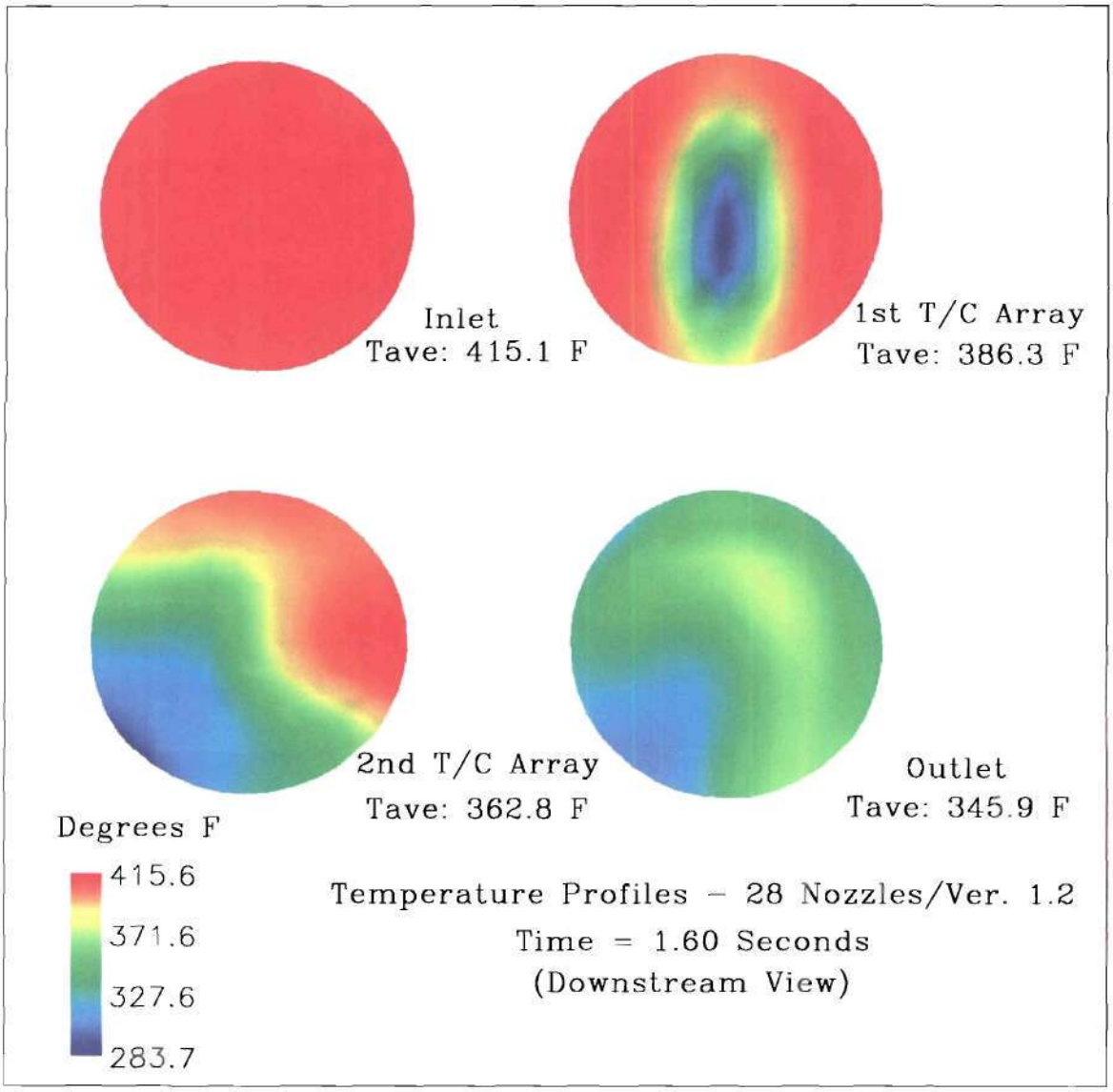
Inlet
Tave: 415.1 F
1st T/C Array
Tave: 386.3 F
2nd T/C Array
Tave: 362.8 F
Outlet
Tave: 345.9 F
Degrees F
415.6
371.6
327.6
283.7
Temperature Profiles - 28 Nozzles/Ver. 1.2
Time = 1.60 Seconds
(Downstream View)

Figure V.31

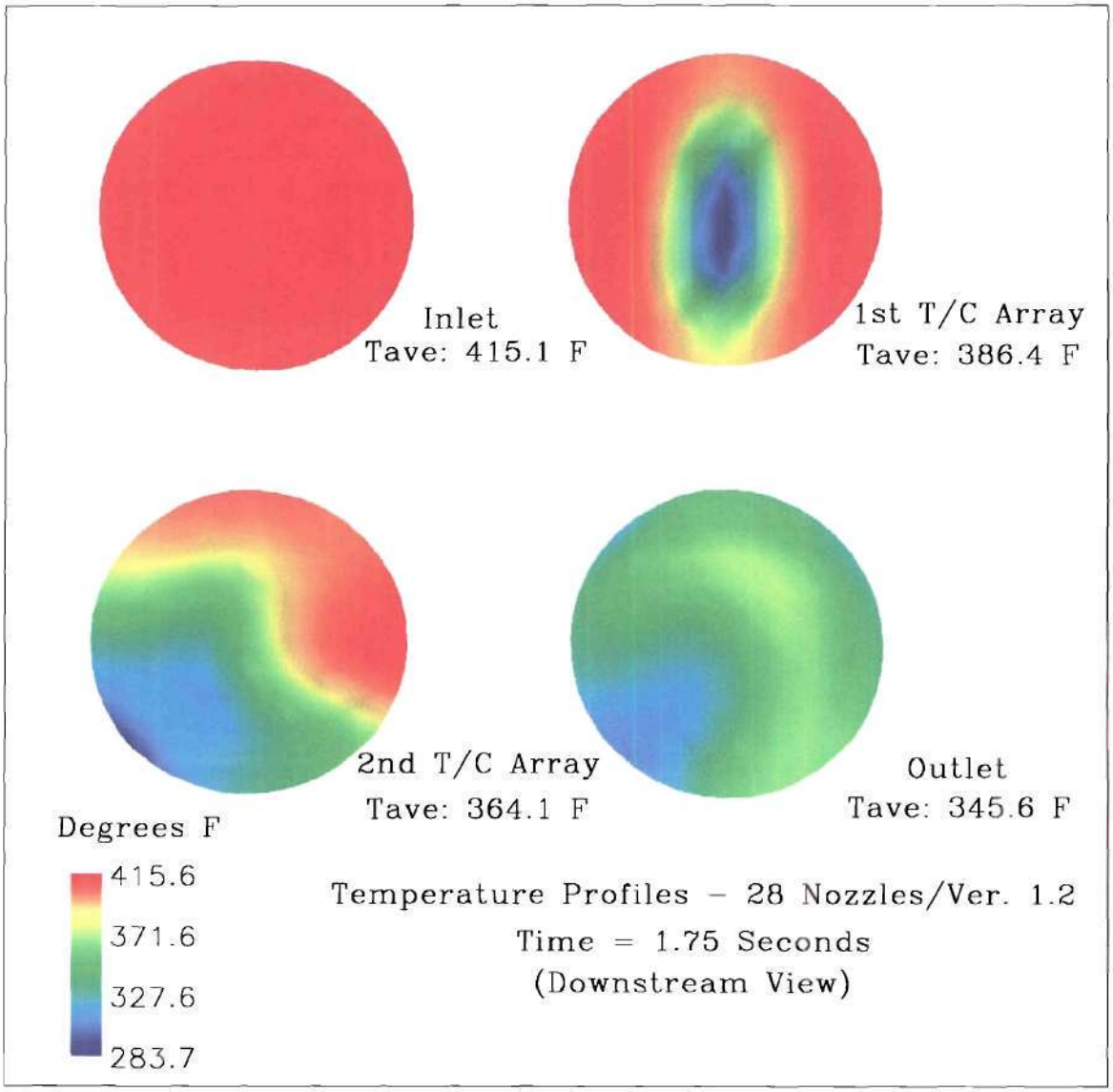
Inlet
Tave: 415.1 F
1st T/C Array
Tave: 386.4 F
2nd T/C Array
Tave: 364.1 F
Outlet
Tave: 345.6 F
Degrees F
415.6
371.6
327.6
283.7
Temperature Profiles - 28 Nozzles/Ver. 1.2
Time = 1.75 Seconds
(Downstream View)

Figure V.32

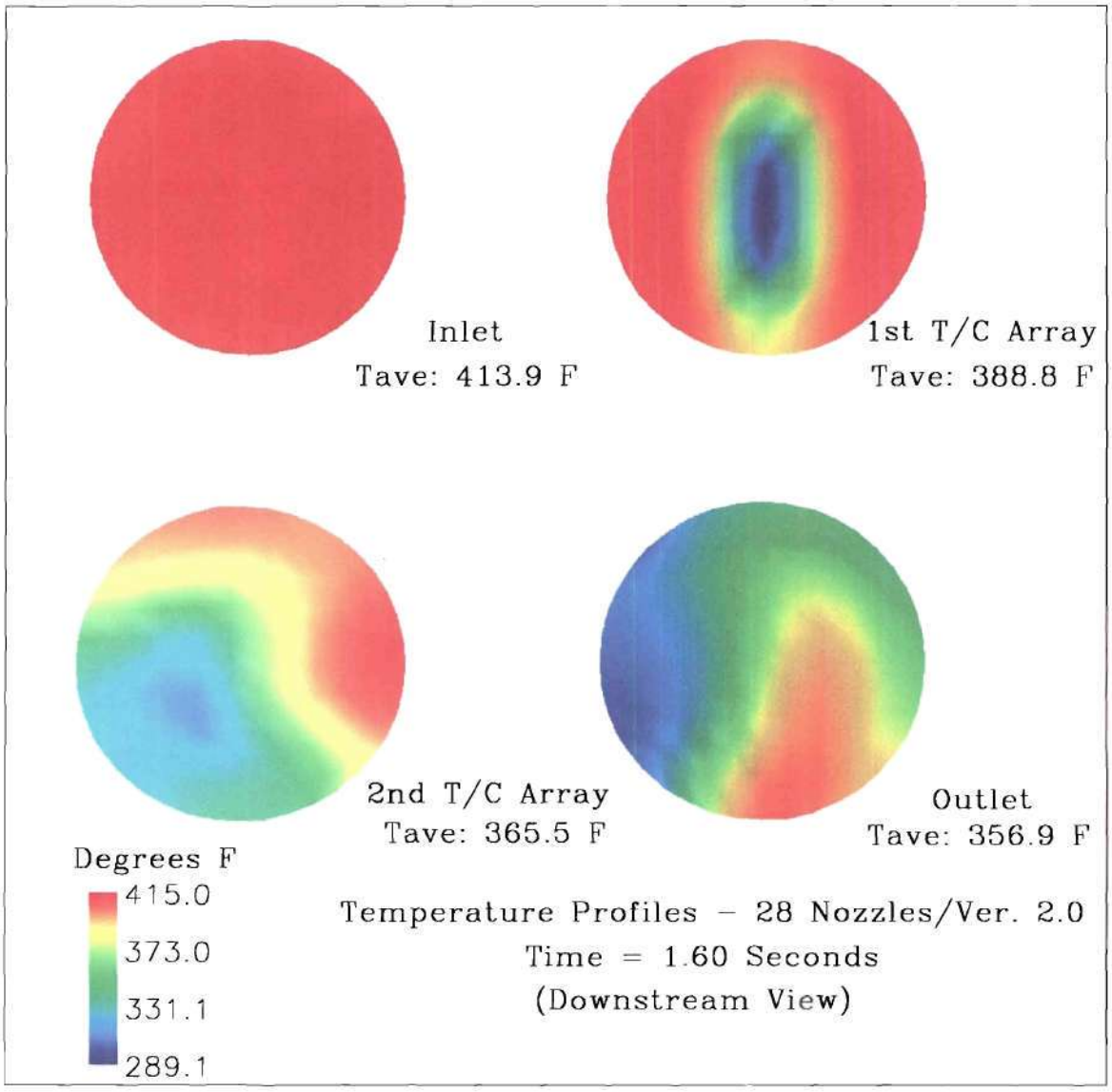
Inlet
Tave: 413.9 F
1st T/C Array
Tave: 388.8 F
2nd T/C Array
Tave: 365.5 F
Outlet
Tave: 356.9 F
Degrees F
415.0
373.0
331.1
289.1
Temperature Profiles - 28 Nozzles/Ver. 2.0
Time = 1.60 Seconds
(Downstream View)

Figure V.33

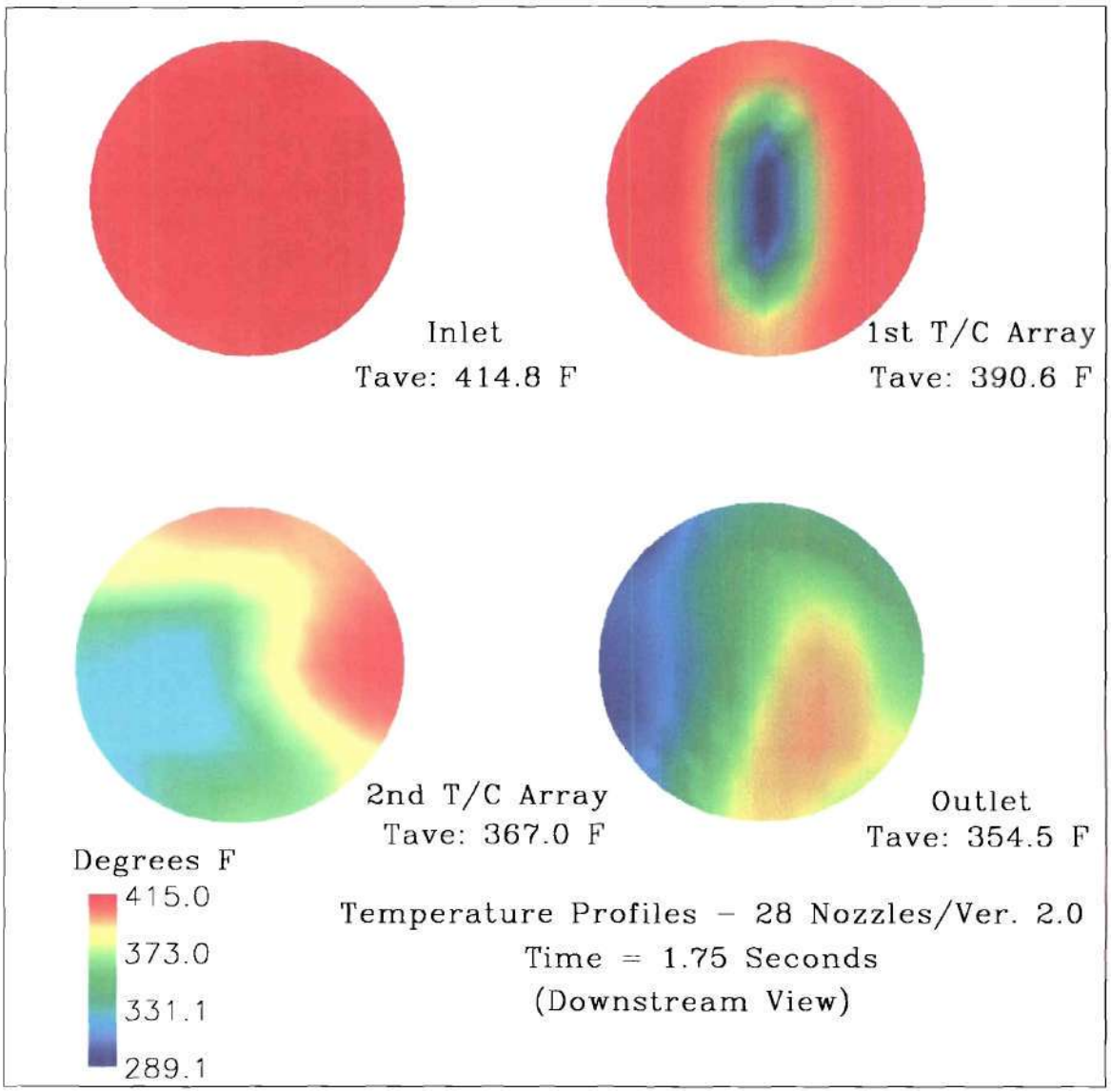
Inlet
Tave: 414.8 F
1st T/C Array
Tave: 390.6 F
2nd T/C Array
Tave: 367.0 F
Outlet
Tave: 354.5 F
Degrees F
415.0
373.0
331.1
289.1
Temperature Profiles - 28 Nozzles/Ver. 2.0
Time = 1.75 Seconds
(Downstream View)

Figure V.34

calculated. Prior to the inclusion of a film model, the particulate was allowed to pool on the pipe walls. Interaction with the flowing steam was limited. In some cases, the pooling was shown to have caused condensing of the surrounding steam, thus producing erroneous thermodynamic properties and temperature profiles.

The complete graphical output of the temperature profiles for the four-nozzle arrangement, using both Version 1.2 and Version 2.0, can be viewed in Appendix D. In each case, the view is always in the direction of flow or looking downstream.

V.3.4 Spray Water Particle Flow

The spray water particle flow graphics do not contribute significantly to the purpose of this work. However, they do assist in graphically depicting the flow and direction of the particulate relative to the piping geometry. By examining the particulate flow, a better understanding of the spray dynamics and interpretation of the thermal profiles can be achieved.

Figures V.35 and V.36 illustrate the initial spray pattern as interpreted by the code at 0.85 seconds. As previously mentioned and depicted in the thermal profiles at the 1st thermocouple array, the flow pattern is very compact and representative of the devices general geometry, i.e., vertically concentrated. It is interesting to examine the break-up of the dense spray pattern as the particulate progresses downstream and the droplets begin to spread and become smaller.

In Figures V.37, and V.38, the control volume is completely filled with the particulate bundles. In viewing the pipeline from this perspective, it is interesting to note the changes in the flow structure. Of particular note is the continuous reduction in

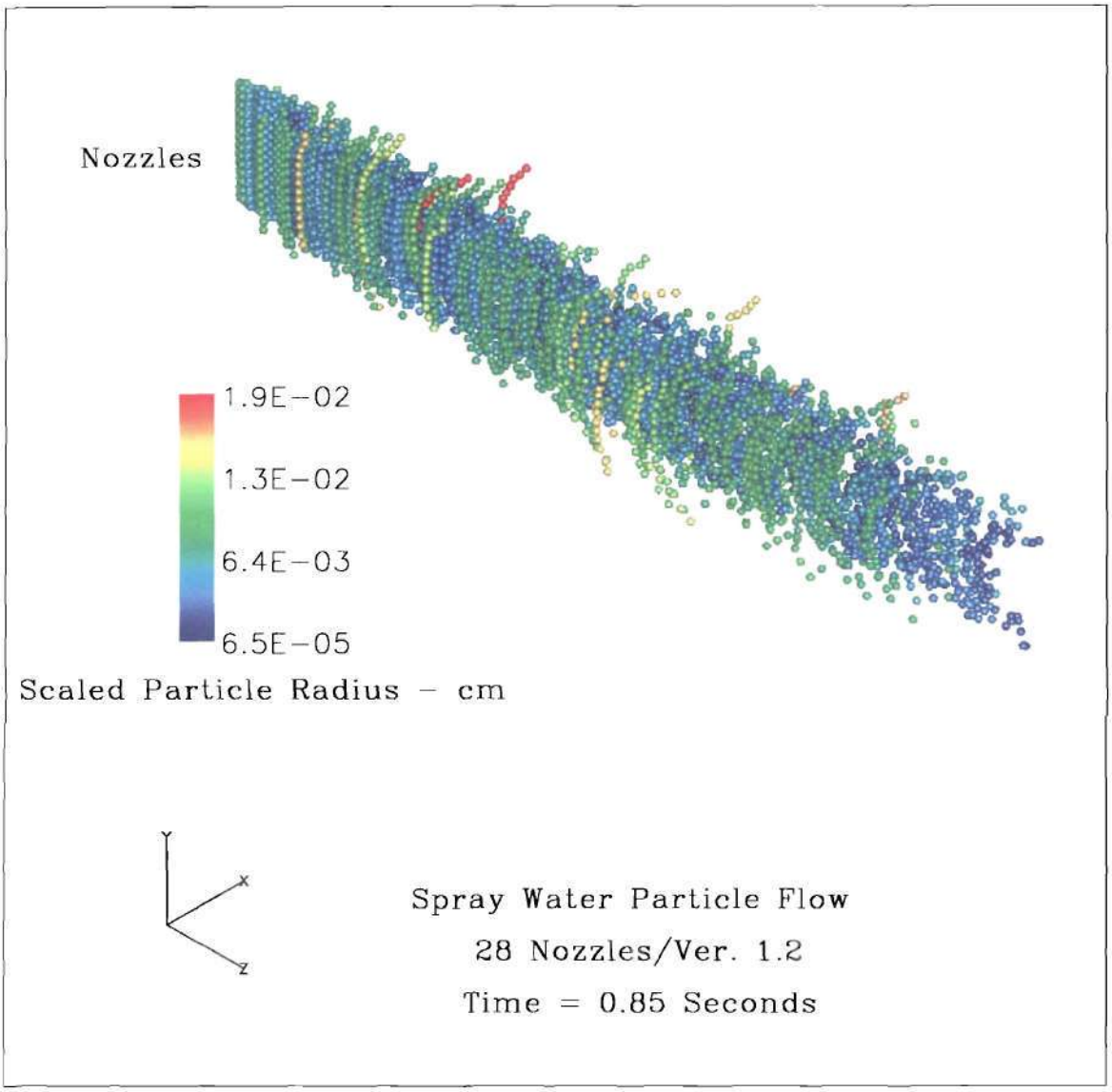
Nozzles
1.9E−02
1.3E−02
6.4E−03
6.5E−05
Scaled Particle Radius − cm
Y
X
Z
Spray Water Particle Flow
28 Nozzles/Ver. 1.2
Time = 0.85 Seconds

Figure V.35

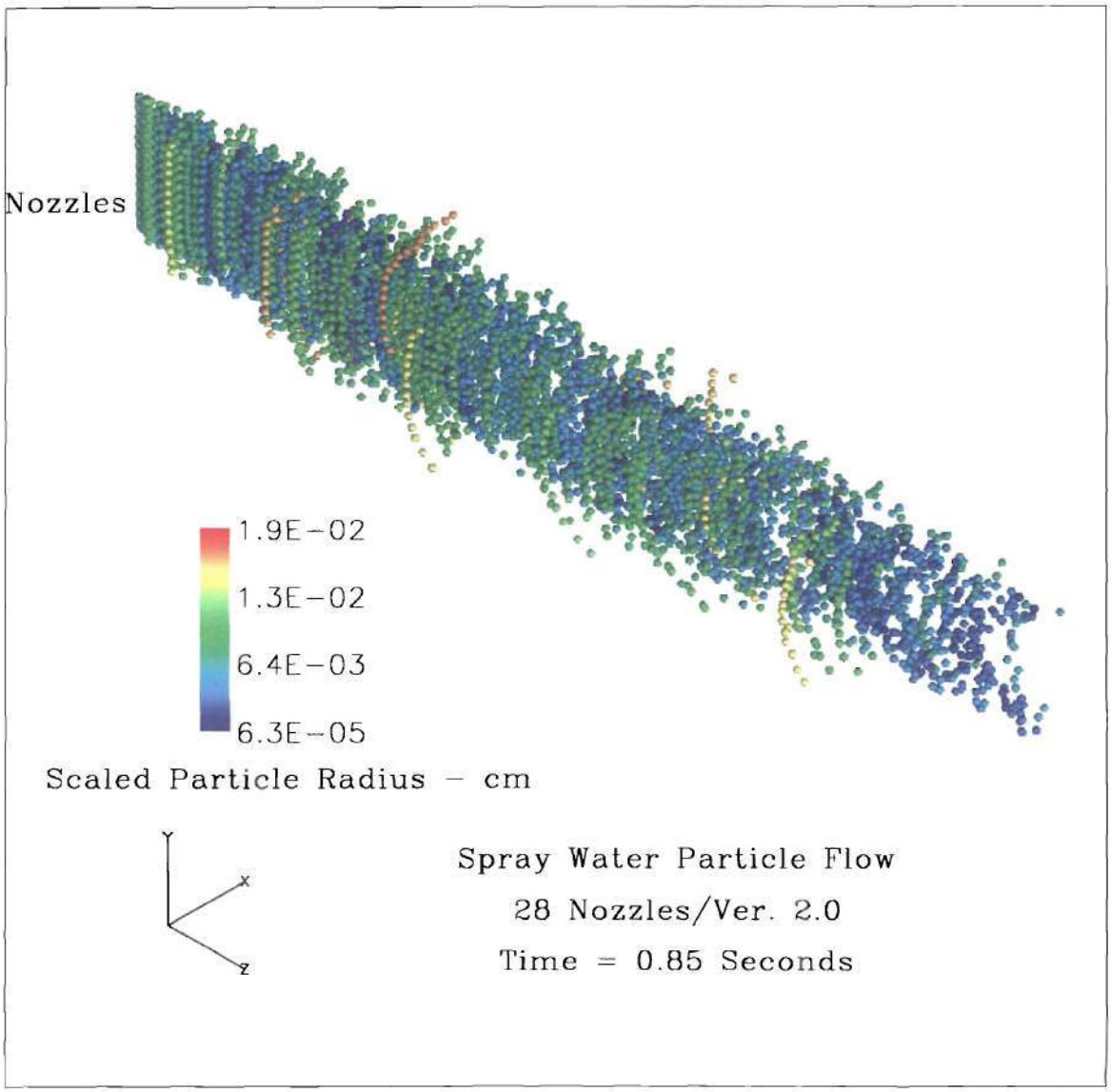
Nozzles
1.9E-02
1.3E-02
6.4E-03
6.3E-05
Scaled Particle Radius - cm
Y
X
Z
Spray Water Particle Flow
28 Nozzles/Ver. 2.0
Time = 0.85 Seconds

Figure V.36

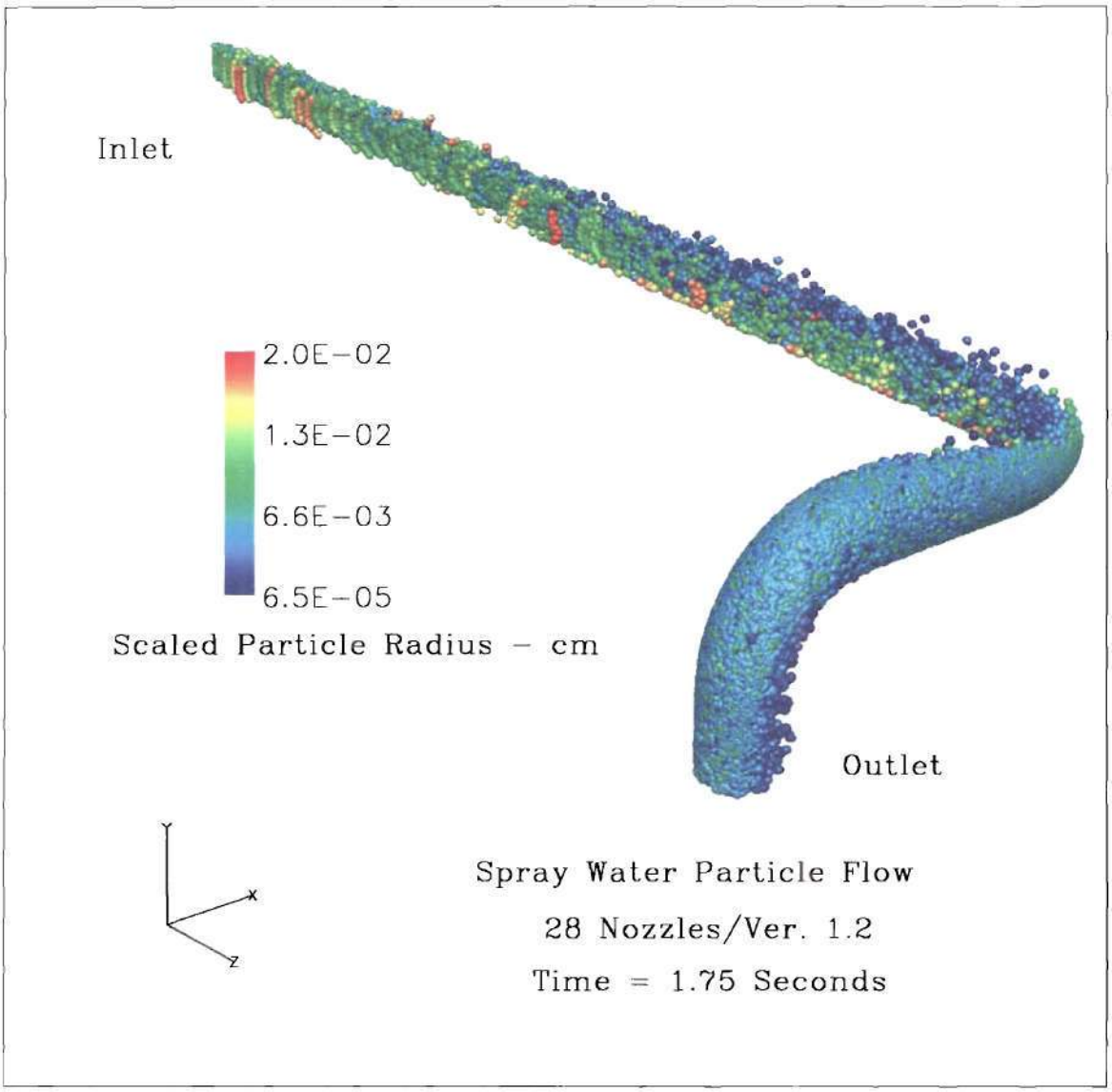
Inlet
2.0E-02
1.3E-02
6.6E-03
6.5E-05
Scaled Particle Radius - cm
Outlet
Y
X
Z
Spray Water Particle Flow
28 Nozzles/Ver. 1.2
Time = 1.75 Seconds

Figure V.37

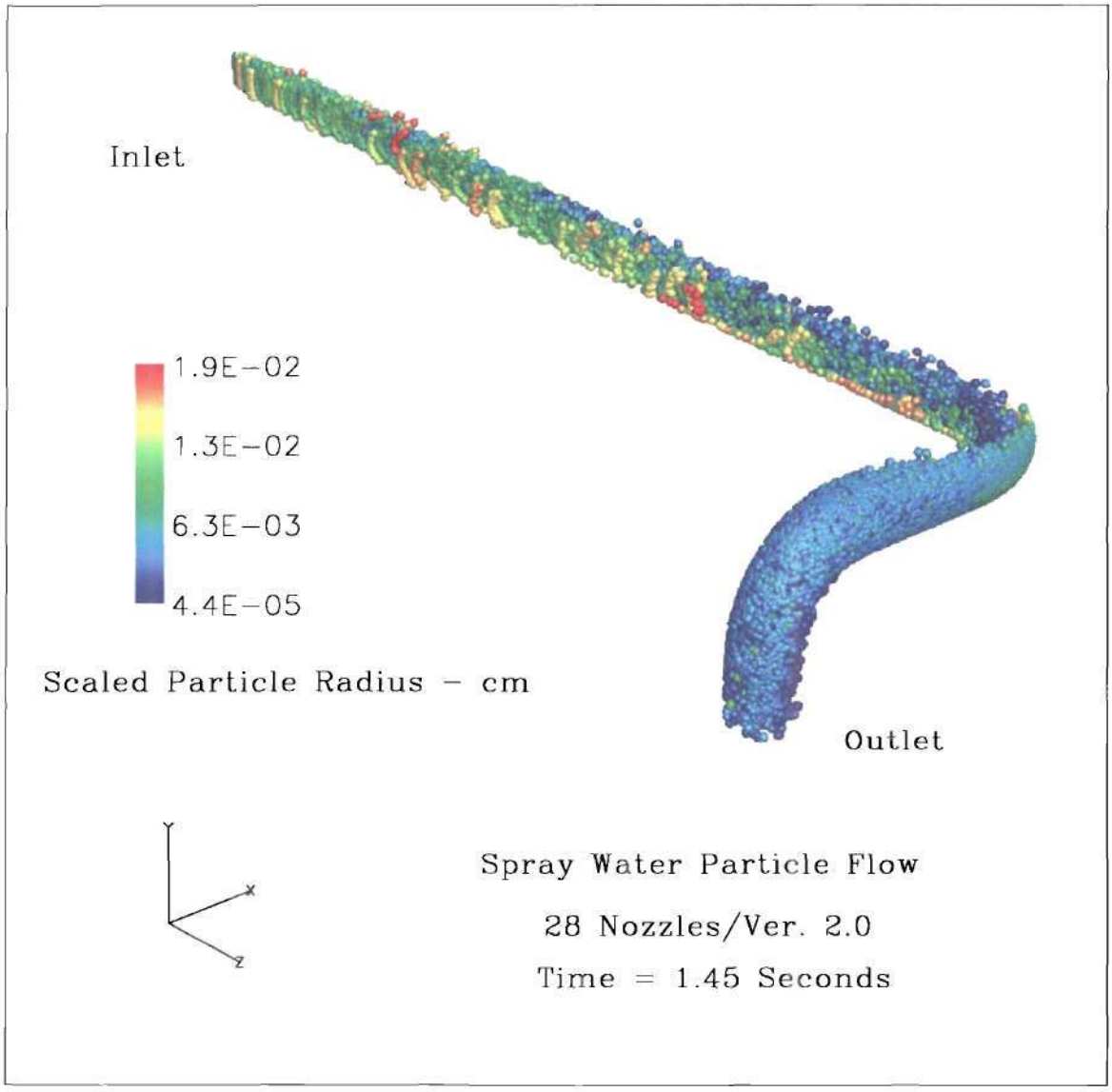
Inlet
1.9E-02
1.3E-02
6.3E-03
4.4E-05
Scaled Particle Radius - cm
Outlet
Y
X
Z
Spray Water Particle Flow
28 Nozzles/Ver. 2.0
Time = 1.45 Seconds

Figure V.38

calculated. Prior to the inclusion of a film model, the particulate was allowed to pool on the pipe walls. Interaction with the flowing steam was limited. In some cases, the pooling was shown to have caused condensing of the surrounding steam, thus producing erroneous thermodynamic properties and temperature profiles.

The complete graphical output of the temperature profiles for the four-nozzle arrangement, using both Version 1.2 and Version 2.0, can be viewed in Appendix D. In each case, the view is always in the direction of flow or looking downstream.

V.3.4 Spray Water Particle Flow

The spray water particle flow graphics do not contribute significantly to the purpose of this work. However, they do assist in graphically depicting the flow and direction of the particulate relative to the piping geometry. By examining the particulate flow, a better understanding of the spray dynamics and interpretation of the thermal profiles can be achieved.

Figures V.35 and V.36 illustrate the initial spray pattern as interpreted by the code at 0.85 seconds. As previously mentioned and depicted in the thermal profiles at the 1st thermocouple array, the flow pattern is very compact and representative of the devices general geometry, i.e., vertically concentrated. It is interesting to examine the break-up of the dense spray pattern as the particulate progresses downstream and the droplets begin to spread and become smaller.

In Figures V.37, and V.38, the control volume is completely filled with the particulate bundles. In viewing the pipeline from this perspective, it is interesting to note the changes in the flow structure. Of particular note is the continuous reduction in

generated by the two versions of the SteamCFD code. The graphs used to relate the data refer to the specific thermocouples by a position number from 1 to 6. In our test apparatus, the outer most ring of thermocouples is designated as 1 and the inner most is 6. The placements of thermocouples are on the vertical and horizontal axis of the measurement plane. In every case, the view is always downstream. For further clarification, refer to Figure II.8.

Figures V.39 and V.40 illustrate the 1st thermocouple array experimental results as compared to the computational results obtained from Version 1.2 and 2.0, respectively, for the 28 nozzle device. Unfortunately, it is quite apparent that the use of thermocouples for the measurement of a particle-laden two-phase vapor-liquid flow stream is not acceptable. The thermocouples installed in this first array could only detect the saturation temperature of the unevaporated droplets. In contrast, the code was designed to only register the temperature of the superheated vapor. However, even with these differences, some notable observations can be rendered.

In positions 1-4 there is good symmetry associated with the computational results from both versions. In positions 5 and 6, the innermost thermocouples, we see the formation of an asymmetric pattern as the left side of the graph indicates a more rapid cooling then the right side. One possible reason for this to occur relates to pressure variations generated by the downstream elbow. In order for continuity to be maintained, the flow on the left side of the pipe must increase to coincide with the flow on the inside. As a result, the pressure decreases and thus improves the heat transfer and vaporization process on the left side only. However, as one observes the actual data, as plotted in

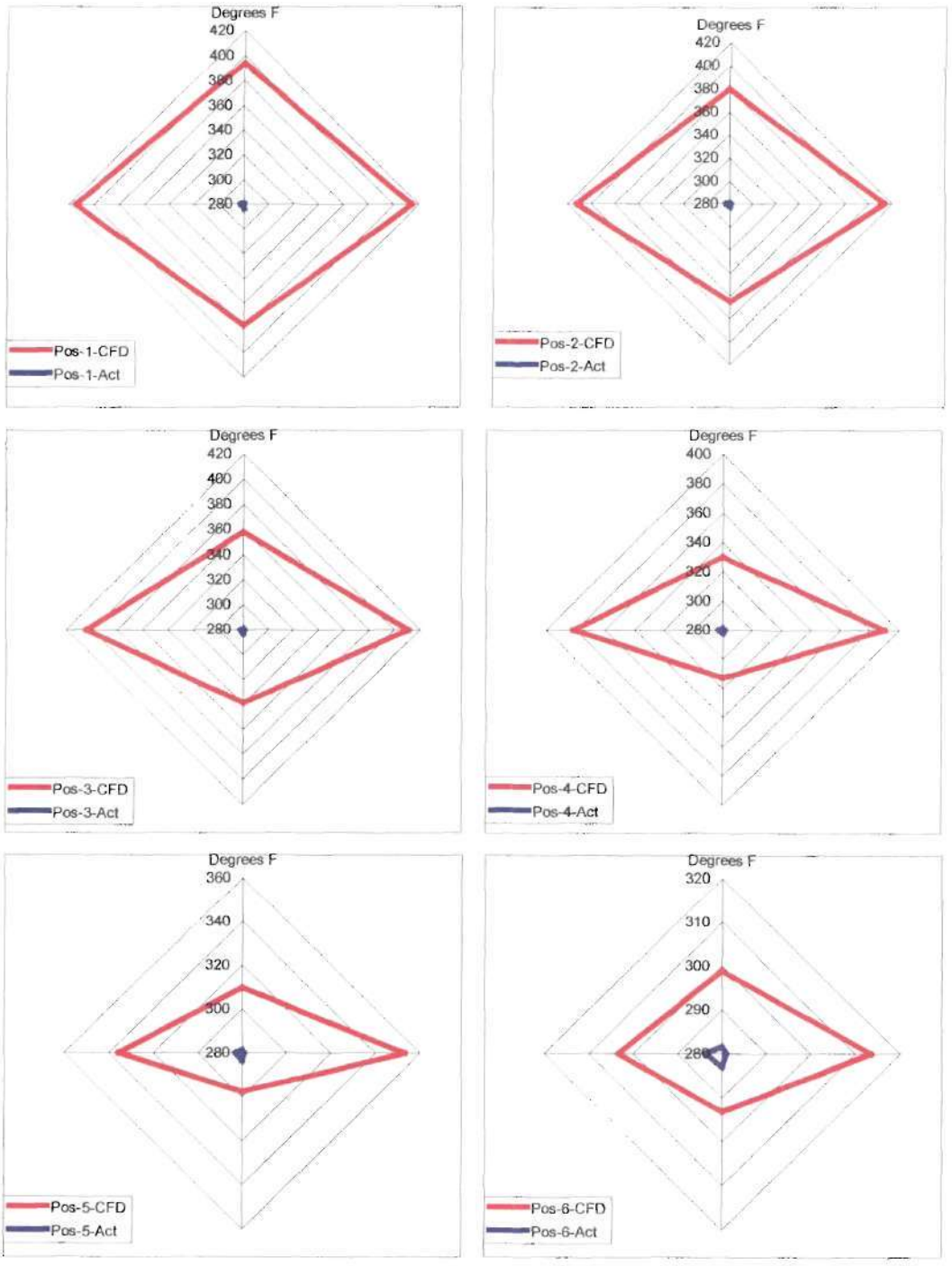

Comparison of Actual vs. Computational Thermocouple Readings - 1st Array, 28 Nozzles, Version 1.2

Figure V.39

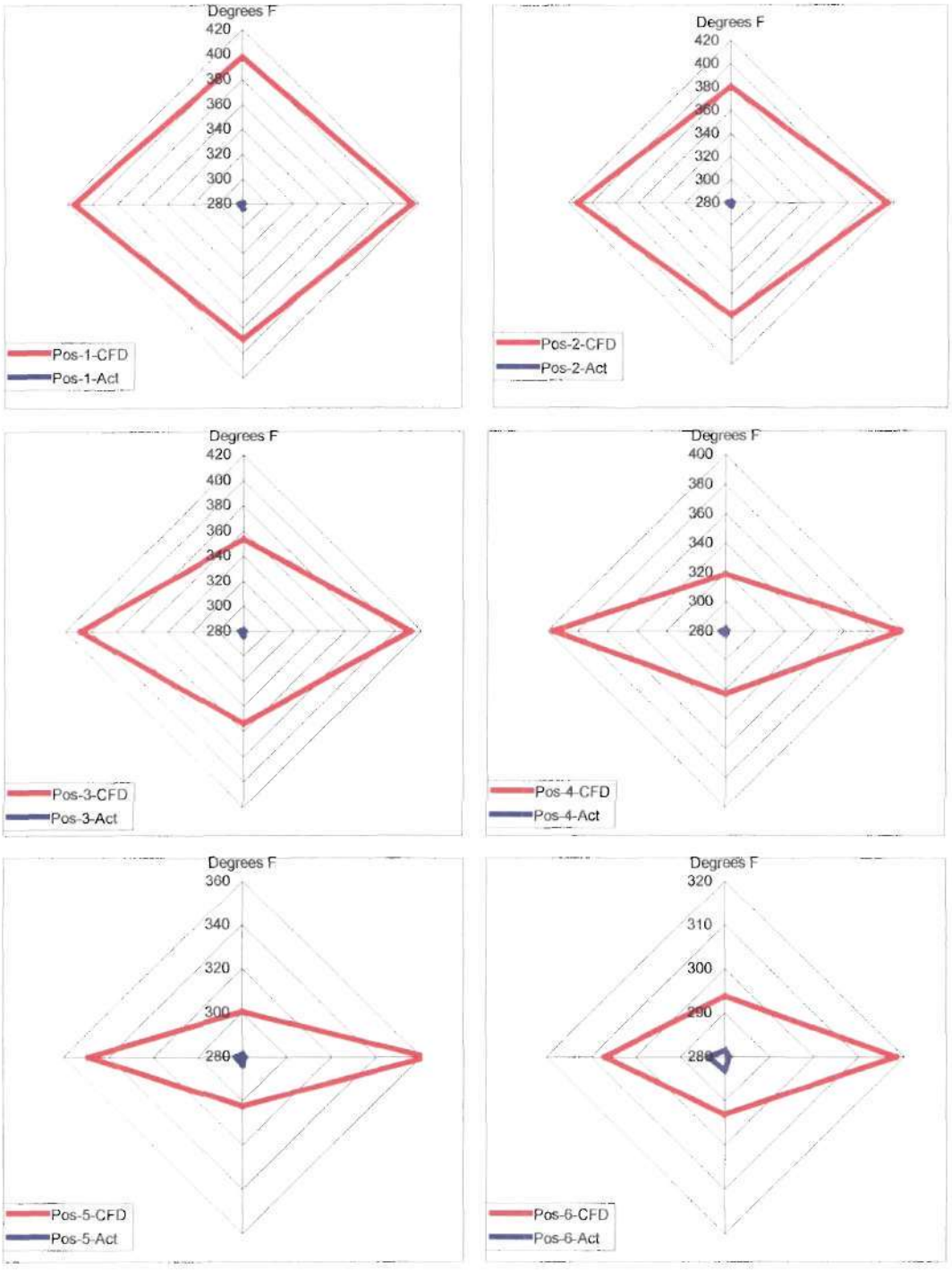

Comparison of Actual vs. Computational Thermocouple Readings - 1st Array, 28 Nozzles, Version 2.0

Figure V.40

position 5 and 6 with the scale reduced, the shape of the actual profile is opposite to that which is computationally created. In viewing position 6, the left side of the actual data is registering the highest values of actual data for the 1st array. Once again, this is not significant and is attributed to pressure fluctuations and flow instability created by an upstream elbow that was not included in the computational model. In all positions, the geometric affects of the device and gravity are exhibited. The temperatures are lower along the vertical axis and the peak values are higher at the top of the pipe then at the bottom. This complies well with the other computational graphics presented previously.

In Figures V.41 and V.42 the results are substantially different. By the time the steam reaches the 2nd thermocouple array, there is sufficient vaporization and flow disruption to provide temperature outputs from the sensing devices. The graphics here clearly show the impact of the liquid separation due to the first elbow. The temperature on the left side of the graphs are severely depressed, while the right side is at or near the initial inlet temperature, particularly in the outer rings of measurement. What is most interesting about these graphs is the fact that the general shapes of the thermal profiles for the actual data very closely resembles those of the computational results for both versions. The actual data does show further reduction in steam temperature then the computational output. This can be caused by a number of potential differences including secondary effects of the cooling water impinging on the probes, particle size and distribution differences in the computational model versus reality, and refinement in the heat transfer routines presently in place. In contrast to the differences, it is important to note that the actual data was fully contained with the boundary of the computational

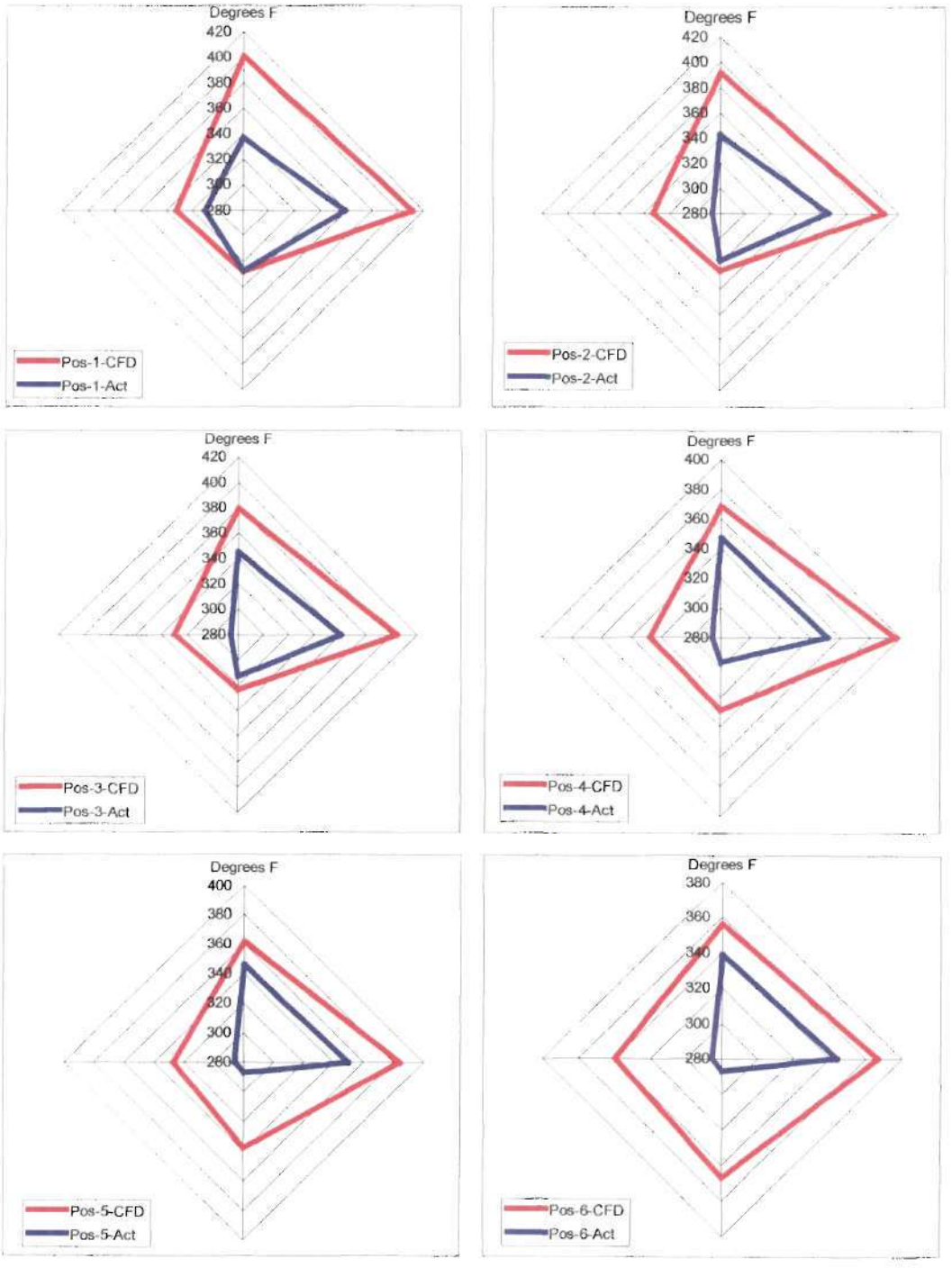

Comparison of Actual vs. Computational Thermocouple Readings - 2nd Array, 28 Nozzles, Version 1.2

Figure V.41

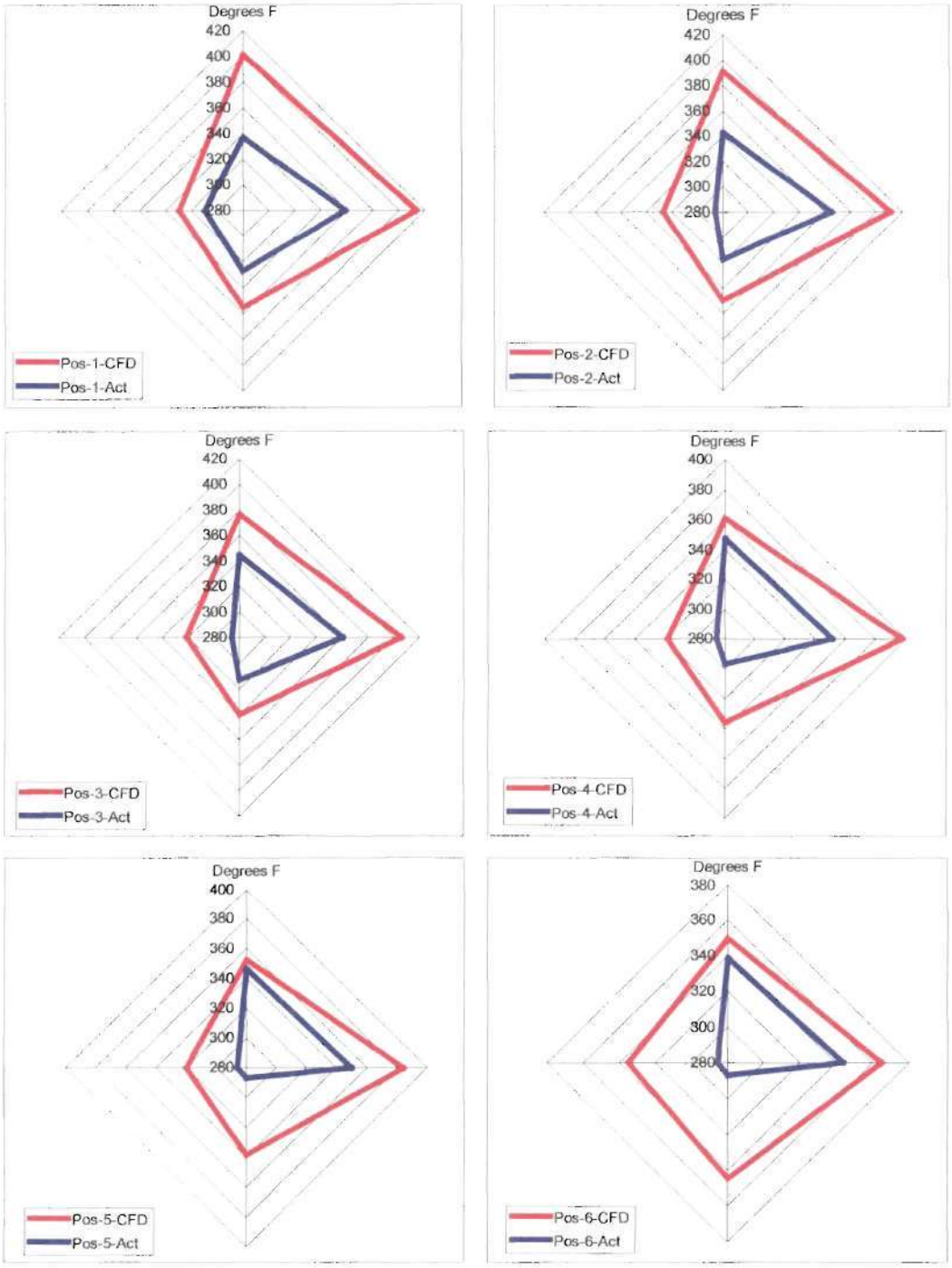

Comparison of Actual vs. Computational Thermocouple Readings - 2nd Array, 28 Nozzles, Version 2.0

Figure V.42

results, thus indicating that no major mass, momentum, or energy discrepancies existed within the program logic.

V.4 The Single Nozzle Device

V.4.1 Thermal Equilibrium

As in the case for the previous arrangement, the first task was to establish thermal equilibrium for each of the four coordinate surfaces. These surfaces were integrated to determine the average profile temperature at time increments of 0.1 seconds between 0.75 to 1.80 seconds. The results of this exercise can be seen in Figures V.43. Since no experimental data were available for this case, it was decided to only run it for one set of conditions, namely that of the four-nozzle device, and use the latest version of the code. All comparisons will be made based on relating the computational four nozzle results to the single nozzle ones. Both cases reached equilibrium at about the same time. The inlet provided a near constant value of 377° F throughout the prescribed time period. The 1st and 2nd array of thermocouples reached equilibrium at approximately 1.15 and 1.35 seconds respectively. The outlet plane reached apparent thermal equilibrium at approximately 1.60 seconds, however it is noted in both cases that the slope of the outlet temperature line continues to have a slight negative gradient and more run time may be required to assure outlet stability is achieved. For comparison purposes, the outlet plane is not strictly required, thus all the surfaces achieved relatively constant average temperature profiles within the 1.75-second period of analysis.

While the time to equilibrium was relatively constant between the two cases, the actual equilibrium temperature was not. Each coordinate plane exhibited at least a 5° F

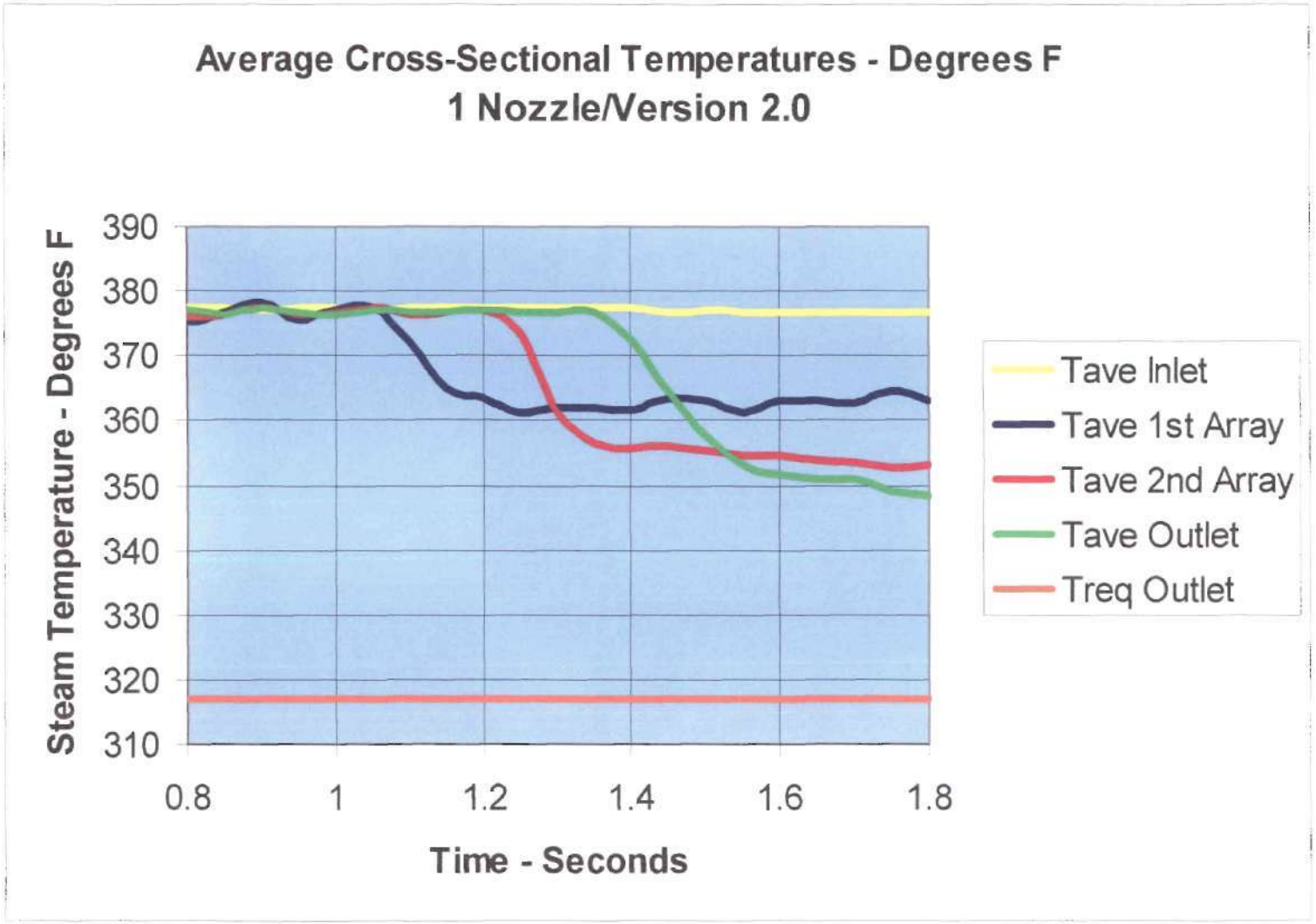
Average Cross-Sectional Temperatures - Degrees F
1 Nozzle/Version 2.0
Steam Temperature - Degrees F
390
380
370
360
350
340
330
320
310
0.8
1
1.2
1.4
1.6
1.8
Time - Seconds
Tave Inlet
Tave 1st Array
Tave 2nd Array
Tave Outlet
Treq Outlet

Figure V.43

difference between the two cases. The outlet plane showed the greatest differential with an 8° F temperature variance. In all cases, the single nozzle arrangement resulted in higher calculated temperatures. Since both cases were run using the same initial flow conditions and the same version of the code, all the differences would have to be contributed to geometric variances in nozzle size and distribution. This differential could have been expected and was one of the goals of this project. Since the only difference between the two runs was nozzle placement and geometry, the net result indicates that placement, spray injection coverage, and reduced particle size, associated with smaller nozzles, did impact positively the overall performance. Unfortunately, the same could not be said for the 28 nozzle arrangement which did not show a proportionate improvement in performance even though the same parameters were exaggerated by a factor of 7 times. To the contrary, the calculated results were worse then for the four-nozzle device.

V.4.2 Boundary Temperature Conditions

The boundary temperature conditions appear to be relatively constant between the two cases until we reach 1.25 seconds. In viewing Figures V.44 and V.45, both at 1.25 seconds, thermal differences at the top and bottom of the initial horizontal pipe run can be detected. This is probably caused by the more complete coverage of the cross-sectional flow area by the four-nozzle device then with the single nozzle. The single nozzle device is centrally located and further away from the upper pipe walls, thus the cooling we are seeing is most probably caused by particulate fall-out due to gravity. This is further evident in Figures V.46 and V.47 at 1.45 seconds. Here the lower surfaces of the

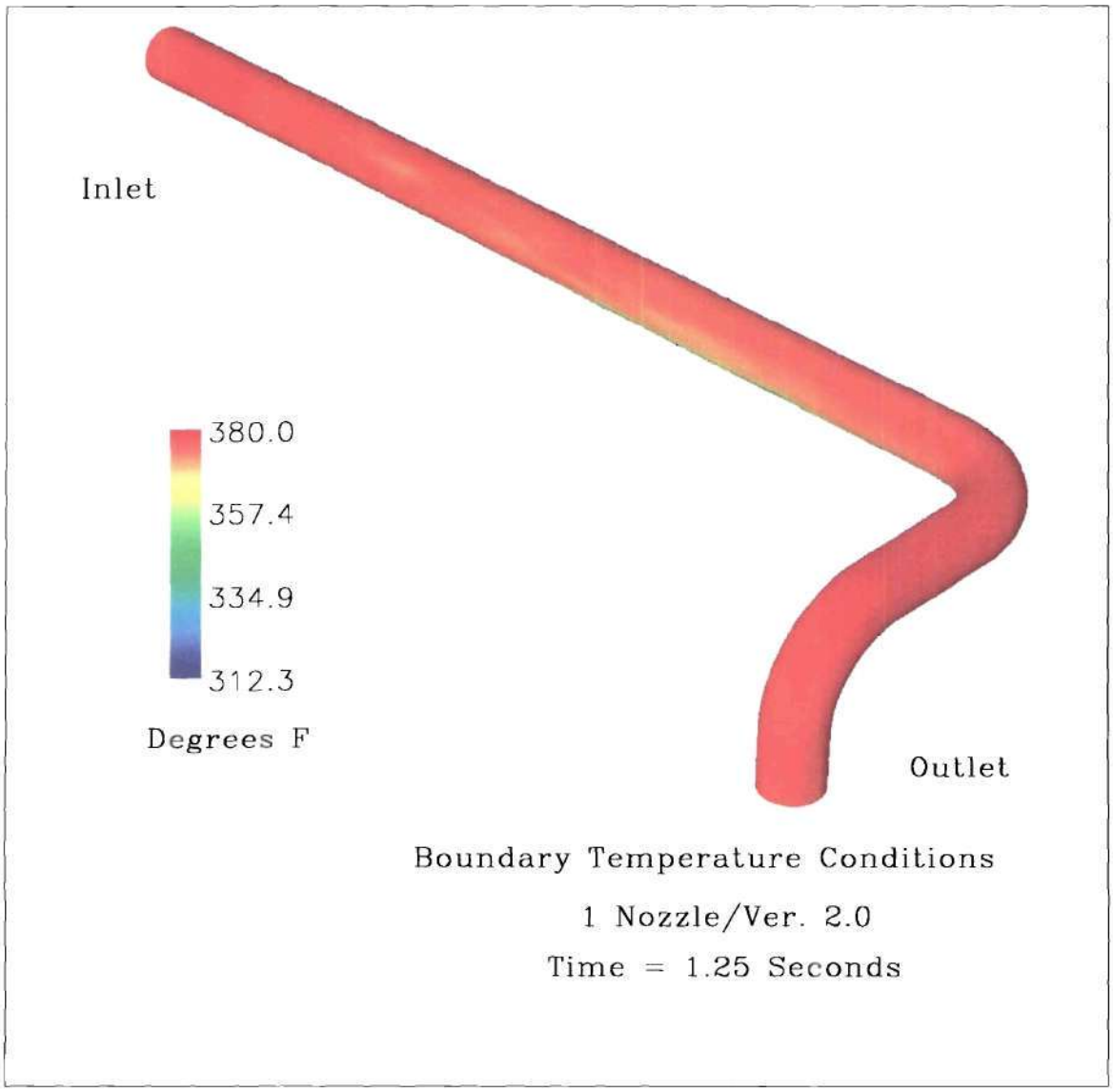
Inlet
380.0
357.4
334.9
312.3
Degrees F
Outlet
Boundary Temperature Conditions
1 Nozzle/Ver. 2.0
Time = 1.25 Seconds

Figure V.44

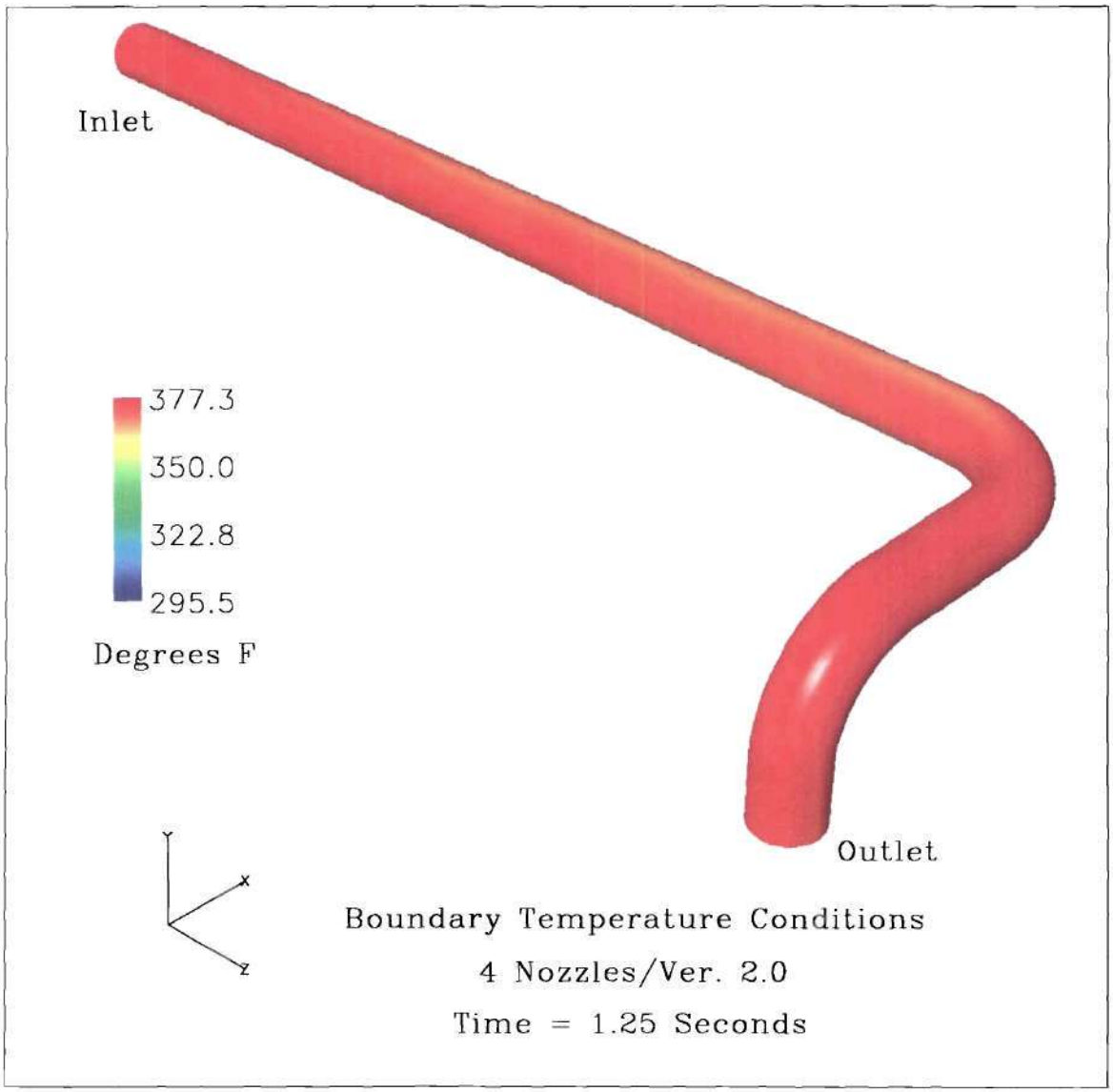
Inlet
377.3
350.0
322.8
295.5
Degrees F
Outlet
Boundary Temperature Conditions
4 Nozzles/Ver. 2.0
Time = 1.25 Seconds

Figure V.45

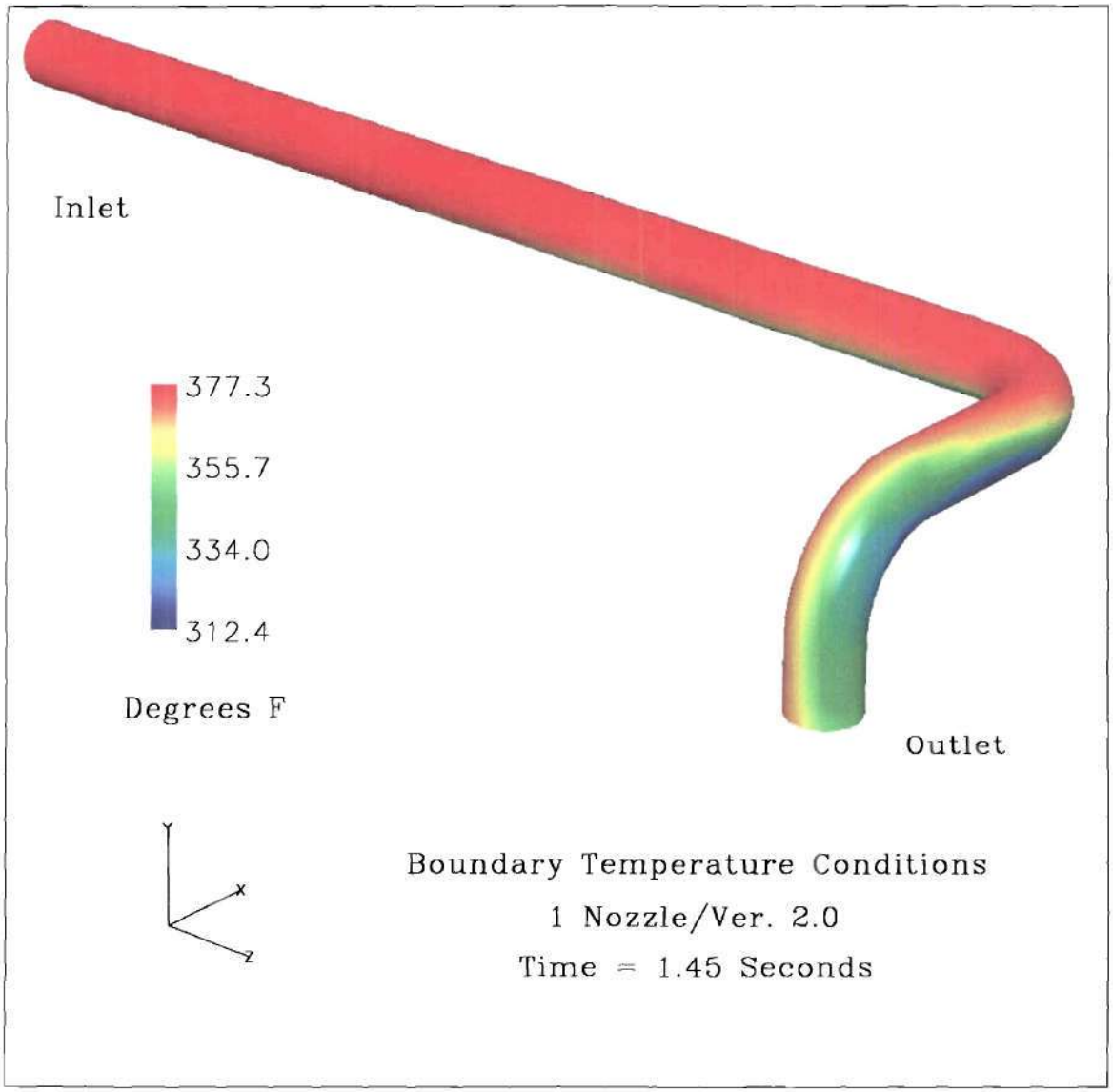
Inlet
377.3
355.7
334.0
312.4
Degrees F
Outlet
Y
X
Z
Boundary Temperature Conditions
1 Nozzle/Ver. 2.0
Time = 1.45 Seconds

Figure V.46

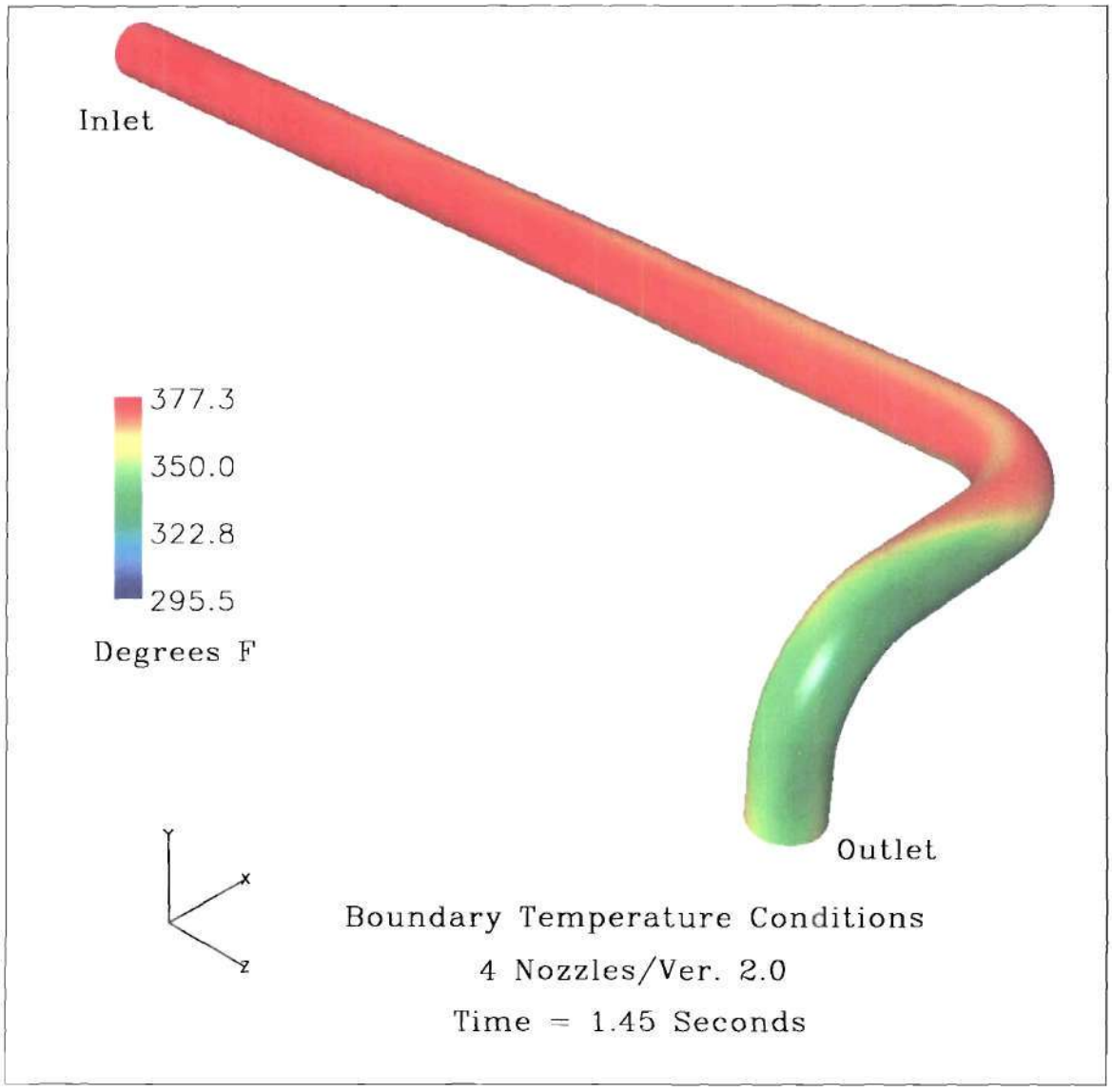
Inlet
377.3
350.0
322.8
295.5
Degrees F
Outlet
Y
X
Z
Boundary Temperature Conditions
4 Nozzles/Ver. 2.0
Time = 1.45 Seconds

Figure V.47

pipeline, just after the first elbow, is significantly colder then the four-nozzle arrangement. Once again, this would be the result of gravity and pooling of water on the lower pipe surfaces.

The boundary temperatures at 1.75, see Figures V.48 and V.49, are nearly identical within the respective cases. However, it appears that we continue to see the affects of particulate fall-out as the lower edge of the pipe downstream of the first elbow remains colder in the single nozzle arrangement then in the four-nozzle arrangement. This observation, once again, reinforces the opinion that the use of more nozzles that are strategically placed provides improved performance.

A complete set of temperature boundary condition graphics for the single nozzle arrangement can be found in Appendix E.

V.4.3 Temperature Profiles

Viewing the thermal profiles at 1.10 seconds, one can already see the obvious geometric difference between the two cases. In Figures V.50 and V.51, the shape of the initially cooled region closely resembles the shape of the injection pattern. For the single nozzle case, the pattern is round and symmetric. For the four-nozzle case, the shape is elongated along the vertical axis. In Figures V.52 and V.53, at 1.25 seconds, the previously mentioned affects of gravity on the single nozzle case can clearly be seen as compared to the four-nozzle configuration. There is significant lower edge cooling and particulate fall-out over a wide region at the 1st thermocouple array for the single nozzle device. As we proceed along in our examination of these two cases, the overwhelming difference is the substantially cooler temperatures and regions along the pipe surfaces that

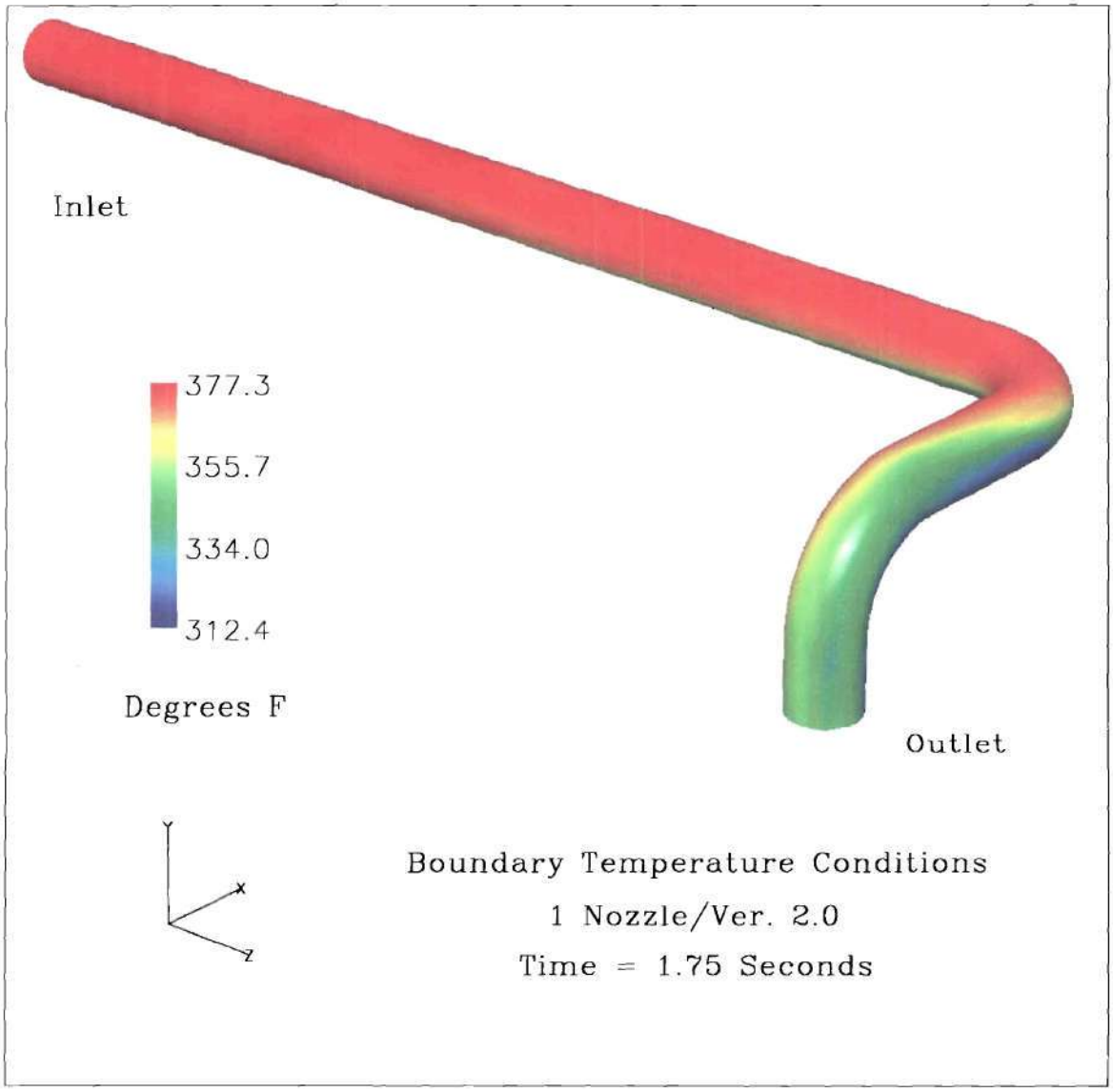
Inlet
377.3
355.7
334.0
312.4
Degrees F
Outlet
Y
X
Z
Boundary Temperature Conditions
1 Nozzle/Ver. 2.0
Time = 1.75 Seconds

Figure V.48

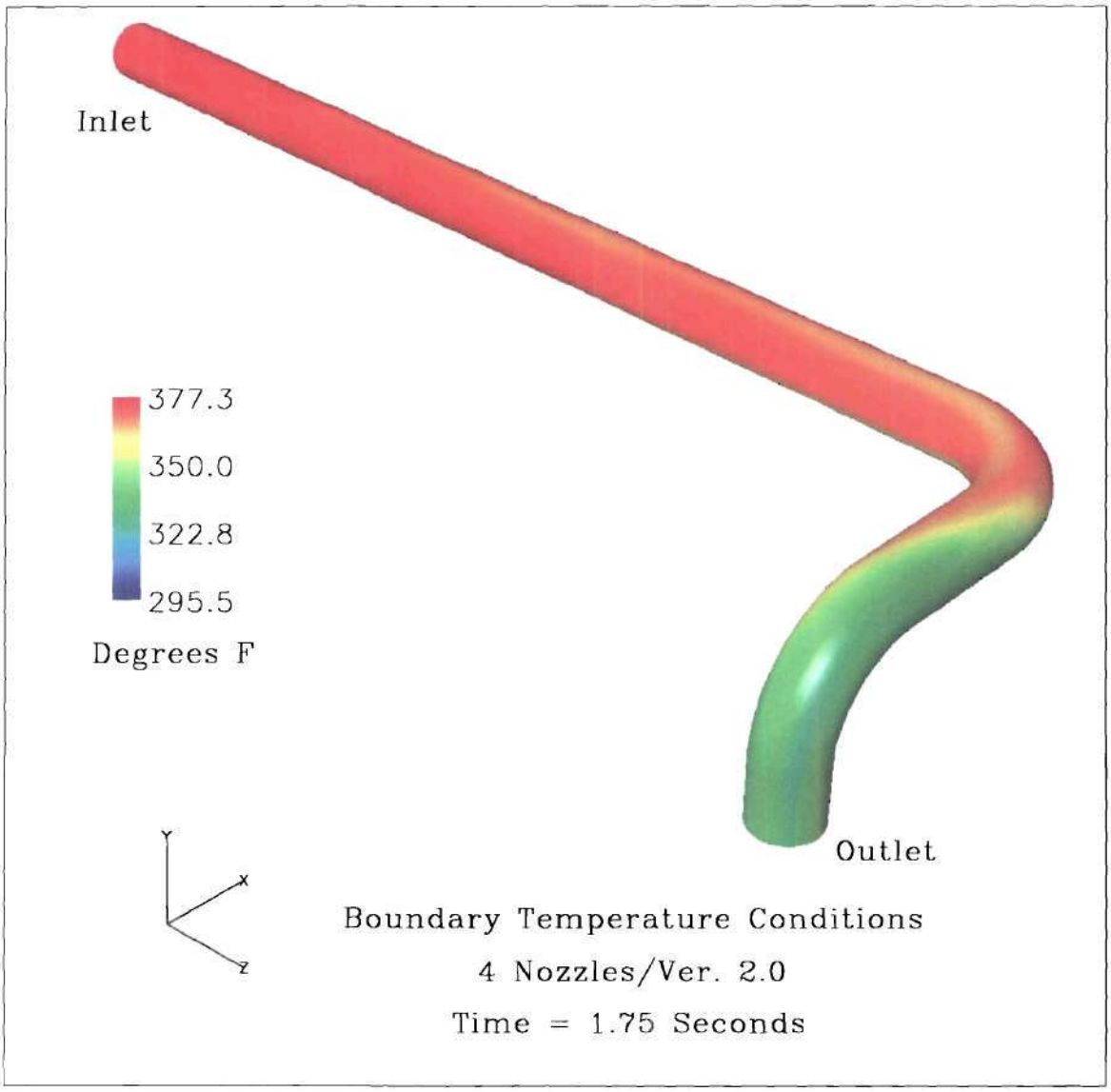
Inlet
377.3
350.0
322.8
295.5
Degrees F
Outlet
Boundary Temperature Conditions
4 Nozzles/Ver. 2.0
Time = 1.75 Seconds

Figure V.49

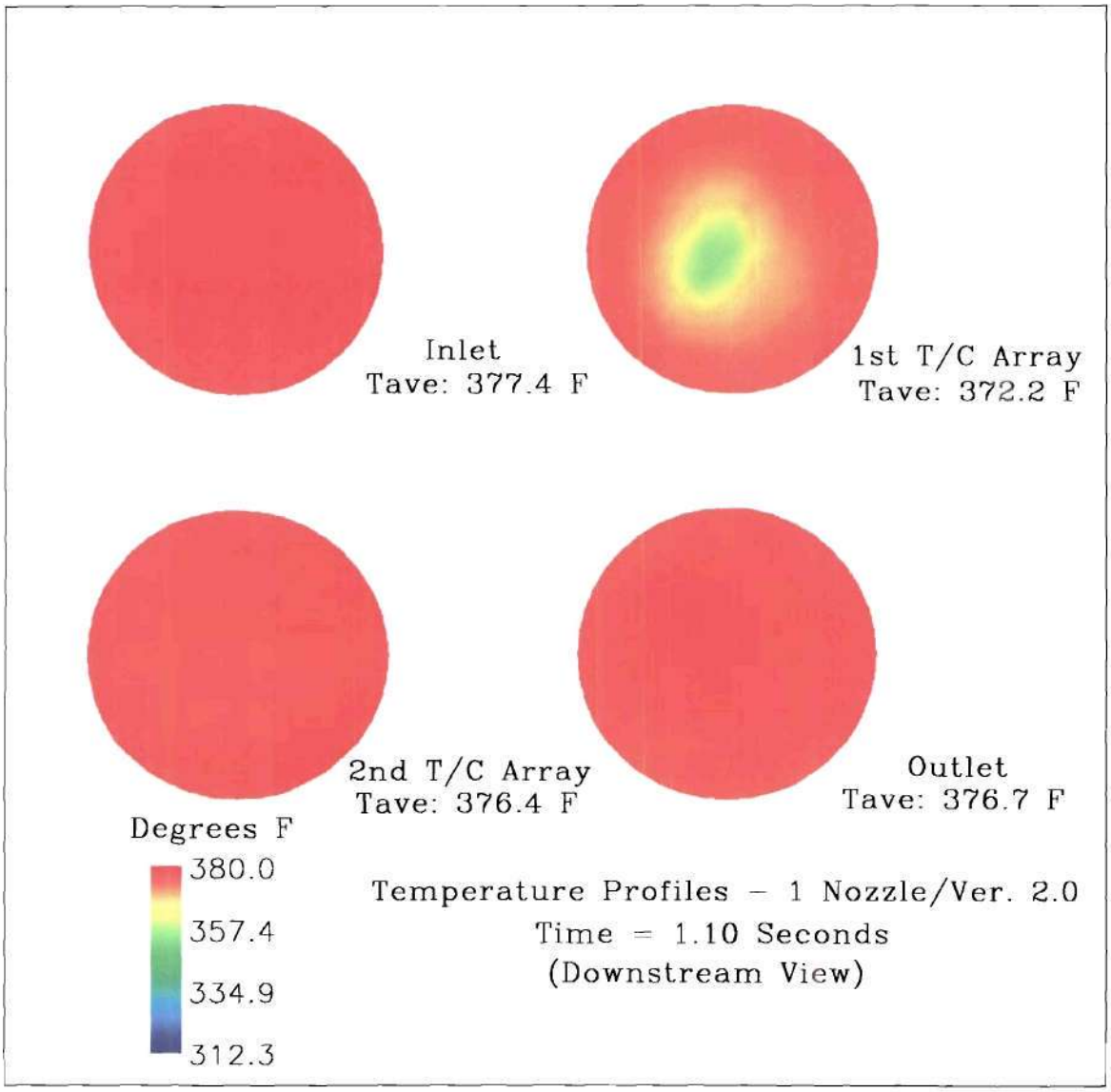
Inlet
Tave: 377.4 F
1st T/C Array
Tave: 372.2 F
2nd T/C Array
Tave: 376.4 F
Outlet
Tave: 376.7 F
Degrees F
380.0
357.4
334.9
312.3
Temperature Profiles - 1 Nozzle/Ver. 2.0
Time = 1.10 Seconds
(Downstream View)

Figure V.50

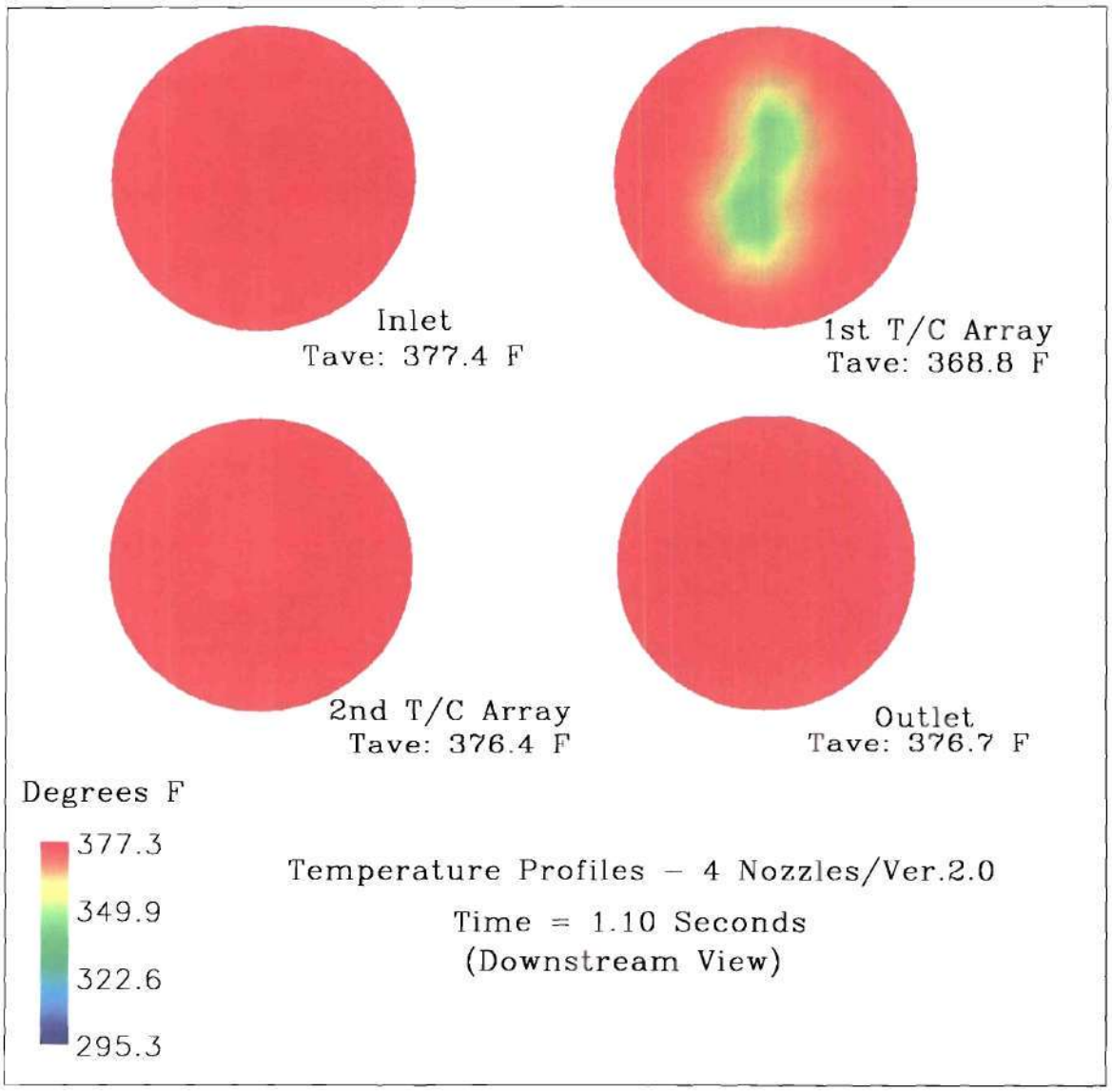
Inlet
Tave: 377.4 F
1st T/C Array
Tave: 368.8 F
2nd T/C Array
Tave: 376.4 F
Outlet
Tave: 376.7 F
Degrees F
377.3
349.9
322.6
295.3
Temperature Profiles - 4 Nozzles/Ver.2.0
Time = 1.10 Seconds
(Downstream View)

Figure V.51

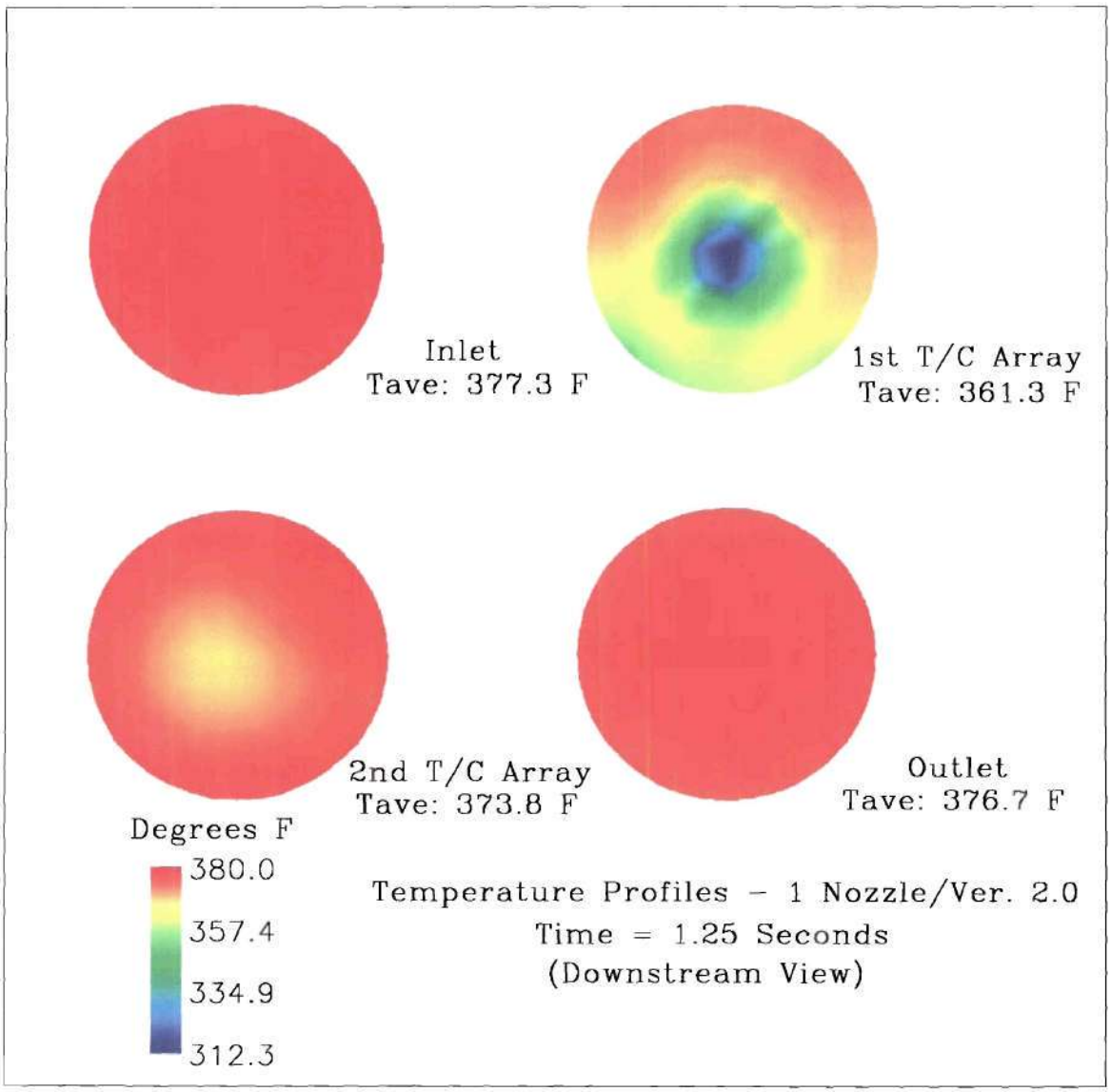
Inlet
Tave: 377.3 F
1st T/C Array
Tave: 361.3 F
2nd T/C Array
Tave: 373.8 F
Outlet
Tave: 376.7 F
Degrees F
380.0
357.4
334.9
312.3
Temperature Profiles - 1 Nozzle/Ver. 2.0
Time = 1.25 Seconds
(Downstream View)

Figure V.52

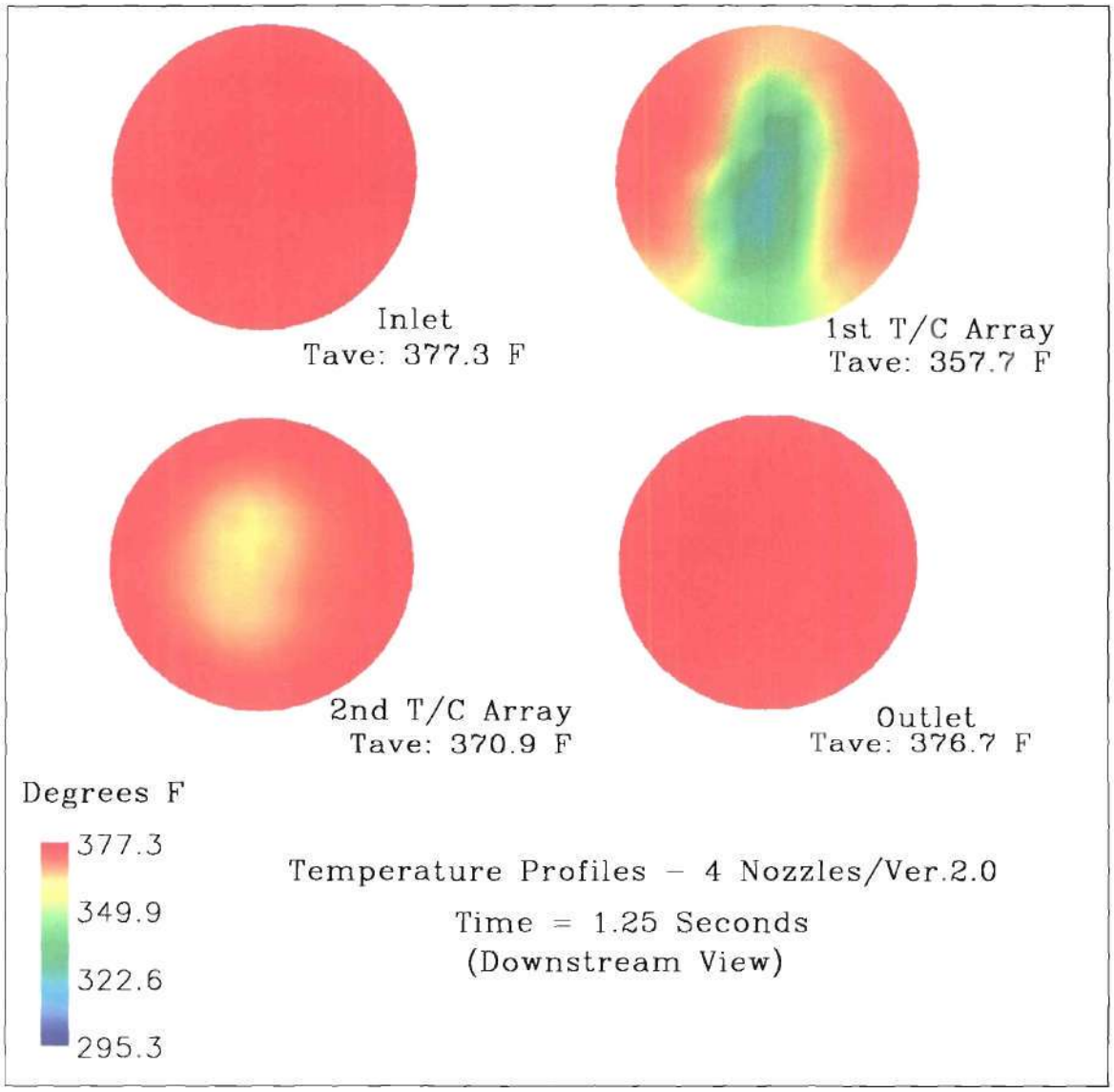
Inlet
Tave: 377.3 F
1st T/C Array
Tave: 357.7 F
2nd T/C Array
Tave: 370.9 F
Outlet
Tave: 376.7 F
Degrees F
377.3
349.9
322.6
295.3
Temperature Profiles - 4 Nozzles/Ver.2.0
Time = 1.25 Seconds
(Downstream View)

Figure V.53

would be most affected by momentum changes and forced fluid separation from the vapor. This is especially evident when viewing the temperature profiles at 1.75 seconds, see Figures, V.54 and V.55. The case using the single nozzle is 9.0° F warmer then the corresponding four-nozzle case, but yet has significantly more profiling in the lower temperature color regions.

A complete set of temperature profile graphics for the single nozzle arrangement can be found in Appendix E.

V.4.4 Spray Water Particle Flow

Figures V.56 and V.57 illustrate the initial spray pattern for each of the two cases as interpreted by the code at 0.85 seconds. Here, the advantages of the multiple nozzle arrangement can be clearly observed. The multiple nozzles far better support the general coverage of the cross-sectional flow area. Additionally, with the use of the smaller nozzles, the same mass flow can be introduced but in a smaller droplet size configuration. From the scale utilized, the single nozzle device produced a maximum droplet radius of $4.0e^{-2}$, more then 33% larger then the four-nozzle arrangement. This would equate to the four-nozzle device as providing 77% more surface area, based on radius alone, for heat transfer then the single nozzle arrangement.

As the ensuing graphic depictions of the spray water particle flows are examined for the single nozzle device, the comments previously mentioned and depicted in the thermal profiles are clearly evident. In Figures V.58 and V.59, time equals 1.45 seconds, the flow pattern differences for the two cases is quite evident. Of particular note is the lack of particles in the flow area just before the first elbow. When compared to the four-

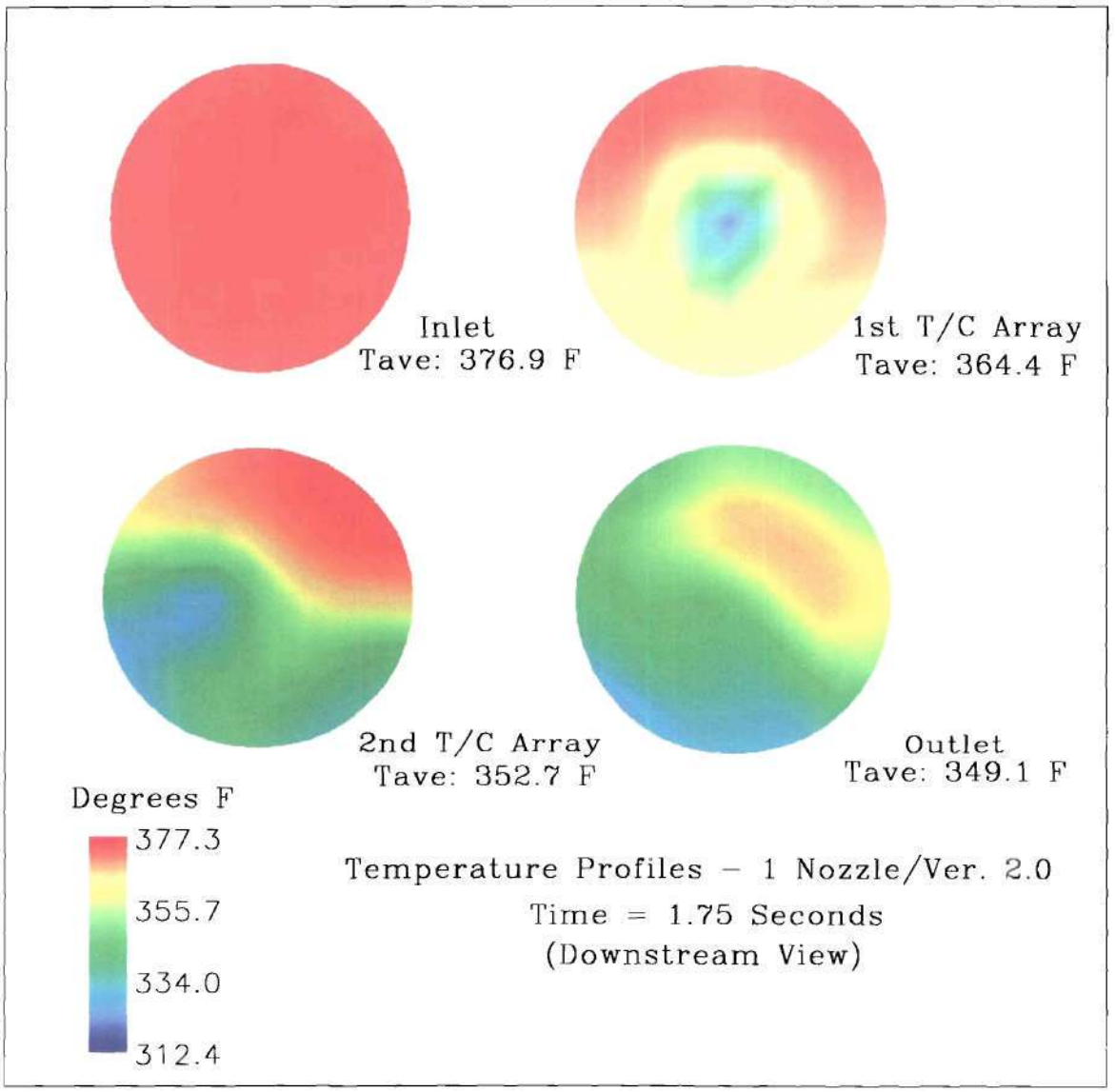
Inlet
Tave: 376.9 F
1st T/C Array
Tave: 364.4 F
2nd T/C Array
Tave: 352.7 F
Outlet
Tave: 349.1 F
Degrees F
377.3
355.7
334.0
312.4
Temperature Profiles - 1 Nozzle/Ver. 2.0
Time = 1.75 Seconds
(Downstream View)

Figure V.54

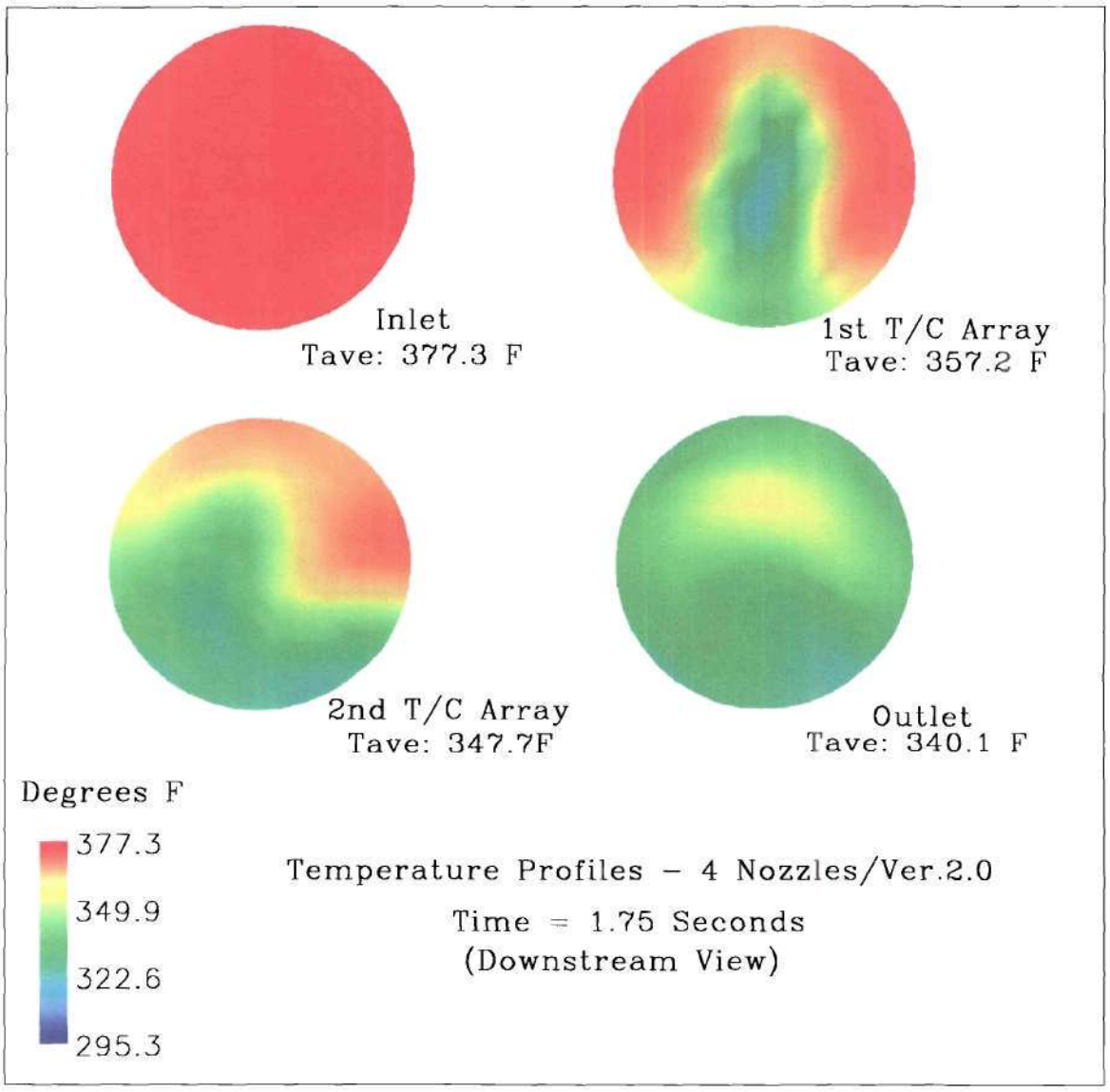
Inlet
Tave: 377.3 F
1st T/C Array
Tave: 357.2 F
2nd T/C Array
Tave: 347.7F
Outlet
Tave: 340.1 F
Degrees F
377.3
349.9
322.6
295.3
Temperature Profiles - 4 Nozzles/Ver.2.0
Time = 1.75 Seconds
(Downstream View)

Figure V.55

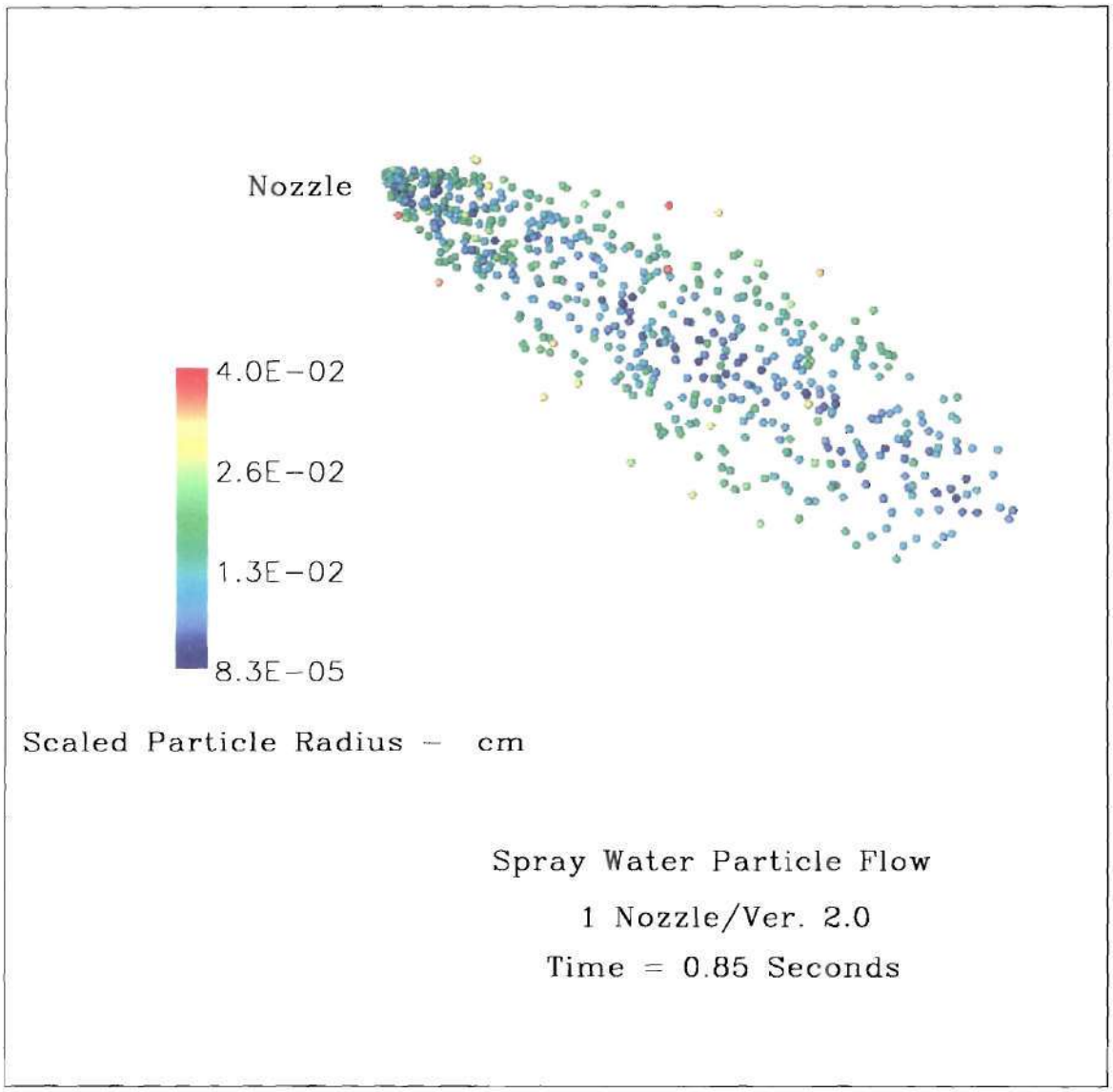
Nozzle
4.0E-02
2.6E-02
1.3E-02
8.3E-05
Scaled Particle Radius - cm
Spray Water Particle Flow
1 Nozzle/Ver. 2.0
Time = 0.85 Seconds

Figure V.56

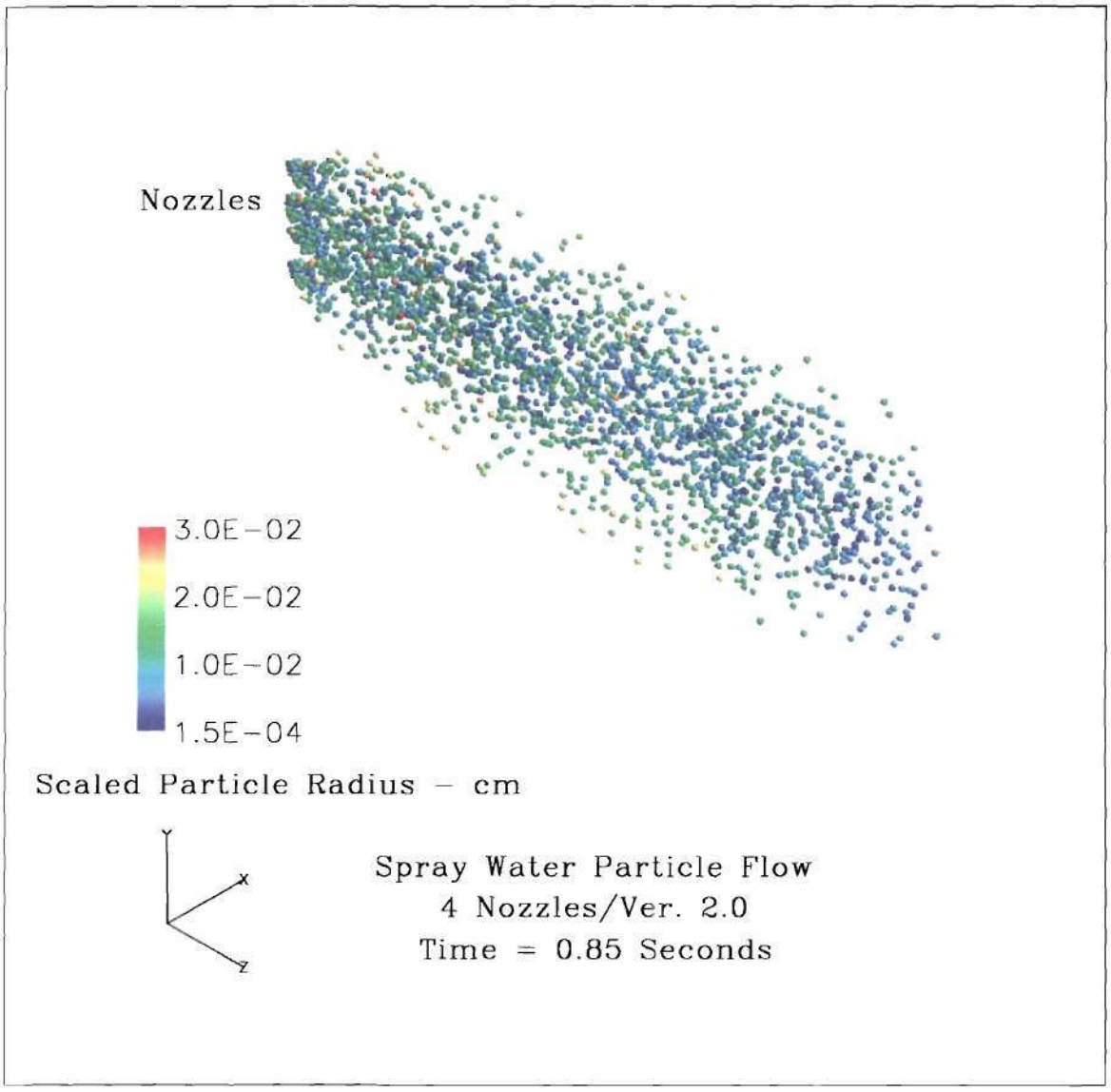
Nozzles
3.0E-02
2.0E-02
1.0E-02
1.5E-04
Scaled Particle Radius - cm
Y
X
Z
Spray Water Particle Flow
4 Nozzles/Ver. 2.0
Time = 0.85 Seconds

Figure V.57

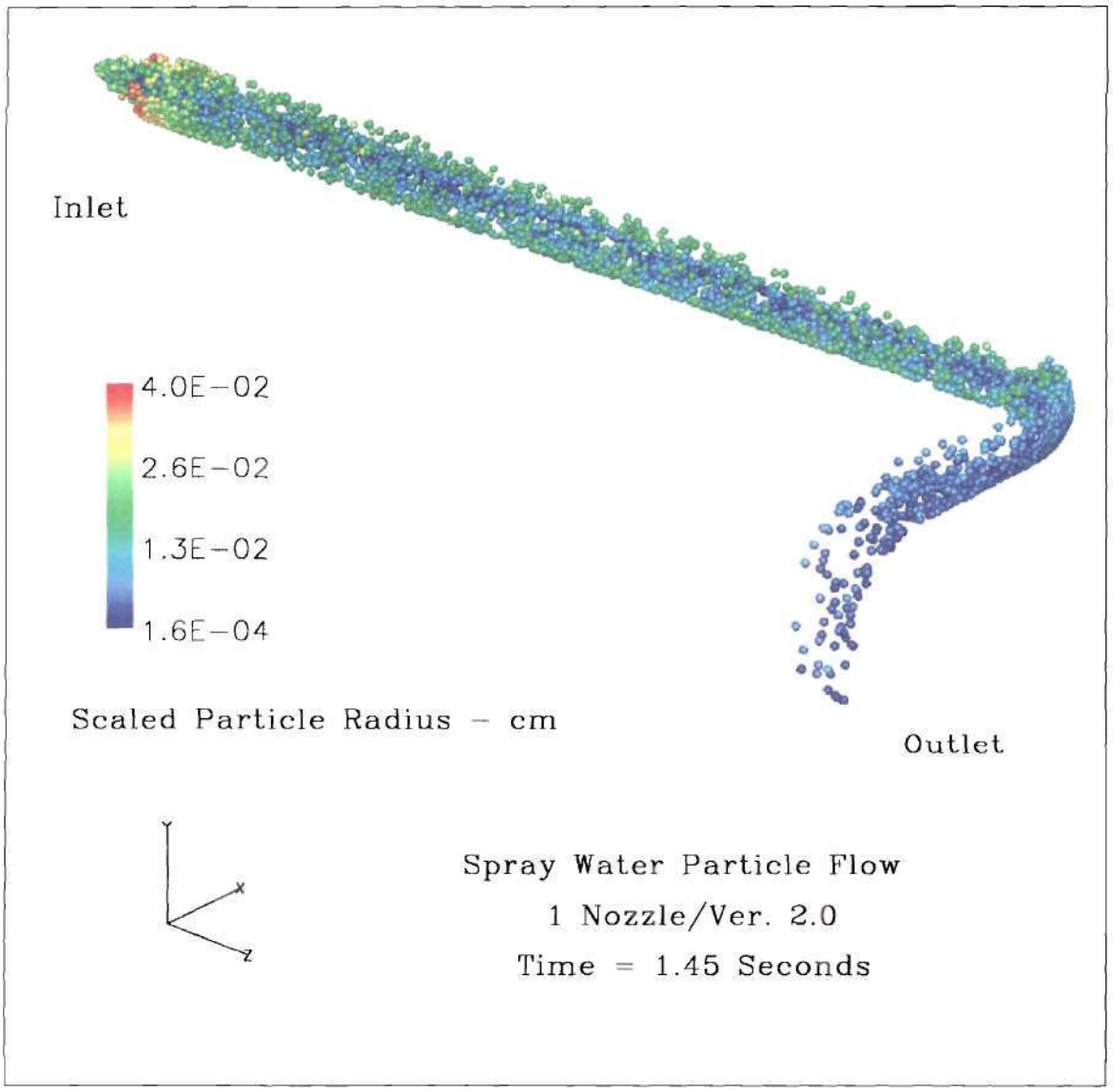
Inlet
4.0E-02
2.6E-02
1.3E-02
1.6E-04
Scaled Particle Radius - cm
Outlet
Y
X
Z
Spray Water Particle Flow
1 Nozzle/Ver. 2.0
Time = 1.45 Seconds

Figure V.58

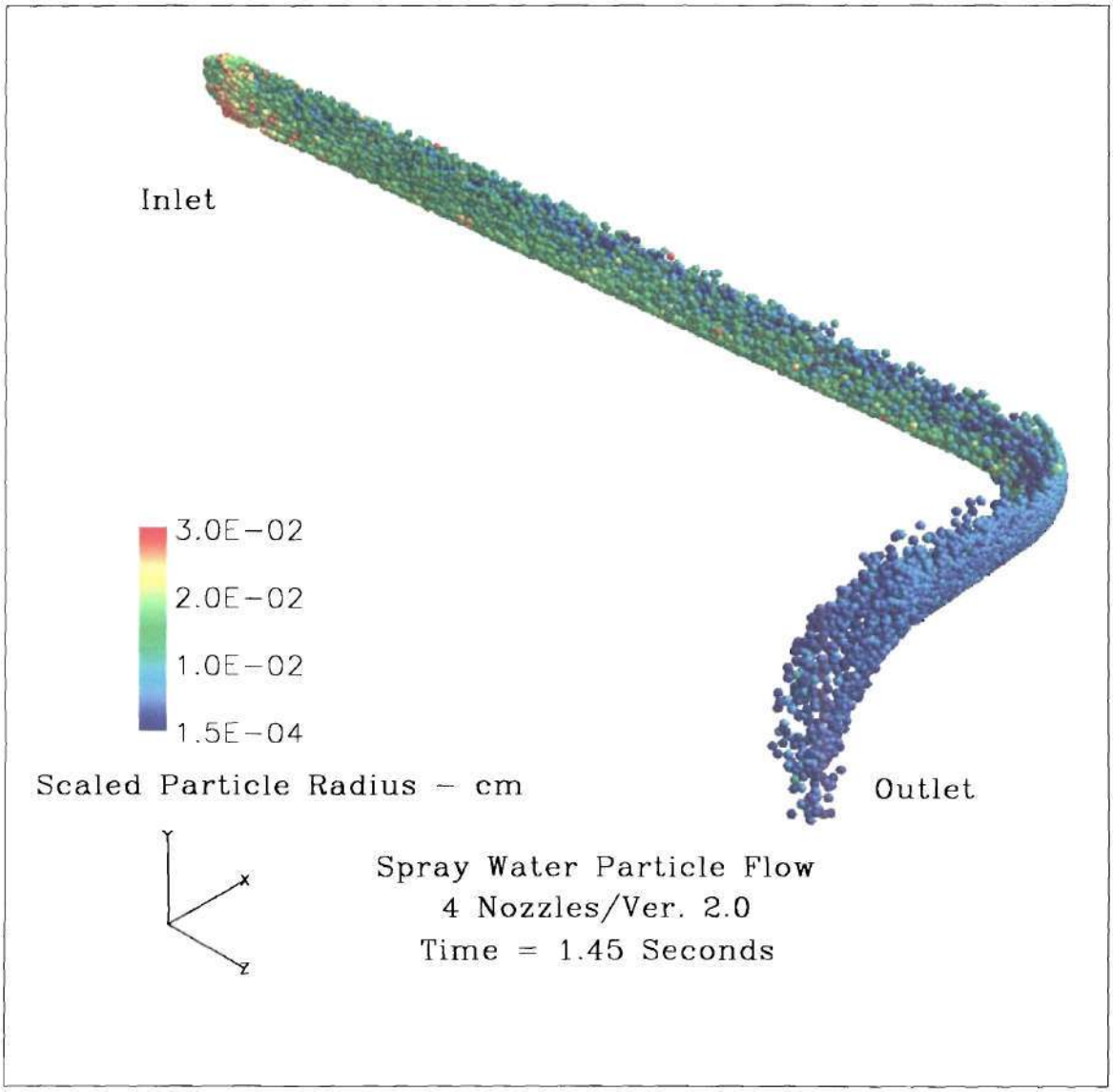
Inlet
3.0E-02
2.0E-02
1.0E-02
1.5E-04
Scaled Particle Radius - cm
Outlet
Spray Water Particle Flow
4 Nozzles/Ver. 2.0
Time = 1.45 Seconds

Figure V.59

nozzle arrangement, the single nozzle pipeline appears only half full. Likewise, the number and additional mass associated with the larger single nozzle has prevented them from progressing as far down the pipeline as with the four-nozzle arrangement. Even after steady state conditions are achieved, the density and distribution of the particles is far inferior for the single as compared to the multiple nozzle configurations.

V.4.5 Computational Temperature Data

In this section, the computational thermocouple outputs of the single nozzle device will be compared to the four-nozzle arrangement. The graphs used to relate the data are similar to the ones used in the previous analyses except for the elimination of actual readings. The specific thermocouple positions and nomenclature are the same as well, i.e., 1 to 6.

In Figure V.60, the results at the 1st thermocouple array can be seen. As expected, the variations at this point are slight and more related to the physical geometry of the device. Due to its symmetry on both axes, the single nozzle device provides a more evenly distributed thermal profile at all of the thermocouple positions. The four-nozzle configuration distorts the symmetry due to its placement of the nozzles along the vertical axis of the flow cross-section. This is clearly depicted when viewing positions 3 and 4. The vertical axis is considerably cooler for the four-nozzle arrangement but the horizontal axis is almost the same. This would indicate that the smaller flow particles, associated with the multiple nozzles, are better able to mix with the flowing steam vapor and evaporate more quickly. However, as we reach the center of the flow stream, position 6, both configurations appear to provide the same degree of temperature control.

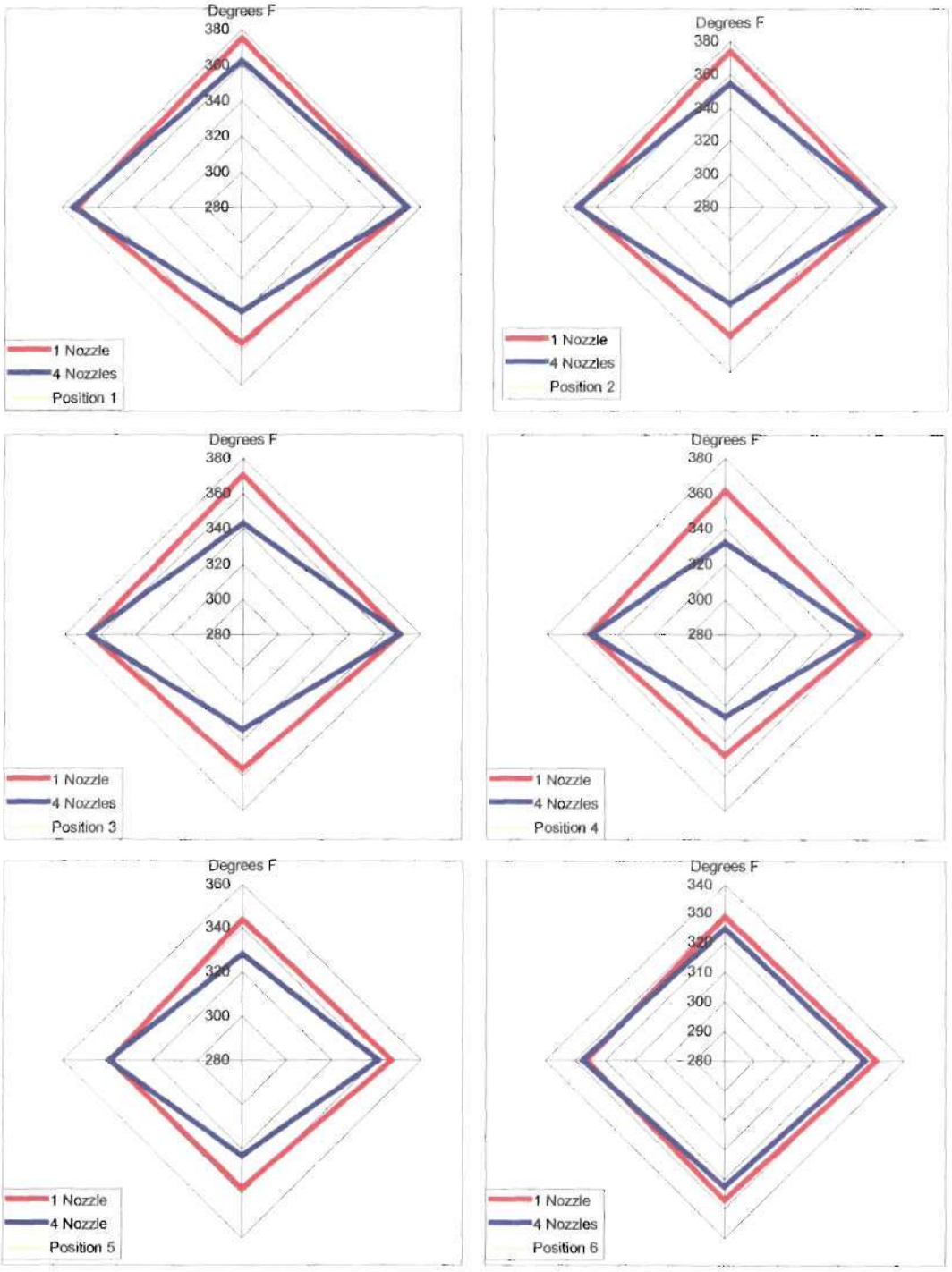

Comparison of Computational Thermocouple Readings - 1st Array, 1 Vs. 4 Nozzles, Version 2.0

Figure V.60

In Figure V.61, the results from the location of the 2nd thermocouple array can be examined. The four-nozzle arrangement appears to provide slightly better overall performance than does the single nozzle device. In almost every position, the calculated temperature of the multi-nozzle unit is lower than that for the single nozzle arrangement. The symmetry of the two configurations is surprising close, with only minor discrepancies noted in the vertical axis. The lower temperatures, along this axis, are associated with the four-nozzle unit's ability to provide a more distributed particle flow pattern across the flow area. In both configurations, the devices exhibit a common profile and illustrate the effects of fluid separation as a result of drag and directional flow changes. Thus, the left edge of the pipe is much cooler then the other surfaces due to water separation and build-up.

In general, the four-nozzle device did perform better, at least computationally, than the single nozzle configuration. The profiles were less erratic and the associated temperatures at fixed points were lower, thus confirming the validity of using more and smaller nozzles, within specific limits, as a means of achieving improved performance.

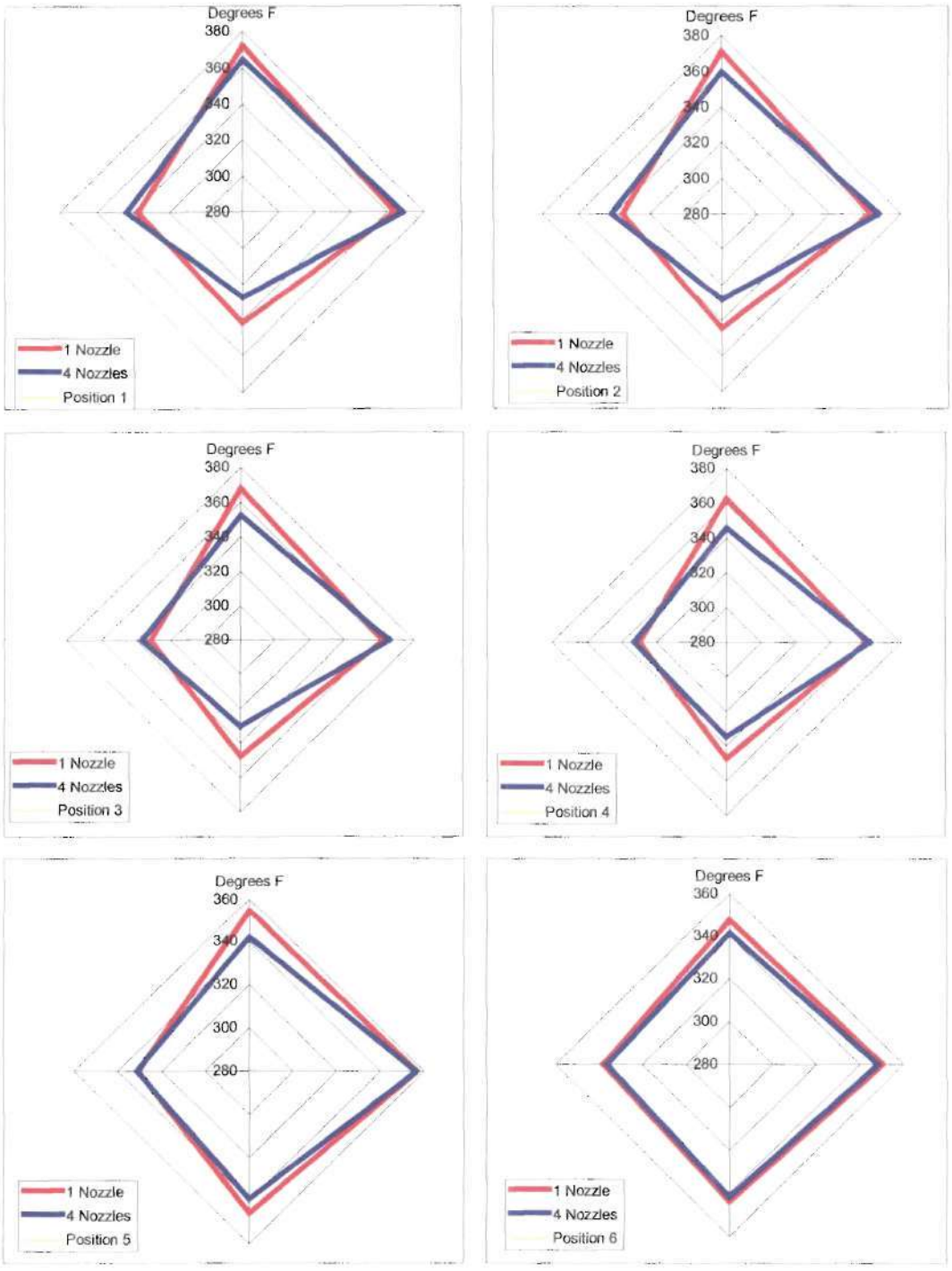

Comparison of Computational Thermocouple Readings - 2nd Array, 1 Vs. 4 Nozzles, Version 2.0

Figure V.61

CHAPTER VI

CONCLUSIONS AND RECOMMENDATIONS

VI.1 Introduction

An experimental and numerical investigation of evaporating water sprays injected into flowing superheated steam was conducted. The experimental phase of the investigation made use of the low-pressure steam turbine extraction system at the UNC-Chapel Hill Cogeneration Facility for the source of superheated steam flow. The pipeline itself was instrumented with an arrangement of 48 thermocouple placed both axially and radially. Their locations was selected so as to permit the measurement of steam temperatures at various locations along the length of the pipe as well as radially across the flow cross-section, i.e., both vertically and horizontally. The water sprays were created by the use of a self-contained water injection device. This device was configured in three different ways in order to measure and determine vaporization performance with respect to different injection parameters, such as injection nozzle location, spray particle size, spray pattern geometry & distribution, and nozzle size. Tests were then conducted while the injection device sprayed water into the flowing superheated flow stream. Measurements were continuously taken over the course of several days and with varying flow, pressure, and temperature conditions. The results were examined and plotted to illustrate the vaporization performance of each of the three devices within the experimental control volume.

The numerical portion of the investigation was conducted using the SteamCFD Code developed at Georgia Tech. The physical geometry of the UNC piping system was computationally generated and an appropriate grid for numerical analysis created. The input file for the program was loaded with data that modeled the performance of the injection device and the flowing conditions of the steam within the pipeline. This data included the spray water mass flow, the spray particle size, the spray injection velocity, cone angle, & thickness, inlet steam velocity, and steam temperature. The program was run until a steady state solution was achieved for each of the three nozzle configurations relative to the specific steam conditions that the experimental investigation experienced. The output data from the program was then computationally transformed into a graphical format for interpretation and analysis. The results of the numerical simulation were compared to the results obtained from the experimental cases.

VI.2 Conclusions

VI.2.1 Thermal Stratification

The results presented here clearly illustrate the thermal stratification phenomenon. Even within a highly turbulent compressible flow stream, there are regions that extend *axially for great lengths* where the steam temperature does not appreciably change. Even when disrupted by the presence of an elbow, these regions remain intact but are slowly reduced in size as the flow streams are homogenized mechanically rather than thermally. Depending on the pipe size, it is anticipated that it will take several more bends or flow disruptions before the flow stream reaches thermal equilibrium.

VI.2.2 Number of Nozzles

One of the premises for this paper was to examine ways of eliminating or reducing the effects of thermal stratification. One attempt was to change the operating parameters within the system by changing the size and number of nozzles being used to introduce the spray water. The premise was that the increased number of nozzles would improve spray pattern and generate smaller droplets to aid in vaporization. In this case, the number of nozzles was increased from one to four, and finally, to 28. The conclusion drawn here is that while the number of nozzles did improve the overall performance of the heat transfer process, a point of diminishing returns was achieved at which time further increases in the number of nozzles provided no further improvement in the vaporization rate.

In the two main cases, the 28 nozzle arrangement did provide better performance after the first elbow than did the unit with four nozzles. This may in fact bring into question the performance of the code itself as the earlier version of the code did a better job of emulating the experimental data then did the latter version that included the film model improvements.

VI.2.3 System Performance

Another premise of this project was to examine the desuperheating process and determine ways to improve its performance within normal piping constraints. As a result of this analysis, it is clear that many of the practices and estimations provided by the industry are insufficient to describe the process and evaluate its effectiveness. The goal in the specific system examined here was to reduce the steam temperature to 317° F at the

outlet of the pipe. The best that was achieved was nearly 23° F short of this mark. The degree and complexity of the process dynamics goes well beyond the scope of this one example, but important information was still gathered for future enhancement. This includes the size and numbers of nozzles, large pipeline dynamics, the impact of flow disruptions, and vaporization rates of injected particulate of known physical characteristics.

VI.3 Recommendations

VI.3.1 Spray Nozzle Data

While the experimental data proved that the physical changes in the system were insufficient to significantly improve the operating performance of the system, the computational model was able to simulate the nozzle performance. This included inputting the Sauter Mean Radius of the particles formed and then using a fixed function to determine their distribution within the pipeline. In order obtain better results, more analysis and measurements of the respective nozzles must be conducted to create more detailed and realistic models of the nozzles.

VI.3.2 SteamCFD Code

Clearly, Version 2.0 of the SteamCFD Code showed greater robustness and more stable operation then the earlier Version 1.2. However, as already mentioned, additional changes in the code must be investigated relative to nozzle descriptions and performance parameters. In addition, it would be interesting to run these problems again but with a finer grid. In this way, more details of particulate flow and thermal changes could be monitored, especially in the regions in close proximity to the elbows and the

thermocouples. Additionally, more cases need to be run using alternate nozzle geometry's, nozzle types, as well as water temperatures and possibly nozzle flow direction.

VI.3.3 Temperature Measurements

From the data collected, it is obvious that the thermocouples are not the best choice for measuring the temperature of the flowing particle-laden steam flow. In the future, alternate means of determining the vapor temperature within the two-phase mixture must be determined. Recent advances by several companies into creating a device that can actually record steam qualities may be substituted for the thermocouples once they are completely developed and become commercially available.

APPENDIX A

EXPERIMENTAL DATA FOR CASE 1

Graphical representations of experimental data collected from the UNC Cogeneration Facility. This data is restricted to the time period of 1170-1200 minutes elapsed time from midnight on October 30, 2000. The data in this time increment was used to develop the input conditions for the computational analysis for the one and four nozzle desuperheater configurations. It was also used in both versions of the SteamCFD Code.

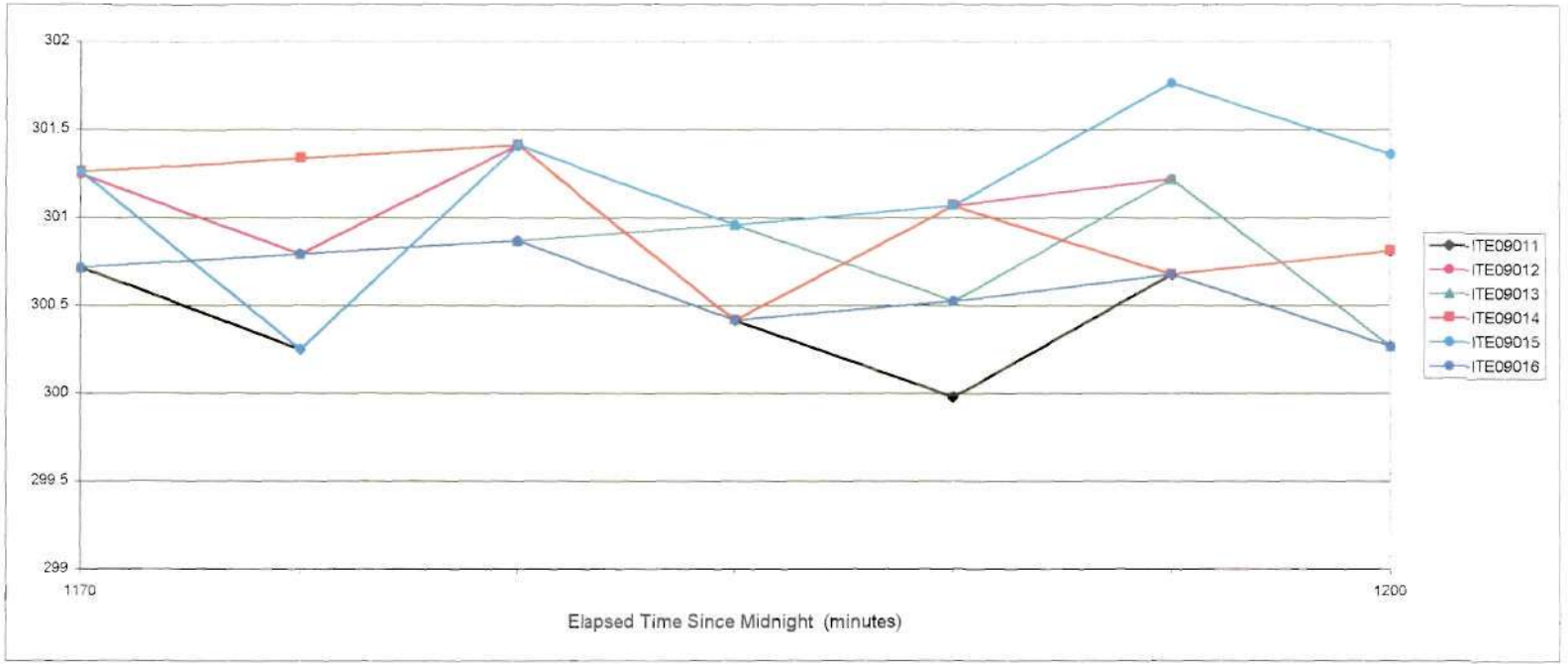

Zoom
Scroll

Data from file:
C:\Old Data Files\Tecra 750CDT\C-Drive\My Docu

Turn series ON/OFF

Select Y-Axis PRI/SEC

\10-30tc

Series 1	ITE09011	Temperature - Con-Tek radial probe, station 1, element 1	F	22	
Series 2	ITE09012	Temperature - Con-Tek radial probe, station 1, element 2	F	23	
Series 3	ITE09013	Temperature - Con-Tek radial probe, station 1, element 3	F	24	
Series 4	ITE09014	Temperature - Con-Tek radial probe, station 1, element 4	F	25	
Series 5	ITE09015	Temperature - Con-Tek radial probe, station 1, element 5	F	26	
Series 6	ITE09016	Temperature - Con-Tek radial probe, station 1, element 6	F	27	

Autoscale state: ON

Min / Max: 30(35(update

Time Units:

Notes on autoscaling.

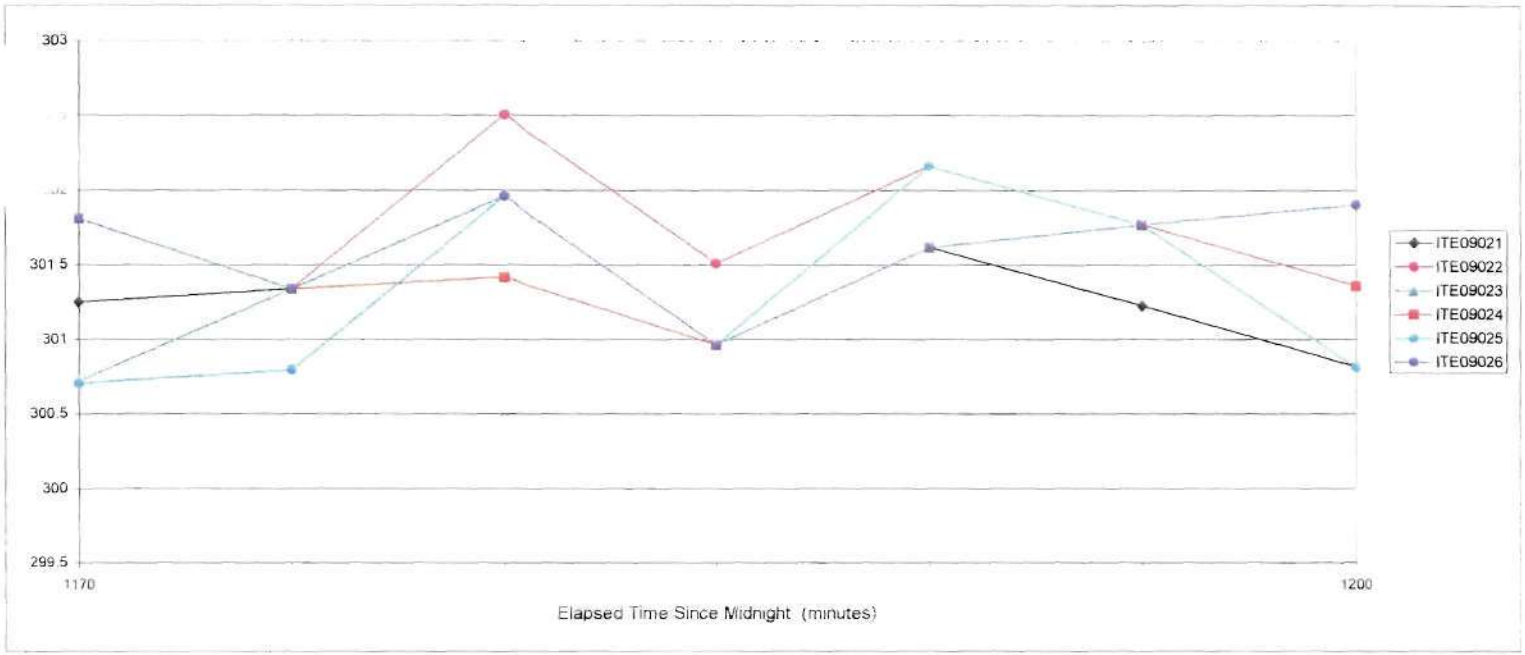

Zoom
Scroll

Data from file:
C:\Old Data Files\Tecra 750CDT\C-Drive\My Docur

					Turn series ON/OFF	Select Y-Axis PRI/SEC
Series 1	ITE09021	Temperature - Con-Tek radial probe, station 2, element 1	F	28		
Series 2	ITE09022	Temperature - Con-Tek radial probe, station 2, element 2	F	29		
Series 3	ITE09023	Temperature - Con-Tek radial probe, station 2, element 3	F	30		
Series 4	ITE09024	Temperature - Con-Tek radial probe, station 2, element 4	F	31		
Series 5	ITE09025	Temperature - Con-Tek radial probe, station 2, element 5	F	32		
Series 6	ITE09026	Temperature - Con-Tek radial probe, station 2, element 6	F	33		

Autoscale state: ON

Min / Max

Time Units: Minutes

Notes on autoscaling.

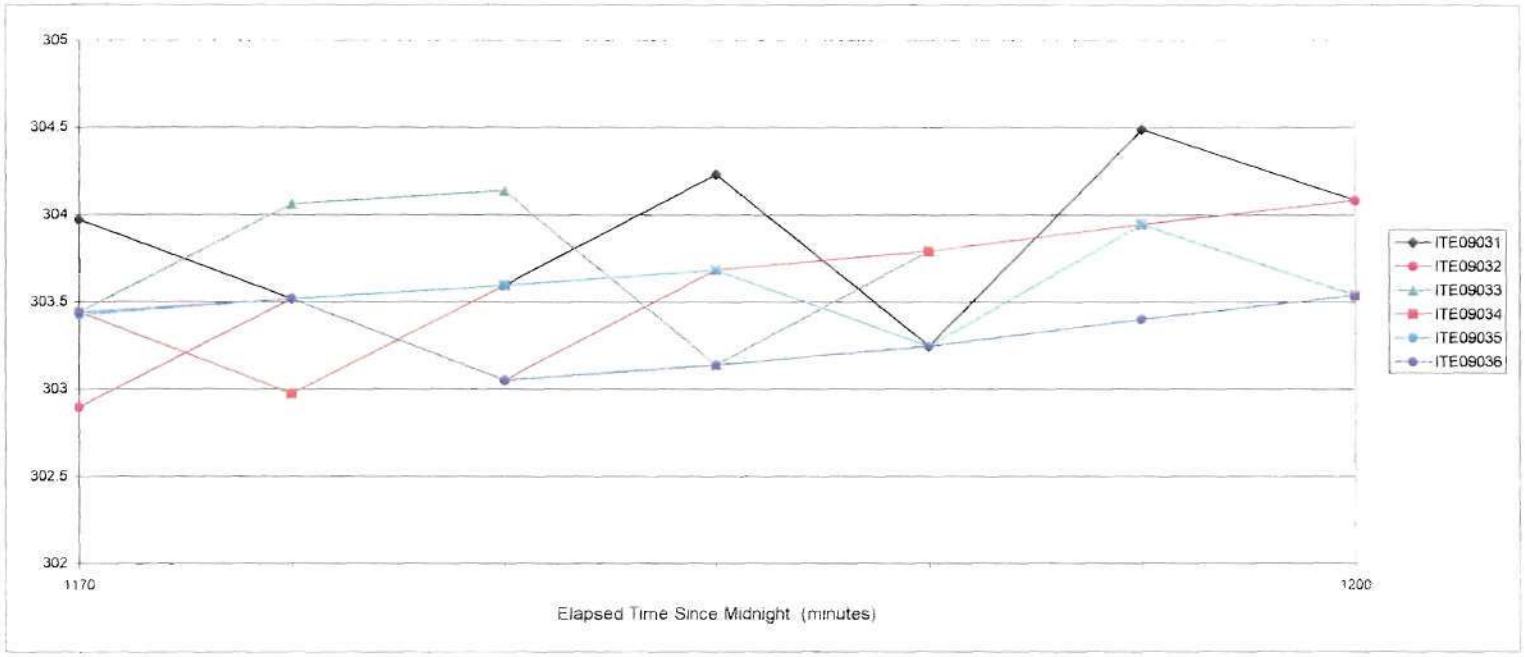

Zoom
Scroll

Data from file: C:\Old Data Files\Tecra 750CDT\C-Drive\My Docur

Turn series ON/OFF

Select Y-Axis PRI/SEC

Series 1	ITE09031	Temperature - Con-Tek radial probe, station 3, element 1	F	34	10-30to1		
Series 2	ITE09032	Temperature - Con-Tek radial probe, station 3, element 2	F	35			
Series 3	ITE09033	Temperature - Con-Tek radial probe, station 3, element 3	F	36			
Series 4	ITE09034	Temperature - Con-Tek radial probe, station 3, element 4	F	37			
Series 5	ITE09035	Temperature - Con-Tek radial probe, station 3, element 5	F	38			
Series 6	ITE09036	Temperature - Con-Tek radial probe, station 3, element 6	F	39			

Autoscale state: ON

Min / Max: 300 355 Update

Time Units: Minutes

Notes on autoscaling

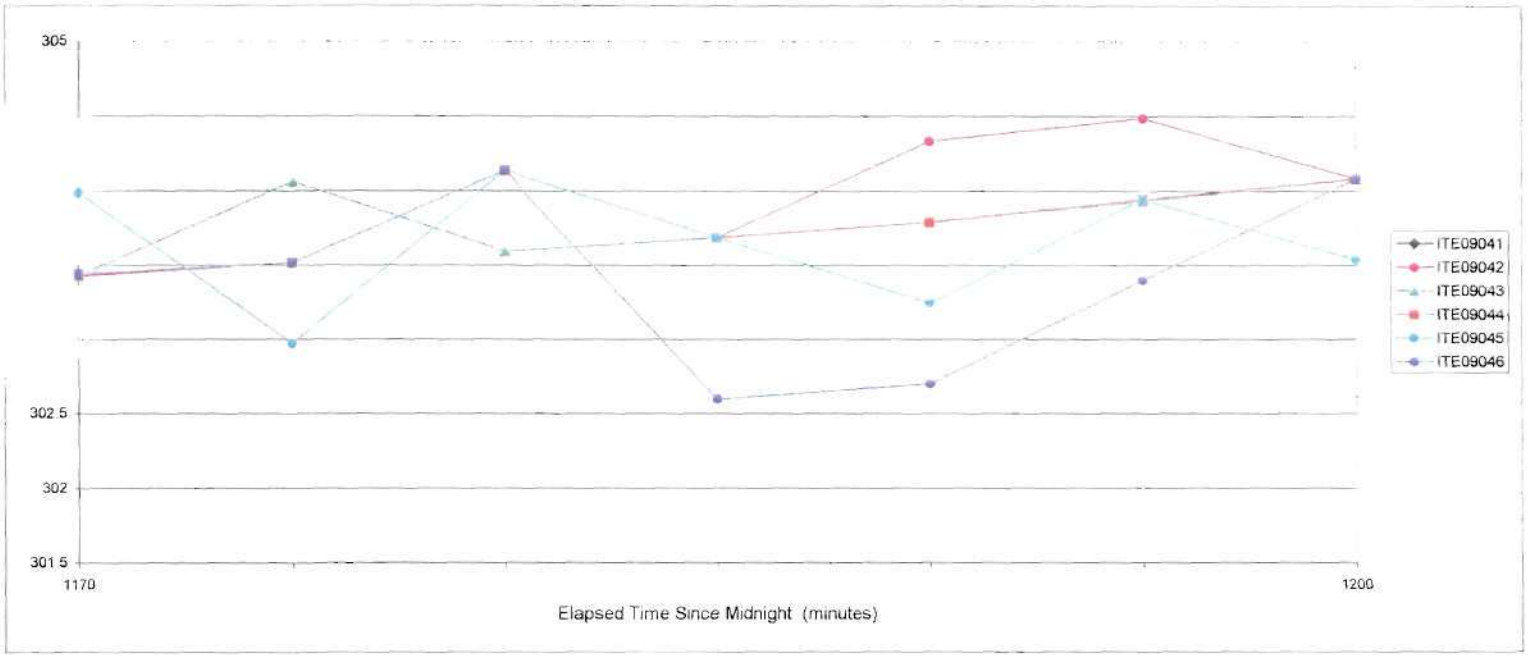

Zoom
Scroll

Data from file:
C:\Old Data Files\Tecra 750CDT\C-Drive\My Docur

Turn series ON/OFF

Select Y-Axis PRI/SEC

10-30to1

Series 1	ITE09041	Temperature - Con-Tek radial probe, station 4, element 1	F	40			
Series 2	ITE09042	Temperature - Con-Tek radial probe, station 4, element 2	F	41			
Series 3	ITE09043	Temperature - Con-Tek radial probe, station 4, element 3	F	42			
Series 4	ITE09044	Temperature - Con-Tek radial probe, station 4, element 4	F	43			
Series 5	ITE09045	Temperature - Con-Tek radial probe, station 4, element 5	F	44			
Series 6	ITE09046	Temperature - Con-Tek radial probe, station 4, element 6	F	45			

Autoscale state: ON

Min / Max

Time Units: Minutes

Notes on autoscaling

OCT 31 2000

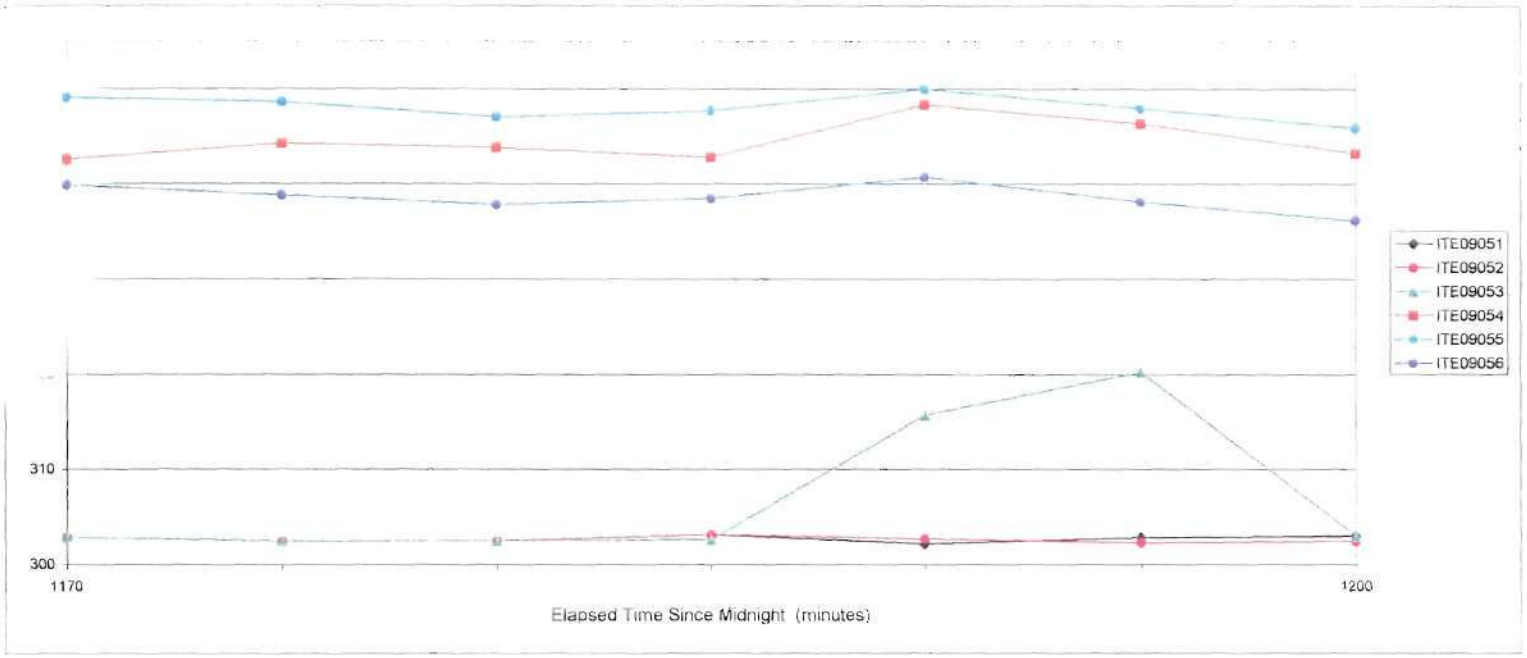

Zoom
Scroll

Data from file
C:\Old Data Files\Tecra 750CDT\C-Drive\My Docur

					Turn series ON/OFF	Select Y-Axis PRI/SEC
Series 1	ITE09051	Temperature - Con-Tek radial probe, station 5, element 1	F	46		
Series 2	ITE09052	Temperature - Con-Tek radial probe, station 5, element 2	F	47		
Series 3	ITE09053	Temperature - Con-Tek radial probe, station 5, element 3	F	48		
Series 4	ITE09054	Temperature - Con-Tek radial probe, station 5, element 4	F	49		
Series 5	ITE09055	Temperature - Con-Tek radial probe, station 5, element 5	F	50		
Series 6	ITE09056	Temperature - Con-Tek radial probe, station 5, element 6	F	51		

Autoscale state: OFF
Min / Max: 300 | 355 Update
Time Units: Minutes
Notes on autoscaling

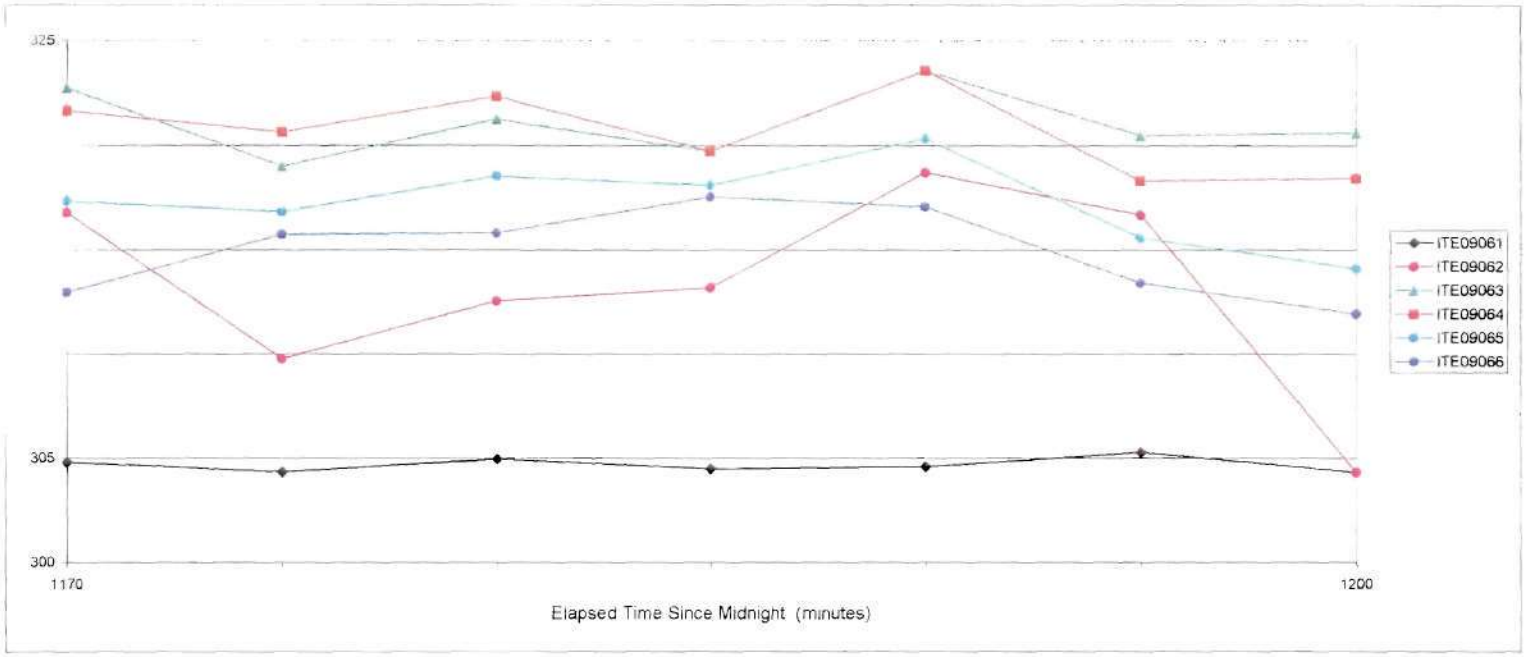

Zoom
Scroll

Data from file: C:\Old Data Files\Tecra 750CDT\C-Drive\My Docur

					Turn series ON/OFF	Select Y-Axis PRI/SEC
Series 1	ITE09061	Temperature - Con-Tek radial probe, station 6, element 1	F	52	N	10-30to1
Series 2	ITE09062	Temperature - Con-Tek radial probe, station 6, element 2	F	53		
Series 3	ITE09063	Temperature - Con-Tek radial probe, station 6, element 3	F	54		
Series 4	ITE09064	Temperature - Con-Tek radial probe, station 6, element 4	F	55		
Series 5	ITE09065	Temperature - Con-Tek radial probe, station 6, element 5	F	56		
Series 6	ITE09066	Temperature - Con-Tek radial probe, station 6, element 6	F	57		

Autoscale state: OFF Min / Max: 300 325 Update

Time Units: Minutes

Notes on autoscaling

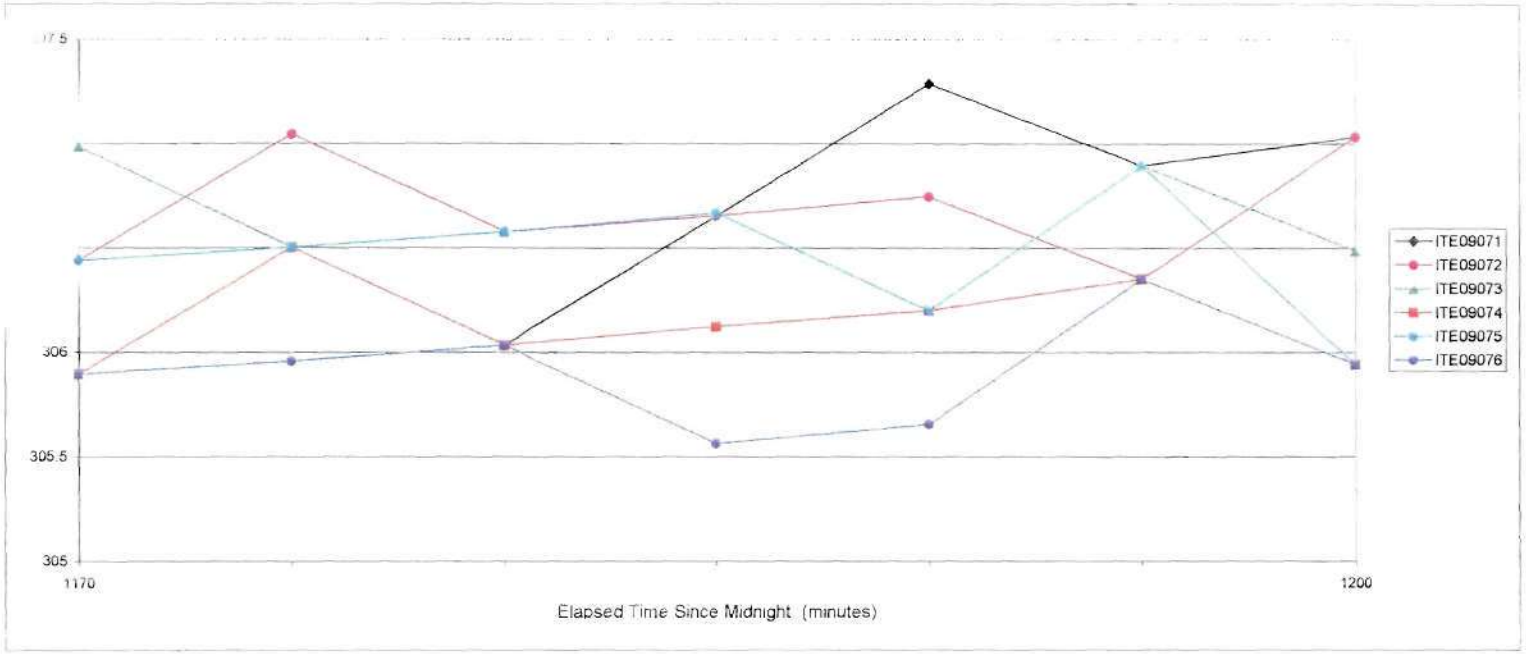

Zoom
Scroll

Data from file:
C:\Old Data Files\Tecra 750CDT\C-Drive\My Docur

					Turn series ON/OFF	Select Y-Axis PRI/SEC
Series 1	ITE09071	Temperature - Con-Tek radial probe, station 7, element 1	F	58		
Series 2	ITE09072	Temperature - Con-Tek radial probe, station 7, element 2	F	59		
Series 3	ITE09073	Temperature - Con-Tek radial probe, station 7, element 3	F	60		
Series 4	ITE09074	Temperature - Con-Tek radial probe, station 7, element 4	F	61		
Series 5	ITE09075	Temperature - Con-Tek radial probe, station 7, element 5	F	62		
Series 6	ITE09076	Temperature - Con-Tek radial probe, station 7, element 6	F	63		

Autoscale state: OFF
Min / Max: 305
Update

Time Units: Minutes

Notes on autoscaling

OCT 31 2000

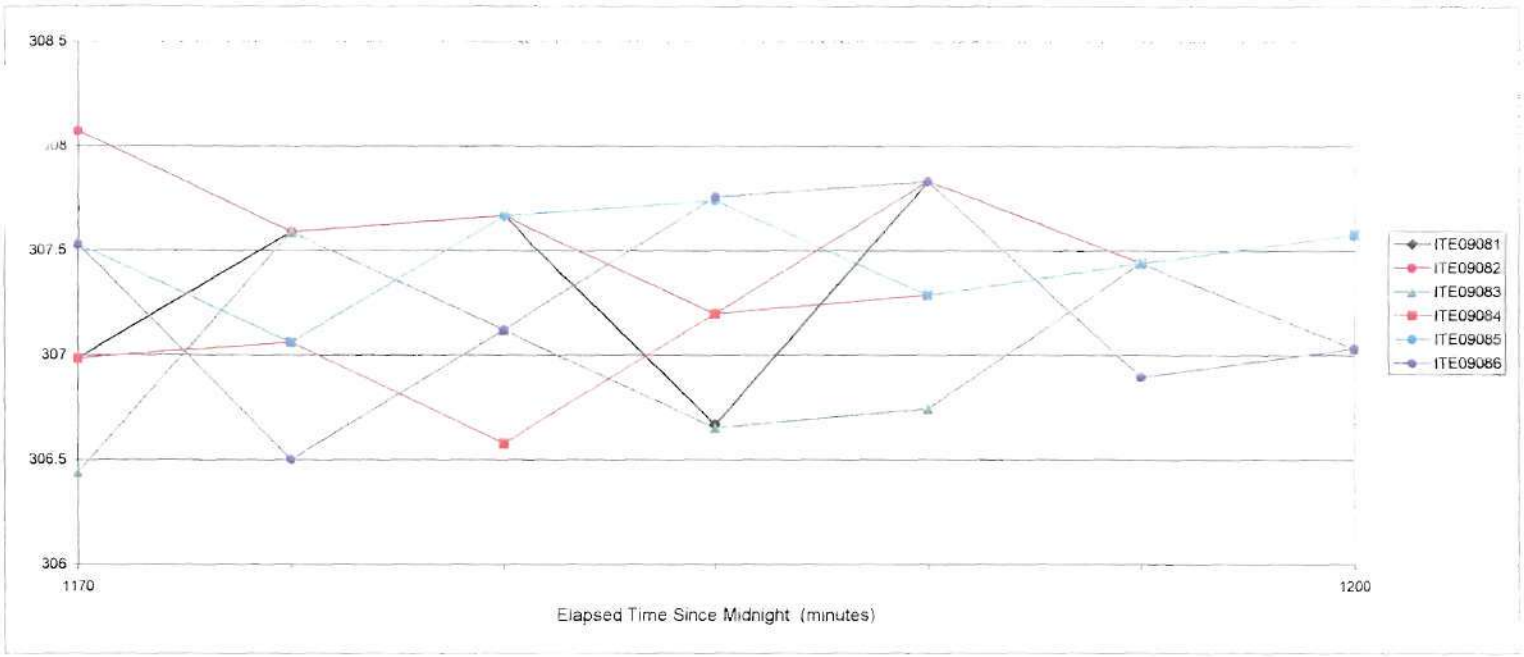

Zoom
Scroll

Data from file:
C:\Old Data Files\Tecra 750CDT\C-Drive\My Docur

Turn series ON/OFF

Select Y-Axis

Series 1	ITE09081	Temperature - Con-Tek radial probe, station 8, element 1	F	64			
Series 2	ITE09082	Temperature - Con-Tek radial probe, station 8, element 2	F	65			
Series 3	ITE09083	Temperature - Con-Tek radial probe, station 8, element 3	F	66			
Series 4	ITE09084	Temperature - Con-Tek radial probe, station 8, element 4	F	67			
Series 5	ITE09085	Temperature - Con-Tek radial probe, station 8, element 5	F	68			
Series 6	ITE09086	Temperature - Con-Tek radial probe, station 8, element 6	F	69			

Autoscale state: OFF

Min / Max: 306

Update

Time Units: Minutes

Notes on autoscaling

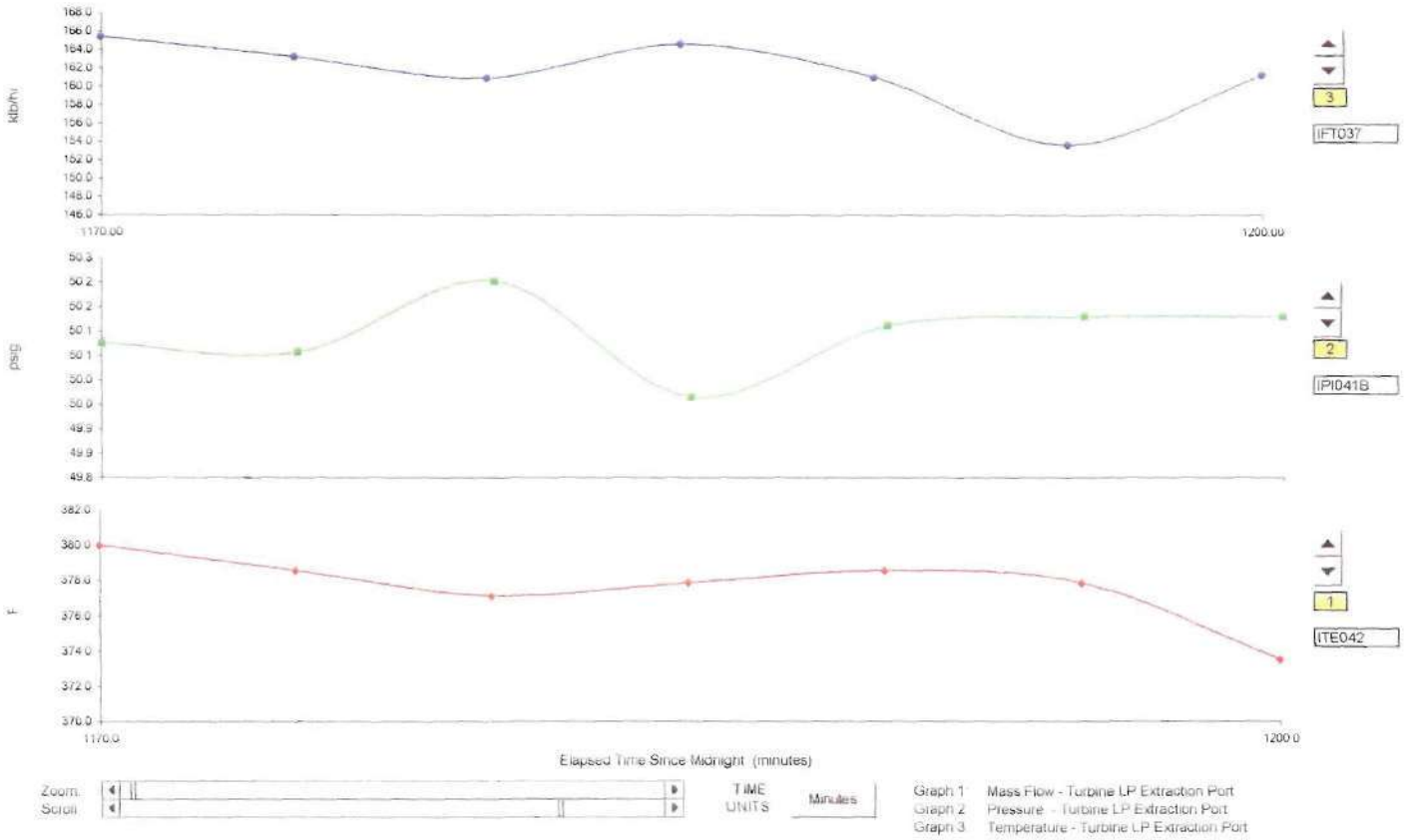
klb/hr
168.0
166.0
164.0
162.0
160.0
158.0
156.0
154.0
152.0
150.0
148.0
146.0
1170.00
1200.00
3
IFT037
psig
50.3
50.2
50.2
50.1
50.1
50.0
50.0
49.9
49.9
49.8
2
IPI041B
F
382.0
380.0
378.0
376.0
374.0
372.0
370.0
1170.0
1200.0
1
ITE042
Elapsed Time Since Midnight (minutes)
Zoom
Scroll
TIME UNITS
Minutes
Graph 1 Mass Flow - Turbine LP Extraction Port
Graph 2 Pressure - Turbine LP Extraction Port
Graph 3 Temperature - Turbine LP Extraction Port

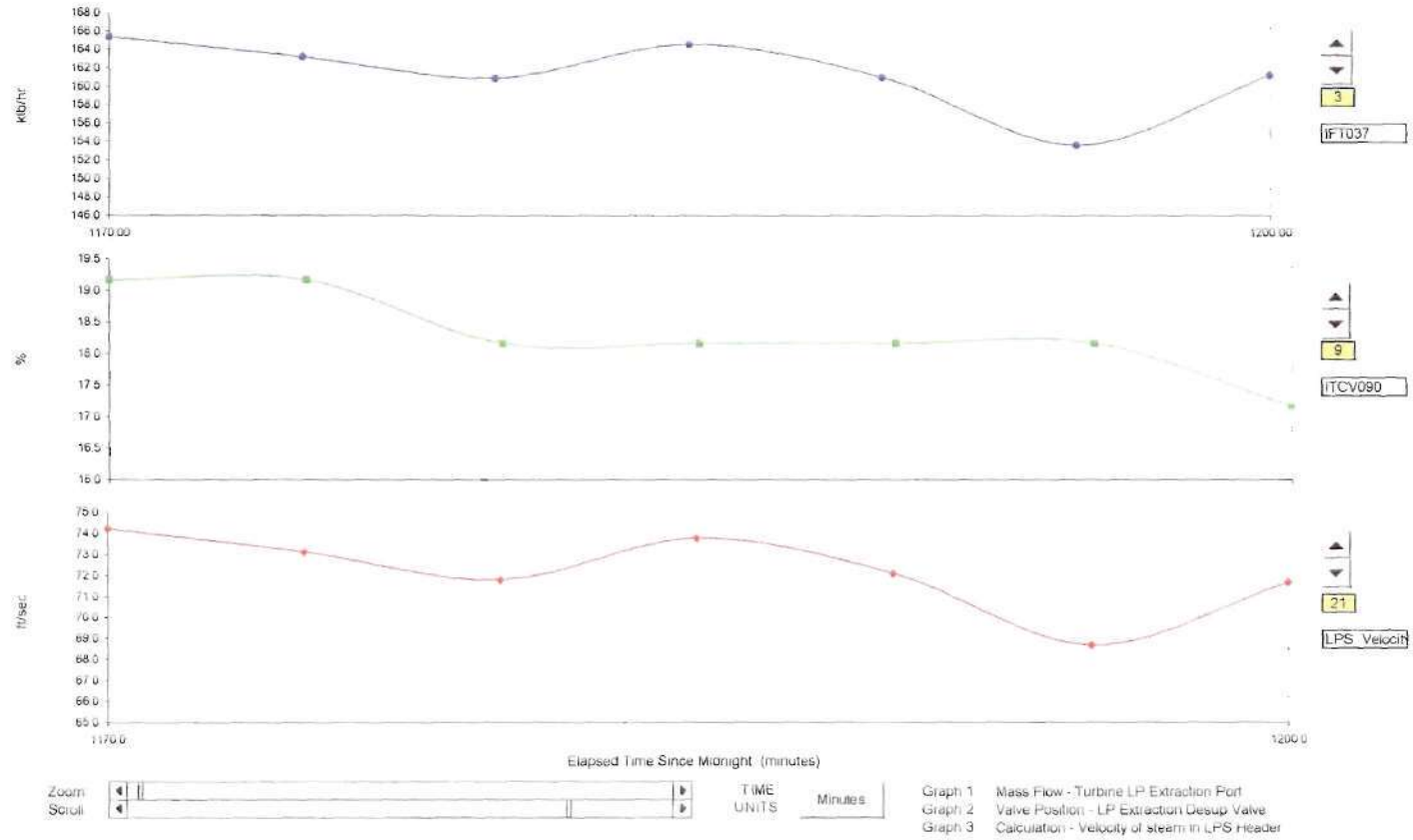
Klb/hr
168.0
166.0
164.0
162.0
160.0
158.0
156.0
154.0
152.0
150.0
148.0
146.0
1170.00
1200.00
3
IFT037
%
19.5
19.0
18.5
18.0
17.5
17.0
16.5
16.0
9
ITCV090
ft/sec
75.0
74.0
73.0
72.0
71.0
70.0
69.0
68.0
67.0
66.0
65.0
1170.0
1200.0
21
LPS_Velocity
Elapsed Time Since Midnight (minutes)
Zoom
Scroll
TIME UNITS
Minutes
Graph 1 Mass Flow - Turbine LP Extraction Port
Graph 2 Valve Position - LP Extraction Desup Valve
Graph 3 Calculation - Velocity of Steam in LPS Header

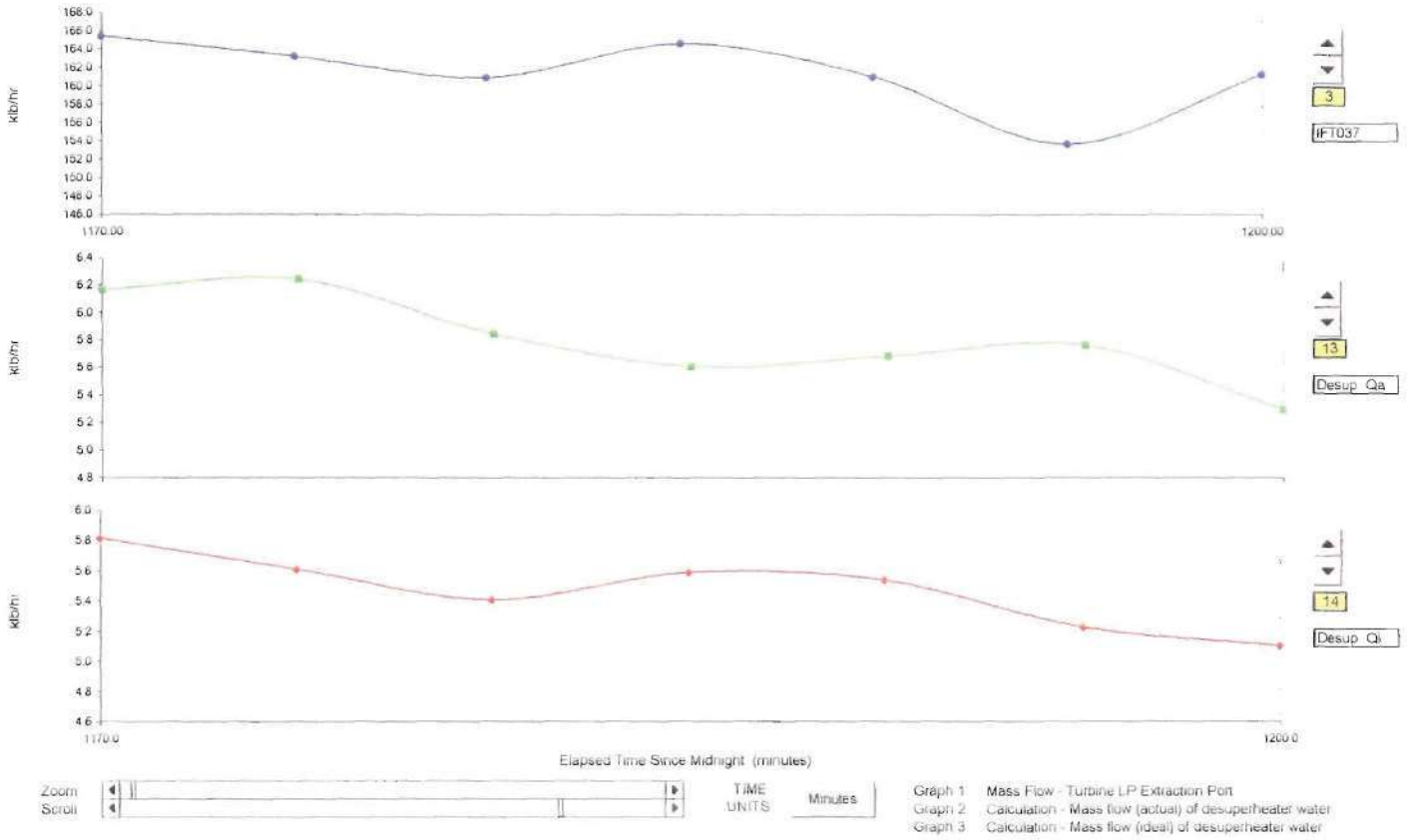
168.0
166.0
164.0
162.0
160.0
158.0
156.0
154.0
152.0
150.0
148.0
146.0
klb/hr
1170.00
1200.00
3
IFT037
6.4
6.2
6.0
5.8
5.6
5.4
5.2
5.0
4.8
klb/hr
13
Desup Qa
6.0
5.8
5.6
5.4
5.2
5.0
4.8
4.6
klb/hr
1170.0
1200.0
14
Desup Qi
Elapsed Time Since Midnight (minutes)
Zoom
Scroll
TIME UNITS
Minutes
Graph 1 Mass Flow - Turbine LP Extraction Port
Graph 2 Calculation - Mass flow (actual) of desuperheater water
Graph 3 Calculation - Mass flow (ideal) of desuperheater water

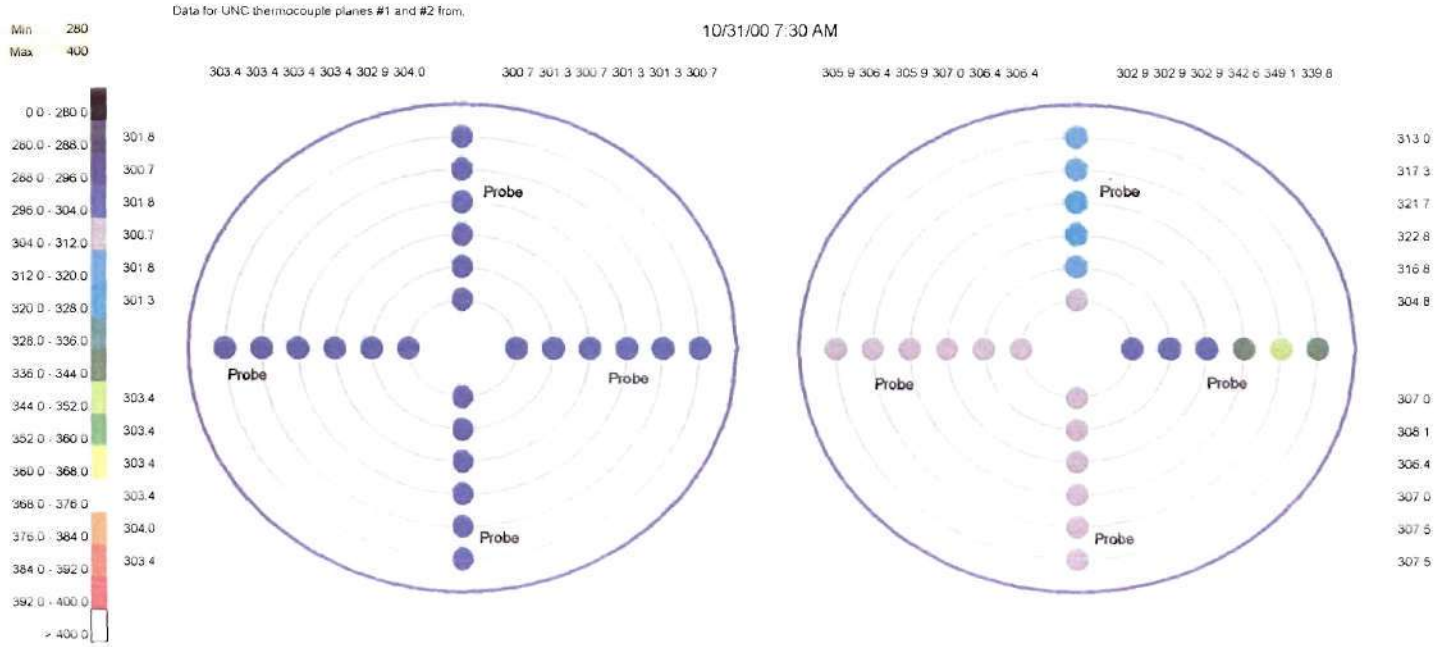
Data for UNC thermocouple planes #1 and #2 from,
10/31/00 7:30 AM
Min 280
Max 400
0.0 - 280.0
280.0 - 288.0
288.0 - 296.0
296.0 - 304.0
304.0 - 312.0
312.0 - 320.0
320.0 - 328.0
328.0 - 336.0
336.0 - 344.0
344.0 - 352.0
352.0 - 360.0
360.0 - 368.0
368.0 - 376.0
376.0 - 384.0
384.0 - 392.0
392.0 - 400.0
> 400.0
303.4 303.4 303.4 303.4 302.9 304.0
300.7 301.3 300.7 301.3 301.3 300.7
305.9 306.4 305.9 307.0 306.4 306.4
302.9 302.9 302.9 342.6 349.1 339.8
301.8
300.7
301.8
300.7
301.8
301.3
303.4
303.4
303.4
303.4
304.0
303.4
313.0
317.3
321.7
322.8
316.8
304.8
307.0
308.1
306.4
307.0
307.5
307.5
Probe
Probe
Probe
Probe
Probe
Probe

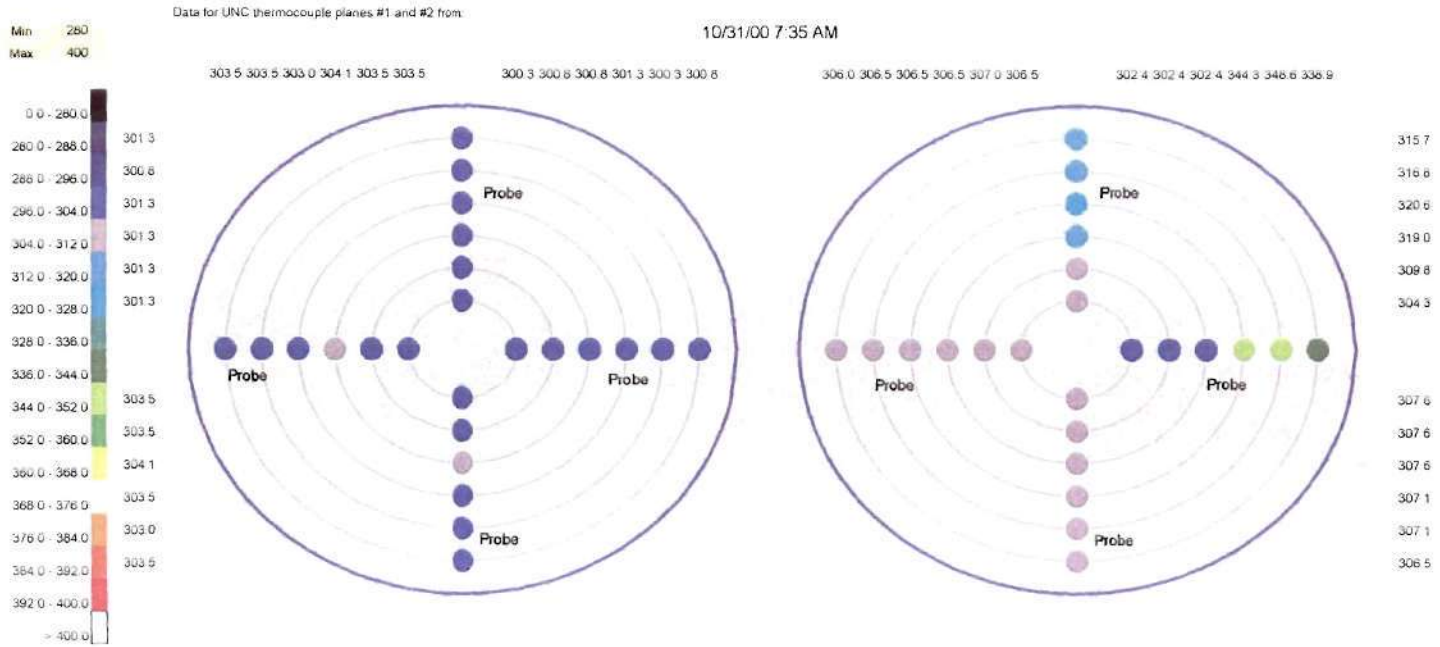
Data for UNC thermocouple planes #1 and #2 from:
10/31/00 7:35 AM
Min 280
Max 400
0.0 - 280.0
280.0 - 288.0
288.0 - 296.0
296.0 - 304.0
304.0 - 312.0
312.0 - 320.0
320.0 - 328.0
328.0 - 336.0
336.0 - 344.0
344.0 - 352.0
352.0 - 360.0
360.0 - 368.0
368.0 - 376.0
376.0 - 384.0
384.0 - 392.0
392.0 - 400.0
> 400.0
303.5 303.5 303.0 304.1 303.5 303.5
300.3 300.8 300.8 301.3 300.3 300.8
306.0 306.5 306.5 306.5 307.0 306.5
302.4 302.4 302.4 344.3 348.6 338.9
301.3
300.8
301.3
301.3
301.3
301.3
303.5
303.5
304.1
303.5
303.0
303.5
315.7
316.6
320.6
319.0
309.8
304.3
307.6
307.6
307.6
307.1
307.1
306.5
Probe
Probe
Probe
Probe
Probe
Probe

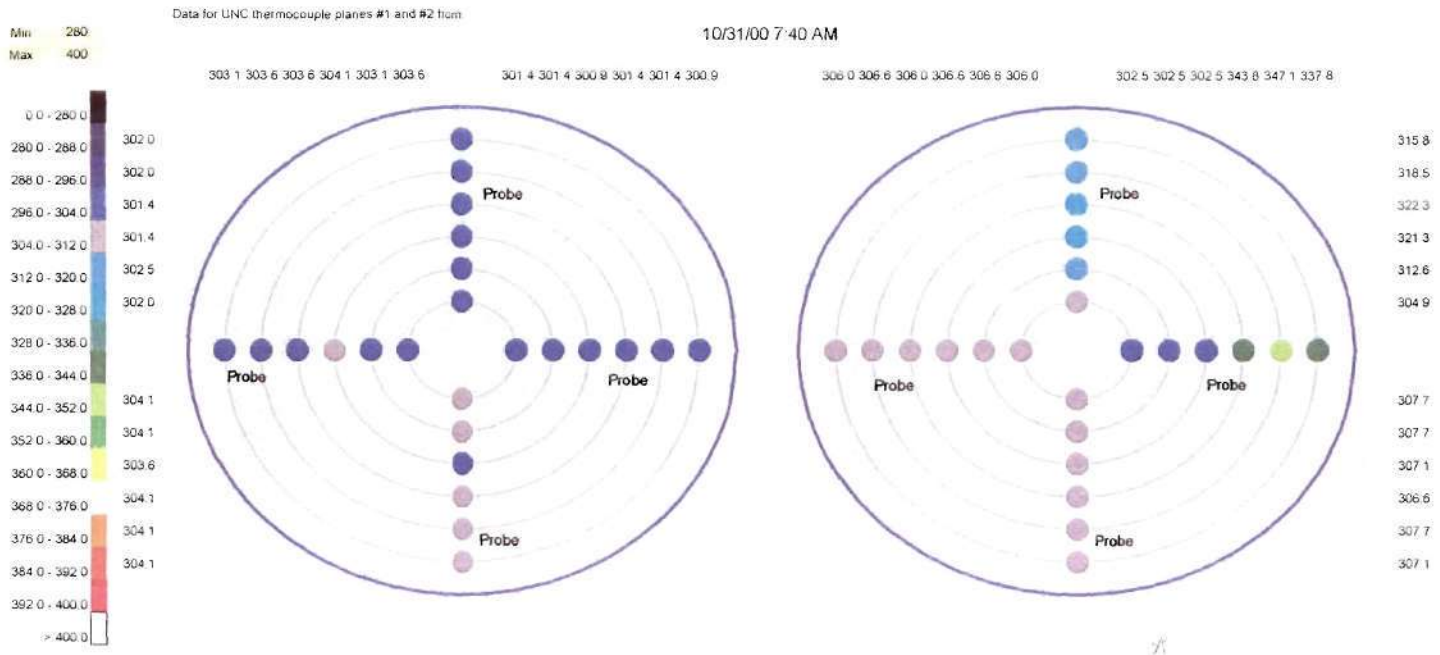
Data for UNC thermocouple planes #1 and #2 from
10/31/00 7:40 AM
Min 280
Max 400
0.0 - 280.0
280.0 - 288.0
288.0 - 296.0
296.0 - 304.0
304.0 - 312.0
312.0 - 320.0
320.0 - 328.0
328.0 - 336.0
336.0 - 344.0
344.0 - 352.0
352.0 - 360.0
360.0 - 368.0
368.0 - 376.0
376.0 - 384.0
384.0 - 392.0
392.0 - 400.0
> 400.0
303.1 303.6 303.6 304.1 303.1 303.6
301.4 301.4 300.8 301.4 301.4 300.9
306.0 306.6 306.0 306.6 306.6 306.0
302.5 302.5 302.5 343.8 347.1 337.8
302.0
302.0
301.4
301.4
302.5
302.0
304.1
304.1
303.6
304.1
304.1
304.1
315.8
318.5
322.3
321.3
312.6
304.9
307.7
307.7
307.1
306.6
307.7
307.1
Probe
Probe
Probe
Probe
Probe
Probe

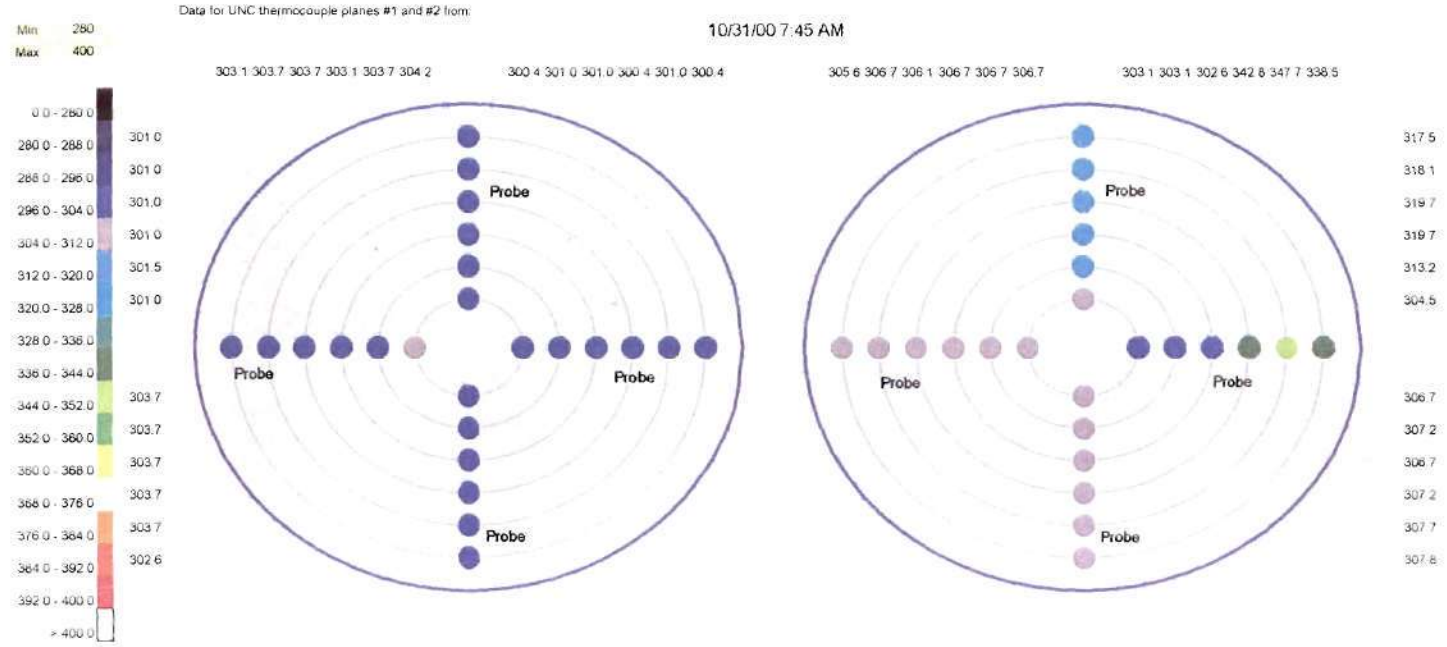
Data for UNC thermocouple planes #1 and #2 from:
10/31/00 7:45 AM
Min 280
Max 400
0.0 - 280.0
280.0 - 288.0
288.0 - 296.0
296.0 - 304.0
304.0 - 312.0
312.0 - 320.0
320.0 - 328.0
328.0 - 336.0
336.0 - 344.0
344.0 - 352.0
352.0 - 360.0
360.0 - 368.0
368.0 - 376.0
376.0 - 384.0
384.0 - 392.0
392.0 - 400.0
> 400.0
303.1 303.7 303.7 303.1 303.7 304.2
300.4 301.0 301.0 300.4 301.0 300.4
305.6 306.7 306.1 306.7 306.7 306.7
303.1 303.1 302.6 342.8 347.7 338.5
301.0
301.0
301.0
301.0
301.5
301.0
303.7
303.7
303.7
303.7
303.7
302.6
Probe
Probe
Probe
Probe
Probe
Probe
317.5
318.1
319.7
319.7
313.2
304.5
306.7
307.2
306.7
307.2
307.7
307.8

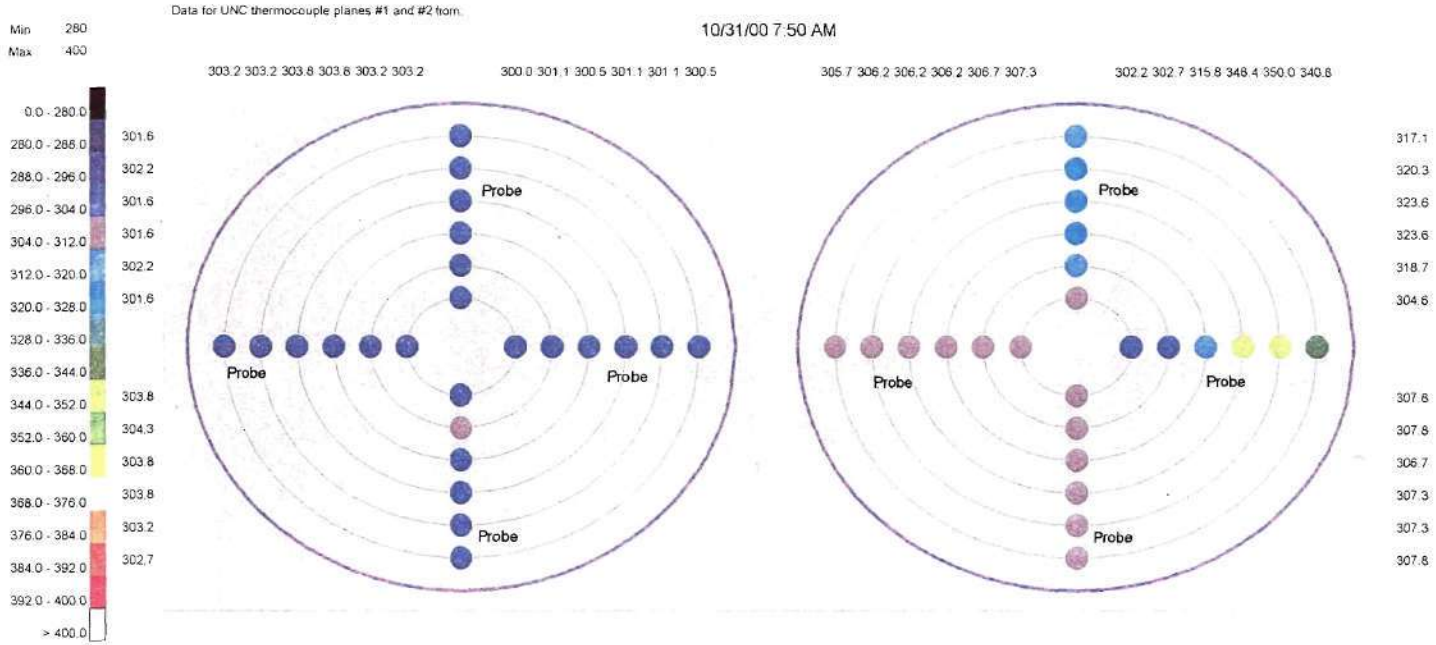
Data for UNC thermocouple planes #1 and #2 from
10/31/00 7:50 AM
Min 280
Max 400
0.0 - 280.0
280.0 - 288.0
288.0 - 296.0
296.0 - 304.0
304.0 - 312.0
312.0 - 320.0
320.0 - 328.0
328.0 - 336.0
336.0 - 344.0
344.0 - 352.0
352.0 - 360.0
360.0 - 368.0
368.0 - 376.0
376.0 - 384.0
384.0 - 392.0
392.0 - 400.0
> 400.0
303.2 303.2 303.8 303.6 303.2 303.2
300.0 301.1 300.5 301.1 301 1 300.5
305.7 306.2 306.2 306.2 306.7 307.3
302.2 302.7 315.8 348.4 350.0 340.8
301.6
302.2
301.6
301.6
302.2
301.6
303.8
304.3
303.8
303.8
303.2
302.7
317.1
320.3
323.6
323.6
318.7
304.6
307.6
307.8
306.7
307.3
307.3
307.8
Probe
Probe
Probe
Probe
Probe
Probe

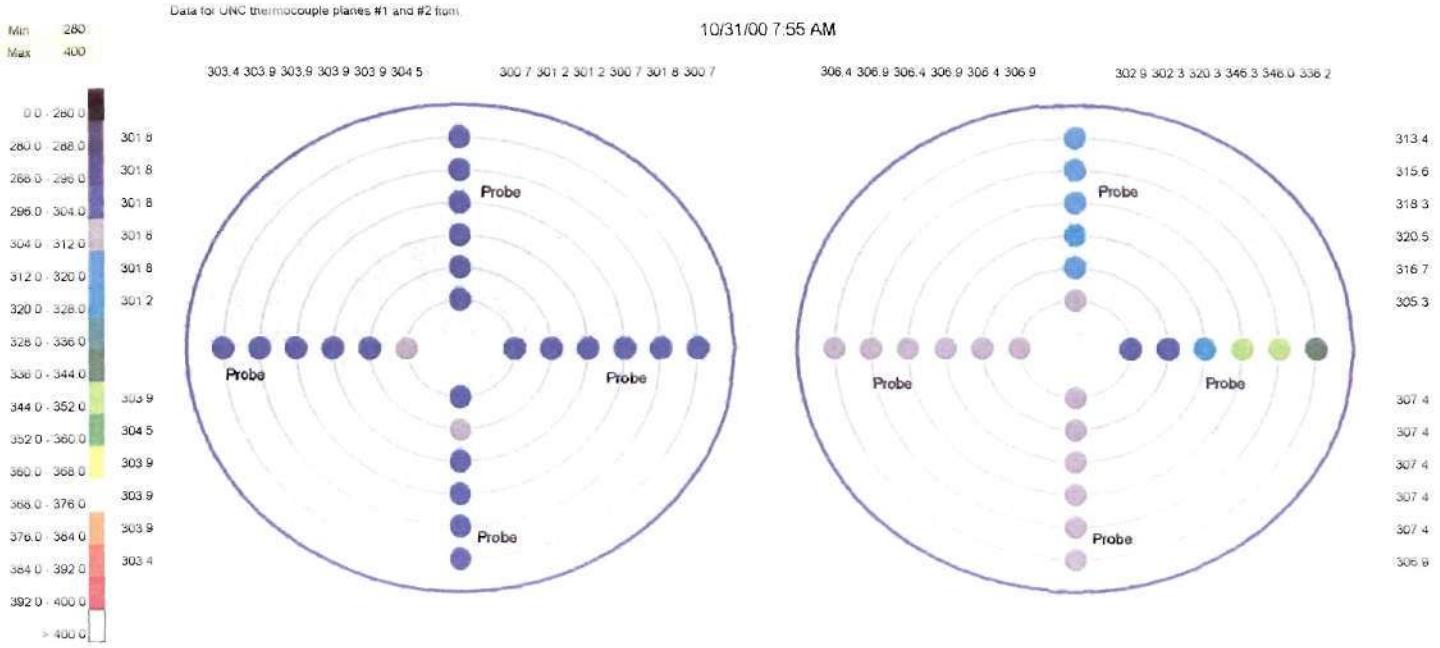
Data for UNC thermocouple plates #1 and #2 from
10/31/00 7:55 AM
Min 280
Max 400
0.0 - 280.0
280.0 - 288.0
288.0 - 296.0
296.0 - 304.0
304.0 - 312.0
312.0 - 320.0
320.0 - 328.0
328.0 - 336.0
336.0 - 344.0
344.0 - 352.0
352.0 - 360.0
360.0 - 368.0
368.0 - 376.0
376.0 - 384.0
384.0 - 392.0
392.0 - 400.0
> 400.0
303.4 303.9 303.9 303.9 303.9 304.5
300.7 301.2 301.2 300.7 301.8 300.7
306.4 306.9 306.4 306.9 306.4 306.9
302.9 302.3 320.3 346.3 346.0 336.2
301.8
301.8
301.8
301.6
301.8
301.2
303.9
304.5
303.9
303.9
303.9
303.4
313.4
315.6
318.3
320.5
316.7
305.3
307.4
307.4
307.4
307.4
307.4
306.9
Probe
Probe
Probe
Probe
Probe
Probe

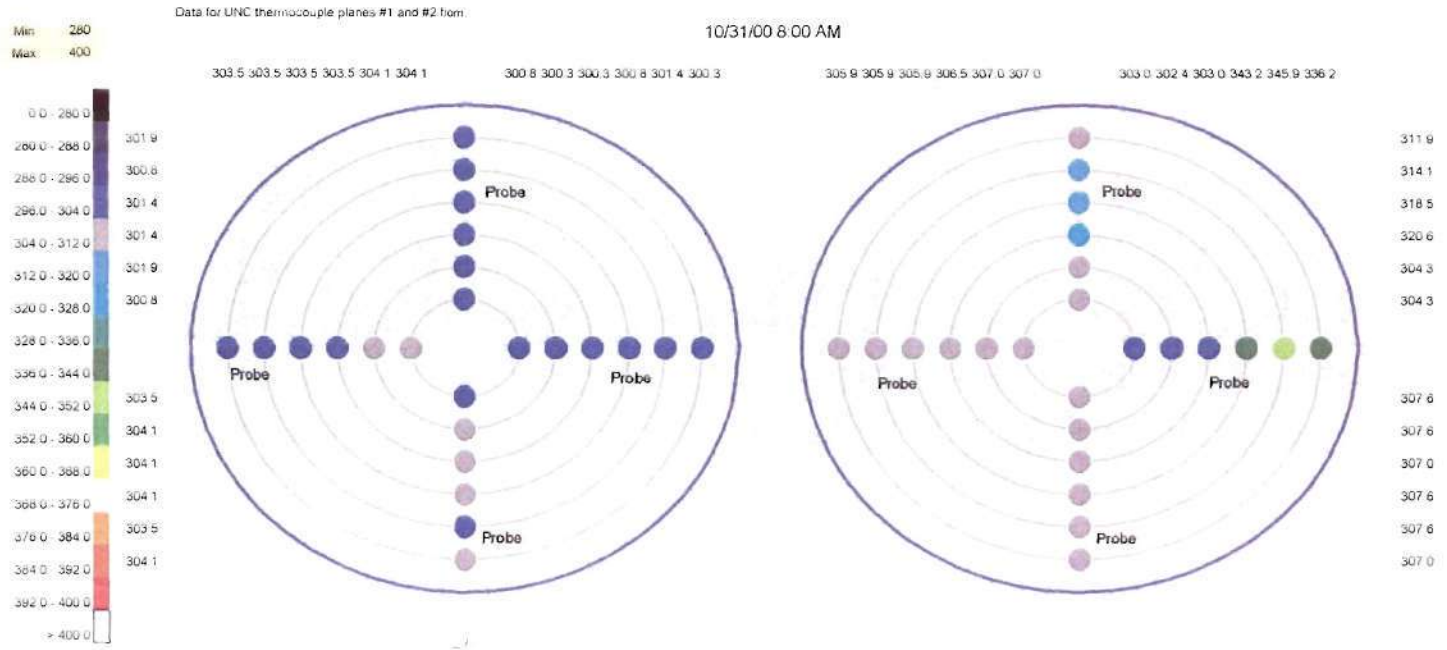
Data for UNC thermocouple planes #1 and #2 from
10/31/00 8:00 AM
Min 280
Max 400
0.0 - 280.0
280.0 - 288.0
288.0 - 296.0
296.0 - 304.0
304.0 - 312.0
312.0 - 320.0
320.0 - 328.0
328.0 - 336.0
336.0 - 344.0
344.0 - 352.0
352.0 - 360.0
360.0 - 368.0
368.0 - 376.0
376.0 - 384.0
384.0 - 392.0
392.0 - 400.0
> 400.0
303.5 303.5 303.5 303.5 304.1 304.1
300.8 300.3 300.3 300.8 301.4 300.3
305.9 305.9 305.9 306.5 307.0 307.0
303.0 302.4 303.0 343.2 345.9 336.2
301.9
300.8
301.4
301.4
301.9
300.8
303.5
304.1
304.1
304.1
303.5
304.1
Probe
Probe
Probe
Probe
Probe
Probe
311.9
314.1
318.5
320.6
304.3
304.3
307.6
307.6
307.0
307.6
307.6
307.0

APPENDIX B

EXPERIMENTAL DATA FOR CASE 2

Graphical representations of experimental data collected from the UNC Cogeneration Facility. This data is restricted to the time period of 1170-1200 minutes elapsed time from midnight on October 30, 2000. The data in this time increment was used to develop the input conditions for the computational analysis for the one and four nozzle desuperheater configurations. It was also used in both versions of the SteamCFD Code.

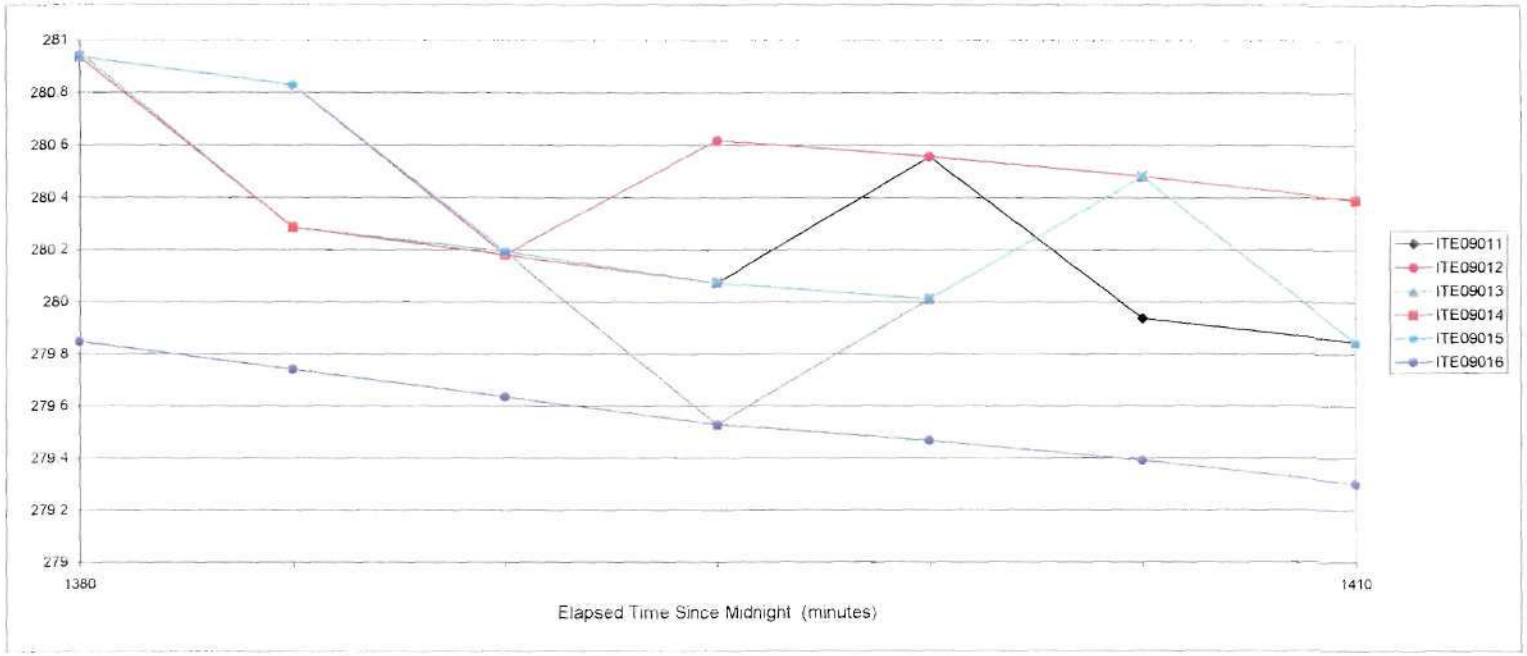

Zoom
Scroll

Data from file
C:\Old Data Files\Tecra 750CDT\C-Drive\My Docur

Turn series ON/OFF

Select Y-Axis PRI/SEC

s\Excel\

Series 1	ITE09011	Temperature - Con-Tek radial probe, station 1, element 1	F	22			
Series 2	ITE09012	Temperature - Con-Tek radial probe, station 1, element 2	F	23			
Series 3	ITE09013	Temperature - Con-Tek radial probe, station 1, element 3	F	24			
Series 4	ITE09014	Temperature - Con-Tek radial probe, station 1, element 4	F	25			
Series 5	ITE09015	Temperature - Con-Tek radial probe, station 1, element 5	F	26			
Series 6	ITE09016	Temperature - Con-Tek radial probe, station 1, element 6	F	27			

Autoscale state: OFF

Min / Max: 279 | 281 Update

Time Units: Minutes

Notes on autoscaling

MAY 2 2001

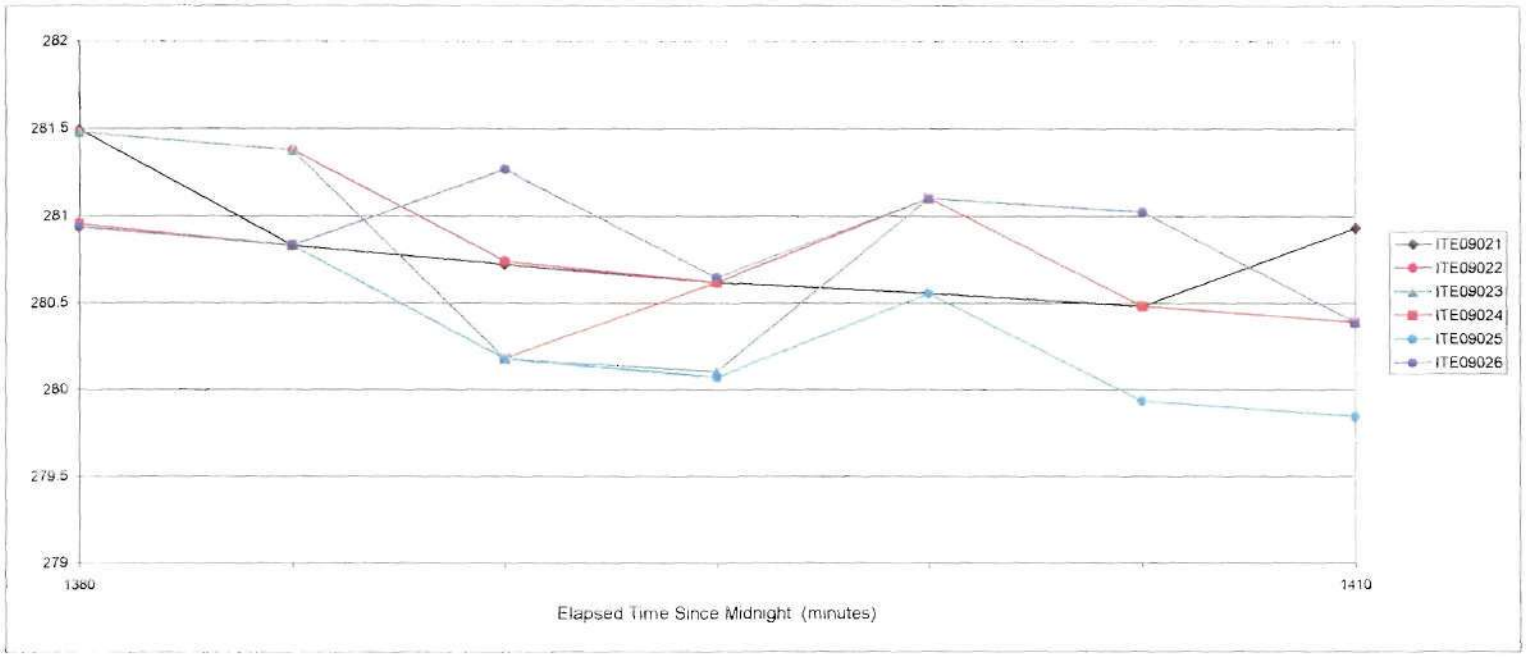

Zoom
Scroll

Data from file:
C:\Old Data Files\Tecra 750CDT\C-Drive\My Docur

Turn series ON/OFF

Select Y-Axis PRI/SEC

s\Excel\

Series 1	ITE09021	Temperature - Con-Tek radial probe, station 2, element 1	F	28		
Series 2	ITE09022	Temperature - Con-Tek radial probe, station 2, element 2	F	29		
Series 3	ITE09023	Temperature - Con-Tek radial probe, station 2, element 3	F	30		
Series 4	ITE09024	Temperature - Con-Tek radial probe, station 2, element 4	F	31		
Series 5	ITE09025	Temperature - Con-Tek radial probe, station 2, element 5	F	32		
Series 6	ITE09026	Temperature - Con-Tek radial probe, station 2, element 6	F	33		

Autoscale state: OFF

Min / Max: 279 | 282 | Update

Time Units: Minutes

Notes on autoscaling

MAY 2 2001

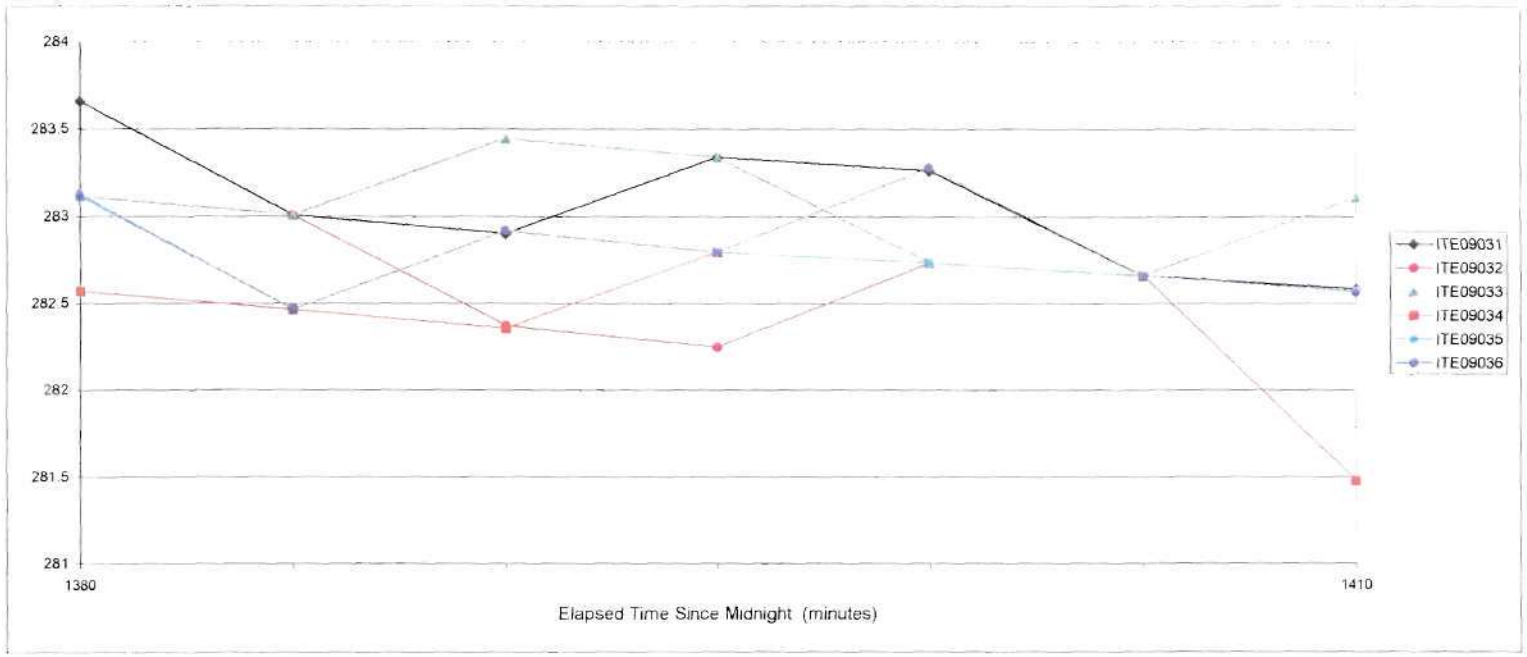

Zoom
Scroll

Data from file:
C:\Old Data Files\Tecra 750CDT\C-Drive\My Docur

Turn series ON/OFF

Select Y-Axis 0PRI/SEC

s\Excel\

Series 1	ITE09031	Temperature - Con-Tek radial probe, station 3, element 1	F	34			
Series 2	ITE09032	Temperature - Con-Tek radial probe, station 3, element 2	F	35			
Series 3	ITE09033	Temperature - Con-Tek radial probe, station 3, element 3	F	36			
Series 4	ITE09034	Temperature - Con-Tek radial probe, station 3, element 4	F	37			
Series 5	ITE09035	Temperature - Con-Tek radial probe, station 3, element 5	F	38			
Series 6	ITE09036	Temperature - Con-Tek radial probe, station 3, element 6	F	39			

Autoscale state: OFF

Min / Max: 281 284 Update

Time Units: Minutes

Notes on autoscaling

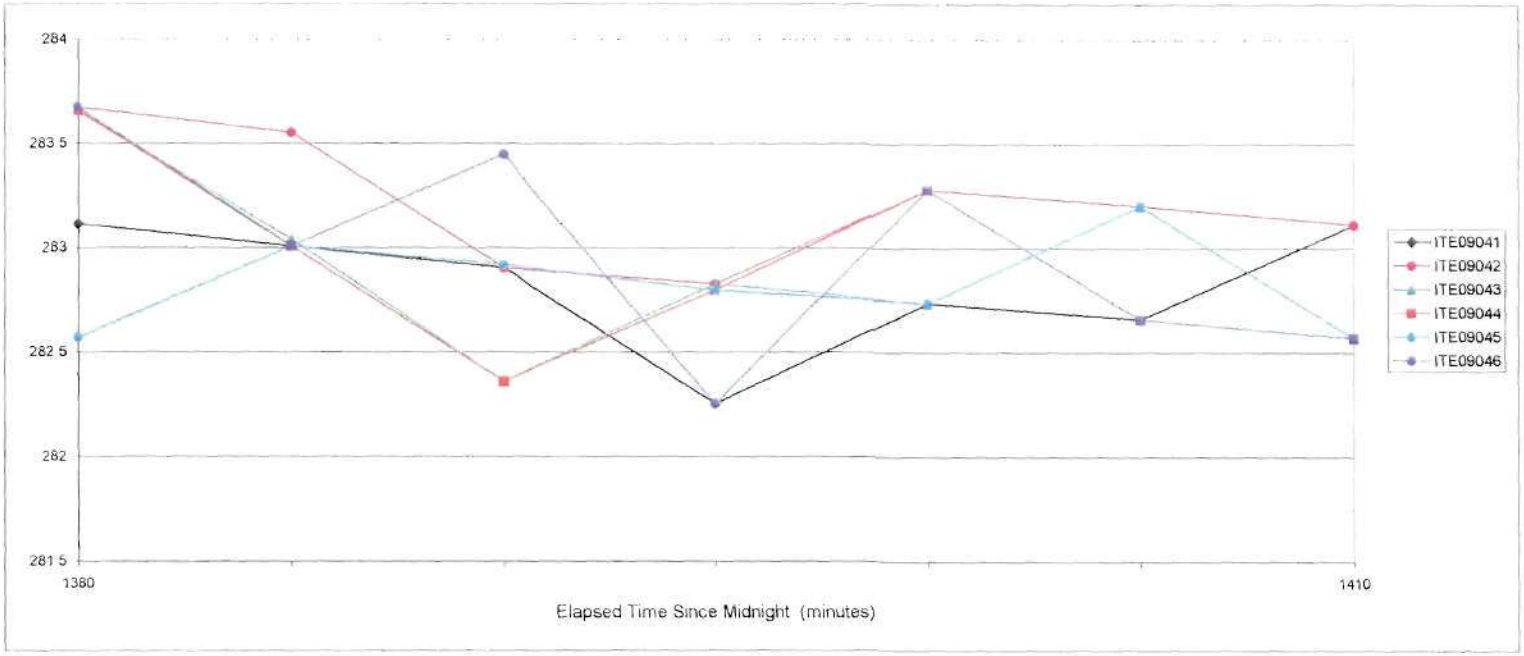

Zoom
Scroll

Data from file:
C:\Old Data Files\Tecra 750CDT\C-Drive\My Docur

			Turn series ON/OFF	Select Y-Axis PRI/SEC
Series 1	ITE09041	Temperature - Con-Tek radial probe, station 4, element 1	F 40	s\Excel\
Series 2	ITE09042	Temperature - Con-Tek radial probe, station 4, element 2	F 41	
Series 3	ITE09043	Temperature - Con-Tek radial probe, station 4, element 3	F 42	
Series 4	ITE09044	Temperature - Con-Tek radial probe, station 4, element 4	F 43	
Series 5	ITE09045	Temperature - Con-Tek radial probe, station 4, element 5	F 44	
Series 6	ITE09046	Temperature - Con-Tek radial probe, station 4, element 6	F 45	

Autoscale state: ON | Min / Max | Update | Time Units: Minutes | Notes on autoscaling

MAY 2 2001

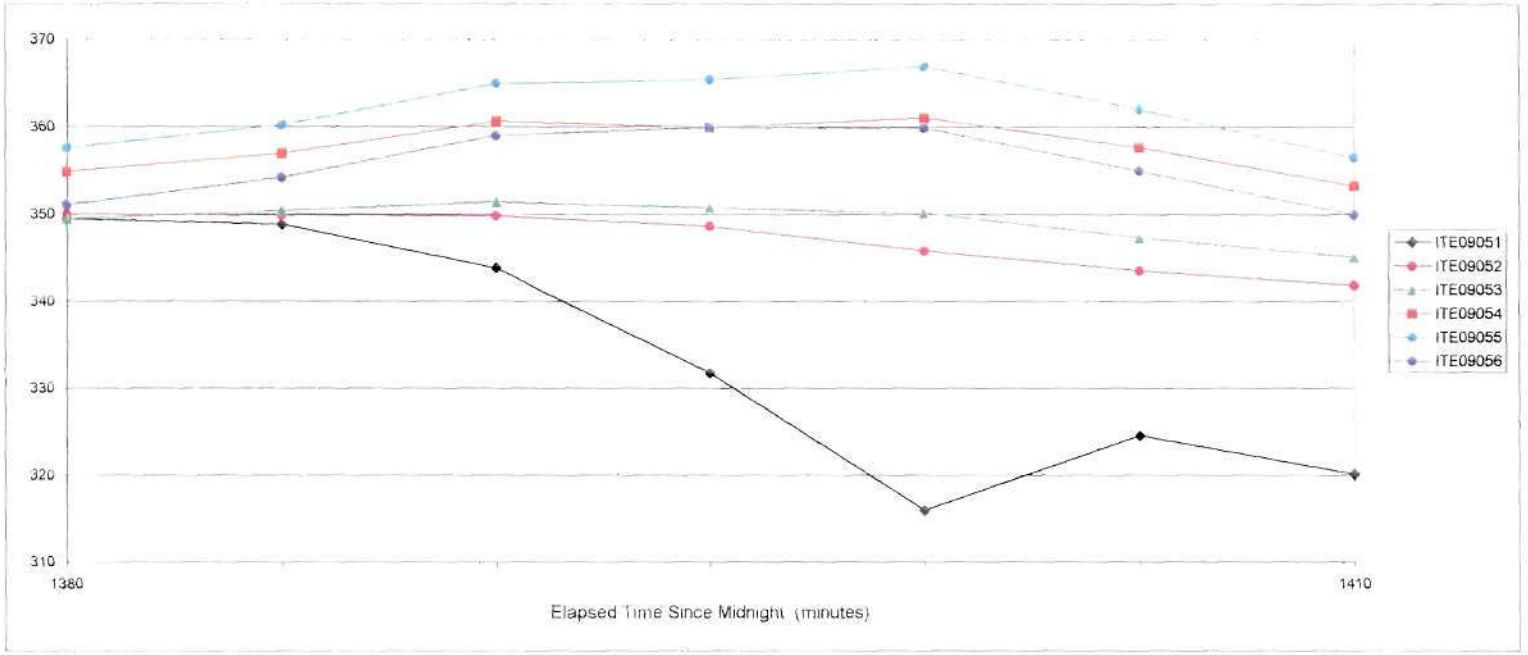

Zoom
Scroll

Data from file:
C:\Old Data Files\Tecra 750CDT\C-Drive\My Docur

					Turn series ON/OFF	Select Y-Axis PRI/SEC
Series 1	ITE09051	Temperature - Con-Tek radial probe, station 5, element 1	F	46		
Series 2	ITE09052	Temperature - Con-Tek radial probe, station 5, element 2	F	47		
Series 3	ITE09053	Temperature - Con-Tek radial probe, station 5, element 3	F	48		
Series 4	ITE09054	Temperature - Con-Tek radial probe, station 5, element 4	F	49		
Series 5	ITE09055	Temperature - Con-Tek radial probe, station 5, element 5	F	50		
Series 6	ITE09056	Temperature - Con-Tek radial probe, station 5, element 6	F	51		

Autoscale state: OFF
Min / Max: 310 370 Update
Time Units: Minutes
Notes on autoscaling

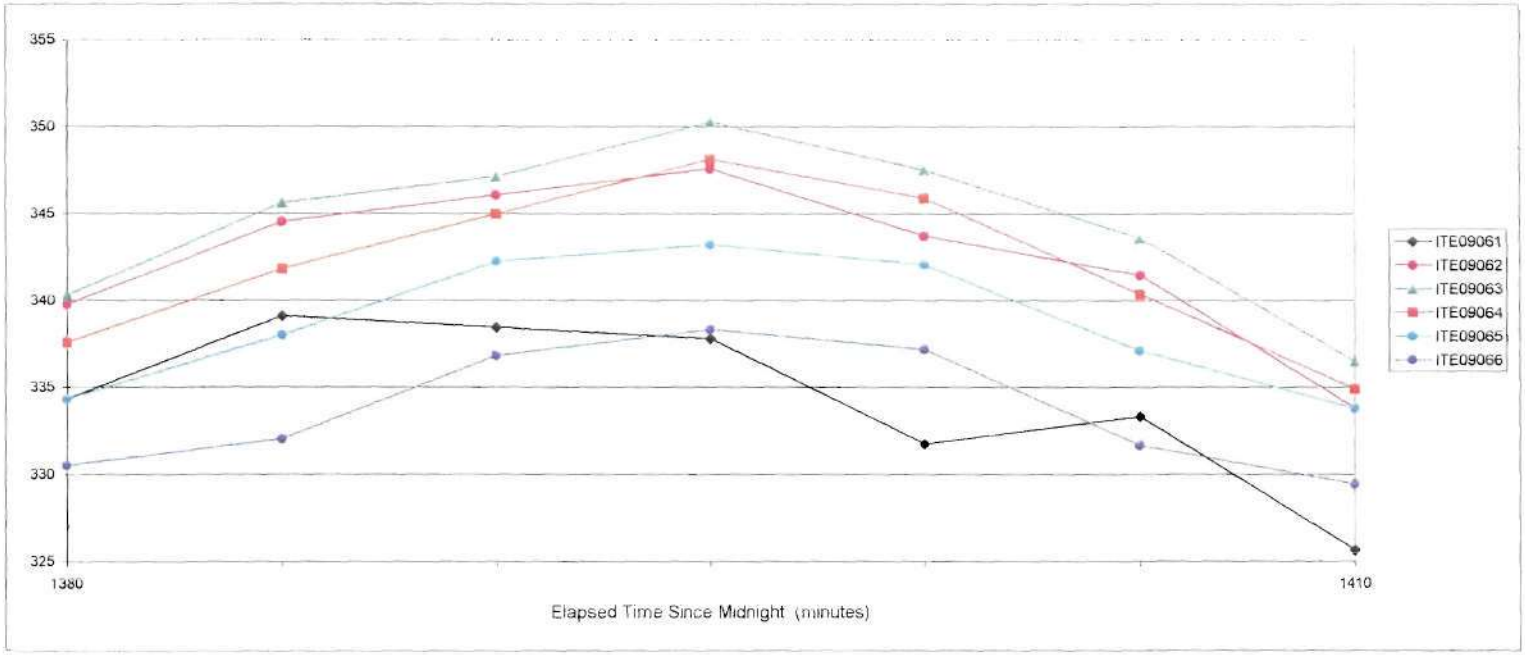

Zoom
Scroll

Data from file:
C:\Old Data Files\Tecra 750CDT\C-Drive\My Docur

Turn series ON/OFF

Select Y-Axis PRI/SEC

s\Excel\

Series 1	ITE09061	Temperature - Con-Tek radial probe, station 6, element 1	F	52			
Series 2	ITE09062	Temperature - Con-Tek radial probe, station 6, element 2	F	53			
Series 3	ITE09063	Temperature - Con-Tek radial probe, station 6, element 3	F	54			
Series 4	ITE09064	Temperature - Con-Tek radial probe, station 6, element 4	F	55			
Series 5	ITE09065	Temperature - Con-Tek radial probe, station 6, element 5	F	56			
Series 6	ITE09066	Temperature - Con-Tek radial probe, station 6, element 6	F	57			

Autoscale state: OFF

Min / Max: 325 355 Update

Time Units: Minutes

Notes on autoscaling

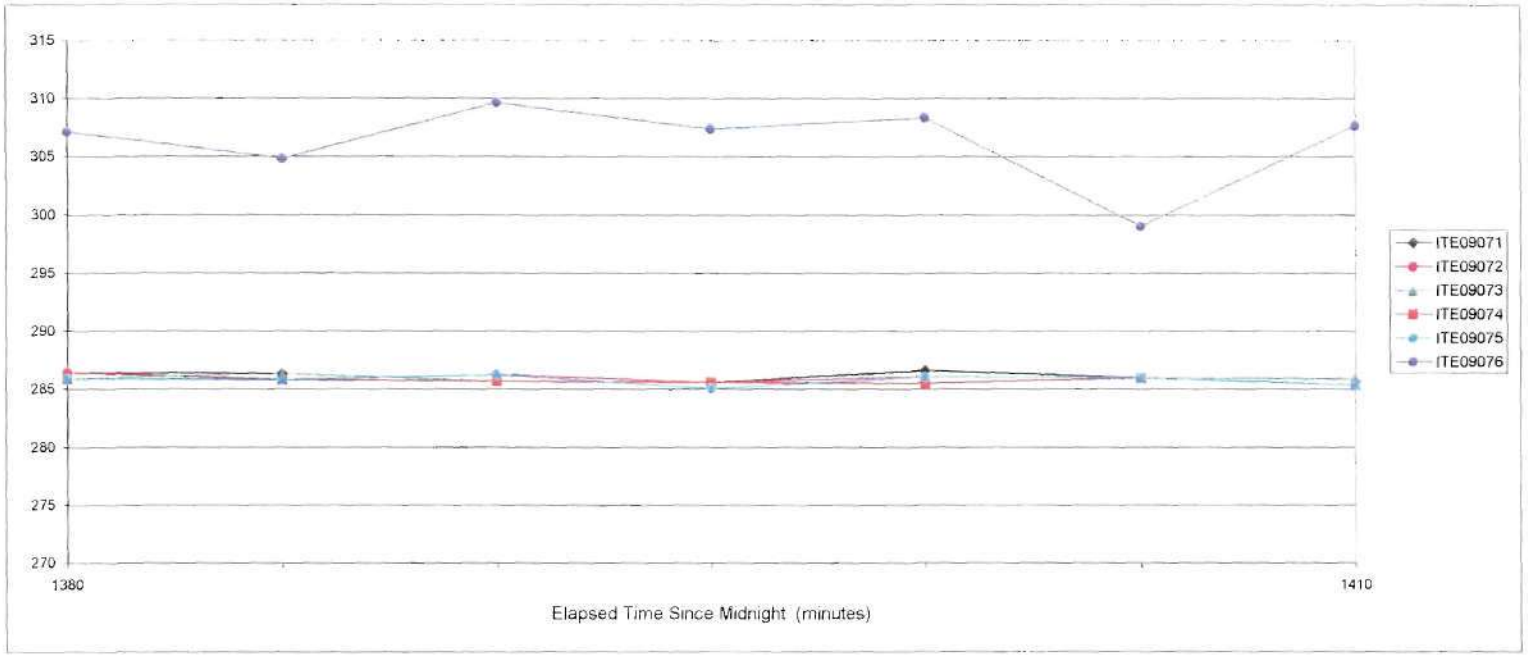

Zoom
Scroll

Data from file:
C:\Old Data Files\Tecra 750CDT\C-Drive\My Docur

					Turn series ON/OFF	Select Y-Axis 0PRI/SECS
Series 1	ITE09071	Temperature - Con-Tek radial probe, station 7, element 1	F	58		
Series 2	ITE09072	Temperature - Con-Tek radial probe, station 7, element 2	F	59		
Series 3	ITE09073	Temperature - Con-Tek radial probe, station 7, element 3	F	60		
Series 4	ITE09074	Temperature - Con-Tek radial probe, station 7, element 4	F	61		
Series 5	ITE09075	Temperature - Con-Tek radial probe, station 7, element 5	F	62		
Series 6	ITE09076	Temperature - Con-Tek radial probe, station 7, element 6	F	63		

Autoscale state: OFF Min / Max: 280 315 Update

Time Units: Minutes

Notes on autoscaling.

MAY 2 2001

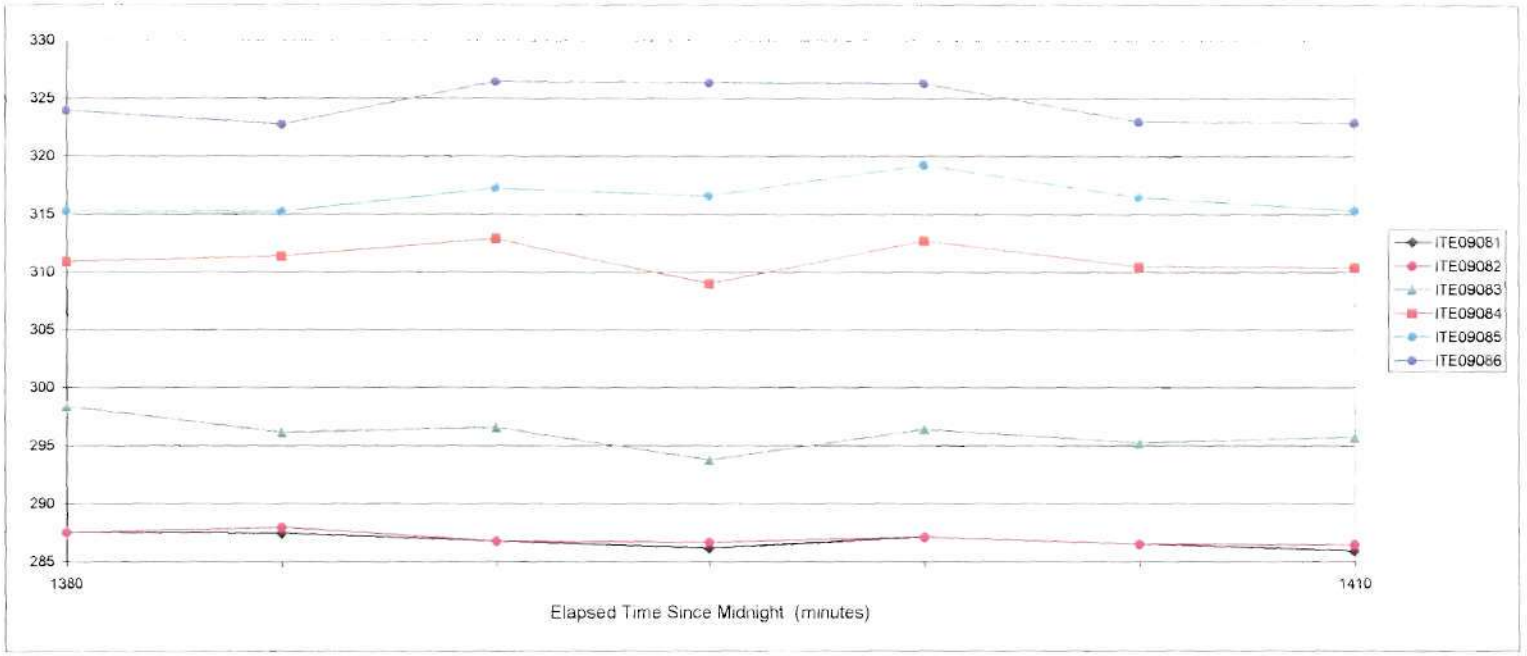

Zoom
Scroll

Data from file:
C:\Old Data Files\Tecra 750CDT\C-Drive\My Docur

					Turn series ON/OFF	Select Y-Axis PRI/SEC
Series 1	ITE09081	Temperature - Con-Tek radial probe, station 8, element 1	F	64		
Series 2	ITE09082	Temperature - Con-Tek radial probe, station 8, element 2	F	65		
Series 3	ITE09083	Temperature - Con-Tek radial probe, station 8, element 3	F	66		
Series 4	ITE09084	Temperature - Con-Tek radial probe, station 8, element 4	F	67		
Series 5	ITE09085	Temperature - Con-Tek radial probe, station 8, element 5	F	68		
Series 6	ITE09086	Temperature - Con-Tek radial probe, station 8, element 6	F	69		

Autoscale state: OFF Min / Max: 285 330 Update

Time Units: Minutes

Notes on autoscaling.

MAY 2 2001

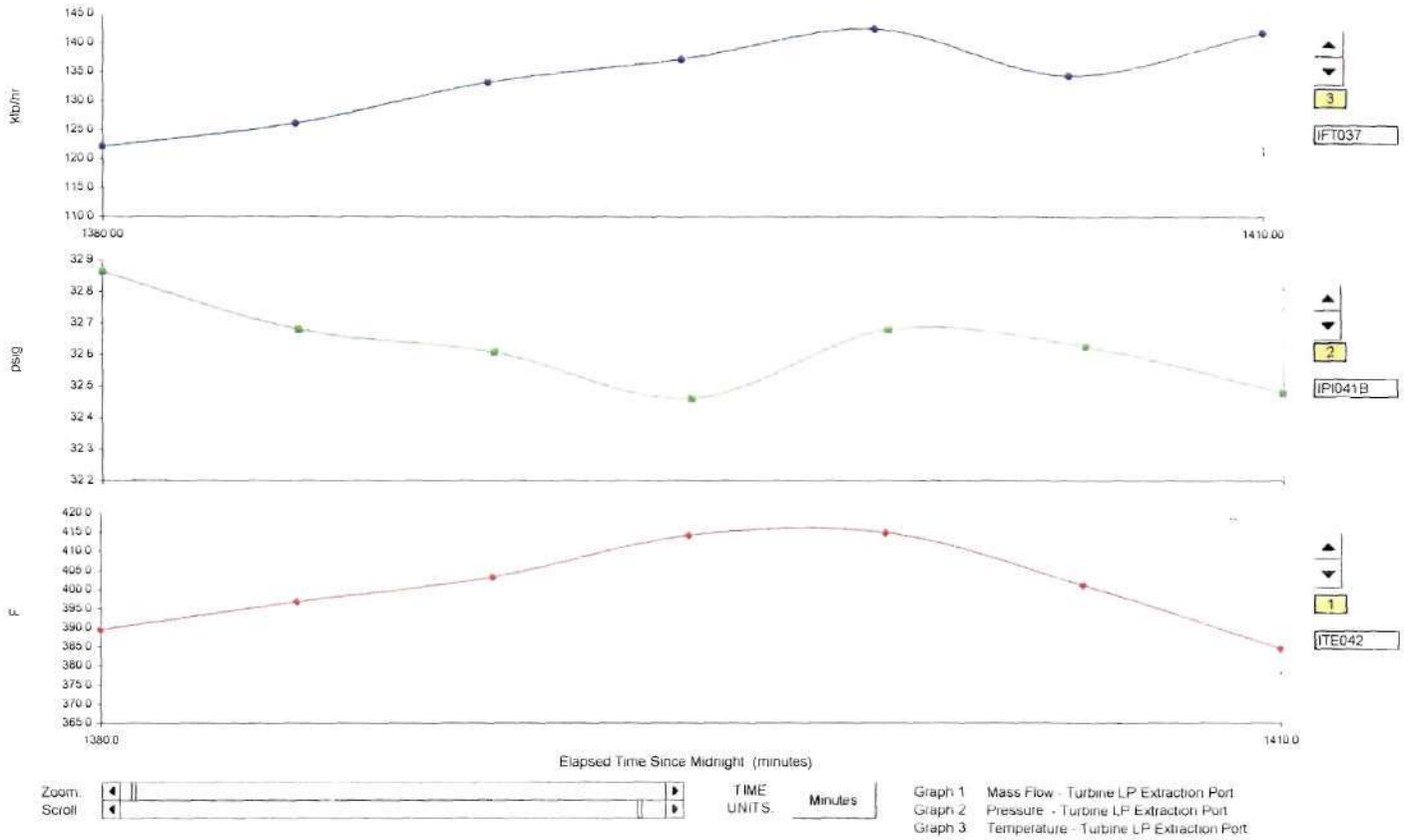
klb/hr
145.0
140.0
135.0
130.0
125.0
120.0
115.0
110.0
1380.00
1410.00
3
IFT037
psig
32.9
32.8
32.7
32.6
32.5
32.4
32.3
32.2
2
IPI041B
F
420.0
415.0
410.0
405.0
400.0
395.0
390.0
385.0
380.0
375.0
370.0
365.0
1380.0
1410.0
1
ITE042
Elapsed Time Since Midnight (minutes)
Zoom
Scroll
TIME UNITS
Minutes
Graph 1 Mass Flow - Turbine LP Extraction Port
Graph 2 Pressure - Turbine LP Extraction Port
Graph 3 Temperature - Turbine LP Extraction Port

MAY 2 2001

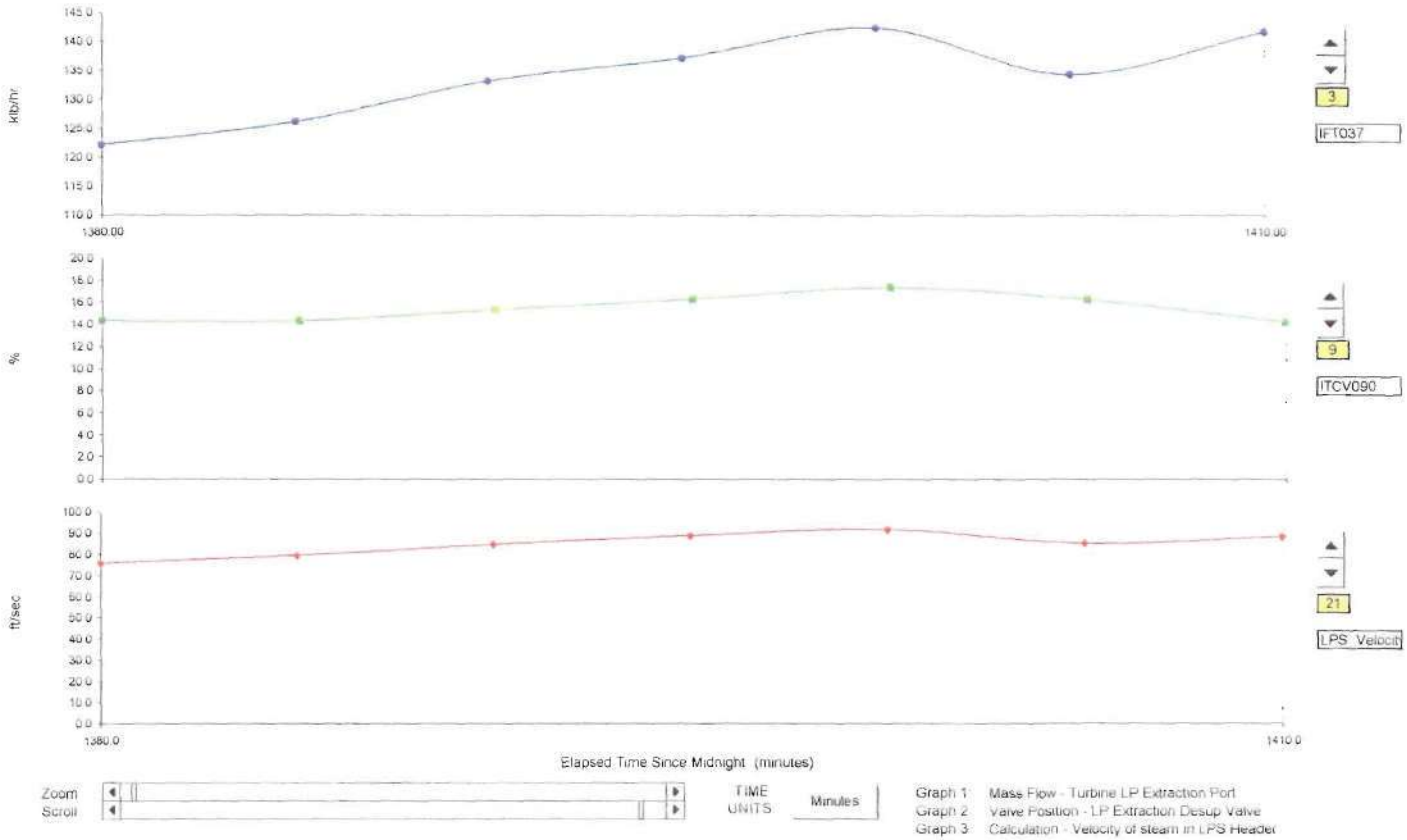
145.0
140.0
135.0
130.0
125.0
120.0
115.0
110.0
klb/hr
1380.00
1410.00
3
IFT037
20.0
18.0
16.0
14.0
12.0
10.0
8.0
6.0
4.0
2.0
0.0
%
9
ITCV090
100.0
90.0
80.0
70.0
60.0
50.0
40.0
30.0
20.0
10.0
0.0
ft/sec
1380.0
1410.0
21
LPS Velocit
Elapsed Time Since Midnight (minutes)
Zoom
Scroll
TIME UNITS
Minutes
Graph 1 Mass Flow - Turbine LP Extraction Port
Graph 2 Valve Position - LP Extraction Desup Valve
Graph 3 Calculation - Velocity of steam in LPS Header

MAY 2 2001

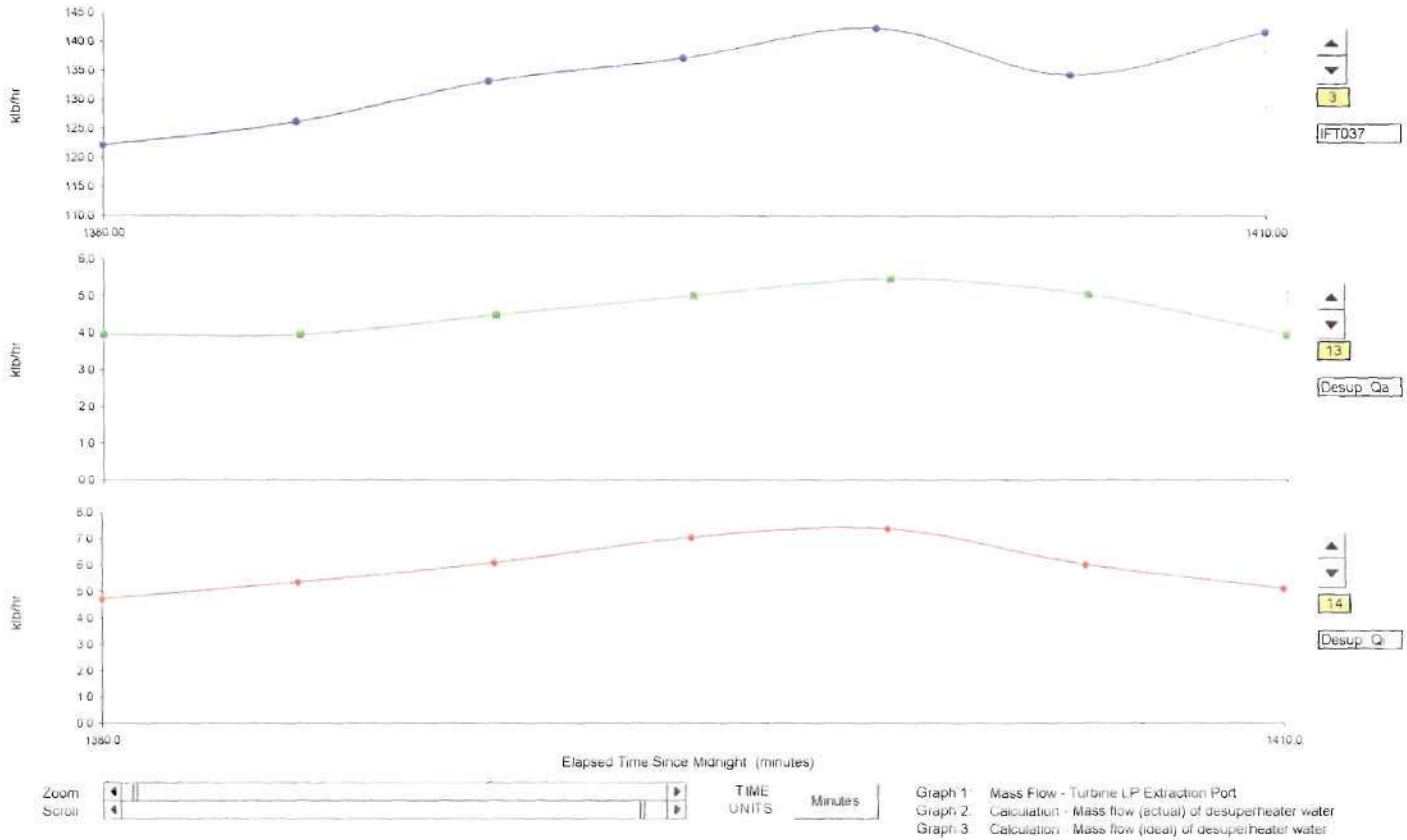
klb/hr
145.0
140.0
135.0
130.0
125.0
120.0
115.0
110.0
1360.00
1410.00
3
IFT037
klb/hr
6.0
5.0
4.0
3.0
2.0
1.0
0.0
13
Desup_Qa
klb/hr
8.0
7.0
6.0
5.0
4.0
3.0
2.0
1.0
0.0
1360.0
1410.0
14
Desup_Qi
Elapsed Time Since Midnight (minutes)
Zoom
Scroll
TIME UNITS
Minutes
Graph 1 Mass Flow - Turbine LP Extraction Port
Graph 2 Calculation - Mass flow (actual) of desuperheater water
Graph 3 Calculation - Mass flow (ideal) of desuperheater water

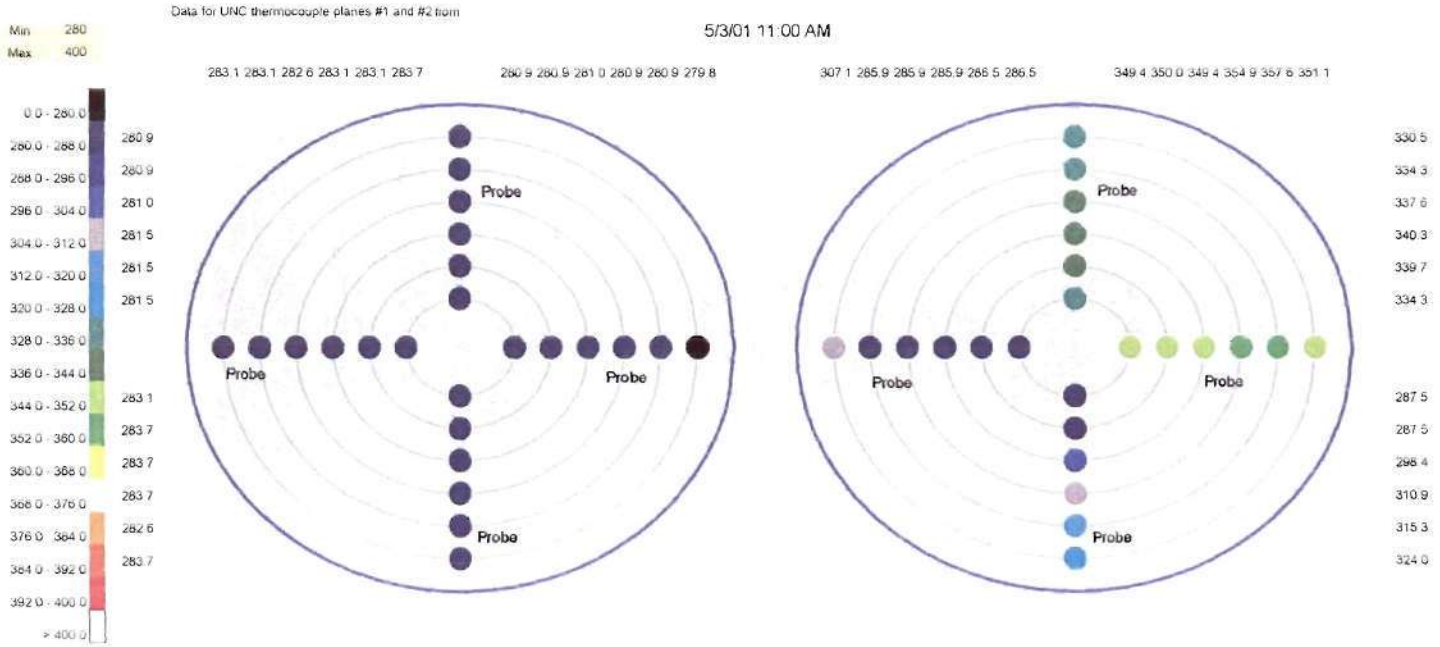
Data for UNC thermocouple planes #1 and #2 from
5/3/01 11:00 AM
Min 280
Max 400
0.0 - 280.0
280.0 - 288.0
288.0 - 296.0
296.0 - 304.0
304.0 - 312.0
312.0 - 320.0
320.0 - 328.0
328.0 - 336.0
336.0 - 344.0
344.0 - 352.0
352.0 - 360.0
360.0 - 368.0
368.0 - 376.0
376.0 - 384.0
384.0 - 392.0
392.0 - 400.0
> 400.0
283.1 283.1 282.6 283.1 283.1 283.7
280.9 280.9 281.0 280.9 280.9 279.8
307.1 285.9 285.9 285.9 285.5 286.5
349.4 350.0 349.4 354.9 357.6 351.1
280.9
280.9
281.0
281.5
281.5
281.5
283.1
283.7
283.7
283.7
282.6
283.7
330.5
334.3
337.6
340.3
339.7
334.3
287.5
287.5
298.4
310.9
315.3
324.0
Probe
Probe
Probe
Probe
Probe
Probe

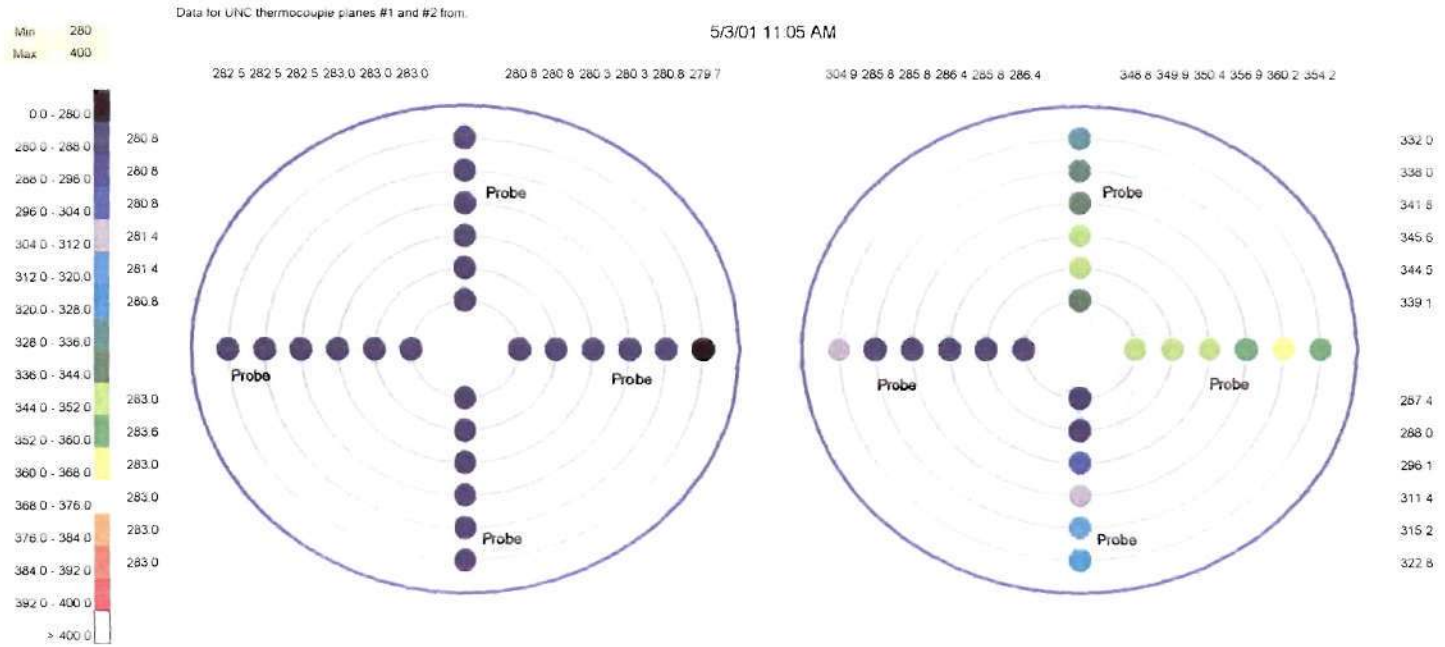
Data for UNC thermocouple planes #1 and #2 from:
5/3/01 11:05 AM
Min 280
Max 400
0.0 - 280.0
280.0 - 288.0
288.0 - 296.0
296.0 - 304.0
304.0 - 312.0
312.0 - 320.0
320.0 - 328.0
328.0 - 336.0
336.0 - 344.0
344.0 - 352.0
352.0 - 360.0
360.0 - 368.0
368.0 - 376.0
376.0 - 384.0
384.0 - 392.0
392.0 - 400.0
> 400.0
282.5 282.5 282.5 283.0 283.0 283.0
280.8 280.8 280.8 280.3 280.3 280.8 279.7
304.9 285.8 285.8 286.4 285.8 286.4
346.8 349.9 350.4 356.9 360.2 354.2
280.8
280.8
280.8
281.4
281.4
280.8
283.0
283.6
283.0
283.0
283.0
283.0
332.0
338.0
341.8
345.6
344.5
339.1
287.4
288.0
296.1
311.4
315.2
322.8
Probe
Probe
Probe
Probe
Probe
Probe

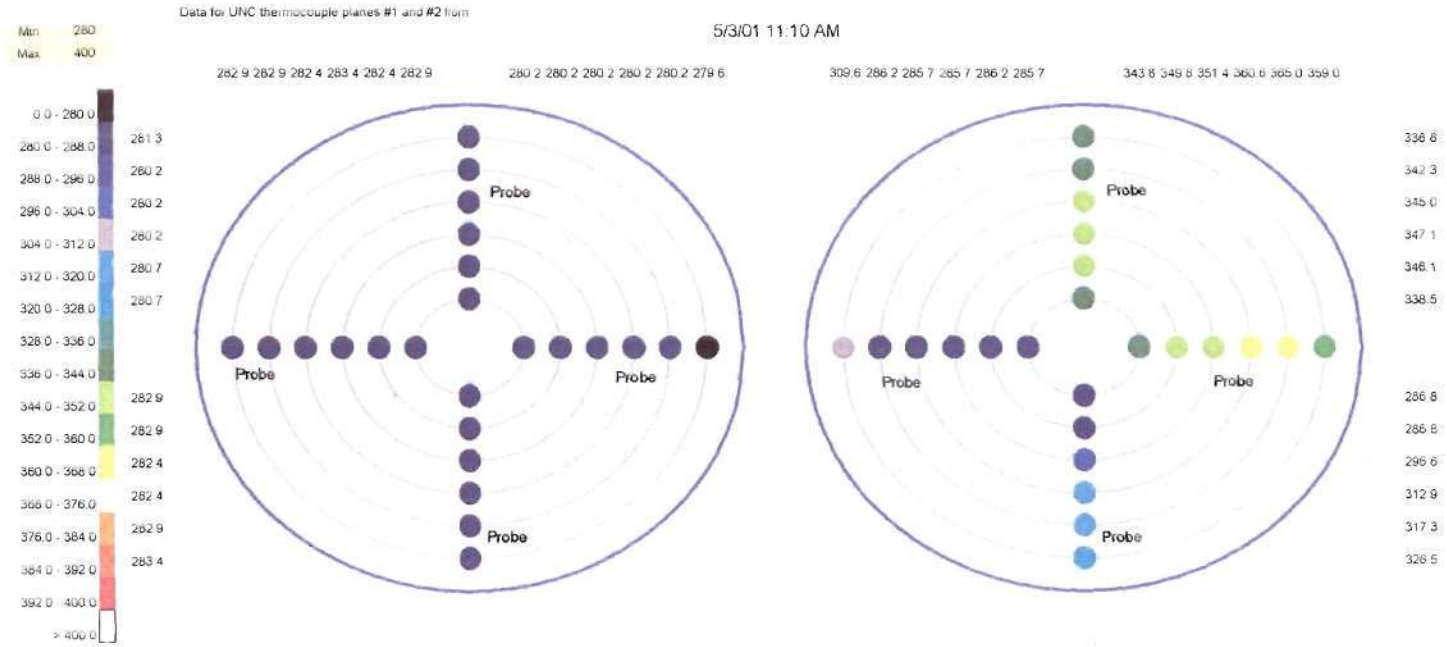
Data for UNC thermocouple planes #1 and #2 from
5/3/01 11:10 AM
Min 280
Max 400
0.0 - 280.0
280.0 - 288.0
288.0 - 296.0
296.0 - 304.0
304.0 - 312.0
312.0 - 320.0
320.0 - 328.0
328.0 - 336.0
336.0 - 344.0
344.0 - 352.0
352.0 - 360.0
360.0 - 368.0
368.0 - 376.0
376.0 - 384.0
384.0 - 392.0
392.0 - 400.0
> 400.0
282.9 282.9 282.4 283.4 282.4 282.9
280.2 280.2 280.2 280.2 280.2 280.2 279.6
309.6 286.2 285.7 285.7 286.2 285.7
343.8 349.8 351.4 360.6 365.0 359.0
281.3
280.2
280.2
280.2
280.7
280.7
282.9
282.9
282.4
282.4
282.9
283.4
336.8
342.3
345.0
347.1
346.1
338.5
286.8
286.8
296.6
312.9
317.3
328.5
Probe
Probe
Probe
Probe
Probe
Probe

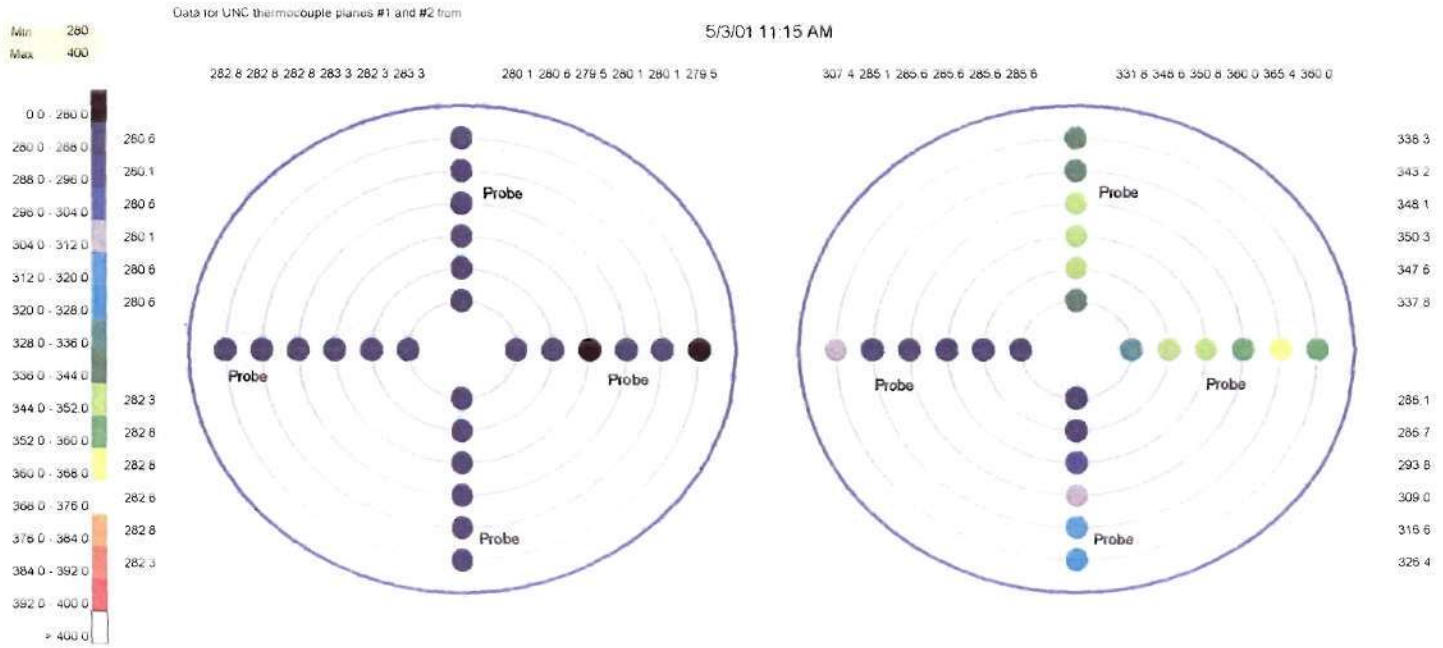
Data for UNC thermocouple planes #1 and #2 from
5/3/01 11:15 AM
Min 280
Max 400
0.0 - 280.0
280.0 - 288.0
288.0 - 296.0
296.0 - 304.0
304.0 - 312.0
312.0 - 320.0
320.0 - 328.0
328.0 - 336.0
336.0 - 344.0
344.0 - 352.0
352.0 - 360.0
360.0 - 368.0
368.0 - 376.0
376.0 - 384.0
384.0 - 392.0
392.0 - 400.0
> 400.0
282.8 282.8 282.8 283.3 282.3 283.3
280.1 280.6 279.5 280.1 280.1 279.5
307.4 285.1 285.6 285.6 285.6 285.6
331.6 348.6 350.8 360.0 365.4 360.0
280.6
280.1
280.6
280.1
280.6
280.6
282.3
282.8
282.8
282.6
282.8
282.3
338.3
343.2
348.1
350.3
347.6
337.8
286.1
286.7
293.8
309.0
316.6
326.4
Probe
Probe
Probe
Probe
Probe
Probe

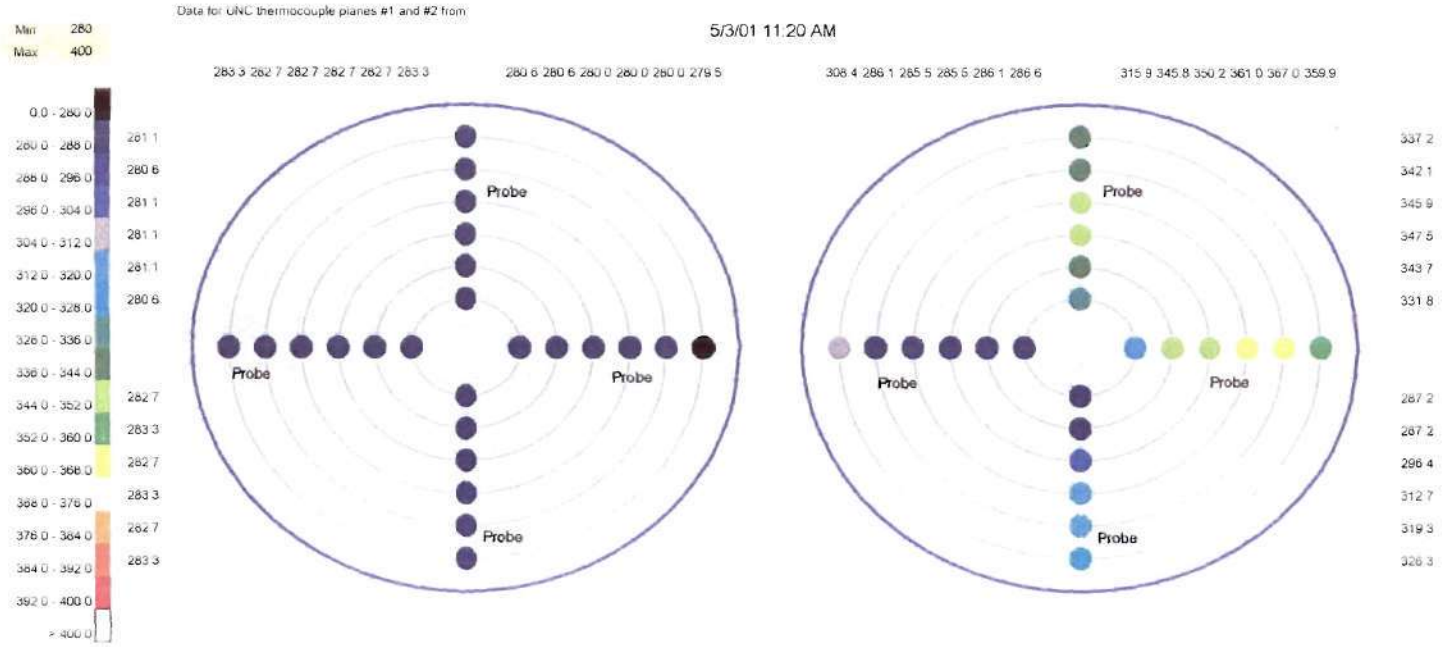
Min 280
Max 400
0.0 - 280.0
280.0 - 288.0
288.0 - 296.0
296.0 - 304.0
304.0 - 312.0
312.0 - 320.0
320.0 - 328.0
328.0 - 336.0
336.0 - 344.0
344.0 - 352.0
352.0 - 360.0
360.0 - 368.0
368.0 - 376.0
376.0 - 384.0
384.0 - 392.0
392.0 - 400.0
> 400.0
Data for UNC thermocouple planes #1 and #2 from
5/3/01 11:20 AM
283.3 282.7 282.7 282.7 282.7 283.3
280.6 280.6 280.0 280.0 280.0 279.5
308.4 286.1 285.5 285.5 286.1 286.6
315.9 345.8 350.2 361.0 367.0 359.9
281.1
280.6
281.1
281.1
281.1
280.6
282.7
283.3
282.7
283.3
282.7
283.3
337.2
342.1
345.9
347.5
343.7
331.8
287.2
287.2
296.4
312.7
319.3
326.3
Probe
Probe
Probe
Probe
Probe
Probe

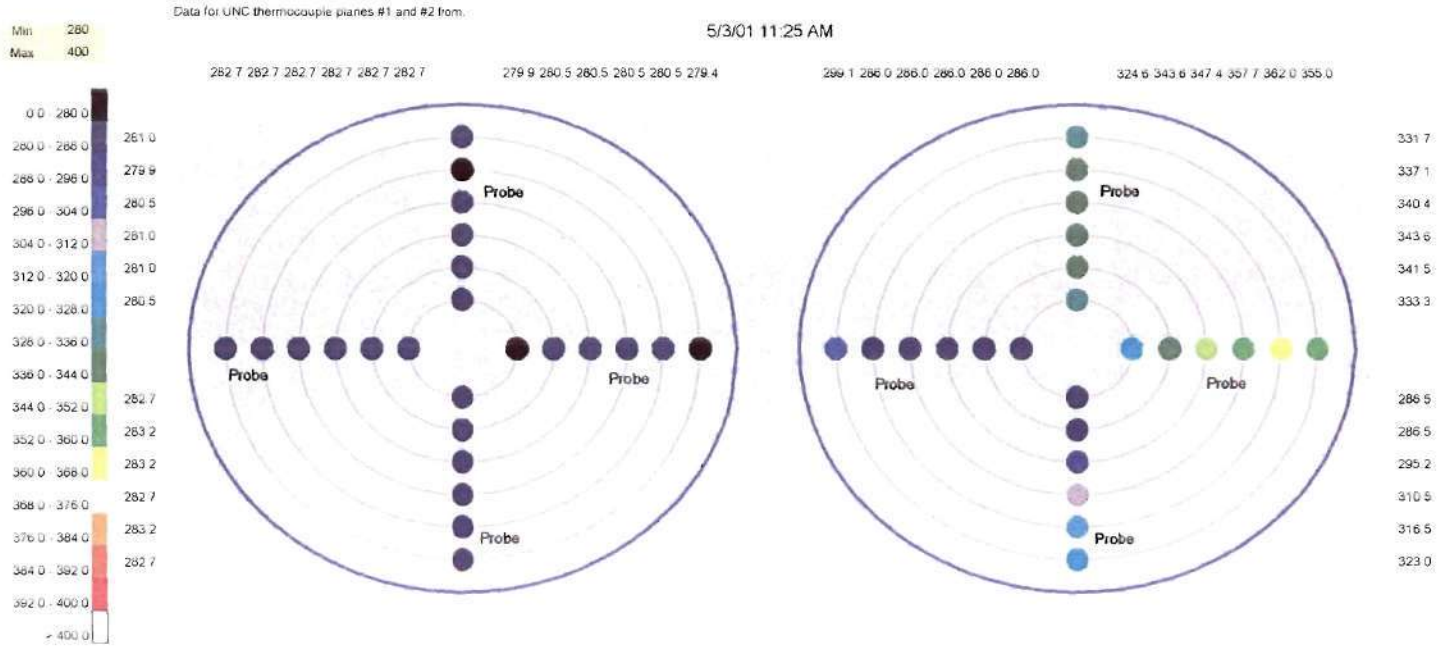
Data for UNC thermocouple planes #1 and #2 from:
5/3/01 11:25 AM
Min 280
Max 400
0.0 - 280.0
280.0 - 288.0
288.0 - 296.0
296.0 - 304.0
304.0 - 312.0
312.0 - 320.0
320.0 - 328.0
328.0 - 336.0
336.0 - 344.0
344.0 - 352.0
352.0 - 360.0
360.0 - 368.0
368.0 - 376.0
376.0 - 384.0
384.0 - 392.0
392.0 - 400.0
> 400.0
282.7 282.7 282.7 282.7 282.7 282.7
279.9 280.5 280.5 280.5 280.5 279.4
299.1 286.0 286.0 286.0 286.0 286.0
324.6 343.6 347.4 357.7 362.0 355.0
261.0
279.9
280.5
281.0
281.0
280.5
282.7
283.2
283.2
282.7
283.2
282.7
331.7
337.1
340.4
343.6
341.5
333.3
286.5
286.5
295.2
310.5
316.5
323.0
Probe
Probe
Probe
Probe
Probe
Probe

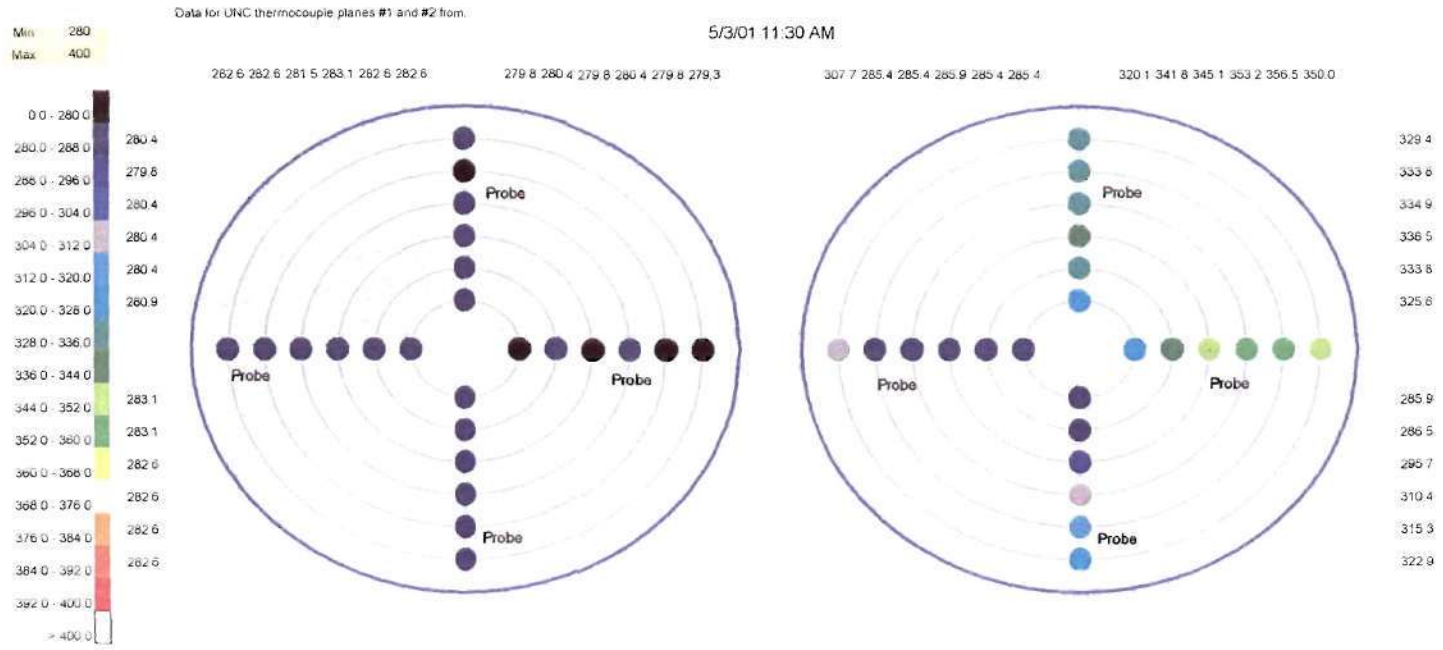
Data for UNC thermocouple planes #1 and #2 from
5/3/01 11:30 AM
Min 280
Max 400
0.0 - 280.0
280.0 - 288.0
288.0 - 296.0
296.0 - 304.0
304.0 - 312.0
312.0 - 320.0
320.0 - 328.0
328.0 - 336.0
336.0 - 344.0
344.0 - 352.0
352.0 - 360.0
360.0 - 368.0
368.0 - 376.0
376.0 - 384.0
384.0 - 392.0
392.0 - 400.0
> 400.0
282.6 282.6 281.5 283.1 282.6 282.6
279.8 280.4 279.8 280.4 279.8 279.3
307.7 285.4 285.4 285.9 285.4 285.4
320.1 341.8 345.1 353.2 356.5 350.0
280.4
279.8
280.4
280.4
280.4
280.9
283.1
283.1
282.6
282.6
282.6
282.6
329.4
333.6
334.9
336.5
333.6
325.6
285.9
286.5
285.7
310.4
315.3
322.9
Probe
Probe
Probe
Probe
Probe
Probe

APPENDIX C

STEAMCFD OUTPUT FOR CASE 1

This appendix contains the graphical representations of computational data collected from the SteamCFD Code. This data examines the results obtained when utilizing the four-nozzle desuperheater arrangement and experimental data from the time period of 1170-1200 minutes elapsed time from midnight on October 30, 2000, i.e., 07:30 to 08:00 AM. The graphical representations include output from both Version 1.2 and Version 2.0 of the SteamCFD Code.

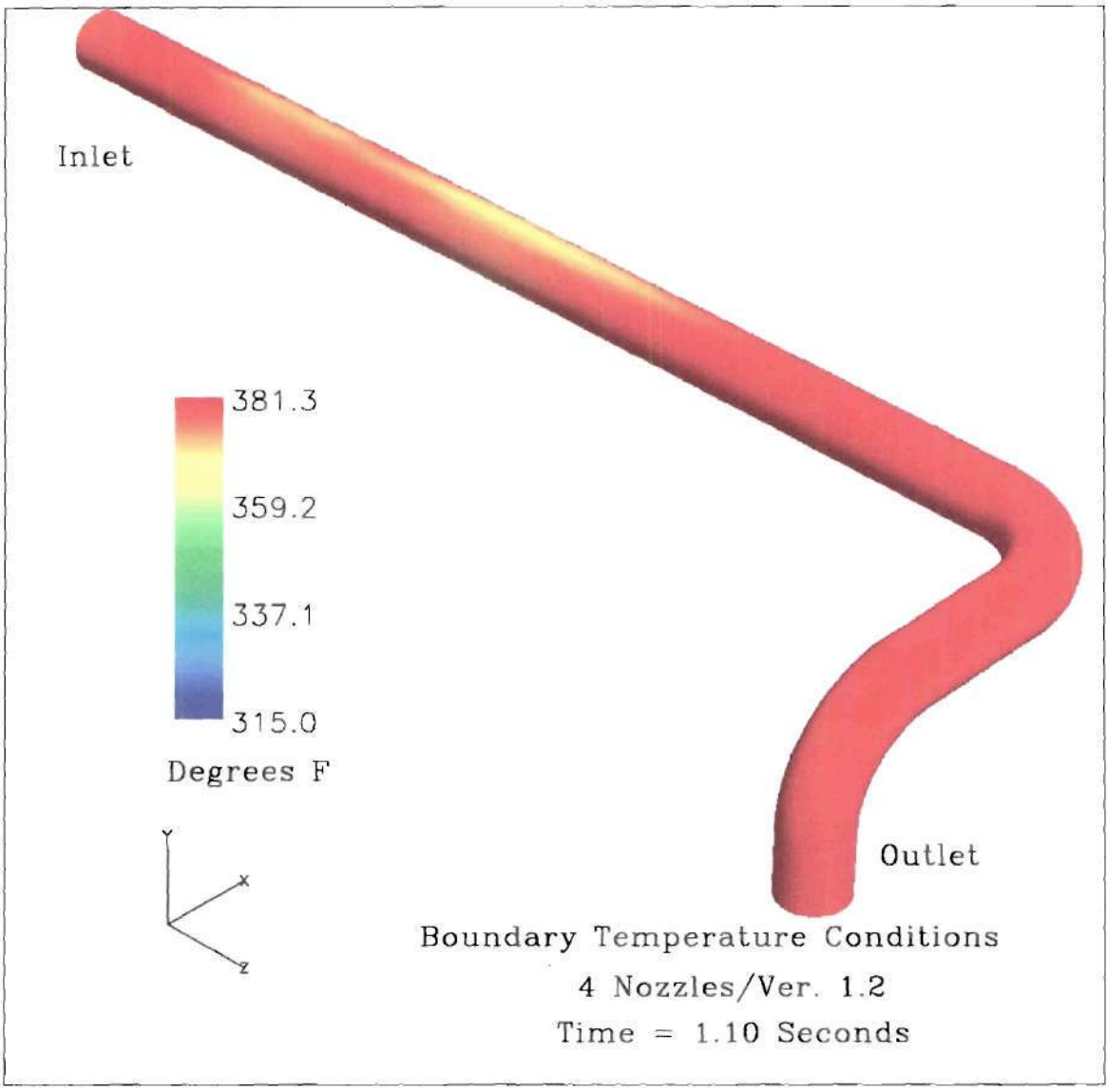
Inlet
381.3
359.2
337.1
315.0
Degrees F
Y
X
Z
Outlet
Boundary Temperature Conditions
4 Nozzles/Ver. 1.2
Time = 1.10 Seconds

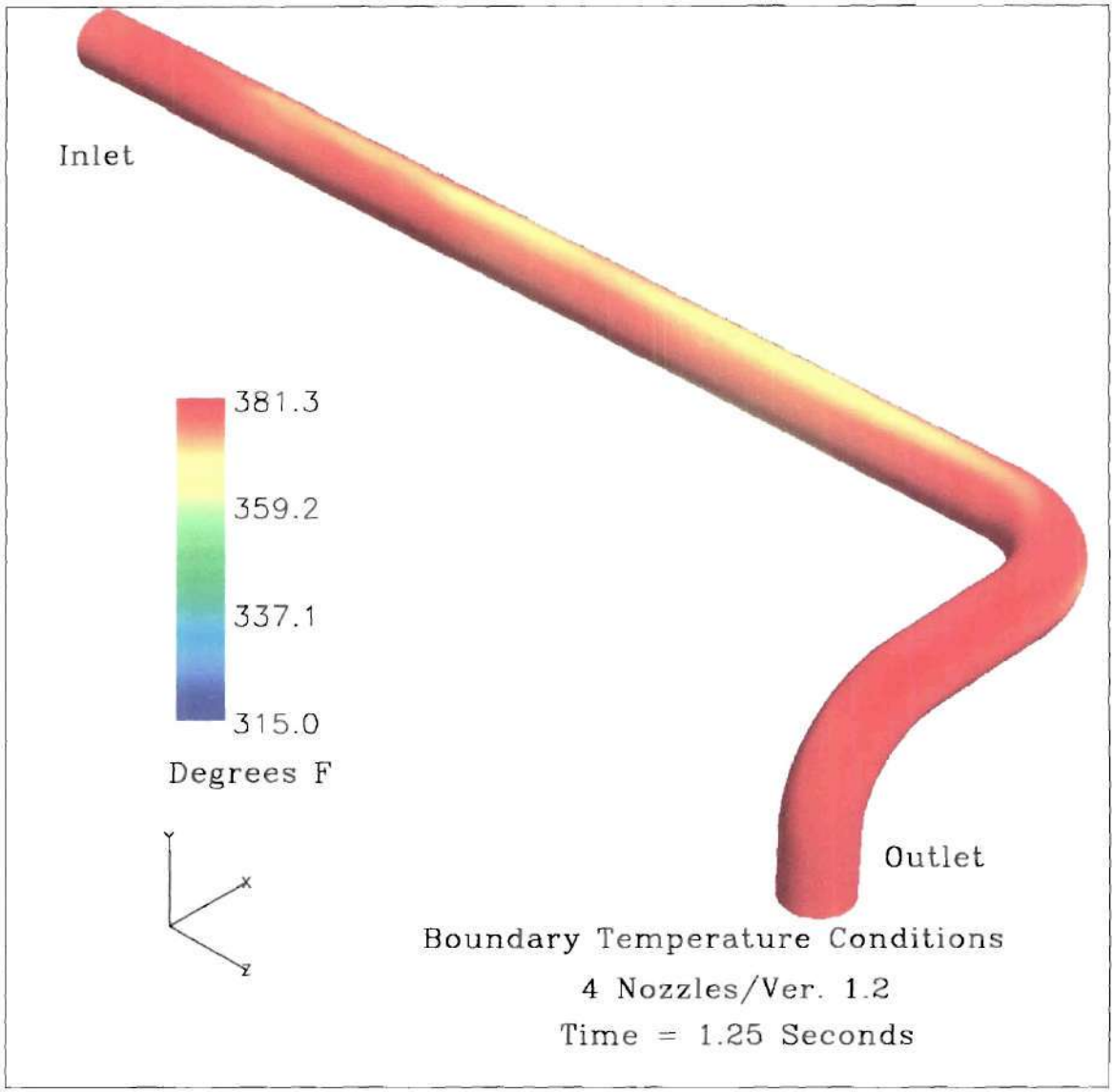
Inlet
381.3
359.2
337.1
315.0
Degrees F
Y
X
Z
Outlet
Boundary Temperature Conditions
4 Nozzles/Ver. 1.2
Time = 1.25 Seconds

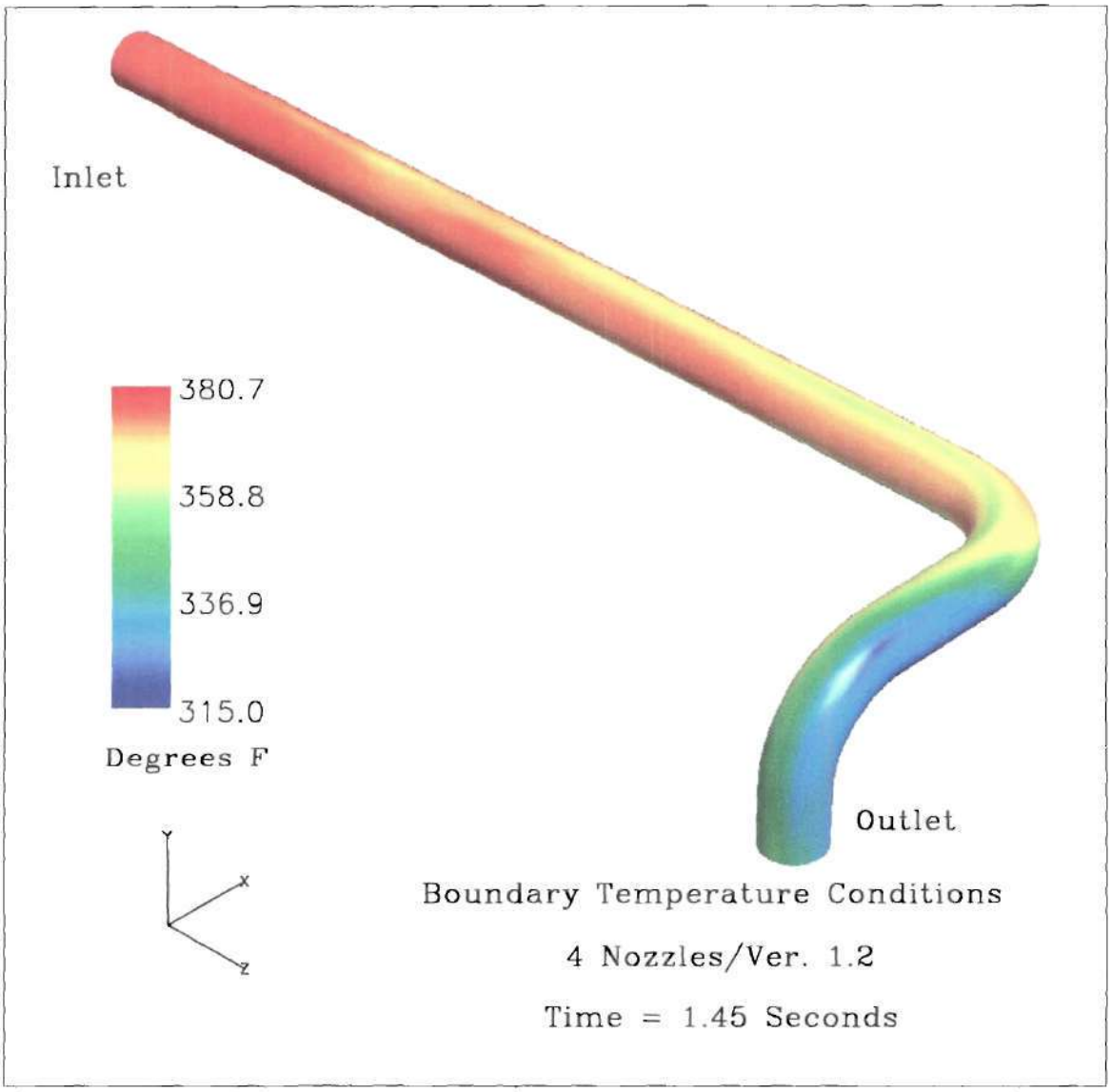
Inlet
380.7
358.8
336.9
315.0
Degrees F
Y
X
Z
Outlet
Boundary Temperature Conditions
4 Nozzles/Ver. 1.2
Time = 1.45 Seconds

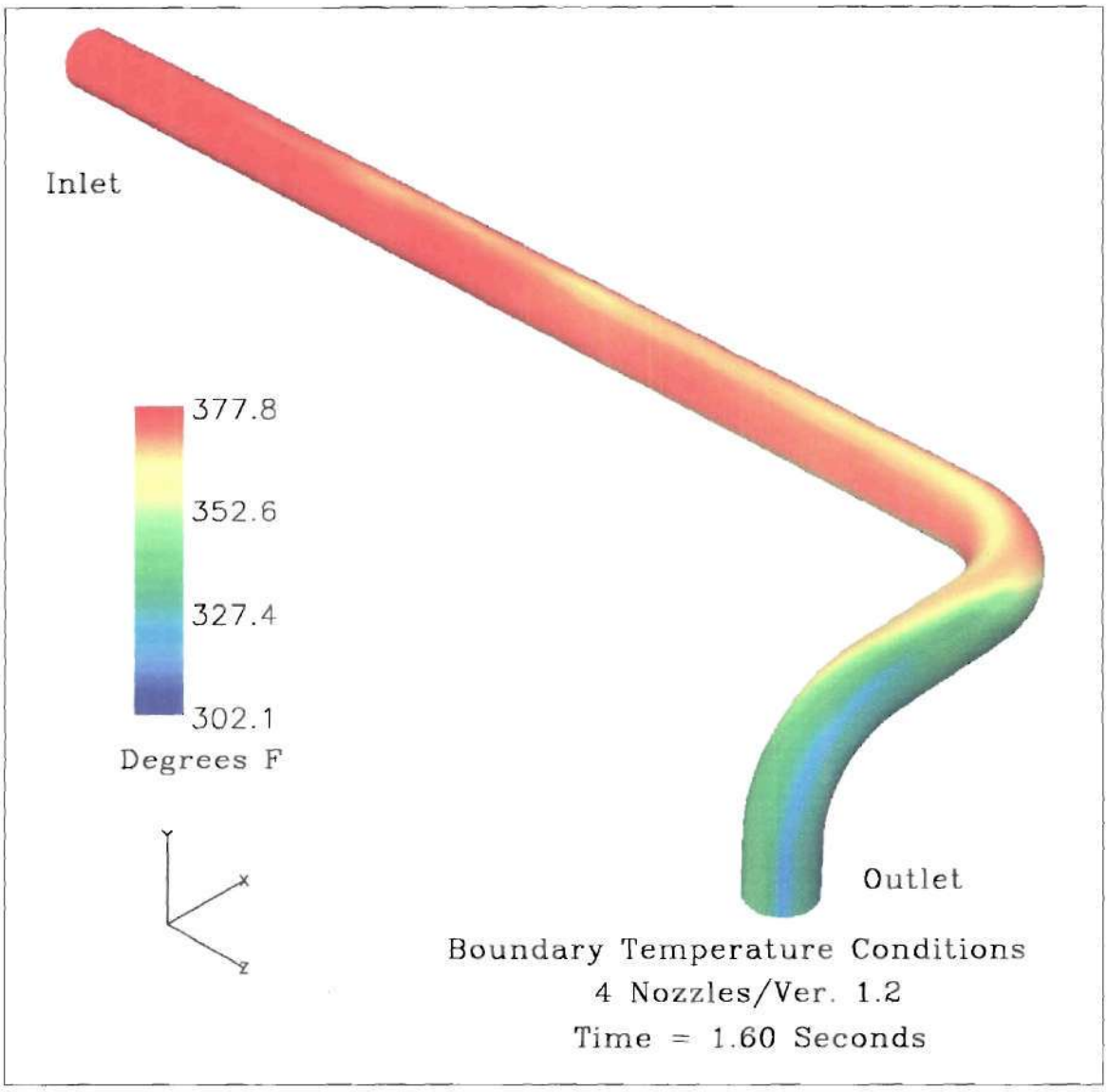
Inlet
377.8
352.6
327.4
302.1
Degrees F
Y
X
Z
Outlet
Boundary Temperature Conditions
4 Nozzles/Ver. 1.2
Time = 1.60 Seconds

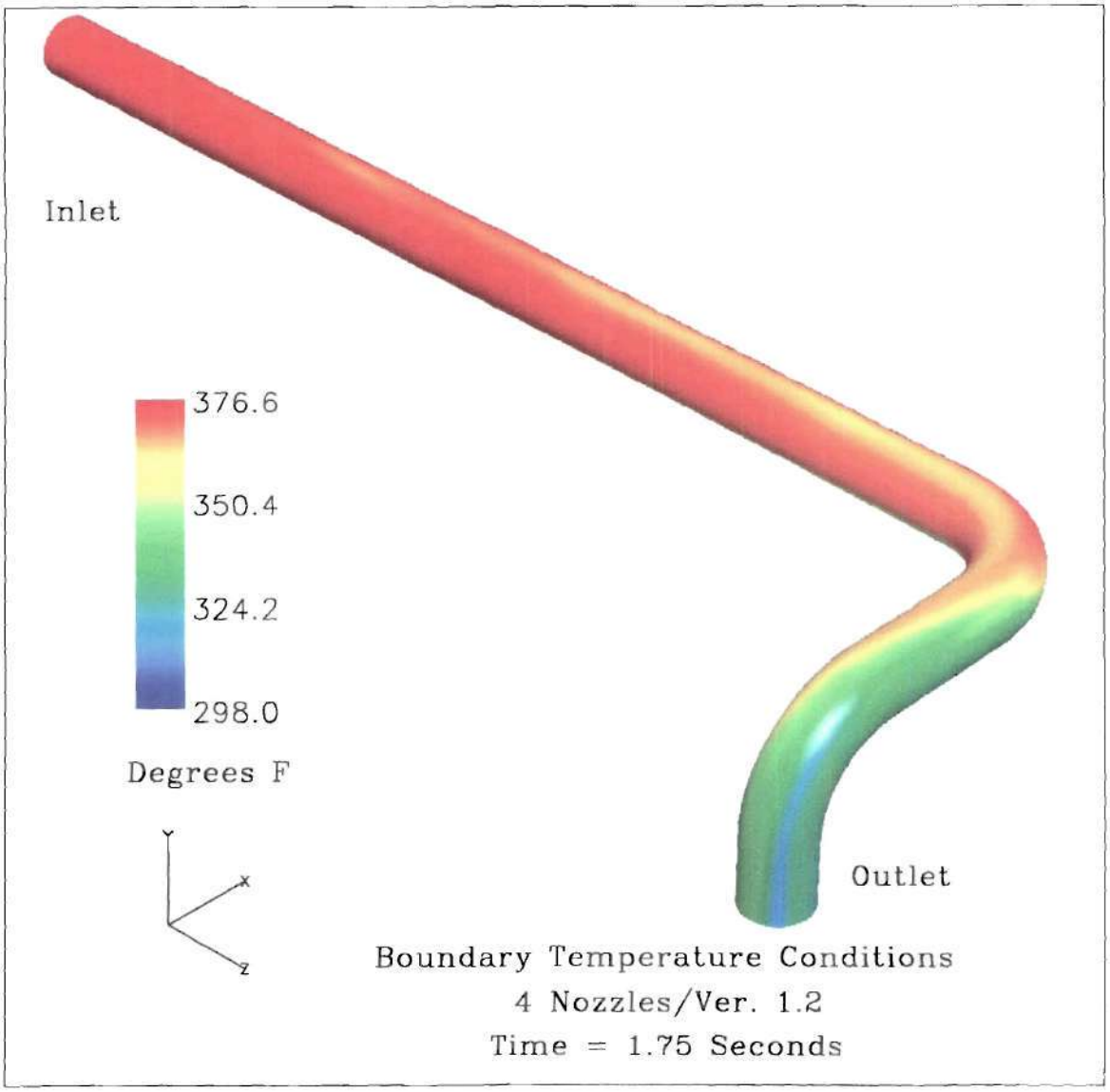
Inlet
376.6
350.4
324.2
298.0
Degrees F
Y
X
Z
Outlet
Boundary Temperature Conditions
4 Nozzles/Ver. 1.2
Time = 1.75 Seconds

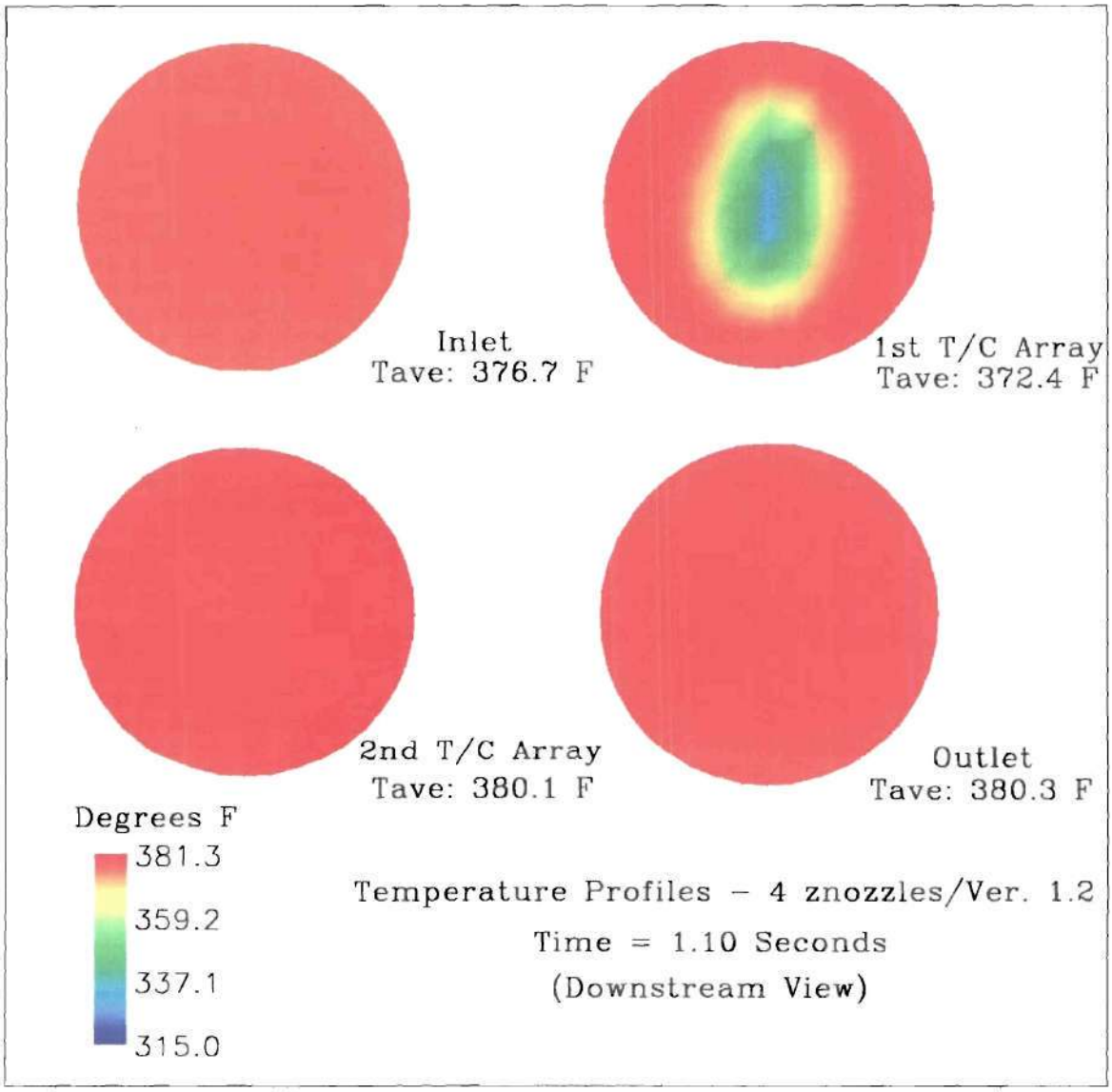
Inlet
Tave: 376.7 F
1st T/C Array
Tave: 372.4 F
2nd T/C Array
Tave: 380.1 F
Outlet
Tave: 380.3 F
Degrees F
381.3
359.2
337.1
315.0
Temperature Profiles - 4 znozzles/Ver. 1.2
Time = 1.10 Seconds
(Downstream View)

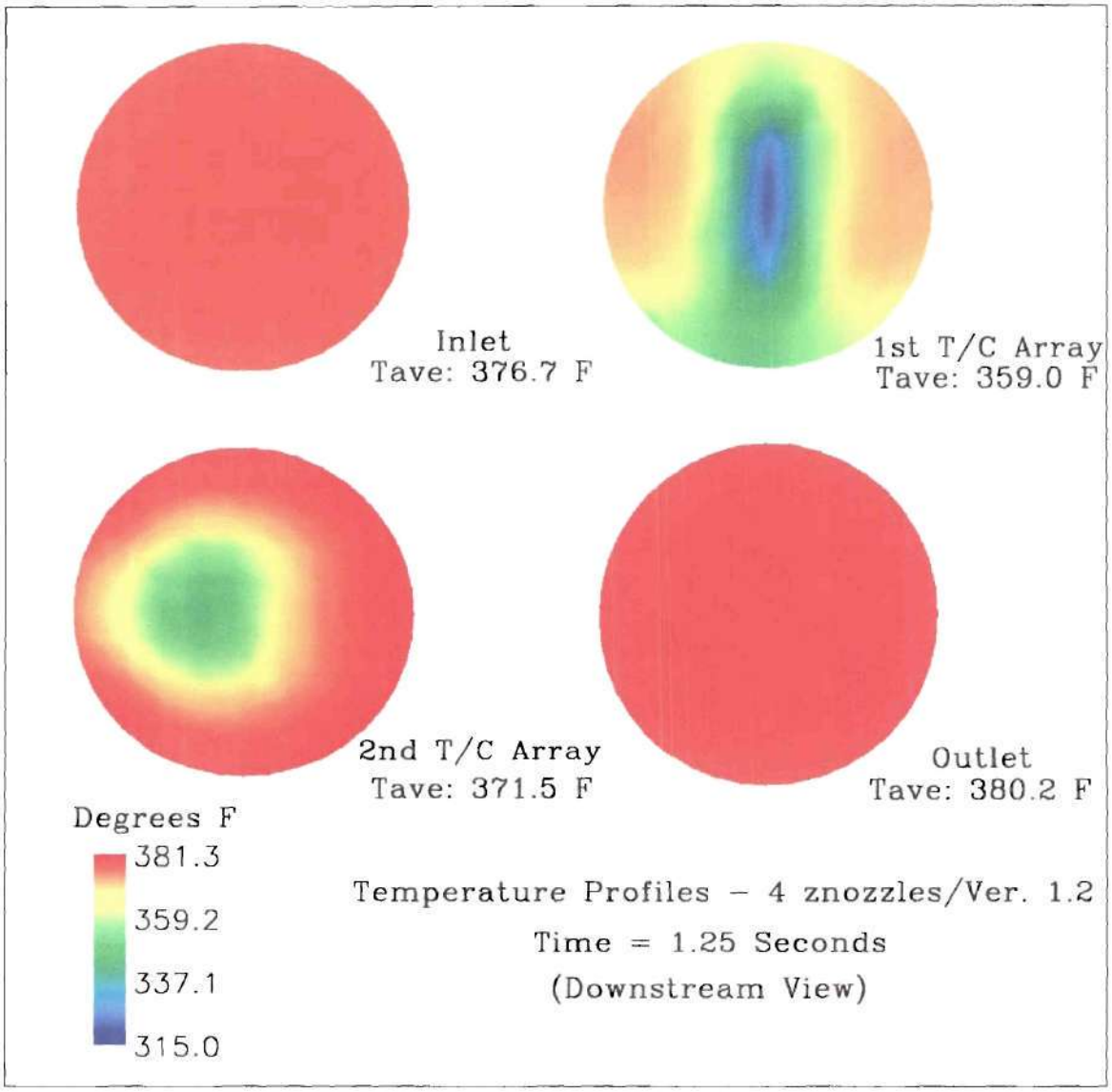
Inlet
Tave: 376.7 F
1st T/C Array
Tave: 359.0 F
2nd T/C Array
Tave: 371.5 F
Outlet
Tave: 380.2 F
Degrees F
381.3
359.2
337.1
315.0
Temperature Profiles - 4 znozzles/Ver. 1.2
Time = 1.25 Seconds
(Downstream View)

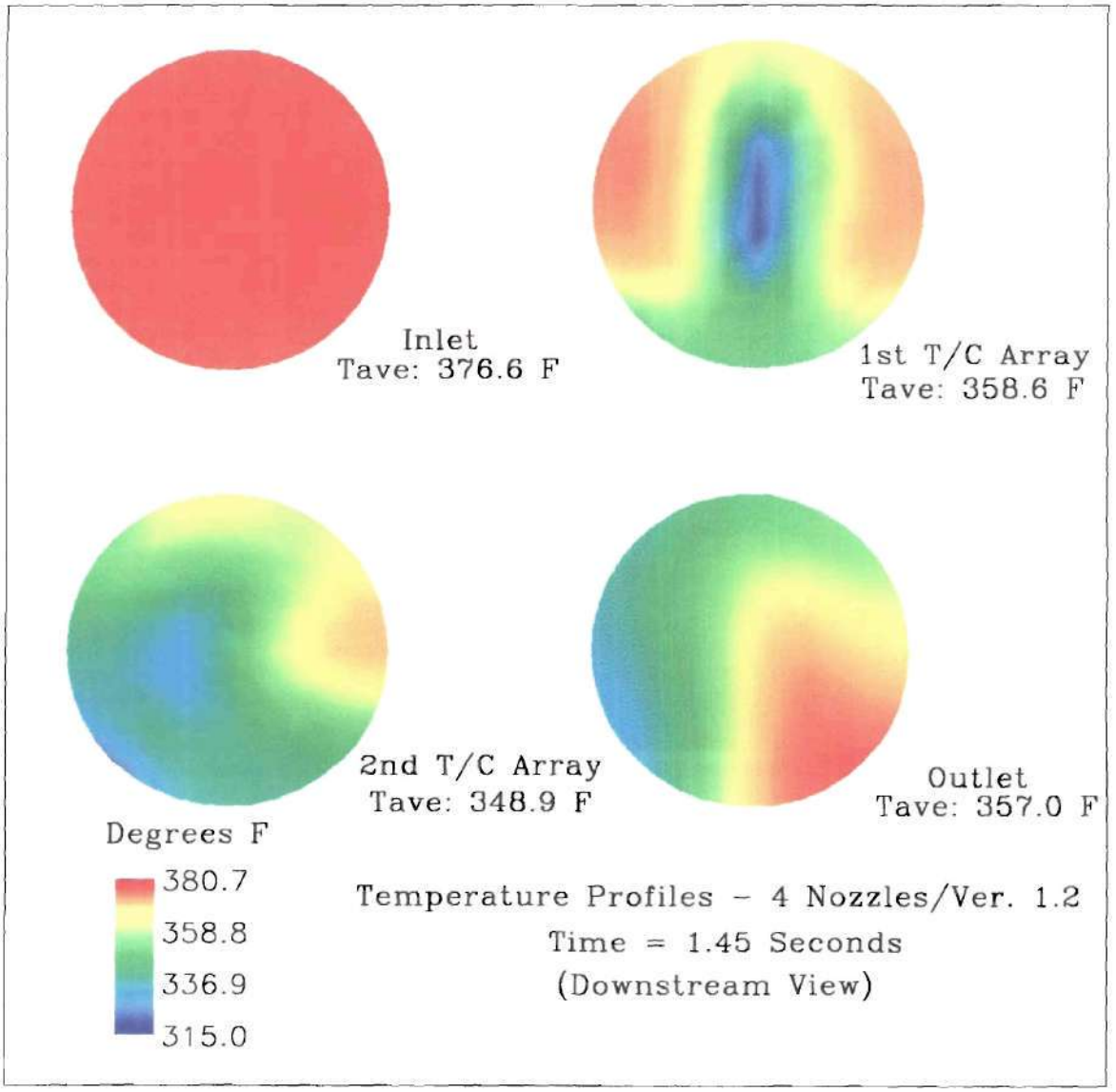
Inlet
Tave: 376.6 F
1st T/C Array
Tave: 358.6 F
2nd T/C Array
Tave: 348.9 F
Outlet
Tave: 357.0 F
Degrees F
380.7
358.8
336.9
315.0
Temperature Profiles - 4 Nozzles/Ver. 1.2
Time = 1.45 Seconds
(Downstream View)

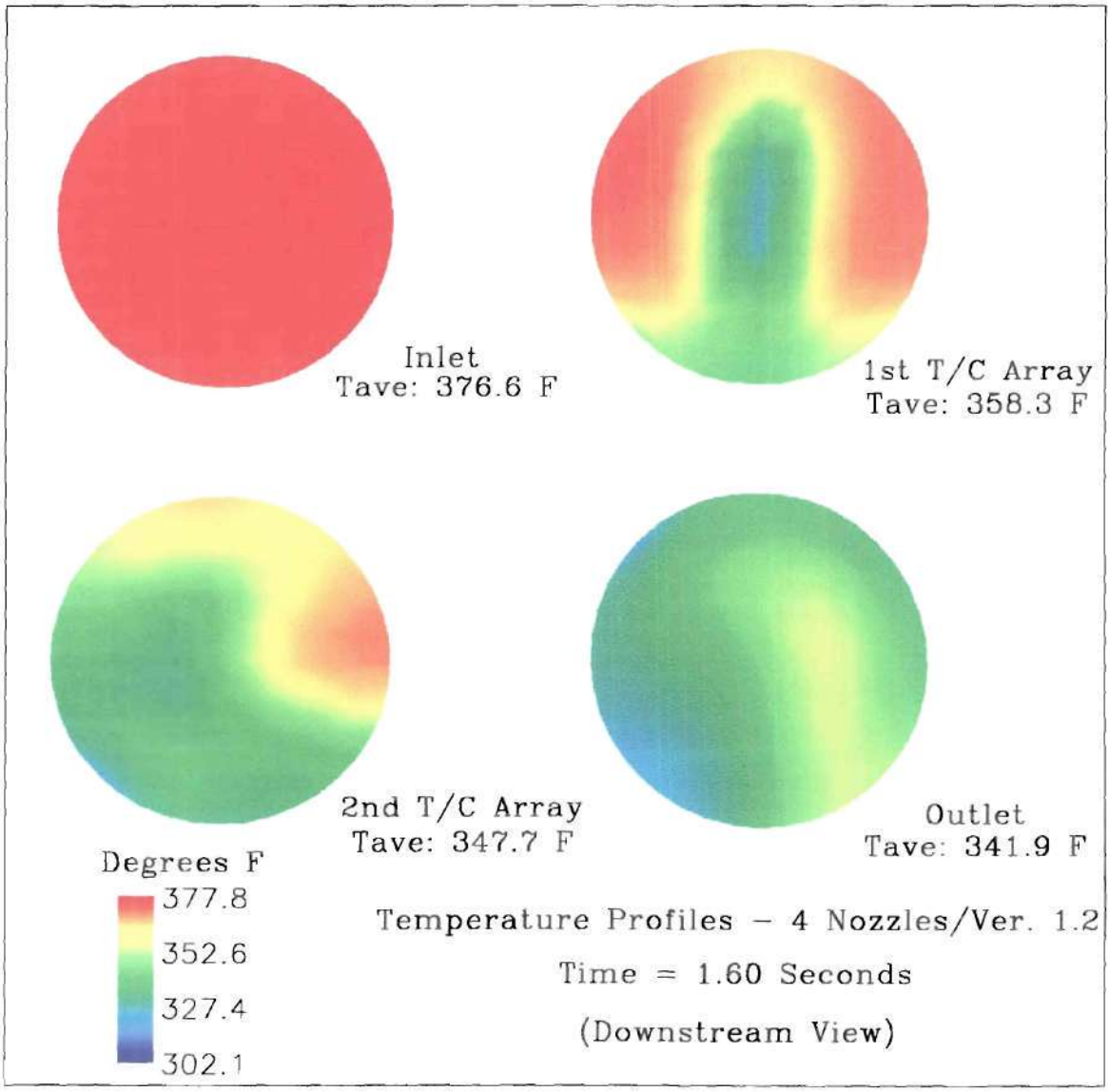
Inlet
Tave: 376.6 F
1st T/C Array
Tave: 358.3 F
2nd T/C Array
Tave: 347.7 F
Outlet
Tave: 341.9 F
Degrees F
377.8
352.6
327.4
302.1
Temperature Profiles - 4 Nozzles/Ver. 1.2
Time = 1.60 Seconds
(Downstream View)

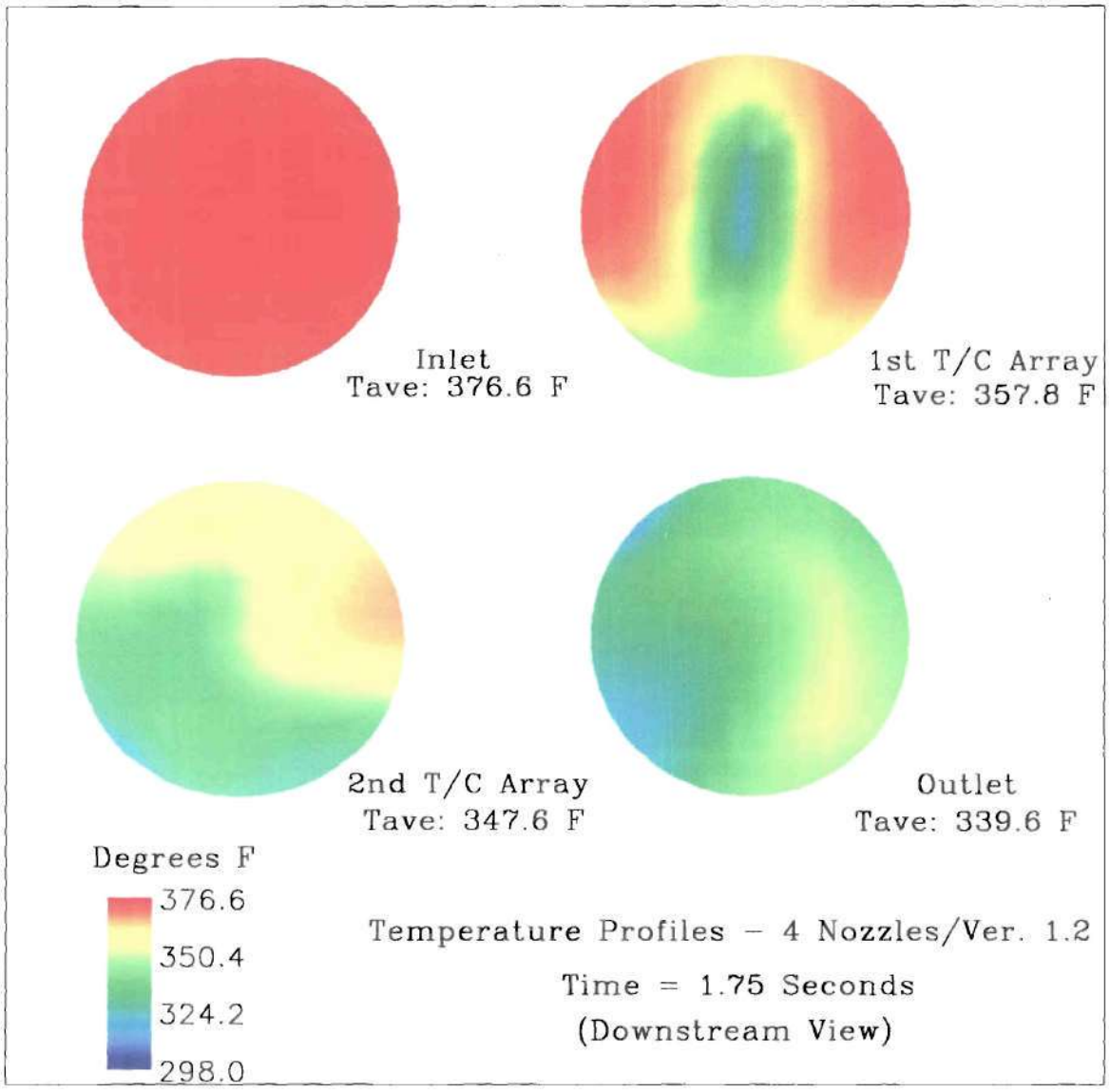
Inlet
Tave: 376.6 F
1st T/C Array
Tave: 357.8 F
2nd T/C Array
Tave: 347.6 F
Outlet
Tave: 339.6 F
Degrees F
376.6
350.4
324.2
298.0
Temperature Profiles - 4 Nozzles/Ver. 1.2
Time = 1.75 Seconds
(Downstream View)

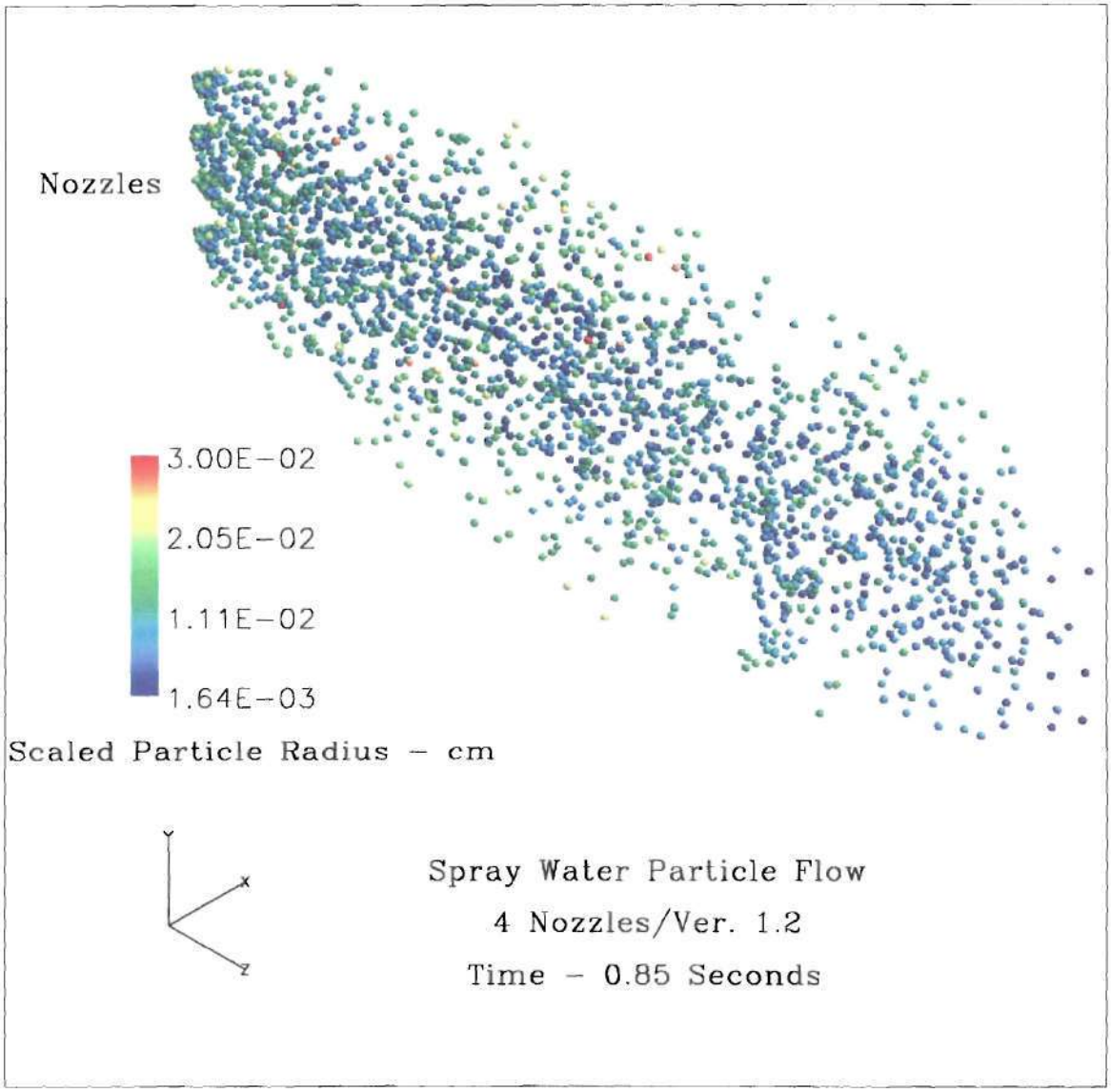
Nozzles
3.00E-02
2.05E-02
1.11E-02
1.64E-03
Scaled Particle Radius - cm
Y
X
Z
Spray Water Particle Flow
4 Nozzles/Ver. 1.2
Time - 0.85 Seconds

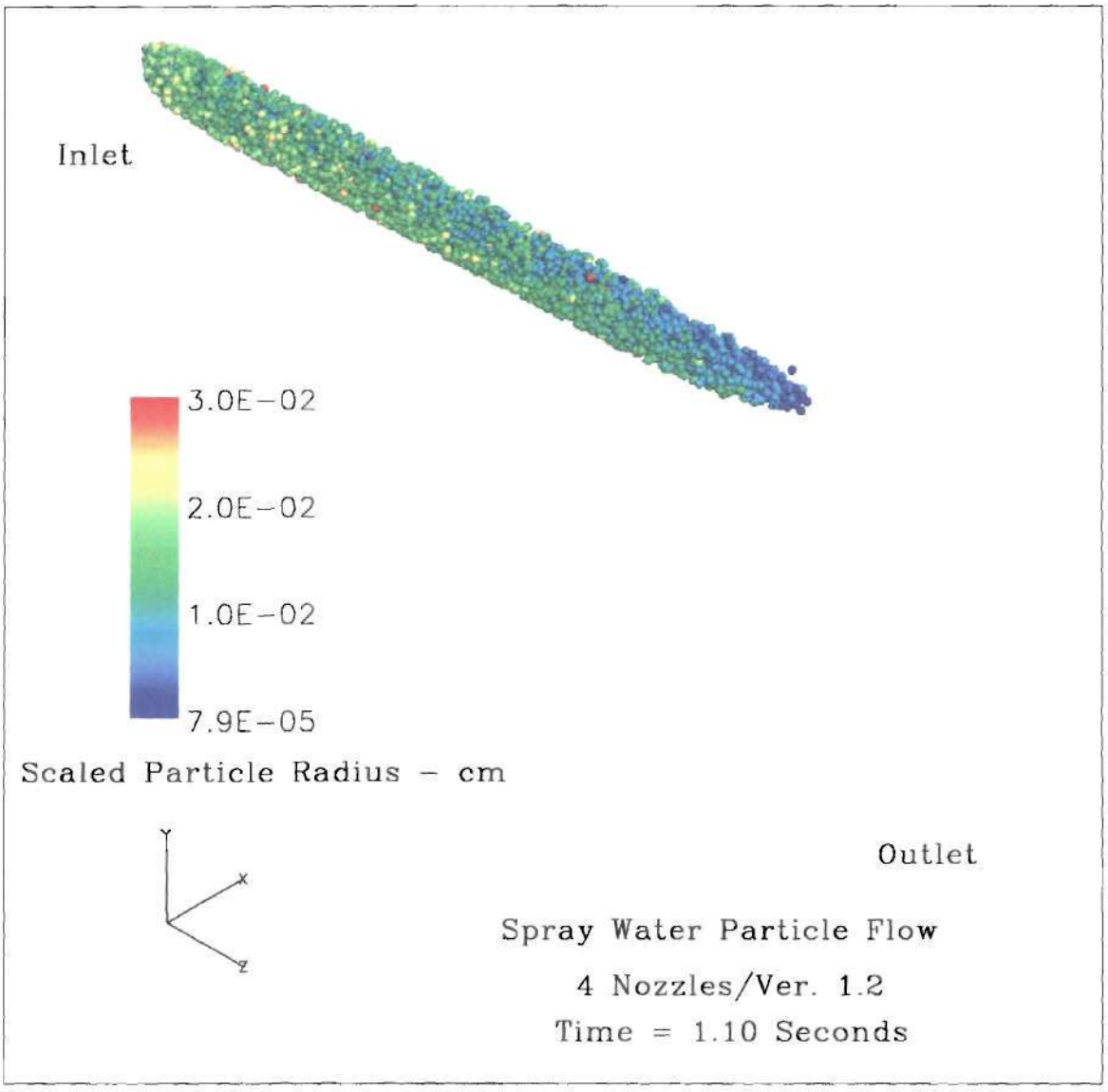
Inlet
3.0E-02
2.0E-02
1.0E-02
7.9E-05
Scaled Particle Radius - cm
Y
X
Z
Outlet
Spray Water Particle Flow
4 Nozzles/Ver. 1.2
Time = 1.10 Seconds

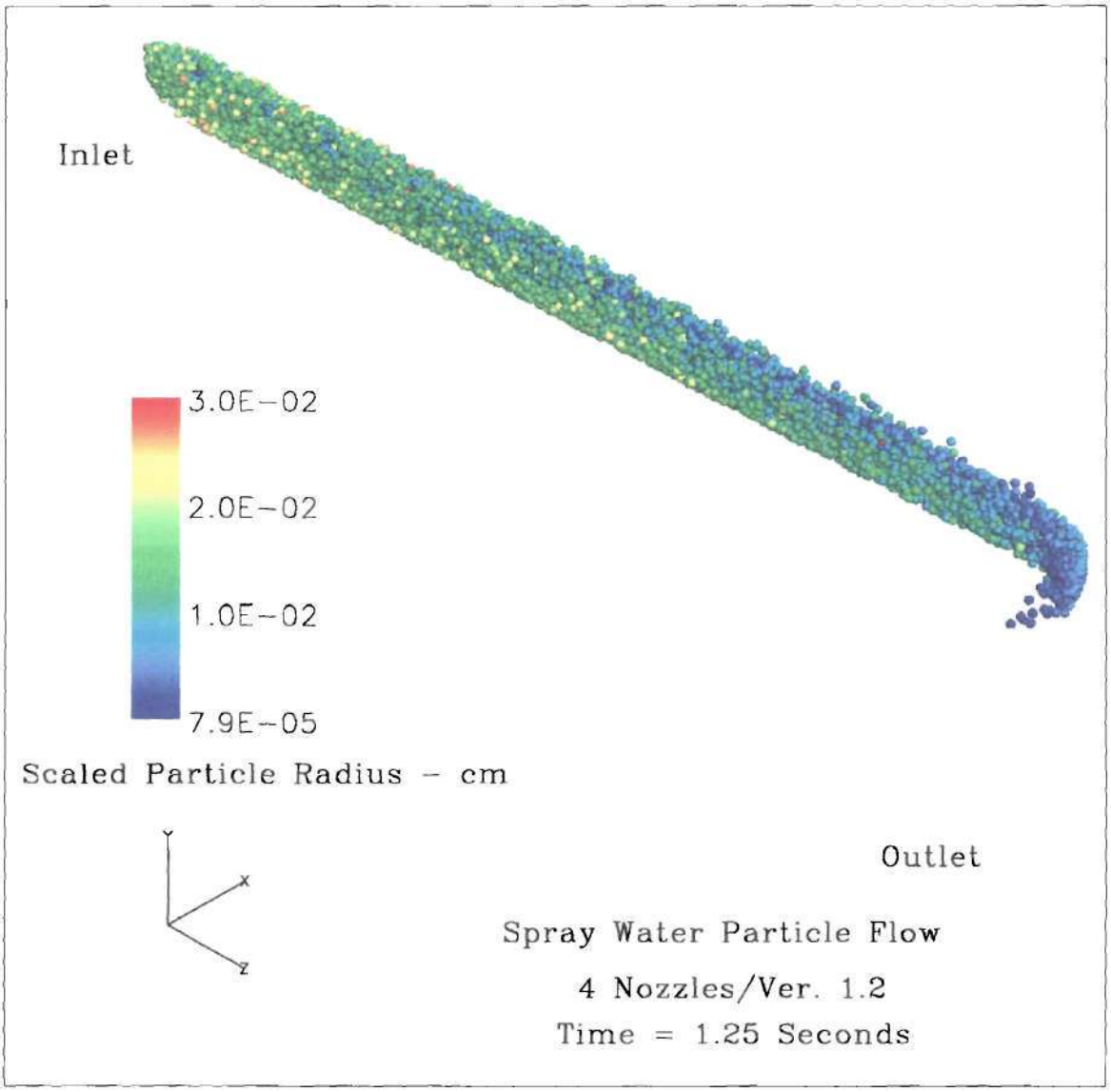
Inlet
3.0E-02
2.0E-02
1.0E-02
7.9E-05
Scaled Particle Radius - cm
Y
X
Z
Outlet
Spray Water Particle Flow
4 Nozzles/Ver. 1.2
Time = 1.25 Seconds

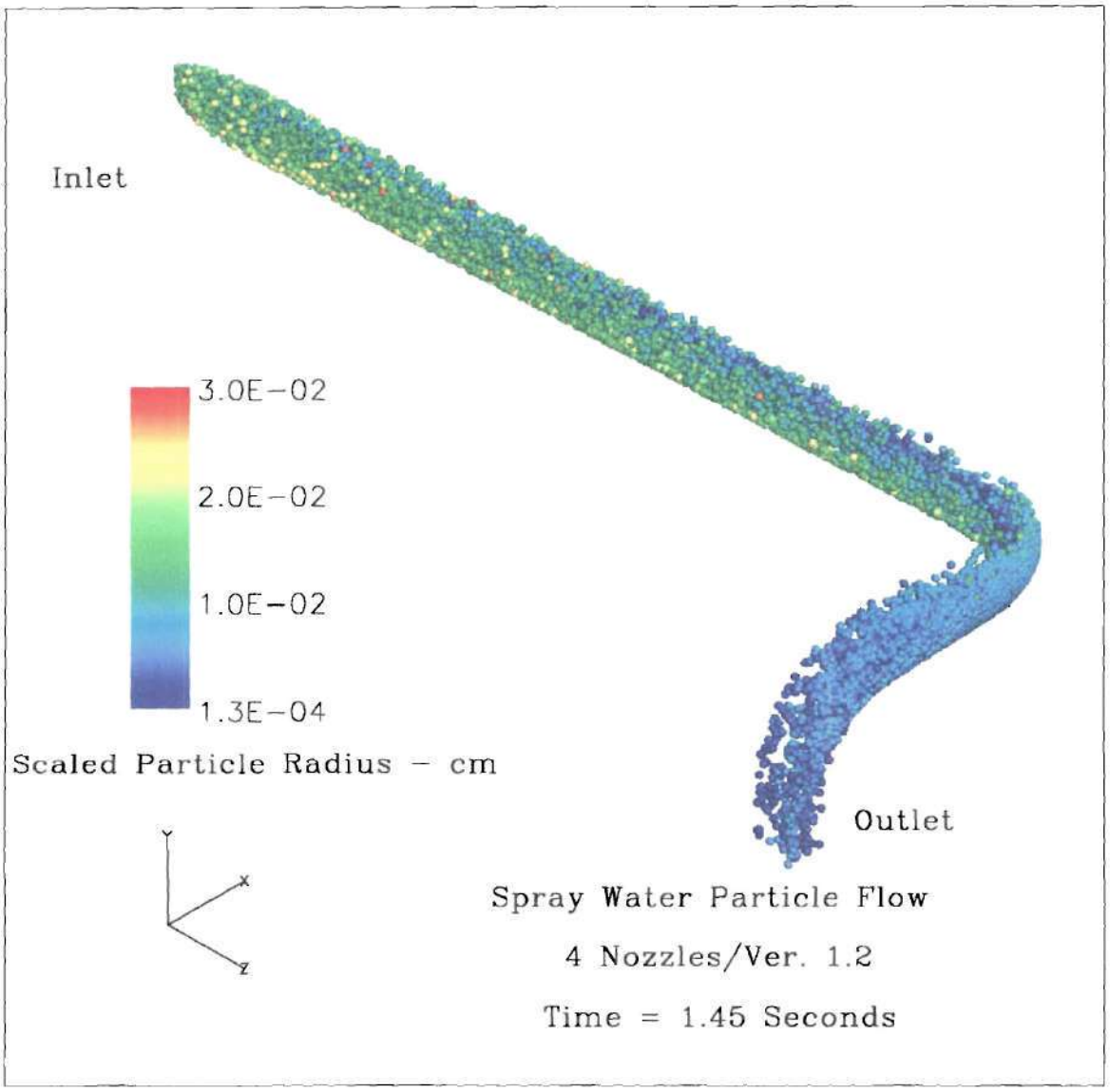
Inlet
3.0E−02
2.0E−02
1.0E−02
1.3E−04
Scaled Particle Radius − cm
Outlet
Y
X
Z
Spray Water Particle Flow
4 Nozzles/Ver. 1.2
Time = 1.45 Seconds

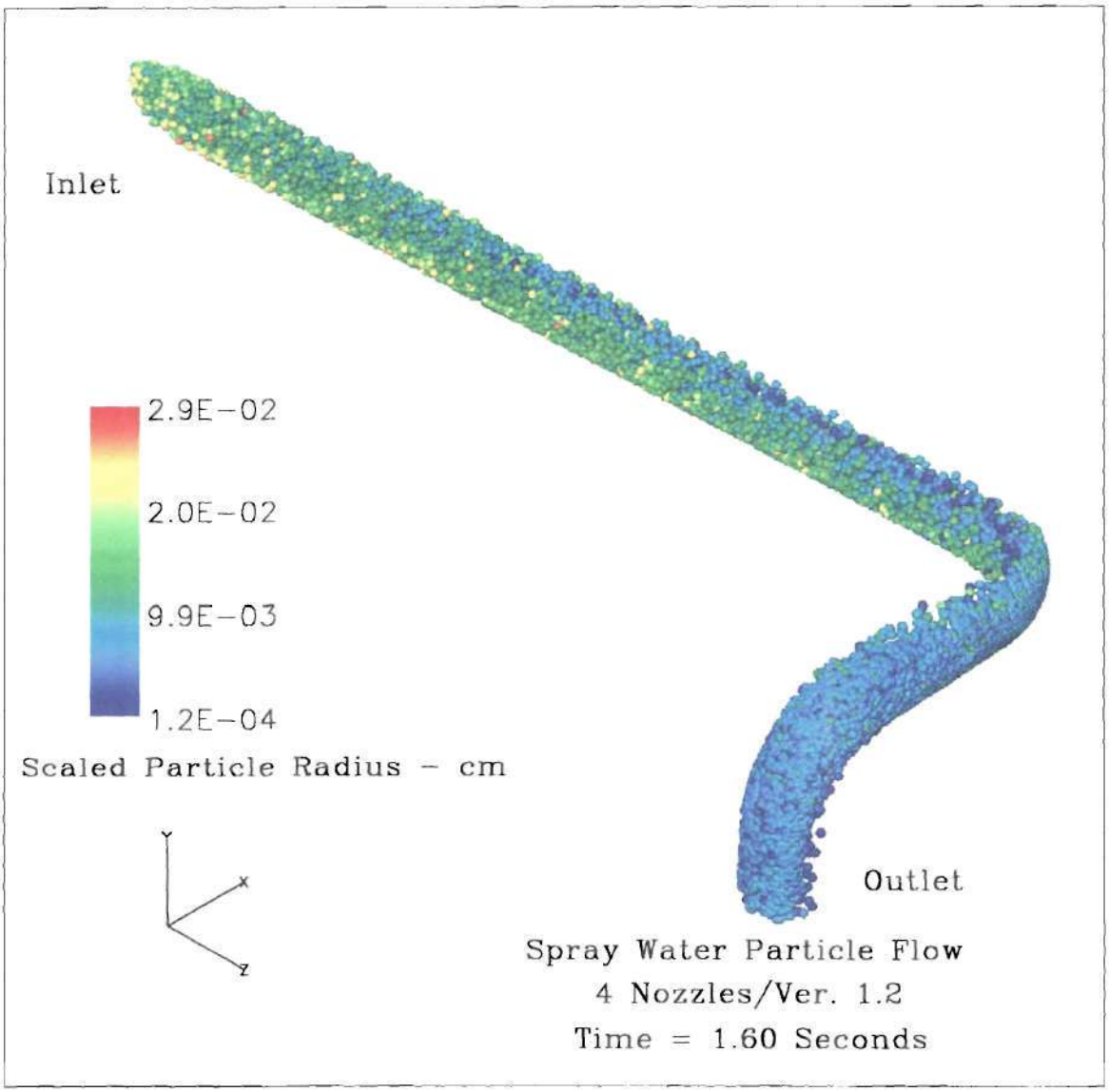
Inlet
2.9E-02
2.0E-02
9.9E-03
1.2E-04
Scaled Particle Radius - cm
Y
X
Z
Outlet
Spray Water Particle Flow
4 Nozzles/Ver. 1.2
Time = 1.60 Seconds

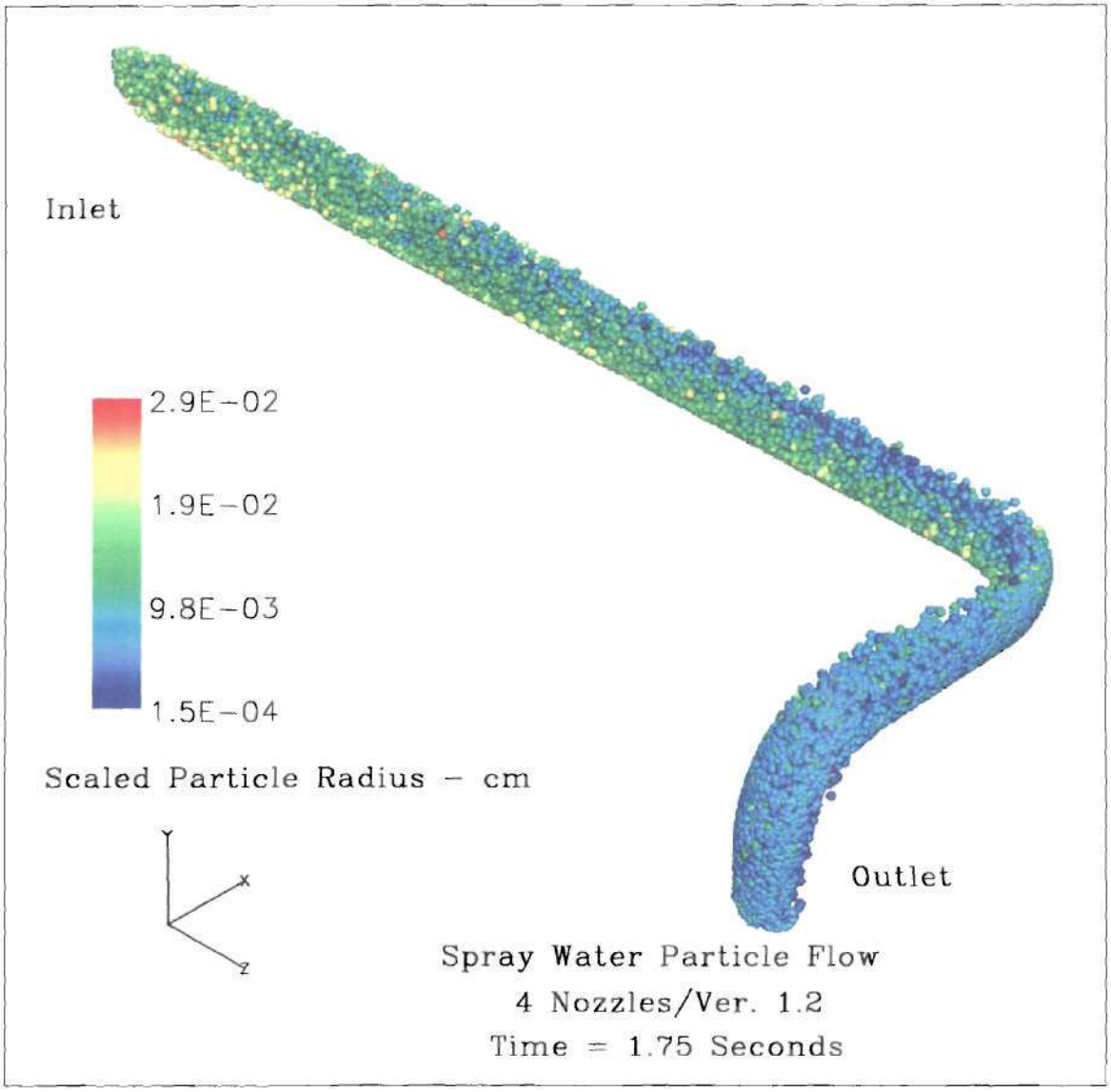
Inlet
2.9E-02
1.9E-02
9.8E-03
1.5E-04
Scaled Particle Radius - cm
Y
X
Z
Outlet
Spray Water Particle Flow
4 Nozzles/Ver. 1.2
Time = 1.75 Seconds

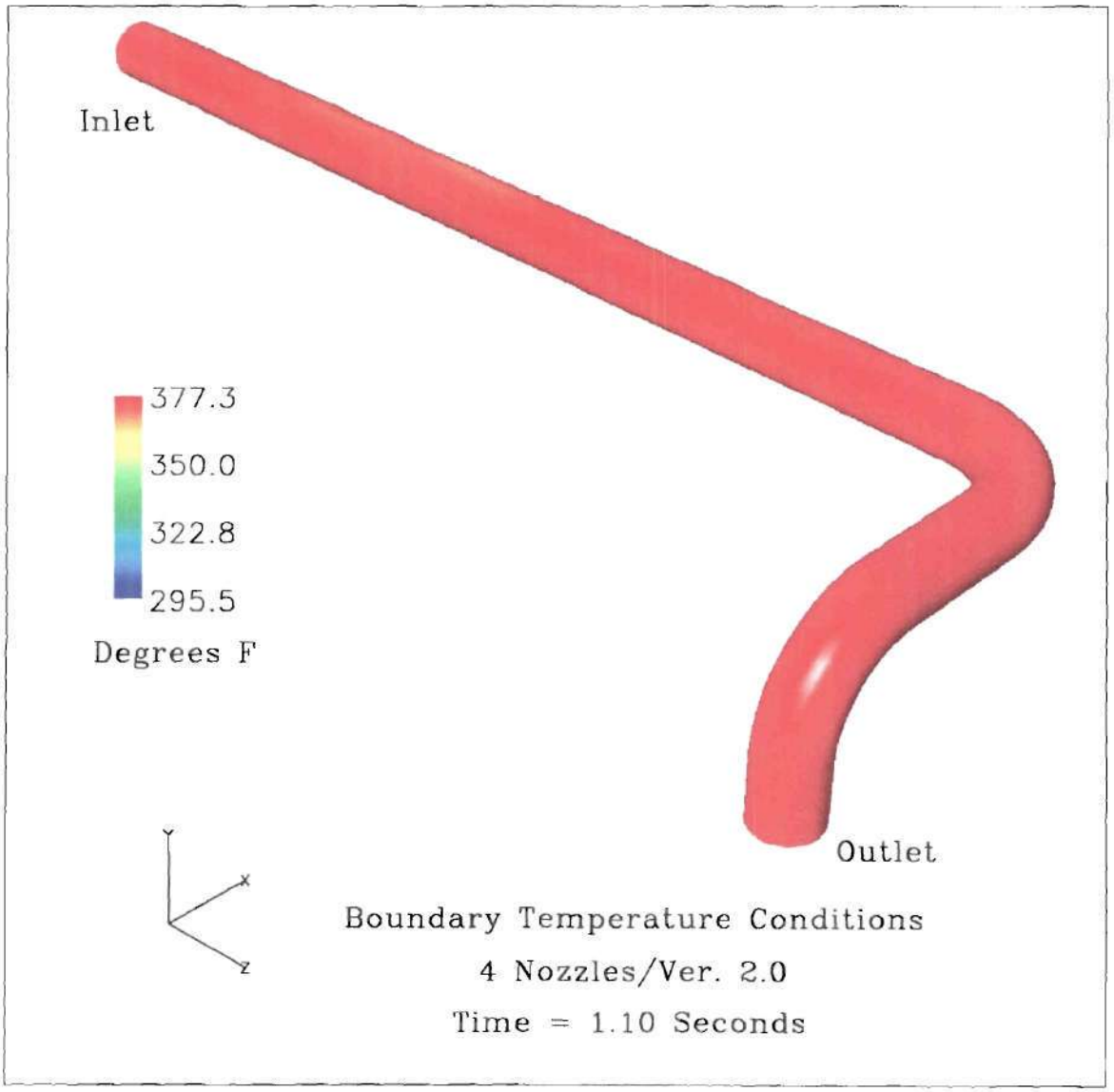
Inlet
377.3
350.0
322.8
295.5
Degrees F
Outlet
Y
X
Z
Boundary Temperature Conditions
4 Nozzles/Ver. 2.0
Time = 1.10 Seconds

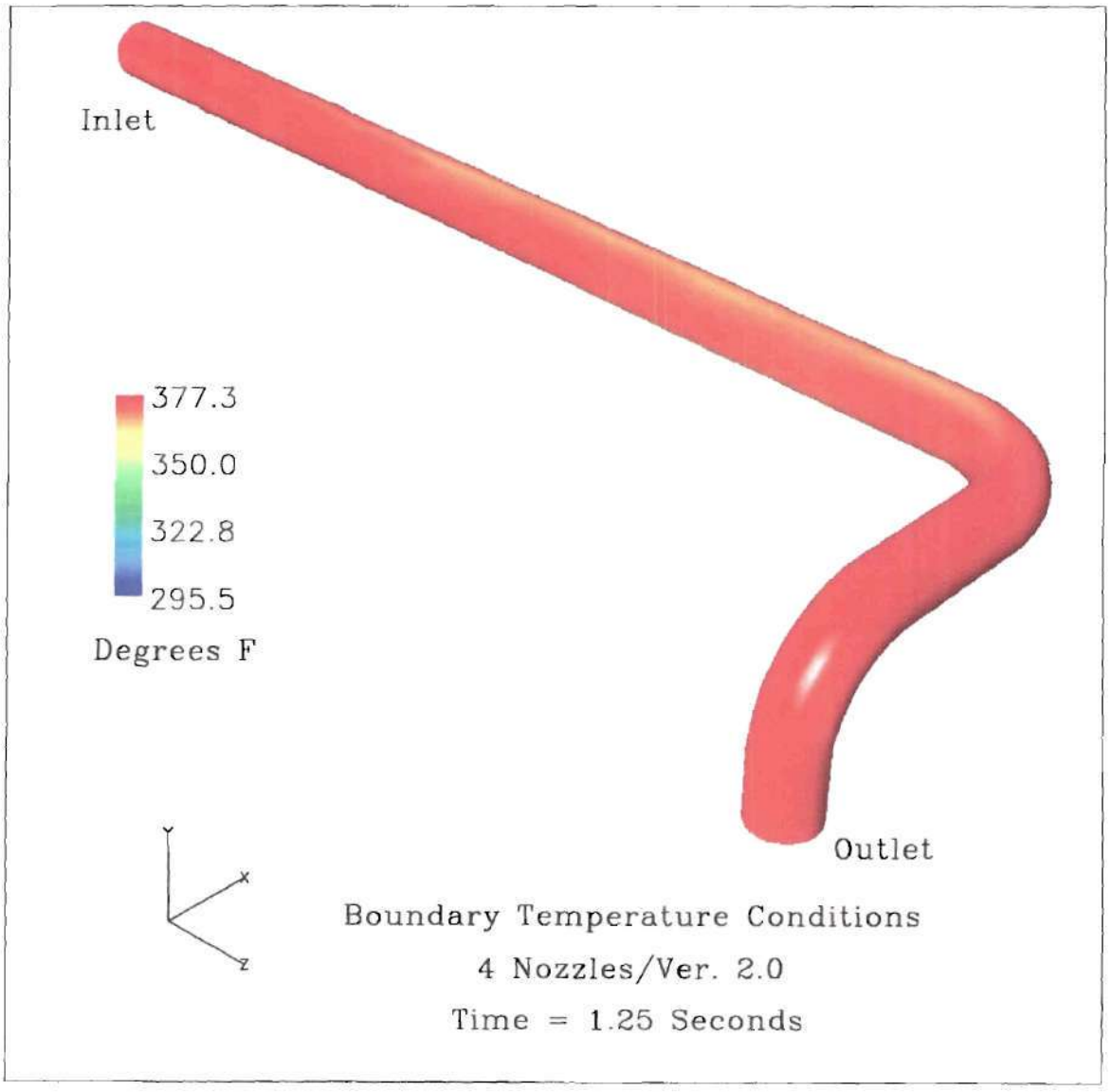
Inlet
377.3
350.0
322.8
295.5
Degrees F
Outlet
Y
X
Z
Boundary Temperature Conditions
4 Nozzles/Ver. 2.0
Time = 1.25 Seconds

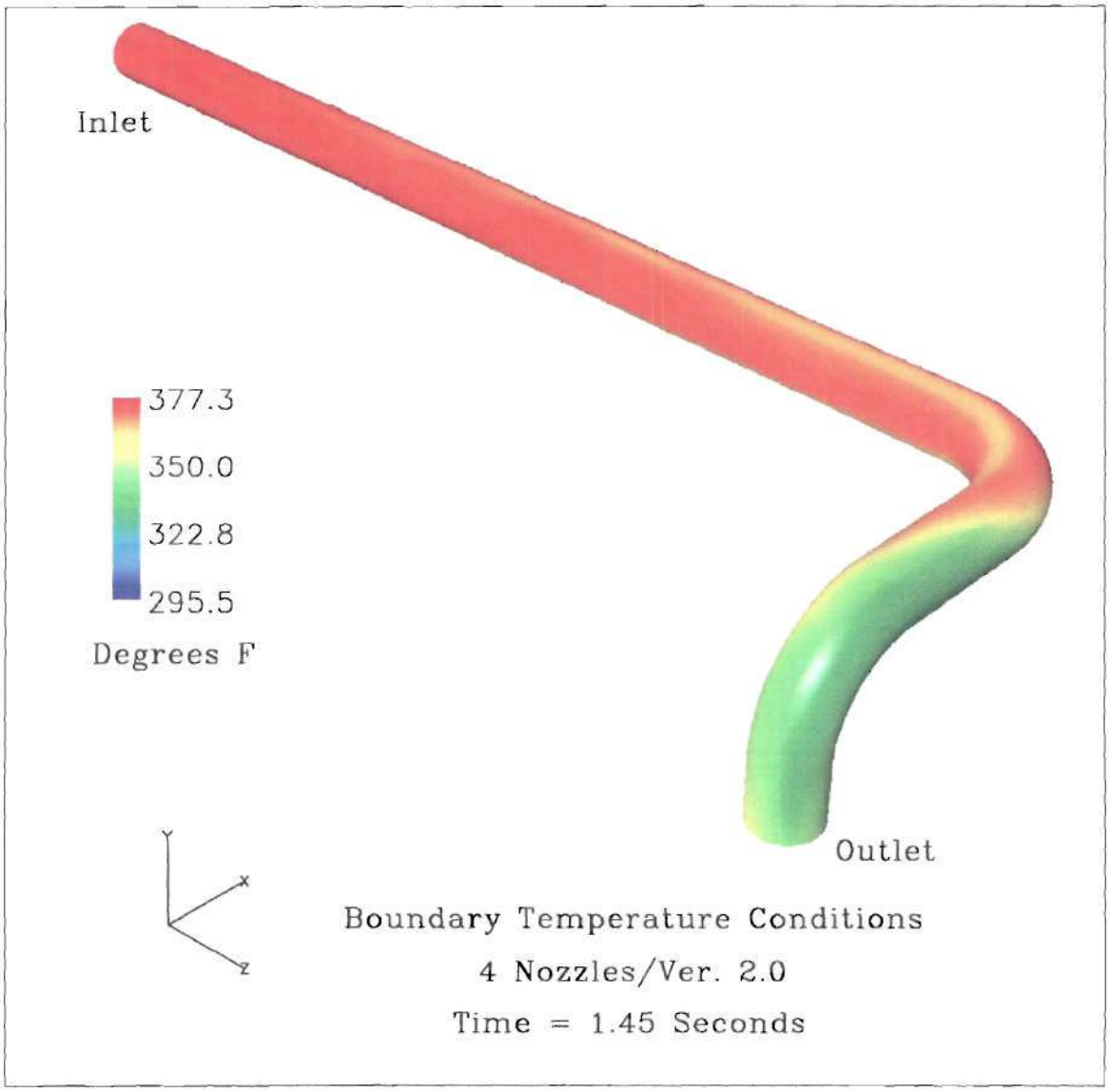
Inlet
377.3
350.0
322.8
295.5
Degrees F
Outlet
Y
X
Z
Boundary Temperature Conditions
4 Nozzles/Ver. 2.0
Time = 1.45 Seconds

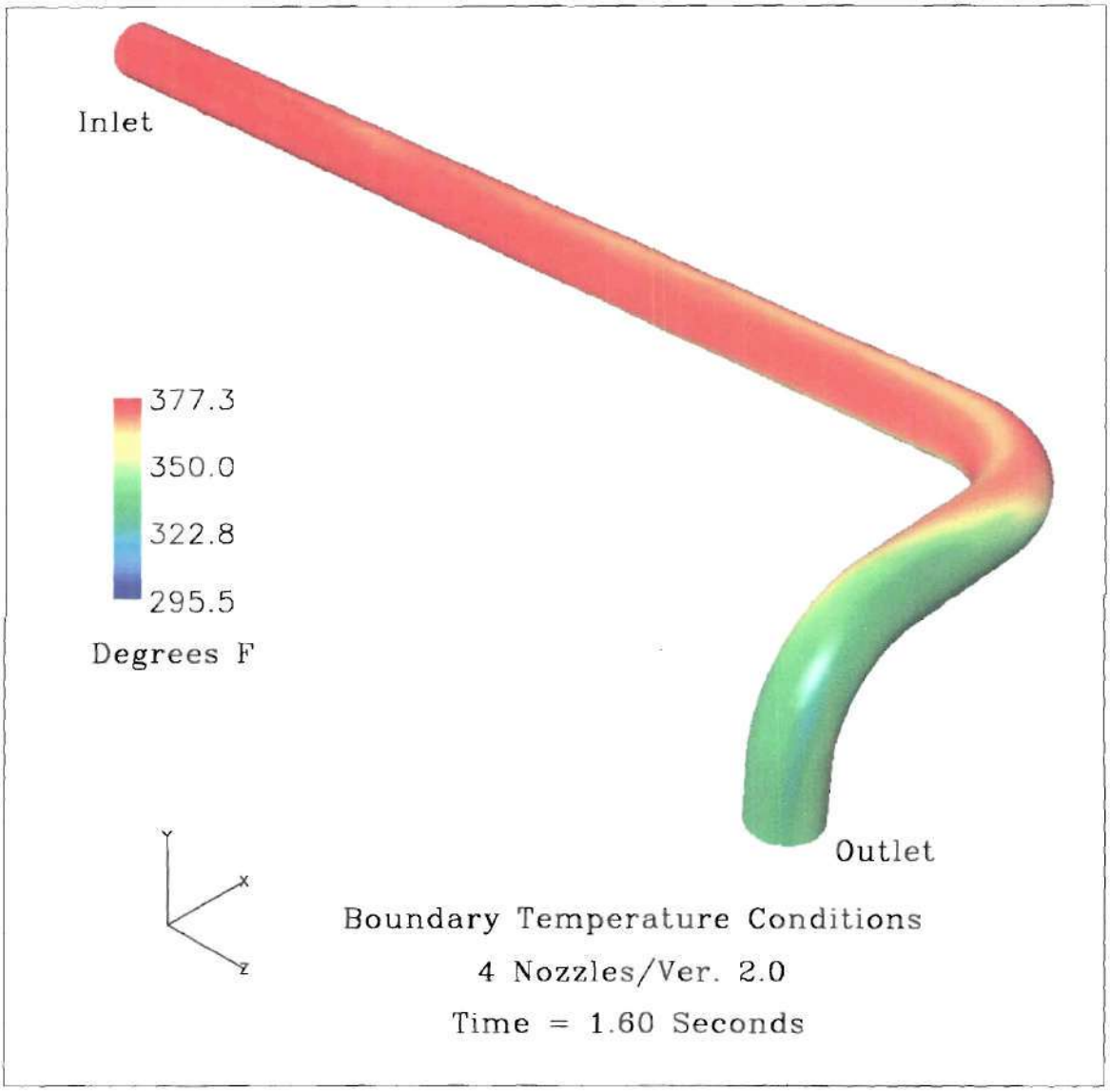
Inlet
377.3
350.0
322.8
295.5
Degrees F
Outlet
Y
X
Z
Boundary Temperature Conditions
4 Nozzles/Ver. 2.0
Time = 1.60 Seconds

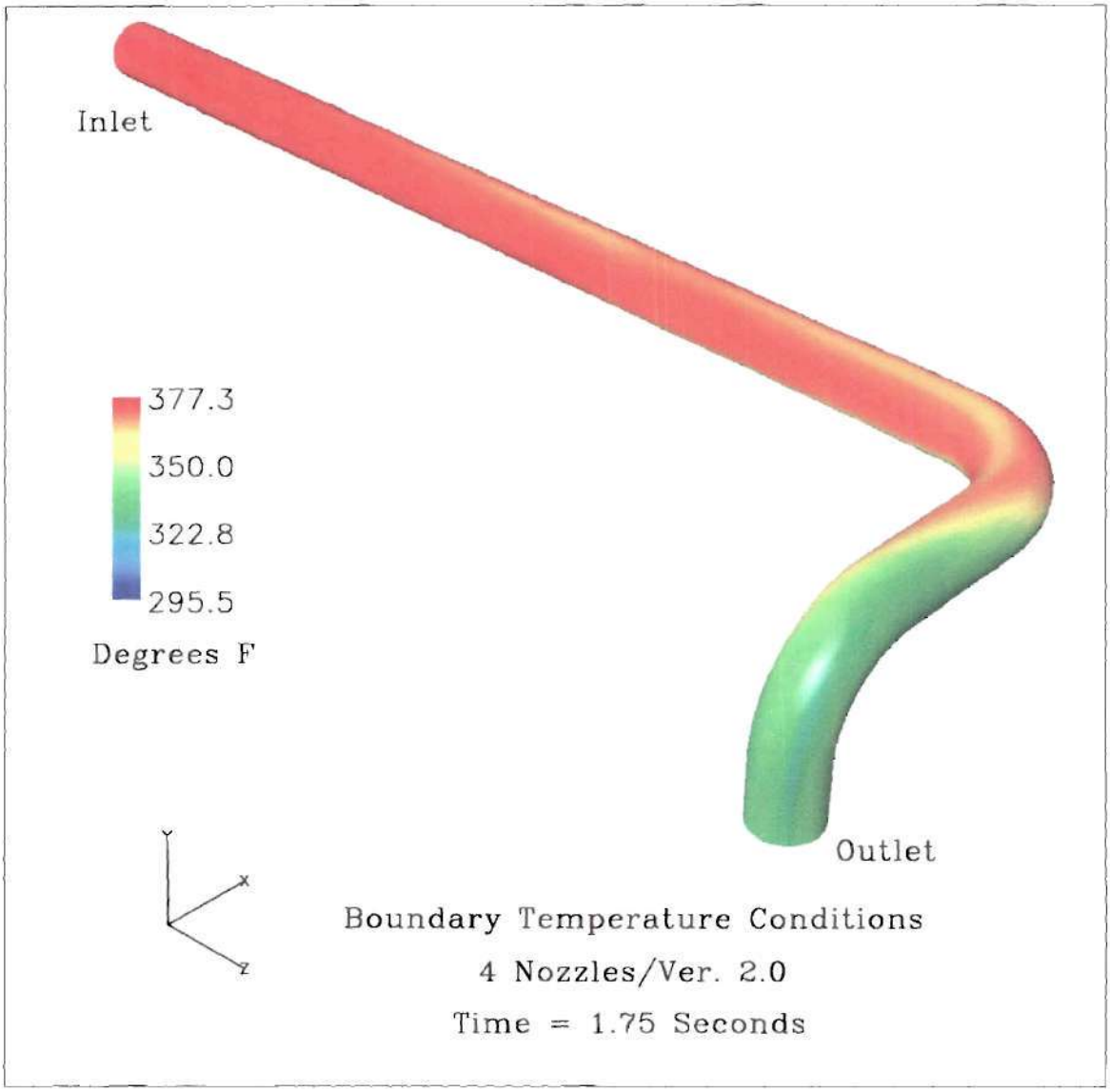
Inlet
377.3
350.0
322.8
295.5
Degrees F
Outlet
Y
X
Z
Boundary Temperature Conditions
4 Nozzles/Ver. 2.0
Time = 1.75 Seconds

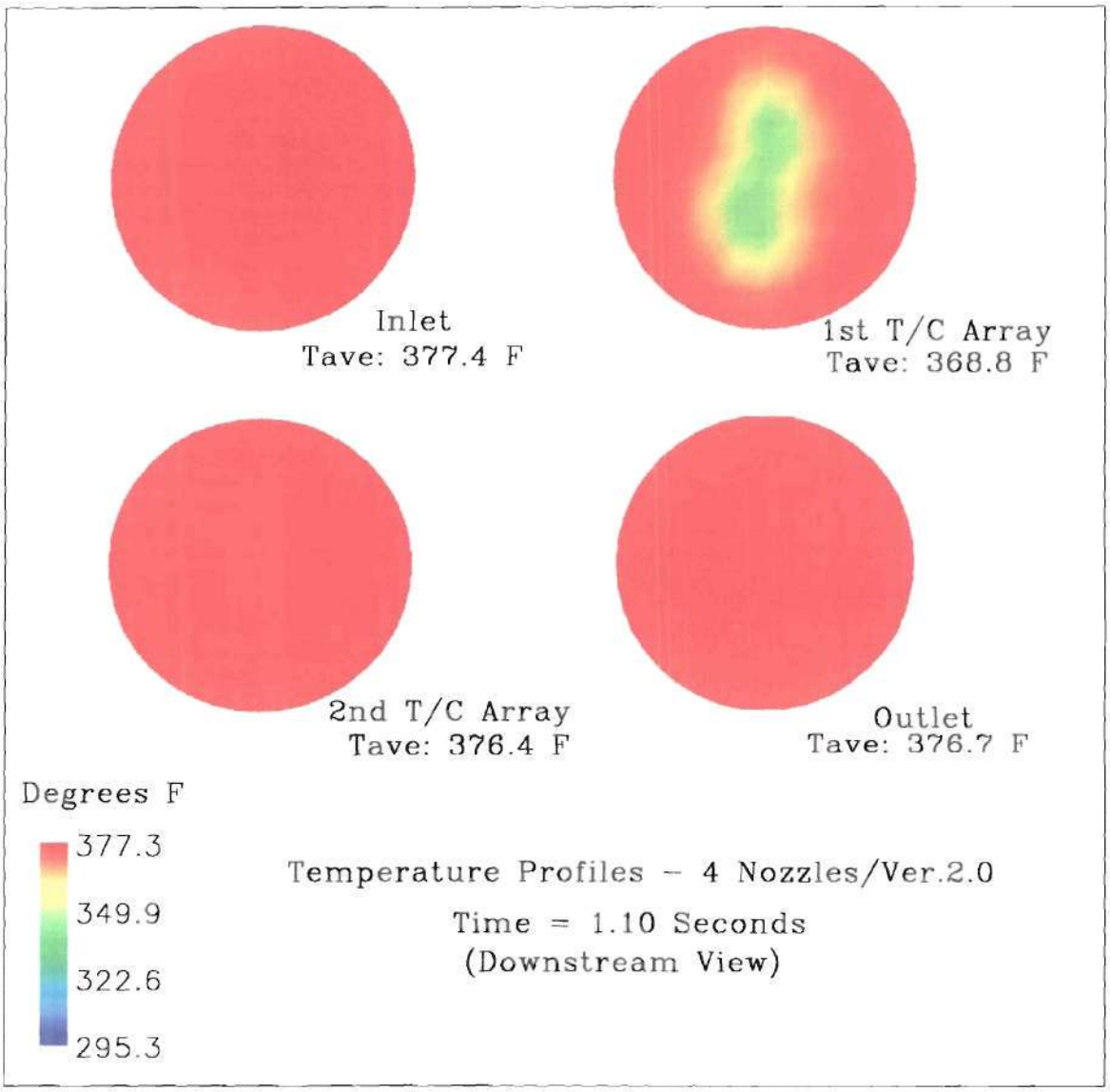
Inlet
Tave: 377.4 F
1st T/C Array
Tave: 368.8 F
2nd T/C Array
Tave: 376.4 F
Outlet
Tave: 376.7 F
Degrees F
377.3
349.9
322.6
295.3
Temperature Profiles - 4 Nozzles/Ver.2.0
Time = 1.10 Seconds
(Downstream View)

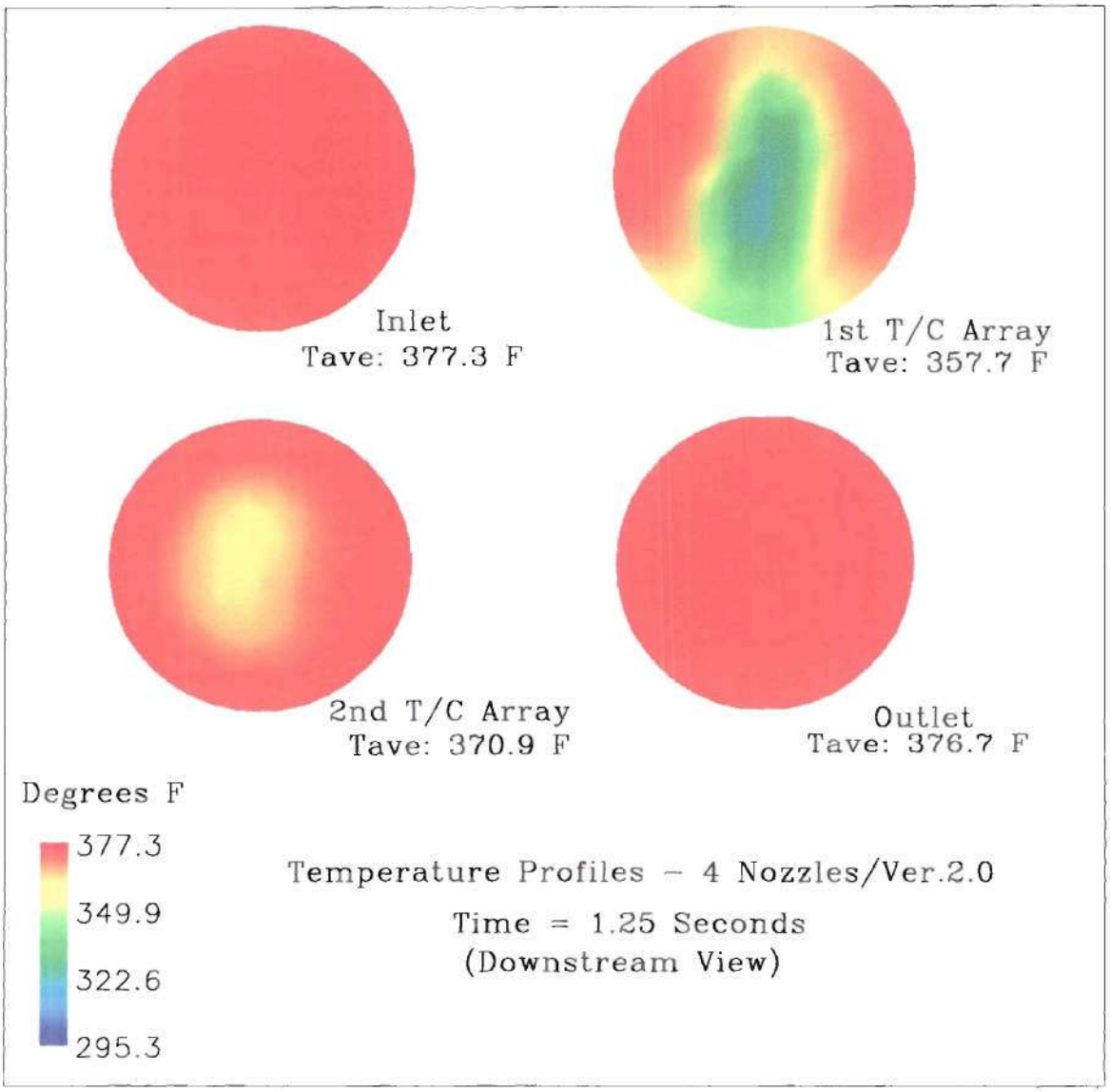
Inlet
Tave: 377.3 F
1st T/C Array
Tave: 357.7 F
2nd T/C Array
Tave: 370.9 F
Outlet
Tave: 376.7 F
Degrees F
377.3
349.9
322.6
295.3
Temperature Profiles - 4 Nozzles/Ver.2.0
Time = 1.25 Seconds
(Downstream View)

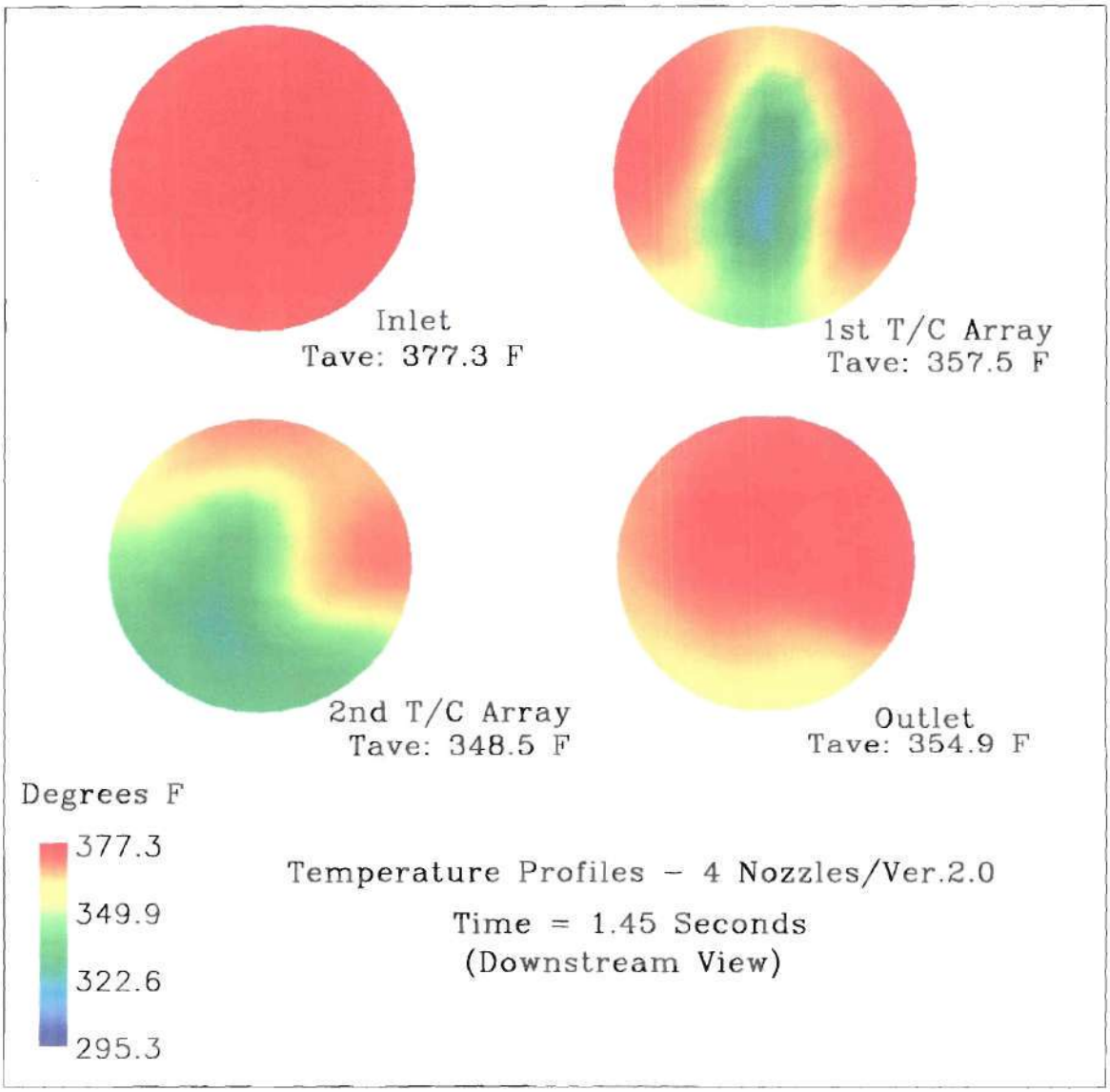
Inlet
Tave: 377.3 F
1st T/C Array
Tave: 357.5 F
2nd T/C Array
Tave: 348.5 F
Outlet
Tave: 354.9 F
Degrees F
377.3
349.9
322.6
295.3
Temperature Profiles - 4 Nozzles/Ver.2.0
Time = 1.45 Seconds
(Downstream View)

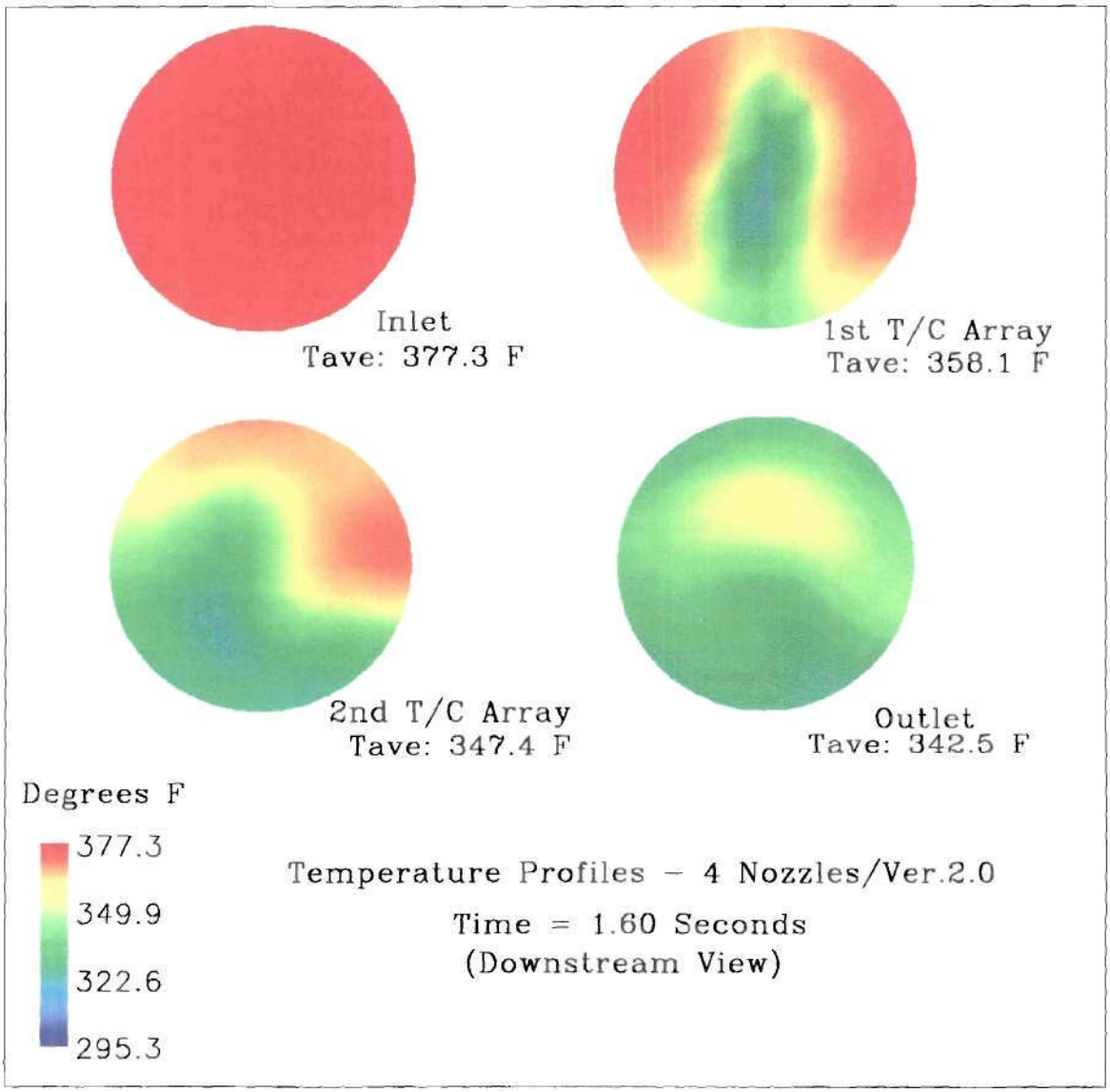
Inlet
Tave: 377.3 F
1st T/C Array
Tave: 358.1 F
2nd T/C Array
Tave: 347.4 F
Outlet
Tave: 342.5 F
Degrees F
377.3
349.9
322.6
295.3
Temperature Profiles - 4 Nozzles/Ver.2.0
Time = 1.60 Seconds
(Downstream View)

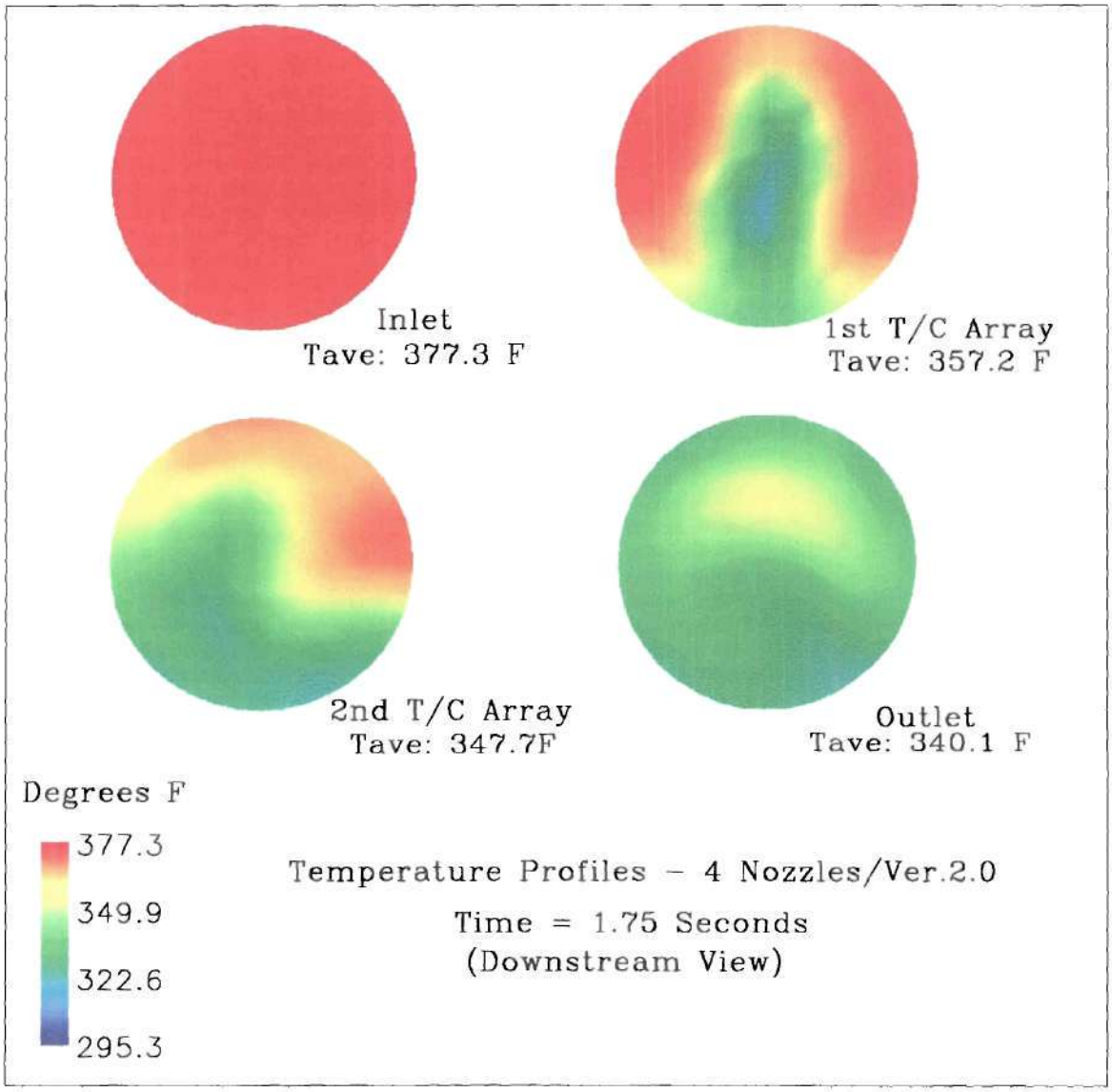
Inlet
Tave: 377.3 F
1st T/C Array
Tave: 357.2 F
2nd T/C Array
Tave: 347.7F
Outlet
Tave: 340.1 F
Degrees F
377.3
349.9
322.6
295.3
Temperature Profiles - 4 Nozzles/Ver.2.0
Time = 1.75 Seconds
(Downstream View)

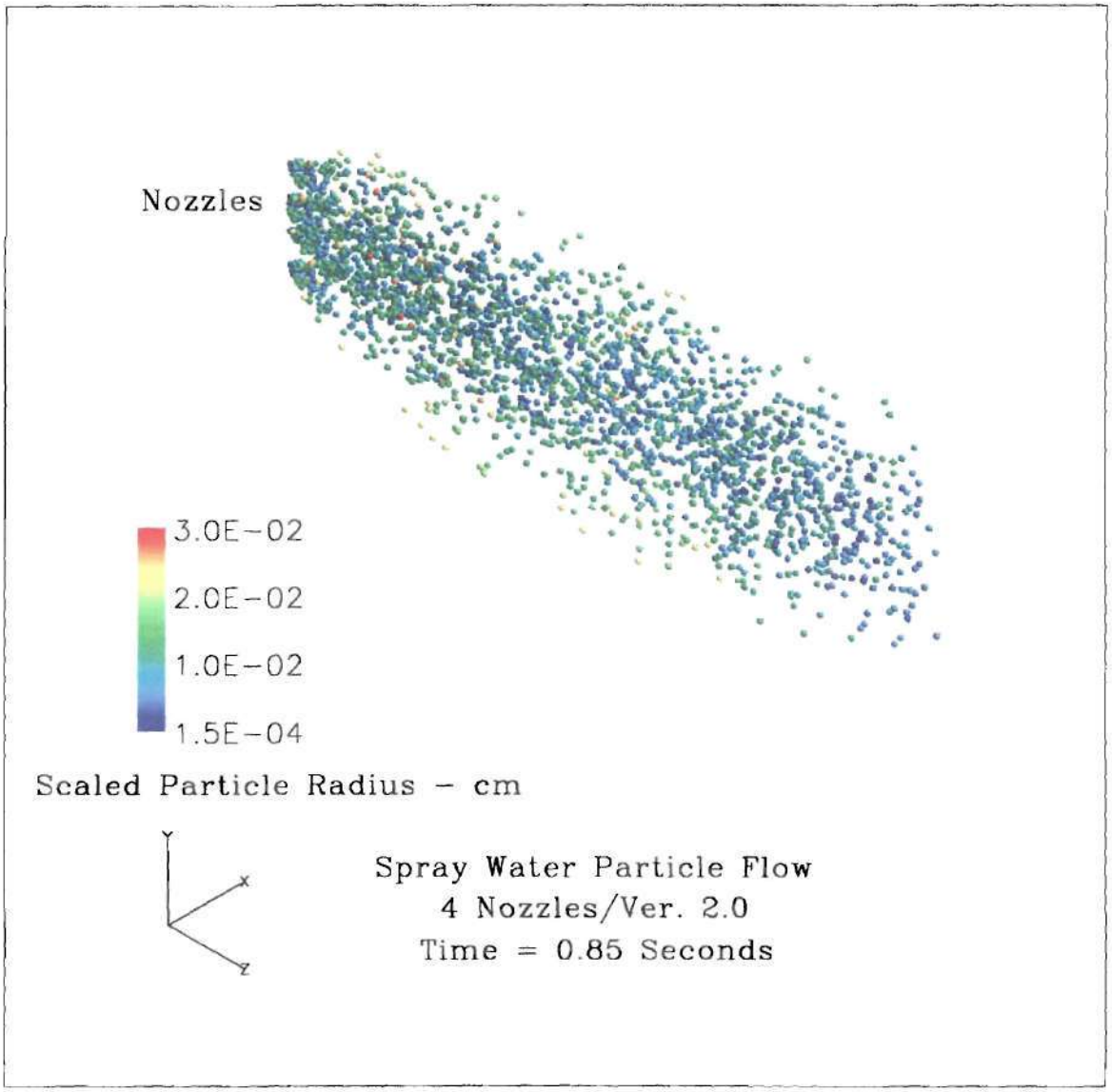
Nozzles
3.0E-02
2.0E-02
1.0E-02
1.5E-04
Scaled Particle Radius - cm
Y
X
Z
Spray Water Particle Flow
4 Nozzles/Ver. 2.0
Time = 0.85 Seconds

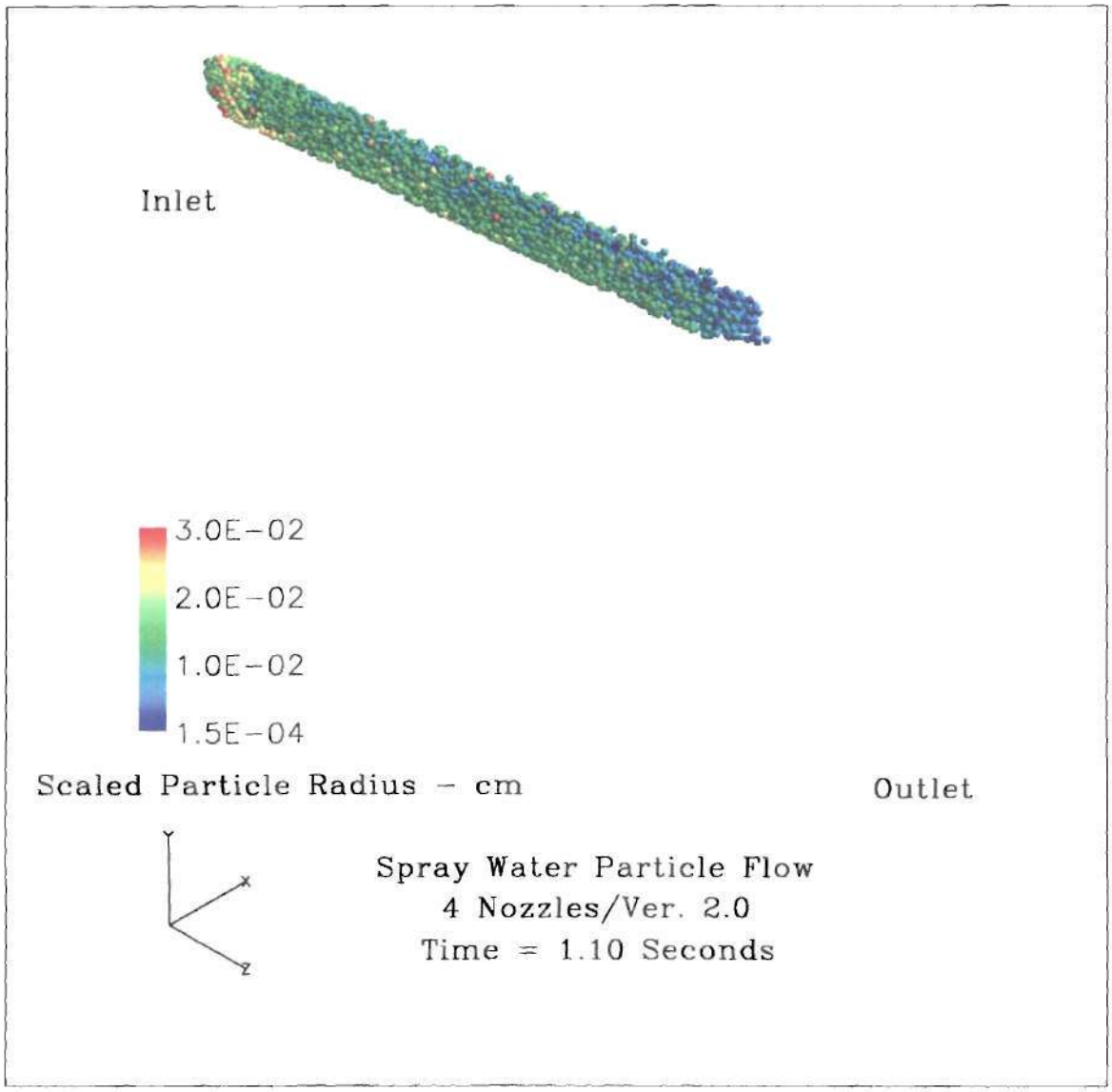
Inlet
3.0E-02
2.0E-02
1.0E-02
1.5E-04
Scaled Particle Radius - cm
Outlet
Y
X
Z
Spray Water Particle Flow
4 Nozzles/Ver. 2.0
Time = 1.10 Seconds

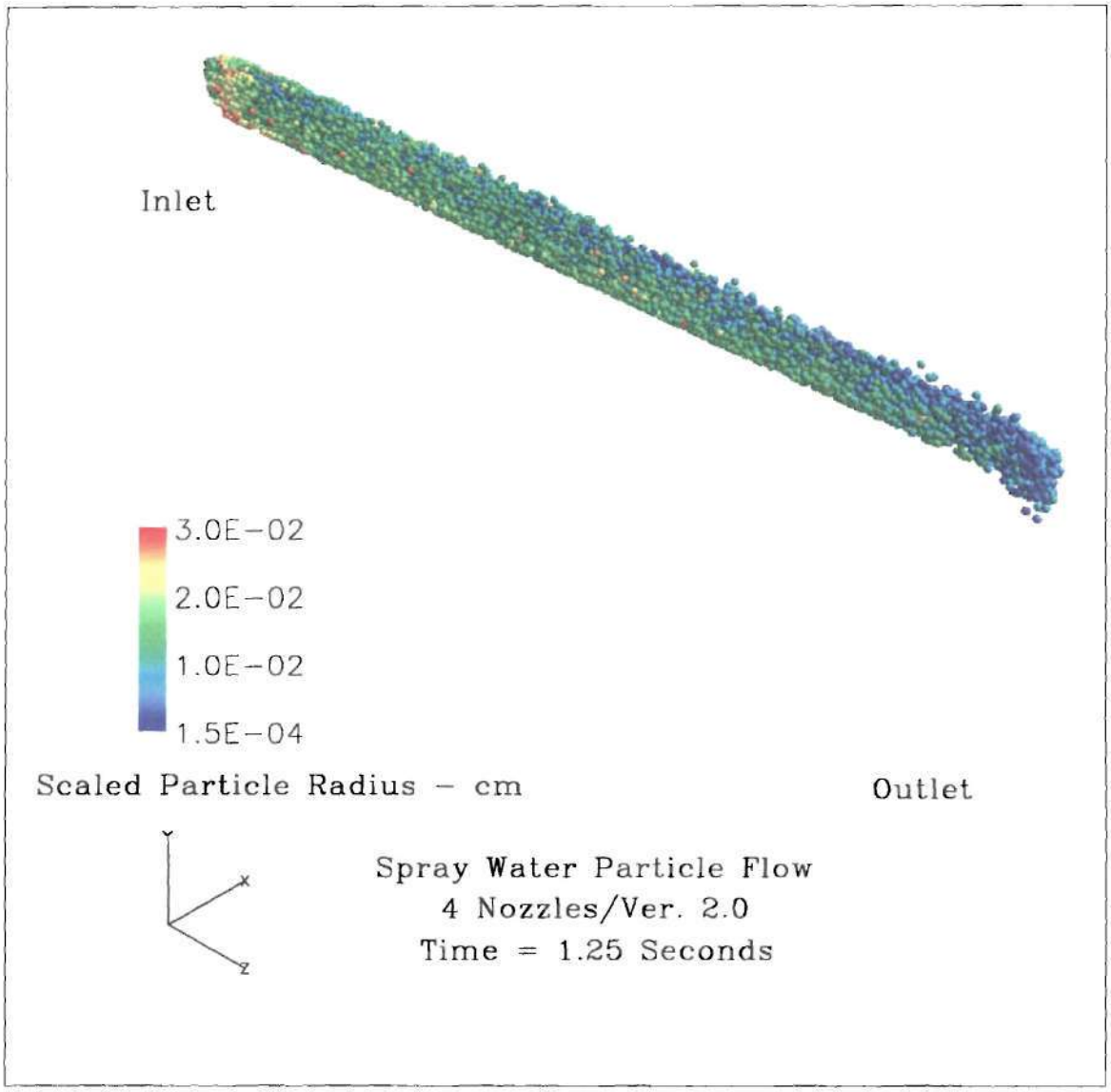
Inlet
3.0E−02
2.0E−02
1.0E−02
1.5E−04
Scaled Particle Radius − cm
Outlet
Y
X
Z
Spray Water Particle Flow
4 Nozzles/Ver. 2.0
Time = 1.25 Seconds

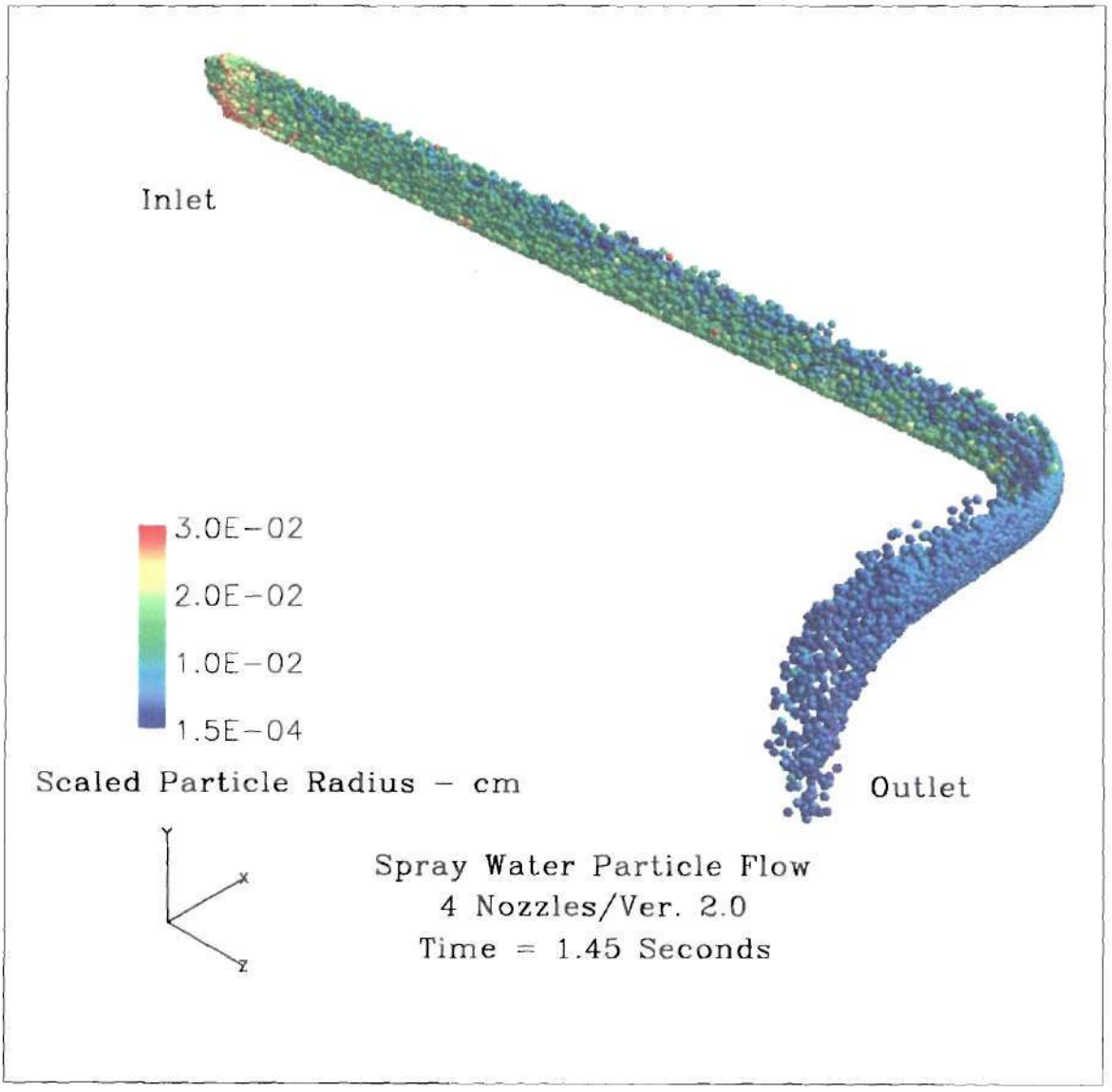
Inlet
3.0E-02
2.0E-02
1.0E-02
1.5E-04
Scaled Particle Radius - cm
Outlet
Y
X
Z
Spray Water Particle Flow
4 Nozzles/Ver. 2.0
Time = 1.45 Seconds

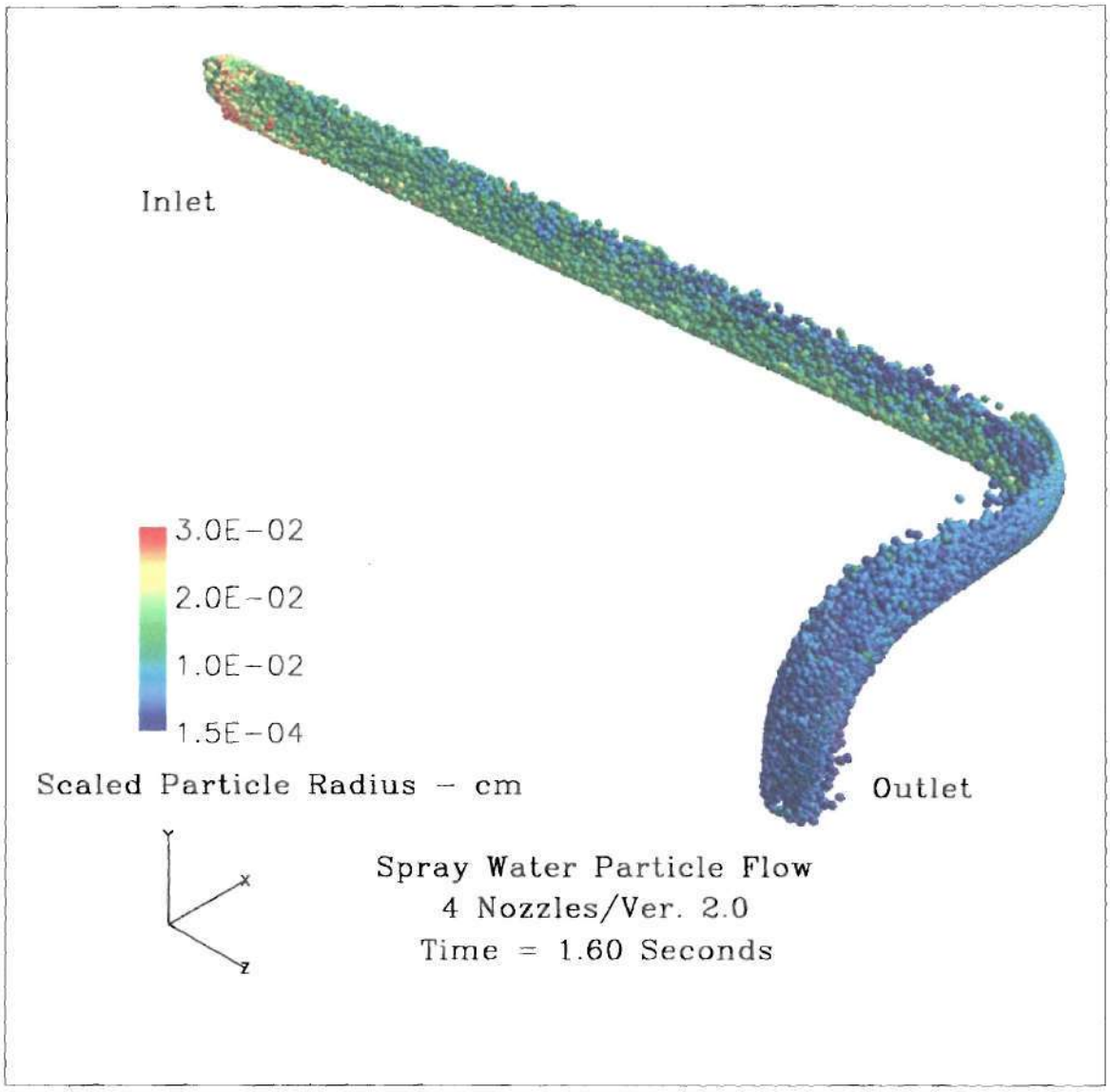
Inlet
3.0E-02
2.0E-02
1.0E-02
1.5E-04
Scaled Particle Radius - cm
Outlet
Y
X
Z
Spray Water Particle Flow
4 Nozzles/Ver. 2.0
Time = 1.60 Seconds

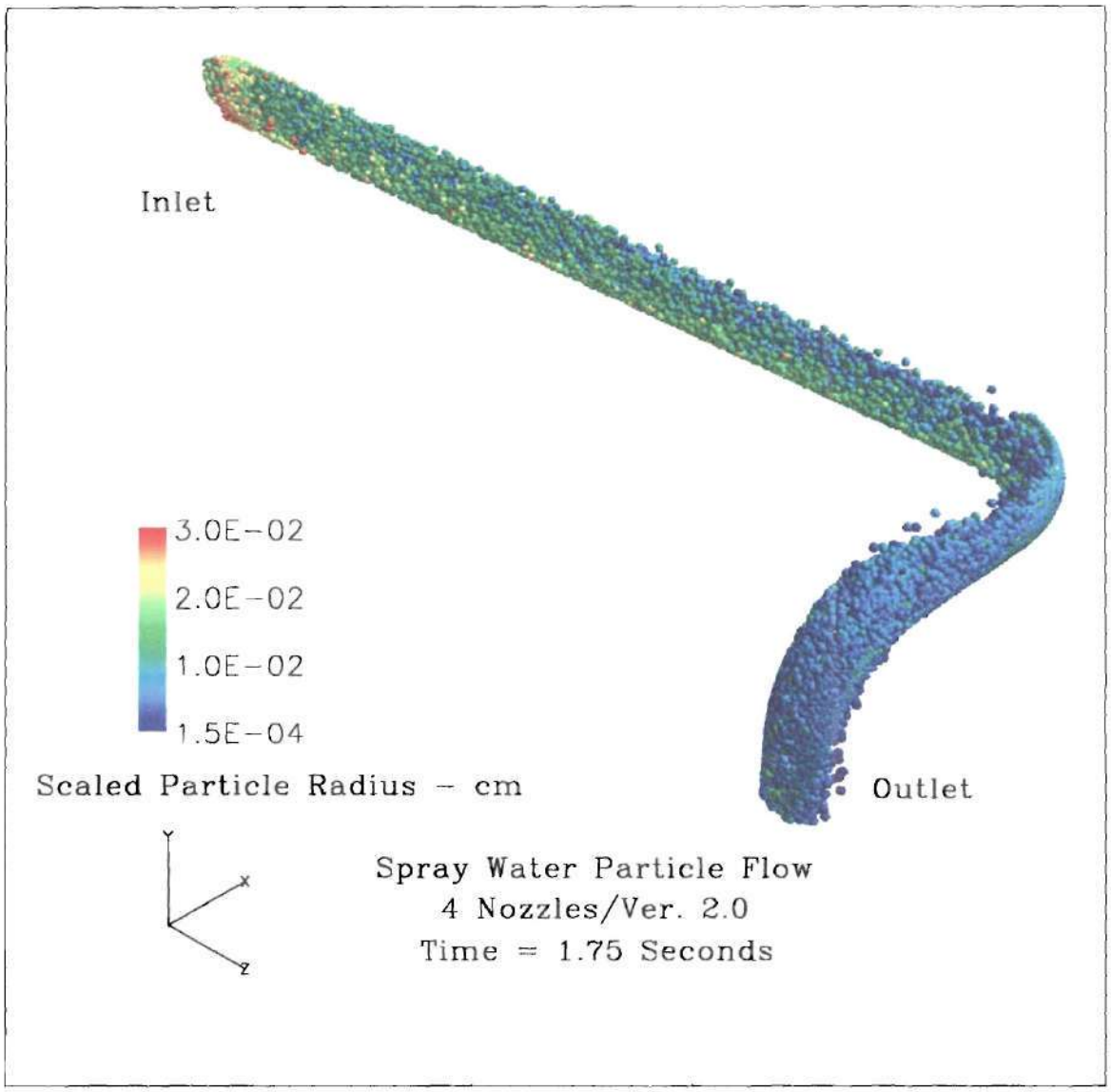
Inlet
3.0E-02
2.0E-02
1.0E-02
1.5E-04
Scaled Particle Radius - cm
Outlet
Y
X
Z
Spray Water Particle Flow
4 Nozzles/Ver. 2.0
Time = 1.75 Seconds

APPENDIX D

STEAMCFD OUTPUT FOR CASE 2

This appendix contains the graphical representations of computational data collected from the SteamCFD Code. This data examines the results obtained when utilizing the 28-nozzle desuperheater arrangement and experimental data from the time period of 1380-1410 minutes elapsed time from midnight on May 2, 2001, i.e., 11:00 to 11:30 AM. The graphical representations include output from both Version 1.2 and Version 2.0 of the SteamCFD Code.

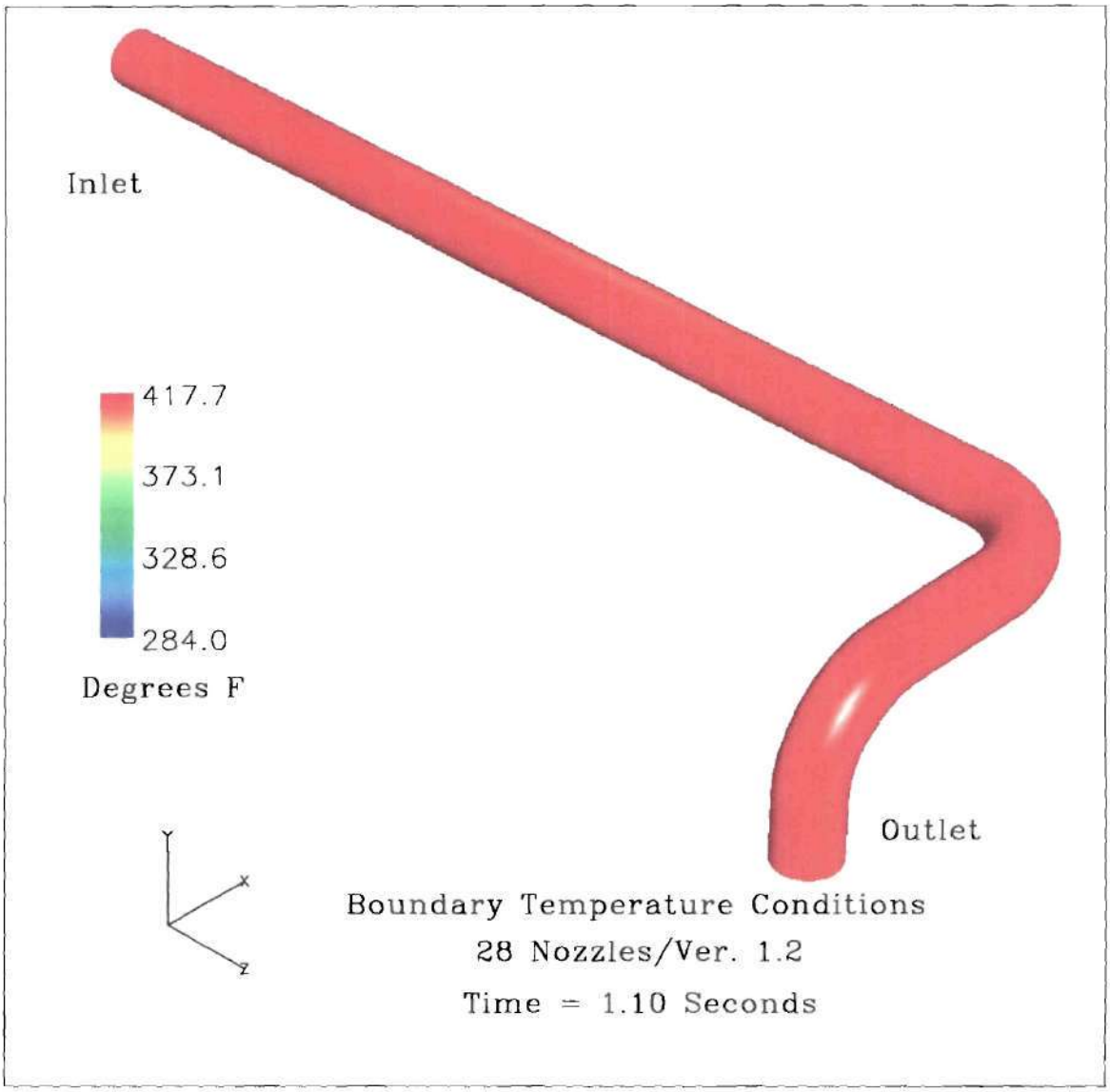
Inlet
417.7
373.1
328.6
284.0
Degrees F
Outlet
Y
X
Z
Boundary Temperature Conditions
28 Nozzles/Ver. 1.2
Time = 1.10 Seconds

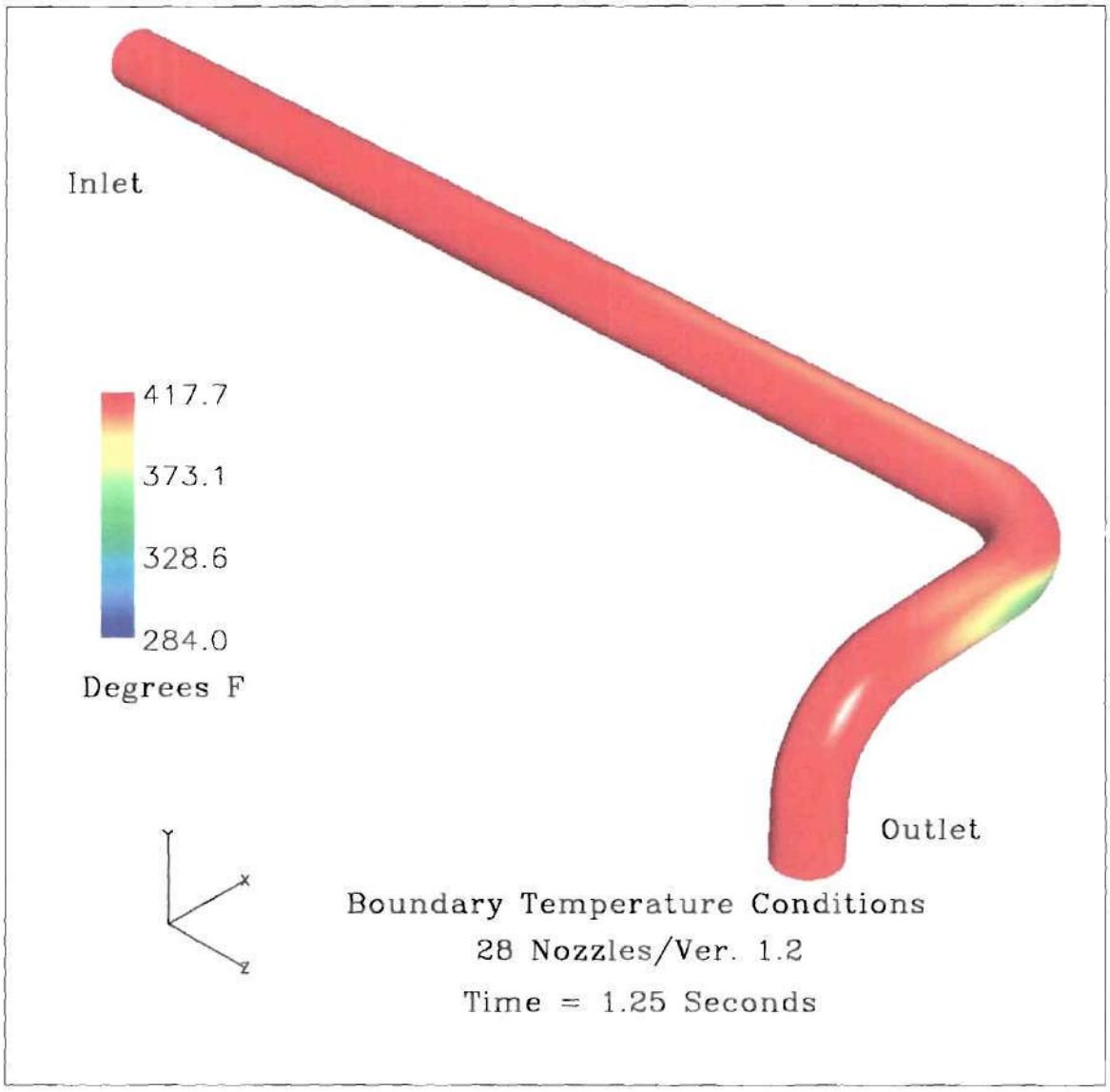
Inlet
417.7
373.1
328.6
284.0
Degrees F
Outlet
Y
X
Z
Boundary Temperature Conditions
28 Nozzles/Ver. 1.2
Time = 1.25 Seconds

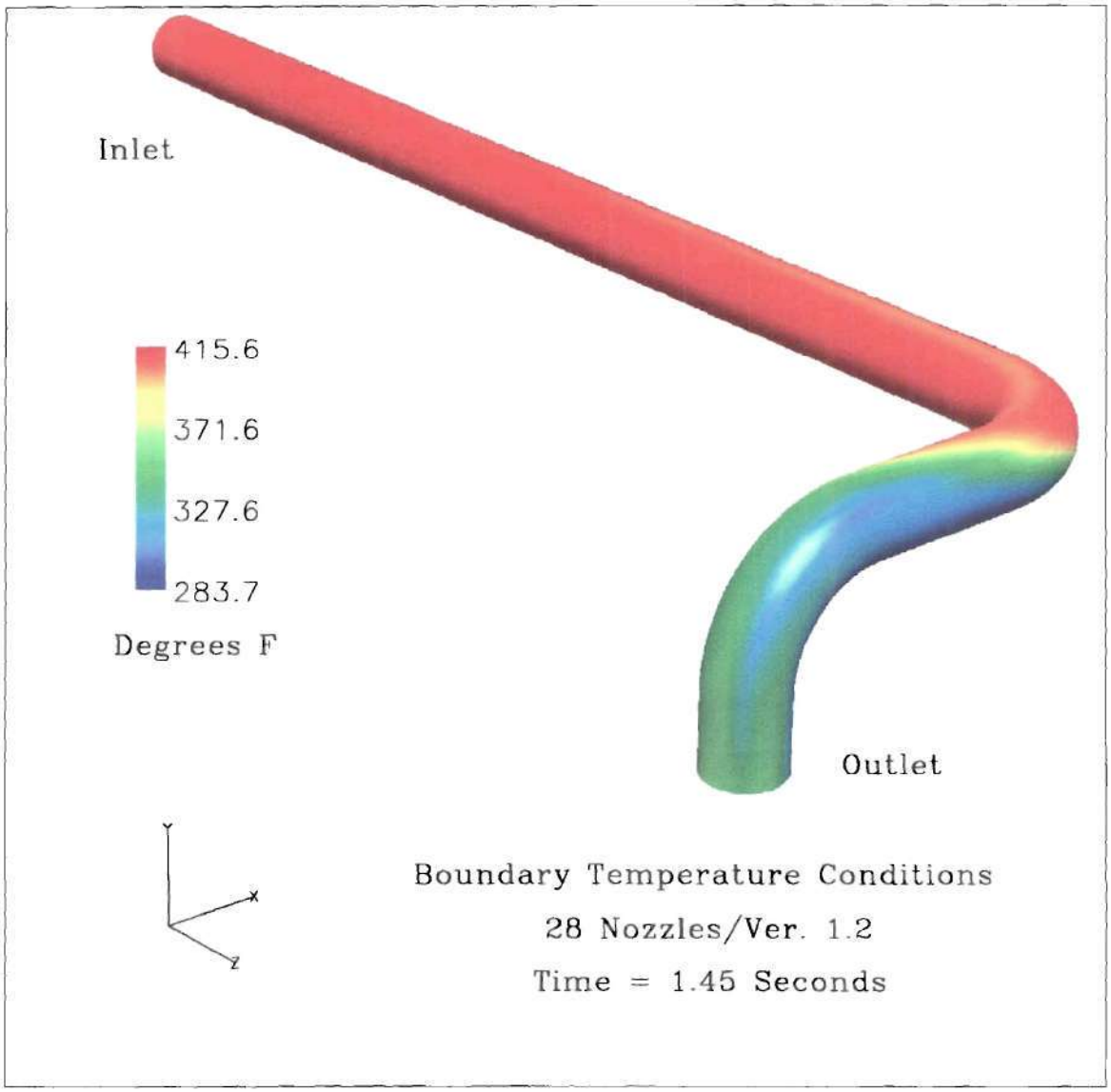
Inlet
415.6
371.6
327.6
283.7
Degrees F
Outlet
Y
X
Z
Boundary Temperature Conditions
28 Nozzles/Ver. 1.2
Time = 1.45 Seconds

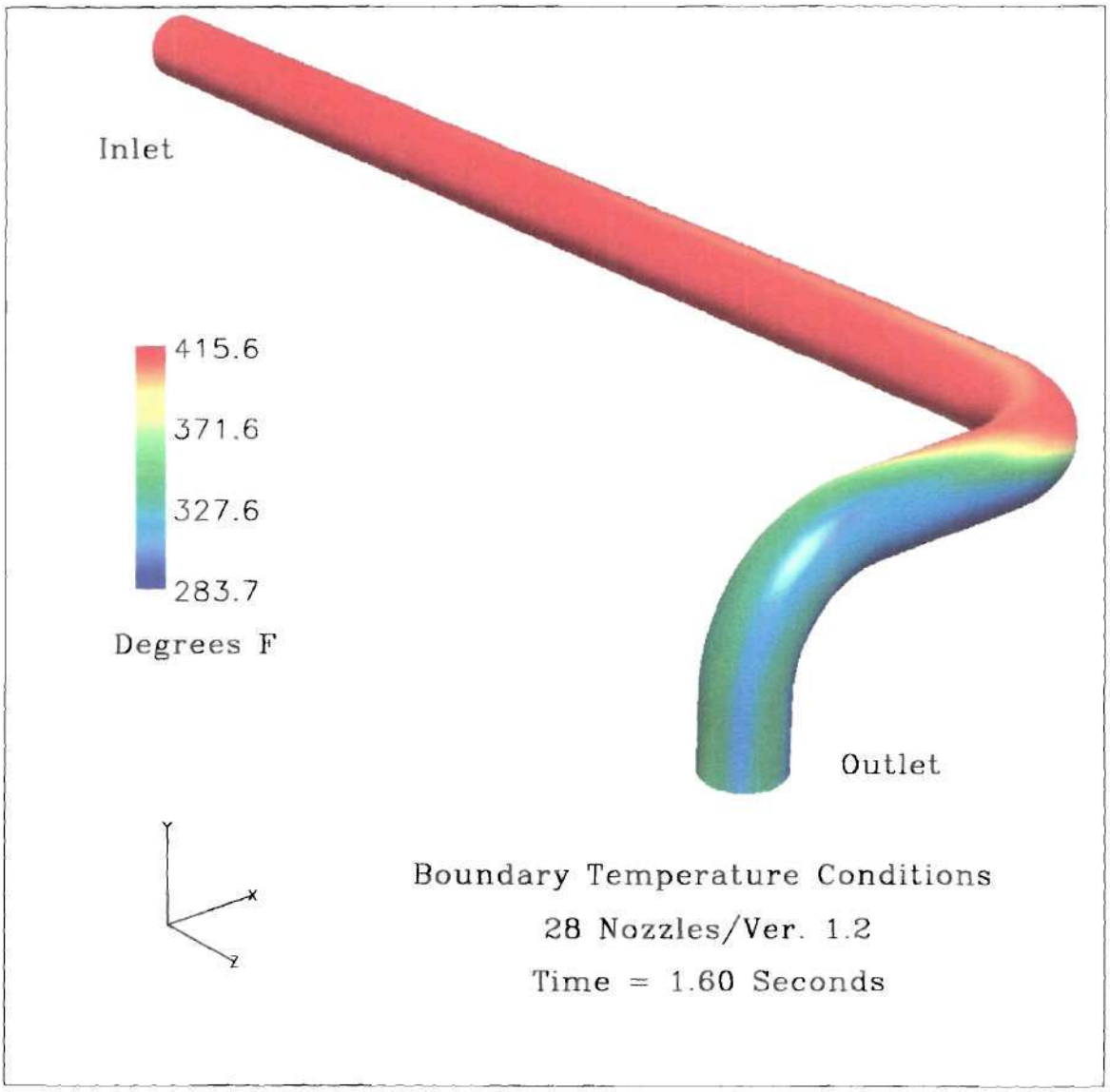
Inlet
415.6
371.6
327.6
283.7
Degrees F
Outlet
Y
X
Z
Boundary Temperature Conditions
28 Nozzles/Ver. 1.2
Time = 1.60 Seconds

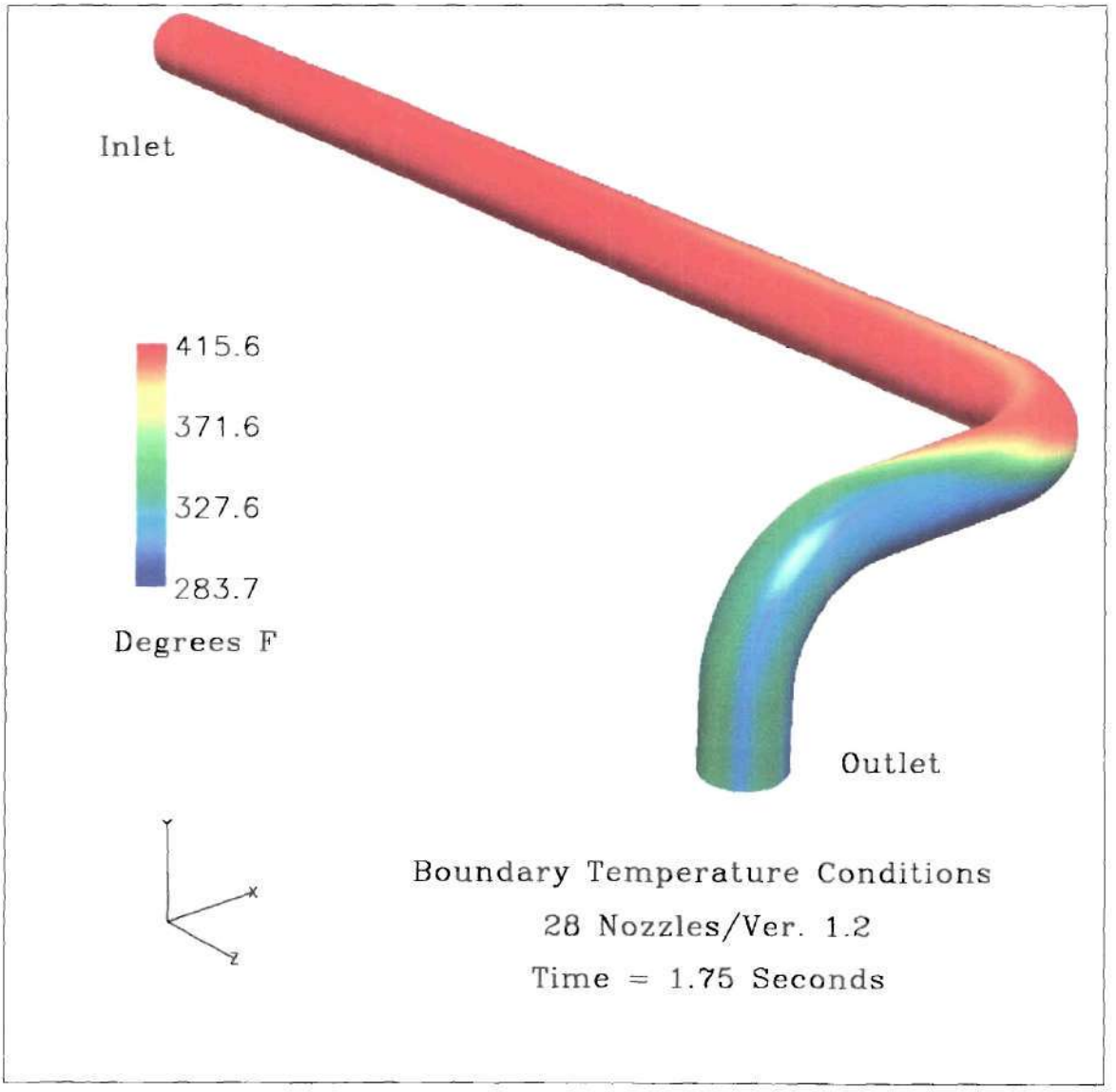
Inlet
415.6
371.6
327.6
283.7
Degrees F
Outlet
Y
X
Z
Boundary Temperature Conditions
28 Nozzles/Ver. 1.2
Time = 1.75 Seconds

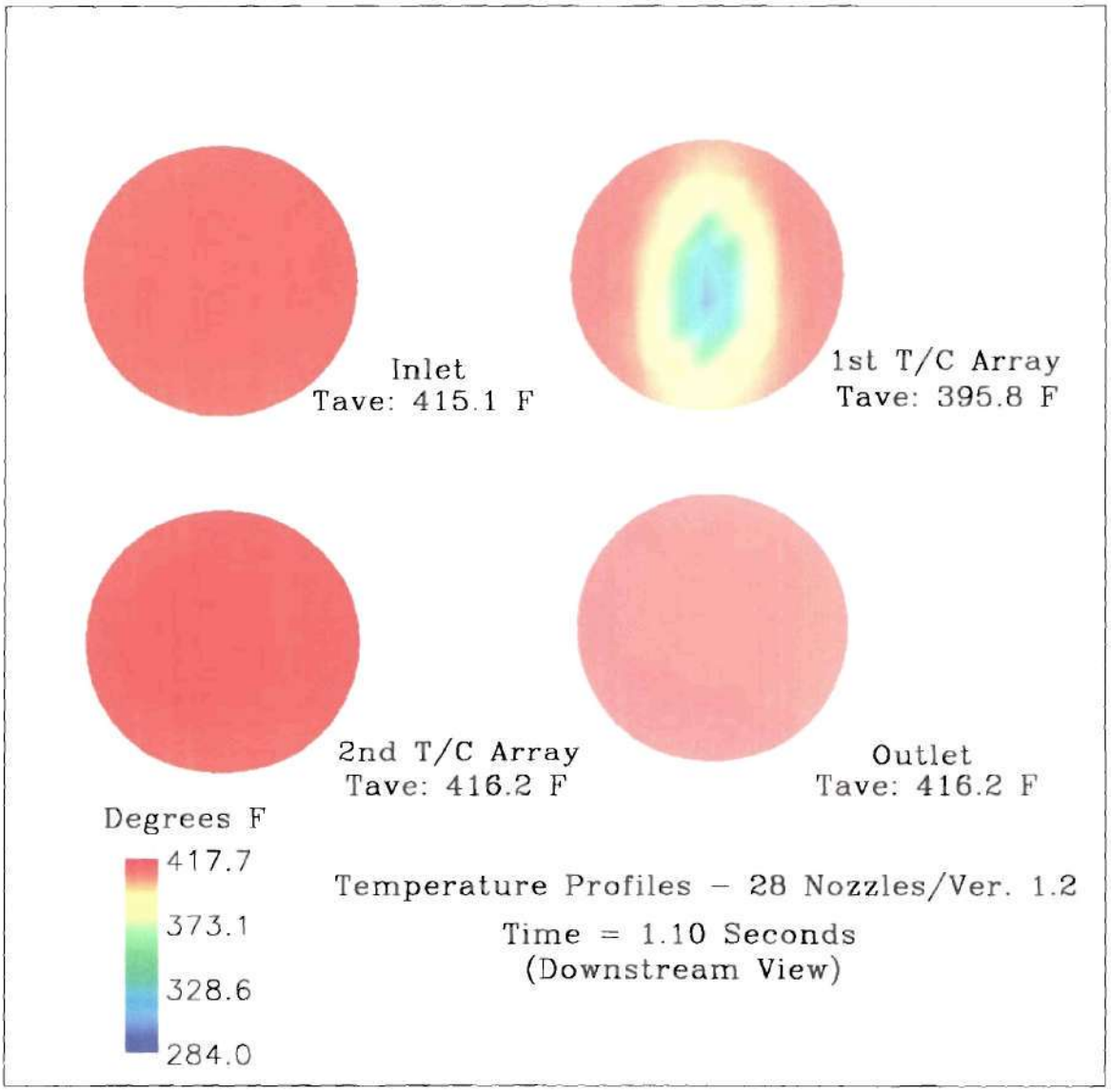
Inlet
Tave: 415.1 F
1st T/C Array
Tave: 395.8 F
2nd T/C Array
Tave: 416.2 F
Outlet
Tave: 416.2 F
Degrees F
417.7
373.1
328.6
284.0
Temperature Profiles - 28 Nozzles/Ver. 1.2
Time = 1.10 Seconds
(Downstream View)

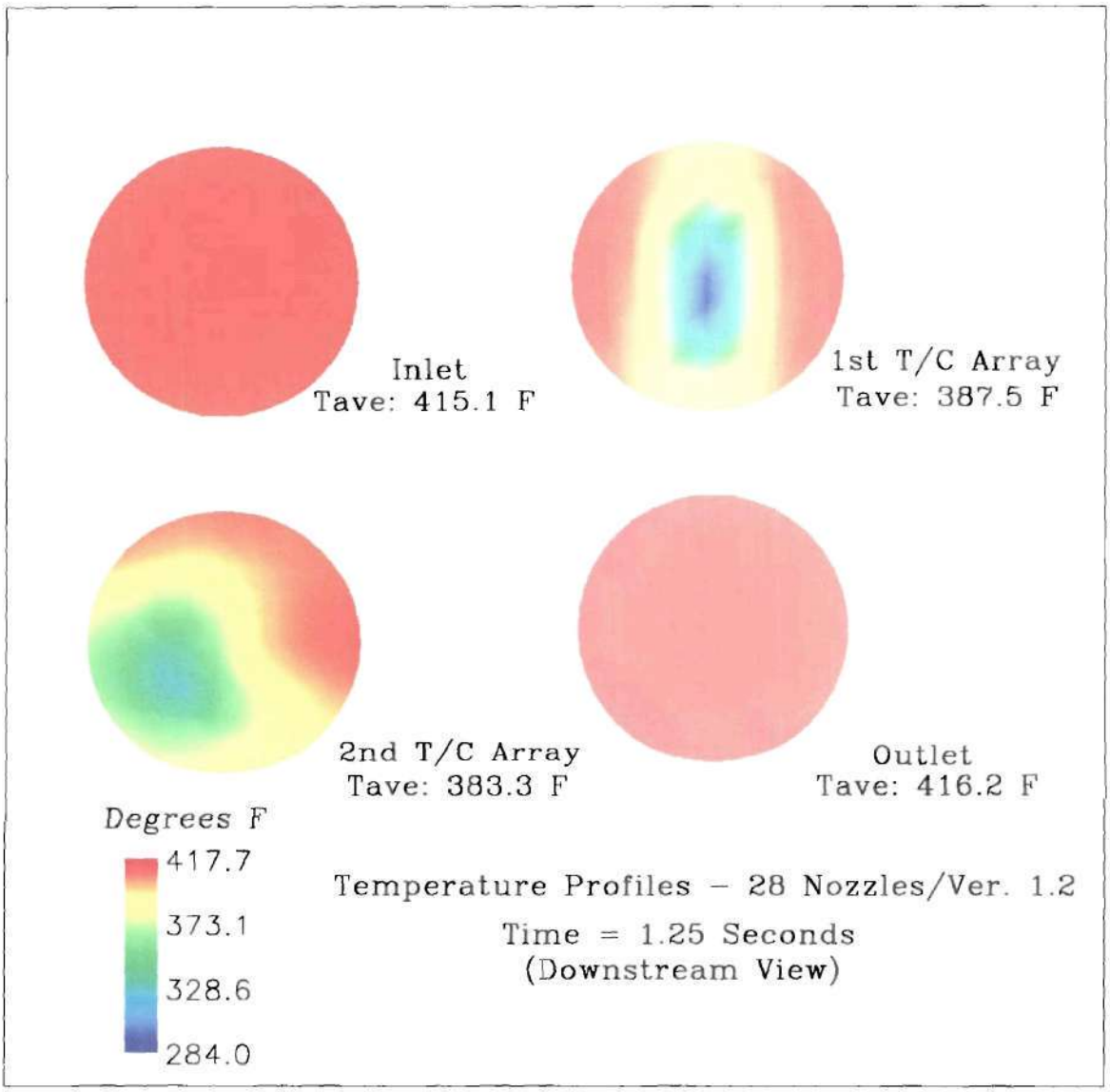
Inlet
Tave: 415.1 F
1st T/C Array
Tave: 387.5 F
2nd T/C Array
Tave: 383.3 F
Outlet
Tave: 416.2 F
Degrees F
417.7
373.1
328.6
284.0
Temperature Profiles - 28 Nozzles/Ver. 1.2
Time = 1.25 Seconds
(Downstream View)

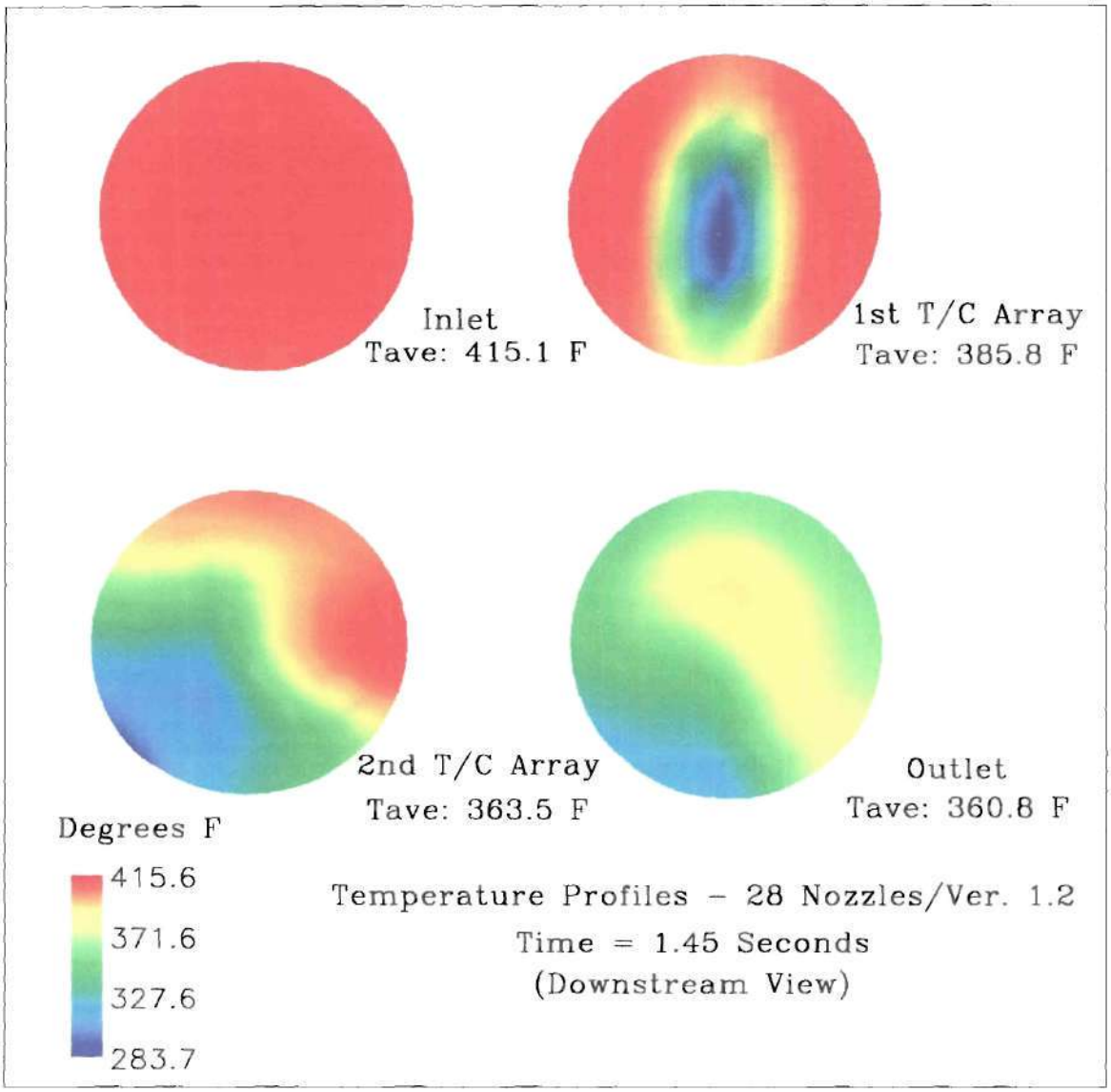
Inlet
Tave: 415.1 F
1st T/C Array
Tave: 385.8 F
2nd T/C Array
Tave: 363.5 F
Outlet
Tave: 360.8 F
Degrees F
415.6
371.6
327.6
283.7
Temperature Profiles - 28 Nozzles/Ver. 1.2
Time = 1.45 Seconds
(Downstream View)

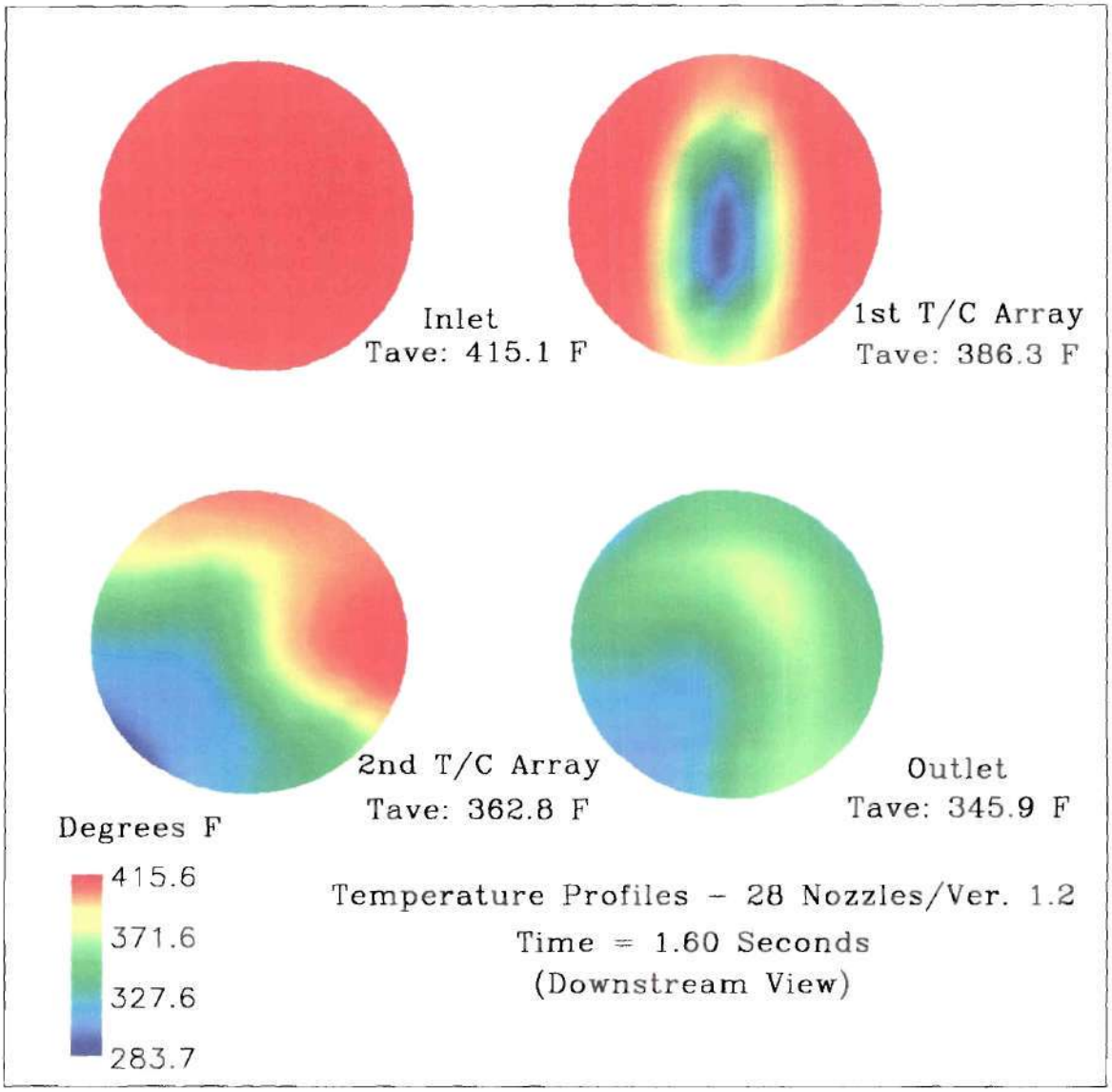
Inlet
Tave: 415.1 F
1st T/C Array
Tave: 386.3 F
2nd T/C Array
Tave: 362.8 F
Outlet
Tave: 345.9 F
Degrees F
415.6
371.6
327.6
283.7
Temperature Profiles - 28 Nozzles/Ver. 1.2
Time = 1.60 Seconds
(Downstream View)

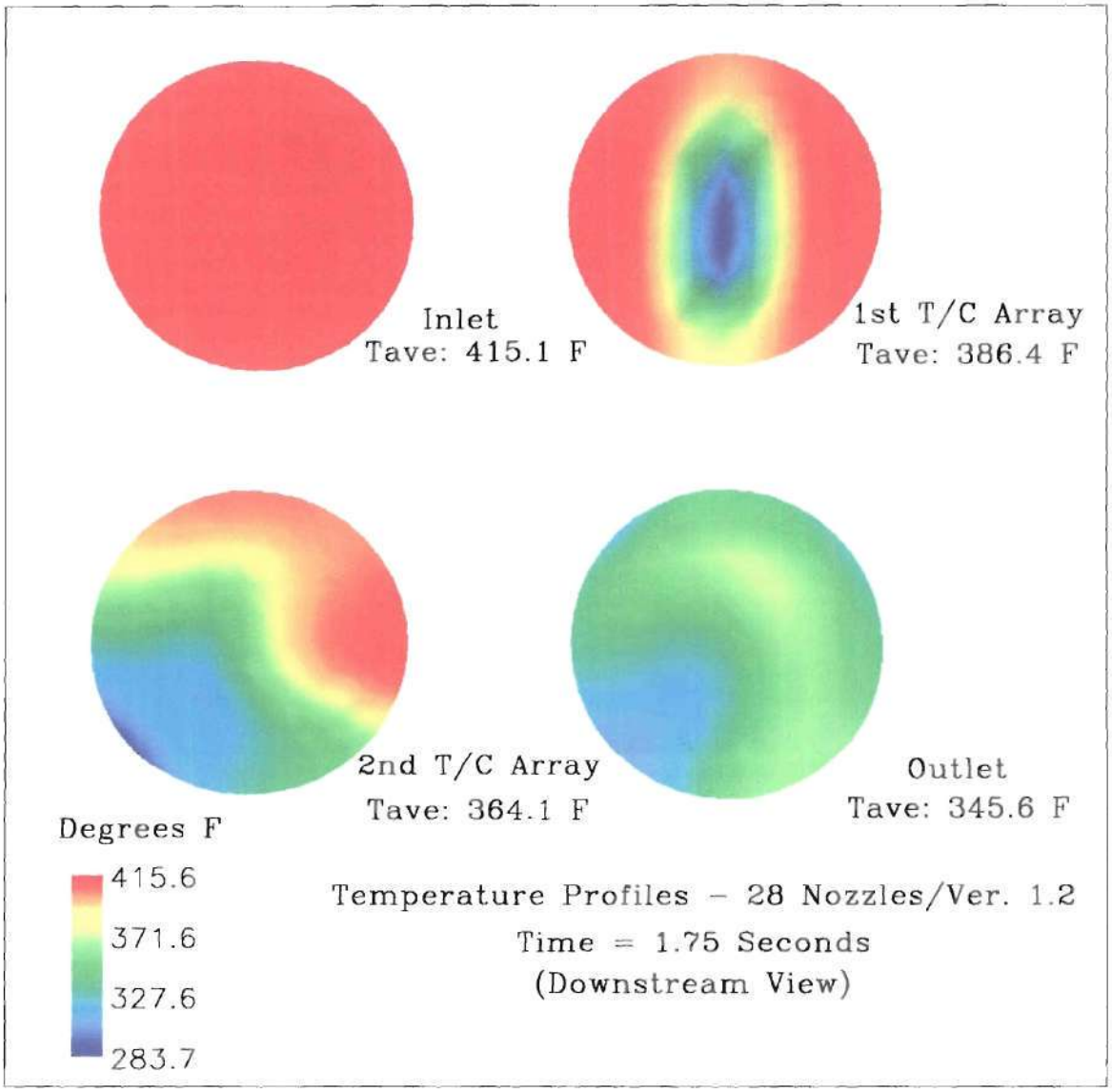
Inlet
Tave: 415.1 F
1st T/C Array
Tave: 386.4 F
2nd T/C Array
Tave: 364.1 F
Outlet
Tave: 345.6 F
Degrees F
415.6
371.6
327.6
283.7
Temperature Profiles - 28 Nozzles/Ver. 1.2
Time = 1.75 Seconds
(Downstream View)

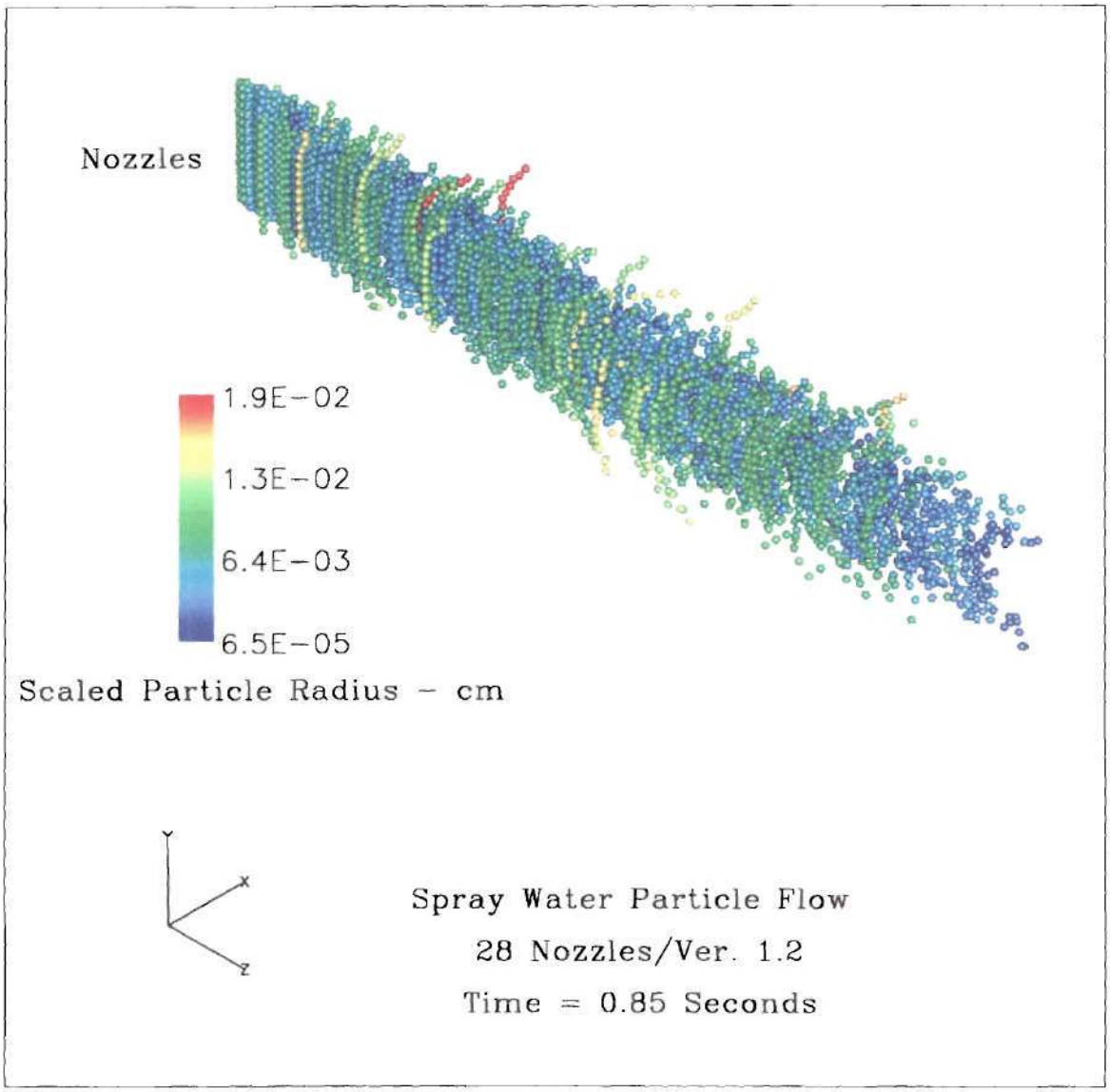
Nozzles
1.9E-02
1.3E-02
6.4E-03
6.5E-05
Scaled Particle Radius - cm
Y
X
Z
Spray Water Particle Flow
28 Nozzles/Ver. 1.2
Time = 0.85 Seconds

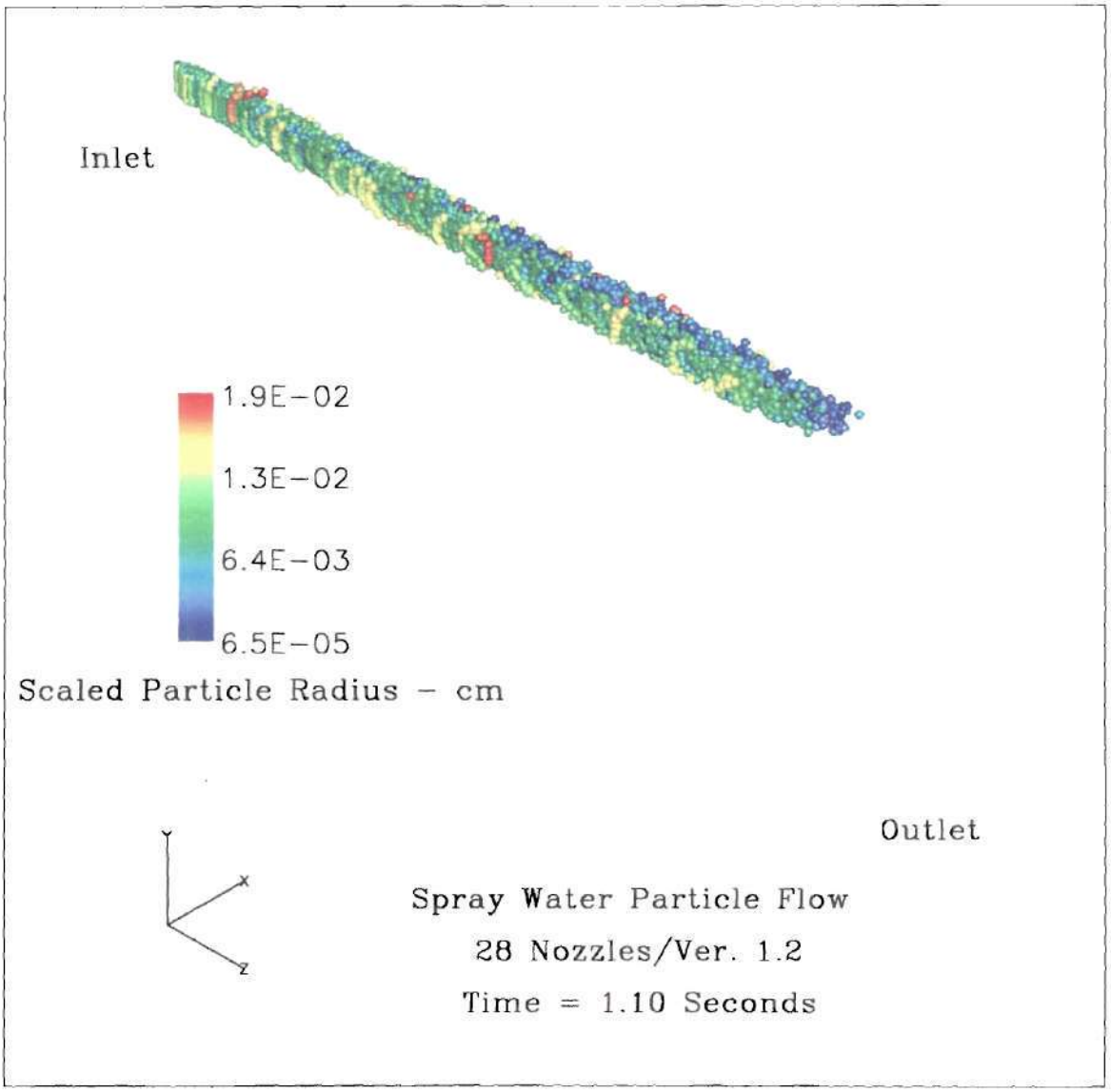
Inlet
1.9E-02
1.3E-02
6.4E-03
6.5E-05
Scaled Particle Radius - cm
Outlet
Spray Water Particle Flow
28 Nozzles/Ver. 1.2
Time = 1.10 Seconds

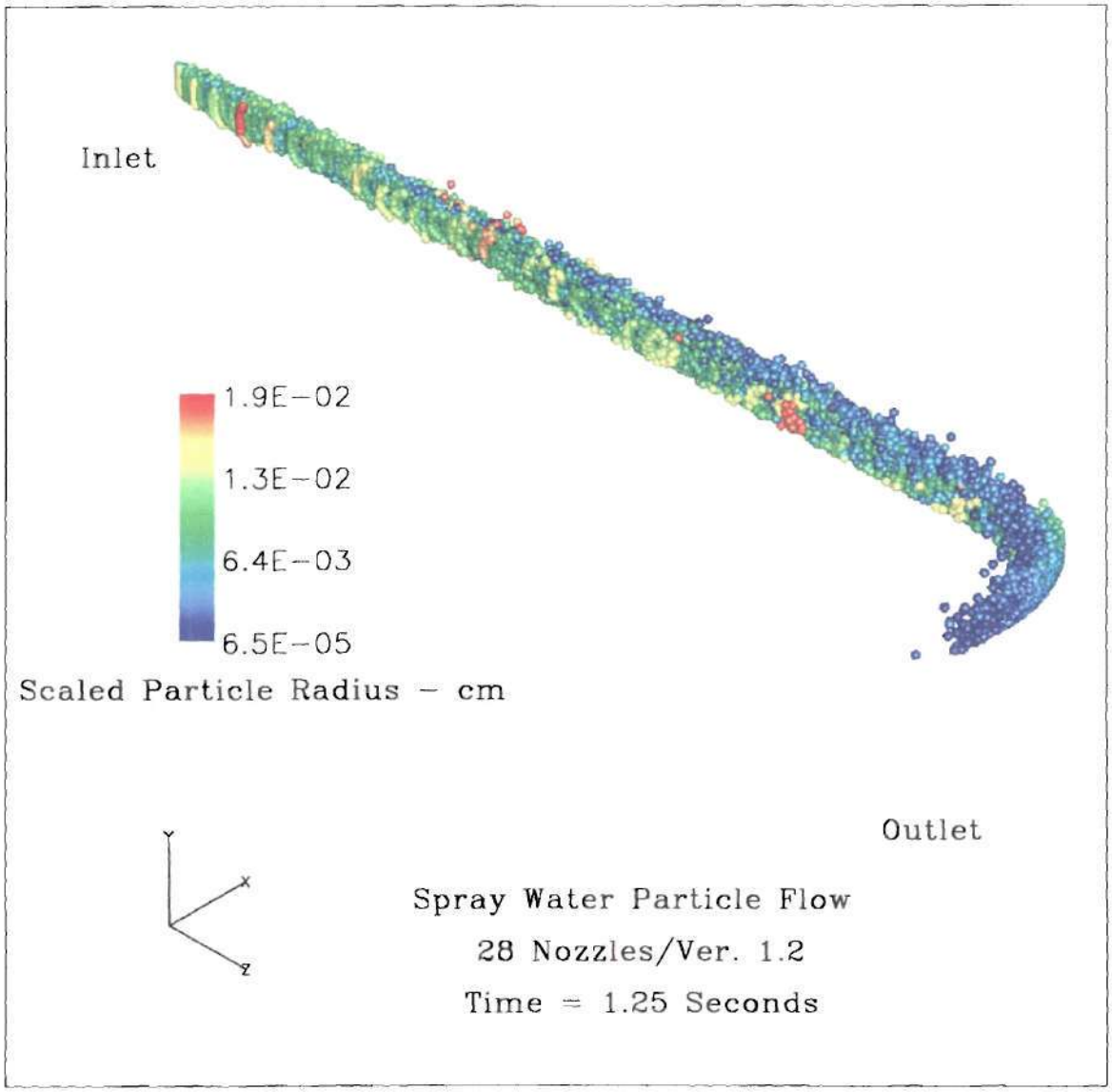
Inlet
1.9E-02
1.3E-02
6.4E-03
6.5E-05
Scaled Particle Radius - cm
Outlet
Y
X
Z
Spray Water Particle Flow
28 Nozzles/Ver. 1.2
Time = 1.25 Seconds

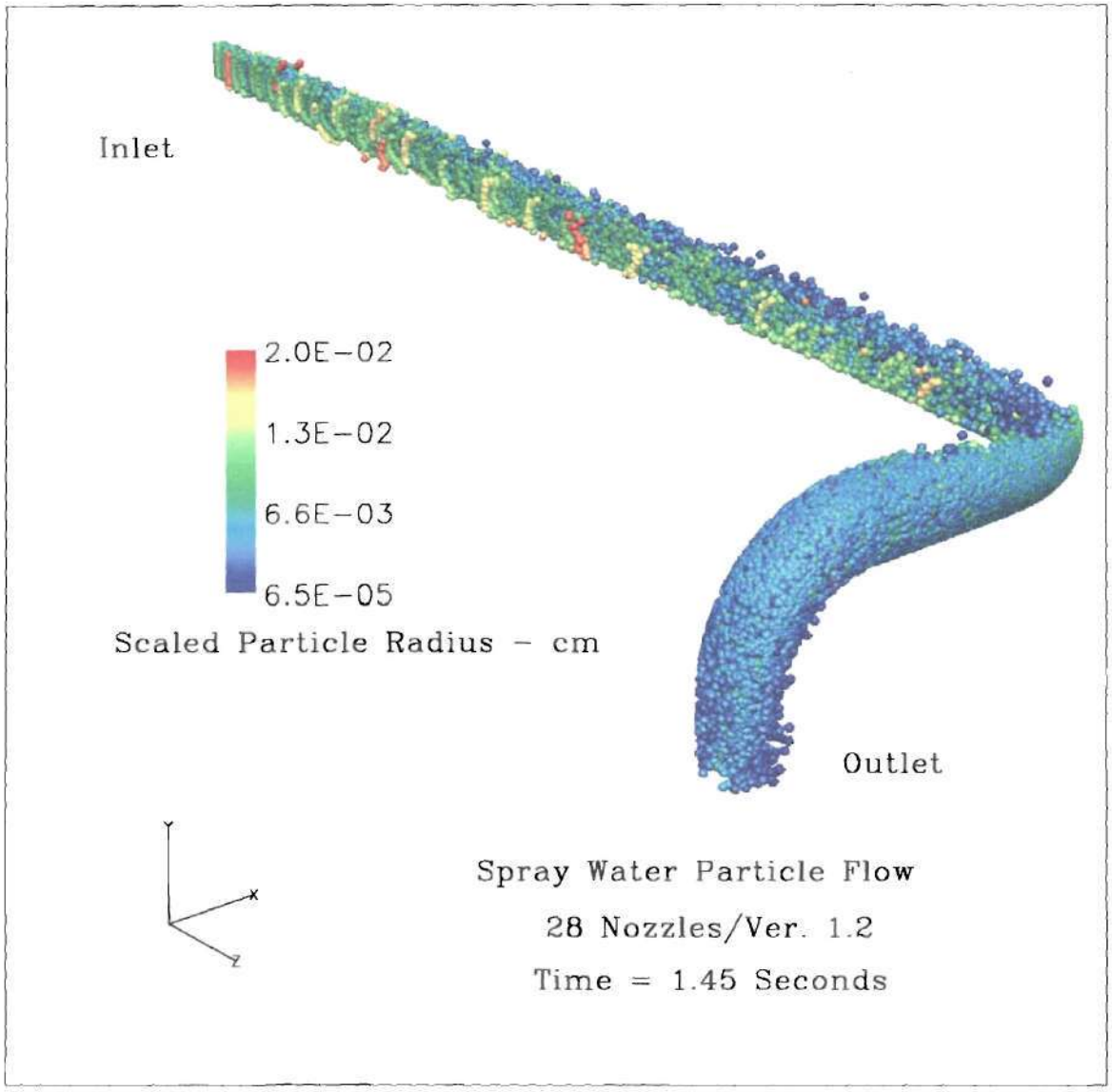
Inlet
2.0E-02
1.3E-02
6.6E-03
6.5E-05
Scaled Particle Radius - cm
Outlet
Y
X
Z
Spray Water Particle Flow
28 Nozzles/Ver. 1.2
Time = 1.45 Seconds

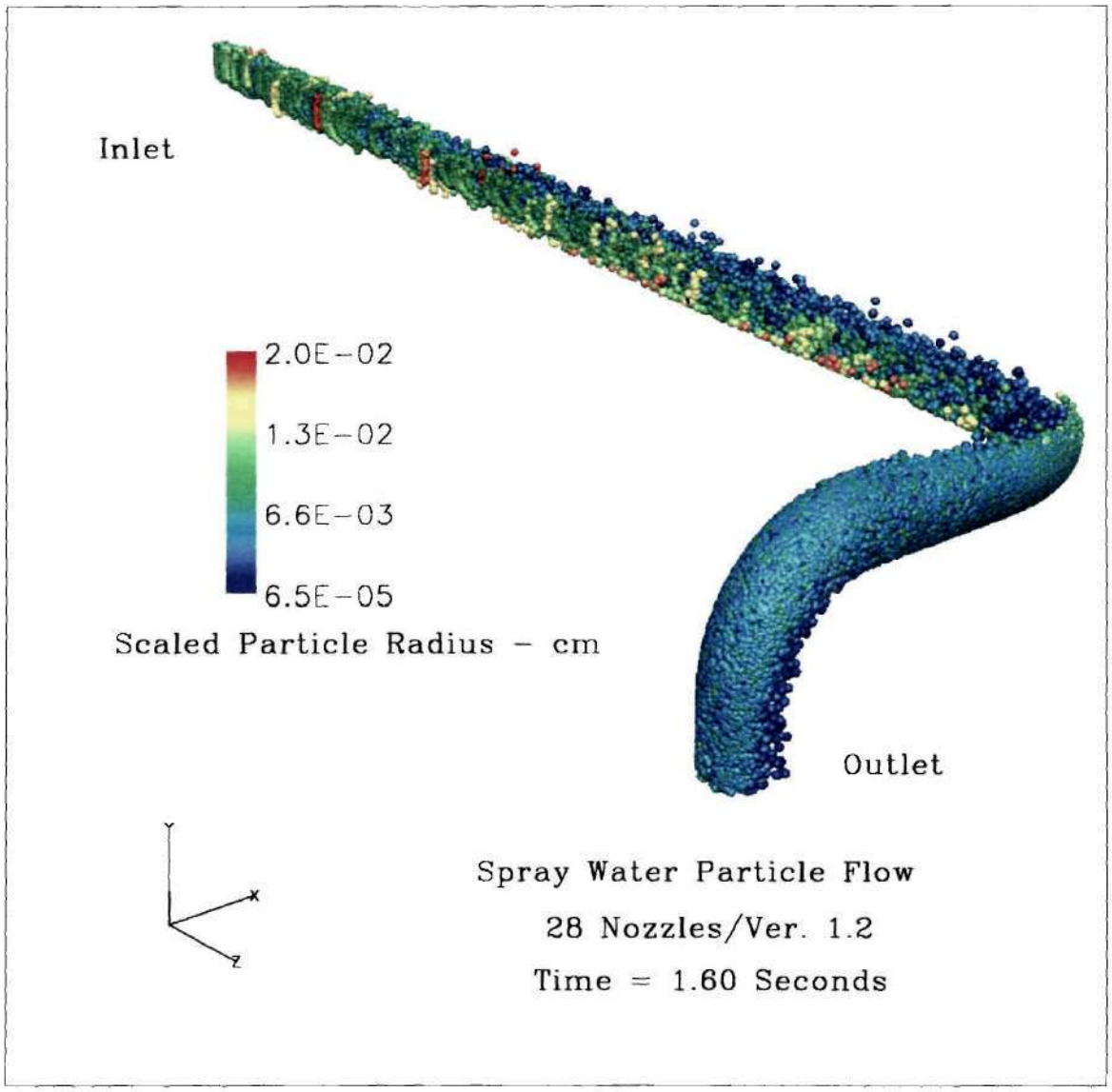
Inlet
2.0E-02
1.3E-02
6.6E-03
6.5E-05
Scaled Particle Radius - cm
Outlet
Y
X
Z
Spray Water Particle Flow
28 Nozzles/Ver. 1.2
Time = 1.60 Seconds

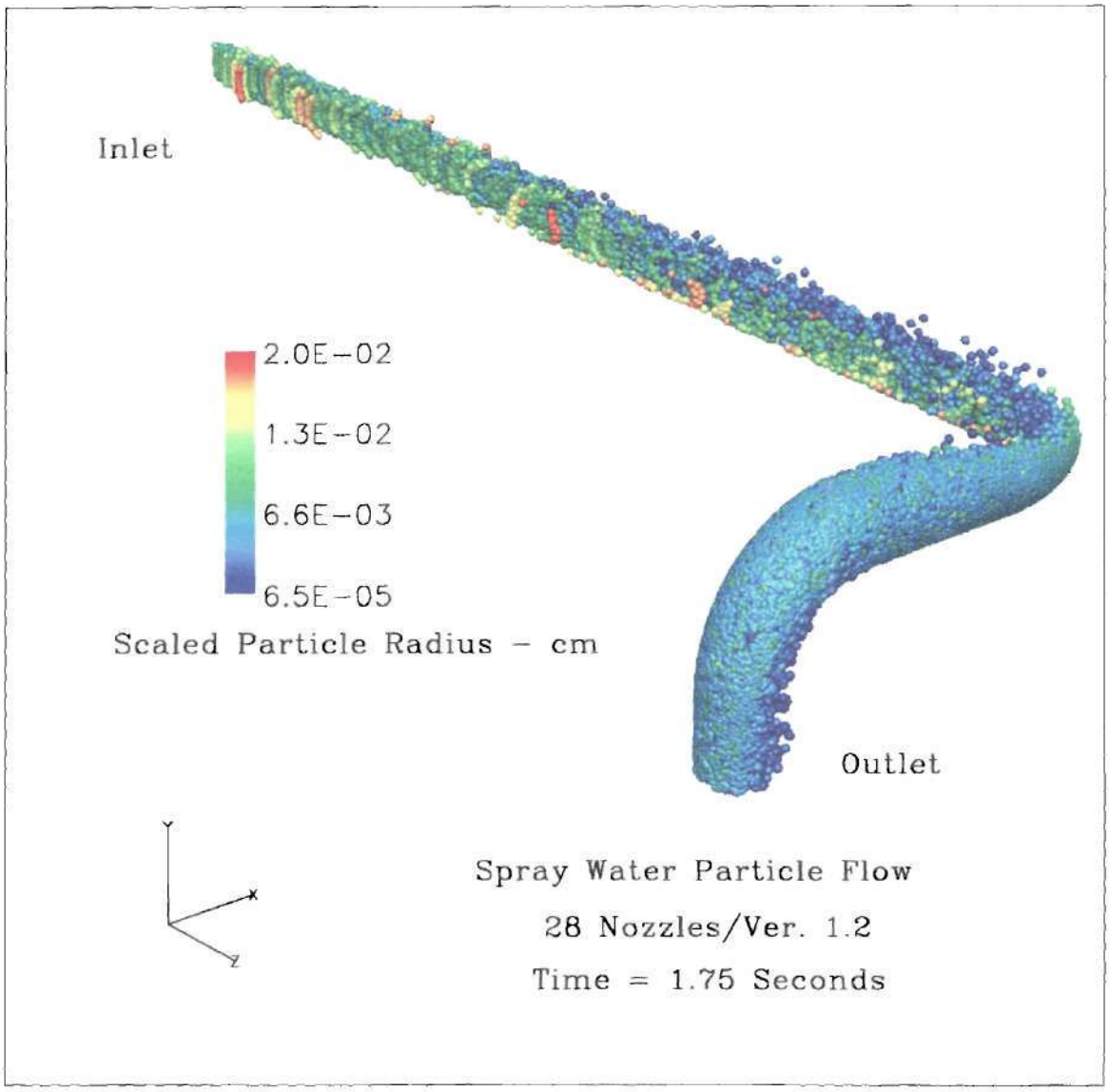
Inlet
2.0E-02
1.3E-02
6.6E-03
6.5E-05
Scaled Particle Radius - cm
Outlet
Y
X
Z
Spray Water Particle Flow
28 Nozzles/Ver. 1.2
Time = 1.75 Seconds

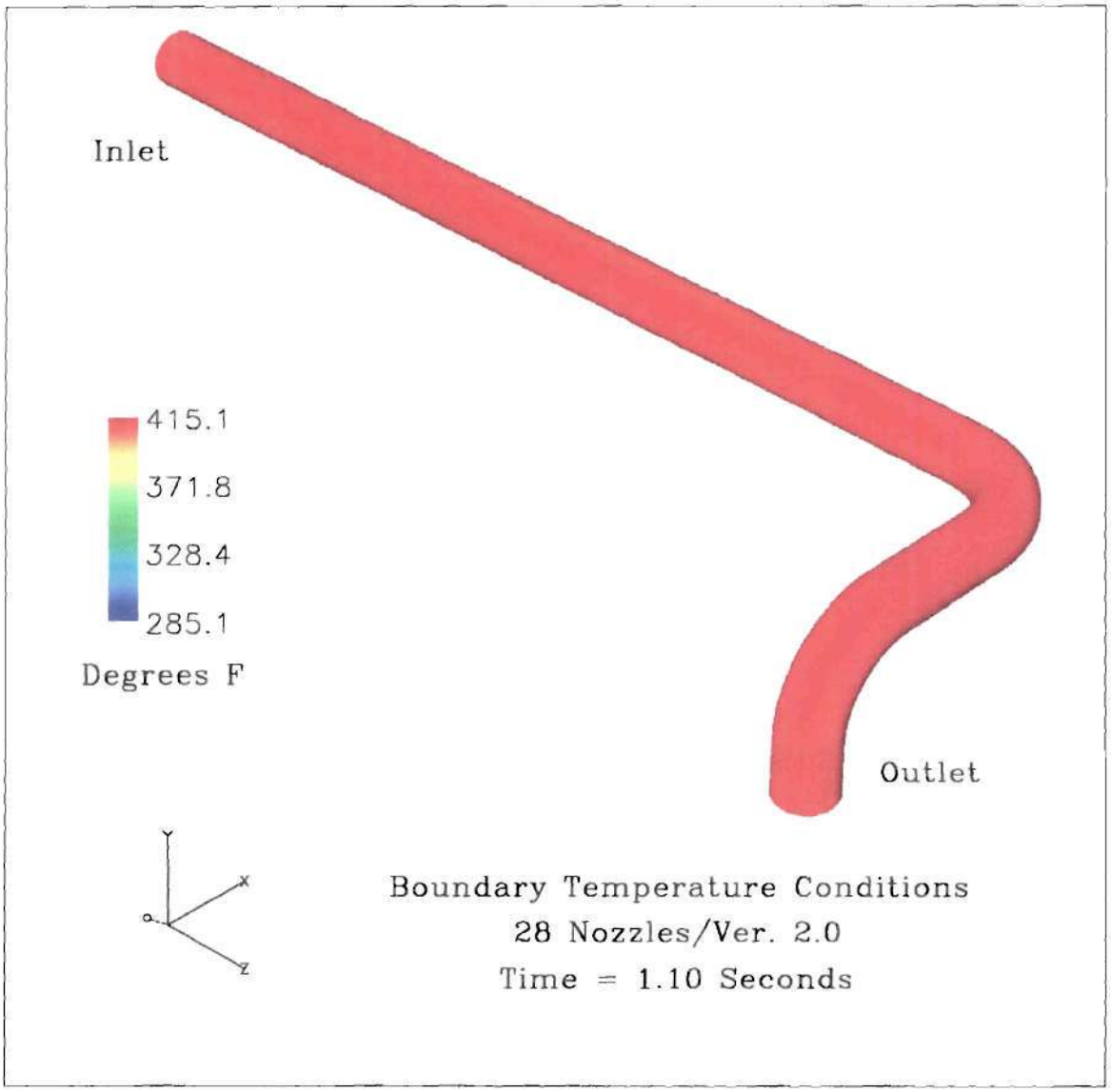
Inlet
415.1
371.8
328.4
285.1
Degrees F
Outlet
Y
X
Z
Boundary Temperature Conditions
28 Nozzles/Ver. 2.0
Time = 1.10 Seconds

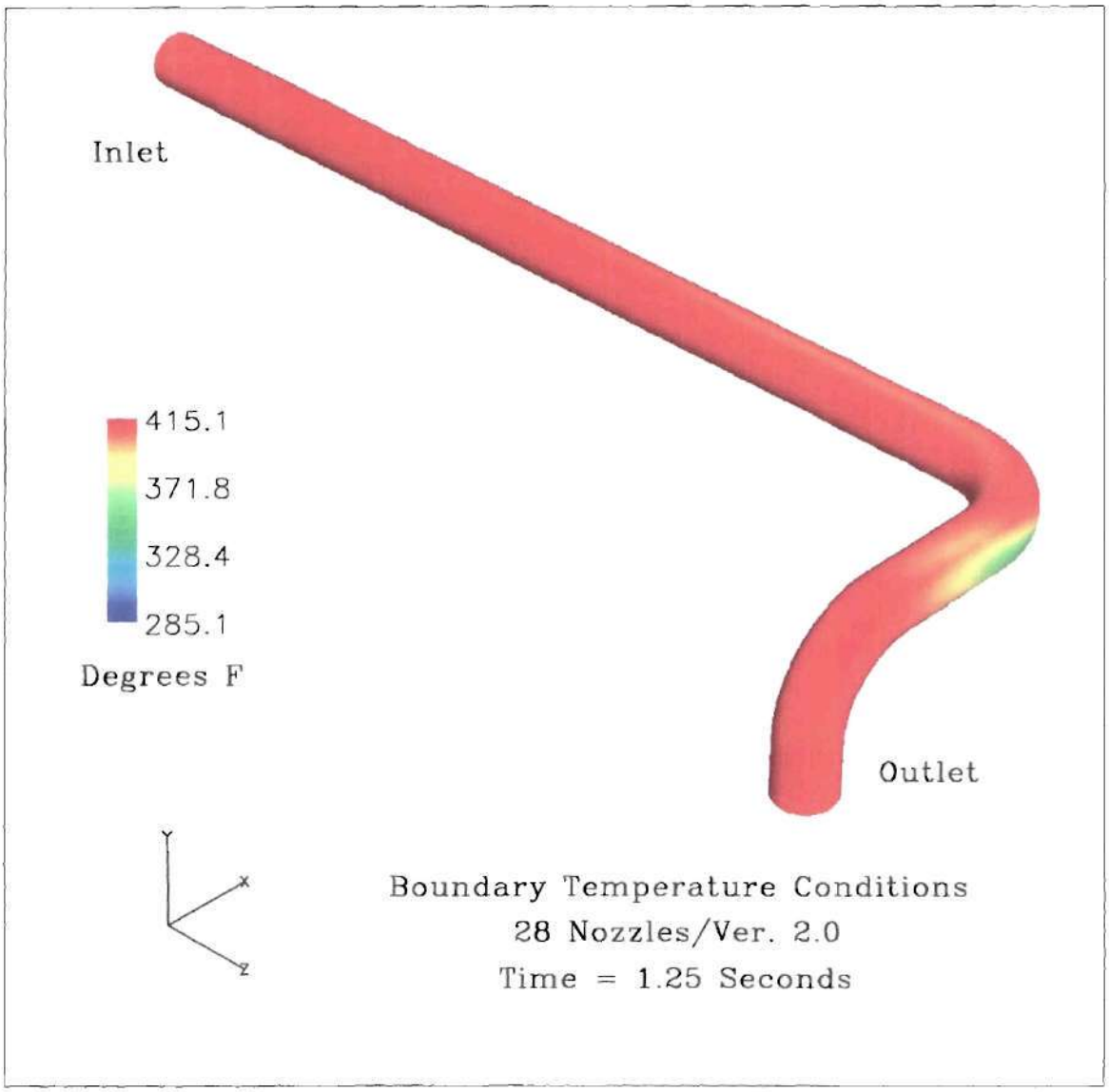
Inlet
415.1
371.8
328.4
285.1
Degrees F
Outlet
Y
X
Z
Boundary Temperature Conditions
28 Nozzles/Ver. 2.0
Time = 1.25 Seconds

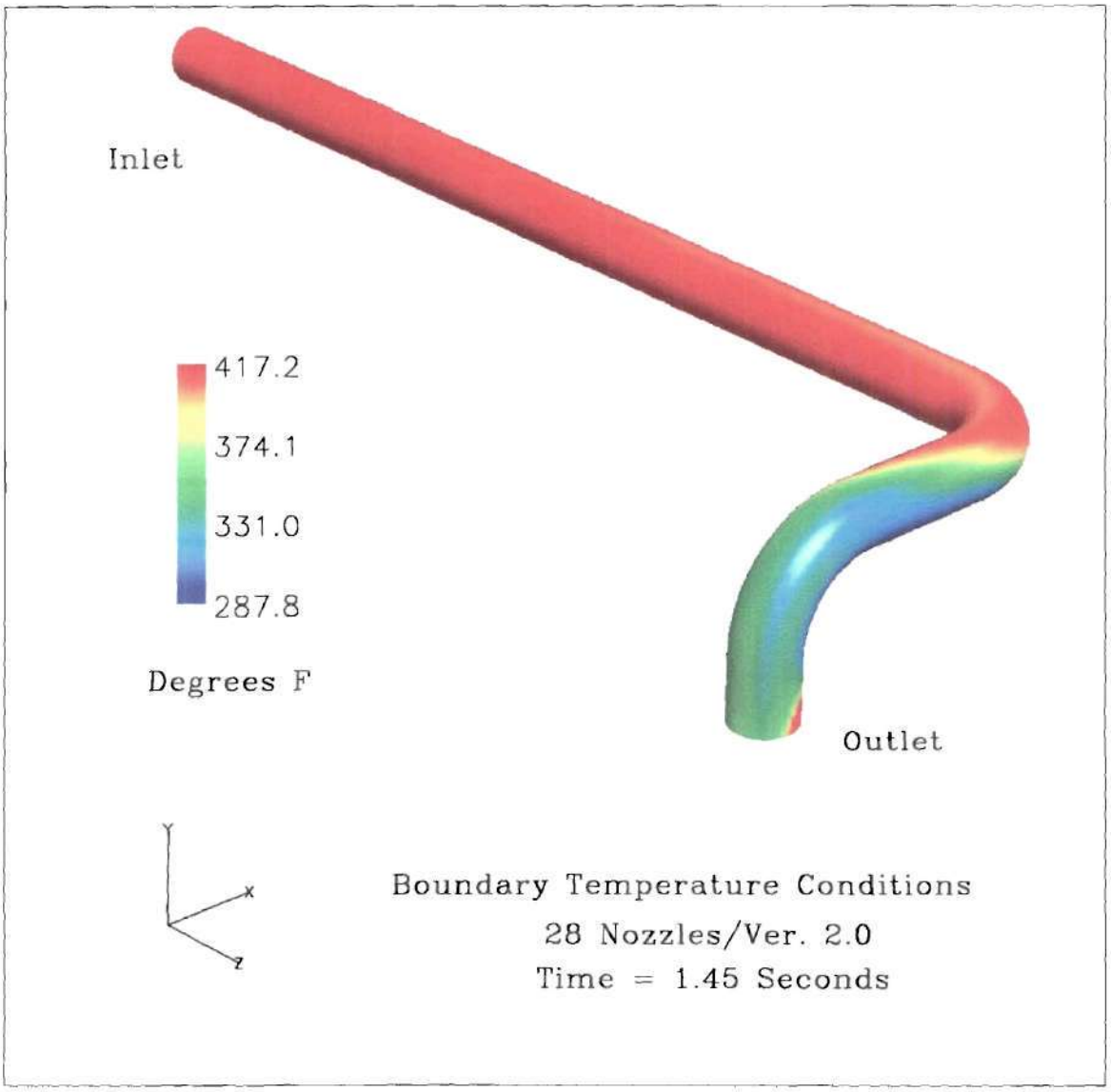
Inlet
417.2
374.1
331.0
287.8
Degrees F
Outlet
Y
X
Z
Boundary Temperature Conditions
28 Nozzles/Ver. 2.0
Time = 1.45 Seconds

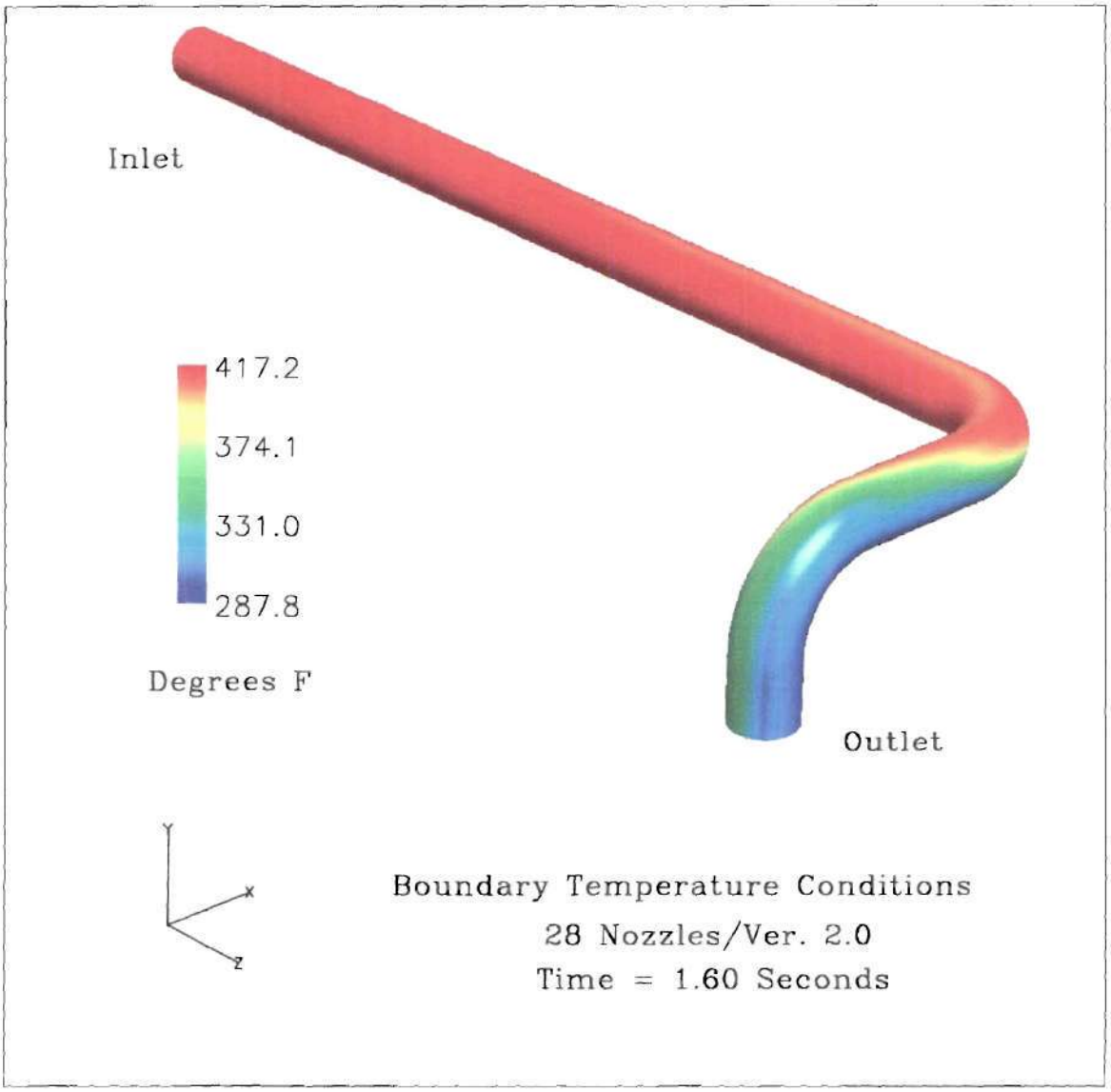
Inlet
417.2
374.1
331.0
287.8
Degrees F
Outlet
Y
X
Z
Boundary Temperature Conditions
28 Nozzles/Ver. 2.0
Time = 1.60 Seconds

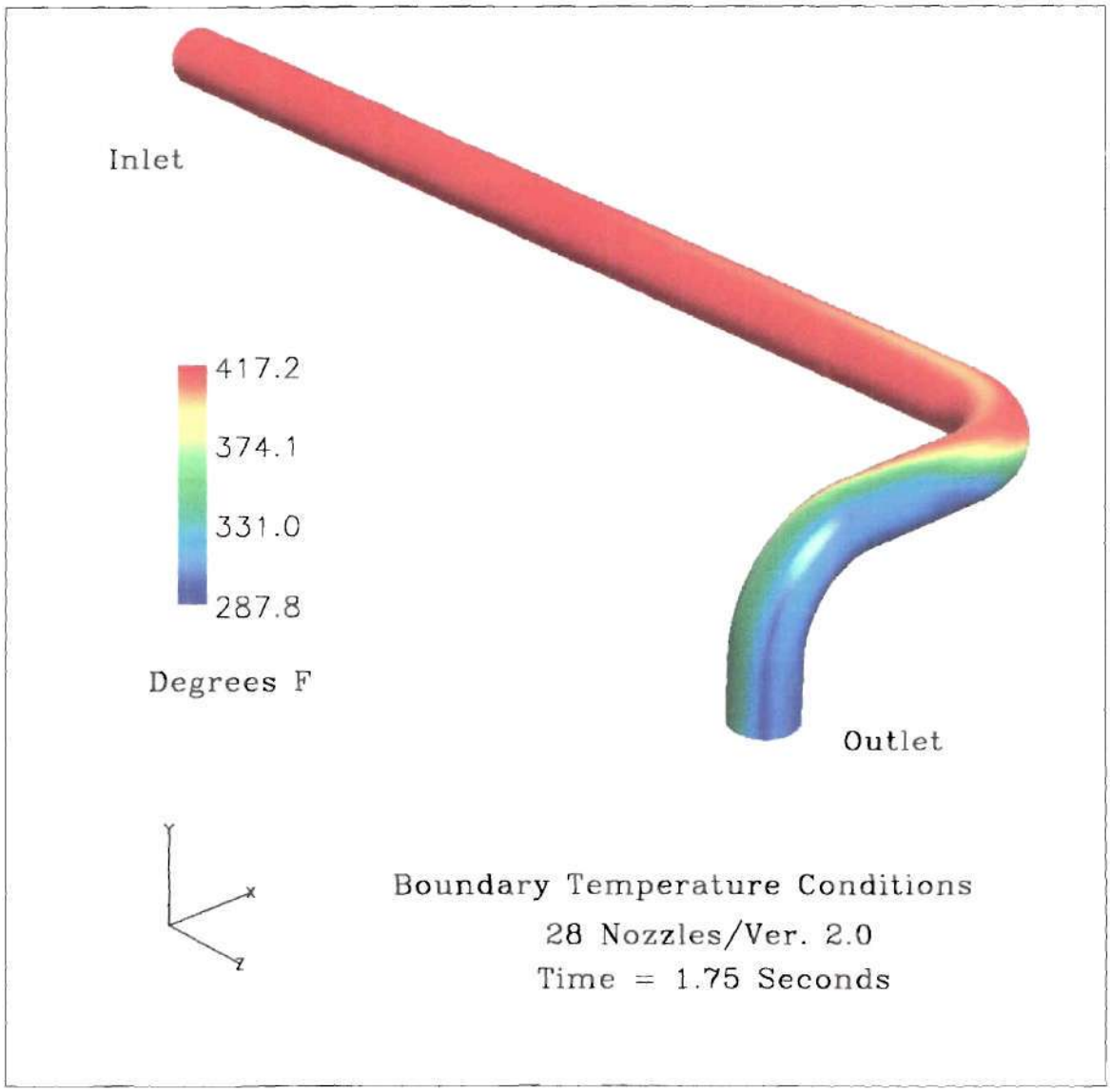
Inlet
417.2
374.1
331.0
287.8
Degrees F
Outlet
Y
X
Z
Boundary Temperature Conditions
28 Nozzles/Ver. 2.0
Time = 1.75 Seconds

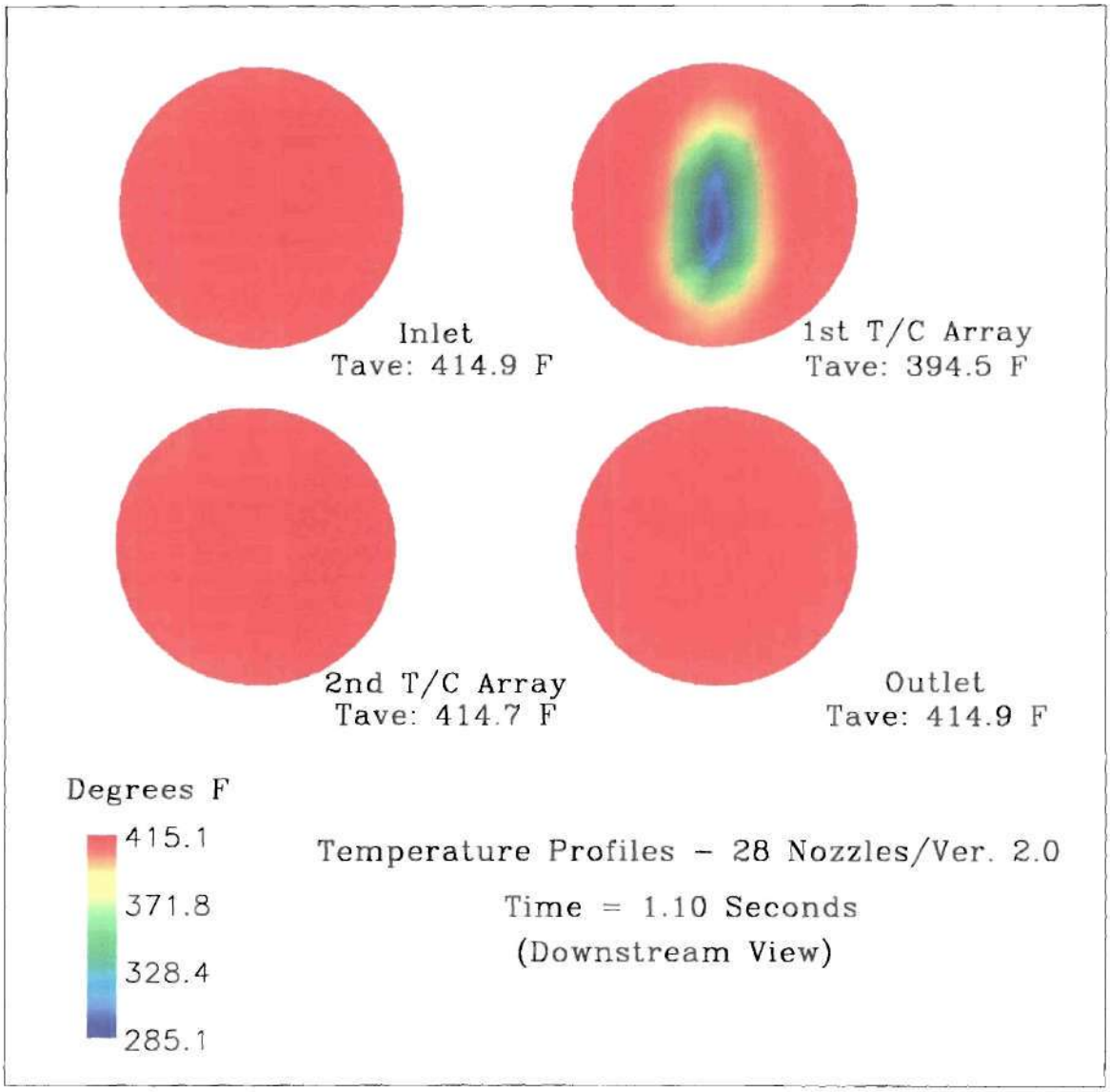
Inlet
Tave: 414.9 F
1st T/C Array
Tave: 394.5 F
2nd T/C Array
Tave: 414.7 F
Outlet
Tave: 414.9 F
Degrees F
415.1
371.8
328.4
285.1
Temperature Profiles - 28 Nozzles/Ver. 2.0
Time = 1.10 Seconds
(Downstream View)

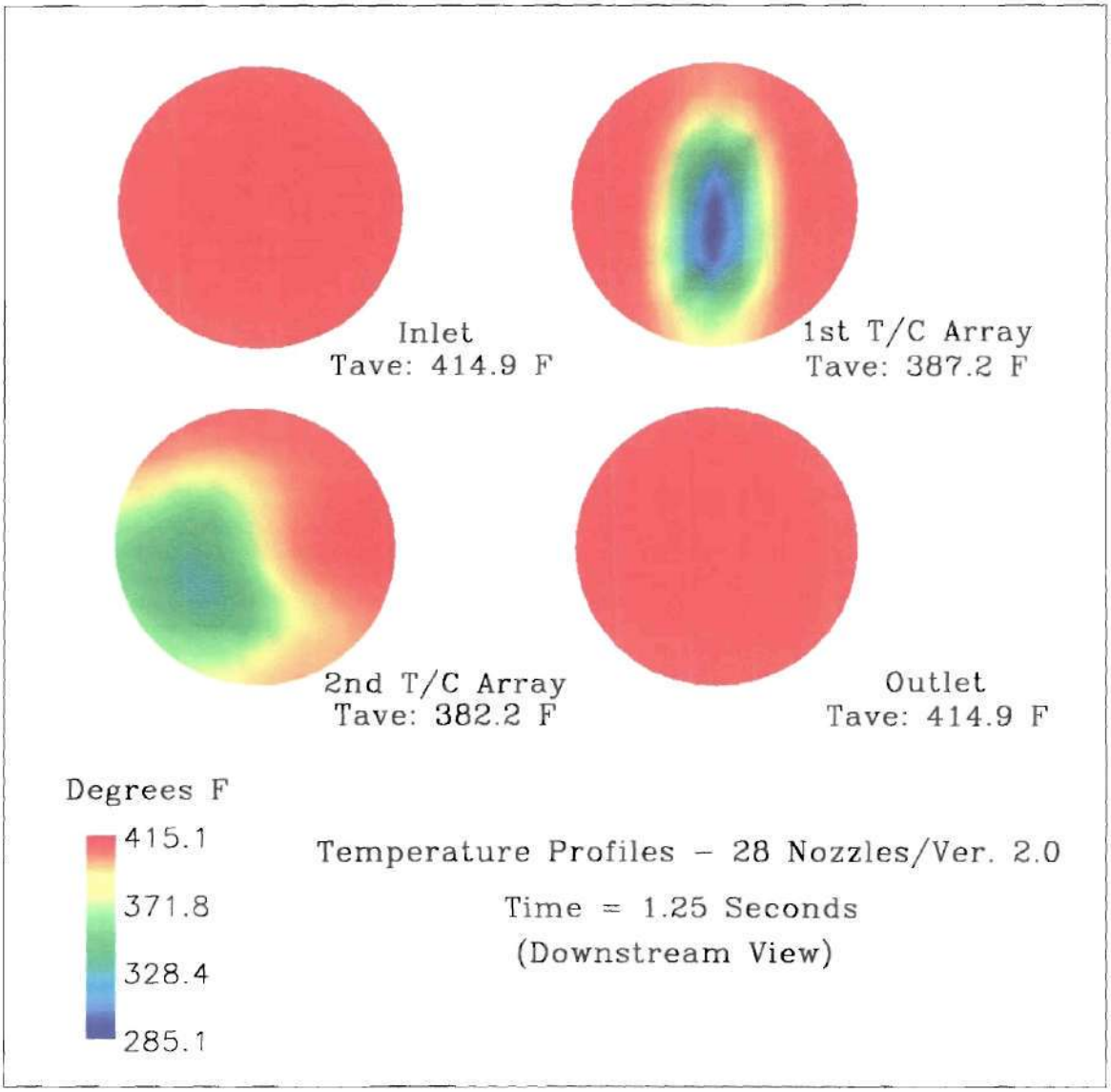
Inlet
Tave: 414.9 F
1st T/C Array
Tave: 387.2 F
2nd T/C Array
Tave: 382.2 F
Outlet
Tave: 414.9 F
Degrees F
415.1
371.8
328.4
285.1
Temperature Profiles - 28 Nozzles/Ver. 2.0
Time = 1.25 Seconds
(Downstream View)

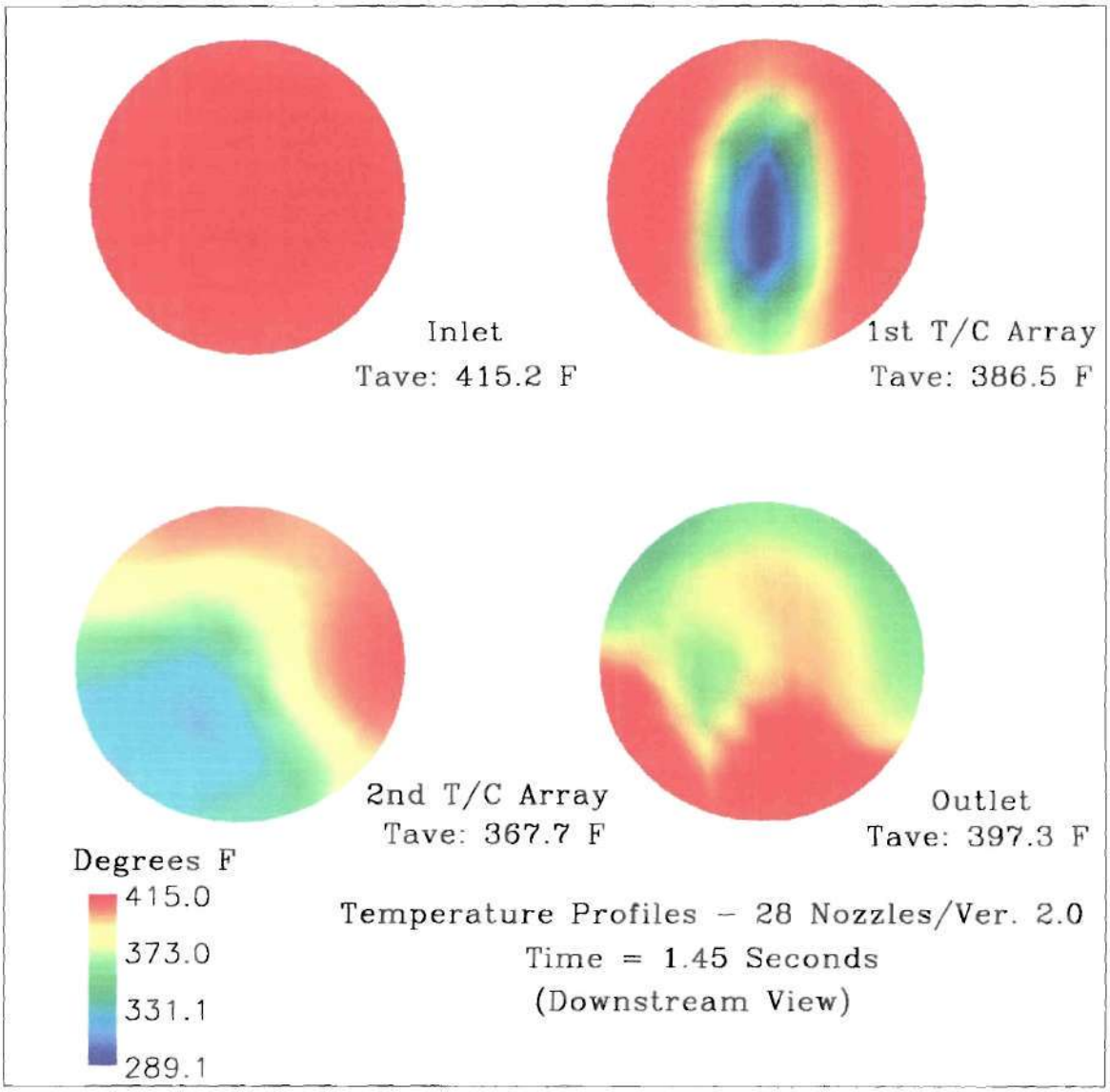
Inlet
Tave: 415.2 F
1st T/C Array
Tave: 386.5 F
2nd T/C Array
Tave: 367.7 F
Outlet
Tave: 397.3 F
Degrees F
415.0
373.0
331.1
289.1
Temperature Profiles - 28 Nozzles/Ver. 2.0
Time = 1.45 Seconds
(Downstream View)

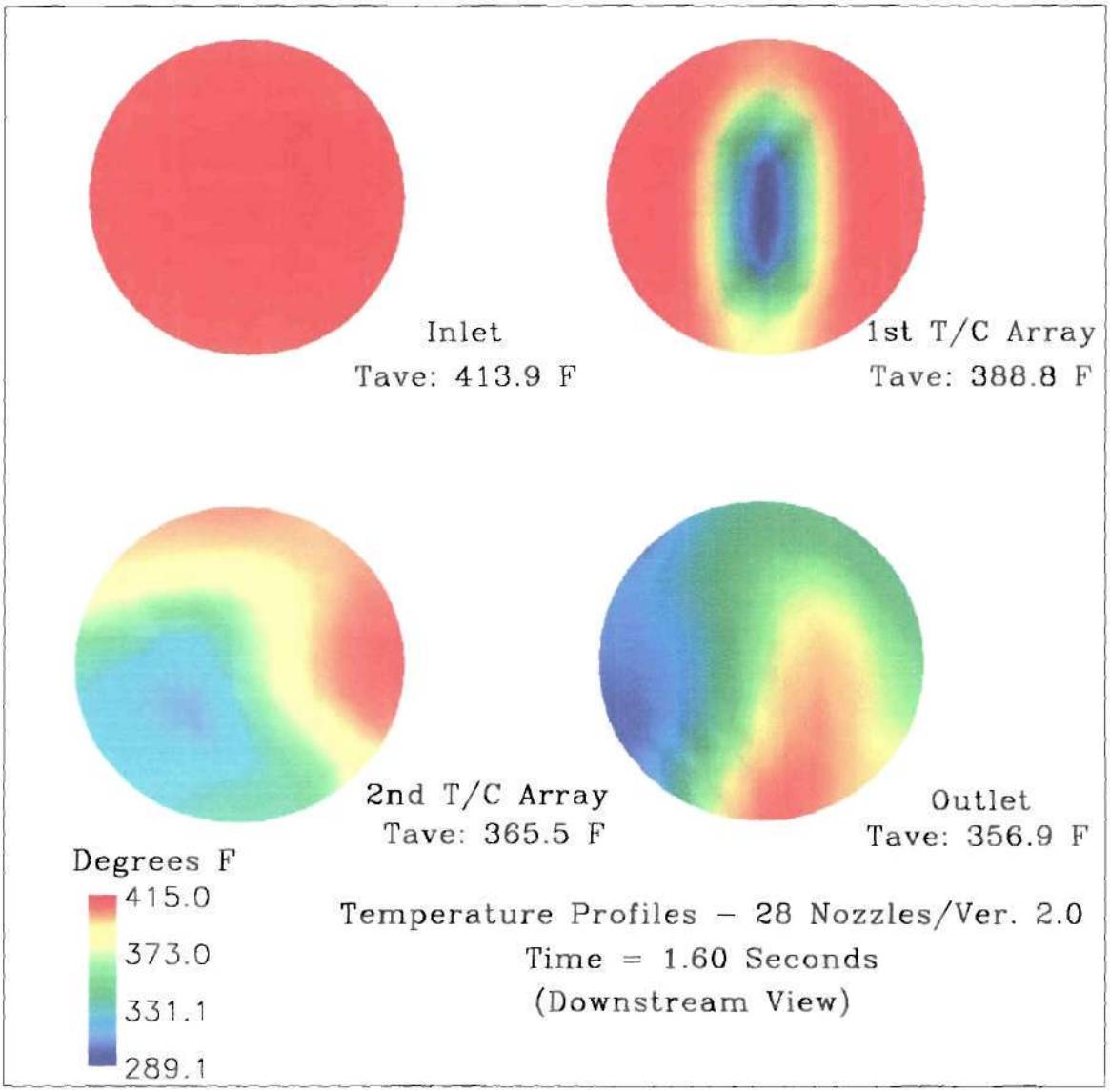
Inlet
Tave: 413.9 F
1st T/C Array
Tave: 388.8 F
2nd T/C Array
Tave: 365.5 F
Outlet
Tave: 356.9 F
Degrees F
415.0
373.0
331.1
289.1
Temperature Profiles - 28 Nozzles/Ver. 2.0
Time = 1.60 Seconds
(Downstream View)

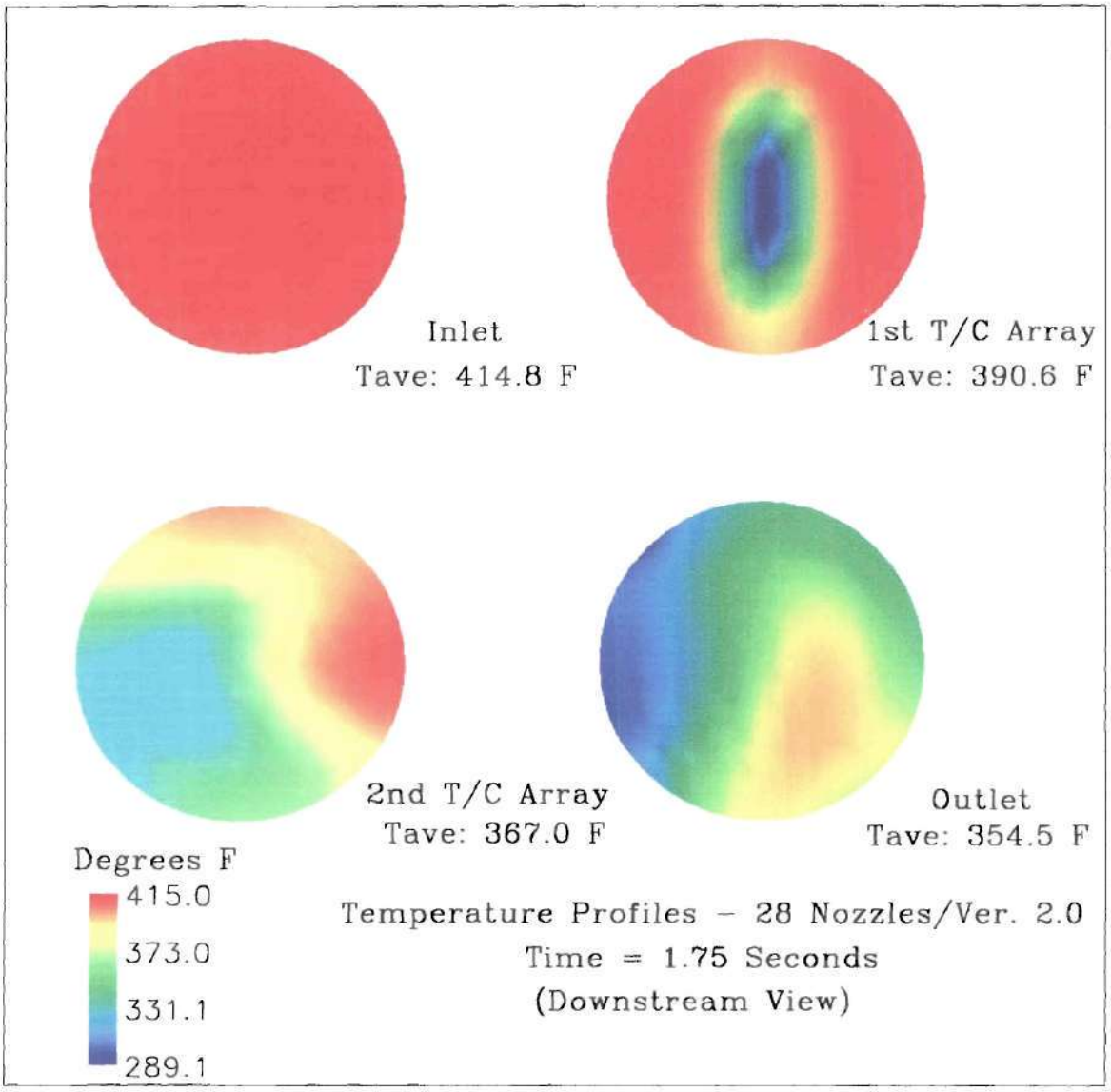
Inlet
Tave: 414.8 F
1st T/C Array
Tave: 390.6 F
2nd T/C Array
Tave: 367.0 F
Outlet
Tave: 354.5 F
Degrees F
415.0
373.0
331.1
289.1
Temperature Profiles - 28 Nozzles/Ver. 2.0
Time = 1.75 Seconds
(Downstream View)

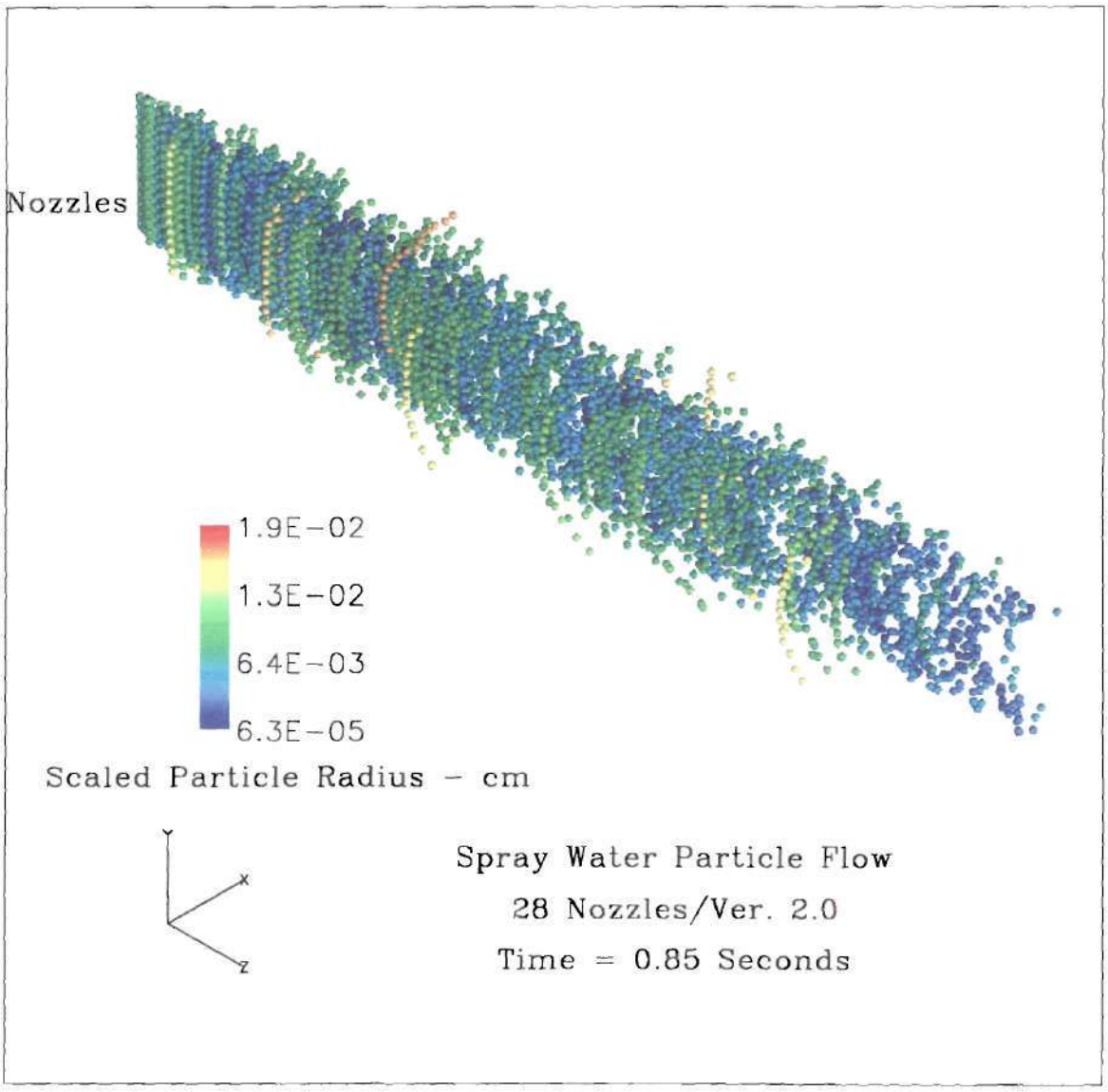
Nozzles
1.9E-02
1.3E-02
6.4E-03
6.3E-05
Scaled Particle Radius - cm
Y
X
Z
Spray Water Particle Flow
28 Nozzles/Ver. 2.0
Time = 0.85 Seconds

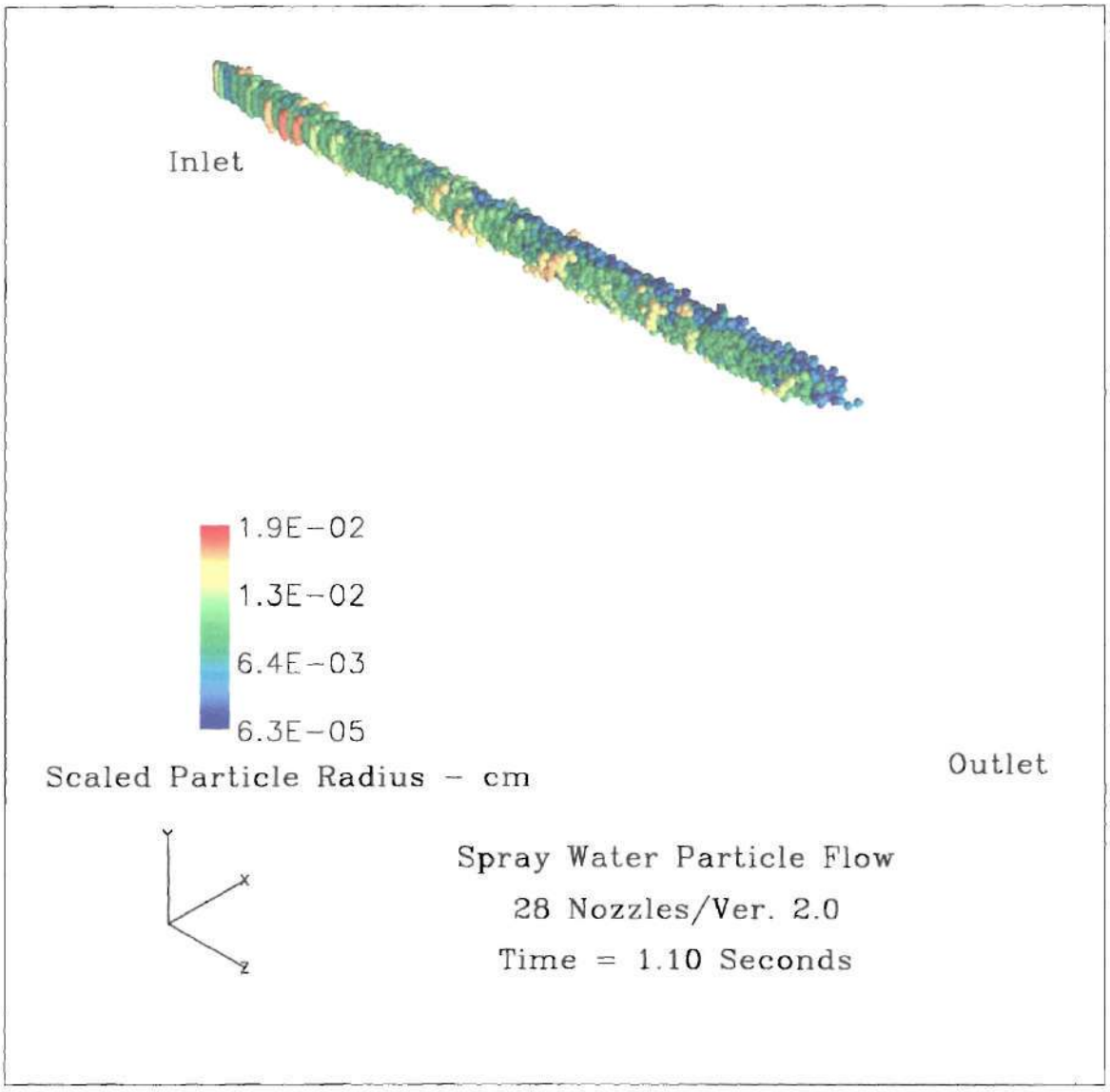
Inlet
1.9E-02
1.3E-02
6.4E-03
6.3E-05
Scaled Particle Radius - cm
Outlet
Y
X
Z
Spray Water Particle Flow
28 Nozzles/Ver. 2.0
Time = 1.10 Seconds

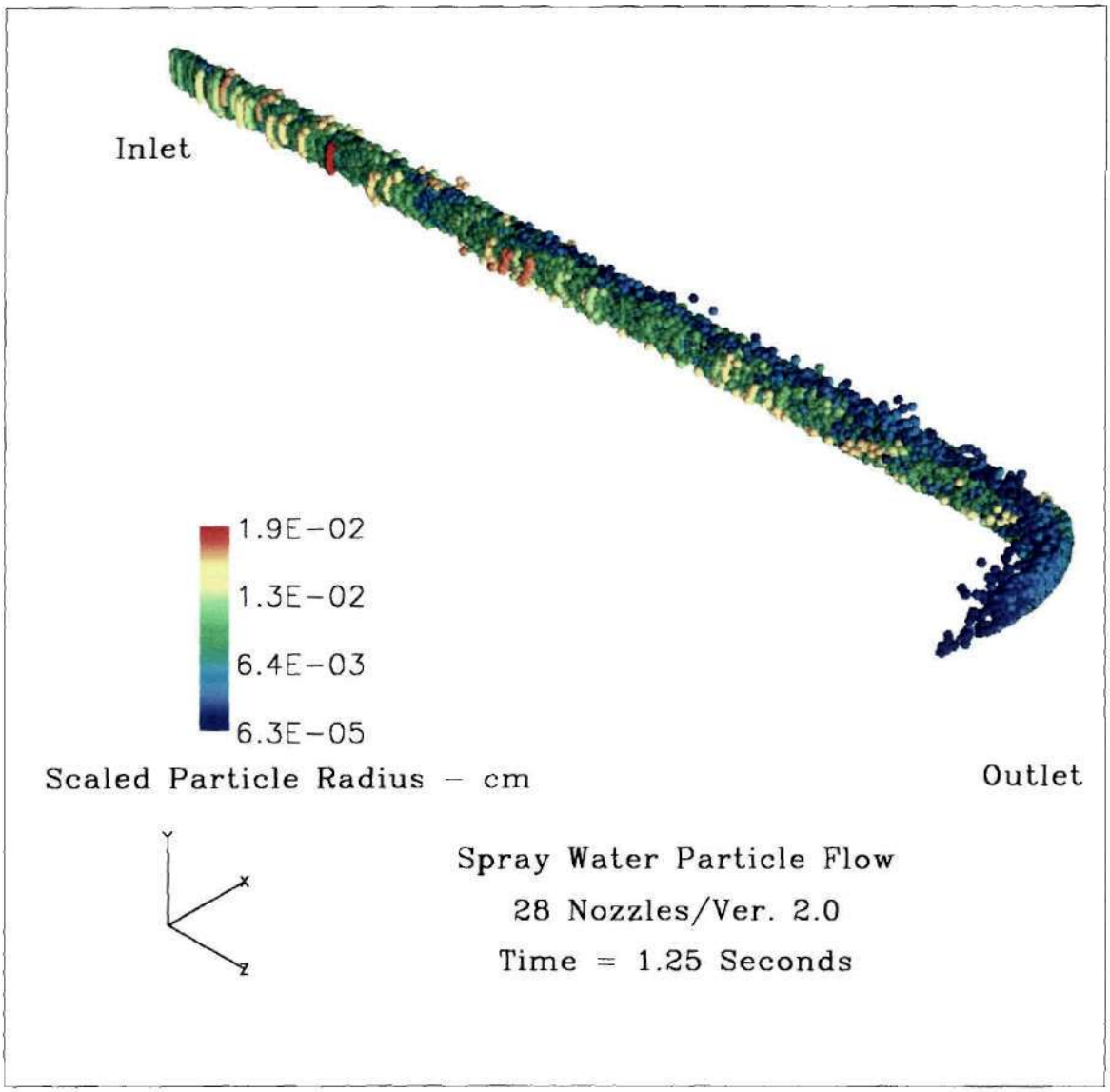
Inlet
1.9E-02
1.3E-02
6.4E-03
6.3E-05
Scaled Particle Radius - cm
Outlet
Y
X
Z
Spray Water Particle Flow
28 Nozzles/Ver. 2.0
Time = 1.25 Seconds

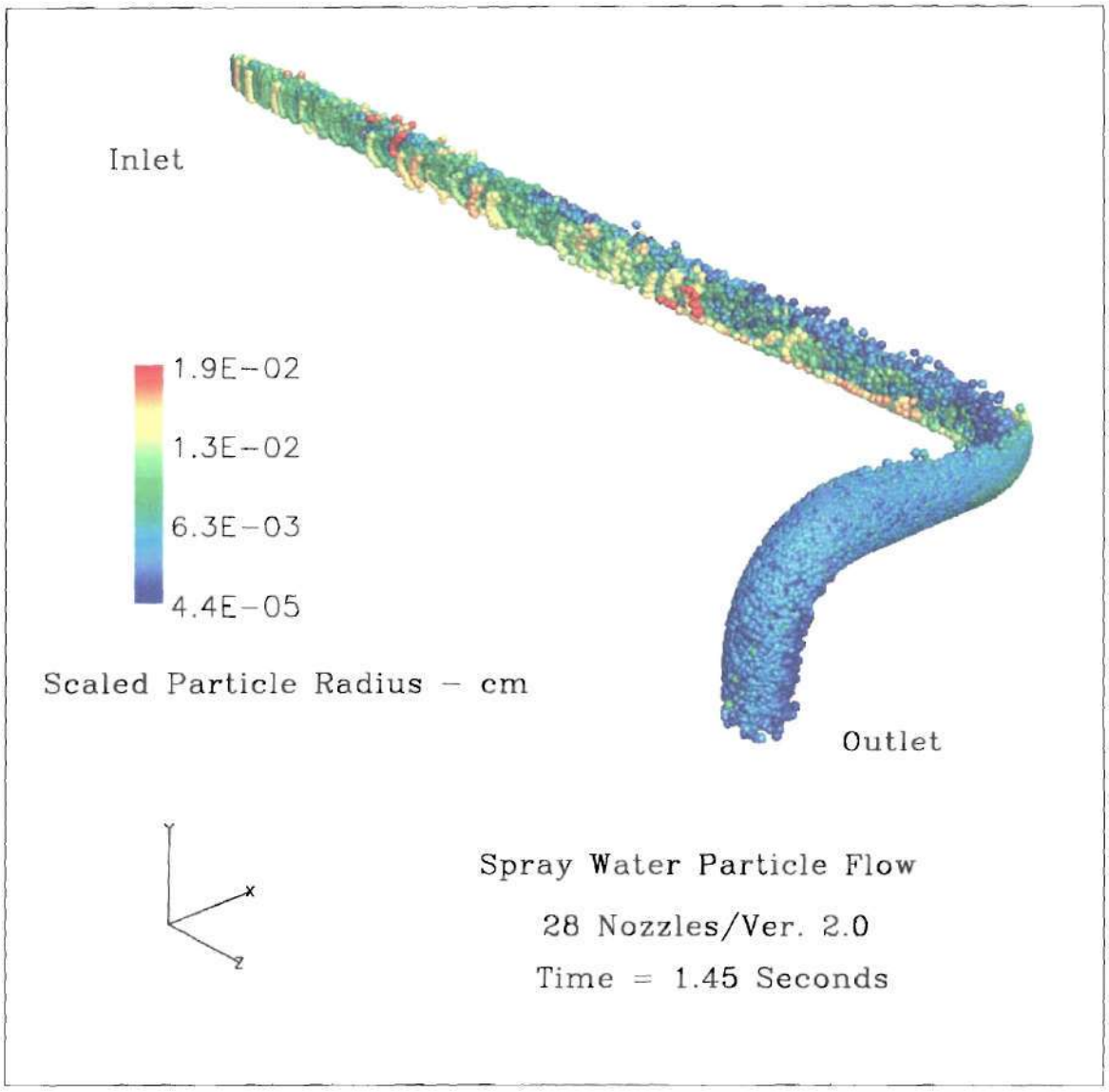
Inlet
1.9E-02
1.3E-02
6.3E-03
4.4E-05
Scaled Particle Radius - cm
Outlet
Y
X
Z
Spray Water Particle Flow
28 Nozzles/Ver. 2.0
Time = 1.45 Seconds

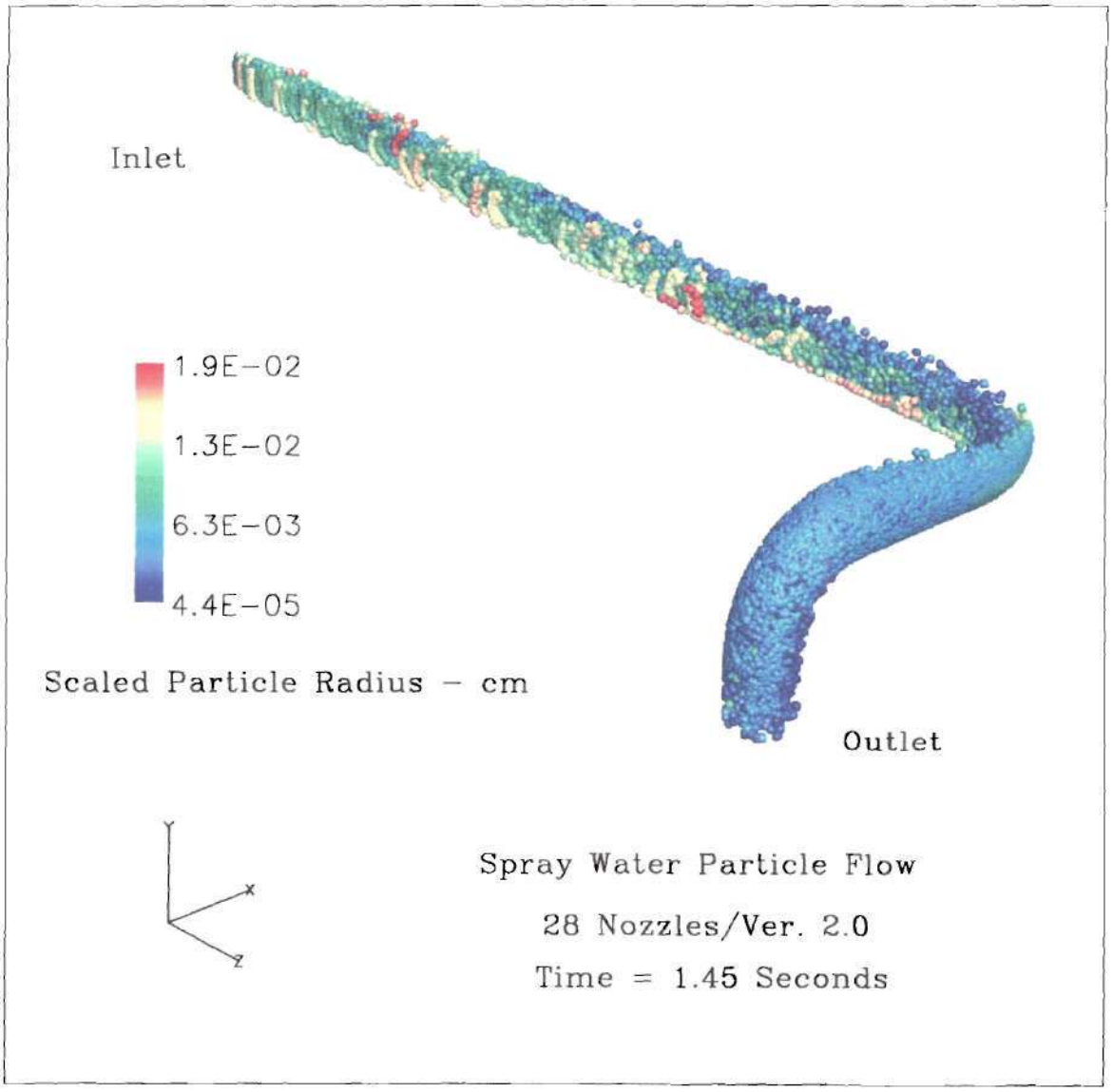
Inlet
1.9E-02
1.3E-02
6.3E-03
4.4E-05
Scaled Particle Radius - cm
Outlet
Y
X
Z
Spray Water Particle Flow
28 Nozzles/Ver. 2.0
Time = 1.45 Seconds

APPENDIX E

STEAMCFD OUTPUT FOR CASE 3

This appendix contains the graphical representations of computational data collected from the SteamCFD Code. This data examines the results obtained when utilizing the single nozzle desuperheater arrangement and experimental data from the time period of 1170-1200 minutes elapsed time from midnight on October 30, 2000, i.e., 07:30 to 08:00 AM. Only Version 2.0 of the SteamCFD Code was used in this case.

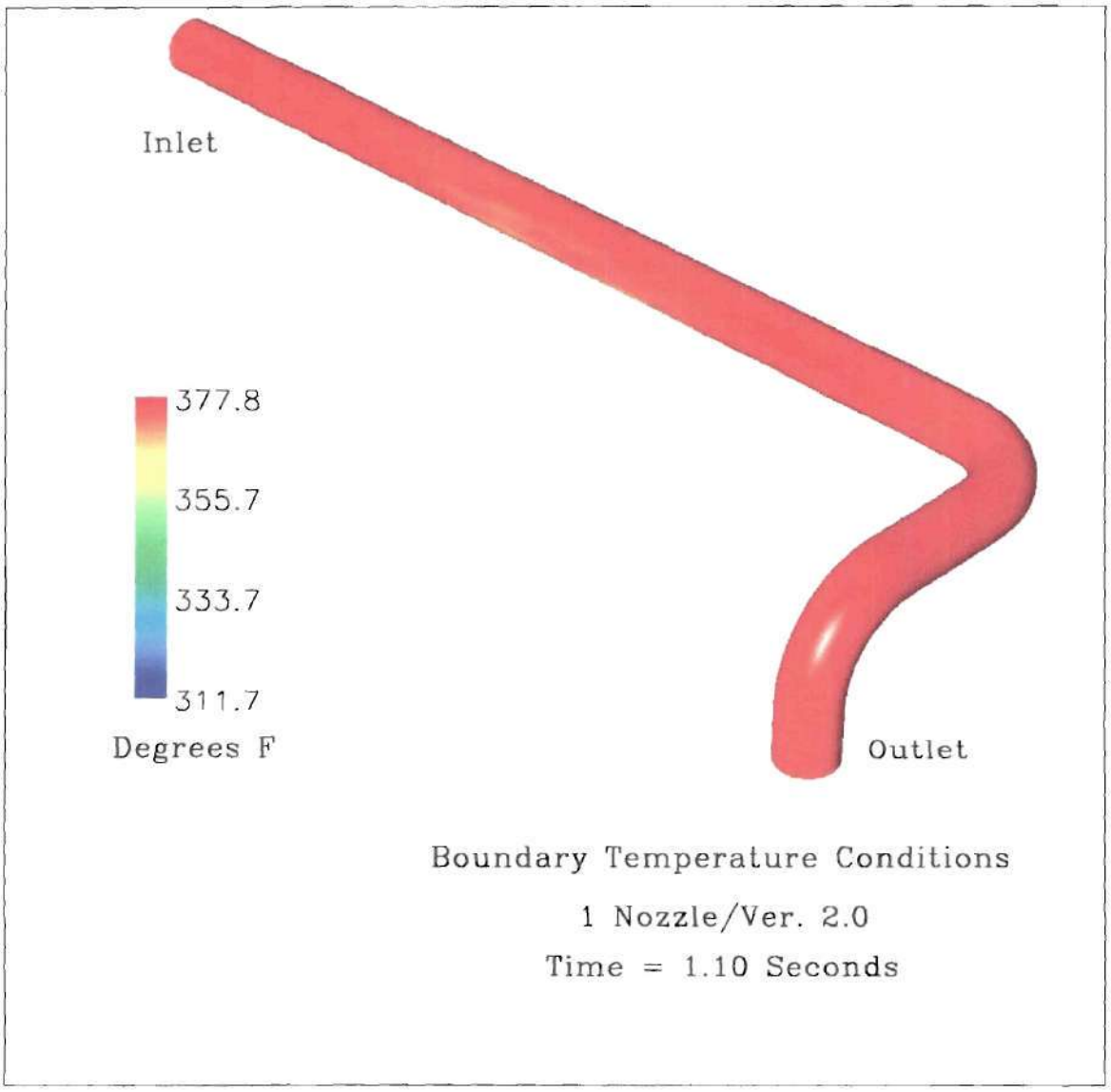
Inlet
377.8
355.7
333.7
311.7
Degrees F
Outlet
Boundary Temperature Conditions
1 Nozzle/Ver. 2.0
Time = 1.10 Seconds

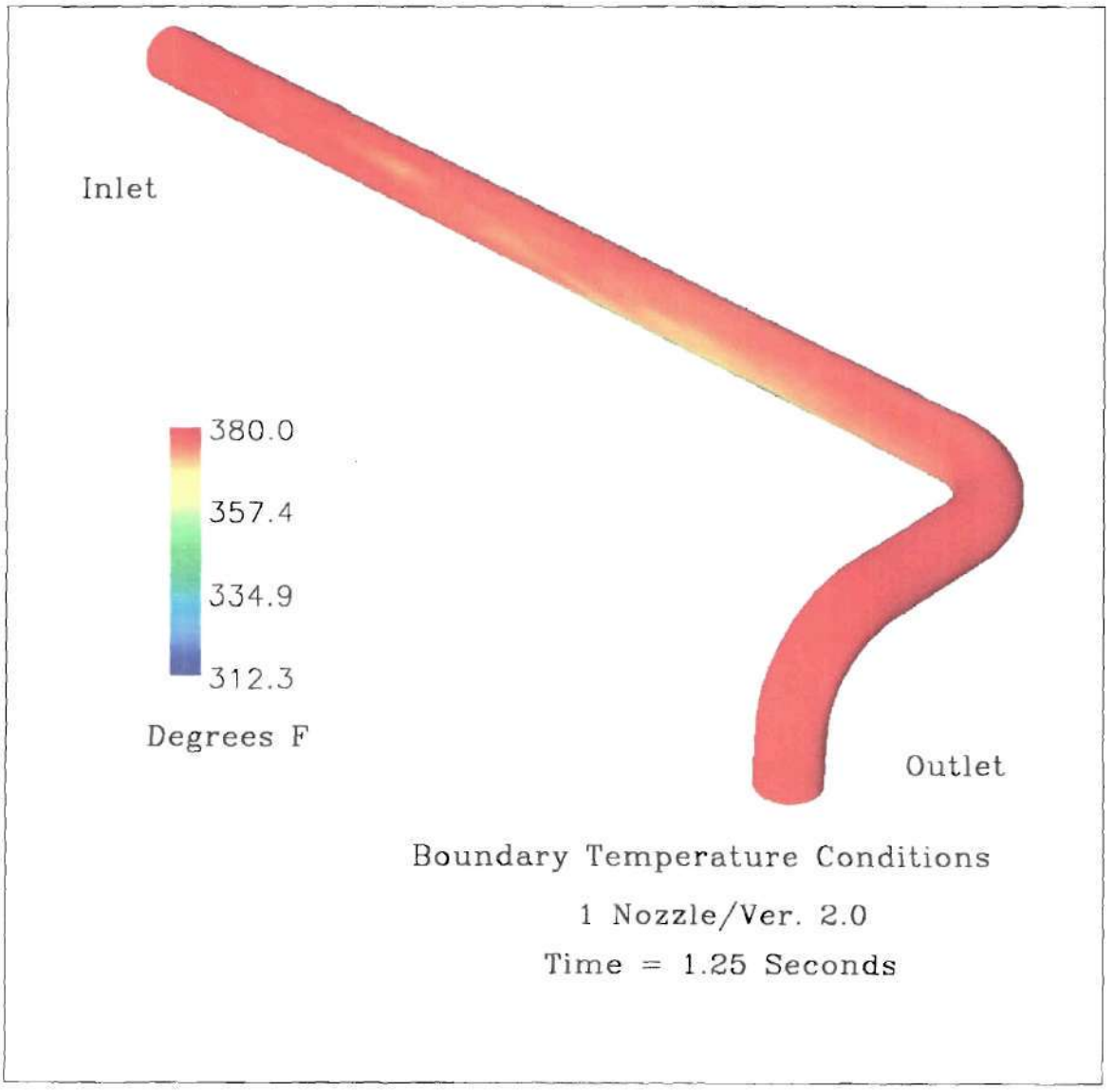
Inlet
380.0
357.4
334.9
312.3
Degrees F
Outlet
Boundary Temperature Conditions
1 Nozzle/Ver. 2.0
Time = 1.25 Seconds

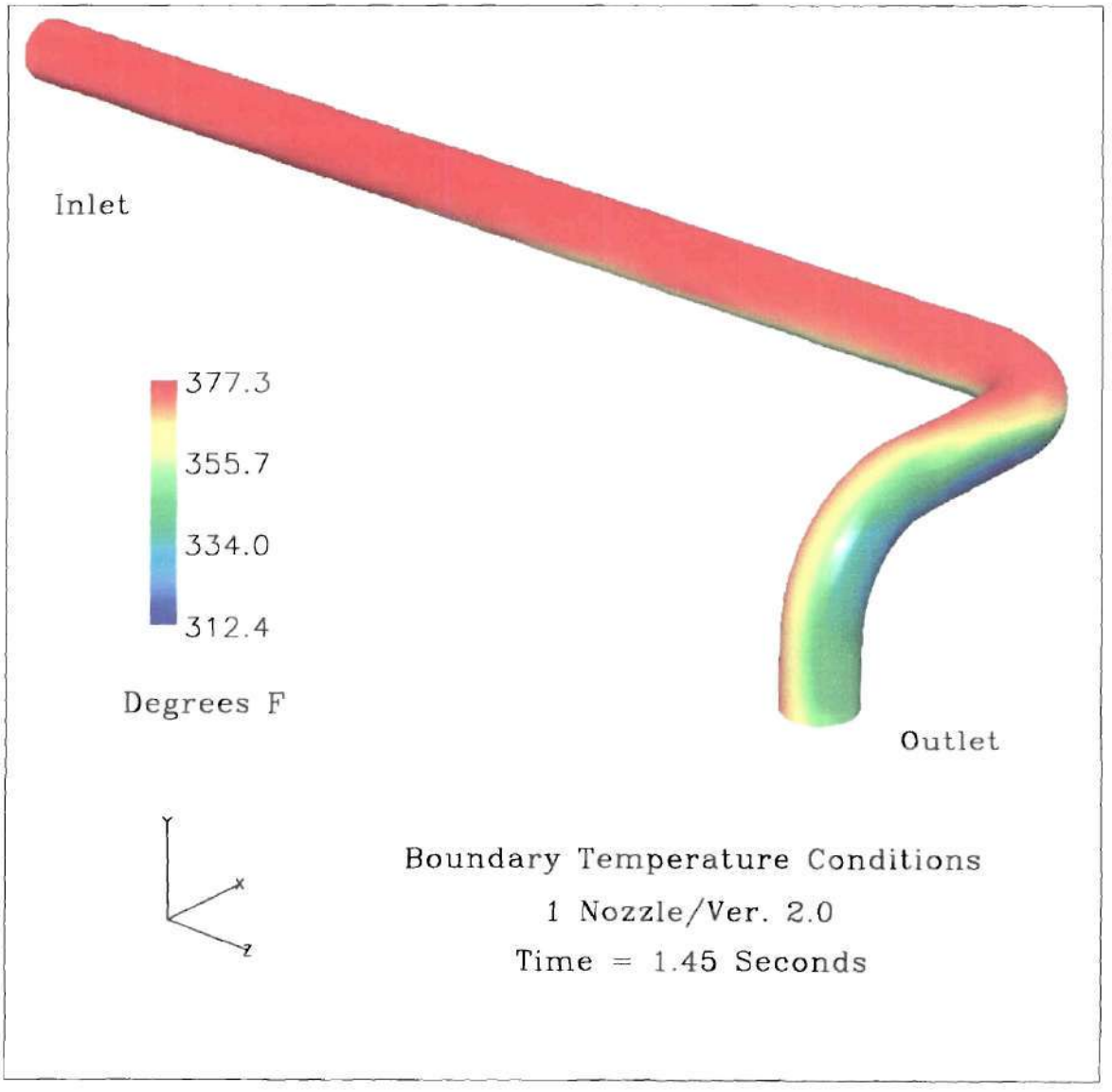
Inlet
377.3
355.7
334.0
312.4
Degrees F
Outlet
Y
X
Z
Boundary Temperature Conditions
1 Nozzle/Ver. 2.0
Time = 1.45 Seconds

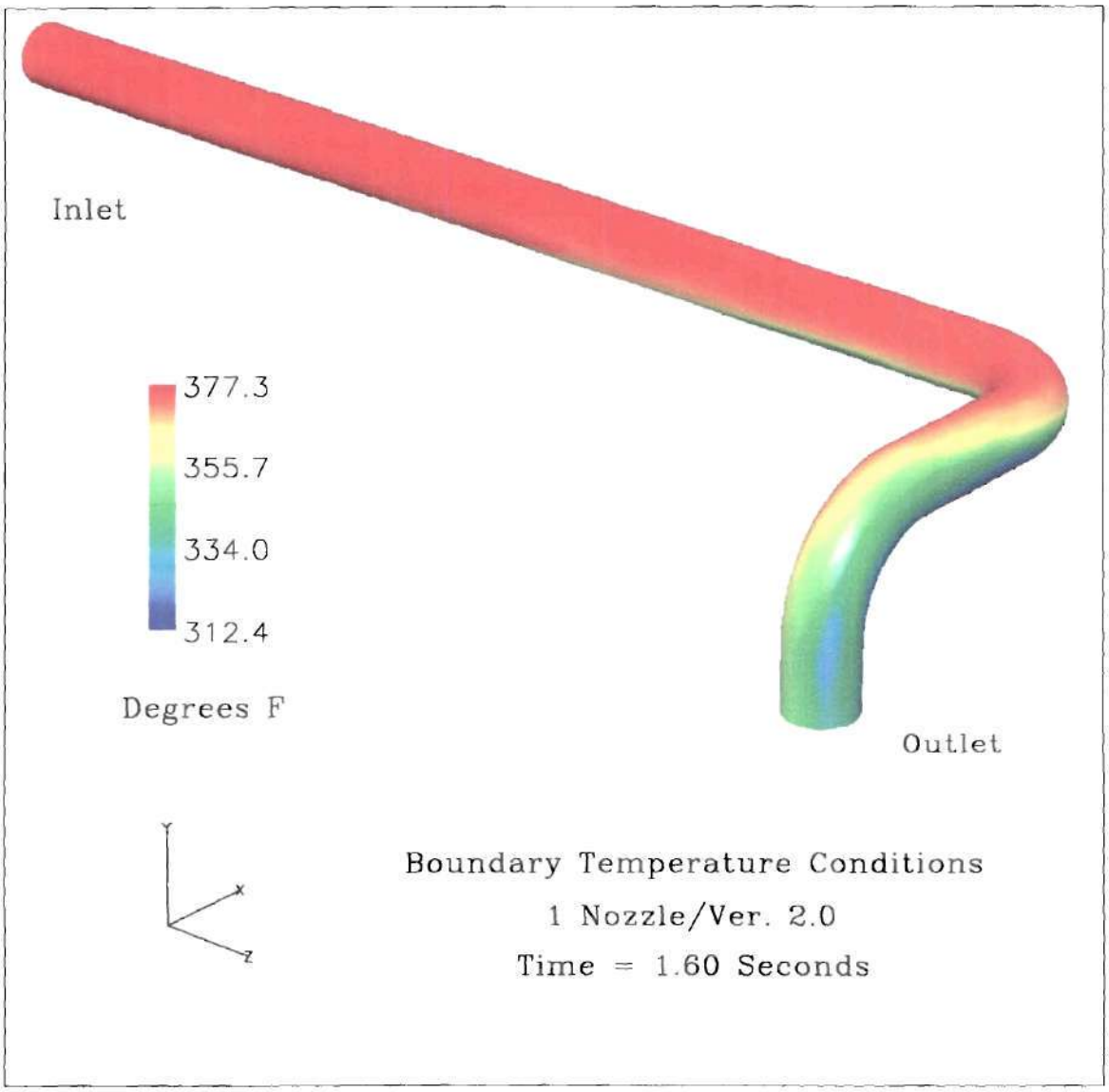
Inlet
377.3
355.7
334.0
312.4
Degrees F
Outlet
Y
X
Z
Boundary Temperature Conditions
1 Nozzle/Ver. 2.0
Time = 1.60 Seconds

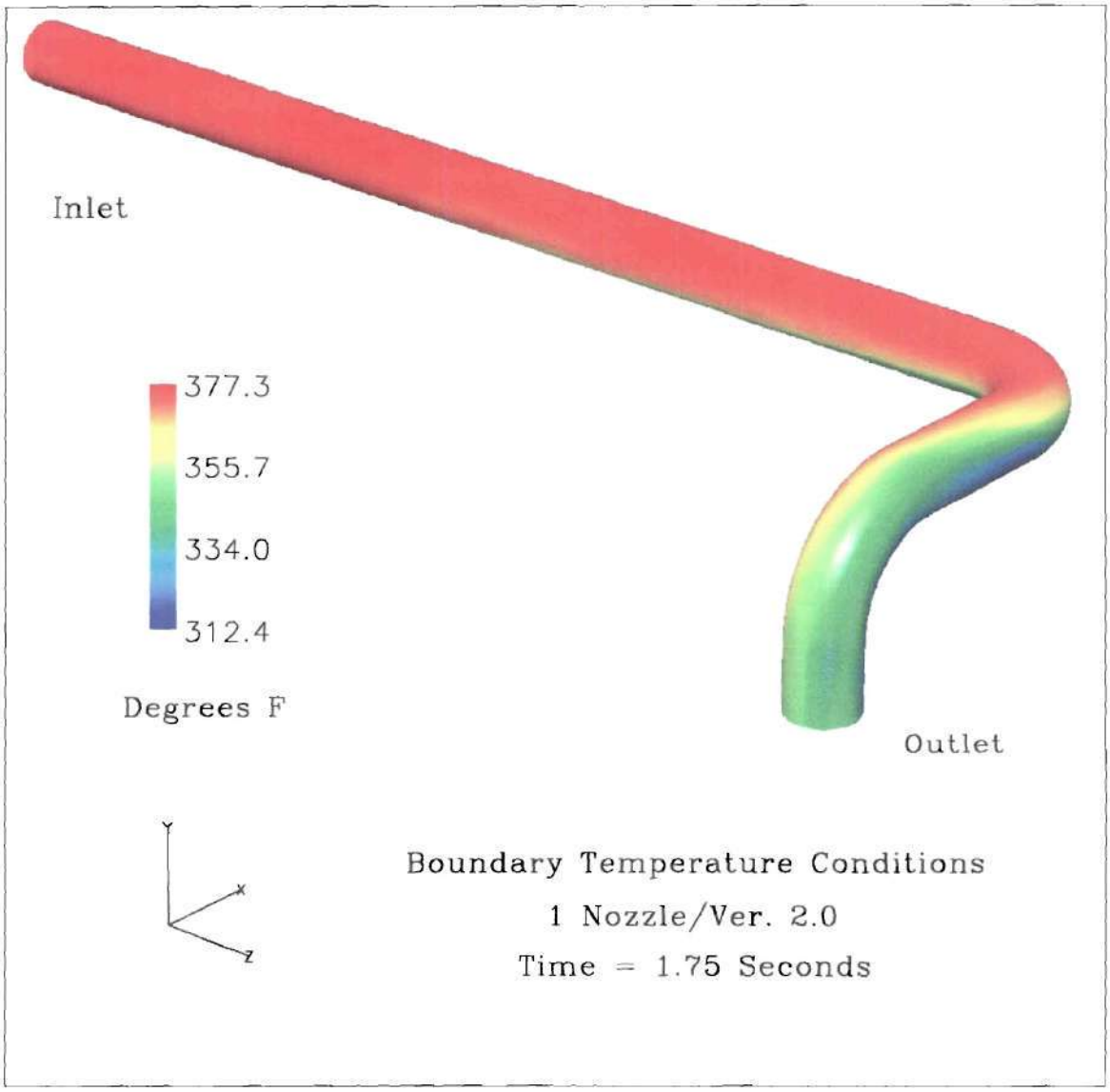
Inlet
377.3
355.7
334.0
312.4
Degrees F
Outlet
Y
X
Z
Boundary Temperature Conditions
1 Nozzle/Ver. 2.0
Time = 1.75 Seconds

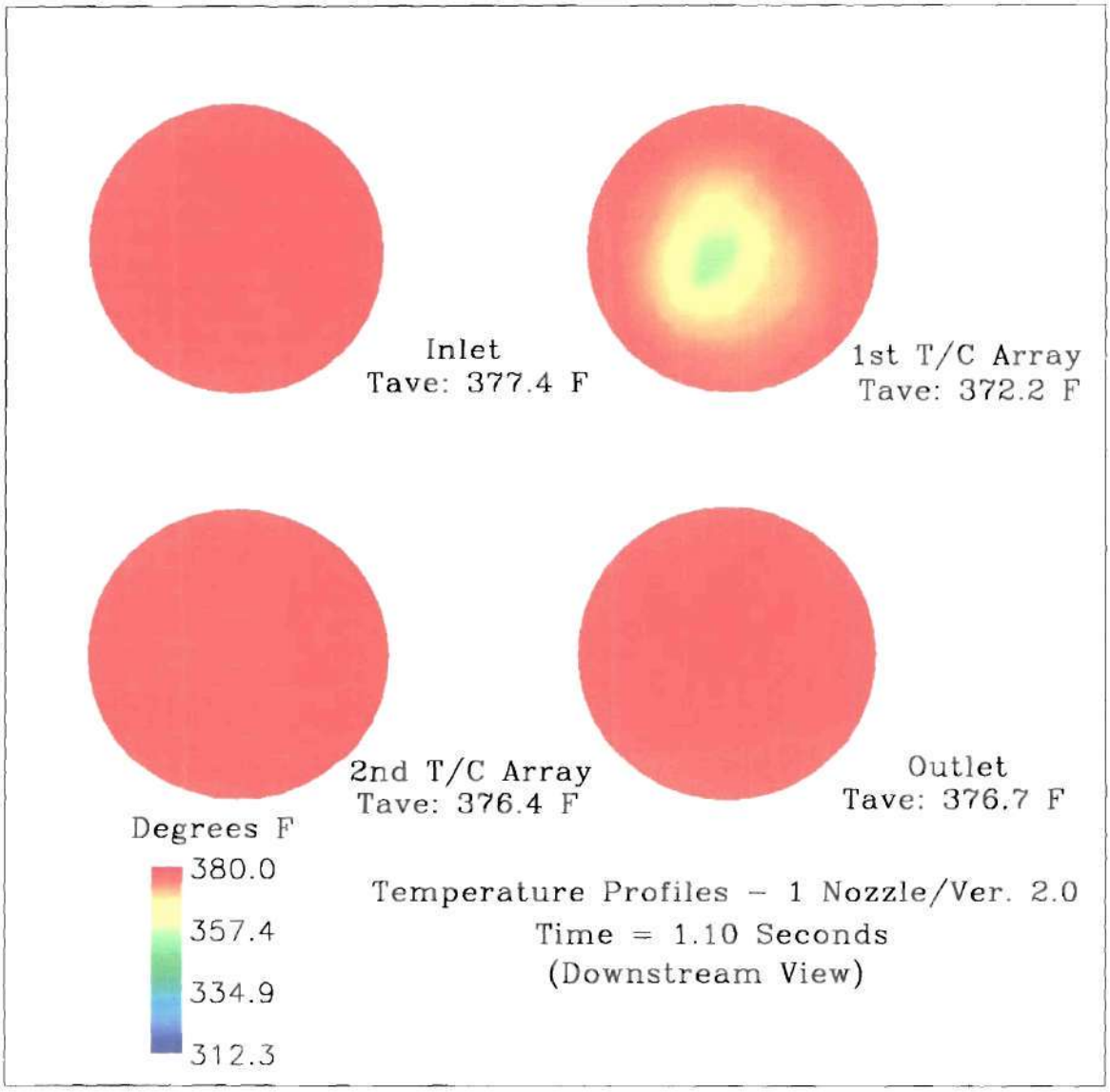
Inlet
Tave: 377.4 F
1st T/C Array
Tave: 372.2 F
2nd T/C Array
Tave: 376.4 F
Outlet
Tave: 376.7 F
Degrees F
380.0
357.4
334.9
312.3
Temperature Profiles - 1 Nozzle/Ver. 2.0
Time = 1.10 Seconds
(Downstream View)

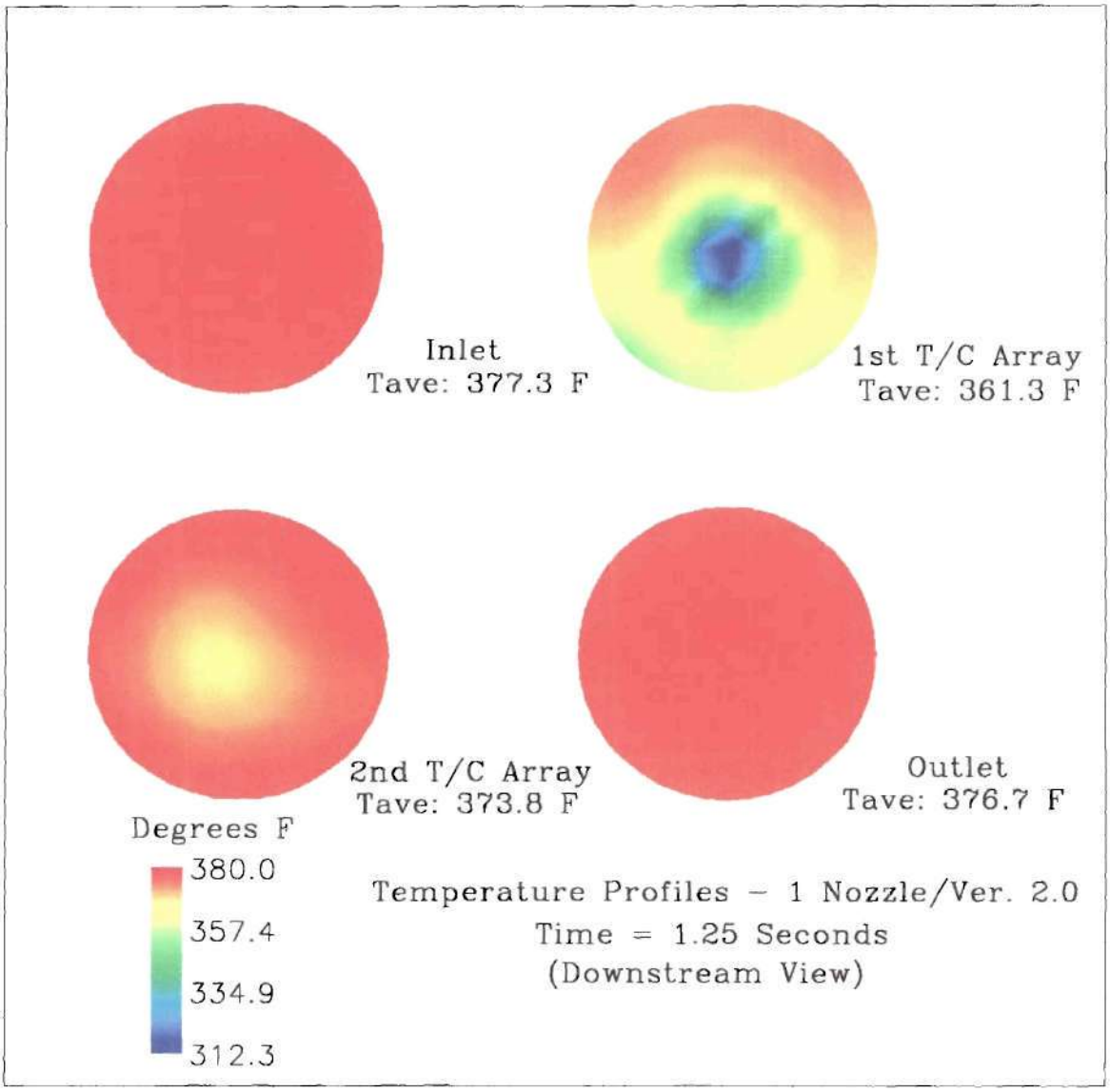
Inlet
Tave: 377.3 F
1st T/C Array
Tave: 361.3 F
2nd T/C Array
Tave: 373.8 F
Outlet
Tave: 376.7 F
Degrees F
380.0
357.4
334.9
312.3
Temperature Profiles - 1 Nozzle/Ver. 2.0
Time = 1.25 Seconds
(Downstream View)

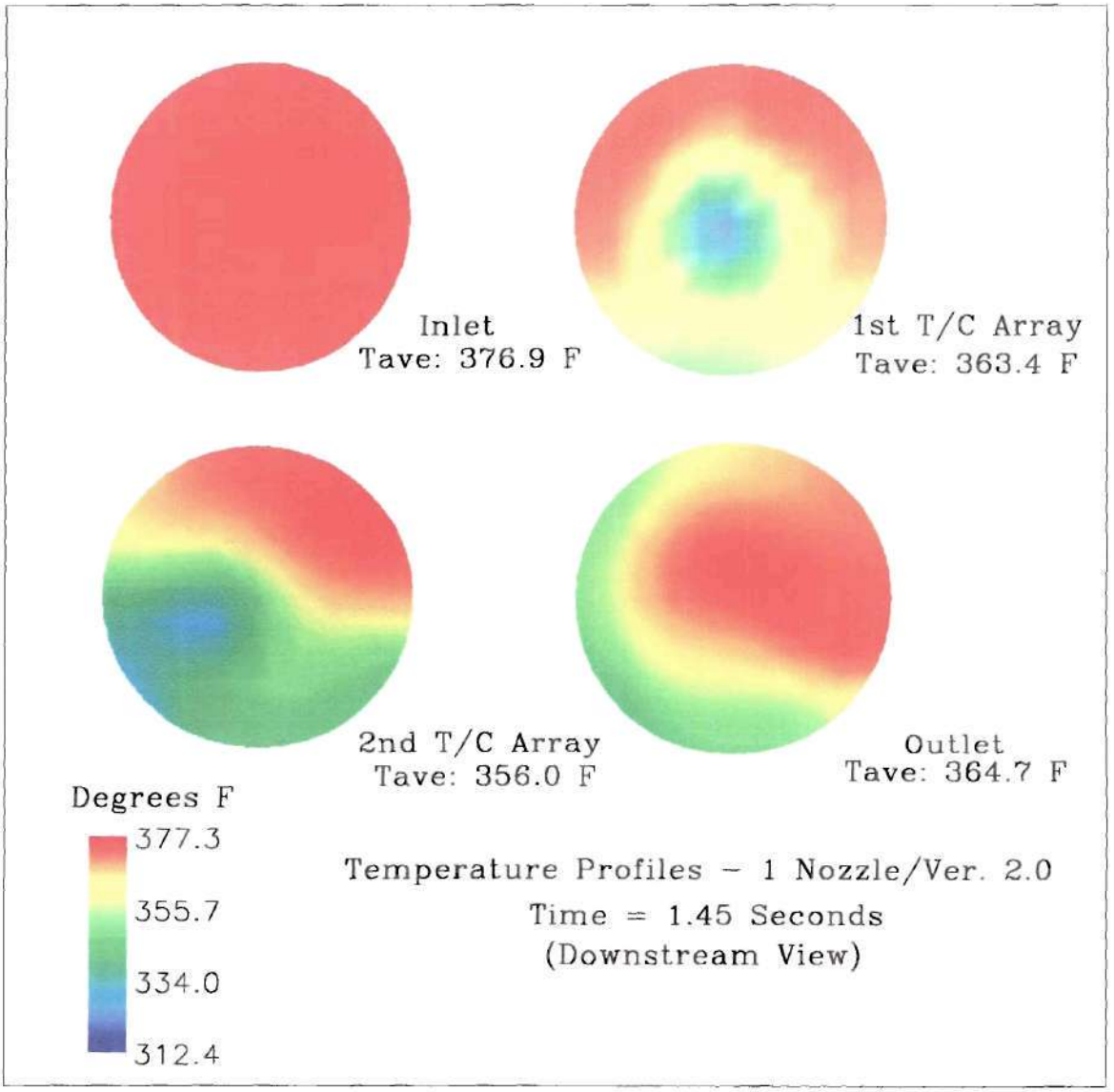
Inlet
Tave: 376.9 F
1st T/C Array
Tave: 363.4 F
2nd T/C Array
Tave: 356.0 F
Outlet
Tave: 364.7 F
Degrees F
377.3
355.7
334.0
312.4
Temperature Profiles - 1 Nozzle/Ver. 2.0
Time = 1.45 Seconds
(Downstream View)

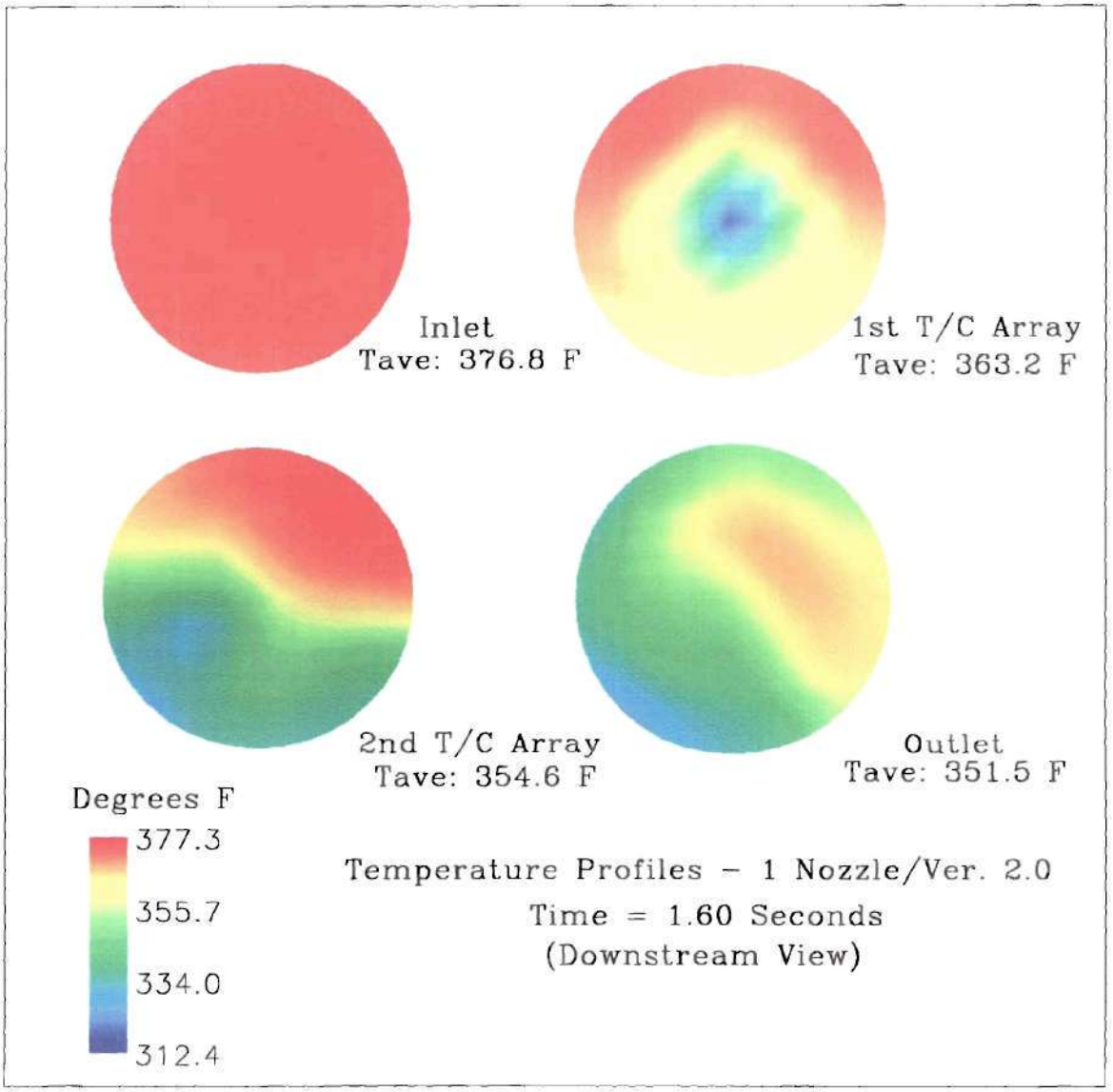
Inlet
Tave: 376.8 F
1st T/C Array
Tave: 363.2 F
2nd T/C Array
Tave: 354.6 F
Outlet
Tave: 351.5 F
Degrees F
377.3
355.7
334.0
312.4
Temperature Profiles - 1 Nozzle/Ver. 2.0
Time = 1.60 Seconds
(Downstream View)

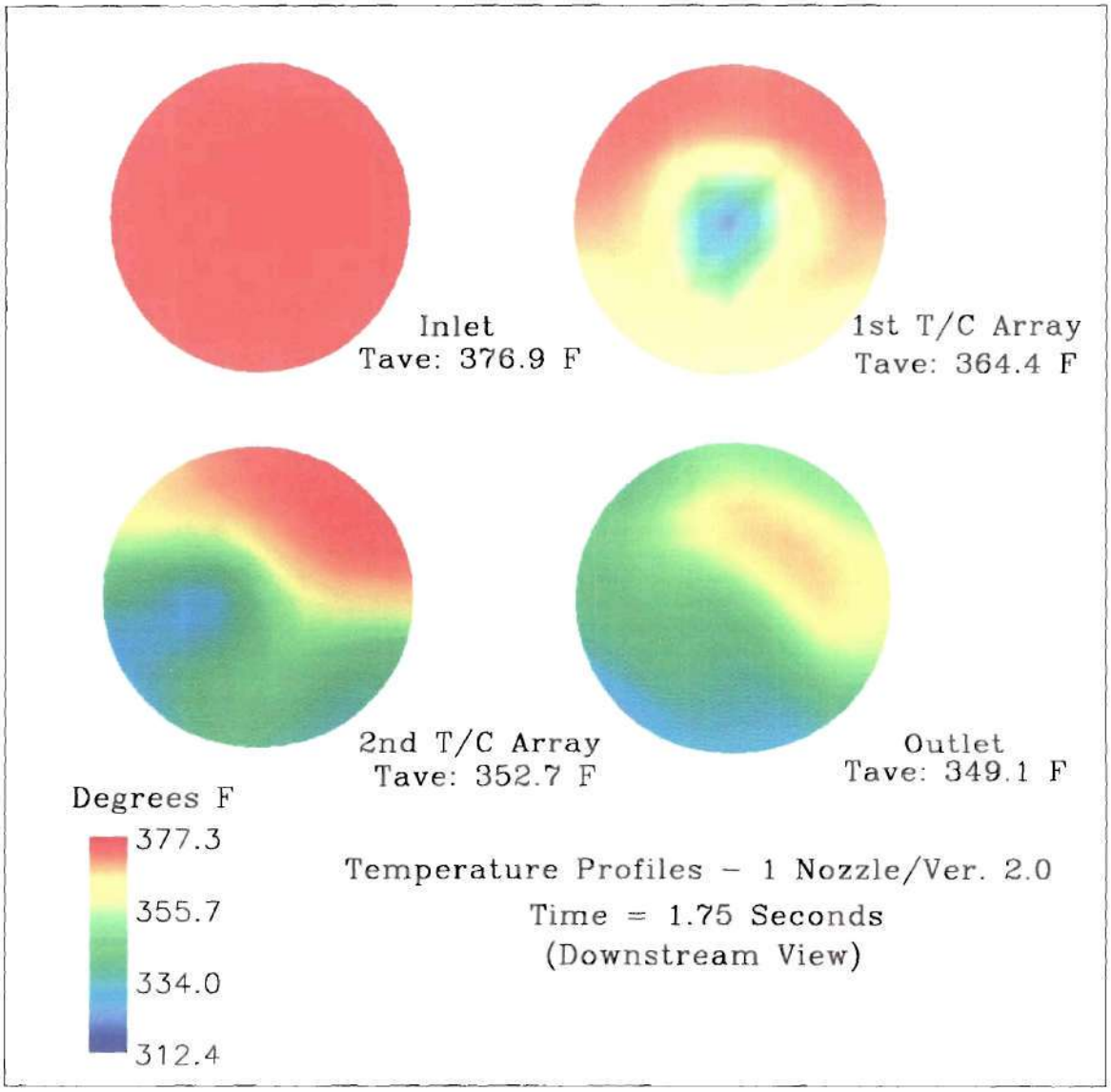
Inlet
Tave: 376.9 F
1st T/C Array
Tave: 364.4 F
2nd T/C Array
Tave: 352.7 F
Outlet
Tave: 349.1 F
Degrees F
377.3
355.7
334.0
312.4
Temperature Profiles - 1 Nozzle/Ver. 2.0
Time = 1.75 Seconds
(Downstream View)

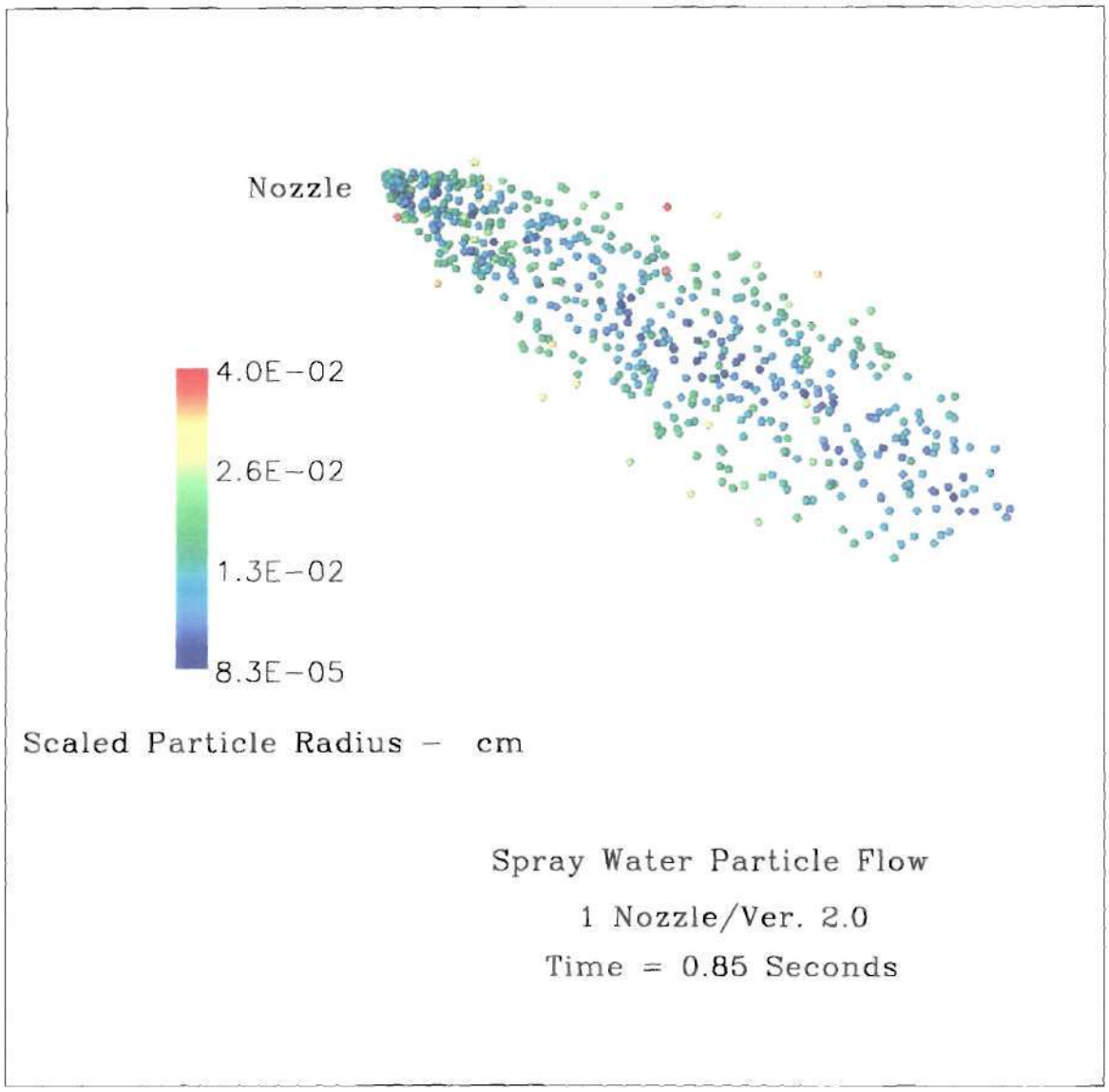
Nozzle
4.0E-02
2.6E-02
1.3E-02
8.3E-05
Scaled Particle Radius - cm
Spray Water Particle Flow
1 Nozzle/Ver. 2.0
Time = 0.85 Seconds

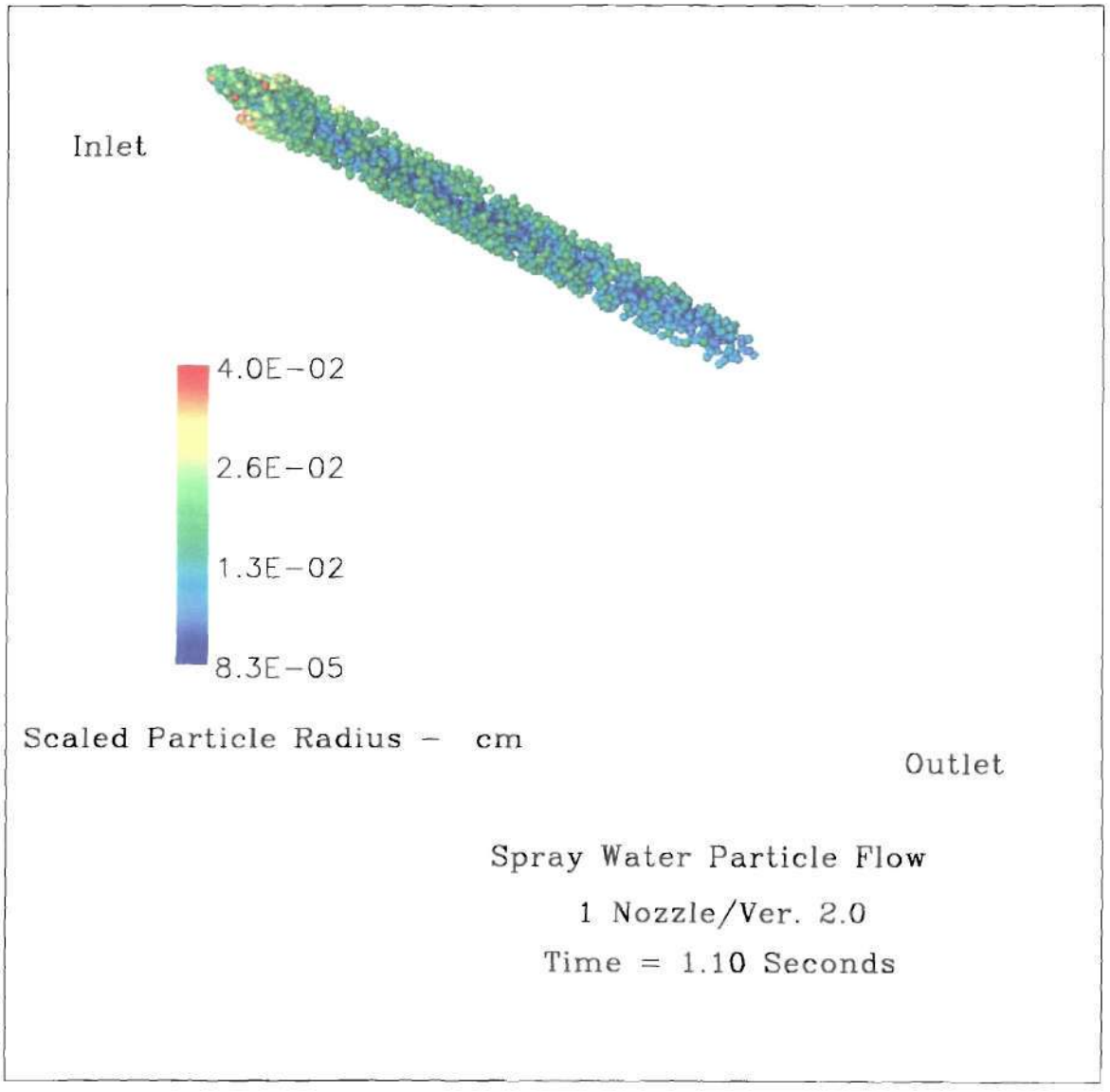
Inlet
4.0E-02
2.6E-02
1.3E-02
8.3E-05
Scaled Particle Radius - cm
Outlet
Spray Water Particle Flow
1 Nozzle/Ver. 2.0
Time = 1.10 Seconds

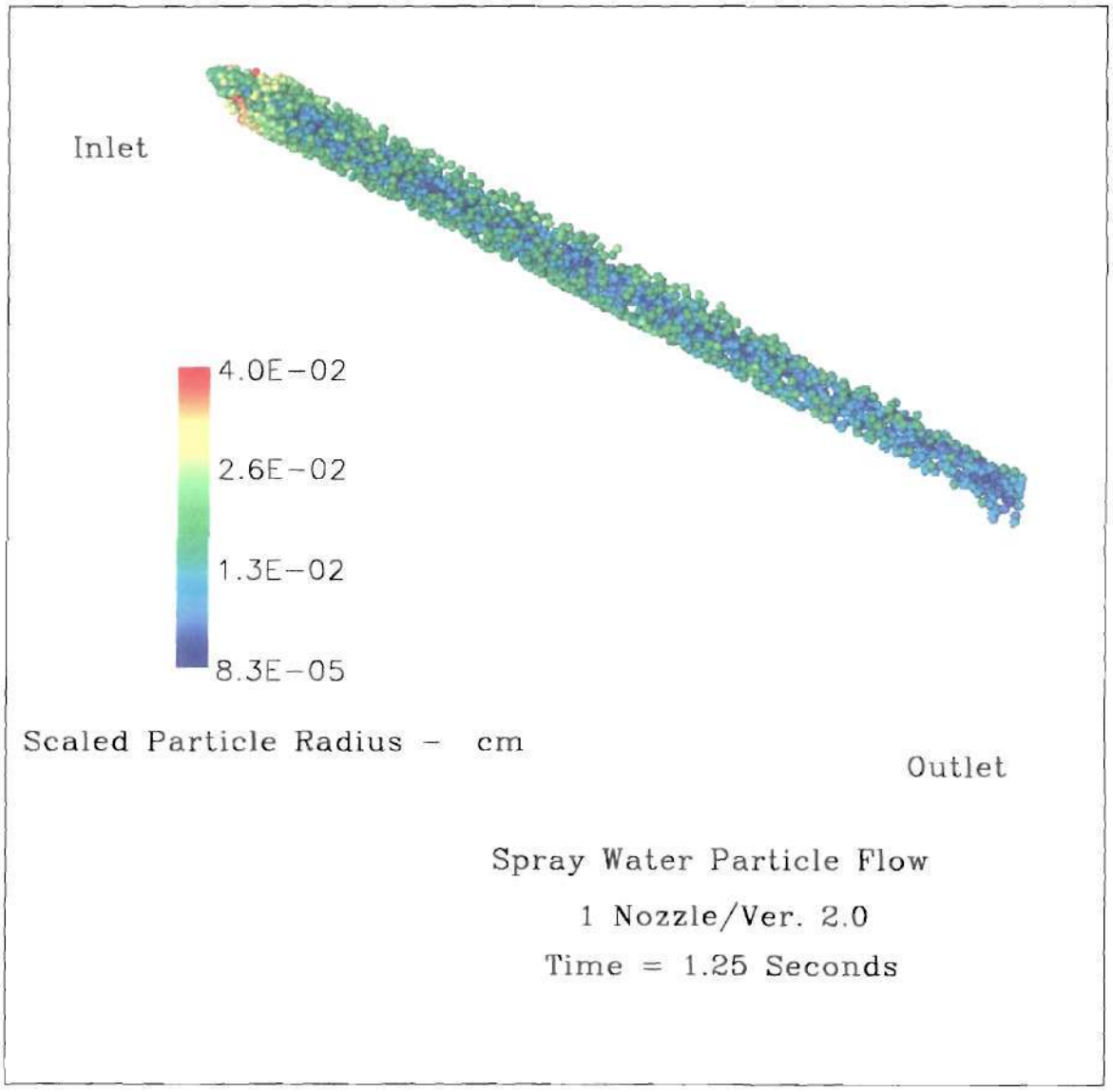
Inlet
4.0E-02
2.6E-02
1.3E-02
8.3E-05
Scaled Particle Radius - cm
Outlet
Spray Water Particle Flow
1 Nozzle/Ver. 2.0
Time = 1.25 Seconds

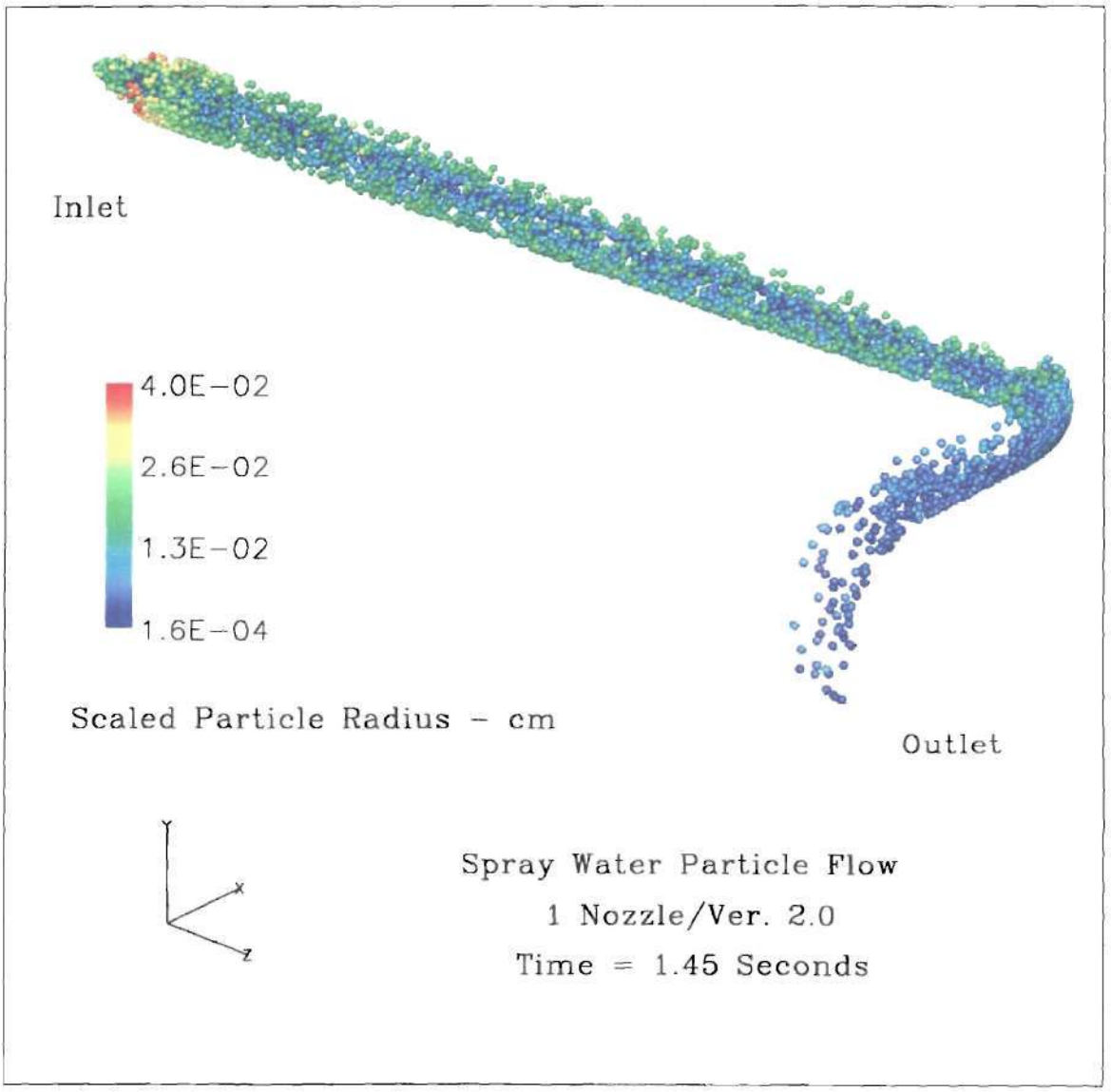
Inlet
4.0E-02
2.6E-02
1.3E-02
1.6E-04
Scaled Particle Radius - cm
Outlet
Y
X
Z
Spray Water Particle Flow
1 Nozzle/Ver. 2.0
Time = 1.45 Seconds

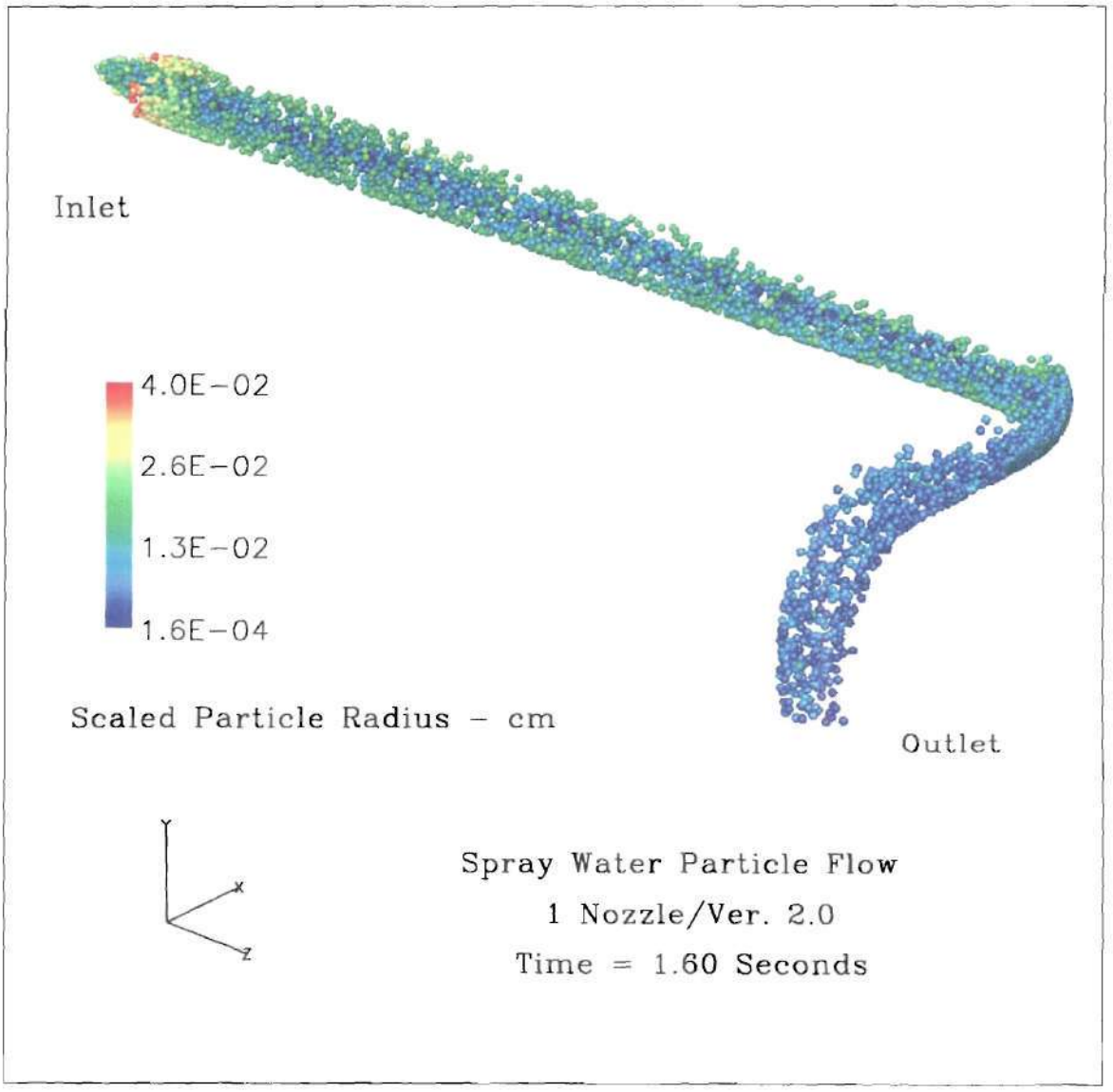
Inlet
4.0E-02
2.6E-02
1.3E-02
1.6E-04
Scaled Particle Radius - cm
Outlet
Y
X
Z
Spray Water Particle Flow
1 Nozzle/Ver. 2.0
Time = 1.60 Seconds

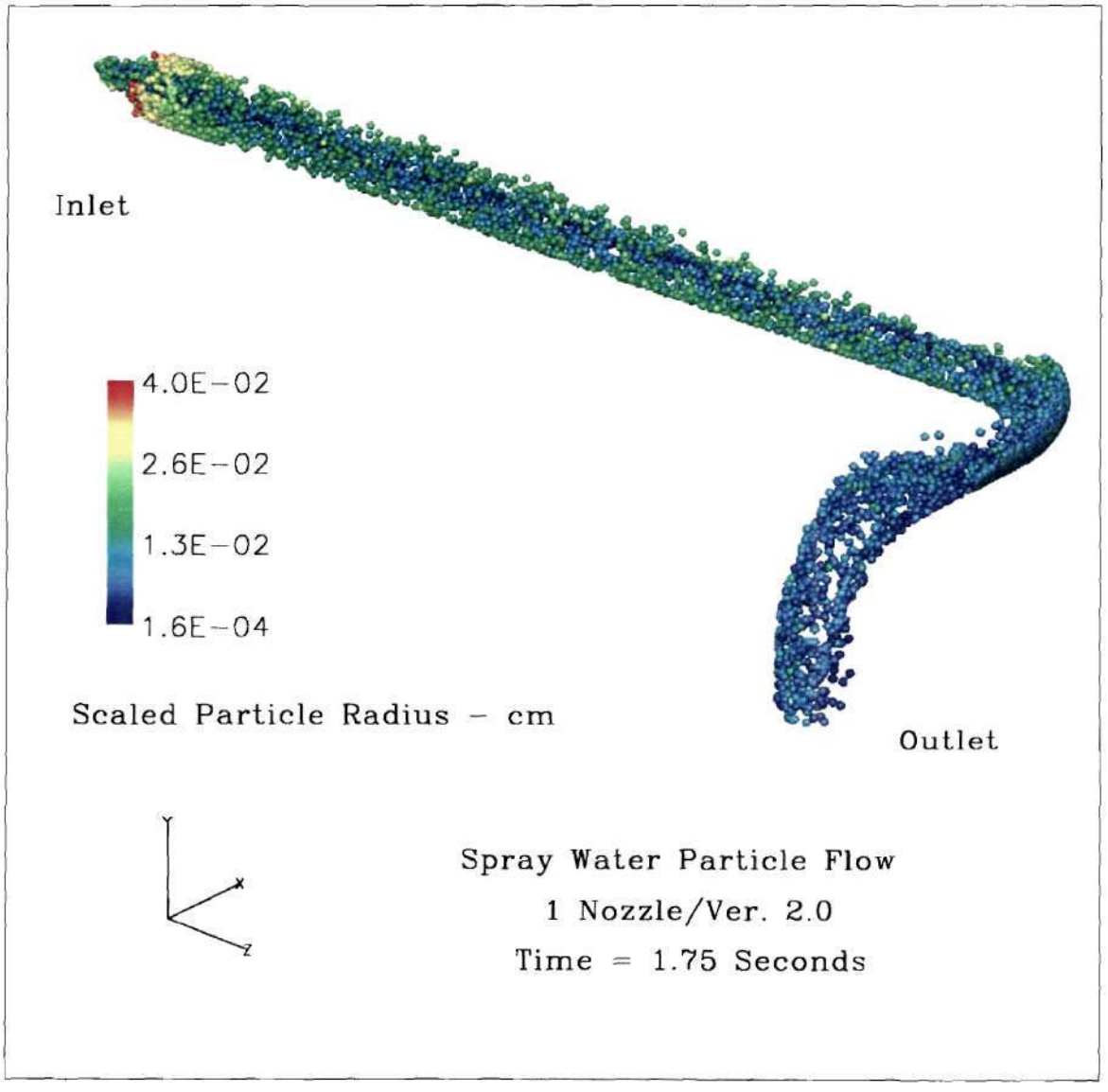
Inlet
4.0E-02
2.6E-02
1.3E-02
1.6E-04
Scaled Particle Radius - cm
Outlet
Y
X
Z
Spray Water Particle Flow
1 Nozzle/Ver. 2.0
Time = 1.75 Seconds

Bibliography

Aggarwal, S.K., Chitre, S., 1991 "Computations of Turbulent Evaporating Sprays", *AIAA Jet Propulsion*, Vol. 7, No. 2, 213-220.

Aggarwal, S.K., Peng, F., 1995 "A Review of Droplet Dynamics and Vaporization Modeling for Engineering Calculations", *Journal of Engineering for Gas Turbines and Power*, Vol. 117, 453-461.

Amano, R.S., Draxler, G.R., Golembiewski, J.M., 1997 "Turbulent Heat Transfer in a Steam Turbine Bypass Pipe Flow", Proceedings of the ASME Heat Transfer Division HTD-Vol. 353, 37-45.

Bowie, G.E., 1985 "Specifying and Operating Desuperheaters", *Chemical Engineering* May 27 1985, 119-124.

Chow, L.C., Chung, J.N., 1982 "Evaporation of Water into a Laminar Stream of Air and Superheated Steam", *ASME Journal of Heat Transfer*, 82-HT-73, 1-8.

Chow, L.C., Chung, J.N., 1983 "Water Evaporation into a Turbulent Stream of Air, Humid Air, and Superheated Steam", *ASME Journal of Heat Transfer*, 83-HT-2, 1-7.

Dent, J.C., 1971 "A Basis for the Comparison of Various Experimental Methods for Studying Spray Penetration", *Loughborough University of Technology TP-710571*, 1881-1885.

Dwyer, H.A., 1989, "Calculations of Droplet Dynamics in High Temperature Environments", *Progressive Energy Combustion Science*, Vol. 15, 131-158.

Elkotb, M.M., Rafat, N.M., 1978 "Fuel Spray Trajectory in Diesel Engines", *ASME Journal of Power* April 1978, Vol. 100, 326-332.

Gokalp, I., Chauveau, C., Morin, C., Vieille, B., Birouk, M., 2000 "Improving Droplet Breakup and Vaporization Models by Including High Pressure and Turbulence Effects", *Atomization & Sprays* Vol. 10, 475-510.

Guo, T., Wang, T., Gaddis, J.L., 2000 "Mist/Steam Cooling in a 180-Degree Tube Bend", *ASME Journal of Heat Transfer* Vol. 122, 749-756.

Hardalupas, Y., Whitelaw, J.H., 1996 "Interaction Between Sprays From Multiple Coaxial Airblast Atomizers", Journal of Fluid Engineering, Vol. 118, 762-771.

Hellingman, A., 1985 "Steam Cycle Control with the use of Desuperheaters", International Power Generation, July/August 1985, 23-27.

Hubbard, G.L., Denny, V.E., Mills, A.F., 1975 "Droplet Evaporation: Effects of Transients and Variable Properties", *International Journal of Heat Transfer*, Vol. 18, 1003-1008.

Ingebo, R.D., 1953 "Study of Pressure Effects on Vaporization Rate of Drops in Gas Stream", *National Advisory Committee for Aeronautics* – Technical Note 2850.

Ingebo, R.D., 1953 "Vaporization Rates and Heat Transfer Coefficients for Pure Liquid Drops", *National Advisory Committee for Aeronautics* – Technical Note 2368.

Kals, W., 1992 "Condensing the Dumped Steam During a Turbine Bypass", Journal of Engineering for Gas Turbines and Power, Vol. 114, 621-631.

Kauer, G., 1998 "Steam Desuperheating by Spray Water Injection in Thermal Plants", *VBG Power Tech* 9/98, 37-44.

Kunkle, T.E., 1999 "Evaluating Desuperheater Performance", Valve Magazine Summer 1999, 18-25.

Lasheras, J.C., Villermaux, E., Hopfinger, E.J., 1998 "Break-Up and Atomization of a Round Water Jet by a High Speed Annular Air Jet", *Journal of Fluid Mechanics*, Vol. 357, 351-379.

Liao, Y., Sakman, A.T., Jeng, S.M., Jog, M.A., 1999 "A Comprehensive Model to Predict Simplex Atomizer Performance", *Journal of Engineering for Gas Turbines and Power*, Vol. 121, 285-294.

Mott, W.W., 1997 "Basic Principles & Practices of Desuperheating", *Valve Magazine*, Spring 1997, 18-26.

Palaszewski, S.J., Jiji, L.M., Weinbaum, S., 1981 "A Three-Dimensional Air-Vapor-Droplet Local Interaction Model for Spray Units", *ASME Journal of Heat Transfer*, 81-HT-18, 1-9.

Ranz, W.E., Marshall, W.R., 1952 "Evaporation From Drops", *Chemical Engineering Progress* Vol. 48, No. 3, 141-146.

Reitz, R.D., Bracco, F.V., 1979 "On the Dependence of Spray Angle and Other Spray Parameters on Nozzle Design and Operating Conditions", *SAE Technical Paper 790494*, 1-19.

Reitz, R.D., Bracco, F.V., 1982 "Mechanism of Atomization of a Liquid Jet", *Physical Fluids*, Vol. 25, No. 10, 1730-1742.

Rizkalla, A.A., Lefebvre, A.H., 1975 "The Influence of Air and Liquid Properties on Airblast Atomization", *ASME Journal of Fluid Engineering*, September 1975, 316-320.

Schelling, J., 1998 "Atomization In a Co-Current Downward Air Stream", *Swiss Federal Institute of Technology Zurich – Diss. ETH No. 12883.*

Sebald J.F., Phillips, N.A., Haman, L.L., 1982 "Recommended Guidelines for the Admission of High-Energy Fluids to Steam Surface Condensers", *EPRI Research Project 1689-1, Report CS-2251.*

Sirignano, W.A., 1983 "Fuel Droplet Vaporization and Spray Combustion Theory", *Prog. Energy Combustion Science* Vol. 9, 291-322.

Stanton, D.W. and Rutland, C.J., 1998 "Multi-Dimensional Modeling of Thin Liquid Films and Spray-Wall Interactions Resulting from Impinging Sprays", *International Journal of Heat and Mass Transfer* 41, 3037-3054.

Stelz, W.G., Rosard, D.D., 1984 "Assessment of Fossil Steam Bypass Systems", *EPRI Research Project 1879-1, Report CS-3717.*

Tropea, C., Roisman, I.V., 2000 "Modeling of Spray Impact on Solid Surfaces", *Atomization & Sprays* Vol. 10, 387-408.

Van Paassen, C.A.A., 1995 "Verstuiven En Verdampen Met Energie", *Technische Universiteit Deft WbMT198*, Holland.

Vara Prasad, C.M., Kar, S., 1978 "An Investigation of the Influence of Back Pressure on the Diffusion of Mass and Momentum of Fuel in Diesel Spray", *ASME Journal of Power* April 1978, Vol. 100, 241-251.

Yao, G.F., Ghiaasiaan, S.M., Abdel-Khalek, S.I., Schoonover, K.G., 1999 "Computational Modeling of Spray Cooling in Vapor Conditioning Equipment", *Proceedings of 2nd International Symposium on Computational Technologies for Fluid/Thermal/Chemical/Systems with Industrial Applications*, Vol. 2, 107-116.